LBL-900

ACCELERATOR HEALTH PHYSICS

H. Wade Patterson

Certified Health Physicist
Group Leader, Health Physics Department

and

Ralph H. Thomas Ph.D. F. Inst. P.

Certified Health Physicist
Health Physics Department

Lawrence Berkeley Laboratory
University of California
Berkeley, California

DISCLAIMER

"The desire for safety stands against every great and noble enterprise."

TACITUS: *Annals,* XV, c.110

Health Physics studies at Berkeley were under the guidance of Professor Burton J. Moyer during the period 1947–1970, and his leadership and wisdom in selecting fruitful avenues of research have led, in a large measure, to our present understanding of the radiation protection problems associated with particle accelerators. It is to him that we dedicate this volume, with respect and admiration.

ACCELERATOR HEALTH PHYSICS

TABLE OF CONTENTS

PREFACE

Accelerator Health Physics is a part of Health Physics--the profession devoted to the protection of man and his environment from unwarranted radiation exposures. Until comparatively recently it has engaged the attention of only a small number of people, principally in the major nuclear physics and high energy physics laboratories throughout the world, where particle accelerators are used largely for fundamental research.

Experience shows us, however, that the research instruments of today are rapidly modified and adapted to become the work-a-day tools of tomorrow. This is undoubtedly happening now with particle accelerators.

In the past few years, there has been a steady increase in the application of particle accelerators to industry and medicine. Recent estimates have indicated that their number is presently increasing at the rate of 200 per year (or roughly 10% per annum of the world total of 2000); about half are being constructed within the United States. Concurrently there is also a trend toward application of accelerators of the higher intensity and energy which are now technically feasible to a host of new and diverse problems throughout a wide range of disciplines.

This increasing use of accelerators demands a corresponding increase in the number of persons familiar with the problems of accelerator radiation protection. The challenge presented to the health physicist is nowhere greater than at accelerator installations, where the radiation environment may be extremely complex and the technique of measurement unfamiliar. If pitfalls are to be avoided, special attention must be given to the problems of shielding and dosimetry at new facilities.

This need was first recognized by E. J. Vallario of the Division of Operational Safety, USAEC, who suggested in 1966 that the Lawrence Berkeley Laboratory, Berkeley, California, be asked to develop a flexible training program in accelerator health physics.

The first course was held in 1967, and over the past 6 years a viable scheme of organization has been developed. Since the needs of the students vary from year to year, the precise set of studies is worked out only after the makeup of the classes is known. In this way we attempt to prepare a "custom-made" course for the student, whether he be from industry, university, National Laboratory, or government agency. This flexibility is provided by having a basic "home team" of lecturers and instructors drawn from the Health Physics group at Berkeley. To prevent presentation of any "parochial" view or "party line"--particularly in matters of administration and philosophy--visiting lecturers are invited to present alternative (or even contrary) views. In this way the student is provided with a sound technical base for accelerator health physics coupled with a broad view of the administrative problems.

The entire course lasts approximately 4 weeks and consists of roughly 60 hours of formal lectures supplemented by some 60 hours of practical work, which includes operational surveys of laboratory accelerators. Adequate time is available for discussion, both among students and between students and instructors. This course is intended to develop a group of health physicists who specialize in accelerator radiation safety problems and who will all have the same training in advanced accelerator radiation monitoring. The variety of accelerators (cyclotrons, both frequency-modulated and sector-focused; proton synchrotrons; heavy-ion accelerators; electron accelerators of a wide range of energies), and the more than 30 years' experience of the Lawrence Radiation Laboratory staff in accelerator radiation measurements, instrument design, shielding radiobiology, and accelerator design, make this laboratory an ideal site for the course. We hope that greater uniformity of health physics measurements and their easier intercomparison throughout the field of accelerator protection will result from this course.

Because no suitable text was available it was quickly recognized that a special manual was needed. In this volume is distilled the almost 50 years of combined experience in working with accelerators shared by the authors as well as their considerable familiarity with training in accelerator health physics for the AEC Special Fellowship Program and the Berkeley Accelerator Health Physics Training Course. General principles are emphasized and material necessary for a clear understanding of accelerator radiation problems, unfamiliar to the average health physicist, has been brought together in convenient form for the first time. The text includes a comprehensive bibliography.

We are aware of the magnitude of the task we have attempted and have approached it with some trepidation, recognizing our limitations in a field already so vast and so rapidly expanding. The general understanding of accelerator radiation problems is continually improving, and a book such as this is to some extent obsolete before it is written. However, we share the views of the thirteenth century chinese author Tai T'ung, who wrote (to paraphrase)

"Were I to await perfection, my book would never be finished, so I have made shift to collect the fruits of my labors as I find them,"*

We have been encouraged, however, by the favorable comments on preliminary drafts of this book by some students who have previously attended the training course. If this volume proves helpful in stimulating the study of Accelerator Health Physics we shall be satisfied.

No work of this nature could have been attempted without the encouragement and support of a very large number of people. Our colleagues in the Health Physics group at the Lawrence Berkeley Laboratory have

---

*The authors are grateful to James Benet, formerly of the San Francisco Chronicle staff, for drawing their attention to this quotation.

been instrumental in developing the Accelerator Health Physics Training Course and making helpful comments on this volume. J. B. McCaslin, A. J. Miller, A. Rindi, J. T. Routti, A. R. Smith, L. D. Stephens, and H. W. Wollenberg all contributed to the preparation of the Appendix.

Roger Wallace assisted in developing the outline for the text and in addition has arranged the format of the lectures offered in the training course. Several other colleagues have freely given us the benefits of their experience in several specialized aspects of Accelerator Health Physics. Many of these have delivered lectures to the Berkeley Accelerator Health Physics Training Course: Mr. H. Howe, of the National Accelerator Laboratory, Batavia, on LET Spectrometry and the Use of Bonner Spheres; Mr. T. M. Jenkins, of the Stanford Linear Accelerator Center (SLAC), on Radiation Protection at Electron Linear Accelerators; Prof. L. H. Lanzl, of the Argonne Cancer Hospital, on Radiation Accidents; and Prof. G. K. Svensson, formerly of SLAC, now of the Harvard Medical School, on ionization chamber theory. For our text we have relied heavily on their lectures and their supplemental notes. Prof. R. Madey of Kent State University gave permission for us to use an extract of his article "Nucleon Accelerators in General" published by Springer-Verlag; Dr. D. Nachtigall, of Euratom, gave us helpful advice on rem-meters; and Dr. J. T. Routti, formerly of Berkeley, now of CERN II, provided the treatment of spectrum unfolding techniques. Dr. R. Budnitz of the Lawrence Berkeley Laboratory is to be thanked for his helpful comments and constructive criticism.

Our sincere thanks are due to Ellen E. Cimpher and Mary L. Long for their cooperation and patience in typing and retyping the manuscripts for this volume. Last but not least the generous and cheerful assistance of the Technical Information Division of Lawrence Berkeley Laboratory, without which this text could not have been produced, is gratefully acknowledged. Charlotte E. Mauk, as editor, with quiet tact and great good humor has striven to improve the literary style of the manuscript; Marthamae Snyder was responsible for the mammoth task of setting the final version on the Composer; Evelyn Grant, Barbara Atkinson, and Robert Stevens drew the diagrams; and Loretta Lizama coordinated the publishing. Our thanks too, to all who have been omitted here to avoid a long catalog, for help on many phases of the work.

We gratefully recognize the foresight and initiative of Mr. Edward J. Vallario, of the USAEC Division of Operational Safety, in suggesting and supporting the Accelerator Health Physics training program, and his encouragement of the writing of this book. We are indebted to the Division of Nuclear Education and Training for encouragement and financial support.

Work done under the auspices of the U. S. Atomic Energy Commission.

CHAPTER 1.

FUNDAMENTAL PARTICLES AND THEIR INTERACTIONS WITH MATTER.

TABLE OF CONTENTS

FUNDAMENTAL PARTICLES AND THEIR INTERACTIONS WITH MATTER

INTRODUCTION

In its most fundamental form a radiation field may be considered in terms of the particles of which it is comprised. "The simplest way to describe a radiation field is to count the number of quanta or particles ('rays') in some way. To describe the field at different points one can count the number of rays per unit area and per unit time of each point" (ROE W 68).

In most branches of health physics it has been customary to quantify radiation fields in terms of integral quantities such as exposure, absorbed dose, and dose equivalent. The reader will discover that a recurring theme of this text is that such a procedure is inadequate in accelerator health physics. In order to properly perform the tasks required of a health physicist at an accelerator--personal dosimetry, the design and construction of radiation-measuring instruments, general radiation and particle beam dosimetry, shielding design or determination of induced activity--it is vital that the detailed composition of the radiation environment be understood "in terms of the particles of which it is comprised." This fact was perhaps first recognized for accelerators by Moyer (MOY B 52a, MOY B 52b, MOY B 54, MOY B 58), and several authors have subsequently discussed this matter (LAD M 69, RIN A 72).

Over the past ten years techniques have been developed for determination of the neutron spectra produced by particle accelerators, with accuracy sufficient for dose-equivalent determinations (GIL W 68, ROU J 69). The conversion of these spectra to dose equivalent is now well understood (PAT H 71, GIL W 68, SHA K 69). This approach to the problem of radiation measurement is also finding increasing favor at reactors, and, indeed wherever neutrons are to be measured (STO D 71, IAEA 63). Sidwell and Wheatley (SID J 68) have indicated the advantages of such an approach to photon dosimetry.

FUNDAMENTAL PARTICLES

Segrè has warned of the difficulties of the concept of a fundamental or elementary particle:

"The whole concept of 'elementary particle,' including its definition, is not clearly settled. Attempts have been made to classify particles in various ways, attributing to some of them a more fundamental role than to others. . . Until now, however, none of these ambitious themes has been able to make enough predictions to establish itself solidly." [Emilio Segrè, in "Nuclei and Particles--An Introduction to Nuclear and Subnuclear Physics."] Nevertheless, despite his warning we list in Table 1.1 the principal properties of the known "fundamental" particles of physics.

Table 1.1. The Fundamental particles.

Class	Symbol and name: Particle	Symbol and name: Anti-particle	Spin (h)	Strangeness (for particle)	Mass (MeV)	Mass (m_c)	Mean life (sec)
BARYONS							
Hyperons	Ξ^- (Xi − or cascade −)	$\bar{\Xi}^+$	1/2	-2	1320.8±0.2	2584.7	$(1.74\pm0.05)\times10^{-10}$
	Ξ^0 (Xi 0 or cascade 0)	$\bar{\Xi}^0$	1/2	-2	1314.3±1.0	2572.0	$(3.06\pm0.40)\times10^{-10}$
	Σ^- (sigma −)	$\bar{\Sigma}^+$	1/2	-1	1197.08±0.19	2342.6	$(1.58\pm0.05)\times10^{-10}$
	Σ^0 (sigma 0)	$\bar{\Sigma}^0$	1/2	-1	1192.3±0.3	2333.2	$<1.0\times10^{-14}$
	Σ^+ (sigma +)	$\bar{\Sigma}^-$	1/2	-1	1189.41±0.14	2327.6	$(0.788\pm0.027)\times10^{-10}$
	Λ (lambda or Λ^0)	$\bar{\Lambda}$ or $\bar{\Lambda}^0$	1/2	-1	1115.40±0.11	2182.8	$(2.62\pm0.02)\times10^{-10}$
Nucleons	n (neutron)	$\bar{n}$	1/2	0	939.550±0.005	1838.6	$(1.01\pm0.03)\times10^{3}$
	p (proton)	$\bar{p}$	1/2	0	938.256±0.005	1836.1	stable
MESONS							
Kaons	K^0	$\bar{K}^0$	0	1	498.0±0.5	974.5	50% K_1, 50% K_2
	K_1^0 or K_1	$\bar{K}^0$					$(0.92\pm0.02)\times10^{-10}$
	K_2^0 or K_2						$(5.62\pm0.008)\times10^{-8}$
	K^+	K^-	0	1	493.8±0.2	996.3	$(1.229\pm0.008)\times10^{-8}$
Pions	π^+	π^-	0	0	139.60±0.05	273.2	$(2.551\pm0.026\times10^{-8}$
	π^0	(π^0)	0	0	135.01±0.05	264.2	$(1.80\pm0.29)\times10^{-16}$
LEPTONS							
Muons	μ^-	μ^+	1/2		105.659±0.002	206.8	$2.2001\pm0.0008)\times10^{-6}$
Electrons	e^-	e^+	1/2		0.511006±0.000002	1.000	stable
Neutrinos	ν_μ	$\bar{\nu}_\mu$	1/2		0 (< 4 keV)		stable
	ν_e	$\bar{\nu}_e$	1/2		0 (< 0.2 keV)		stable
PHOTONS	γ	(γ)	1		0		stable

It is convenient to classify the fundamental particles in four groups, in order of ascending mass:

a. Photons.
b. Leptons.
c. Mesons.
d. Baryons.

The first group contains only one member, the photon, the quantum of electromagnetic radiation. The second group contains all the particles of spin 1/2 that are lighter than the proton. The third group consists of particles of mass intermediate between the leptons and the proton; all members have spin 0. The fourth group consists of heavy particles, of mass equal to or greater than that of the proton.

CONCEPTS

In addition to specifying the species of particles comprising a radiation field it is necessary to describe their energy and spatial distribution. In order to measure radiation fields and to shield them one must understand their interaction with matter. A brief review of the basic concepts needed is given here. More comprehensive discussions are found in publications of the ICRU (ICRU 69, ICRU 70, ICRU 71) or in review articles such as those by Roesch and Attix (ROE W 68) or Kase and Nelson (KAS K 72).

KINETIC ENERGY, TOTAL ENERGY, AND MOMENTUM

Many early accelerators operated on the principle of voltage drop, in which the electrical potential of a charged particle is converted to kinetic energy by acceleration across a potential difference. A typical example is the Van de Graaff accelerator (see Chapter 3).

It became customary therefore to measure kinetic energies in units of electron volts (eV)--corresponding to the kinetic energy acquired by a particle of electron charge crossing a potential difference of 1 volt:

$$1 \text{ eV} \equiv 1.602 \times 10^{-12} \text{ ergs.}$$

The multiple units most frequently used are keV, MeV, and GeV (10^9 eV).

In accelerator health physics many of the particles to be measured are sufficiently energetic that their motion is subject to relativistic kinematics.

The rest energy, W_0, of the particle is defined as

$$W_0 = m_0 c^2, \tag{1}$$

where m_0 = particle rest mass,
c = velocity of light,

and the total energy, W, of the particle is given by

$$W = mc^2 \tag{2a}$$

$$= m_0 c^2 (1-\beta^2)^{-1/2} \tag{2b}$$

where m = observed mass of particle,

$$\beta = \frac{v}{c} .$$

The kinetic energy, E, of the particle is given by

$$E = W - W_0 = (m-m_0)c^2. \tag{3}$$

From Eqs. 1a and 2 it follows that

$$\beta = \frac{v}{c} = \left[1 - \left(\frac{W_0}{W}\right)^2\right]^{1/2} \tag{4}$$

The momentum, p, of a particle is

$$p = mv = m\beta c = \frac{1}{c} (W^2 - W_0^2)^{1/2}$$

$$= \frac{1}{c} \left[E(E + 2W_0)\right]^{1/2} . \tag{5}$$

We see from Eq. 5 that at high kinetic energies ($E >> 2W_0$)

$$p \approx \frac{E}{c} \approx \frac{W}{c} . \tag{5a}$$

Equation 5a explains the frequent use of the units MeV/c or GeV/c to express particle momentum in accelerator physics.

FLUX DENSITY

A radiation field may be described by specifying the number of rays (particle paths) crossing unit area in a given time.

The simplest case that may be considered is that in which all the rays are parallel (Fig. 1.1a). The flux density at the point P may be determined by counting the number of rays per unit area over a small area, dA, in the vicinity of P, over which the flux density is essentially uniform. From Fig. 1.1a we see that the number of rays intercepted by the small area, dA, is proportional to $\cos\theta$, where θ is the angle between the normal to dA and the beam direction. When $\theta = 0$ the number of rays, dn, intercepting the area, da, in time dt is a maximum, and the particle flux density, ϕ, which is a scalar quantity, is defined to be

$$\phi = \frac{dn}{dA\, dt} . \tag{6}$$

In radiation fields whose constituent particles move in many directions the flux density is also defined by Eq. 6, but now dn is the number of rays (particle paths) that cross the surface of the sphere of revolution of a small circular area, dA (Fig. 1.1b), in time dt.

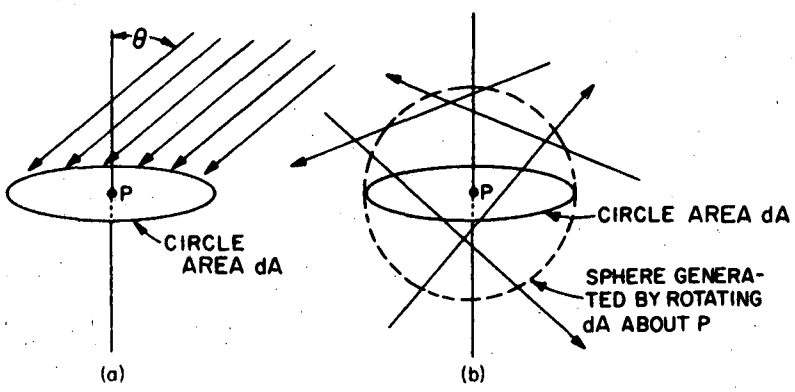

Fig. 1.1. Flux density and fluence in monodirectional and multidirectional fields. (from Roesch and Attix)

ENERGY SPECTRA

The flux density at a point of all particles of one species is usually insufficient for health physics purposes. It is necessary, in addition, to specify the distribution of these particles with energy, and sometimes necessary to specify their distribution in space. The flux density of particles having kinetic energy in the range E and E+dE is written $\phi(E)dE$, and the parameter $\phi(E)$ as a function of E is termed the *differential energy spectrum.*

The flux density over all energies, Φ, is given by

$$\Phi = \int_0^\infty \phi(E)dE, \tag{7}$$

and the *integral flux density*, $\Phi(> E')$, is given by

$$\Phi(>E') = \int_{E'}^\infty \phi\,(E)\,dE. \tag{8}$$

CROSS SECTION

Cross section is an extremely important concept in describing the interactions of particles. Consider a beam of particles of intensity I particles/cm^2 sec incident upon a thin slab of absorber of thickness dx. If the absorbing medium contains N nuclei per cm^3, then the number of incident particles interacting, dI, will be proportional to both I and Ndx:

$$-dI \propto INdx$$

$$\text{or} \quad -dI = \sigma NIdx, \tag{9}$$

where σ is a constant of proportionality, representing the effective interaction cross section of each nucleus.

Integration of Eq. 9 gives

$$I(x) = I(0)\, e^{-N\sigma x}, \tag{10}$$

where $I(x)$ is the particle intensity at depth x,
$I(0)$ is the incident particle intensity.

The product $N\sigma$ is often called the *absorption coefficient*, denoted by μ,

$$\mu = N\sigma, \tag{11}$$

and its reciprocal an *attenuation length*, often denoted by λ,

$$\lambda = \frac{1}{\mu} = \frac{1}{N\sigma}. \tag{12}$$

These concepts are of particular importance in the theory of accelerator shielding (Chapter 6).

Partial Cross Sections

The angular and energy distributions of particles produced in nuclear reactions is expressed by partial cross section. The probability of producing a particle of energy in the range E, E+dE in the solid angle between Ω and Ω+dΩ is denoted by

$$\frac{d^2\sigma}{dEd\Omega}.$$

The integration of these partial cross sections over the appropriate range of energy and in space gives the total cross section defined by Eq. 10 (GRE A 55).

THE INTERACTION OF FUNDAMENTAL PARTICLES

We have seen in the quotation from Segrè on fundamental particles that a full discussion of their properties would inevitably lead to philosophical and speculative areas of knowledge. Moreover, this is beyond the scope of this book and the capacity of the authors!

Fortunately, such a discussion is unnecessary for our purposes, and we may proceed in a strictly pragmatic manner. The four principal types of radiations of concern to the accelerator health physicist are

a. Electromagnetic radiation (photons, e.g., x or γ radiation).
b. Electrons (including positrons).
c. Charged heavy particles of mass comparable to the mass of the hydrogen atom (e.g., protons, deuterons, α particles).
d. Neutrons.

In addition, at higher energies one may have to consider the charged π mesons produced in nuclear interactions and their decay products, the μ mesons (see Table 1.1).

The primary cause of biological damage is production of ions in living tissue by radiation. The establishment of adequate techniques of radiation dosimetry must be based upon an understanding of the physical phenomena by means of which energy is transferred from radiation to matter and the concomitant process of ionization.

At high energies, such as those at particle accelerators, ionization often proceeds via two different mechanisms. High energy particles (including photons) undergo *nuclear interactions* that may produce photons and secondary heavy particles that may be either charged (e.g. protons, deuterons, α particles, $\pi^{\pm}$ mesons) or uncharged (neutrons). Photons, electrons, and charged heavy particles undergo *electromagnetic interactions.* These processes that produce ionization are of major importance in health physics.

ELECTROMAGNETIC INTERACTIONS

Heavy Charged Particles

A characteristic feature of the absorption of slow heavy charged particles is that they have a definite range in matter (Fig. 1.2). This is in constrast to the absorption of photons or neutrons, which is exponential, or of electrons, which have only an ill-defined range in matter.

Energy losses due to ionization are now relatively well understood and are discussed in many fundamental texts on nuclear physics (see bibliography). The interested reader is referred to the literature for a detailed discussion of stopping-power theory. Turner (TUR J 67) has given a brief overview of the contributions of Bohr and Bethe, and Fano (FAN U 63) has discussed the development of Bethe's stopping-power theory to its presently used form. More comprehensive reviews have been given by Bethe and Ashkin (BET H 53), Northcliffe (NOR L 63), Steward (STE P 68), and Kase and Nelson (KAS K 78).

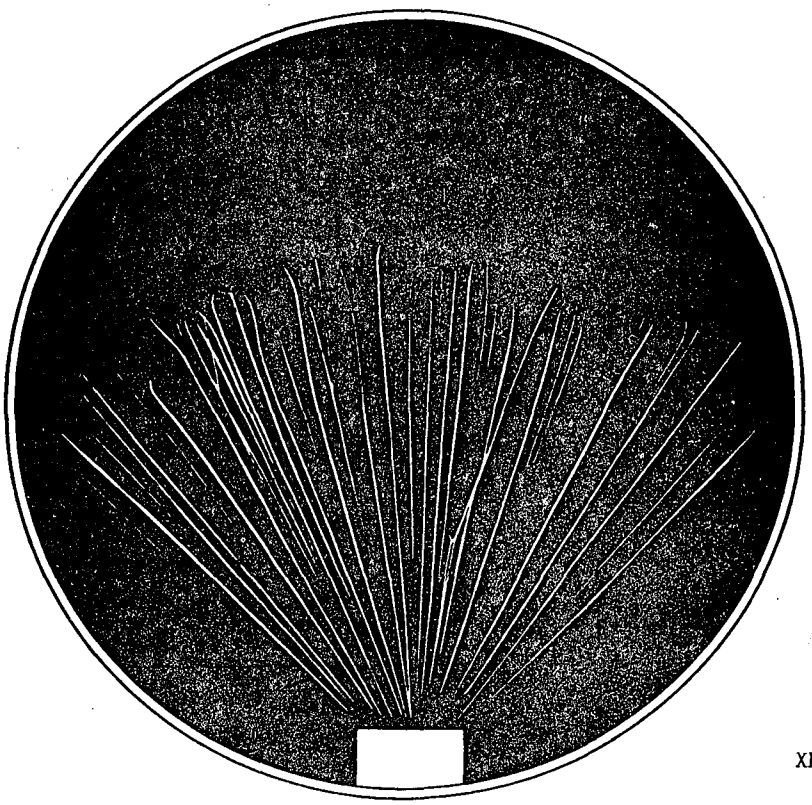

XBL 728-1364

Fig. 1.2 A sketch of some cloud chamber tracks of α particle from ^{210}Po. The definite range of heavy charged particles is clearly seen. (from Halliday.)

For our purposes here it is sufficiently accurate to express the energy losses of heavy particles due to collision processes with atomic electrons by Bethe's formula (LIV M 37):

$$-\left(\frac{dE}{dx}\right)_{coll} = \frac{4\pi z^2 e^4 NZ}{mv^2}\left[\ell n \left(\frac{2mv^2}{I(1-\beta^2)}\right) - \beta^2\right], \qquad (13)$$

where e is the charge of the moving particle,
v is the velocity of the moving particle,
m is the rest mass of the electron,
N is the atomic density of the absorber,
Z is the atomic number of the absorber.,
I is the effective ionization potential of the medium.

We may write Eq. 13 in the form

$$-\left(\frac{dE}{dx}\right) = z^2 f(v), \qquad (14)$$

where f(v) is some function of velocity. From Eq. 14 it is self-evident that particles with the *same velocity* have collision energy losses proportional to z^2. Remembering that the kinetic energy of a particle, E, is given by

$$E = M\, g(v), \tag{15}$$

where g (v) is a function of velocity alone,
we conclude that

$$\left(\frac{dE}{dx}\right)_{coll} = z^2 h\left(\frac{E}{M}\right), \tag{16}$$

where h(E/M) is a function of (E/M) alone.
Thus particles with energy expressed in units of kinetic energy per unit mass have stopping powers proportional to z^2.

Consequently, once the energy loss of protons as a function of kinetic energy is known, the foregoing considerations make it possible for us to write the energy loss as a function of kinetic energy of any heavy particle. Fig. 1.3 shows the stopping power of air (at STP) for several particles as a function of kinetic energy. (No account is taken of nuclear collisions, which are important for protons, α particles, and deuterons above $\approx$ 50 MeV--see Chapter 3.) Extensive tabulation of collision stopping power for heavy charged particles may be found, for example, in Rich and Madey (RIC M 54), Atkinson and Willis (ATK J 57), Bichsel (BIC H 63), Barkas and Berger (BAR W 64), Fano (FAN U 64), and Janni (JAN J 66). These calculated tabulations are in excellent agreement with available experimental data. Figure 1.4 shows the collision stopping power of water (similar in atomic composition to human tissue) for protons of kinetic energy between 1 MeV and 1 GeV.

Once the collision energy loss is known as a function of energy for a particular heavy particle, its range in an absorbing medium may be determined. The mean range, $\bar{R}$, may be written

$$\bar{R} = \int_0^R dx = \int_0^R dE \Big/ \left(\frac{dE}{dx}\right)_{coll} \tag{17}$$

The mean range, $\bar{R}$, may then be simply determined by performing the integration of Eq. 17. At particle energies well above 1 MeV/amu the use of the Bethe formula above (Eq. 13) leads to good estimates of mean range. However, at low energies the Bethe formula fails. As a heavy particle slows down the collision stopping power must eventually fall to zero, whereas Eq. 13 predicts a steady increase. This inaccuracy arises because no account is taken of the random capture and loss of electrons by the moving particle as it slows down to velocities comparable to those of orbiting electrons of the atoms of the absorbing medium. In the energy range between 0.01 and

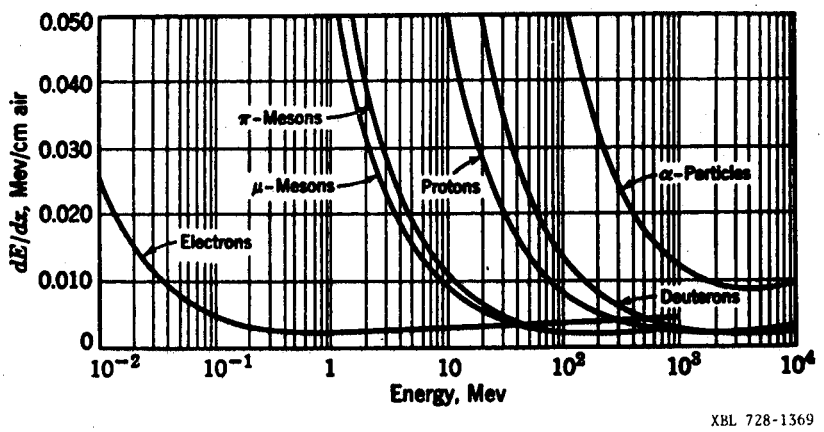

Fig. 1.3. The stopping power of air (at STP) for several particles. (from Halliday.)

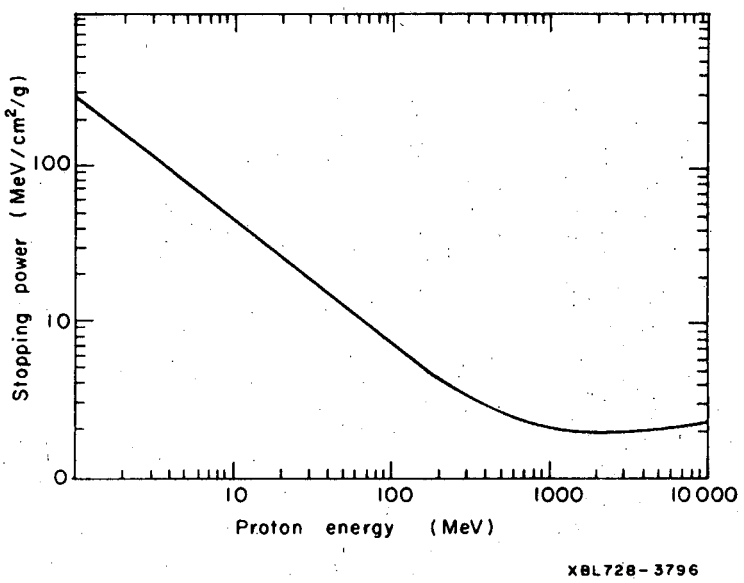

Fig. 1.4. The stopping power of water for protons. (after Rich and Madey.)

I MeV/amu we are dependent upon experimental measurements; these have been summarized by Whaling (WHA W 58) [derived from data due to Phillips (PHI J 53), Reynolds et al. (REY H 53), Milani et al. (MIL S 58), and Northcliffe (NOR L 63).] Figure 1.5 shows the stopping power of aluminum for various ions, according to Northcliffe's evaluation of the experimental data. When these data are combined with the data of the tabulations above 1 MeV/amu, extremely reliable estimates of stopping power over the range from 0.01 MeV/amu to more than 10 MeV/amu are obtained.

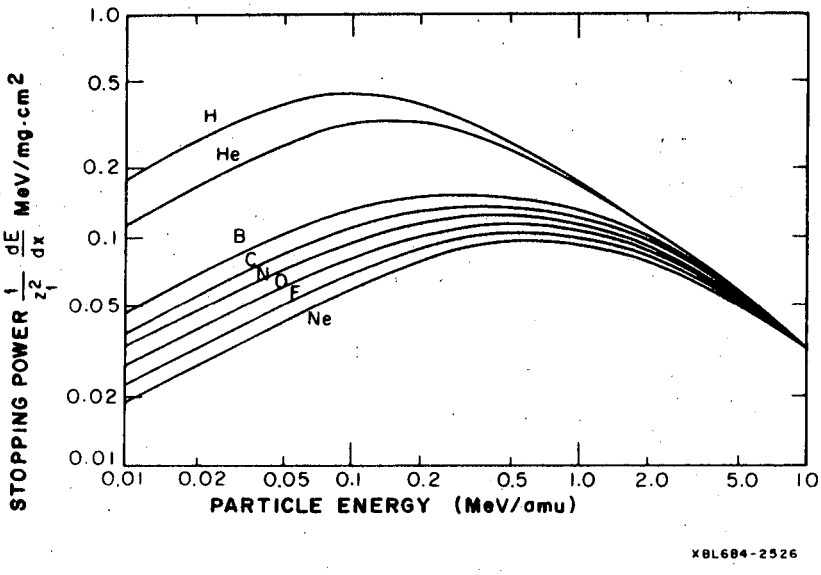

Fig. 1.5. The stopping power for various ions in aluminum. (from Steward, after Northcliffe.)

Electrons

The absorption of electrons in matter is much more complicated than that of heavy particles. This complexity arises because two mechanisms contribute to the energy-loss process. In addition to atomic collisions, radiation losses occur when an electron is deflected by the electromagnetic field of a nucleus.

The total energy loss, dE/dx_{tot}, may now be written

$$\left(\frac{dE}{dx}\right)_{tot} = \left(\frac{dE}{dx}\right)_{coll} + \left(\frac{dE}{dx}\right)_{rad} \qquad (18)$$

where the latter term represents radiation losses. Figure 1.6 illustrates the relative importance of these two mechanisms as functions of electron energy.

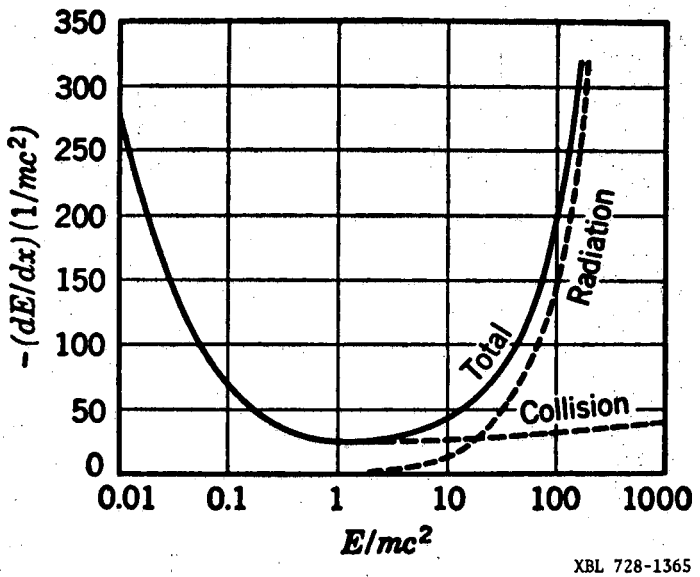

Fig. 1.6. Energy-loss mechanisms for electrons in lead. (from Halliday.)

COLLISION LOSSES

At low energies ($\leq 2\ mc^2$, corresponding to about 1 MeV) the energy loss due to ionization is seen to be more important than that due to radiation.

The collision energy loss is very similar to that for heavy charged particles (Eq. 13):

$$\left(\frac{dE}{dx}\right)_{coll} = \frac{4\pi e^4 N}{mc^2}\left\{\log\ \frac{2\,mc^2}{I} - \frac{3}{2}\ \log(1-\beta^2)^{1/2} - 0.9772\right\}. \quad (19)$$

At identical values of particle velocity, β, Eq. 19 never differs by more than 10% from the equivalent expression for heavy particles (of the same velocity) up to energies of 10 GeV/amu.

RADIATION LOSSES

An accelerated charged particle radiates electromagnetic energy. Acceleration occurs when a charged particle passes close to an atomic nucleus. For electrons, which are of relatively small mass, this acceleration is often sufficient to deflect the electron, in which case radiation will be emitted. This radiation is termed bremsstrahlung. The continuous spectrum emitted by x-ray tubes is a good example of this type of radiation. (See also chapter 3, p. 3-13 et seq.)

Another situation in which bremsstrahlung is emitted occurs when electrons are deflected in a circular orbit, as, for example, in a betatron. Usually this bremsstrahlung intensity is so low that it can be neglected so far as health physics is concerned; however, Shurcliffe (SHU W 72) has shown that it is not always negligible. He has estimated that the theoretical dose rate that could exist in accessible areas near the stored electron beam (5 ma average current and 3 GeV energy) at the Cambridge Electron Accelerator is as high as 10^4 rem/sec.

Radiative energy losses are theoretically well understood. Bethe and Heitler (BET H 34) give the energy loss at high energy ($E \gg 0.5$ MeV for the electron) as

$$\left(\frac{dE}{dx}\right)_{rad} = \frac{4Z(Z+\zeta)\,e^4N}{137\,m^2c^4}\,E\,[\ell n\,(183\,X^{-1/3}) + 1/18]. \qquad (20)$$

In this equation all the symbols are familiar except the parameter ζ, which gives the contribution due to the influence of orbital electrons. Values of ζ are given by Bethe and Ashkin (BET H 53), who show the parameter to vary smoothly from 1.40 for hydrogen to 1.14 for uranium.

Equation 20 shows that radiative losses are proportional to kinetic energy E and roughly proportional to $(Z/m)^2$. For a given particle, Eq. 20 may be written

$$-\frac{dE}{dx_{rad}} = \frac{E}{L}, \qquad (21)$$

where L is a constant for a given target material, independent of energy. Integration gives

$$E = E_0\,e^{-x/L},$$

where E_0 is the initial energy of the particle
and L is a quantity known as the radiation length; it is evidently

$$\frac{1}{L} = \frac{4Z(Z+\zeta)\,e^4N\,[\ell n\,(183Z^{-1/3}) + 1/18]}{137\,m^2c^4} \qquad (22)$$

(see Chapters 3 and 6).

[Heavy particles may also lose energy by radiative processes but that these losses are inversely proportional to m^2 makes them extremely small. Several authors have discussed the energy loss of high energy muons (HAY P 63, THO R 64, DES H 68, THE D 70). At energies above 10 GeV radiation losses became significant, particularly in materials of high atomic number. Figure 1.7 shows the energy loss of muons, as a function of energy, in several materials. Radiative energy losses by protons and heavier particles are negligible in the energy range presently achievable.]

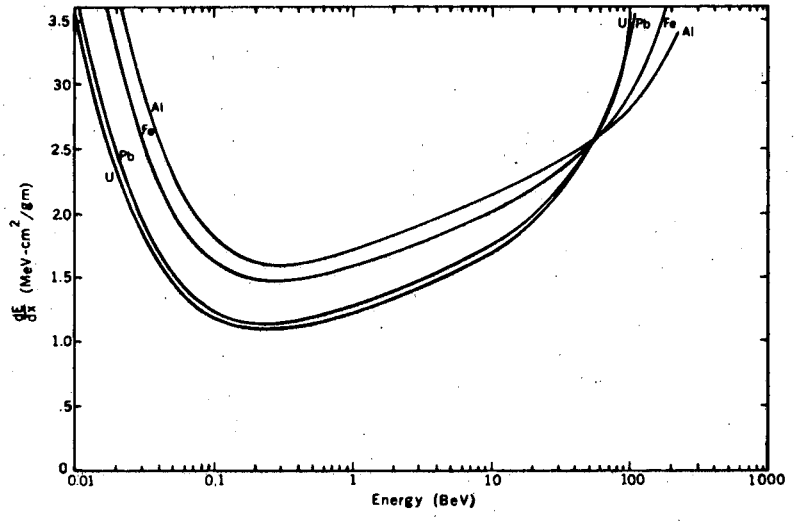

Fig. 1.7. Energy loss of muons. (after Thomas.)

As a consequence of these two mechanisms of energy loss--radiation and collision--electrons do not have as definite a range as do protons and other heavier particles. Firstly, the trajectories of electrons through matter are not straight, electrons suffering large deflections in their collisions with atomic electrons. For this reason the actual amount of material traversed by electrons passing between two points in an absorber may vary significantly. In consequence electrons of the same energy are not stopped by the same amounts of material. Secondly, as we have seen, absorption due to radiative energy losses is exponential.

Figure 1.8 shows typical examples of absorption measurements of monoenergetic electrons in aluminum when an ionization chamber is used as a detector. Various definitions of effective range are evidently possible, but the most reproducible feature of such data is the intercept of the linear

region of the absorption curve with the thickness axis (see Fig. 1.8). This is referred to as the *extrapolated range.* Figure 1.9 shows a typical absorption curve obtained for a continuous β^--particle spectrum. A maximum range, R_{max}, is usually chosen at the rather clearly defined intersection of the absorption curve with the background curve.

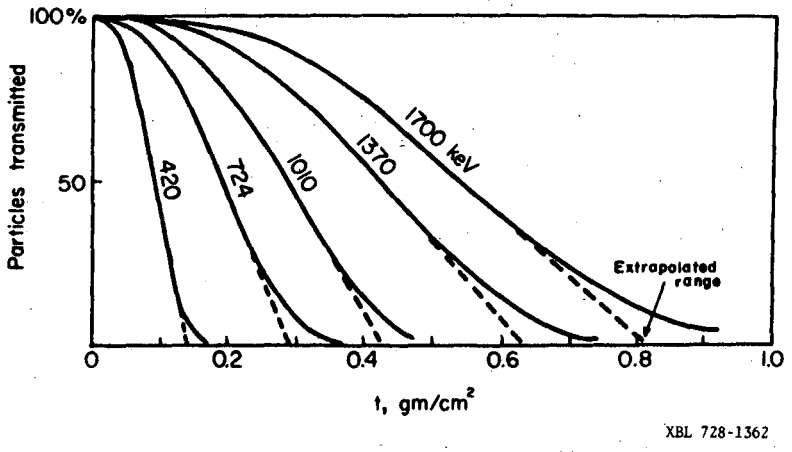

Fig. 1.8. The absorption of monoenergetic electrons. (after Bichsel.)

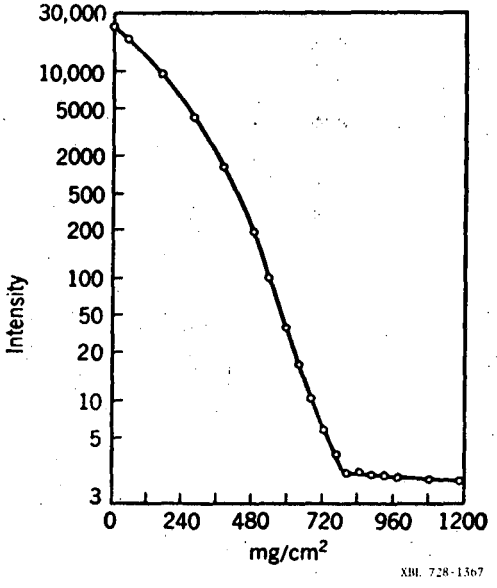

Fig. 1.9. The absorption of β particles emitted by ^{32}P.

The maximum range, R_{max}, for continuous β^--particle spectra is for all practical purposes the same as the extrapolated range of monoenergetic electrons whose energy equals the maximum energy of the β^--particle spectrum. This is seen in Fig. 1.10, which summarizes some empirical determinations of electron range as a function of energy for both monoenergetic electrons and β^- particles. Based on such empirical data, Katz and Penfold (KAT L 52) proposed the empirical range relationships

$$R_0(\text{mg/cm}^2) = 412\, E^n, \text{ for } 0.01 \text{ MeV} \leqslant E \approx 3 \text{ MeV}, \qquad (23a)$$

where $n = 1.265 - 0.0954\, \ell n\, E$,

$$R_0(\text{mg/cm}^2) = 530\, E - 196, \text{ for } 1 \text{ MeV} \approx E \approx 20 \text{ MeV}. \qquad (23b)$$

Figure 1.10 shows how well these formulae represent the experimental data.

The International Commission on Radiation Units and Measurements (ICRU) has recently reviewed the theoretical and experimental information on stopping power and range of electrons (ICRU 70), primarily of interest to the radiation biologist.

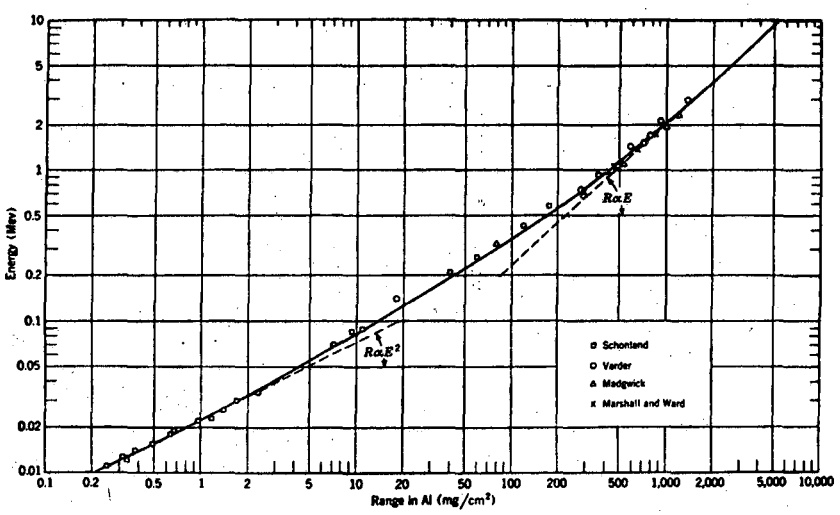

Fig. 1.10. Range-energy data for electrons. (from Evans.)

Figures 1.11 and 1.12, based on ICRU Report 16, summarize the available data on mass stopping power and range for electrons in water.

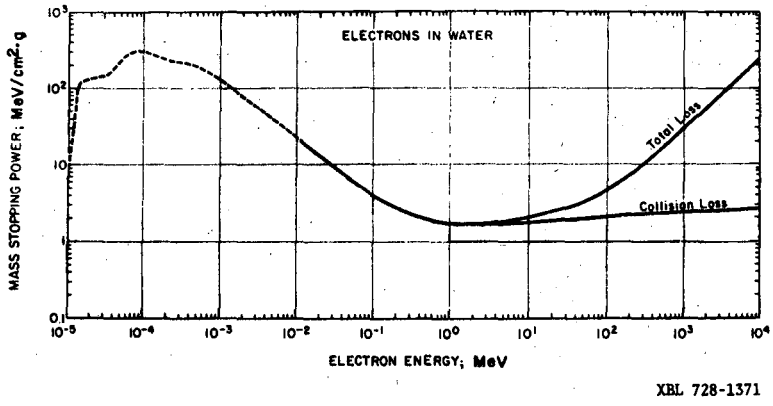

Fig. 1.11. The mass stopping power of water for electrons as a function of energy. Below 10 keV theoretical formulae are inaccurate, only limited experimental data are available (after ICRU Report 16.)

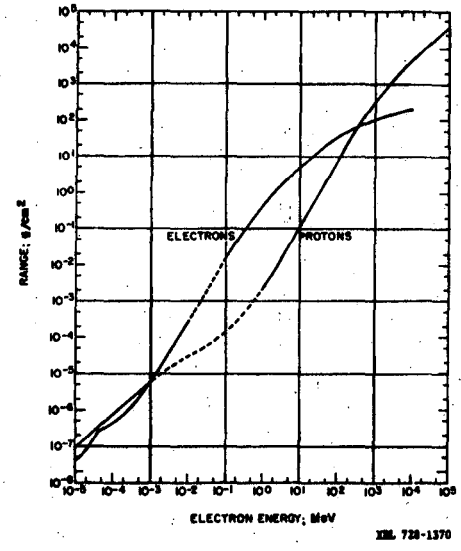

Fig. 1.12. The range of electrons and protons in water as a function of particle energy. For electrons: below 10 keV experimental data have been used, between 10 KeV and 150 keV both experimental and theoretical data have been used and above 100 keV theoretical data only have been used.

For protons theoretical data are used below 1 keV, between 1 keV and 1 MeV theoretical and experimental data are used and above 1 MeV theoretical data are used. (after ICRU report 16.)

For electron energies below 10 keV theoretical mass stopping power formulae are inapplicable, and we are therefore dependent upon experimental data. Above 10 keV it is possible to compare theoretical predictions and experimental measurements, of both stopping power and range; agreement within about 5% is obtained (KAT L 52). Figure 1.11 shows both the collision and total energy loss for electrons. The importance of radiation losses above 10 MeV is clearly seen.

Photons

The absorption of photons in matter is a complex process, because three mechanisms are involved, each of which, being accompanied by secondary processes, is itself quite complex.

The three important phenomena are

a. photoelectric effect,
b. Compton scattering, and
c. pair production.

Space does not permit thorough discussion of these phenomena here; they are comprehensively discussed in texts referred to in the bibliography. A brief discussion, however, is given in Section 10 of the Laboratory Manual (Appendix). Excellent reviews of x and γ ray interactions have been given by Evans (EVA R 68) and Kase and Nelson (KAS K 72). Briefly, in the *photoelectric effect* a photon dissipates its entire energy by knocking out an orbiting electron from an atom. In Compton scattering the photon scatters on a free electron, imparting some kinetic energy to it. The essential difference between the photoelectric effect and the Compton effect is that in the former the photon disappears whereas in the latter a photon remains, albeit of lower energy than the incident photon. In pair production a photon is absorbed in the field of a nucleus to create an electron-positron pair.

The attenuation of photons in matter is exponential, basically because a photon is "removed" by a single interaction. At the same depth x in the absorber the rate-dI at which photons are removed in a thickness dn of absorber is given by

$$-dI = \mu_0 I(x) dx, \tag{24}$$

where I(x) is the photon intensity at depth x,

μ_0 is the total linear attenuation coefficient.

Integration of Eq. 24 yields

$$I(x) = I(0)\, e^{-\mu_0 x}. \tag{25}$$

[A mass absorption coefficient, μ, is defined by

$$\mu = \mu_0/\rho \tag{26}$$

where ρ is the density of the absorber.]

The total linear absorption coefficient, μ_0, may be resolved into three coefficients representing the three basic phenomena:

$$\mu_0 = \tau + \sigma + \kappa, \tag{27}$$

where τ, σ, and κ represent the linear absorption coefficients for the photoelectric process, Compton scattering, and the pari-production process, respectively. Figure 1.13 shows schematically the relative importance of the three major types of photon interaction, as a function of photon energy and absorber atomic number.

There are, of course, corresponding mass-attenuation coefficients, and the total mass-attenuation coefficient is defined by

$$\mu = \frac{\tau}{\rho} + \frac{\sigma}{\rho} + \frac{\kappa}{\rho} \quad . \tag{28}$$

Figure 1.14 summarizes the total mass-attenuation coefficients, and the individual coefficients in water, as a function of photon energy.

Estimates of the actual absorption of energy in an absorbing material are of importance in health physics. The total mass-attenuation coefficient, which is a measure of the probability of photon interaction is always greater than the mass absorption coefficient, which is a measure of energy absorption. It is necessary therefore to estimate the proportions of energy locally deposited by the three interactions. The loss of energy from the point of interaction is most important. (In Compton scattering, a substantial fraction of the energy of the interacting photon is not absorbed at the point of interaction but is re-emitted as a photon of lower energy.)

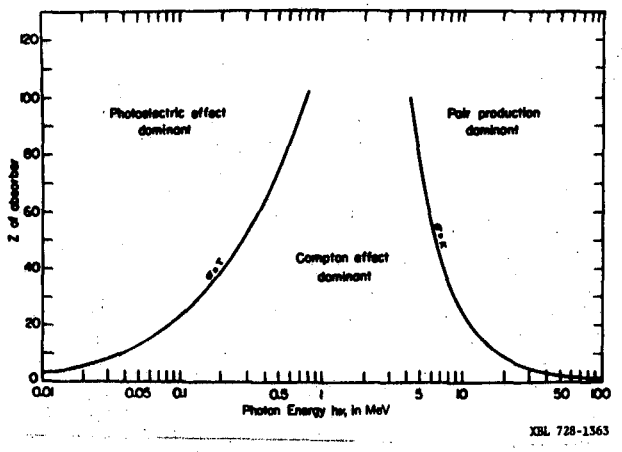

Fig. 1.13. Schematic diagram showing the relative importance of the three major types of γ-ray interaction. The lines indicate the values of z and photon energy at which the two neighboring effects are equal. (from Evans.)

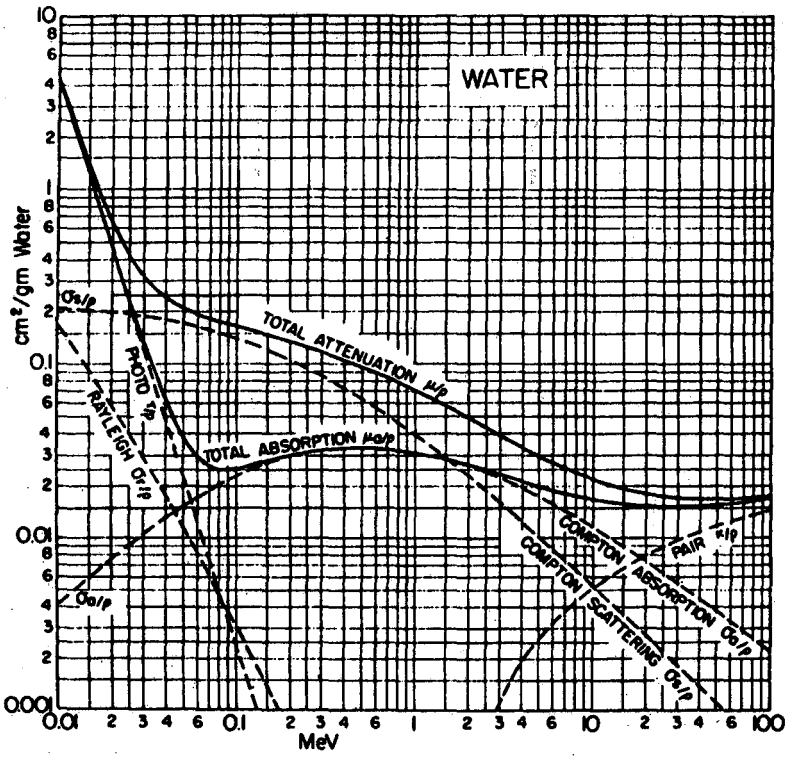

Fig. 1.14. The mass attenuation coefficients for photons in water. (from Evans.)

ATTENUATION OF BREMSSTRAHLUNG

When shielding against the bremsstrahlung produced by an electron accelerator is required, one must first determine the forward intensity and angular distribution of the source or sources; information on this if found in Chapter 3. In principle, one whould then divide the bremsstrahlung spectrum into appropriate energy intervals and treat each separately by means of the applicable absorption coefficients for narrow-beam condition (good geometry) and the necessary buildup factors. Use of narrow-beam coefficients alone results, in most cases, in a substantial underestimate in the thickness of shield material required. This is because the primary radiation produces secondaries, which can leave the shield and contribute to the radiation field outside it. Buildup factors are defined as the ratio of some quantity associated with the beam such as dose or energy flux when all

particles and photons are considered to that same quantity when only the primary photons are considered. Tables of buildup factors, B, are available as a function of μx, where μ is the mass-absorption coefficient and x is the shield thickness in g/cm^2. B appears in the familiar exponential absorption equation,

$$I = I_0 B(\mu x) e^{-\mu x}. \quad (24)$$

Narrow-beam mass-absorption coefficients are given in Table 1.II, taken from NBS Handbook 97 (NBS 64). Figure 1.15 presents similar data in a different form; it is taken from Price, Horton, and Spinney (PRI B 57). The method of calculating buildup factors for many energies and quantities and in many materials has been extensively described by Goldstein and Wilkins (GOL H 54). For purposes of accelerator shielding, use of the dose-buildup factors for point isotropic sources is somewhat conservative. Values of these factors are given in Table 1.III, taken from NBS Handbook 97 after Fano (FAN O 53).

Instead of dealing with each energy interval in the bremsstrahlung spectrum separately, it is sometimes sufficient to replace the whole spectrum with a single value of "effective photon energy." MacGregor (MAC M 57) states that for 20-MeV electrons the effective photon energy is about 7 MeV; for 6-MeV electrons, it is about 3 MeV. As a rule of thumb the effective energy is about 1/3 of the peak energy. It is always desirable to check calculations against available experimental data. A well known example of such data is shown in Fig. 1.16, after Kirn and Kennedy (KIR F 54). At high energies, at which scattering is strongly peaked in the forward direction, it may appear attractive to take advantage of this peaking and specify thin side shielding walls. However, unless it is certain that the forward direction will always be the same, it is better to have thick enough side walls so that there will be adequate latitude for different beam-loss points and direction. The interested reader who needs more detailed information on these and other topics, such as skyshine and scattering, should consult the references cited. Also, Chapter VI presents information on attenuation at high energies, at which the electromagnetic cascade can develop. Neutron production from electron accelerators is discussed in Chapter III, and should always be considered at energies $>$ 20 MeV.

Table 1.II. Mass absorption coefficients (cm^2/g)[a]

Photon energy (MeV)	Material			
	H_2O	OAl	Fe	Pb
0.5	0.0967	0.0844	0.0840	0.152
0.6	0.0894	0.0779	0.0769	0.119
0.8	0.0786	0.0683	0.0668	0.0866
1.0	0.0708	0.0614	0.0598	0.0703
1.5	0.0576	0.0500	0.0484	0.0523
2.0	0.0493	0.0431	0.0422	0.0456
3.0	0.0396	0.0353	0.0359	0.0413
4.0	0.0339	0.0310	0.0330	0.0416
5.0	0.0302	0.0284	0.0314	0.0430
6.0	0.0277	0.0266	0.0305	0.0445
8.0	0.0242	0.0243	0.0298	0.0471
10.0	0.0221	0.0232	0.0300	0.0503
15.0	0.0194	0.0219	0.0308	0.0567
20.0	0.0180	0.0217	0.0321	0.0625
30.0	0.0170	0.0221	0.0346	0.0709
40.0	0.0167	0.0228	0.0366	0.0773
50.0	0.0167	0.0230	0.0384	0.0817
60.0	0.0168	0.0237	0.0399	0.0855
80.0	0.0170	0.0246	0.0419	0.0907
180.0	0.0173	0.0254	0.0436	0.0945

[a]Values from G. R. White as quoted by C. M. Davisson in Appendix 1, *Beta and Gamma-Ray Spectroscopy*, edited by K. Siegbahn (Interscience Publishers, Amsterdam, 1955).

Table 1.III. Dose buildup factors for point isotropic sources from NBS Handbook 97 after Fano (FAN U 53)

E_0 (MeV)	2	4	7	10	15	20
			Water			
0.5	5.14	14.3	38.8	77.6	178	–
1	3.50	7.21	14.6	24.0	44.7	–
2	2.77	4.88	8.46	12.4	19.5	–
3	2.42	3.91	6.23	8.63	12.8	–
4	2.17	3.94	5.12	6.94	9.97	–
6	1.91	2.80	4.08	5.33	7.34	–
8	1.77	2.49	3.51	4.50	6.05	–
10	1.63	2.22	3.04	3 82	5.07	–
			Aluminum			
0.5	4.24	9.47	21.5	38.9	80.8	141
1	3.31	6.57	13.1	21.2	37.9	58.5
2	2.61	4.62	8.05	11.9	18.7	26.3
3	2.32	3.78	6.15	8.65	13.0	17.7
4	2.08	3.22	5.01	6.88	10.1	13.4
6	1.85	2.70	4.06	5.49	7.96	10.4
8	1.68	2.37	3.45	4.58	6.56	8.52
10	1.55	2.12	3.01	3.96	5.63	7.32
			Iron			
0.5	3.09	5.98	11.73	19.23	35.42	55.6
1	2.88	5.39	10.21	16.18	28.31	42.7
2	2.38	4.08	6.99	10.47	16.83	24.0
3	2.12	3.44	5.74	8.35	13.25	18.8
4	1.94	3.03	4.91	7.11	11.23	16.00
6	1.72	2.58	4.14	6.02	9.89	14.7
8	1.56	2.23	3.49	5.07	8.50	13.0
10	1.42	1.95	2.98	4.35	7.54	12.4
			Lead			
0.5	1.42	1.69	2.00	2.27	2.65	–
1	1.69	2.26	3.02	3.74	4.81	–
2	1.76	2.51	3.66	4.84	6.86	–
3	1.68	2.43	3.75	5.30	8.44	–
4	1.56	2.25	3.61	5.44	9.80	–
5.11	1.46	2.08	3.44	5.55	11.74	–
6	1.40	1.97	3.34	5.69	13.80	–
8	1.30	1.74	2.89	5.07	14.05	–
10	1.23	1.58	2.52	4.34	12.54	–

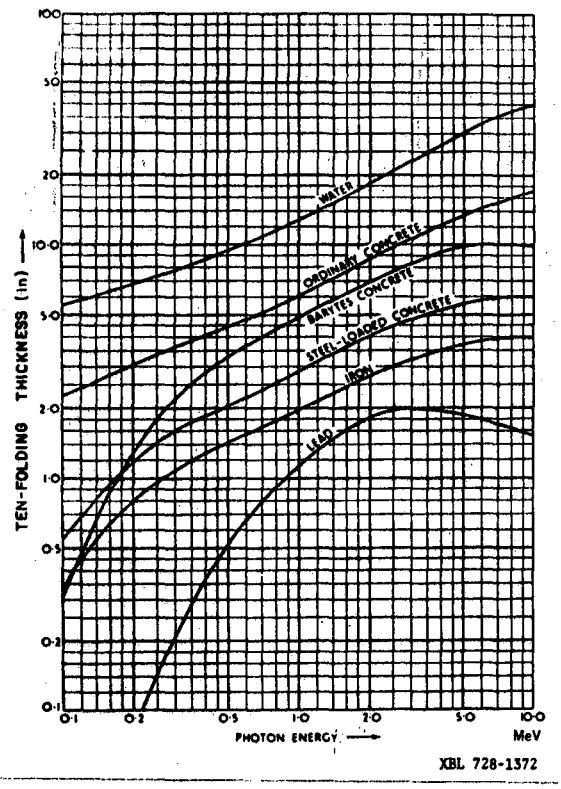

Fig. 1.15. Ten folding lengths for common shielding materials. The curves are based on narrow-beam coefficients and do not include any allowance for multiple scattering. They were calculated assuming the following densities and compositions:
Shot concrete: Density 5.3 g/cm^3 (79.5% Fe by weight).
Ordinary concrete: Density 2.35 g/cm^3. Composition (wt. %): Ca, 8.6; Si, 35.8; Fe, 1.2; Al, 2.0; Na, 0.33; H, 0.63; C, 0.4; O, 51.1.
Barytes concrete: Density 3.1 g/cm^3. Composition (wt %): Ba, 35.8; Ca, 7.4; S, 9.0; Si, 8.9; Fe, 1.5; H, 0.44; C, 1.1; O, 35.4.
Lead: Density 11.4 g/cm^3.
Iron: Density 7.8 g/cm^3.

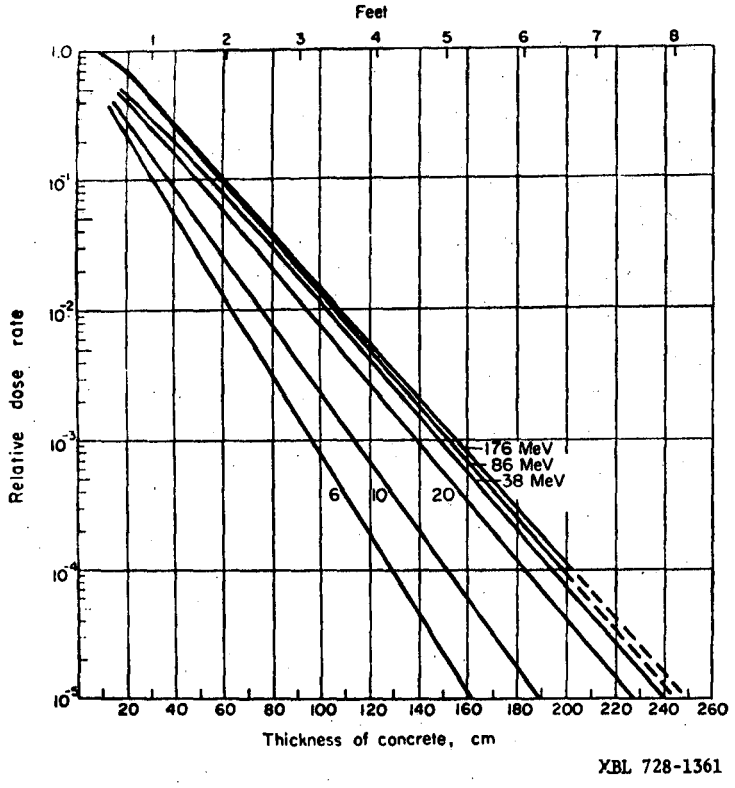

Fig. 1.16. Broad-beam absorption of x rays in concrete (ρ=2.35 g/cm^3) peak photon energies. (after Kirn and Kennedy.)

NEUTRONS

The interactions of neutrons with matter are complex, but the concepts of cross section for interaction and the process of exponential attenuation arising therefrom are identical with photons. Important types of neutron interactions are elastic and inelastic scattering, capture (with either the emission of a charged particle or a photon or photons, and the n, 2n reaction. Each of these is involved to some extent with neutron detection and measurements, the production of induced radioactivity, and shielding; full discussion is found in Chapters II, III, VI, and VII.

REFERENCES

ATK J 57 J. H. Atkinson and B. H. Willis, High Energy Particle Data, Vol. 2, University of California Radiation Laboratory report, UCRL-2426 (Rev.), 1957.

BAR W 64 Walter H. Barkas and Martin J. Berger, Tables of Energy Losses and Ranges of Heavy Charged Particles, in *Studies in Penetration of Charged Particles in Matter,* Ed. U. Fano, Report No. 39, Nuclear Science Series Publication 1133, (National Academy of Sciences, National Research Council, Washington, 1964.

BET H 34 H. A. Bethe and W. Heitler, The Stopping of Fast Particles and the Reaction of Positive Electrons. Proc. Roy. Soc. (London) *A146,* 83 (1934).

BET H 53 H. A. Bethe and J. Ashkin, Passage of Radiation Through Matter, in *Experimental Nuclear Physics,* Ed. E. Segre, Vol. 1, (John Wiley and Sons, Inc., New York, 1953), p. 166.

BIC H 68 H. Bichsel, Charged Particle Interactions, in *Radiation Dosimetry,* Ed. F. H. Attix and W. C. Roesch, Vol. 1 (Academic Press, New York, 1968), p. 157.

DES H 68 H. de Staebler, T. M. Jenkins, and W. R. Nelson, Shielding and Radiation, in *The Stanford Two-Mile Accelerator,* Ed. R. B. Neal, (W. A. Benjamin, Inc., New York, 1968), Chap. 26.

EVA R 68 R. D. Evans, X-Ray and γ-Ray Interactions, in *Radiation Dosimetry,* Ed. F. H. Attix and W. C. Roesch, Vol. 1 (Academic Press, New York, 1968), p. 94.

FAN U 53 U. Fano, Gamma Ray Attenuation, Nucleonics *11* [9], 55 (1953).

FAN U 63 U. Fano, Penetration of Protons, Alpha Particles, and Mesons, Ann. Rev. Nucl. Sci. *13,* 1 (1963).

FAN U 64 U. Fano, Ed., *Studies in Penetration of Charged Particles in Matter,* Report #39, Nuclear Science Series Publication 1133, (National Academy of Sciences, National Research Council, Washington, 1964.

GIL W 68 W. S. Gilbert et al., 1966 CERN-LRL-RHEL Shielding Experiment at CERN Proton Synchrotron, Lawrence Radiation Laboratory report UCRL-17941, Sept. 1968.

GOL H 54 H. Goldstein and J. E. Wilkins, Calculations of the Penetration of Gamma Rays, USAEC Report NYO-3075, 1954.

GRE A 55 A. E. S. Green, *Nuclear Physics* (McGraw-Hill, New York, 1955).

HAY P 63 P. J. Hayman, N. S. Palmer, and A. W. Wolfendale, The Rate of Energy Loss of High-Energy Cosmic Ray Muons, Proc. Roy. Soc. *275A,* 391 (1963).

IAE A 63 See for example: *Neutron Dosimetry*, Vols. 1 and 2, *Proceedings of the Symposium on Neutron Detection, Dosimetry, and Standardization, Harwell, 10-14 December 1962* (IAEA, Vienna, 1963).

ICR U 69 ICRU Report 13, Neutron Fluence, Neutron Spectra, and Kerma (International Commission on Radiation Units and Measurements, Washington, D.C., 1969).

ICR U 70 ICRU Report 16, Linear Energy Transfer (International Commission on Radiation Units and Measurements, Washington, D.C., 1970).

ICR U 71 ICRU Report 19, Radiation Quantities and Units (International Commission on Radiation Units and Measurements, Washington, D.C., 1971).

JAN J 66 J. F. Janni, Calculations of Energy Loss, Range, Pathlength, Straggling, Multiple Scattering, and the Probability of Inelastic Nuclear Collisions for 0.1- to 1000-MeV Protons, Air Force Weapons Lab. Kirtland A. F. B., NM, Technical Report No. AFWL-TR-65-150, Sept. 1966.

KAS K 72 K. R. Kase and W. R. Nelson, Concepts of Radiation Dosimetry, Stanford Linear Accelerator Report No. 153, June 1972.

KAT L 52 L. Katz and A. S. Penfold, Range-Energy Relations for Electrons and the Determination of Beta-Ray End-Point Energies by Absorption. Rev. Mod. Phys. *24*, 28 (1952).

KIR F 54 F. S. Kirn and R. J. Kennedy, Betatron X-Rays: How Much Concrete for Shielding? Nucleonics *12* [6], 44 (1954).

LAD M 69 M. Ladu, Problems of Safety and Radiation Protection Around High Energy Accelerators, in *Health Physics* Vol. 2 Part I, Ed., A.M.F. Duhamel (Pergamon Press, Oxford, 1969), p. 365.

LIV M 37 M. S. Livingston and H. A. Bethe, The Range-Energy Relationship, Rev. Mod. Phys. *9*, 261 (1937).

MAC M 57 M. H. MacGregor, Production of Gamma Radiation With a Linear Electron Accelerator, Applied Radiation Corporation Report AM-100, March 1957.

MIL S 58 S. Milani, J. N. Cooper, and J. C. Harris, personal communication to W. Whaling (WHA W 58).

MOY B 52a B. J. Moyer, Survey Methods for Slow Neutrons, Nucleonics *10* [4], 14 (1952).

MOY B 52b B. J. Moyer, Survey Methods for Fast and High Energy Neutrons, Nucleonics *10* [5], 14 (1952).

MOY B 54 B. J. Moyer, Neutron Physics of Concern to the Biologist, Radiation Res. *1*, 10 (1954).

MOY B 58 B. J. Moyer, Practical Control of Radiation Hazards in Physics Research, Ann. Rev. Nucl. Sci. *8*, 327 (1958).

NBS 64 National Bureau of Standards Handbook 97, Shielding for High-Energy Electron Accelerator Installations, July 1964.

NOR L 63 Lee C. Northcliffe, Passage of Heavy Ions Through Matter, Ann. Rev. Nucl. Sci. *13*, 67 (1963).

PAT H 71 H. W. Patterson, J. T. Routti, and R. H. Thomas, What Quality Factor? Health Phys. *20*, 517 (1971).

PHI J 53 J. A. Phillips, The Energy Loss of Low Energy Protons in Some Gases, Phys. Rev. *90*, 532 (1953).

PR B 57 B. T. Price, C. C. Horton and K. T. Spinney, Radiation Shielding (Pergamon Press, Oxford, 1957).

REY H 53 H. K. Reynolds, D. N. F. Dunbar, W. A. Wenzel, and W. Whaling, The Stopping Cross Section of Gases For Protons, 20-600 KeV, Phys. Rev. *92*, 742 (1953).

RIC M 54 M. Rich and R. Madey, Range Energy Tables, University of California Radiation Laboratory report UCRL-2301, 1954.

RIN A 71 A. Rindi and R. H. Thomas, Absorbed Dose--An Unfortunate Red Herring in Radiation Protection, in *Radiation Protection Standards: Quo Vadis* Vol II, Proceedings of the Sixth Annual Health Physics Society Topical Symposium, Richland, Washington, Nov. 1971.

RIN A 72 A. Rindi and R. H. Thomas, Povera et Nuda Vai, Dosimetria, Health Phys. (in press).

ROE W 68 W. C. Roesch and F. H. Attix, Basic Concepts of Dosimetry, in *Radiation Dosimetry* Vol. I, *Fundamentals*, Eds., W. C. Roesch and F. H. Attix((Academic Press, New York, 1968), p. 1.

ROU J 69 Jorma T. Routti, High Energy Neutron Spectroscopy With Activation Detectors, Lawrence Radiation Laboratory report UCRL-18514, April 1969.

SHA K 69 K. B. Shaw, G. R. Stevenson, and R. H. Thomas, Evaluation of Dose Equivalent from Neutron Energy Spectra, Health Phys. *17*, 459 (1969).

SHU W 72 W. A. Shurcliff, Calculations as to How Large a Dose-Rate of Synchrotron Radiation Would be Received by a Person Standing Close to the CEA Ring or By-Pass When There is a 5-mA ave. 3-GeV Beam Stored There, Cambridge Electron Accelerator report CEAL-1057, March 1972.

SID J 68 J. M. Sidwell and B. M. Wheatley, Br. J. Radiol. *42*, 522 (1968).

STE P 68 P. G. Steward, Stopping Power and Range for Any Nucleus in the Specific Energy Interval 0.01 to 500 MeV/amu in any Nongaseous Material, Lawrence Radiation Laboratory report UCRL-18127, May 1968.

STO D 71 D. R. Stone and John H. Thorngate, The Development of a Spectrometer and the Measurement of the Neutron Spectrum from the Health Physics Research Reactor between 50 KeV and 450 KeV. Health Phys. *21*, 441 (1971).

THE D 70 D. Theriot, Muon dE/dx and Range Tables, National Accelerator Report TM 229, March 1970.

THO R 64 R. H. Thomas, Energy Loss of High Energy Muons, Lawrence Berkeley Laboratory internal document UCID-10010, July 1964.

TUR J 67 J. E. Turner, Calculation of Stopping Power of a Heavy Charged Particle in Matter, Health Phys. *13*, 1255 (1967).

WHA W 58 W. Whaling, The Energy Loss of Charged Particles in Matter, in *Encyclopedia of Physics*, Vol. 34 (Springer-Verlag, Berlin, 1958), p. 193.

BIBLIOGRAPHY

H. A. Bethe, and Philip Morrison, *Elementary Nuclear Theory*, 2nd ed. (Wiley, New York, 1956).

L. R. B. Elton, *Introductory Nuclear Theory* (Wiley-Interscience, New York, 1959).

R. D. Evans, *The Atomic Nucleus* (McGraw-Hill, New York, 1955).

Enrico Fermi, *Nuclear Physics* (University of Chicago Press, Chicago, 1950).

A. E. S. Green, *Nuclear Physics* (McGraw-Hill, New York, 1955).

David Halliday, *Introductory Nuclear Physics*, 2nd ed. (Wiley, New York, 1953).

K. Kase, W. R. Nelson, Concepts of Radiation Dosimetry, Stanford Linear Accelerator Report 153, June 1972.

B. Rossi, *High Energy Particles* (Prentice-Hall, New York, 1952).

E. Segrè, *Nuclei and Particles* (Benjamin, New York 1965).

CHAPTER 2.

RADIATION FIELDS: THEIR SPECIFICATION AND MEASUREMENT.

TABLE OF CONTENTS

RADIATION FIELDS: THEIR SPECIFICATION AND MEASUREMENT

INTRODUCTION

One of the most important duties of a health physicist is to make measurements from which the dose equivalent (or dose-equivalent rate) may be derived. This may be difficult at particle accelerators because of the possible complexity of their external radiation fields, particularly at the highest energies, at which it is possible for every known particle--as well as those yet to be discovered--to be created!

Fortunately, experience has shown that in most practical situations the dose equivalent delivered by particles other than neutrons and γ rays is often negligibly small (THO R 65). Therefore it devolves primarily upon the health physicist to make measurements of these two types of radiation.

Unfortunately, except in a very limited and theoretical way, it is not possible to measure dose equivalent directly, nor is it possible to make a single measurement from which the dose equivalent can be derived, unless perhaps one has extensive prior knowledge of the radiation field.

Historically the first measurements of accelerator radiation fields were made with air-ionization chambers, by the same techniques as had been successful with x and γ rays. In time, the marked differences between the nature of neutron interactions in air and in tissue (LEA D 46) were seen to result in severe deficiencies when these measurement techniques were applied to health physics. Alternative methods were sought, and two somewhat different procedures are now in common use. The first method utilizes an ionization chamber constructed with "tissue-equivalent materials" to measure the energy absorbed in tissue placed in a radiation field. The second procedure involves measurement of the number and energy distribution of the components of the radiation field. Thus basically the first technique specifies the radiation field in terms of its interaction with tissue, whereas the second method specifies the field in physical terms, independently of any interaction with matter. Whichever technique is used, however, the experimental data must often be converted into terms appropriate to radiation protection--the dose equivalent.

Measurements of absorbed dose alone have limited value in health physics. Thus, although they are valuable for radiation protection in x- or γ-radiation fields, or those radiation fields for which the necessary modifying factors are known, measuring only the absorbed dose is inadequate in other areas of accelerator health physics, such as shielding specification or prediction of changes in the radiation field associated with accelerator operation.

Conversely, if particle spectra are determined and related to accelerator operation, sufficient information is available to implement many aspects of a health physics program, and, in addition, to establish routine monitoring procedures suitable for controlling radiation exposures. The dose equivalent may be obtained from spectral information by direct conversion (GIL W 68, ROU J 69a, ROU J 69b). This technique has thus far been employed with success in radiation fields dominated by neutrons; there is no basic reason why it may not be extended to photon radiation fields (SID J 69, WHE B 70).

CONCEPTS AND UNITS

The first attempts to quantify radiation fields began with x and γ radiation. Although the *energy absorbed* by irradiated material is important in determining the biological response of living organisms, in practice these energies are typically too small to measure directly. Energy absorption in air, however, produces ionization and provides a convenient method of measurement. Therefore the concept of *exposure* was developed (ICRU 38, ICRU 57, ICRU 62), which is a measure of the radiation based upon its ability to produce ionization. The special unit of exposure is the roentgen--one roentgen being that exposure that produces one electrostatic unit of charge of both positive and negative signs in one cubic centimeter of air at standard conditions of temperature and pressure.

It should be noted here that in this brief review of radiation units our discussion cannot be of great depth, our purpose being only to paint a broad canvas indicating points of special importance. The reader interested in more detail is referred to texts on radiation dosimetry--for example, that edited by Attix, Roesch, and Tochilin, (ATT F 66, ATT F 68, ATT F 69), or the authoritative reports of ICRU.

Despite its great utility, dissatisfaction with the concept of exposure arose because of its exclusiveness--it is, for example, inappropriate for neutron irradiation--and the fact that exposure is not linearly related to energy absorption in tissue. Both disadvantages are due to the basic difference in atomic composition of air and tissue. This difference is most striking for neutrons, since the production of recoil protons is the main mechanism for energy transfer to tissue, but even for photons the different chemical compositions of various tissues--fat, muscle, bone-compared with air become important at low energies (JOH H 56). A concept more widely applicable to radiation protection was needed. Since energy absorption seemed to be related to biological response, it was natural to define *absorbed dose.*

Absorbed dose due to any ionizing radiation is the energy imparted to matter by ionizing particles per unit mass of irradiated material at the place of interest. The unit of absorbed dose is the "rad" and is equal to an energy absorption of 100 ergs/g.

Most portable survey instruments for electromagnetic radiation depend for their operation on the measurement of ionization produced in air or other gas, and are usually either ionization chamber or Geiger-Müller tube instruments. However, it is only by the application of the Bragg-Gray principle (BUR T 68) that absorbed dose can be measured with such instruments. (This is discussed more fully in the Section on Techniques of Radiation Field Measurement.)

In the discussion of energy absorption in tissue irradiated by indirectly ionizing radiation (e.g., photons, neutrons) it is important to note that energy is deposited in two steps. Energy is transferred to charged particles, which then lose energy by Coulomb interactions.

Another concept in dosimetry, which has recently appeared, is *Kerma.* Kerma is defined as the kinetic energy of charged particles released by the primary radiation per unit mass of the material. It is not a practical unit, for although Kerma can be calculated, no instrument has thus far been built to measure Kerma directly. In theory, Kerma may be measured in any units of energy absorption per unit mass.

These concepts of exposure, absorbed dose, and Kerma describe only the gross properties of the ionizing radiation field. Precise physical specification of radiation fields, however, requires the concept of flux density. *Particle fluence* is the time integral of particles that enter a sphere of unit cross sectional area. *Particle flux density* is the time derivative of fluence, and is expressed in units of particles per unit area per unit time.

In radiation protection we are concerned with preventing all unnecessary radiation exposure and limiting necessary exposure to tolerable levels. This necessitates some estimates of probable risks involved in exposure to low doses of ionizing radiations. The biological effects resulting from exposure to ionizing radiation are not a simple function of absorbed dose alone, but depend as well upon a large number of physical and biological factors. It is convenient to find some standard way to relate the biological effects due to a variety of radiations. This is achieved by selecting a standard radiation (e.g., 200-kV x rays) to which radiation effects can be related and by application of the concept of relative biological effectiveness (RBE).

Relative biological effectiveness is the ratio of the absorbed dose of reference radiation to the absorbed dose of a different radiation required to produce the same biological effect. An RBE may be specified for any kind of radiation or condition of exposure.

The RBE for radiation of type i is, then,

$$(\mathrm{RBE})_i = D_X/D_i, \qquad (1)$$

where D_X, D_i are absorbed doses of 200-keV x rays and of radiation of type i to produce the same biological effect. Thus the biological effect of irradiation by n different types of radiation would be identical to that from

$$\sum_{i=1}^{n} (RBE)_i D_i \text{ rads of 200-keV x rays.}$$

This concept was first introduced for radiation protection purposes by Parker (PAR H 48), who used the unit rem (roentgen equivalent man) to quantify an absorbed dose so modified. This hybrid quantity was first referred to as RBE dose (ICRU 57), later becoming modified to *dose equivalent* (ICRU 62).

In radiation protection we are concerned with whole-body chronic low-level exposures. The biological effects are not completely defined, but include cancer induction, cataract formation, life-span shortening, and deleterious mutations. With this in mind we are led to the concept of a special RBE for the purposes of radiation protection, which has been termed a modifying factor (MF). Thus dose equivalent (DE, in rem) may be related to the absorbed dose (D, in rad) resulting from mixed radiation fields by the equation

$$DE = (MF)D. \tag{2}$$

The modifying factor (MF) is theoretically separable into several subsidiary modifying factors each representing a separate variable of irradiation. Thus

$$DE = (M_1 M_2 M_3 \ldots M_i)D. \tag{3}$$

One of the most important of these factors influencing the biological efficiency of radiation is the linear energy transfer (ZIR R 52). *Linear energy transfer* (LET) is the average energy locally imparted to the medium by the passage of a charged particle. The units of LET are normally keV per micron. Soon after the original definition was promulgated, it became clear that a limit had to be placed on the region in which energy could be considered to be locally deposited. This has been discussed by Madey (MAD R 67), who pointed out that in general the concept of linear energy transfer is different from that of stopping power, L_∞. However, it is sufficiently accurate for radiation protection purposes to use values of stopping power--as is done in the ICRP-ICRU definition of the QF-LET relationship (QF is defined below) in which the values of LET used are stopping power in water. It might further be argued that the definition should be made in terms of stopping power in tissue, and, in fact, calculations have been made for these conditions. However, the differences so obtained in LET values are small and are far outweighed by the absolute errors attached to radiobiological experimental data.

Thus if a separate modifying factor that is a function only of LET may be identified, we may modify Eq. 3 to

$$DE = (QF)(M_1 M_2 \ldots M_{i-1})D, \tag{4}$$

where QF is the LET-dependent modifying factor and is known as *quality factor.*

To some extent this formalism is theoretical, because in actual practice use is seldom made of the additional factors M_1, M_2, · · ·, etc., and thus the DE for any type of radiation and for any exposure condition is put, numerically equal to the product of the absorbed dose in rads and the quality factor, QF. The interested reader is referred to the NCRP report on Dose-Effect Modifying Factors in Radiation Protection (NCRP 67), which discusses other modifying factors, such as those concerned with the energy of the radiation or the portion of the body involved.

It should be pointed out that some inconsistencies occur in the literature concerning the use of the term "quality factor" (NEU J 69b, NEU J 70, PAT H 70).

The confusion arises because of the simultaneous use of the term "quality factor" for (a) a quantity defined in terms of linear energy transfer (in effect, stopping power) for charged particles, and (b) the product of the modifying factors (QF) (DF)· · · and other necessary modifying factors as expressed in ICRU Report 11 (ICRU 68). In certain special circumstances the two definitions may be numerically identical, but in the general sense they are distinct quantities.

In this text we use the term "modifying factor" for the factor that converts absorbed dose to dose equivalent. Values of "quality factor" as a function of LET have been derived from radiobiological experiments, and the interested reader is referred to the report of the joint ICRP/IRCU committee on RBE (ICRP 63). Figure 2.1, taken from the NCRP report on Dose-Effect Modifying Factors, summarizes experimental values of RBE as a function of LET for different end-point ratios in a variety of organisms. These results are further summarized in Fig. 2.2, which shows the typical response of mammalian cells and gives the currently recommended QF values for comparison. It may be seen that these are somewhat conservative but not unduly restrictive.

Table 2.1 summarizes the stopping power quality factor (L_∞–QF) relationship recommended by the ICRP 70.)

Table 2.1. L_∞–QF relationship.

L_∞ in water (keV/μ)	QF
3.5 (and less)	1
7	2
23	5
53	10
175 (and more)	20

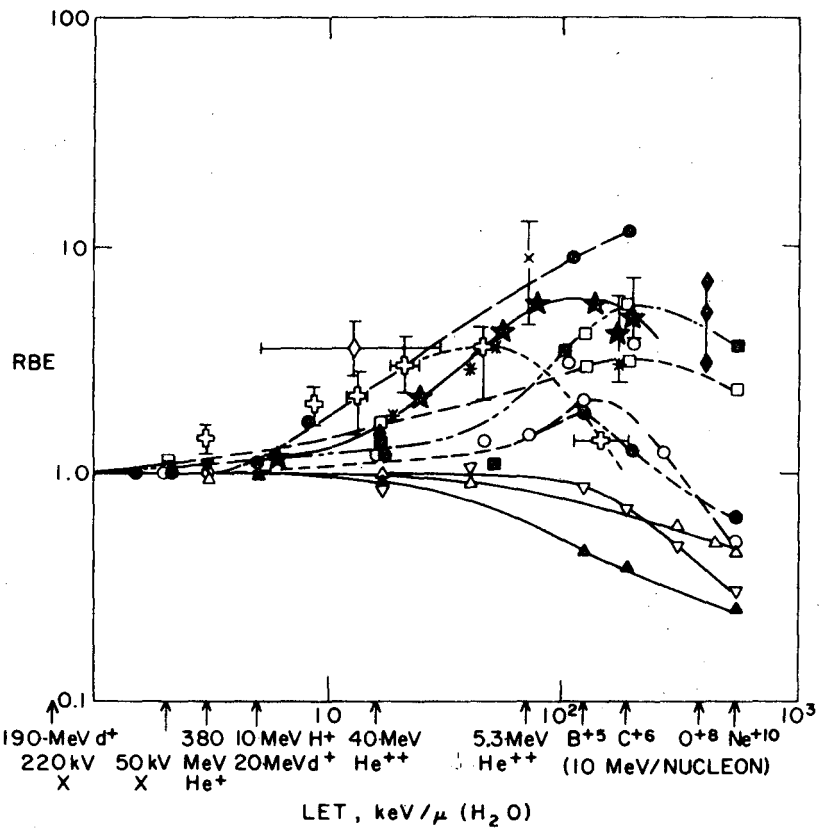

XBL 708-1764

Fig. 2.1. Experimental curves of RBE versus LET. ▲, T1 bacteriophage in broth. ▽, Shigella sonnei in O_2 (in N_2, behaves like type 2). △, Trypsin, lysozyme, DNase, dry, --●. Haploid yeast survival in air, induced reversions in diploid S. cerevisiae, survival. □, Diploid yeast survival in air. ■, Haploid or diploid S. cerevisiae in N_2. ♦, Artemia eggs, hatching or emergence. ★, Mammalian tissues, various. ⁎, Mammalian tissues, various. X, Broad bean root, various effects on growth and survival. Tradescantia microspores, chromatid and isochromatid breaks. Rabbit crystalline lens cells, destruction and division effects, mammalian injury up to LET 20. ●, Stichococcus, survival. (From BNL - 50073.)

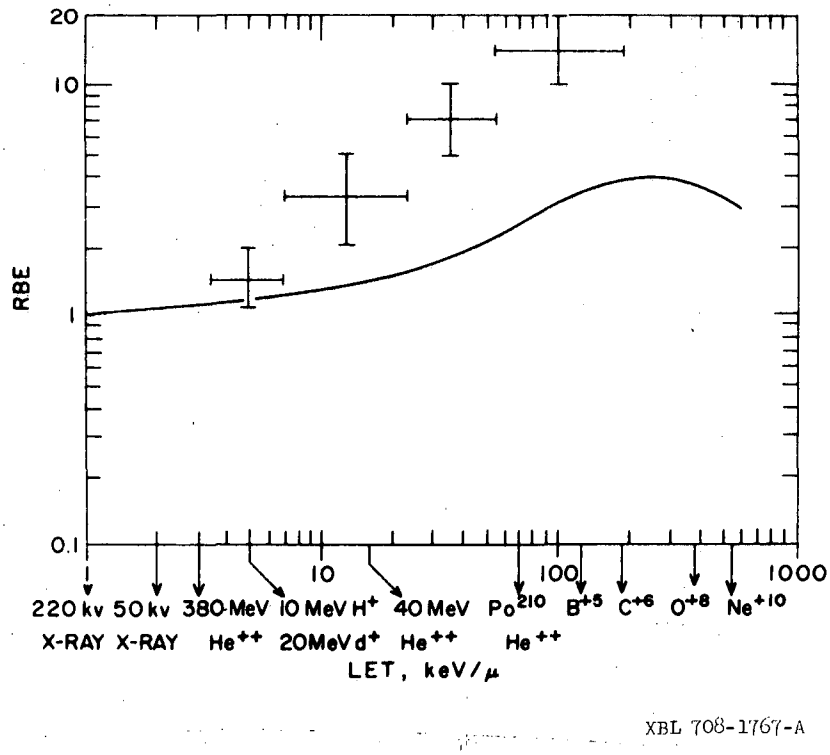

Fig. 2.2. Schematic curve summarizing the response of mamalian cells shown in Fig. 2.1. The crosses identify current values of Quality Factors recommended by ICRP. (After BNL - 50073.)

Intermediate values of QF obtained by interpolation are presented in Fig. 2.3. It should be noted that this relationship applies only to the charged particles, and that average QF's are not specified for distributions of LET.

Many calculations of stopping power for charged particles have been made, such as those by Rich and Madey (RIC M 54), Atkinson and Willis (ATK J 66) Barkas and Berger (BAR W 64), and the National Academy of Science report number 39 (NASc 64). For protons of less than 1 MeV theoretical calculations are no longer reliable, but measurements of stopping power have been reported down to 10 keV (PHI J 53, REY H 53, WHA W 58).

Figure 2.4 summarizes theoretical and experimental data for protons and electrons between 10 keV and 1 GeV. The stopping power of other heavy charged particles in water may be calculated with accuracy sufficient for health physics purposes from the data for protons. For a particle of mass M and charge ZE the energy scale of Fig. 2.4 should be multiplied by a factor M/M_p, where M_p is the proton mass, and the stopping-power scale should be multiplied by a factor of Z^2. It follows that any given charged particle has varying values of L_∞, and therefore QF, along its path. From the interpolated values of quality factor derived from Fig. 2.3 and values of stopping power derived either from Fig. 2.4 or tabulated data, it is a simple matter to deduce the values of QF as a function of particle residual energy (COW F 64).

Figure 2.5 plots values of QF as a function of residual energy for muons, pions, kaons, protons, deuterons, tritons, ^{3}He, and α particles. The curves given in Fig. 2.5 take account only of ionization processes. In estimating the quality factor appropriate to irradiation by charged particles, an averaging procedure must be carried out along the particle track: Cowan et al. (1964) report such average values for pions, protons, deuterons, and α particles.

Thus, in summary, the formalism of

$$DE = QF\,(M_1\,M_2\,.\,.\,.\,M_i)D, \tag{4}$$

together with the $QF-L_\infty$ relationship as defined by ICRP/ICRU (Table 2.1), allows measurements of absorbed dose to be converted to dose equivalent.

For a mixed radiation field the dose equivalent must be obtained from an average quality factor $\langle QF\rangle$, obtained by integration over the LET spectrum in tissue:

$$\langle QF\rangle = \int_0^\infty QF(L)\,D(L)\,dL \Big/ \int_0^\infty D(L)\,dL, \tag{5}$$

where quality factor QF(L) is assumed to be a continuous function of stopping power, L, and D(L) is the distribution of absorbed dose as a function of L (ICRU 70).

Thus, if we consider a small volume of tissue (of unit mass to facilitate discussion) traversed by n particles, the dose equivalent may be represented

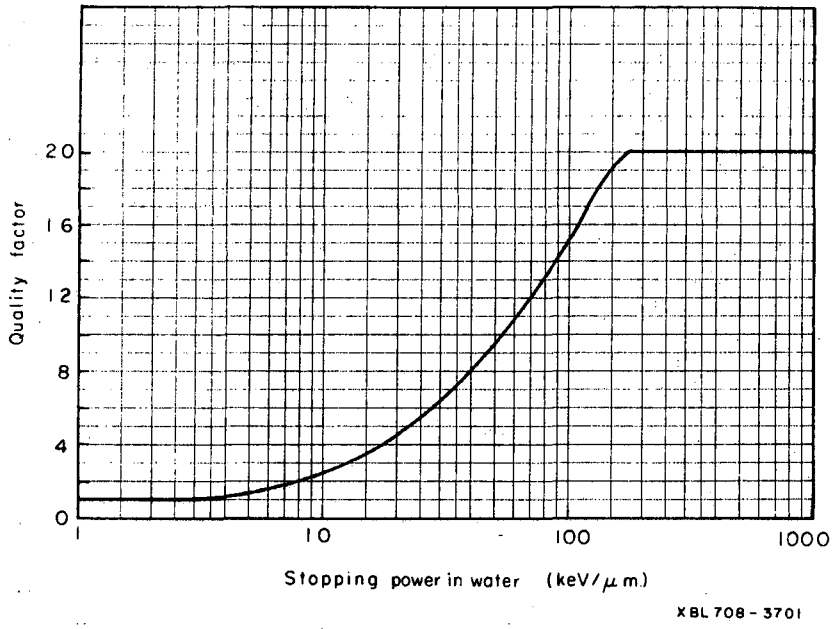

Fig. 2.3. Quality Factor as a function of stopping power in water. (interpolated from ICRP recommendations).

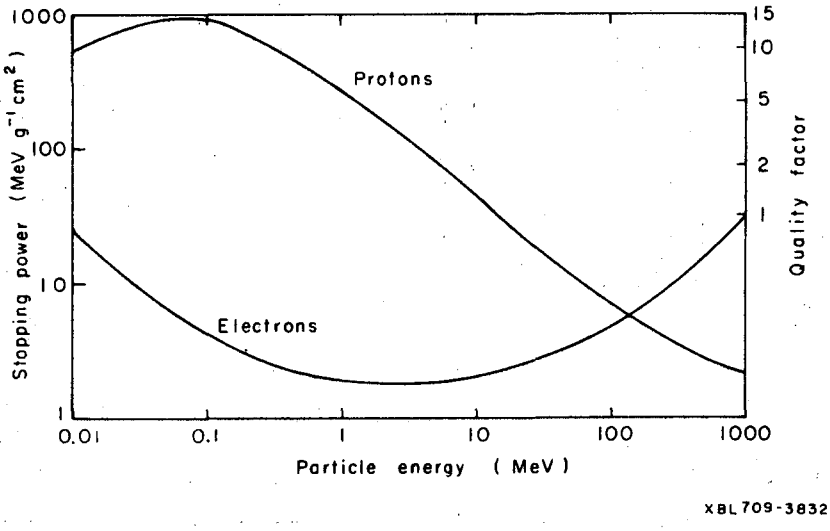

Fig. 2.4. Stopping power of electrons and protons in water as a function of energy.

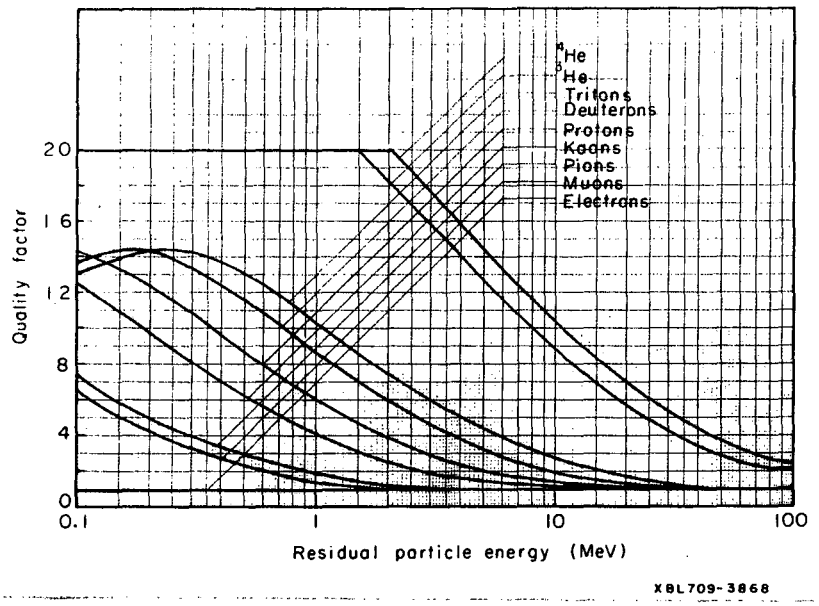

Fig. 2.5. Quality factors of charged particles as a function of energy.

by

$$DE = \sum_{i=1}^{n} \int QF(L)\, L\, dz, \qquad (6)$$

where Σ represents summation over n particles and the integral is a line integral along each track within the volume of tissue.

Alternatively, if the radiation field is specified in terms of its n components, the dose equivalent is given by

$$DE = \sum_{i=1}^{n} \int_{E_{max}}^{E_{min}} P_i(E)\, N_i(E)\, dE, \qquad (7)$$

where Σ represents summation over the n radiation components of type i (that is, n, p, γ, etc.), $N_i(E)\, dE$ is the number of particles of type i with energy between E and E+dE, and $P_i(E)$ is a parameter that converts fluence to dose equivalent.

TECHNIQUES OF RADIATION FIELD MEASUREMENT

Few techniques have found practical application in the evaluation of accelerator radiation fields. Perhaps the most directly appealing, at least conceptually, is the use of a class of instruments collectively known as "rem meters." These instruments attempt to measure dose equivalent directly and can do so under certain limited conditions. The advantages of such instruments in radiation protection are obvious: a single direct reading of the radiation field, providing instantaneous information, allowing swift reaction. On the other hand the disadvantages are equally clear--even if dose equivalent is measured directly, the health physicist is given no information on which to base recommendations for shielding or otherwise modifying the radiation field. In x- or γ-radiation fields instruments calibrated in rads also read directly in rem--thus over a wide range of photon energies air ionization chambers may be regarded as "gamma rem meters." Rem meters used to measure neutrons usually utilize a thermal neutron detector surrounded by a moderating material such as paraffin or polyethylene in some special configuration. Examples of such instruments are the Andersson--Braun (AND I 63) counter, the Hankins (HAN D 62) sphere, the Dvorak-Dyer (DVO R 65) sphere, or the Leake (LEA J 67) ball. Without exception these instruments are limited to energies from a few keV to about 15 MeV. The most careful study and evaluation of the different commercially available detectors is due to Nachtigall (NAC D 67). He reports, "The deviations of the sensitivity curves of rem meters from the dose equivalent curve specified by the ICRP amount to as much as a factor of 5 in the intermediate energy region and dose

equivalent measurements in the same neutron field with different rem meters calibrated under the same conditions also show deviations as great as a factor of 5. Therefore, especially necessary is information on the spectra and flux density. If this information is not available for corrections, one must assume that the error in a rem meter reading is in most cases larger than a factor of two."

Tesch (TES K 70) has reported the use of liquid scintillators in conjunction with a photomultiplier for neutron dosimetry in the energy range 10 to 100 MeV. The effective threshold of the instrument is selected at about 5 MeV when it has a rem response within ±15% up to about 100 MeV. Pulse-shaping techniques are used to discriminate against other particles. Coleman (COL F 69) has shown that in typical radiation environments around high energy electron accelerators the response of plastic scintillators to neutrons or photons of energy greater than 20 MeV differs by only ±30% over a wide range of energy spectra. Thus the instrument described by Tesch may be useful in a variety of mixed photon and neutron irradiation fields, but some development studies are still needed.

The universal "rem meter" has not yet been developed, and the limitations of presently available instruments necessitate alternative procedures if fair accuracy is required. Baum (BAU J 67, BAU J 68, BAU J 70a, BAU J 70b) has, however, suggested using a modified spherical tissue-equivalent chamber to construct a rem meter. By use of a nonlinear amplifier the pulse-height distribution may be modified to give an output proportional to dose equivalent. On the other hand, Dvorak (DVO R 69) has made calculations that indicate such an instrument would have poor response to intermediate-energy neutrons.

In a strict sense, however, since dose equivalent is a defined quantity, it is not directly measurable with an instrument.

An alternative procedure involves measuring absorbed dose and weighting by an appropriate modifying factor. Absorbed dose may be measured with a tissue-equivalent ionization chamber by meeting the Bragg-Gray requirements that the tissue-equivalent wall be thick enough so that charged-particle equilibrium is achieved, and that the density of the gas in the cavity be small enough so that charged particles do not lose an appreciable fraction of their energy in traversing the cavity. Clearly, to insure that these requirements are met, one must either have prior knowledge of the quality of the radiation or make assumptions (ROS H 56, COW F 65). When such absorbed-dose measurements are made there still remains the problem of selecting an appropriate weighting factor. This selection may be achieved by:

(a) a second measurement for estimating the appropriate modifying factor with, for example, an instrument such as the recombination chamber (ZEL M 62, ZEL M 64, SUL A 63, SUL A 64), or

(b) determination of the LET spectrum of the radiation field (recently the ICRU has discussed the difficulties in measuring LET spectra, and indicated that in general full LET distributions may be obtained only by calculation. This of course presupposes *a priori* knowledge of the radiation field) and calculation of an appropriate modifying factor (ROS H 55 a,b, ROS H 62, PHI L 65), or

(c) knowledge of the spectrum of the radiation field, which permits calculation of the appropriate modifying factor (later we show how knowledge of neutron spectra is used for this purpose), or

(d) choice of some prudently conservative estimate of modifying factor (because it never underestimates dose equivalent, this approximation usually results in unnecessary restrictions in operational procedures).

The use of recombination chambers depends on creating operating conditions in a tissue-equivalent ionization chamber, filled with tissue-equivalent gas, in which current collected is a known function of the quality factor of the radiation being measured. Sullivan and Baarli (SUL A 63) have described a parallel-plate ionization chamber for which the saturation curves may be represented by

$$i = kV^n, \tag{8}$$

where i is the collected current, V the applied voltage, k a proportionality factor, and n the recombination coefficient, which may be related to quality factor. Figure 2.6 shows the response of such a chamber to radium γ rays, Po-Be neutrons, 14-MeV neutrons, and α particles from Pu. An accuracy within ±20% is claimed for the evaluation of QF in a mixed radiation field (SUL A 63).

The use of LET spectrometers in practice was first described by Rossi at al. (ROS H 62), and the technique has since been used in a number of laboratories with good success. From the measured LET distribution appropriate quality factors can be selected for each part of the LET spectrum, and the absorbed-dose measurement previously or simultaneously made weighted accordingly.

Phillips et al. (PHI L 65) have described the principles of the LET spectrometer in the following terms:

"In brief, the LET spectrometer is a TE proportional counter whose output signal is dependent upon the energy loss of individual particles traversing it. The product of the particle's LET and path length yields its energy loss; the resultant output pulse may best be analyzed using a spherical counter. Uniform gas multiplication along the center wire of this counter is established by means of a concentric correcting electrode (helix) upon which a suitable voltage is applied. Operation at a low pressure is required to minimize the variation in LET for individual traversals. The derivation of the equations for computing the absorbed dose as a function of LET is relatively complex.

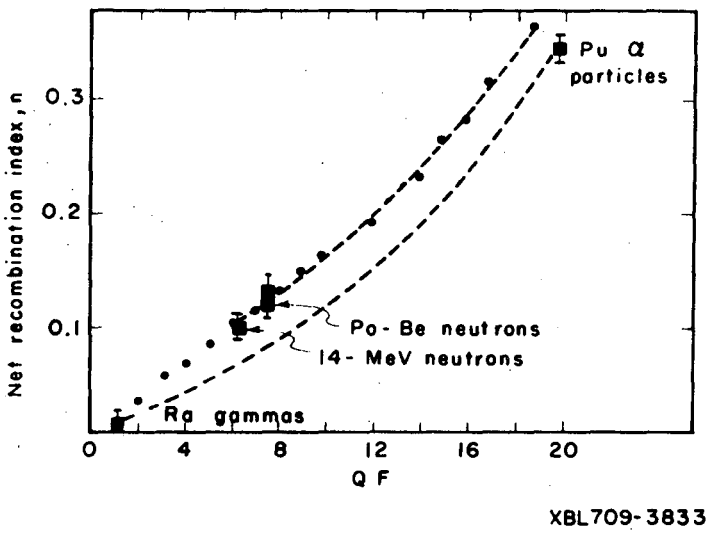

Fig. 2.6. Response of a high pressure parallel-plate recombination chamber as a function of quality factor. ●–●–●– shows the normalized response predicted from Jaffé theory. – – – – shows the response to mixed points (after Sullivan and Baarli).

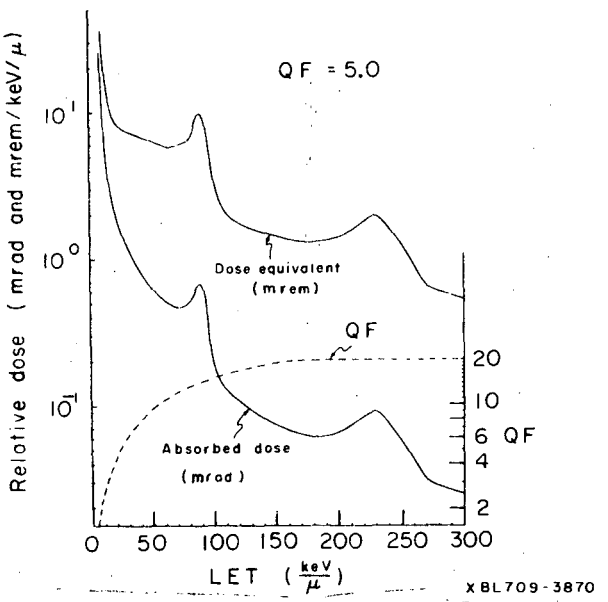

Fig. 2.7. Example of dose and dose-equivalent distribution as a function of linear energy transfer measured at the Brookhaven AGS. (After Phillips et al.)

However, an analytical technique has been developed" (ROS W 60) "which simplifies this LET analysis. The equation for determining dose as a function of LET reduces to

$$D(L) = \frac{1.6 \times 10^{-7}}{2\pi r^2}\left[-h^3 \frac{d}{dh}\left(\frac{Q}{h}\right)\right] \frac{\text{rads}}{\text{keV}/\mu} \qquad (9)$$

where

$D(L)$ = absorbed dose per LET interval, $\frac{\text{rads}}{\text{keV}/\mu}$,

r = radius of spherical proportional counter (cm),

h = pulse height (keV/μ),

Q = total counts in a given pulse height interval"

. . .[For the BNL chamber]

"$D(L) = 9.87 \times 10^{-7} D(h)$ $\frac{\text{mrad}}{\text{keV}/\mu}$,

$D(h) = hQ(1-S)$,

S = the slope of the log Q vs log h curve.

"For the actual computation of the absorbed dose above 3.5 keV/μ, the area under the D(L) vs h curve is determined and multiplied by the keV/μ per channel as determined by the collimated alpha source calibration. A similar treatment is used to obtain the dose equivalent.

Knowing the QF for each LET interval (as defined by the ICRP) one can derive the DE distribution with LET. Although the device is capable of measuring radiations whose LET is less than 3.5 keV/μ, the present study follows the ICRP recommendation. Thus, a QF of one is applied to all LET intervals below this value. The previously mentioned TE ionization chamber is employed for dose determination in this low LET interval.

"The effective QF is determined as follows:

$$QF = \frac{(D_i - D_p)\, QF_{3.5} + R}{D_i}, \qquad (10)$$

where

D_i = total absorbed dose as measured by the TE ionization chamber (mrad),

D_p = total absorbed dose as computed from the proportional counter data, for LET values greater than 3.5 keV/μ (mrad),

R = total DE as computed from the proportional counter data for LET values greater than 3.5 keV/μ (mrem),

$QF_{3.5}$ = quality factor for LET values less than 3.5 keV/μ (equal to unity)."

Figure 2.7 shows a representative dose distribution measured at the Brookhaven National Laboratory AGS. The presence of a heavy-ion peak at approximately 250 keV/μ should be noted.

As previously discussed, Baum et al. have recently reported studies that may facilitate the construction of a portable rem survey meter based upon the principles of the LET spectrometer.

A third technique--neutron spectrometry--largely used around accelerators and to some extent at nuclear reactors, also is of value when the radiation field is dominated by neutrons. The principle here is to determine each component of the radiation field separately and evaluate its contribution to the total dose equivalent. Neutron flux density measurements are normally made over a wide energy range with a number of different detectors, all of which have different response functions and thresholds. Such a detector, i, gives response, A_i, of the form

$$A_i = K_i \int_{E_{min}}^{E_{max}} R_i(E)\, \phi(E)\, dE, \qquad (11)$$

where E_{min} and E_{max} are appropriate energy limits, $\phi(E)$ is the differential energy spectrum, and $R_i(E)$ the response function (e.g., cross section in the case of activation detectors). When the response is thus measured for a number of detectors, it is possible to closely estimate a neutron spectrum that could produce the measured response in the series of detectors (GIL W 68, ROU J 69a, ROU J 69b).

In most practical stiuations this estimated neutron spectrum is a sufficiently accurate representation for health physics purposes. In typical accelerator conditions, for which neutrons and photons are the dominant components of the radiation field, it is usually necessary only to measure the neutron spectrum and evaluate the gamma contribution to the total dose equivalent.

Nuclear emulsion can be used to measure a proton recoil spectrum for spectroscopy of neutrons between 1 MeV and about 20 MeV (LEH R 64). For higher-energy neutrons a measurement of the average number of gray prongs per neutron star is useful in making crude estimates of the shape of the neutron spectrum (PAT H 69). This latter technique--neutron spectrometry--not only can be used to estimate the dose equivalent by use of the flux-to-dose conversion factors given in the following section, but also gives valuable information about the quality of the radiation field. It can be used by the health physicist to specify shielding for personnel and for other detectors, as well as specifying proper wall thickness for tissue-equivalent ionization chambers and evaluating the response of any other detectors that may be used. If it is known--as, for example, for low-energy electron

accelerators--that the radiation field is entirely electromagnetic in character, then the problem of dose-equivalent evaluation is greatly simplified. By definition the QF for low-LET radiation is unity, and it is merely necessary to check for wall thickness within the correct range before using a tissue-equivalent ion chamber. Other detectors useful in this situation are thermoluminescent and glass dosimeters. All these techniques are fully discussed in Part II of this text.

THE CONVERSION OF RADIATION MEASUREMENTS TO DOSE EQUIVALENT

DOSE-DEPTH CALCULATIONS

We have seen in the preceding sections that absolute radiation measurements are of two types, which may be formally characterized by

$$DE = (MF)\, D \tag{2}$$

when absorbed-dose measurements are made, and by

$$DE = \sum_{i=1}^{n} \int_{E_{max}}^{E_{min}} p_i(E)\, N_i(E)\, dE \tag{7}$$

when particle fluence is measured.

It has become conventional, when particle spectra are measured, to quote measured flux densities (in units of particles/cm^2 sec) and to use conversion factors to get flux density to dose equivalent rate (conversion factors: g(E) in units of n/cm^2 sec/per millirem/h.) Thus Eq. 7 becomes modified to

$$DER = \sum_{i=1}^{n} \int_{E_{min}}^{E_{max}} \frac{\phi_i(E)}{g_i(E)}\, dE \tag{7a}$$

where $\phi_i(E)$ is the flux density of particles between energies E and E+dE.

It is necessary therefore, to facilitate the conversion of experimental data to dose equivalent, that values of modifying factors (MF) or flux–to–dose equivalent conversion factors be defined both for monoenergetic particles and for particle spectra.

In general the evaluation of conversion and modifying factors is a complex matter involving the calculation of particle spectra produced within irradiated tissue. Given the details of particle spectra within the tissue, one can calculate the absorbed dose from the known stopping power of each charged particle in tissue. Finally, from the quality factor–LET relationship (as defined on p. 5), one can weight each segment of charged-particle track by the appropriate quality factor and calculate the dose equivalent. The

absorbed dose and dose equivalent are averaged over small volumes of tissue (typically 1 cm^3), and from a knowledge of the distribution of these parameters in an irradiated human body, it is a simple matter to calculate the appropriate conversion and modifying factors. Such detailed calculations, involving as they do complex details of geometry and nuclear interactions, in general need a large digital computer for their execution. Extensive effort has been devoted by the Health Physics and Neutron Physics divisions of Oak Ridge National Laboratory to the calculation of absorbed dose and dose-equivalent distributions in water and tissue phantoms. In general such calculations have been principally in semi-infinite uniform tissue slabs, although some work has been carried out on finite tissue cylinders and parallelipipeds. Budinger et al. (BUD T 70), in preliminary neutron radiography studies at 14 MeV, have described calculations that take into account the different composition of muscle, fat, and bone. Auxier et al. (AUX J 68) have recently reviewed such calculations for neutrons and discussed their limitations. Table 2.11 summarizes published calculations of dose distributions in anthropomorphic phantoms irradiated by electrons, neutrons, photons, or protons. Interested readers should consult the original papers for details.

Figure 2.8 shows examples of dose-equivalent–depth curves for neutrons calculated by several Oak Ridge groups. The influence of incident-particle angular distribution has been investigated by calculating the upper and lower bounds on doses in cases of practical interest. Irradiation of the body by particles incident normally produces, in general, the largest dose equivalent per unit fluence. As Fig. 2.8 shows, the position of the maximum dose equivalent is a function of particle energy. From dose equivalent and absorbed dose-depth curves it is possible to evaluate modifying and conversion factors: it is conventional to evaluate these at the maximum dose equivalent (MADE) in the irradiated phantom.

Thus, if the MADE per unit fluence is Q particles/cm^2, then g(E), the flux density equivalent to a DE rate of 1 mrem/h, is given by

$$g(E) = \frac{1}{3600\ (\text{sec/h})} \times \frac{1}{10^3\ (\text{mrem/rem})} \times \frac{1}{Q\ (\text{rem/particle/cm}^2)}$$

$$= (2.778 \times 10^{-7}/Q)\ \text{particles/cm}^2\ \text{sec/mrem/h}, \qquad (12)$$

and if the absorbed dose per unit fluence is P at the maximum dose equivalent, then the modifying factor MF(E) is given by

$$MF(E) \equiv Q/P\,. \qquad (13)$$

Table 2.11. Summary of depth-dose calculations in tissue for electrons, neutrons, photons, and protons.

	Particle	Energy range	Incident angular distribution	Author(s)	Phantom	Reference
1.	Neutrons	Thermal	Normal	Snyder (1952)	Semi-infinite slab	SNY W 52
2.	Neutrons	Thermal – 10 MeV	Normal	Snyder (1957)	Semi-infinite slab	SNY W 57
3.	Neutrons	Thermal – 15 MeV	Normal	Auxier et al. (1968)	Cylinder	AUX J 68
4.	Neutrons	Thermal – 14 MeV	Normal	Snyder (1968)	Cylinder	SNY W 68
5.	Neutrons	0.5 - 60 MeV	Normal and isotropic	Irving et al. (1967)	Semi-infinite slab	IRV D 67
6.	Neutrons	60 - 400 MeV	Normal and isotropic	Zerby, Kinney (1965); Turner et al. (1964)	Semi-infinite slab	ZER C 65 TUR J 64
7.	Neutrons	60 - 3000 MeV	Normal	Alsmiller et al.(1970)	Semi-infinite slab	ALS R 70
8.	Neutrons	600 - 2000 MeV	Normal and isotropic	Neufeld et al. (1969)	Semi-infinite slab	NEU J 69a
9.	Protons	100 - 400 MeV	Normal	Turner et al. (1964)	Semi-infinite slab	TUR J 64
10.	Protons	100 - 400 MeV	Normal and isotropic	Neufeld et al. (1966)	Semi-infinite slab	NEU J 66
11.	Protons	400 - 3000 MeV	Normal	Alsmiller et al. (1970).	Semi-infinite slab	ALS R 70
12.	Protons	600 - 2000 MeV	Normal and isotropic	Neufeld et al. (1969)	Semi-infinite slab	NEU J 69a
13.	Electrons	100 MeV – 20 GeV	Normal	Alsmiller and Moran (1967)	Semi-infinite slab	ALS R 67
14.	Electrons	100 MeV – 20 GeV	Normal	Beck (1970)	Semi-infinite slab	BEC H 70
15.	Photons	10 MeV – 20 GeV	Normal	Alsmiller and Moran (1967)	Semi-infinite slab	ALS R 67
16.	Photons	150 MeV – 20 GeV	Normal	Beck (1970)	Semi-infinite slab	BEC H 70

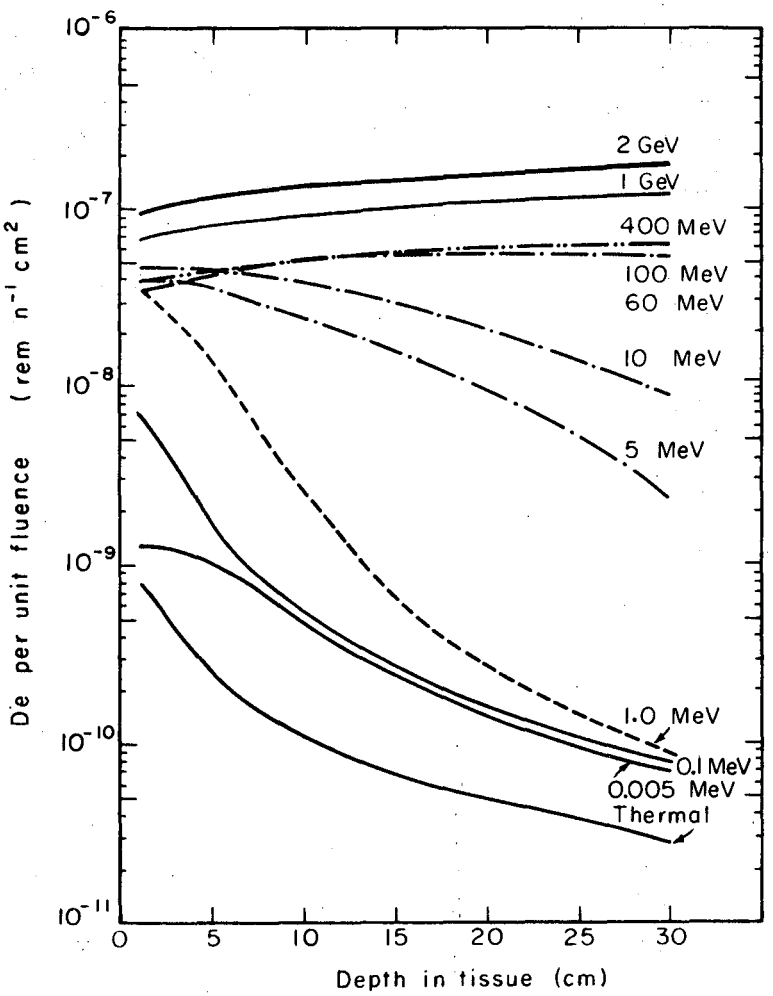

Fig. 2.8. Dose-equivalent depth distributions in a 30-cm semi-infinite tissue slab for normally incident neutrons.

EVALUATION OF FLUX-TO-DOSE CONVERSION FACTORS IN SIMPLE SPECIAL CASES

It is necessary to utilize digital computers to perform these calculations, and it is unfortunate that the complexity of the computer methods often obscures the underlying physical principles. Thus the reader may gain more physical insight by reading the early (but inaccurate) estimates of dose deposition by neutrons and protons. Thus, Sykes (SYK J 58) and Randolph (RAN M 57) reported early estimates for 14- and 20-MeV neutrons and 14-MeV neutrons respectively. These early estimates are basically calculations of "first collision dose" in tissue crudely corrected for backscattering effects.

Somewhat later Neary and Mulvey (NEA G 58) estimated the average dose deposition through the body by neutrons and protons between 40 and 1000 MeV. Estimates were made both for monoenergetic particles and for particles accompanied by their equilibrium cascade. These latter became the basis for conversion factors recommended by ICRP (ICRP 64) for neutrons and protons.

Goussev (GOU N 68) has discussed simple analytical expressions that relate particle flux density to absorbed dose rate in an approximate way. For photons, under conditions of electronic equilibrium, the flux density, ϕ, equivalent to an absorbed dose rate of 1 m rad/h, is given by

$$\phi = 17.34/E\chi, \tag{14}$$

where E is the photon energy, and χ is the mass energy-absorption coefficient in water. (For derivation see below.)

Such a simple relationship extends only to a few MeV, but its use gives good agreement with more sophisticated calculations even up to 100 MeV (THO R 69).

For charged particles the dose deposition rate, P, is given by

$$P = 1.6 \times 10^{-8} \times \phi \left(\frac{dE}{dx}\right) \text{ rads/sec}, \tag{15}$$

where ϕ is the charged particle flux density (in particles/cm^2 sec),

$\left(\frac{dE}{dx}\right)$ is the stopping power in water (in MeV/g/cm^2),

and 1.6×10^{-8} converts MeV/g to rads.
If P is 10^{-3} rad/h, then

$$\frac{10^{-3}}{3.6 \times 10^3} = 1.6 \times 10^{-8} \phi \left(\frac{dE}{dx}\right),$$

and, finally,

$$\phi = 17.34 \Big/ \left(\frac{dE}{dx}\right) \quad , \tag{16}$$

with ϕ in particles/cm^2/sec/mrem/h and $\left(\frac{dE}{dx}\right)$ in units of MeV cm^2/g.

When the charged particle is slow enough so that its stopping power in water is greater than 35 MeV/g/cm^2, Eq. 16 must be modified to

$$\phi = 17.34 / \text{QF}\left(\frac{dE}{dx}\right) \times \left(\frac{dE}{dx}\right) \tag{17}$$

where $\text{QF}\left(\frac{dE}{dx}\right)$ is the appropriate quality factor at the given value of $\left(\frac{dE}{dx}\right)$ (see Fig. 2.3). Such a prescription ignores backscattering and nuclear interactions, but is extremely useful for estimating surface dose from low-energy electrons and protons. Goussev has used this formulation to calculate ϕ_β, the flux of β particles equivalent to a dose rate of 1 mrad/h from measurements of β-particle spectra. In this case the average energy loss $\left\langle\frac{dE}{dx}\right\rangle$ is given by

$$\left\langle\frac{dE}{dx}\right\rangle = \int_0^{E_{max}} \frac{dE}{dx} N(E)dE \Big/ \int_0^{E_{max}} N(E)dE, \tag{18}$$

where N(E) is the number of electrons with energy between E and E+dE, and $\left(\frac{dE}{dx}\right)$ is the energy loss at energy E.

Substituting into Eq. 16, one has

$$\phi_\beta = 17.34 \int_0^{E_{max}} N(E)dE \Big/ \int_0^{E_{max}} \frac{dE}{dx} N(E)dE \quad . \tag{19}$$

Table 2.III summarizes the data given by Goussev. Goussev has described the limitations of this technique thus: "The above method of calculating the relationship between absorbed dose and flux density for beta particles possessing a continuous spectrum entails the following errors:

(i) An error due to the fact that the contribution of low-energy (<10 keV) electrons to the absorbed dose is not taken into account. At maximum beta particle energies up to 0.3 MeV the error can reach 20 to 30% (and, consequently, the maximum permissible flux density in this region must be reduced accordingly). For higher maximum energies this contribution may be neglected;

(ii) An error due to the fact that the dependence of the beta particle energy loss, dE/dx, on the atomic number Z of the isotope is not taken into

Table 2.III. Flux density of beta radiation corresponding to a dose rate of 1 mrad/h. (After Goussev.)

Maximum β-particle energy (MeV)	Flux density (β particles/cm^2 sec)
0.2	2.4
0.4	3.6
0.6	4.8
0.8	6.4
1	7.2
1.5	8.4
2	8.8
3	9.2

account. As Z increases from 10 to 80, dE/dx grows by 15 to 20% in the low-energy region (0.1 to 0.4 MeV), and by 7 to 10% in the high-energy region (1.5 to 3 MeV). In the above calculations we have taken the average dependence on Z obtained experimentally with the isotopes in question;

(iii) An error due to the fact that differences in the shape of the spectrum are not taken into account. It is known that energy losses dE/dx for allowed transitions are considerably higher than those for transitions forbidden in the first order. Thus for biological tissue the energy losses (dE/dx) in the energy range 0.1 to 0.4 MeV are greater by a factor of 1.3 to 1.6 for allowed spectra than for forbidden spectra. At higher energies this difference vanishes.

"In the low-energy region, therefore, the relationship between the absorbed dose rate and the flux density for β particles of forbidden spectra will be closer to that for monochromatic electrons than to that for β particles in allowed spectra; accordingly, the maximum permissible particle flux density will also be closer to that of monochromatic electrons."

Such calculations, however, yield only approximate results, because particle buildup and geometric-effects are not taken into account. The possible magnitude of these effects for electrons is discussed beginning on page 27.

CONVERSION FACTORS FOR MONOENERGETIC PHOTONS

As we have seen in the preceding section, the conversion factors for low-energy photons may be calculated from

$$\phi = 17.34/E\chi \qquad (14)$$

where E is the photon energy,

χ is the mass energy-absorption coefficient in cm^2/g of water.

Between 0.01 and 10 MeV Evans (EVA R 68) has tabulated values of these absorption coefficients which have been used in the evaluation of the conversion factors in Table 2.IV. Alsmiller and Moran (ALS R 67) have reported electromagnetic cascade calculations from 10 MeV to 20 GeV which give agreement to within less than 30% with values of conversion factors estimated by using total absorption coefficients in water that are due to Evans (EVA R 63). Recently, however, Beck, (BEC H 70) has converted the calculations by Alsmiller and Moran by including the density effect in the electron stopping power previously omitted. Lower energy absorption resulted, giving conversion factors some 25% higher than obtained by Alsmiller and Moran at 100 MeV, increasing to 70% at 20 GeV. As is discussed more fully beginning on p. 27, experimental studies have not adequately resolved this discrepancy; and although one might intuitively think the data of Beck more accurate, since they include density effect corrections, the data of Alsmiller and Moran have been used in the evaluation of photon conversion factors, since they are more restrictive. Figure 2.9 summarizes the data of Table 2.IV. Of course the quality factor for photons is always unity, so that conversion of absorbed dose to dose equivalent is trivial.

CONVERSION FACTORS FOR MONOENERGETIC ELECTRONS

At energies less than 100 MeV electrons stop in the human body (the range of a 100-MeV electron is 30 cm in water); at energies less then 0.07 MeV they cannot penetrate the epidermis.

Tesch (TES K 66) made one of the first estimates of conversion factors for electrons. He assumed the dimensions of a critical complex cell to be equivalent to the range of a 0.1-MeV electron (0.015 cm in tissue), and thus by using the known value of dE/dx and the relationship

$$\phi = 17.34/dE/dx \text{ electrons/cm}^2 \text{ sec/mrem/h} \qquad (16)$$

he suggested a value of 4.4 e/cm^2 sec/mrem/h as appropriate up to electron energies of 100 MeV. This represents a safe limit, but is probably conservative by nearly a factor of 2 in the region of a few MeV.

At energies beyond 100 MeV cascade effects become important, and Tesch made measurements of the dose deposition of 5.2-GeV electrons in water. By representing the enhanced energy deposition by a "cascade factor," F(E), Tesch writes

$$\phi = 17.34/F(E)\left(\frac{dE}{dx}\right) \quad . \qquad (17)$$

Table 2.IV. Factors for converting photon flux density to dose equivalent.

Photon energy (MeV)	Flux density equivalent to 1 mrem/h (photons/cm^2 sec)*
0.01	362
0.015	903
0.02	1693
0.03	3879
0.04	6215
0.05	8296
0.06	9031
0.08	8272
0.10	6773
0.15	4173
0.20	2919
0.30	1812
0.40	1322
0.50	1051
0.60	878
0.80	675
1.00	561
1.50	410
2.00	333
3.00	255
4.00	210
5.00	182
6.00	161
8.00	131
10.00	114
20.00	64.8
50	28.6
100	14.1
200	9.4
500	5.7
1000	5.0
5200	3.7
10000	3.4
20000	3.2

*See Table 2.VII

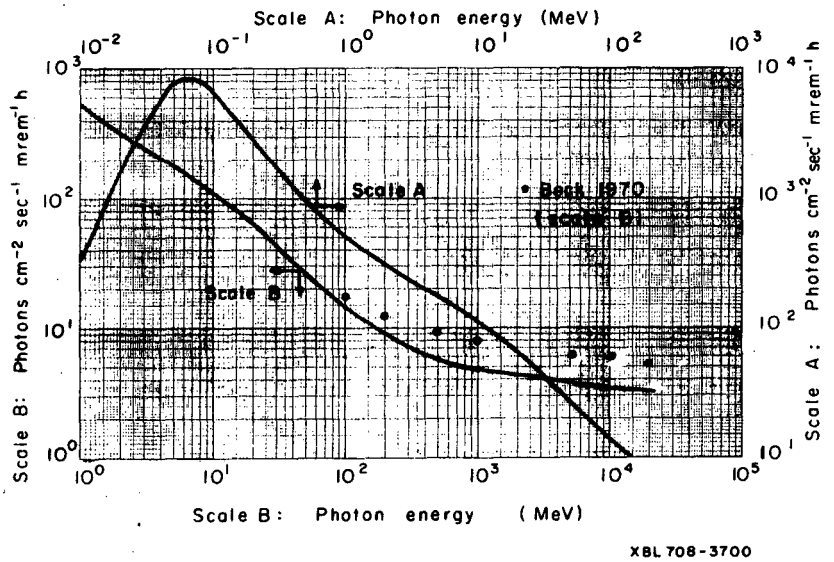

Fig. 2.9. Conversion factors for flux density to dose-equivalent rate for photons.

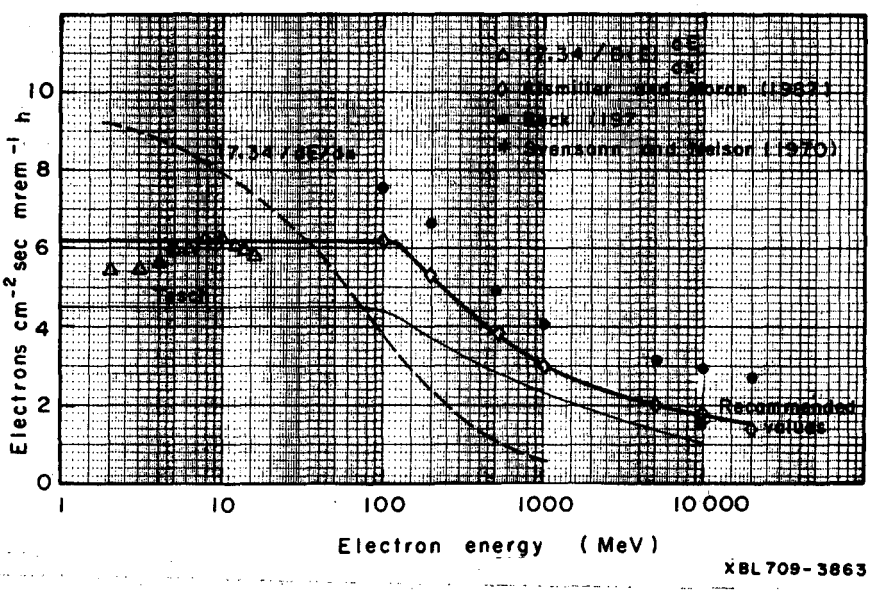

Fig. 2.10. Conversion factors for flux density to dose-equivalent rate for electrons.

At 5.2 GeV Tesch measured F(E) and found it to be 3.5, and by using Ott's (OTT K 53) treatment of the electromagnetic cascade Tesch has suggested values of F(E) up to 10 GeV. However, because the experimental value of F(E) is probably too high by a factor ≈1.6, due to photon contamination of the electron beam, values of derived conversion factors are likely to be conservative.

Monte Carlo calculations by Alsmiller (ALS R 67) of energy deposition in tissue by electrons in the range 100 MeV to 20 GeV have recently been repeated by Beck (BEC H 70), who included the density effect in the electron stopping power. The resultant decreased stopping power produces a significant increase in the conversion factors derived. Although this refinement might be expected to improve the calculations by Alsmiller and Moran, recent experimental studies by Svensson and Nelson (SVE G 70) produce ambivalent results. Measurements of the energy absorption in a water phantom irradiated by 10-GeV electrons shows agreement with calculations by Beck at small depths in the phantom, but better agreement with the results of Alsmiller and Moran at greater depths. A value of 1.61 electrons/cm^2 sec/mrem/h is obtained from interpolating these experimental data to a depth of 30 cm. Since conversion factors are evaluated at the maximum dose equivalent in the body, the findings of Alsmiller and Moran seem more appropriate in defining conversion factors. Further, in the event of unresolved discrepancies it is cautious to use more restricting values.

In the electron energy range from a few MeV to about 30 MeV the dose distribution in water or tissue has been measured under many different geometrical conditions of irradiation. In evaluating conversion factors, data obtained under conditions of maximum buildup within the body should be utilized. Fielder and Holm (FIE E 70) have summarized the values of the ratio of maximum dose to entrance dose in water deposited by electrons between 2 and 16 MeV. Table 2.V gives these values of buildup factor, B(E). Buildup factors above 10 MeV are thus seen to be constant at about 1.25, as also indicated by Jones (JON J 61) in a review article on electron depth-dose measurements. Since Eq. 16 gives the surface dose, we may use the buildup factors of Table 2.V to evaluate conversion factors according to

$$\phi = 17.34/B(E) \frac{dE}{dx} \quad . \qquad (17a)$$

Table 2.VI gives the values so calculated, which are plotted on Fig. 2.10.

In view of the assorted data available, any selection of conversion factors is somewhat arbitrary. Table 2.VI and Fig. 2.10 summarize the various estimates of conversion factors discussed here; values of conversion factors obtained by using Eq. 17a are only approximate at low energies, at which only surface irradiation is achieved. The values by Tesch are certainly

too conservative, and as we have already discussed for the calculations by Alsmiller and Moran, are better supported by experiment at 10 GeV. Therefore we recommend the values given in Table 2.VII, with the conversion factor below 100 MeV to be constant at 6.2 electrons/cm^2 sec/mrem/h and to recommend use of the Alsmiller and Moran data at higher energies. Modifying factors for electrons in this energy range are always 1.0.

Table 2.V. Maximum absorbed dose buildup factors for electrons in water.

Electron energy (MeV)	$\frac{\text{Maximum dose}}{\text{Entrance dose}}$ B(E)
2	1.67
3	1.64
4	1.54
5	1.44
6	1.40
8	1.32
10	1.27
12	1.25
14	1.25
16	1.25

Table 2.VI. Conversion-factor estimates for monoenergetic electrons.

Electron energy (MeV)	Conversion factor $\frac{\text{electrons}}{\text{cm}^2\,\text{sec}}$ / mrem/h	Remarks
0.1	3.9	$\phi = 17.34/\frac{dE}{dx}$ Stopping power data from NAS_C 64
0.2	5.7	
0.5	7.7	
1	8.5	
2	8.7	
0.1-100	4.4	K. Tesch, Nukleonik 8, 264 (1966)
200	3.7	
300	3.2	
500	2.9	
1000	2.4	
2000	2.0	
5000	1.5	
10 000	1.1	
100	6.2	R. G. Alsmiller and H. S. Moran, ORNL-TM 2026 (1967)
200	5.4	
500	3.8	
1000	2.9	
5200	2.1	
10 000	1.8	
20 000	1.5	
100	7.6	H. Beck, Nucl. Instr. Methods 78, 333 (1970)
200	6.6	
500	4.9	
1000	4.1	
5200	3.2	
10 000	2.9	
20 000	2.7	
2	5.5	$\phi = 17.34/B(E)\ dE/dx$. dE/dx from NAS_c 64. B(E) from Table 2.V.
3	5.4	
4	5.6	
5	5.7	
6	5.9	
8	6.1	
10	6.2	
12	6.0	
14	5.9	
16	5.8	

Table 2.VII. Recommended electron conversion factors.

Electron energy (MeV)	Conversion factor* $\frac{\text{electrons}}{\text{cm}^2\,\text{sec}}$ / $\frac{\text{mrem/h}}{}$
0.1-100	6.20
100	6.20
200	5.36
500	3.85
1000	2.94
5200	2.13
10 000	1.82
20 000	1.54

*The number of significant figures given is to facilitate numerical interpolation and does not indicate the accuracy of the recommended factors.

CONVERSION AND MODIFYING FACTORS FOR MONOENERGETIC PROTONS

Table 2.VIII and Fig. 2.11 (also Fig. 2.15) summarize the values of conversion and modifying factors derived from the depth-dose calculations for protons. Below 200 MeV the Bragg peak is always developed in the body, and consequently the conversion factors are constant down to a proton energy of 2 MeV, at which the epidermis cannot be penetrated. At energies greater than 200 MeV, at which the Bragg peak is not developed in the body, the conversion-factor curve shows a sharp rise, followed by a steady decline at higher energies. Modifying factors increase slowly from about 1.3 at 100 MeV to about 2.0 at 2 GeV (see Fig. 2.15).

Table 2.VIII. Summary of conversion-factor (CF) in units of p/cm^2 sec per millirem/hr. and modifying-factor (MF) data for protons.

Proton energy (MeV)	Turner et al.		Neufeld et al.		Alsmiller at al.	
	CF	MF	CF	MF	CF	MF
100	0.41	1.3				
200	0.43	1.3				
300	2.5	1.3				
400	2.5	1.3			2.4	1.6
600			2.4	1.7		
660					2.2	1.8
730					1.8	2.1
1000			2.0	1.9		
1500					1.5	2.4
2000			1.4	1.4	1.2	2.2

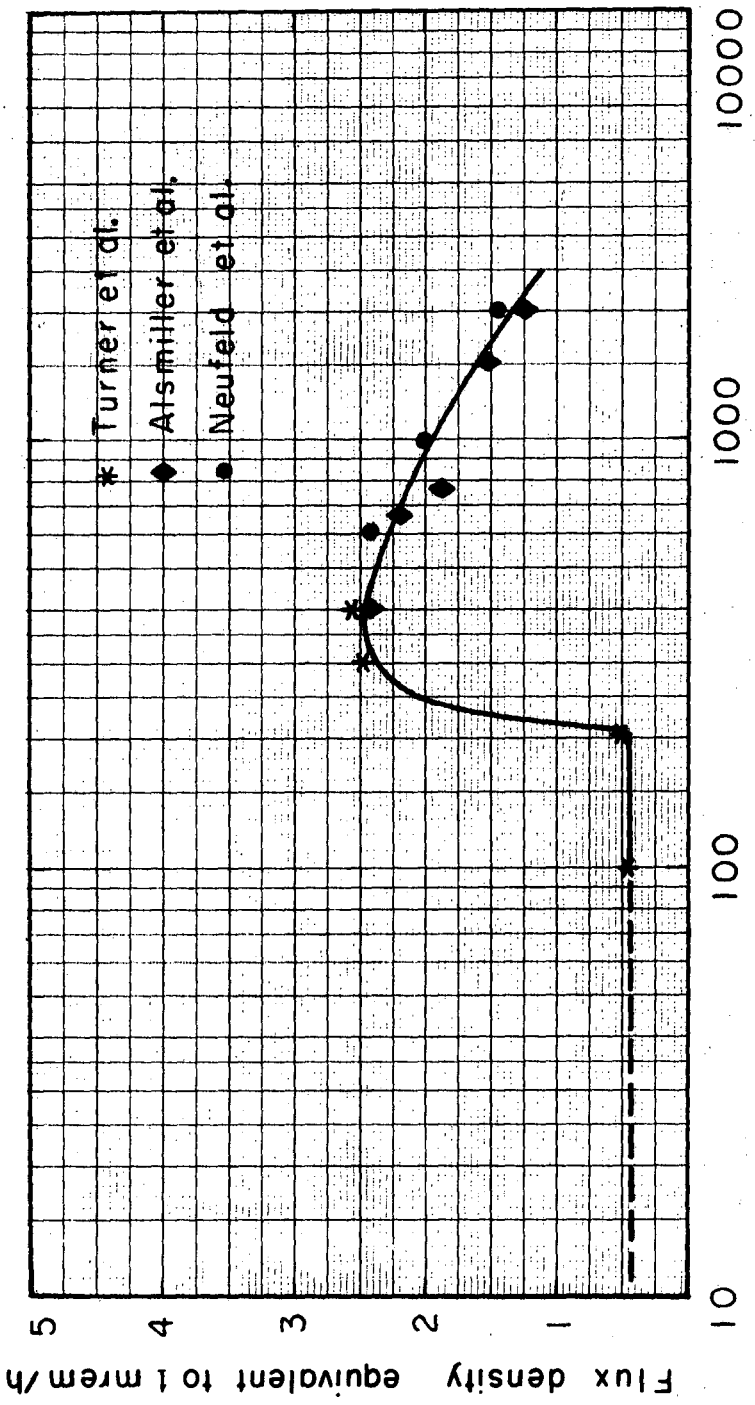

Fig. 2.11. Conversion factors for flux density to dose-equivalent rate for protons.

CONVERSION AND MODIFYING FACTORS FOR MONOENERGETIC NEUTRONS

Until recently the only guidelines available to the health physicist in evaluating neutron dose equivalent were derived from NBS Handbook #63 (NBS 67) and ICRP Publication 4 (ICRP 64). NBS Handbook #63 limits itself to neutron energies of 30 MeV and less. Values of "RBE" as a function of depth in a semi-infinite tissue slab are given for neutrons up to 10 MeV. At these energies the maximum dose equivalent always occurs in the first 1 cm of tissue, or effectively at the body surface.

The deficiencies of ICRP Publication 4 for energies above 10 MeV were suggested as early as 1965 (THO R 65). ICRP 4 gives conversion factors and modifying factors for neutrons and protons between 40 MeV and 1 GeV based upon calculations by Neary and Mulvey (NEA G 58) of the average dose deposited in the body when it is irradiated by primary particles accompanied by their equilibrium cascades. It is more convenient in practice to have values of conversion and modifying factors for monoenergetic particles.

Table 2.III summarizes the depth-dose calculations from which conversion and modifying factors for neutrons may be derived. The only data available until recently for low energies were published in NBS Handbook #63. Recently a revision of this handbook has been undertaken, and Auxier et al. (AUX J 68) and Snyder (SNY W 68) have made calculations in a finite cylindrical tissue phantom. These calculations are limited to neutrons below 15 MeV and for irradiation in a unidirectional beam. Such a phantom better represents the human body, and the calculations have the advantage of the currently best available cross-section data. Furthermore, in the calculations by Snyder, high statistical accuracy was obtained in adequately small volumes of tissue; the newer data are therefore to be preferred. In general, comparison of the newer data with the older NBS 63 data gives close agreement (generally to within less than 20%). A recent semiexperimental determination of the conversion factor for thermal neutrons by Boot and Dennis (BOO S 68) is of interest. Using an elliptical phantom, these workers estimated the thermal neutron flux density equivalent to 1 mrem/h to be 366 $n/cm^2 sec$.

Data between 0.5 and 60 MeV have been provided by calculations due to Irving et al. (IRV D 67), which are in good agreement up to about 10 MeV with the NBS 63 data and with the newer calculations by Snyder and Auxier et al. At 60 MeV, however--for which four alternative calculations are available, due to Irving et al., Turner et al. (TUR J 64), Zerby and Kinney (ZER C 65), and Alsmiller at al. (ALS R 70)--some discrepancies are in evidence. The fundamental difference between the calculation by Irving et al.

and the other three is in the nuclear model used to describe particle production from nonelastic interactions. Although at present insufficient information is available to make an objective choice between the different calculations, the evidence strongly suggests that the recent calculations by Alsmiller et al. (ALS R 70) are the most reliable. Thus the discontinuity in the conversion factor–energy and modifying factor–energy curves indicated by the Irving et al. data may be ignored. It is perhaps unfortunate, in view of these remarks, that the recent calculations by Snyder show a large reduction in conversion factor (from 7.1 to 5.0 n/cm^2 sec/mrem/hr) between 10 and 14 MeV, but if it is borne in mind that the individual accuracy on such points is $\approx \pm 10\%$, such a fluctuation may be interpreted as statistical. It is clear, however, that more work is needed in the neutron energy region 10 to 150 MeV if these anomalies are to be removed. In the energy range 100 to 3000 MeV the situation is much clearer. Calculations by Zerby and Kinney, Turner et al., and Alsmiller are essentially in agreement to within less than 20%.

Table 2.1X summarizes the recommended values of conversion and modifying factors based on the published data; these are shown graphically in Figs. 2.12 and 2.13. The smooth curves drawn through the data indicate the presently available best estimates from the wide variety of data published. In the use of these factors the accuracy of the calculations upon which they are based and the inherent limitations in their definition should be firmly kept in mind.

CONVERSION AND MODIFYING FACTORS FOR MONOENERGETIC PARTICLES--A SUMMARY

We have seen how the assignment of conversion and modifying factors is to some extent an arbitrary matter. It is important to bear in mind, however, that the evaluation of dose equivalent consists of two separable elements--a physical measurement capable of some precision (say, to within 10% or less for external radiation fields), and the conversion of this physical measurement to units appropriate to radiation protection. This conversion is limited by our basic lack of knowledge in radiobiology. It is important to recognize, however, that the final expression of physical measurements in rem depends on a choice of factors and therefore is in essence an *administrative decision;* there is no reason why the basic precision of the physical measurements should not be preserved in such a step. Provided general agreement may be reached on the steps to be taken during conversion, there seems to be no reason why all adequate techniques of radiation measurement will not give dose-equivalent estimates essentially in agreement. The steps outlined in this chapter facilitate such procedures.

Table 2.1X. Conversion and modifying factors for neutrons.
(The number of significant digits given facilitates convenient numerical interpolation, and does not indicate the accuracy of the recommended factors.)

Neutron energy (MeV)	Conversion factor (n/cm^2 sec/mrem/h)	Modifying factor
2.5×10^{-8}	265	2.3
5×10^{-8}	254	2.2
1×10^{-7}	242	2.0
2×10^{-7}	234	2.0
5×10^{-7}	226	2.0
1×10^{-6}	222	2.0
2×10^{-6}	224	2.0
5×10^{-6}	228	2.0
1×10^{-5}	231	2.0
2×10^{-5}	233	2.0
5×10^{-5}	237	2.0
1×10^{-4}	239	2.0
2×10^{-4}	248	2.0
5×10^{-4}	261	2.0
1×10^{-3}	272	2.0
2×10^{-3}	278	2.0
5×10^{-3}	281	2.0
1×10^{-2}	283	2.0
2×10^{-2}	170	3.3
5×10^{-2}	82	5.7
1×10^{-1}	48	7.4
2×10^{-1}	28	9.2
5×10^{-1}	14	11.0
1×10^{0}	8.5	10.6
2×10^{0}	7.0	9.3
5×10^{0}	6.8	7.8
1×10^{1}	6.8	6.8
2×10^{1}	6.5	6.0
5×10^{1}	6.1	5.0
1×10^{2}	5.55	4.4
2×10^{2}	5.10	3.8
5×10^{2}	3.60	3.2
1×10^{3}	2.25	2.8
2×10^{3}	1.55	2.6

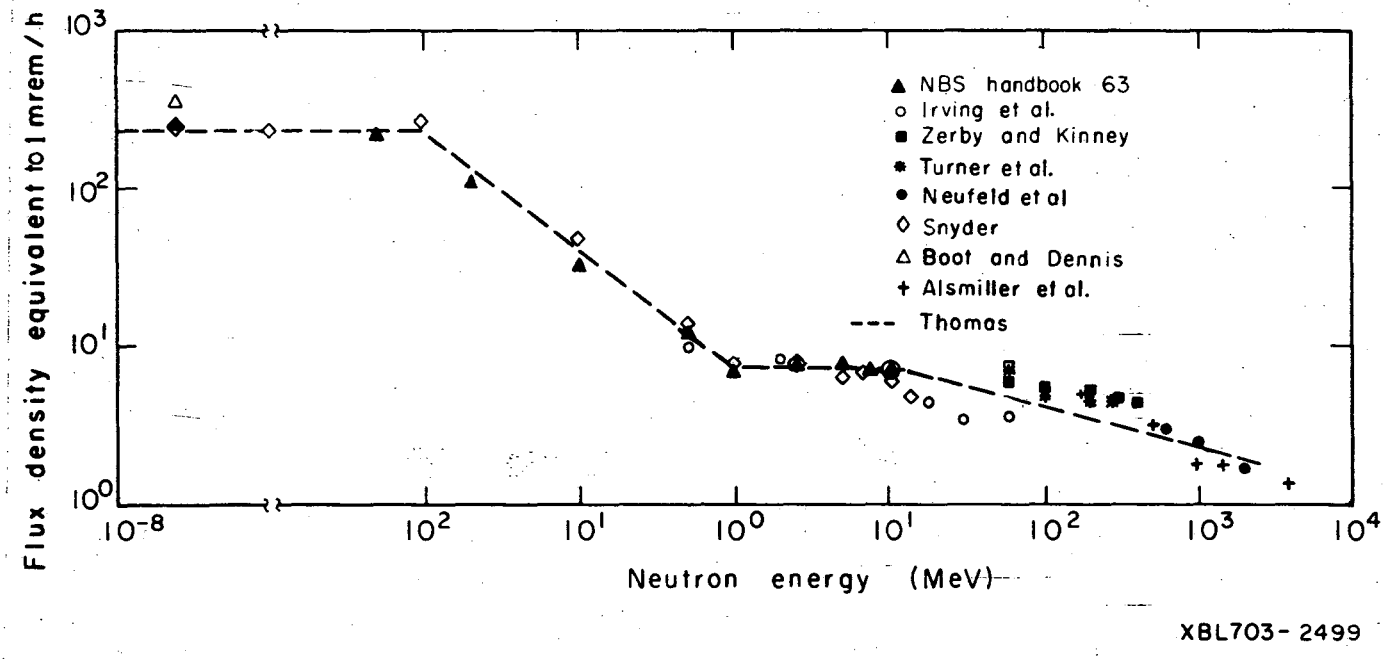

Fig. 2.12. Conversion factors for flux density to dose-equivalent rate for neutrons.

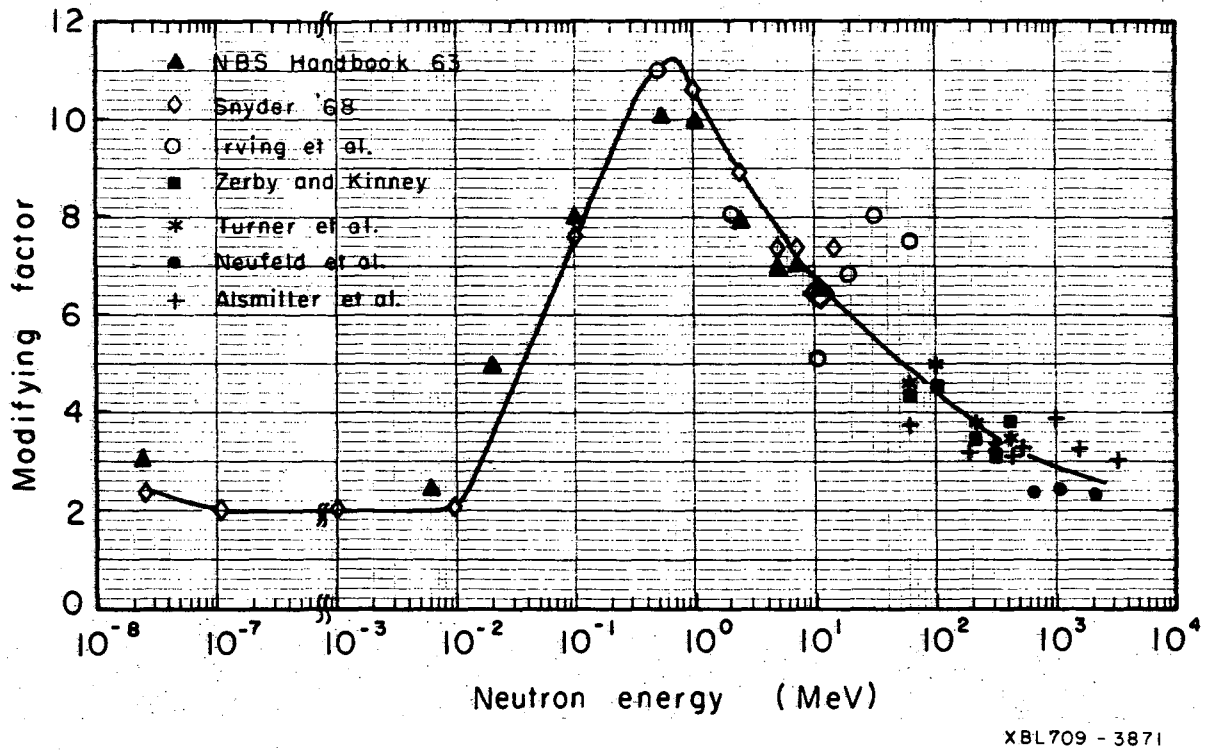

Fig. 2.13. Neutron modifying ("quality") factors.

Figures 2.14 and 2.15 summarize the conversion and modifying factors for monoenergetic photons, electrons, protons, and neutrons derived from currently available data. It is important to discuss how these might be used in some practical instances.

CONVERSION AND MODIFYING FACTORS FOR PARTICLE SPECTRA

We have seen in the seven preceding subsections how conversion and modifying factors may be selected for monoenergetic particles from dose-depth calculations. In practice, however, measurements at particle accelerators are made in particle spectra having a wide energy span. Thus, for example, at high-energy particle accelerators the energy spectrum extends from thermal energies to several GeV. Figure 2.16 shows typical examples of such spectra measured outside shielding at the CERN 25-GeV proton synchrotron and LRL 6-GeV Bevatron. For comparison, the spectrum of neutrons generated in the lower atmosphere by cosmic radiation is shown. (The flux density scale is of no significance--the curves have been vertically displaced for clarity.) The practical problem therefore arises: given such a wide energy span, what average conversion or modifying factors are appropriate?

If only tables of conversion and modifying factors are available as a function of particle energy an average may be specified for particle spectra defined by the equations

$$\langle MF \rangle = \int_{E_{min}}^{E_{max}} MF(E)\,\phi(E)dE \Big/ \int_{E_{min}}^{E_{max}} \phi(E)dE, \qquad (18)$$

$$\frac{1}{\langle g \rangle} = \int_{E_{min}}^{E_{max}} \frac{\phi(E)}{g(E)}\,dE \Big/ \int_{E_{min}}^{E_{max}} \phi(E)dE, \qquad (19)$$

where $\langle MF \rangle$, $\langle g \rangle$ are the average modifying and conversion factors,

$\phi(E)\,dE$ is particle differential energy spectrum,

and E_{min}, E_{max} are appropriate energy limits.

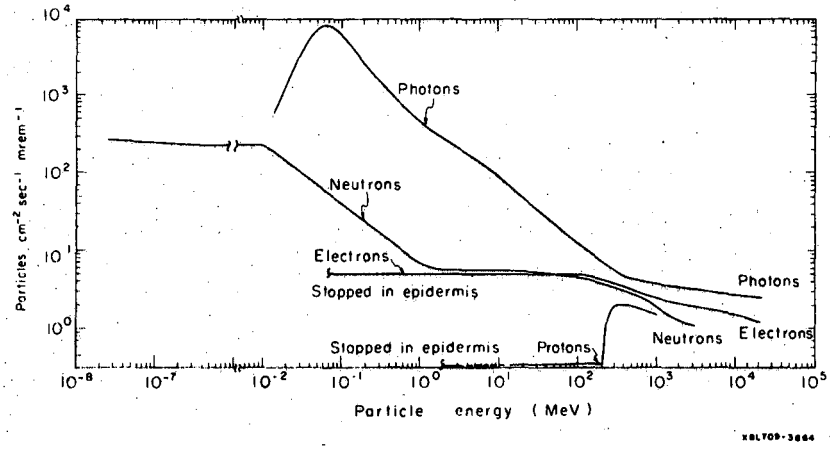

Fig. 2.14. Conversion factors -- a summary.

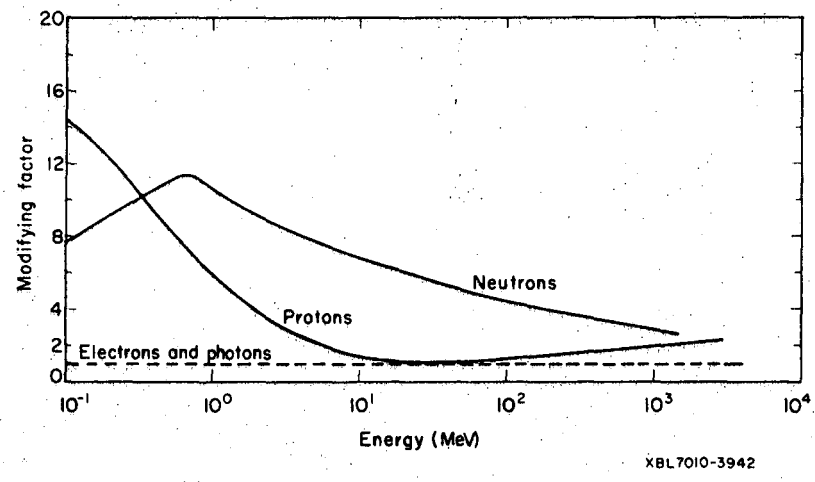

Fig. 2.15. Modifying ("quality") factors - A summary.

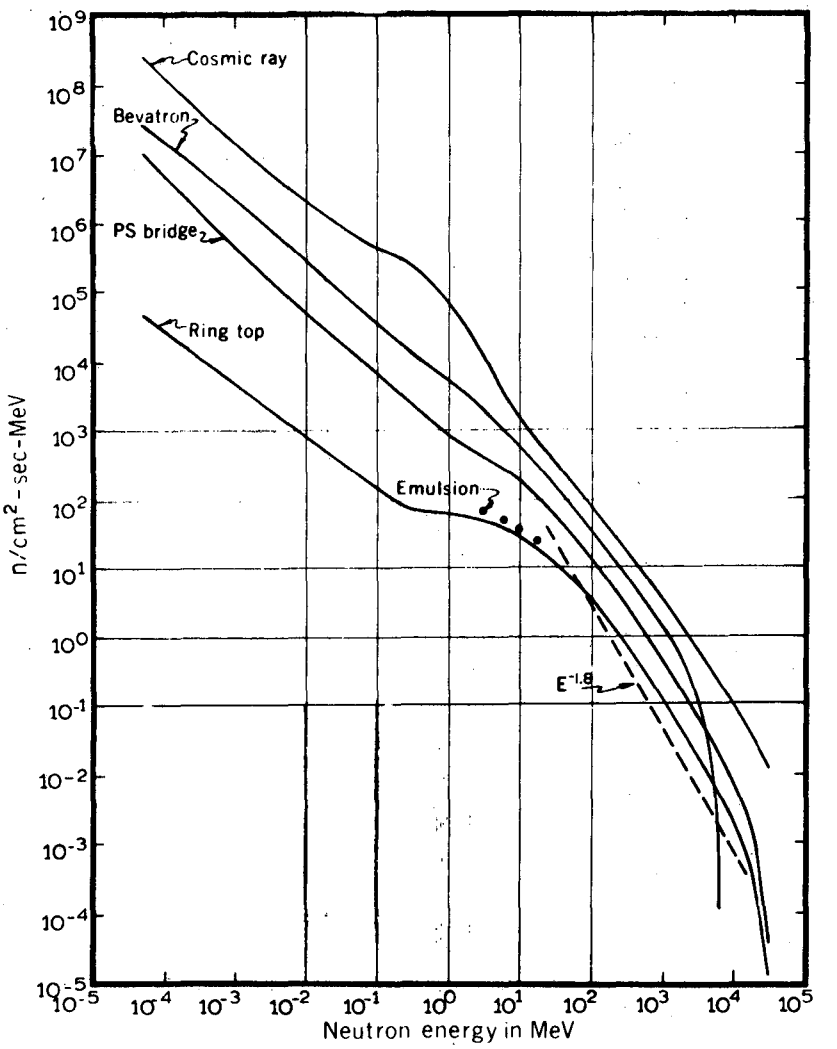

Fig. 2.16. Typical high energy accelerator neutron spectra obtained by threshold detectors. In the case of the "Ring top" spectrum Ilford L4 emulsions were exposed. The experimental points labelled emulsion are derived from proton recoil track analysis while the line with negative slope 1.8 was obtained from star prong counting.

Patterson et al. (PAT H 70) have thus evaluated average modifying factors, for use when tissue equivalent chambers are used to measure absorbed dose in several different neutron spectra. ⟨MF⟩s were calculated for the three accelerator spectra (shown in Fig. 2.16), the Hess cosmic ray spectrum (HES W 59a), the Watt fission spectrum (WAT B 52), and the PuBe(α,n) spectrum (HES W 59b, STE L 55) (Figure 2.17). Results are summarized in Table 2.X).

Table 2.X. Modifying factors calculated for typical neutron spectra (after Patterson et al., PAT H 70).

Spectrum	⟨MF⟩
CERN PS ring top	5.4
CERN PS shield bridge	4.9
Bevatron	5.6
Cosmic-ray spectrum (Hess)	6.5
PuBe spectrum (Hess)	8.1
PuBe spectrum (Stewart)	7.9
Fission spectrum (Watt)	9.0
"1/E spectrum"	cutoff-dependent; 2.9 at E_{max} = 10 GeV

In an attempt to study the variation of ⟨MF⟩ with neutron spectrum characteristics in a more formal manner Patterson et al. also evaluated ⟨MF⟩ for spectra expressed in simple exponential form. Thus $\phi(E)$ was expressed as

$$\phi(E) \propto E^{-\gamma} \qquad (20)$$

and ⟨MF⟩ was evaluated as a function of γ or values between 0 and 2 and as a function of maximum neutron energy, E_{max}. (The interested reader is referred to the original paper for precise details of the mathematical techniques used.) Figure 2.18 summarizes the results of these calculations and leads to the following conclusions:

(a) For very steep spectra ($\gamma > 1.3$), ⟨MF⟩ is independent of energy cutoff, being determined by the dominance of neutrons in the eV range.

(b) For low values of upper-energy cutoff, ⟨MF⟩ is a weakly varying function of E_{max} (for the same reasons as in a), changing only from 2 to 3 in the energy range thermal to 20 keV.

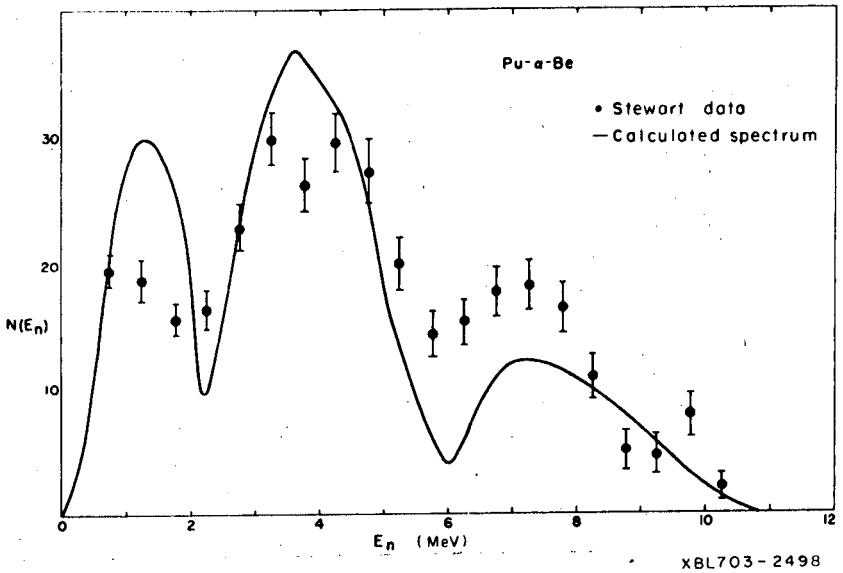

Fig. 2.17. Pu - α - Be neutron spectrum. (After Hess.)

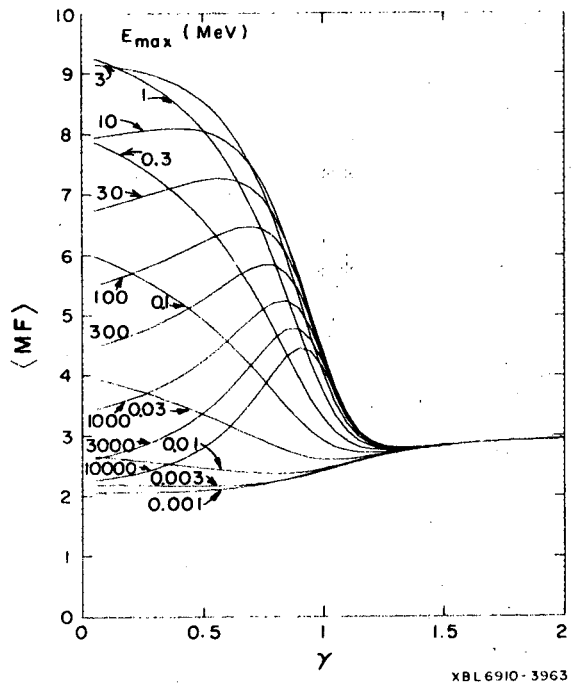

Fig. 2.18. Average modifying ("quality") factors for neutron spectra as a function of cutoff energy and spectrum slope. (After Patterson et al.)

(c) Beyond values of E_{max} of 20 keV the variation of ⟨MF⟩ becomes significant, reaching a peak at $E_{max} \approx 1$ MeV, where ⟨MF⟩ values of 9 are observed at low values of slope.

(d) For values of γ close to 1 (i.e., 1/E spectra), ⟨MF⟩ varies rapidly with spectrum slope for cutoff energies greater than about 0.01 MeV.

As expected from an inspection of Fig. 2.12, neutron spectra relatively rich in neutrons between a few tenths MeV and a few MeV have a high effective modifying factor. It is thus evident that careful evaluation of the radiation fields is needed if accurate dosimetry is to be accomplished by using a tissue-equivalent chamber in neutron fields with maximum neutron energies less than 100 MeV or slopes close to $\gamma = 1$, or both.

In evaluating dose-equivalent rate from neutron spectra Gilbert et al. (GIL W 68) have described the use of analytical expressions for the conversion factors g(E), first suggested by Thomas (THO R 65), which are summarized in Table 2.XI.

Table 2.XI. Analytical expressions for neutron conversion factors as a function of energy.

Energy range (MeV)	g(E) $\frac{n/cm^2\ sec}{mrem/h}$
$< 10^{-2}$	232
$10^{-2} - 10^{0}$	$7.20\ E^{-3/4}$
$10^{0} - 10^{1}$	7.20
$> 10^{1}$	$12.8\ E^{-1/4}$

These expressions were selected when much of the information summarized in Table 2.II. was unavailable, and have proved extremely useful in routine dosimetry at Berkeley. Even today the analytical expressions are remarkably close to current best values of conversion factors (see Fig. 2.12), and their use for broad accelerator spectra is adequate for routine dosimetry.

Under certain conditions conversion factors derived from the maximum dose equivalent (g_{MADE}) may lead to serious overestimates, and in any event they always represent an upper limit. Such overestimates may be important when accumulated personnel doses approach maximum permissible and more precise evaluation may be required. An overestimate results because the equation for the dose-equivalent rate,

$$DER = \int_{E_{min}}^{E_{max}} \phi(E)\, dE/g_{MADE}(E), \tag{7b}$$

expresses the sum of the maxima of the dose-equivalent depth curves at each energy rather than the maximum of the sum of the dose equivalents from each component of the spectrum. This is perhaps best seen in the example given in Fig. 2.19, which shows the DE depth distribution in the body irradiated by two groups of protons of 100 and 200 MeV in energy.

The integral of Eq. 7 then reduces to a simple summation,

$$DER = \sum_{i=1}^{2} \phi_i(E) dE/g_{i_{MADE}}(E), \tag{21}$$

which in our case reduces to

$$DER = \frac{\phi_{100}}{0.44} + \frac{\phi_{200}}{0.44} \quad \text{mrem/h}, \tag{9}$$

where ϕ_{100} and ϕ_{200} are the flux densities of each proton group. If we take unit flux density for each group, then

$$\phi_{100} = \phi_{200} = 1 \text{ proton/cm}^2 \text{ sec} \tag{22}$$

and

$$DER = 2.3 + 2.3 \tag{23}$$

$$= 4.6 \text{ mrem/h}.$$

However, as can be seen from Fig. 2.19, the combined irradiation produces a dose-equivalent rate of

$$DER = \frac{7.3 \times 10^{-7}}{2.8 \times 10^{-7}} \tag{24}$$

$$= 2.6 \text{ mrem/h},$$

or some 80% lower than estimated by use of Eq. (21)

On occasion, therefore, it may be necessary to evaluate dose equivalent more precisely. Goebel et al. (GOE K 67) have suggested an alternative procedure, influenced, primarily by their measurement of absorbed dose, essentially at the body surface. If it is assumed that particle equilibrium is

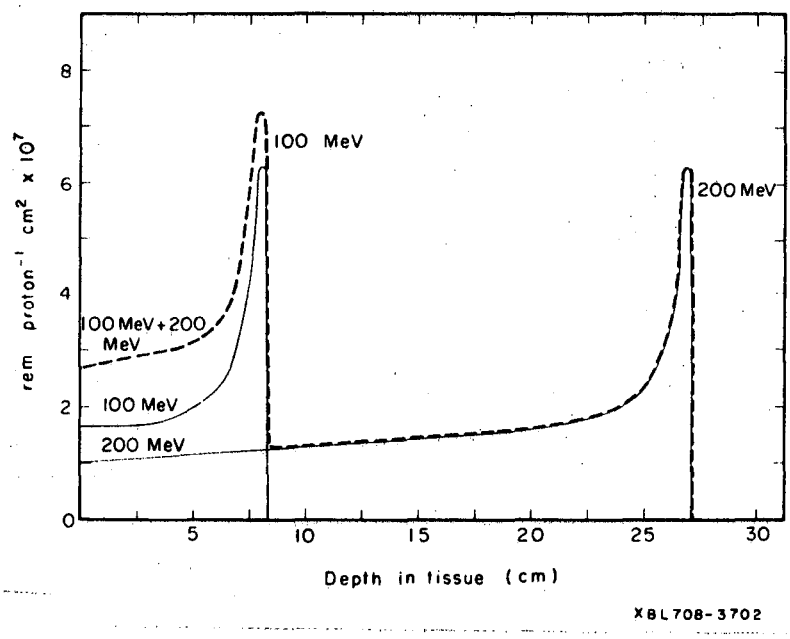

Fig. 2.19. Composite effect of irradiation by 100- and 200-MeV protons.

established in radiation shielding, then it is plausible that this equilibrium will be maintained in a body irradiated outside the shield: No dose buildup would then be detected. Dose-depth measurements in paraffin phantoms irradiated in several radiation environments at the Cosmotron do not entirely support this assumption. Phillips et al. (PHI L 63) reported a buildup in dose of 40% to 60% when the phantom was irradiated in high energy beams, but found dose attenuations of a factor of 3 in regions of highly degraded radiation. In certain special cases, however, no buildup is observed, and in these cases conversion factors evaluated at the body surface, $g_{surface}(E)$, might be more appropriate. It is clear that in general the true dose equivalent rate, DER, lies between the two limits

$$\int_{E_{min}}^{E_{max}} \frac{\phi(E)\,dE}{g_{surface}(E)} \leqslant DER \leqslant \int_{E_{min}}^{E_{max}} \frac{\phi(E)}{g_{MADE}(E)}\,dE \tag{25}$$

where $\phi(E)dE$ is the flux spectrum *incident* on the body.

In order to evaluate the dose equivalent resulting from irradiation by a broad spectrum it is necessary to construct the resultant dose-equivalent depth curve in the body and evaluate conversion and modifying factors at the actual maximum in the dose-equivalent distribution. Shaw et al. (SHA K 69) have reported such calculations for typical accelerator neutron spectra Shaw et al. (SHA K 68) first compiled then available depth-dose and depth-dose equivalent data. Curves were drawn through the data over the neutron energy range 0.025 eV to 2 GeV, and the "smoothed" data so obtained were tabulated for various depths in the body. By folding the measured neutron spectra with the depth-dose data it was possible to construct depth-dose curves in the body for irradiation by eight different neutron spectra. Four of these spectra are shown in Fig. 2.15; the others were two spectra measured at the Rutherford Laboratory 7-GeV proton synchrotron, one at that laboratory's 50-MeV proton linear accelerator, and, finally, a "1/E" spectrum for purposes of comparison. These spectra range from "very soft" to "very hard," and are typical of those that could be encountered outside thick shields of high-energy proton accelerators. Figures 2.20 and 2.21 show the depth dose and dose-equivalent curves calculated by Shaw et al., and their data are given in Table 2.XII.

For the 1/E spectrum a buildup of a factor of 4 is seen, but for high-energy accelerator spectra the buildup is less than 1.6 in all cases. For the soft cosmic ray spectrum the dose equivalent is reduced by a factor of 3.5 through the body, while the attenuation for the PLA spectrum is 5.4. By

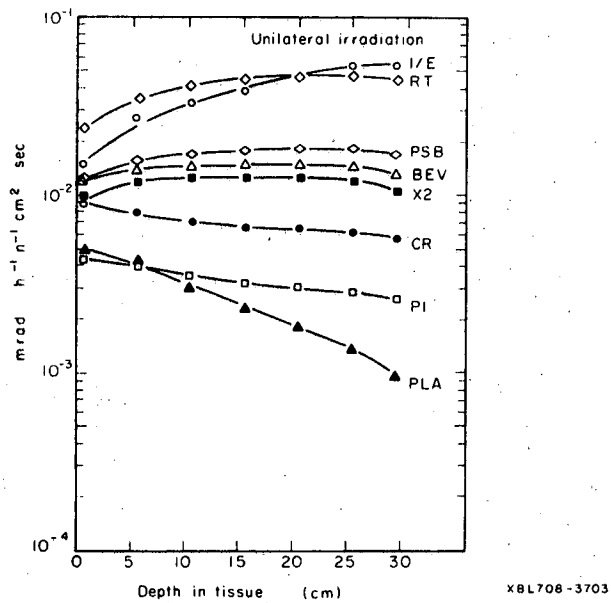

Fig. 2.20. Depth dose distribution for unilateral irradiation by typical accelerator neutron spectra. (After Shaw et al.)

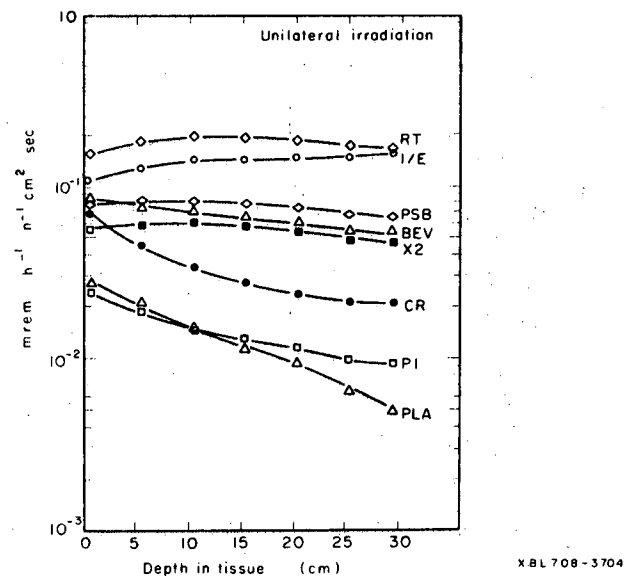

Fig. 2.21. Depth-dose equivalent distribution for unilateral irradiation by typical accelerator neutron spectra. (After Shaw et al.)

Table-2.XII. Depth-dose equivalent rate and depth-dose rate per unit flux density (from Shaw et al.)

Spectrum			Depth (cm.) 0.5	5.5	10.5	15.5	20.5	25.5	29.5
1/E		mrem/hr	0.107	0.126	0.141	0.141	0.148	0.149	0.157
		mrad/hr	0.0142	0.0280	0.0344	0.0400	0.0473	0.0535	0.0544
Ring Top at CERN, Geneva	(RT)	mrem/hr	0.163	0.185	0.195	0.188	0.184	0.167	0.167
		mrad/hr	0.0244	0.0356	0.0408	0.0445	0.0462	0.0474	0.0442
Synchrotron Bridge at CERN, Geneva	(PSB)	mrem/hr	0.0788	0.0818	0.0824	0.0777	0.0751	0.0671	0.0662
		mrad/hr	0.0125	0.0161	0.0173	0.0180	0.0185	0.0187	0.0171
Bevatron, LRL Berkeley	(BeV)	mrem/hr	0.0838	0.0763	0.0712	0.0647	0.0604	0.0528	0.0516
		mrad/hr	0.0124	0.0141	0.0145	0.0149	0.0147	0.0145	0.0131
X2 Nimrod from RHEL, Chilton	(X2)	mrem/hr	0.057	0.0594	0.0601	0.0568	0.0548	0.0475	0.0461
		mrad/hr	0.00989	0.0119	0.0125	0.0128	0.0126	0.0122	0.0106
Cosmic Ray.	(CR)	mrem/hr	0.071	0.046	0.0339	0.0275	0.0244	0.0211	0.0206
		mrad/hr	0.00909	0.00808	0.00712	0.00668	0.00644	0.00625	0.00568
P1 Nimrod from RHEL, Chilton	(P1)	mrem/hr	0.0241	0.0187	0.0150	0.0127	0.0114	0.00965	0.00923
		mrad/hr	0.00432	0.00411	0.00347	0.00319	0.00302	0.00286	0.00259
Proton Linear Accelerator from RHEL, Chilton	(PLA)	mrem/hr	0.027	0.0207	0.0151	0.0117	0.00989	0.00634	0.00504
		mrad/hr	0.00501	0.00424	0.0031	0.00234	0.00191	0.0014	0.000981

and large, however, the most significant point is the relative flatness of most of the DE-depth curves and, as pointed out by Shaw et al., this is even more pronounced for uniform body irradiation approximated by Shaw et al. by calculations of bilateral irradiation; see Fig. 2.22.

From such calculations it is possible to evaluate conversion and modifying factors appropriate to different particle spectra.

In considering modifying factors, Shaw et al. derive two values:

a. $MF_{surface}$' defined as the ratio of dose equivalent at the body surface to absorbed dose at the body surface,

b. $MF_{apparent}$' defined as the ratio of the maximum dose equivalent to the absorbed dose at the body surface.

(Attention is principally given to absorbed dose at the body surface, because this parameter is obtained by using a small bare tissue-equivalent ionization chamber.) Shaw et al. show that, for the spectra studied, that values of $MF_{surface}$ and $MF_{apparent}$ differ by as much as 70% for unilateral body irradiation.

Finally, it is conventional, as we have seen, to define modifying factor at the maximum dose equivalent:

c. MF_{MADE}, defined as the ratio of the maximum dose equivalent to the absorbed dose at the depth of the MADE.

It is this latter value of modifying factor which should be compared with the values of Patterson et al. (Table 2.X) to indicate the magnitude of the error in Patterson et al.'s procedure in neglecting the variation of depth of maximum dose equivalent with energy. Table 2.XIII compares different calculated values of modifying factor for various spectra. The discrepancy between $\langle MF \rangle_{MADE}$ and $\langle MF \rangle$ derived by Patterson et al. is seen to be 20% or less for the neutron spectra studied.

The differences possible in estimation of average conversion factors are summarized in Table 2.XIV. Columns 3 and 4 indicate the differences between unilateral and bilateral indication conditions derived from the work of Shaw et al. Columns 2 and 3 show the differences between using the values of conversion factors given in Table 2.XI in conjunction with Eq. 7 and using the method of Shaw et al. for unilateral irradiation. In all cases the routine system described by Gilbert et al. (GIL W 68) gives a comfortable, though not excessive, overestimate of dose equivalent. Thus in most practical situations a useful "cushion" in the control of personnel exposure is available. In special circumstances, however, such as moderate overexposure, special analysis, appropriate to the particular case under review, is required.

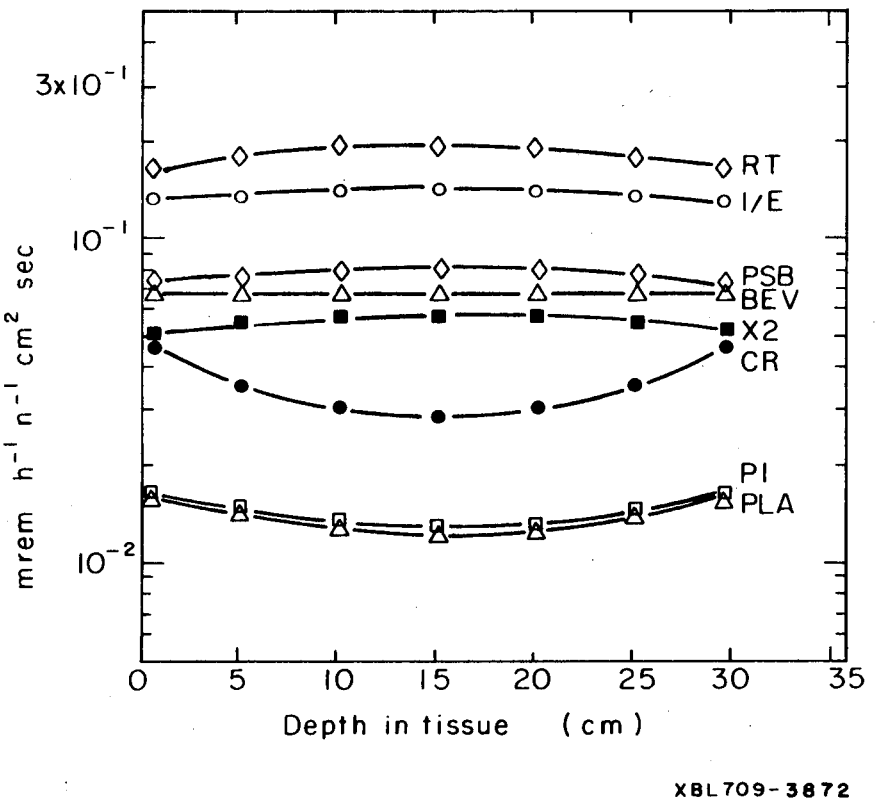

Fig. 2.22. Depth-dose equivalent distribution for bilateral irradiation by typical accelerator neutron spectra. (After Shaw et al.)

Table 2.XIII. Comparison of estimates of modifying factor.

Spectrum	$MF_{apparent}$[a]	$MF_{surface}$[a]	MF_{MADE}[b]	$\langle MF \rangle$[c]
1/E	10.0	7.5	2.9	2.9[d]
Cosmic ray	5.1	7.7	7.7	6.5
Bevatron	5.4	6.8	6.8	5.6
CERN Ring Top	7.8	6.7	4.8	5.4
CERN PSB	6.4	6.3	4.8	4.9

a. Shaw et al., 1969.
b. Shaw et al., 1969.
c. Patterson et al., 1970.
d. At E_{max} = 10 GeV.

Table 2.XIV. Effective conversion factors for neutron spectra.

Spectrum	Effective neutron conversion factors $\frac{n/cm^2\ sec}{nrem/h}$		
	Gilbert et al. (analytic)	Shaw et al. (unilateral irradiation)	Shaw et al. (bilateral irradiation)
Cosmic ray	12.1	14.1	21.8
Bevatron	8.8	11.9	14.9
CERN synchrotron bridge	7.3	12.1	12.5
CERN ringtop	4.3	5.1	5.3
1/E	4.7	6.4	7.0

REFERENCES

ALS R 67 R. G. Alsmiller and H. S. Moran, Dose Rate from High Energy Electrons and Photons, ORNL-TM-2026, October 20, 1967.

ALS R 70 R. G. Alsmiller, T. W. Armstrong, and W. A. Coleman, The Absorbed Dose and Dose Equivalent from Neutrons in the Energy Range 60 to 3000 MeV and Protons in the Energy Range 400 to 3000 MeV, ORNL-2924 Rev., July 15, 1970.

AND I 63 I. O. Andersson and J. Braun, A Neutron Rem Counter with Uniform Sensitivity from 0.025 eV to 10 MeV, in Neutron Dosimetry, Vol. 2, *Proc. Symposium on Neutron Detection, Harwell, December 14, 1962 (IAEA, Vienna, 1963).*

ATK J 66 J. H. Atkinson and B. H. Willis, High Energy Particle Data, Vol. 2, UCRL-2426 Rev. 1966.

ATT F 66 F. H. Attix and W. C. Roesch. Eds., *Radiation Dosimetry*, Vol. 2: (Second Edition), *Instrumentation* (Academic Press, New York, 1966).

ATT F 68 F. H. Attix and W. C. Roesch, Eds., *Radiation Dosimetry*, Vol. 1: (Second Edition), *Fundamentals* (Academic Press, New York, 1968).

ATT F 69 F. H. Attix and E. Tochilin, Eds., *Radiation Dosimetry*, Vol. 3: *Sources, Fields, Measurements, and Applications* (Second Edition) (Academic Press, New York, 1969).

AUX J 68 J. A. Auxier et al., Neutron Interactions and Penetrations in Tissue, Chapter 6 in ATT F 68.

BAR W 64 W. H. Barkas and M. J. Berger, Tables of Energy Losses and Ranges of Heavy Charged Particles, NASA-SP 3013.

BAU J 67 J. Baum, Non-Linear Amplifier for Use in a Mixed Radiation Rem Responding Meter, Health Physics *13*, 775.

BAU J 68 J. Baum et al., Dose-Equivalent Meter Design Based on Tissue-Equivalent Proportional Counters, Health Physics *15*, 195 (1968) (Abstract); paper read at the Annual Health Physics Meeting, Denver, Colorado, June 16-20, 1968.

BAU J 70a J. Baum, A. V. Kuehner, and R. L. Chase, Dose-Equivalent Meter Designs Based on Tissue-Equivalent Proportional Counters (BNL-13378, 1970), Health Physics--in press.

BAU J 70b J. Baum et al., Factors Affecting Pulse Size in Sealed Tissue-Equivalent Counters, in *Proceedings of the Second International Conference in Accelerator Dosimetry and Experience, Stanford Linear Accelerator Center, Nov. 5-7, 1969*, CONF-691101 (USAEC, Division of Technical Information), p. 648.

BEC H 70 H. L. Beck, A New Calculation of Dose Rates from High Energy Electrons and Photons Incident on 30-cm Water Slabs, Instr. Methods *78*, 333-334 (1970).

BOO S 68 S. J. Boot and J. A. Dennis, Phys. Med. Biol. *13*, 573 (1968).

BUD T 70 T. F. Budinger, R. J. Howerton, and E. F. Plechaty, Neutron Radiography and Dosimetry in Humans, in *Proceedings of the Second International Symposium on Accelerator Dosimetry and Experience, Stanford, November 5-7, 1969*, CONF-691101 (USAEC, Division of Technical Information), p. 843.

BUR T 68 T. E. Burlin, Cavity Chamber Theory, in *Radiation Dosimetry*, Vol. 1, F. H. Attix and W. C. Roesch, Eds. (Academic Press, New York, 1968) Chap 8.

COL F 69 F. J. Coleman, The ^{11}C Method Used as a High Energy Mixed Field Rem Detector, Daresbury Nuclear Physics Laboratory Internal Report, DNPL/TM 60, Nov. 1969.

COW F 64 F. P. Cowan, L. F. Phillips, and R. J. King, Some Dosimetry Problems of the Alternating-Gradient Synchrotron, Health Phys. *10*, 33 (1964).

COW F 65 F. P. Cowan, Ultrahigh-Energy Radiation and Uncommon Types of Particles, in *Radiation Dosimetry*, Vol. III, F. H. Attix and E. Tochilin, Eds. (Academic Press, New York, 1969).

DVO R 65 Robert F. Dvorak and Norman C. Dyer, A Neutron Monitor for Simultaneous Measurement of Fluence and Dose Equivalent, ANL-7085, 1965.

DVO R 69 R. F. Dvorak, Calculation of dE/dX and Energy Loss Distributions in Spherical Cavities for Monoenergetic Neutron Fields, Health Phys. *17*, 279 (1969).

EVA R 63 R. D. Evans, in *American Institute of Physics Handbook*, D. E. Gray et al., Eds., 2nd Edition (McGraw-Hill Book Co., 1963), Section 8, pp. 81-106.

EVA R 68 R. D. Evans, X- and γ-Ray Interactions, in *Radiation Dosimetry* Vol. 1, F. H. Attix and W. C. Roesch, Eds. (Academic Press, New York, 1968), Tables 22 and 35.

FIE E 70 E. M. Fielder and N. W. Holm, Dosimetry in Accelerator Research and Processing, in *Manual on Radiation Dosimetry*, N. W. Holm and R. J. Berry, Eds. (Marcel Dekker, New York, 1970), p. 261.

GIL W 68 W. S. Gilbert, H. W. Patterson, and A. R. Smith, Accelerator Neutron Spectra and Spectra-to-Dose Conversion, paper read at Fourteenth Annual Meeting American Nuclear Society, Toronto, Canada, June 1968. Summary, (UCRL-18076, Feb. 1968).
See also W. S. Gilbert et al., Flux to Dose Conversion in Chapt. 9 in 1966 CERN-LRL-RHEL Shielding Experiment at the CERN Proton Synchrotron, Lawrence Radiation Laboratory Report UCRL-17941, Sept. 1968.

GOE K 67 K. Goebel, A. Rindi, A. H. Sullivan, and J. Baarli, The Purpose, Interpretation, and Utilization of Area Monitoring Measurements Near the CERN Accelerators, in *Symposium on Radiation Dose Measurements, Stockholm 1967* (European Nuclear Agency, Paris, 1967), p. 435.

GOU N 68 N. G. Goussev, Relationship Between Dose Equivalent (Absorbed Dose) and Fluence (Flux Density), Section 1.3 in *Engineering Compendium on Radiation Shielding*, R. G. Jaeger, Ed. (Springer-Verlag, Berlin, 1968).

HAN D 62 D. E. Hankins, A Neutron Monitoring Instrument Having a Response Approximately Proportional to the Dose Rate from Thermal to 7 MeV, LA-2717, 1962.

HES W 59a W. N. Hess, The Cosmic Ray Neutron Energy Spectrum, Phys. Rev. ***116***, 445 (1959).

HES W 59b W. N. Hess, Neutrons from (α,n) Sources, Ann. Phys. (N.Y.) *6* [2], 115 (1959).

ICRP 63 Report of the RBE Committee to the International Commission on Radiological Protection and on Radiological Units and Measurements, Health Phys. *9*, 357 (1963),

ICRP 64 ICRP Publication 4, Protection Against Electromagnetic Radiation Above 3 MeV and Electrons, Neutrons, and Protons, (Pergamon Press, Oxford, 1964

ICRP 70 ICRP Publication 15 Protection Against Ionizing Radiation From External Sources (Pergamon Press, Oxford, 1970).

ICRU 38 Recommendations of the International Commission on Radiological Units, Chicago, 1937, Am. J. Roentgenol., Radium Therapy, and Nucl. Med. *39*, 295 (1938).

ICRU 57 Report of the ICRU, 1956, *National Bureau of Standards Handbook 62* (United States Department of Commerce, Washington, D. C., 1957).

ICRU 62 Radiation Quantities and Units, Report 10a of ICRU, *National Bureau of Standards Handbook 84* (United States Department of Commerce, Washington, D. C., 1962).

ICRU 68 Radiation Quantities and Units, ICRU Report 11, (ICRU, Washington, 1968).

ICRU 70 Linear Energy Transfer, ICRU Report 16, ICRU, Washington, June 15, 1970.).

IRV D 67 D. C. Irving et al., Tissue Current-to-Dose Conversion Factors for Neutrons with Energies from 0.5 to 60 MeV, ORNL-4032, 1967.

JOH H 56 H. E. Johns and J. S. Laughlin, Interactions of Radiation With Matter, Chapter 2 in *Radiation Dosimetry*, G. J. Hine and G. L. Brownell, Eds. (Academic Press, New York, 1956).

JON J 61 J. Jones, Brit, J. Radioal. Suppl. 10, 1961.

LEA D 46 D. E. Lea, *Actions of Radiations on Living Cells,* Second Edition (Cambridge University Press, New York, 1955).

LEA J 67 J. W. Leake, Portable Instruments for the Measurements of the Neutron Dose-Equivalent Rate in Steady-State and Pulsed Neutron Fields, in *Neutron Monitoring* (IAEA, Vienna, 1967), p. 313.

LEH R R. L. Lehman and Olga M. Fekula, Some Energy Spectra of Stray Neutrons from the Bevatron, Nucleonics *22,* 11 (1964).

MAD R 67 Richard Madey, Fractional Linear Energy Transfer, in *Proceedings of the First International Symposium on Biological Interpretation of Dose from Accelerator-Produced Radiation, Berkeley, California March 1967,* CONF 670305 (U.S. Atomic Energy Commission Division of Technical Information), p. 63.

NAC D 67 D. Nachtigall, Determination and Accuracy of Results of Rem Counter Measurements, in *Proceedings of the European Nuclear Energy Agency Symposium on Radiation Dose Measurements, Their Purpose, Interpretation and Required Accuracy in Radiological Protection, Stockholm, June 12-16, 1967.*

NASc 64 Studies in Penetration of Charged Particles in Matter, H. Fano (Editor) (Report No. 39 - Nuclear Science Series), Publication 1133 (National Academy of Sciences–National Research Council, Washington, D. C., 1964).

NBS 67 Protection Against Neutron Radiation Up to 30 MeV, in *NBS Handbook #63 (Rev.)* (U.S. Department of Commerce, Washington, D. C., April 1967).

NCRP 67 Dose Effect Modifying Factors in Radiation Protection, Report of Subcommittee M-4 of NCRP, BNL-50073, August 1967.

NEA G 58 G. T. Neary and J. H. Mulvey, Maximum Permissible Fluxes of High Energy Neutrons and Protons in the Range of 40-1000 MeV, Medical Research Council unpublished data, PIRC HP/1, 8, 17, Harwell; Revised by Neary, 1958.

NEU J 66 J. Neufeld et al., Health Phys. *12,* 227 (1966).

NEU J 69a J. Neufeld et al., Health Phys. *17,* 449 (1969).

NEU J 69b J. Neufeld, Comments on Quality Factor, Health Phys. *17,* 625 (1969).

NEU J 70 J. Neufeld, An Alternative Approach to the Formulation of Quality Factor. Paper presented at Second International Congress of IRPA, Brighton, England, May 1970.

OTT K 53 K. Ott, in *Kosmische Strahlung,* W. Heisenberg, Ed. (Springer-Verlag, Berlin, 1953).

PAR H 48 H. M. Parker, Health Physics, Instrumentation, and Radiation Protection, Advan. Biol. Med. Phys. *1*, 243.

PAT H 69 H. Wade Patterson, Harry H. Heckman, and Jorma T. Routti, New Measurements of Star Production in Nuclear Emulsions and Applications to High-Energy Neutron Spectroscopy, in *Proceedings of the second International Conference on Accelerator Dosimetry and Experience, Stanford, California, Nov. 5-7, 1969*, CONF 691101 (U.S. Atomic Energy Commission, Division Technical Information), p. 750.

PAT H 70 H. Wade Patterson, Jorma T. Routti, and Ralph H. Thomas, What Quality Factor? (UCRL-19382 Rev. April 1970), Health Phys.--in press.

PHI J 53 J. A. Phillips, Phys. Rev. *90*, 532 (1953).

PHI L 63 L. F. Phillips, Nucleonics *21*, 12 (1963).

PHI L 65 L. F. Phillips et al., Linear Energy Transfer Spectra and Effective Quality Factors in Stray Radiation Areas of the Brookhaven National Laboratory Proton Synchrotron, in *Proceedings of the USAEC First Symposium on Accelerator Radiation Dosimetry and Experience, Brookhaven National Laboratory*, 1965, CONF. 651109.

RAN M 57 Randolph, M. L., Energy Deposition in Tissue and Similar Material by 14.1-MeV Neutrons, Radiation Res. *7*, 47 (1957).

REY H 53 H. K. Reynolds, Phys. Rev. *92*, 742 (1953).

RIC M 54 M. Rich and R. Madey, Range-Energy Tables, UCRL-2301, Mar. 1954.

ROS H 55a H. H. Rossi and W. Rosenzweig, A Device for the Measurement of Dose as a Function of Specific Ionization, Radiology *64*, 404 (1955).

ROS H 55b H. H. Rossi and W. Rosenzweig, Measurement of Neutron Dose as a Function of Linear Energy Transfer, Radiation Res. *2*, 417 (1955).

ROS H 56 H. H. Rossi and G. Failla, Tissue-Equivalent Ionization Chambers, Nucleonics *14* [2], 32 (1956).

ROS H 62 H. H. Rossi, W. Rosenzweig, M. H. Biaviati, L. Goodman, and L. Phillips, Radiation Protection Surveys at Heavy Particle Accelerators Operating at Energies Beyond Several Hundred Million Electron Volts, Health Phys. *8*, 331 (1962).

ROS W 60 W. Rosenzweig, Calculation of Dose Distribution Measured with the Spherical Proportional Counter, Radiological Research Laboratory, Columbia University, internal report.

ROU J 69a Jorma T. Routti, High Energy Neutron Spectroscopy with Activation Detectors (Ph.D. Thesis), UCRL-18514, April 1969.

ROU J 69b Jorma T. Routti, Mathematical Considerations of Determining Neutron Spectra from Activation Measurements, in *Proceedings of the second International Conference on Accelerator Dosimetry and Experience, Stanford, California, Nov. 5-7, 1969,* CONF 691101 U.S. Atomic Energy Commission Division Technical Information, 1969), p. 494.

SHA K 68 K. B. Shaw, G. R. Stevenson, and R. H. Thomas, Depth Dose and Dose Equivalent Data as Functions of Neutron Energy, Rutherford Laboratory Internal Report, RHEL/M 149, September 1968.

SHA K 69 K. B. Shaw, G. R. Stevenson, and R. H. Thomas, Evaluation of Dose Equivalent from Neutron Energy Spectra, Health Phys. *17,* 459 (1969).

SID J 69 J. M. Sidwell and B. M. Wheatley, Calculations of the Absorbed Dose in a Phantom from Photon Fluence and Some Applications to Radiological Protection, Brit. J. Radiol. *42,* 522 (1969).

SNY W 52 W. S. Snyder, Nucleonics *6,* 46 (1952).

SNY W 57 W. S. Snyder, Protection Against Radiation Up to 30 MeV, in *National Bureau of Standards Handbook #63* (1957) pp. 39-66.

SNY W 68 W. S. Snyder, private communication; data submitted to NCRP.

STE L 55 L. Stewart, Phys. Rev. *98,* 740 (1955).

SUL A 63 A. H. Sullivan and J. Baarli, An Ionization Chamber for the Estimation of the Biological Effectiveness of Radiation, CERN Internal Report CERN 63-17, 1963.

SUL A 64 A. H. Sullivan, An Approach to a Rem Dosimeter Using Ionization Chambers, CERN Internal Report DI/HP/29, 1964.

SVE G 70 G. K. Svensson and W. R. Nelson, Measurement of Radial and Longitudinal Dose Distribution in a Water Phantom Irradiated with a 10-GeV Electron Beam, p. 185, in *Proceedings of the Second International Conference on Accelerator Dosimetry and Experience,* CONF 691101, (U.S. Atomic Energy Commission Division of Technical Information).

SYK J 58 J. B. Sykes, quoted by G. Neary and J. H. Mulvey, Ref. NEA G. 58.

TES K 66 K. Tesch, Nucleonik *8,* 264 (1966).

TES K 70 K. Tesch, Neutron Dosimetry in the Energy Range Between 10 and 100 MeV, Internal report, Deutsches Elecktronen Synchrotron, DESY 70/5, Feb. 1970.

THO R 65 R. H. Thomas, Radiation Field Observed Around High Energy Accelerators, in *Progress in Radiology, Proceedings of XI*

Congress of Radiology, Rome, 1965 (Excerpta Medica Foundation, Amsterdam, 1967).

THO R 69 R. H. Thomas, The Conversion of Particle Fluence to Dose Equivalent, Stanford University Health Physics Department Internal Report, SUHP 69-3, 1969.

TUR J 64 J. E. Turner et al., Health Phys. *10*, 783 (1964).

WAT B 52 B. E. Watt, Energy Spectrum of Neutrons from Thermal Fission of ^{235}U, Harvard University School of Public Health, AECD-3359, 1952).

WHA W 58 W. Whaling, *Handbuch der Physik 34*, (Springer-Verlag, Berlin, 1958), p. 193.

WHE B 70 B. M. Wheatley, A Unified Approach to Problems in Radiological Protection, U. K. Central Electricity Generating Board, Internal Report, RD/B/M1655, March 1970.

ZEL M 62 M. Zelchinskii, Use of Columnar Recombination for Determination of Relative Biological Efficiency of Radiation, Nucleonika 7 (3) 175 (1962).

ZEL M 64 M. Zelchinskii, Instrument for Determination of Recommended Relative Biological Effectiveness of Radiation, Instr. Exptl. Tech. (USSR) No. 6, p. 1217 (1964).

ZER C 65 C. D. Zerby and W. E. Kinney, Nucl. Instr. Methods *36*, 125 (1965).

ZIR R 52 R. E. Zirkle, D. F. Marchbank, and K. D. Kuck, Exponential and Sigmoid Curves Resulting from Alpha and X Irradiation of Aspergillus Spores, J. Cellular Comp. Physiol. *39*, Suppl. 1, 75 (1952).

CHAPTER 3.

PARTICLE ACCELERATORS AND THEIR RADIATION ENVIRONMENT.

TABLE OF CONTENTS

PARTICLE ACCELERATORS AND THEIR RADIATION ENVIRONMENTS

GENERAL INTRODUCTION

Two distinct and separate radiation fields are associated with particle accelerators, and both are of practical concern to health physicists. The first may be described as "prompt," and is directly associated with the operation of the accelerator. All components of this prompt radiation field disappear almost immediately upon accelerator turnoff. The second radiation field may be described as "remanent," since it remains after accelerator operation has ceased; it is due to radioactivity induced in the accelerator structure.

All accelerators, no matter of what energy, produce a prompt radiation field, but induced activity is produced only by particles above the energy threshold for nuclear reactions. Thus, in general, the "remanent field" is not produced by particle accelerators below a few MeV and is in a sense "less fundamental" than the prompt radiation field. It is due to the nuclear interaction of particles produced during existence of the prompt radiation field that induced activity may result. The control of radiation exposure to the "remanent" field is largely an operational health physics problem, generally of concern for a limited number of personnel working directly with the accelerator. These problems are discussed in a later chapter on the problems of induced activity. (Chapter 7)

This chapter deals with the characteristics of the prompt radiation field directly produced by particle accelerators as a result of beam interaction with targets or accelerator components. Such information is necessary for the design of accelerator shielding and for prediction of the radiation field outside the shielding in which radiation surveys will be made. (Subsequent chapters discuss both accelerator shielding and radiation measurements. Chapters 5 and 6)

The prompt radiation field is produced either by the atomic or nuclear interaction of particles during acceleration, or in the utilization of the accelerated particles. Inefficiencies in the acceleration process lead to particle losses during the acceleration cycle (THO R 68). If these particles have sufficient energy they may induce nuclear interactions in the accelerator structure, generating a short-lived radiation field the detailed composition of which is determined by the energy and type of the accelerated particles and the material in which they interact. Beam losses during the acceleration cycle may place severe limitations on beam intensity or may necessitate substantial radiation shielding. Careful studies of beam loss have been made for the most recently designed high energy accelerators (RAN J 69, AND R 69). Superconducting accelerators built in the future will also require low beam losses for maximum efficiency in refrigeration (THO R 69).

Although beam losses may be important, they represent only a small fraction (typically a few percent) of the useful accelerator beam power. In

use the accelerator beam interacts with an experimental target, irradiated specimen, or patient, and it is these interactions that are largely responsible for the general character of the radiation field.

Full understanding of the prompt radiation field generated requires knowledge of (a) the primary interaction in the target material and (b) the subsequent progression of the interaction products through the accelerator structure and surrounding experimental material and shielding. (Such details are discussed shortly.) From general principles it is possible, however, to arrive at many conclusions useful to the Health Physicist.

ACCELERATORS—THEIR GENERAL CHARACTERISTICS AND USES—A BRIEF SURVEY

INTRODUCTION

It is not our purpose here to give a detailed description of the design features, construction, and operation of all accelerators. That has been done with great competence in basic text books (LIV J 61, LIV M 62), review articles (McM E 59, BUR E 68a,b, WID R 68a,b), and technical literature. However, an understanding of the basic features of accelerators and their uses is vital for the health physicist concerned with their operation.

Perhaps the most dramatic feature of accelerator development since the thirties has been the increase in maximum energy achieved. Figure 3.1 shows this growth as a function of time for the principal accelerator families. At present the highest-energy accelerator in operation is the 70-GeV Proton Synchrotron at Serpukhov; 200-GeV operation of the accelerator at Batavia is expected for 1971. It is not uncommon, in the evolution of accelerators, for their energy to stagnate for several years until new technological advances permit further increase in energy. Such features are clearly seen for electron linacs and synchrotrons in Fig. 3.1. Development of the Tandem and Emperor Van de Graaff has increased the upper energy of this constant-voltage machine to about 20 MeV/nucleon at present (FES J 69). Equally dramatic has been the increase in available beam currents. Radiation processing units operate at dc currents of a few hundred mA, and it is not uncommon in certain accelerators to produce currents as high as 10^3 A over a short duration ($\approx$ 10 nanoseconds), e.g., in electron induction accelerators (KEE D 70) and flash x-ray tubes.

The most recent survey of the expanding number of particle accelerators (including low-voltage x-ray machines) and their various uses has been made by E. A. Burrill (BUR E 69). He found that in the last 25 years some 2000 accelerators have been constructed, that almost all are still in use, and that about 100 new accelerators are produced each year. Typical users and applications are in physics, chemistry, and radiobiology research, radiation therapy, radiation processing and sterilization, industrial radiography, and activation analysis. Burrill's survey did not include small sealed-source

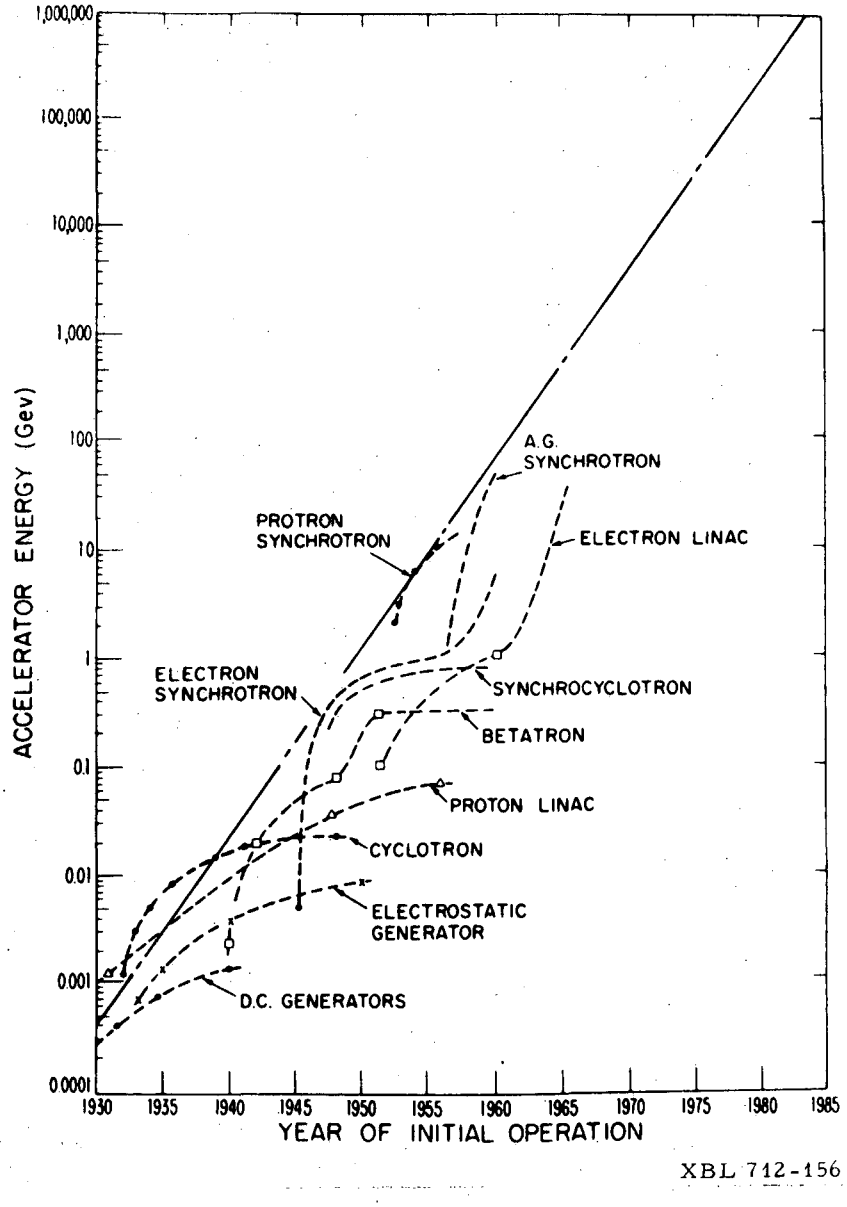

Fig. 3.1. Increase with time in maximum energy achieved by different types of accelerators.

neutron generators of which, he estimates, about 200 are in use today. An upper energy limit of 100 MeV was applied to the accelerators considered by Burrill, since at higher energies all the accelerators are devoted to fundamental research. A recent survey of accelerators operating at or above 1 GeV lists more than 40 accelerators (HOW F 67), 21 proton synchrotrons, 12 electron synchrotrons, 6 linear accelerators, and 2 isochronous cyclotrons. These are formidable numbers for accelerators at such high energies. Previous listings by Adams in 1959 (ADA J 59) and Barton in 1961 (BAR M 61) give details of lower-energy accelerators.

Thus the accelerator health physicist is faced with a bewildering range of accelerators, particles accelerated, energy, intensity, and duty cycles! It is fortunate that despite this array of parameters it is possible to discuss accelerators and their radiation environments in a unified and orderly way.

Particle accelerators are briefly described, and their radiation environments are discussed in general. Prompt radiation fields are discussed in terms of the production of radiation by the interaction of accelerated particles with matter.

Whenever electrons are accelerated in a vacuum there is the possibility of radiation exposure from x-ray production. Only a few months after the discovery of x rays (produced in a simple form of electron accelerator) was announced by Roentgen in 1895, the first radiation burns were reported in the literature (GRU E 33). More recently the radiation exposure of the population at large by the x-ray emission of domestic television receivers has been of concern. x-Ray generators are now widely used in medical centers, in industry, and for research (BUR E 68a). Although such x-ray units present considerable radiation hazards, the methods and techniques of dealing with them are well understood and widely known. The interested reader is referred to the standard texts by Braestrup and Wykcoff (BRA C 58) and Glasser et al. (GLA O 61) and to the relevant NCRP reports for current information (NCRP 68, NCRP 70)

A departure from the conventional x-ray hazards discussed in these documents occurs with the production of neutrons by photonuclear processes. Generally speaking, such reactions have thresholds at a few MeV (though they may occur at energies as low as 1.7 MeV in beryllium or 2.2 MeV in deuterium), therefore it is convenient to discuss radiation problems only for those electron accelerators, above a few MeV in energy, that are potential sources of neutrons. There is no such energy limitation for positive-ion accelerators, because neutrons may be produced by several exoenergetic reactions, e.g., $T(d,n)^4He$. Thus, positive-ion accelerators of very low energy may be intense sources of neutrons. Furthermore, the health physicist must be concerned not only with the primary source of radiation, accelerators in operation, but also with the secondary--usually unwanted--radiation sources that are inevitably encountered.

Although nuclear physicists and chemists may be interested in the accelerators only for their production of particular nuclear reactions under investigation, the physician for their particular diagnostic or therapeutic effects, or the engineer for their use in nondestructive testing, the health physicist cannot be so restrictive. He must address his attention to the broad span of accelerators and understand the radiation characteristics of them all.

It is helpful, in view of the differing uses of the terms low, medium, and high energy, to use the USAEC classifications:

low energy < 50 MeV,

medium energy > 50 MeV < 1 GeV,

high energy > 1 GeV.

We give here a brief description of the principal types of accelerator found in operational health physics, indicating their general radiation-producing characteristics.

VAN de GRAAFF GENERATOR AND SAMES ELECTROSTATIC SYSTEM

The Van de Graff (VAN R 31) electrostatic generator, developed by 1929, is still one of the most practical and widely used accelerators in the energy range 0.4 to 10 MeV (BUR E 68a). Electrical charge is sprayed onto a rapidly moving belt of insulating materials and continuously transported to an insulated high voltage terminal (BUR E 64). The flow of charge provides current for the acceleration tube, which is mounted between the high voltage terminal and ground. Since the polarity of this terminal may be of either sign, generators may be designed to accelerate electrons, negative ions, or positive ions. The earliest generators, situated in the open air, were limited to high voltages of ≈ 500 keV, but in present designs the generator and accelerator tube are insulated in pressurized nitrogen, freon, or carbon dioxide enclosed in a steel pressure vessel.

Typical single-stage Van de Graaff accelerators can produce currents of 1 mA of electrons or about 100μA of positive ions in the energy range 0.5 to 5 MeV. When used as neutron sources they can produce yields of about 5×10^{11} neutrons/sec (MAD R 68). The tandem principle, due to Bennet (BEN R 40), permits ion beams to accelerate to voltages equal to twice the potential of the high voltage terminal. A two-stage acceleration process is utilized in which negative ions are accelerated from ground potential to a positive electrode, where they are stripped of their negative charge by passage through a stripping target of thin foil or gas. The resultant positive ions are then repelled from the positive electrode, gaining additional energy from the voltage drop back to ground potential.

The SAMES electrostatic generator is in many respects similar to the Van de Graaff accelerator, operating in the range of up to several hundred

keV and--if in cascaded form--up to about 1.2 MeV. High voltage is generated by a continuous charge transfer from ground to the high voltage terminal by a segmented rotor inside a cylindrical stator. Concentric cylinders are used for charging, rather than insulating belts as in the Van de Graaff generator.

Van de Graaff electron accelerators have proved themselves of wide application in medical centers for both diagnostic and therapeutic uses, and in most of the areas of research and industrial application described by Burrill. As sources of x-rays in the range 1 to 2 MeV, typical commercially available units produce electron currents of 0.25 mA and exposure rates of 8 to 85 R/min at 1 meter (BUR E 68a). Higher currents are possible, and the units used to provide the high-voltage (2 to 3 MeV) x rays used in deep therapy typically produce currents of 1 mA. The great value of Van de Graaff accelerators in both medical and industrial radiology arises from their comparatively low cost, their extreme reliability, and the rather small size of the x-ray source ($\approx$ 1 to 2 mm diam) that may be obtained by focusing the electron beam on its target. Recent developments of the electron linear accelerator, however, now make it a strong contender in the area of radiotherapy (AUS A 69).

Pulsed ion beams may be generated, of duration from 0.1 to 1000 μsec and with duty cycles up to 5%. Extremely short pulses of only a few nanoseconds' duration may be obtained if the beam produced by the ion source is swept across a small aperture before acceleration (MAD R 68). Pulsed operation of Van de Graaff accelerators has been of great value in certain applications--for example, neutron time-of-flight studies, or pulsed radiolysis studies.

COCKCROFT-WALTON ACCELERATOR AND THE DYNAMITRON

The Cockcroft-Walton electrostatic generator is of historical importance because it was used to produce the first nuclear disintegration by particles accelerated in the laboratory (COC J 32). The now well-known principle of their cascade rectifier is described in the original paper by Cockcroft and Walton and in many textbooks on particle accelerators (LIV J 61, LIV M 62). Cockcroft-Walton accelerators are still widely used, having an upper voltage limit of 1 MV in air or about 2 MV when contained in pressurized gas insulation. Low voltage accelerators in the range 100 to 400 KV have increasing application as relatively inexpensive high-yield neutron sources. If deuterons are accelerated the exoenergetic (d,d) and (d,t) reactions may be used to produce 2.3-MeV or 14-MeV neutrons respectively. Thick-target yields up to 2×10^{11} n/sec may be obtained with tritium targets, but the (d,d) reaction yield is two orders of magnitude lower (DEP J 69).

A modern version of the Cockcroft-Walton accelerator, the Dynamitron, is often used to accelerate electrons in the energy range 500 keV to 4 MeV,

and has found application in the fields of radiation research and radiation processing. "...the Dynamitron utilizes a cascaded rectifier system in which all rectifiers are driven in parallel from a high-frequency oscillator, at 100 kc/sec. Four large rf electrodes surround the rectifier stack and draw power from the oscillator. The resulting rf potential is capacitively coupled to each rectifier tube, through the equipotential ring at each stage of rectification. Since the same rf potential is simultaneously applied to each rectifier, direct current flows through the cascaded rectifiers to establish a constant high voltage on the terminal. A multiple-section acceleration tube is mounted axially in this array, with each electrode connected to a corresponding rectifier. The entire assembly is insulated by pressurized gas and is contained in a steel pressure vessel" (BUR E 68b, CLE M 65). Currents of 10 mA are typically available up to energies of 4 MeV. The Dynamitron principle may be extended to higher voltages.

CYCLOTRON AND SYNCHROCYCLOTRON

Both the Cockcroft-Walton generator and the Van de Graaff accelerator fall in the general category of "potential-drop accelerators," depending as they do upon the production of a large electrostatic potential. Stimulated by the suggestion of resonance acceleration by Wideröe in 1928 (WID R 28) and his work on linear accelerators with Sloan (SLO D 31), Lawrence suggested the principle of the cyclotron. Particles could be accelerated while moving in a spiral path under the constraint of a magnetic field by having them cross an accelerating gap whose field was synchronized with the motion of the accelerated ions. After this principle had been successfully demonstrated in 1932 (LAW E 30, LAW E 31), progress was extremely rapid. By 1937 the 37-inch cyclotron at Berkeley was able to produce 100 μA of 8-MeV deuterons or 3.4 μA of 16-MeV helium ions (McM E 59). There are now many cyclotrons throughout the world that can produce energies typically in the neighborhood of 10 MeV per nucleon at average beam currents between 100 and 1000 μA (GOR H 63).

The upper limit on particle energy due to relativistic mass increase led to development of the synchrocyclotron. Here the accelerating frequency is modulated to compensate for the relativistic increase of the particles being accelerated. Many frequency-modulated cyclotrons have been constructed around the world for the acceleration of protons, deuterons, and α particles. Typical circulating currents are about 1 μA, but extracted beam intensities vary between 10^8 and 10^{11} particles/sec.

"The larger proton synchrocyclotrons in the United States include installations at Harvard University (160 MeV), the University of Rochester (240 MeV), Columbia University (385 MeV), Carnegie Institute of Technology (440) MeV), the University of Chicage (450 MeV), the Langley Research

Center of the National Aeronautics and Space Administration (600 MeV), and ...Lawrence Radiation Laboratory (730 MeV). The California machine also accelerates deuterons to 460 MeV, α particles to 910 MeV, and ^{3}He nuclei to 1140 MeV. The larger proton synchrocyclotrons outside of the United States include installations in Canada at McGill University (100 MeV); in France at Orsay (155 MeV); in England at Harwell (175 MeV) and Liverpool (381 MeV); in Sweden at Uppsala (185 MeV); in Switzerland at Geneva (600 MeV); and in the USSR at Dubna (680 MeV). The Dubna machine also accelerates deuterons to 420 MeV and α particles to 840 MeV" (MAD R 68).

BETATRON

Although the cyclotron was the first cyclic particle accelerator to operate, attempts to accelerate electrons in a circular orbit were also made in the late 20's and early 30's. Slepian (SLE J 27) filed a U.S. patent as early as 1922 on what he called an "induction accelerator"--now generally called a betatron. Although in the period 1928-1929 its principles were thoroughly explored (BRE G 28, WID 28, WAL E 29), it was not until 1941 that Kerst constructed and successfully operated the first betatron(KER D 41).

In simple terms the operation of the Betatron is analogous to that of a transformer in which the secondary windings are replaced by electrons moving in a circular orbit under the influence of a magnetic guide field. Acceleration is obtained from the inductive force supplied by the changing flux linking the electron orbits--obtained through use of coils at a suitable resonant frequency--usually a low multiple of 60 Hz. Wideröe has written an excellent summary of the principles of betatron operation (WID R 68a).

Since the first successful operation of the betatron at 20 MeV many accelerators of this type have been constructed, and improvements in design have increased their maximum energy to about 300 MeV (GOW F 50, WID R 68a). The betatron has proved itself to be a convenient source of x rays and electrons in the energy range of 50 to 100 MeV, and it has found wide application in radiation therapy, nondestructive testing, and research. Typical x-ray outputs from betatrons in the energy region 20 to 30 MeV are 10^3 R/h at 1 meter and at 300 MeV as high as 10^5 R/h at 1 meter.

SYNCHROTRON

Unlike the betatron, synchrotrons may accelerate either electrons or protons (or even heavier ions). First proposed by Oliphant in 1943 (LIV M 49), they were made feasible by the discovery of the principle of phase stability by McMillan (McM E 45) and Veksler (VEK V 45) in 1945. Goward and Barnes (GOW F 46) were the first to demonstrate the operation of a low-energy electron synchrotron a year later, and by 1949 McMillan had successfully accelerated electrons to more than 300 MeV.

The synchrotron in some senses derives from both the cyclotron and the betatron--it has the ac magnet of the latter but uses an rf power source for acceleration. Because the particles are no longer accelerated by an alternating central magnetic flux, the central iron case of the betatron magnet is no longer required, making it economically and technically feasible to accelerate electrons beyond the limit of ≈ 350 MeV set for betatrons by radiation losses. Several strong-focusing electron synchrotrons in the 1-to 10-GeV energy region are in operation with circulating currents of $\approx 5\ \mu$A.

Several constant-gradient synchrotrons have been designed to accelerate protons in the energy range 1 to 10 GeV. Typical circulating intensities are in the range of 10^{12} protons/sec, with repetition rates between 20 pps at Princeton and 0.2 pps at the Bevatron. The successful development of beam-extraction systems permits external proton beams with intensities as high as 5×10^{11} protons/sec over durations between $\approx 200\ \mu$sec and several msec.

For proton energies greater than about 10 GeV strong-focusing synchrotrons are more economic propositions. Typical proton beam intensities are similar to those obtained with weak-focusing accelerators, but the highest energy achieved is 70 GeV, by the accelerator in operation at Serpukhov.

LINEAR ACCELERATOR

Following the suggestion of the principle of resonance acceleration of ions by Wideröe in 1928 (WID R 28), Sloan and Lawrence (SLO D 31) were able to successfully apply it to heavy ions in the laboratory. Serious application, however, had to await the development of intense sources of rf power of short wave-length during World War II.

Toward the end of 1946 two groups--one at Malvern (FRY D 49) and the other at Stanford (GIN E 48)--succeeded in accelerating electrons by the use of traveling waves in disk-loaded guides. The use by the British group of magnetrons as a source of rf power limited the upper energy obtained to a few MeV, but instantaneous currents of ≈ 200 mA were obtained. Accelerators based on these early designs have been widely applied to medical and radiographic uses.

Because work at Stanford was intended to produce higher energies (about several hundred MeV), great attention has been devoted to the development of designs with high shunt impedance and the production of a high-power Klystron amplifier. The Mark III electron linear accelerator has been in operation for many years at the Stanford High Energy Physics Laboratories, and can produce electrons at energies up to 1 GeV at mean currents of up to $10\ \mu$A. Radiation problems with such an accelerator have been quite severe and led to constructing the 20-GeV electron linear at the Stanford Linear Accelerator Center underground.

The first linear accelerator for protons was designed and constructed by Alvarez (ALV L 46), and achieved an energy of 32 MeV. Since then several proton linear accelerators have been successfully constructed and operated--often as injectors to higher-energy accelerators. Thus, typically the Bevatron has a 20-MeV 25-mA (mean) injector, but an energy of 200 MeV is to be used for injection into the 200-MeV proton synchrotron at Batavia. A linear accelerator designed to achieve energies of 800 MeV with beam currents of 1 mA is currently under construction at Los Alamos.

Linear accelerators have also been used to accelerate heavy ions to energies of 10 MeV per nucleon at peak currents of about 50 μA (HUB E 60a).

TIME STRUCTURE OF ACCELERATOR BEAMS

A time structure or bunching of the beam particles as they come out of the accelerator is produced by the particular features of the acceleration process. Those relatively low-energy accelerators, such as Van de Graaffs and Cockcroft-Waltons, which actually produce a constant high voltage equal to the maximum voltage of the accelerated particles have a direct-current beam with only very small purely statistical fluctuations in beam intensity. All the synchronous accelerators such as linear accelerators, cyclotrons, and synchrotrons produce a beam that is variable in time. There is usually a structure of several megacycles per second imposed by the accelerating radio-frequency voltage. Typically, beam pulses might emerge during about 10% of each radio-frequency cycle; this fraction is controlled by phase-stability considerations discussed in some detail in texts on high energy particle accelerators, for example Livingood (LIV J 61) or Livingston and Blewitt (LIV M 62).

There is also a much lower frequency structure imposed on the beam by the overall machine repetition rate. In many cases this is determined by the frequency of the basic power supplies, although it can be a simple harmonic. Thus many accelerators have a basic repetition rate of 50 to 60 cps. The fraction of the time during which beam is produced by the accelerator is called its "duty factor." This term ordinarily does not take into account the additional subdivision of the beam intensity by the radio-frequency accelerating cycle, but takes account only of the repetition rate. Thus, for example, if a radiation detector is influenced by beam fluctuation that occurs in times greater than a millisecond or longer, the "duty factor" satisfactorily describes beam variations. If, however, the detector can detect beam fluctuations in times less than about 0.1 μsec, then the additional fluctuations imposed by the rf voltage have to be taken into account. Radiation-detection difficulties usually arise when the detectors used have a long dead time or when two detectors with long resolving times are used in coincidence.

The bunching of the beam in time, with the attendant high instantaneous count rates during the times when the beam is really on, gives rise to accidental coincidences in the case of coincidence measurements and to lost counts in the case of detectors with significant dead times. The importance of these effects, discussed in Chapter 5, can be easily calculated if the counting rates in single detectors and their dead times are known. Evans (EVA R 55), Price (PRI W 58), and Szelles and Ruby (SZE A 68) have treated these effects in detail.

Few studies of the time structure of accelerator radiation fields have been reported. Studies of the thermalization of fission neutrons induced by using short-duration accelerator beam pulses is a widely known technique (VON G 58). At higher energies Farley et al. (FAR F 64) have studied the time structure of the radiation following passage of a short burst of 24-GeV protons along an external proton beam of the CPS, and Distenfeld (DIS C 64) has measured the time distribution of thermal neutrons during acceleration at the Brookhaven 30-GeV AGS. Essentially, with the exception of thermal neutrons, the radiation pulse generated by the interaction of a primary particle of subsequent reaction products is completed within a few nanoseconds. Thermalization of fast and evaporation neutrons may take from a few tens of microseconds to about a millisecond, depending upon the actual geometrical configuration. Thus the time structure of the radiation field (with the possible exception of thermal neutrons) is essentially controlled by the gross time structure of accelerator operation.

Generally speaking, the more uniform the beam is in time the more useful it is to experimenters, since the uniformity tends to reduce the effect of counter dead time and accidental coincidence. Considerable attempts have been made in the past few years to "debunch" and "stretch" the accelerated particle bunches as they are produced. Thus, for example, in accelerators such as the proton synchrotron that naturally have a low duty cycle, the time distribution of beam is lengthened by letting it interact slowly with an internal target (HER H 65) or by beam-extraction techniques based on the excitation of nonlinear resonances in the accelerated particles' motion (BOV C 64).

At energies sufficiently high that synchronous acceleration must be used, constant-frequency cyclotrons—either of conventional design or the sector-focused type--have the most advantageous beam time structure.

Although it is technically feasible for a linear accelerator to have a constant radio frequency, the power consumption and cooling problems which arise usually dictate that linear accelerators be normally pulsed and an attendant duty factor be imposed on the beam. The development of successful superconducting linear accelerators, too, will provide accelerated beam with a good duty cycle (SLAC 69 , BAN A 61).

The implications of accelerator duty cycle for the health physicist are discussed in some detail in the sections dealing with techniques of measurement. (Chapter 5)

GENERAL CHARACTERISTICS OF ACCELERATOR RADIATION ENVIRONMENTS

It is fortunate that, despite the large variety of particle accelerators and beam characteristics and the many varied tasks to which they are put, there is a great similarity in their radiation environments. In fact it is true that--if we put aside the particular problem of beam dosimetry--the prompt radiation field is dominated by neutrons and electromagnetic radiation. This generalization is particularly apt in discussion of radiation fields produced outside well-shielded accelerators. It is furthermore generally true that, under these conditions, neutrons dominate the external radiation fields of proton accelerators, whereas electromagnetic radiation dominates the fields of electron accelerators.

It is not difficult to understand the basic reasons. The threshold for photodisintegration processes is 1.7 MeV, but for most materials the yields are very low below photon energies of about 10 MeV. Thus the production of neutrons (and subsequent production of radioactivity) does not constitute a problem with electron accelerators up to a few MeV. At electron energies of $\approx$ 300 MeV, photopion production results in the production of high energy neutrons, but it is observed that even at high energies photons dominate the radiation field. Thus, for example, neutrons present a minimal problem at the 7-GeV electron synchrotron at DESY (TES K 69) or at the 20-GeV Stanford Linear Accelerator (BUS D 69). However, at the Stanford Mark III 1-GeV electron accelerator, which is somewhat undershielded, neutrons represent the major component of the radiation field (CAR T 69a, CAR T 69b, CHA V 69). De Staebler (DES H 65) has shown that shielding problems of high-energy high-intensity electron accelerators are very similar to those for high energy proton accelerators. In the use of electron accelerators of high energy and intensity, the high energy neutron production transverse to the beam direction can be sufficiently large to determine the radiation field penetrating a thick shield. In the forward beam direction measurements of induced activity show photoproduction reactions to be dominant at DESY (7 GeV) (TES K 69) and NINA (4 GeV) (COL F 69). However, at very high energies μ mesons produced in π-meson decay may present a serious problem downstream from primary beam targets (DES H 65, NEL W 66a,b, NEL W 68).

With few exceptions neutrons present the dominant problem at proton accelerators up to 10-20 GeV. Below the neutron-production threshold ($\approx$ 8 MeV), x rays produced by electrons accelerated across the potential gradient can be a problem at electrostatic accelerators. As higher energies, however, experience at numerous accelerators confirms neutrons as the significant component. Thus measurements on proton accelerators as diverse as a 50-MeV linear accelerator (THO R 62), 184-inch synchrocyclotron (PAT H 62), 6-GeV and 7-GeV weak-focusing synchrotrons (SMI A 65, PER D 66), and a 25-GeV strong-focusing synchrotron (BAA J 65, GIL W 68)

confirm this finding. At very high energies μ mesons can become a serious problem, at proton accelerators as at electron accelerators. Thus, when the 33-GeV AGS of the Brookhaven National Laboratory first became operational μ mesons presented a problem downstream from experimental targets, but were removed by adequate shielding (COW F 62).

Keefe (KEE D 64, LRL 65) has shown that at higher energies (above 100 GeV) the μ-meson problem takes on dramatic proportions. Extensive studies of this problem are currently under way at the National Accelerator Laboratory in expectation of operation at proton energies up to 500 GeV (THE D 70 a ,b,c).

It is of interest to note that in regions close to the proton beam high photon fluxes have been observed at both the 7-GeV proton synchrotron Nimrod and the 25-GeV CERN Proton Synchrotron (SHA K 67, GIL W 68). The source of this photon field has not been definitely identified, but is probably prompt γ-rays emitted in nuclear reactions and electromagnetic cascades generated by energetic photons produced by π^0 decay. Whatever the cause, however, photons are a dominant component of the radiation field adjacent to a high energy proton beam. Thus at the 7-GeV synchrotron Nimrod, radiation damage phenomena are prinicpally due to photon irradiation (MOR A 66).

Heavy-ion accelerator radiation fields are, from a health physics point of view, similar to those of proton accelerators.

PROMPT RADIATION FIELDS

Bremsstrahlung Production by Electron Accelerators

The production of electromagnetic radiation in a continuous x-ray spectrum, or bremsstrahlung, characterizes electron accelerators. Bremsstrahlung results from inelastic collisons of electrons with nuclei. The deceleration and energy loss consequent upon the encounter of an electron with a nucleus results in radiative emission. (EVA R 55). Space precludes a complete discussion here of the intensity and angular distribution of bremsstrahlung; the interested reader is referred to the definitive articles by Bethe and Ashkin (BET H 52) and Heitler (HEI W 36). However, a general description here will be useful, and complete enough for most health physics work.

The shape of the bremsstrahlung spectrum is discussed in NBS Handbooks 55 and 97 (NBS 54, NBS 64). Few experimental data are available, and one must therefore depend upon theoretical calculations--which, however, are considered reliable. Table 3.1 gives the relative spectrum expressed in terms of the number of photons emitted in each energy increment (either 2 or 5 MeV) per incident high energy electron.

Table 3.1. Relative numbers of photons of various energies in terms of electron energy.

X-Ray photon energy (k) in MeV	Electron energy, E_o, in MeV									
	5.51	6.51	8.51	10.51	12.51	14.51	15.51	16.51	18.51	20.51
2	45.3	69.3	130	208	304	418	481	550	700	800
4	10.6	21.7	50.1	86.2	130	183	213	245	316	396
6	.....	1.36	22.8	46.6	74.7	103	126	147	191	241
8	.....	.....	1.73	25.2	47.1	71.4	84.8	99.1	131	167
10	.....	.....	.....	2.10	28.0	49.1	60.1	71.4	95.9	123
12	.....	.....	.....	.....	2.47	31.0	41.6	52.0	73.0	95.5
14	.....	.....	.....	.....	.....	2.84	21.7	34.1	55.3	75.5
16	.....	.....	.....	.....	.....	.....	.....	3.22	37.3	53.8
18	.....	.....	.....	.....	.....	.....	.....	.....	3.59	40.6
20	.....	.....	.....	.....	.....	.....	.....	.....	.....	3.97
	22.51	24.51	25.51	26.51	28.51	30.51	35.51	40.51	45.51	50.51
2	1056	1261	1370	1484	1725	1934	2712	3554	4510	5579
4	485	583	635	690	806	931	1284	1693	2160	2683
6	298	360	393	428	503	583	811	1077	1380	1721
8	207	251	275	300	354	412	577	771	993	1243
10	154	188	206	226	267	312	439	590	763	958
12	120	147	162	177	210	246	349	471	611	770
14	96.6	119	132	144	171	201	286	387	504	633
16	78.6	98.7	109	120	143	168	240	326	426	540
18	62.6	82.1	91.7	101	122	144	205	279	366	464
20	43.9	66.5	76.3	85.9	105	124	179	243	319	405
22	4.34	47.3	59.6	70.4	89.8	108	157	214	231	358
24	.....	4.72	34.0	50.6	74.4	93.9	140	191	251	319
26	.....	.....	.....	5.10	54.0	78.5	125	172	226	288
28	.....	.....	.....	.....	5.47	57.3	111	156	203	261
30	.....	.....	.....	.....	.....	5.85	97.2	142	187	238
32	.....	.....	.....	.....	.....	.....	78.9	129	172	219
34	.....	.....	.....	.....	.....	.....	46.5	116	159	203
36	.....	.....	.....	.....	.....	.....	.....	99.5	146	189
38	.....	.....	.....	.....	.....	.....	.....	74.3	134	176
40	.....	.....	.....	.....	.....	.....	.....	7.83	119	164
42	.....	.....	.....	.....	.....	.....	.....	.....	93.5	152
44	.....	.....	.....	.....	.....	.....	.....	.....	59.0	138
46	.....	.....	.....	.....	.....	.....	.....	.....	.....	121
48	.....	.....	.....	.....	.....	.....	.....	.....	.....	91.4
50	.....	.....	.....	.....	.....	.....	.....	.....	.....	9.61
	60.51	70.51	80.51	90.51	100.51					
5	1070	4217	5546	7056	8749					
10	1418	1969	2610	3343	4167					
15	877	1229	1641	2115	2648					
20	613	868	1163	1507	1896					
25	460	653	882	1148	1450					
30	362	516	700	914	1158					
35	296	422	573	750	953					
40	250	355	481	631	802					
45	215	305	413	541	689					
50	187	267	361	472	600					
55	153	238	320	417	530					
60	11.5	212	288	374	474					
65	.....	176	262	340	429					
70	.....	13.4	236	311	392					
75	.....	.....	199	286	361					
80	.....	.....	15.3	262	335					
85	.....	.....	.....	222	312					
90	.....	.....	.....	17.1	287					
95	.....	.....	.....	.....	245					
100	.....	.....	.....	.....	19.0					

The relative bremsstrahlung intensity is a parameter frequently used in health physics; it is defined as the product of the relative spectrum and photon energy. Figure 3.2 shows both the photon spectrum and intensity spectrum for bremsstrahlung produced in a thin target bombarded by 16-MeV electrons.

When electrons lose energy raidatively in matter their energy E, at a depth x in the material, is given by

$$E = E_0 \exp(-x/L), \quad (1)$$

where E_0 = initial electron energy and L defines a quantity known as the radiation length.

Equation (1) is obtained by integrating the energy loss term (dE/dx), where

$$\left(\frac{dE}{dx}\right)_{\text{radiation loss}} = CE, \quad (2)$$

where C is a constant for a given target material and it follows that L is the target thickness (usually expressed in g/cm^2) in which, because of bremsstrahlung production, electrons reduce their initial energy by a factor e.

Values of radiation length for different materials are given in Table 3.II and shown in Fig. 3.3 plotted as a function of atomic number.

Table 3.II. Radiation lengths of common elements.

Element	Radiation length (g/cm^2)
Hydrogen	138
Carbon	52
Nitrogen	45
Oxygen	39.7
Aluminum	26.3
Iron	14.4
Copper	13.3
Lead	5.9

Target thickness has an important effect on both bremsstrahlung spectrum and intensity. The data given in Table 3.1 and Fig. 3.2 refer only to thin targets of high atomic number, and in any case are not absolute. Often, in practical cases, the target thickness is not optimum. Rarely will it be too thin for maximum intensity, but often it may be so thick that the spectrum is somewhat degraded in energy as well as lower in intensity. Figure 3.4 shows the typical variation with target thickness of the intensity of bremsstrahlung emitted in the forward direction. The data shown were obtained from 17-MeV electrons on gold (MAC M 57a, LAN L 51), but should apply to all targets of high atomic number and to electron energies above 5 MeV.

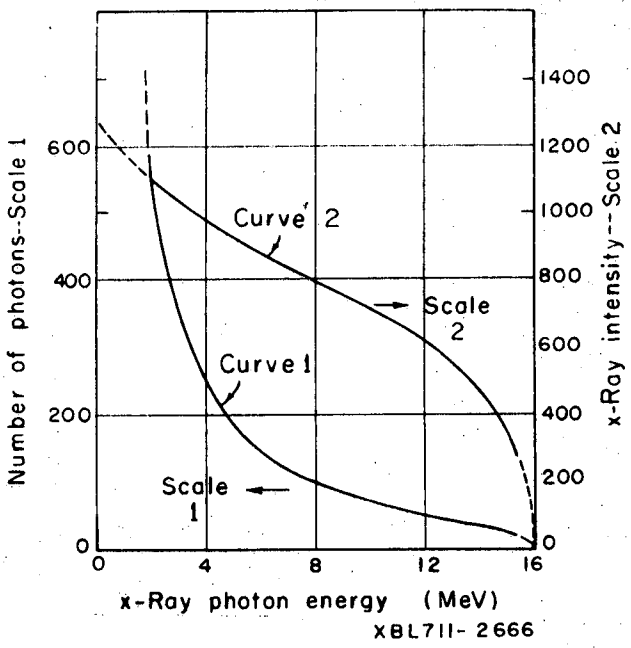

Fig. 3.2. X-Ray photon and intensity spectrum from a thin target bombarded by 16-MeV electrons.

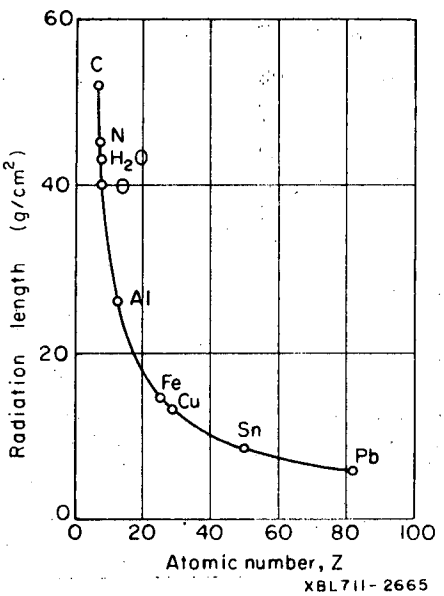

Fig. 3.3. Radiation length as a function of atomic number.

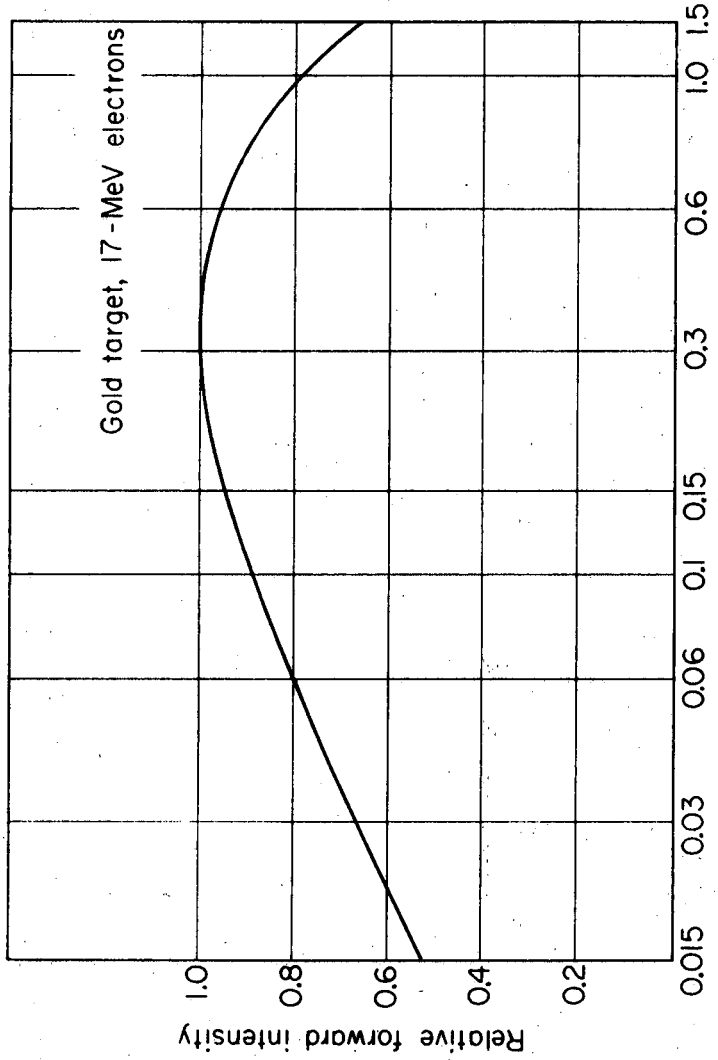

Fig. 3.4. Forward x-ray intensity as a function of target thickness. (After MacGregor, MAC M 57a.)

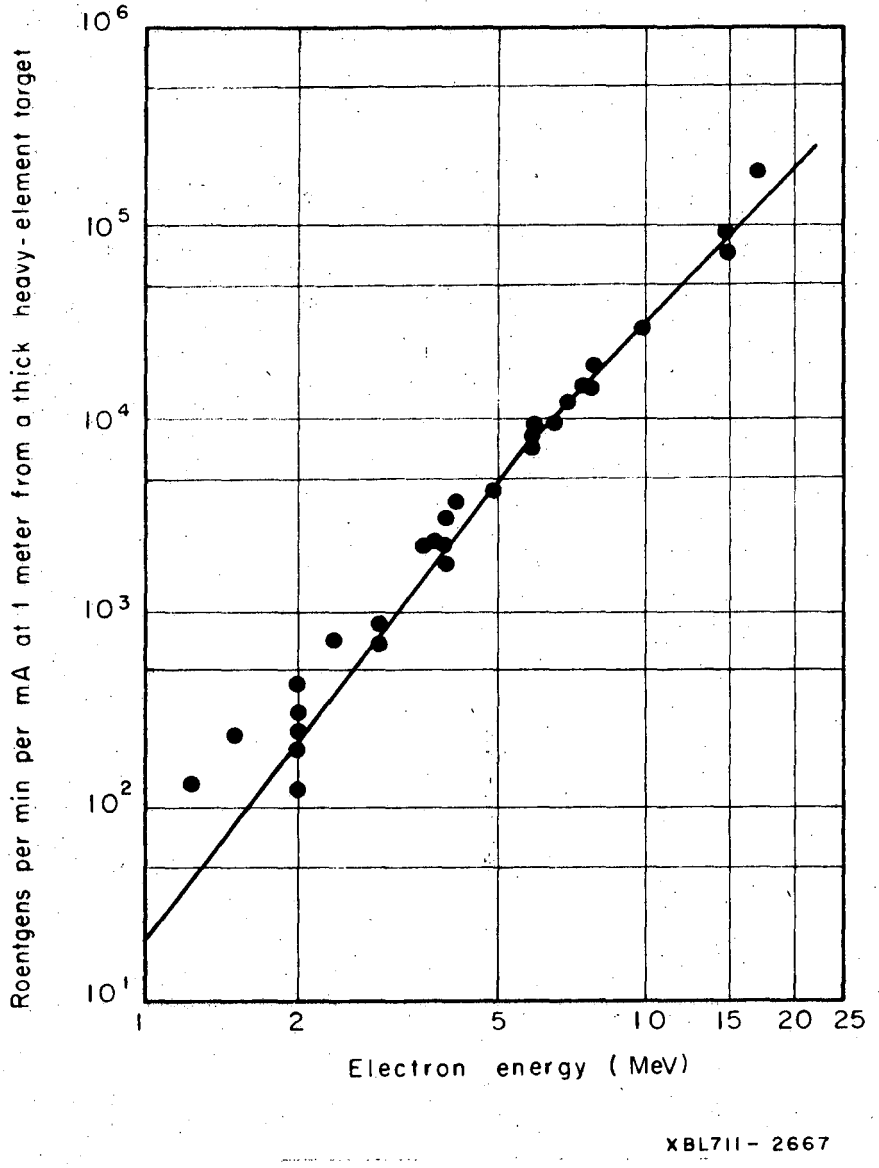

Fig. 3.5. Forward x-ray intensity from an optimum target.

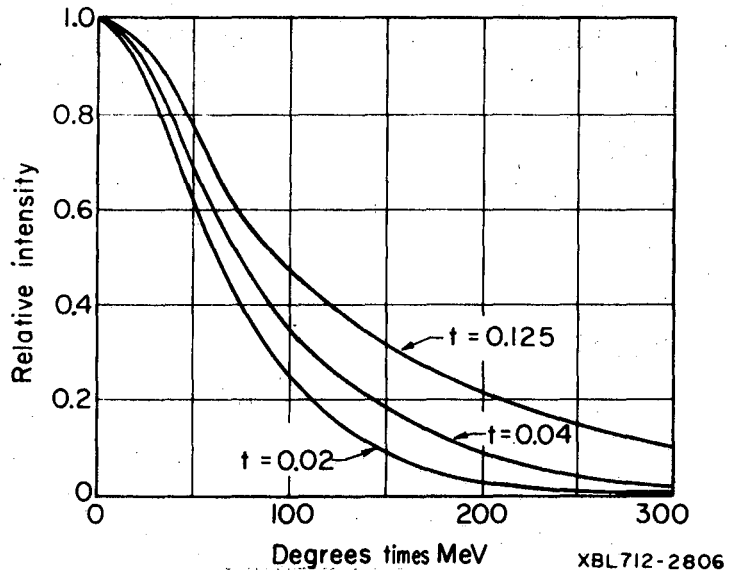

Fig. 3.6. Relative angular distribution of bremsstrahlung from tungsten targets (t - target thickness in radiation lengths). (From NBS Handbook 55, NBS 54.)

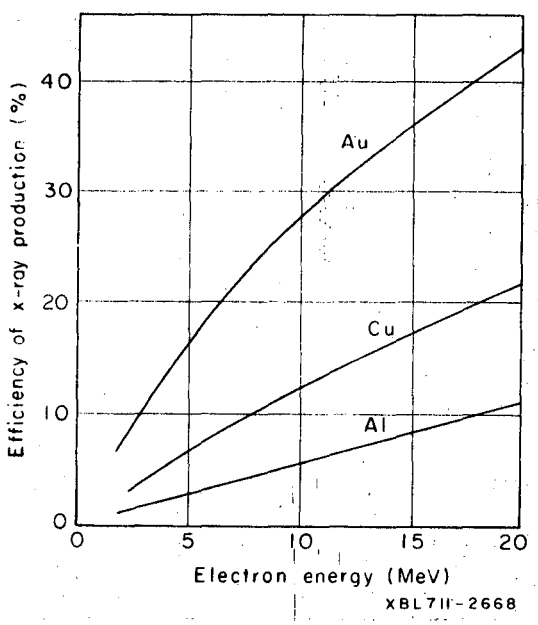

Fig. 3.7. Efficiency of x-ray production. (After Miller, MIL C 53.)

The bremsstrahlung intensity from thick targets as a function of energy is shown in Fig. 3.5. Intensity is expressed in terms of roentgens per mA min at 1 meter, which, although not strictly accurate, is common practice. The roentgen has not been defined above 3 MeV, and it would perhaps be preferable to express output in terms of rads per mA min at 1 meter by multiplying by a factor 0.93. However, although the data are reliable and useful for practical purposes of radiation protection, their intrinsic accuracy probably does not justify this rigor.

Figure 3.6 shows the angular distribution of bremsstrahlung emitted from a tungsten target, based on an equation due to Muirhead et al. (MUI E 52). The relative x-ray intensity for various target thicknesses is plotted as a function of the product of the electron energy and the angle in degrees (MeV-deg). This representation facilitates the use of Fig. 3.6 over a range of electron energies. Although there are no experimental data available for angles greater than those given in the figure at energies above 5 MeV (MAC M 57a), nevertheless in the angular range covered and for the target thicknesses shown, the curves are in good agreement with the data reported by Lanzl and Hanson (LAN L 51) at 17 MeV.

If in doubt it is probably conservative to assume that, for thick targets and large angles ($\theta \geq 90$ deg) the x-ray intensity may be as much as 5% of the forward intensity.

The bremsstrahlung production efficiency is a function of both target Z and target thickness. For targets whose thickness is ≥ 0.2 radiation length (so-called "thick" tagets) the efficiency of production (given in Fig. 3.7) is proportional to Z. The conversion efficiency for thin targets, ≤ 0.1 radiation length, is given in a number of forms by different authors such as Heitler (HEI W 36), Lawson (LAW J 50, 52), and MacGregor (MAC M 57a). However, since the thick targets are the usual concern in health physics practice, the thin-target data are not discussed here, and the interested reader is referred to the literature.

Neutron Production by Electron Accelerators

As we have already seen, neutrons rarely present a major problem at an adequately shielded electron accelerator. This is in contradistinction to the situation around proton or other particle accelerators, where neutrons essentially always dominate the hazard. At electron accelerators the primary concern of the health physicist is for the effects produced by electrons and γ rays, and for this reason extensive discussion of neutron production is not warranted here.

The neutrons produced at electron accelerators are largely due to two processes. Figure 3.8 shows the total photonuclear cross section as a function of photon energy. For photon energies below 50 MeV photodisintegration

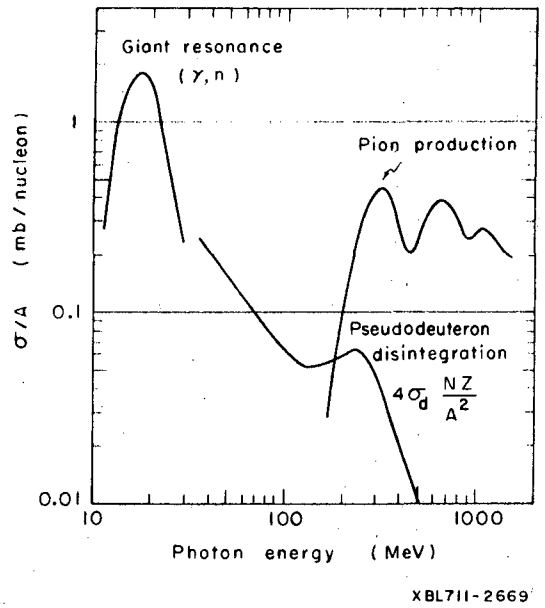

Fig. 3.8. Total photonuclear cross section per nucleon as a function of photon energy. (After De Staebler DES H 65.)

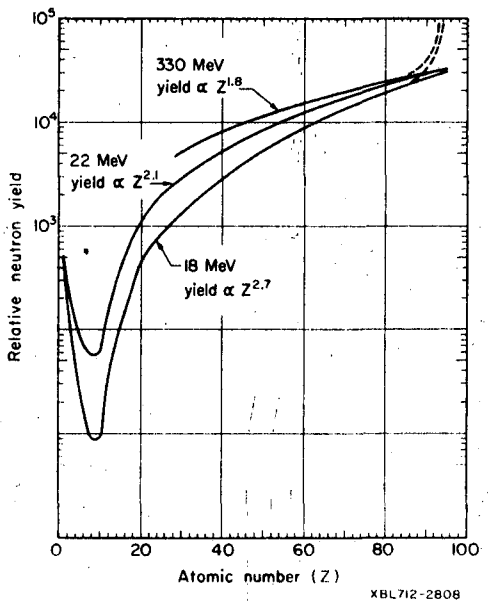

Fig. 3.9. Photoneutron yield as a function of target atomic number.

processes in the so-called "giant resonance" region dominate. These reactions have been extensively reported in the literature (WAT A 57, TOM M 65, IAEA 64). Giant resonance neutrons are of low energy (a few MeV), and the maximum cross section for their production is 1 to 2 mb/neutron. The energy at which the maximum cross section occurs varies with atomic number; for medium-Z nuclei it is found at roughly twice the threshold energy. The width of the resonance varies from 4 to 8 MeV (full width ot half maximum).

At energies between about 20 and 100 MeV photodisintegration of nucleon pairs within the nucleus (the so-called pseudodeuteron) is an important source of neutrons. In De Staebler's apt phrase, however, "the pseudodeuteron reaction always contributes but never dominates" (DES H 65). At photon energies above the pion threshold, high energy neutrons are produced. Figure 3.8 clearly shows the changes in total neutron production cross section at the pion, dipion, and tripion thresholds.

In addition to the references already cited, reports of a number of measurements and calculations of neutron production by bremsstrahlung and direct electron bombardment have been made by Price and Kerst (PRI G 50), Terwilliger, Jones, and Jarmie (TER K 51), Baldwin (BAL F 50), and Bathow, Freytag, and Tesch (BAT G 67). Some of these have been summarized by MacGregor (MAC M 57b).

For the very heavy elements the photofission process supplements the ordinary process of photodisintegration. Thus uranium and thorium yield almost twice as many neutrons as elements just below them in the atomic table, and far more than beryllium and deuterium, as can be seen from Fig. 3.9. For nuclei in the range Z = 30 to 82 the slope of the neutron yield as a fraction of atomic number slowly decreases with maximum photon energy of the bremsstrahlung spectrum. Thus the neutron yield, Y, is expressed in the form

$$Y = aZ^n, \tag{3}$$

where a is a constant, and the exponent n has the value 2.7 at 18 MeV, 2.1 at 22 MeV, and 1.7 at 330 MeV.

Figure 3.10 shows the maximum neutron yield from a thick uranium target as a function of photon energy up to 80 MeV.

When the maximum photon energy is well above the peak for photoneutron production, neutron production is found to be proportional both to electron beam current and to the maximum energy of the electrons (or beam power delivered to the target), as may be seen in Fig. 3.10.

The angular distribution of photoneutrons (including those produced by photofission) is largely isotropic at energies below 50 MeV. Little experimental information is available on the energy and angular distribution above about 100 MeV. De Staebler (DES H 62) has used "fictitious two body reactions to replace the actual complicated reactions." This approach leads to reasonable agreement with the measured spectra of photoprotons in the angular

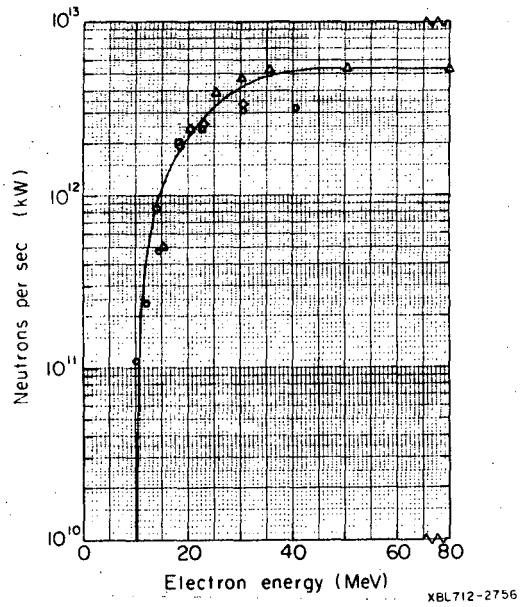

Fig. 3.10. Neutron production for an optimum uranium target as a function of electron energy. (After MacGregor, MAC M 57b.)
O Harwell, AERE T/R 1523
Δ G.E., Phys. Rev. 104, 1652 (1950).
◇ Stanford, Bull. Am. Phys. Soc. 1387 (1950).
□ Cole, from Phys. Rev. 77 806 (1950).

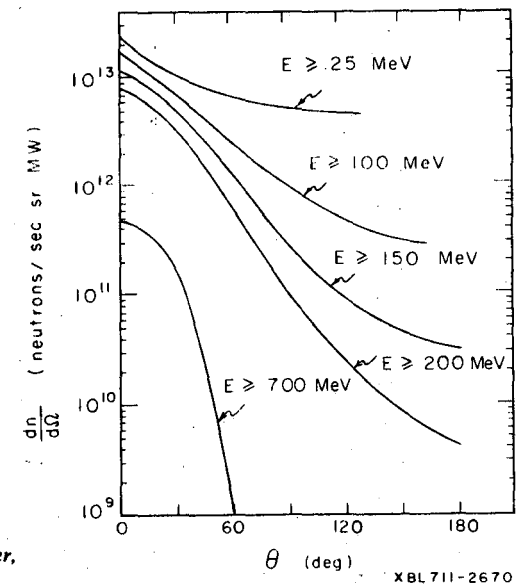

Fig. 3.11. Neutron production by electrons on copper as a function of production angle. The curves indicate the number of neutrons with an energy greater than E. (After De Staebler, DES H 65).

range between 50 and 94 deg to a copper target bombarded by 950-MeV bremsstrahlung (DES H 62), giving some confidence in the calculations. Figure 3.11 shows calculations of the angular distribution of neutrons at photon energies between 25 and 700 MeV.

With the data presented here, it should be possible for the reader to fairly accurately estimate the radiation intensity produced by electron accelerators for most practical situations in which he is likely to have to make shielding calculations or judgments of radiation safety or of proper instrumentation.

Neutron Production by Proton Accelerators and Heavy-Ion Accelerators.

LOW-AND MEDIUM-ENERGY REACTIONS

Health physics problems at heavy-ion accelerators (with the exception of accidental exposure close to or directly in the accelerator beam) are largely due to their neutron production. Thus an understanding of neutron production by charged particles is an essential weapon for the armory of the health physicist, who must design shielding for such accelerators, estimate their production of radioactivity, and measure the radiation field they produce.

Madey (MAD R 68) has summarized neutron production from (p,n), (d,n), (t,n), and (α,n) reactions, and a portion of his article is reproduced here by kind permission of the author and his publisher (Springer-Verlag, Berlin).

"Energy characteristics of neutron source reactions with light nuclei are listed in Table 3.III. With incident charged particles up to 10 MeV, monoenergetic neutron beams in the forward direction are available with energies from about 0.23 to 27 MeV. Figure 3.12 is a plot of the neutron energy in the forward (0 deg) and backward (180 deg) directions for the $^{3}H(p,n)^{3}He$, $^{7}Li(p,n)^{7}Be$, and $^{3}H(p,n)^{4}He$ reactions as a function of the energy of the bombarding particle.

"The (p,n) Reactions

"a. The $^{7}Li(p,n)^{7}Be$ Reaction.

"The $^{7}Li(p,n)^{7}Be$ reaction has been widely used as a source of neutrons with energies in the kilovolt region. Gibbons and Newson (GIB J 60) have tabulated the neutron energy as a function of the proton energy and the emission angle in the laboratory coordinate system. Neutrons with energies below 80 keV must be taken from thin targets at angles greater than 90 deg to the direction of the proton beam. The neutron energy and the relative yield at an angle of 120 deg are shown in Fig. 3.13 as a function of proton energy. Curves c and d in Fig. 3.12 give the energy of neutrons at 0 and 180 deg, respectively, for proton bombarding energies up to 4 MeV.

Table 3.III. Energy characteristics of neutron source reactions with light nuclei (from Brolley and Fowler (BRO J 60).

	Reaction						
	Endothermic			Exothermic			
	^{12}C (d,n)	T (p,n)	^{7}Li (p,n)	^{13}C (χ,n)	D (d,n)	^{9}Be (α,n)	T (d,n)
Q value [MeV]	-0.281	-0.764	-1.646	+2.201	+3.266	+5.708	+17.586
Threshold [MeV]	0.328	1.019	1.882	–	–	–	–
Neutron energy at threshold [keV]	3.4	63.9	29.9	–	–	–	–
Energy of bombarding particle [MeV]	Neutron energy at 0 deg [MeV]						
0	–	–	–	2.070	2.448	5.266	14.046
1	0.693	–	–	3.198	4.137	6.678	16.752
2	1.681	1.201	0.229	4.163	5.238	7.707	18.259
3	2.668	2.215	1.305	5.112	6.265	8.687	19.579
4	3.654	3.221	2.322	6.055	7.261	9.644	20.806
5	4.641	4.224	3.331	6.995	8.239	10.598	21.978
6	5.627	5.226	4.336	7.994	9.207	11.525	23.111
7	6.614	6.277	5.340	8.871	10.167	12.456	24.217
8	7.600	7.228	6.342	9.808	11.123	13.383	25.301
9	8.586	8.229	7.345	10.744	12.074	14.308	26.370
10	9.573	9.229	8.347	11.680	13.023	15.227	17.424

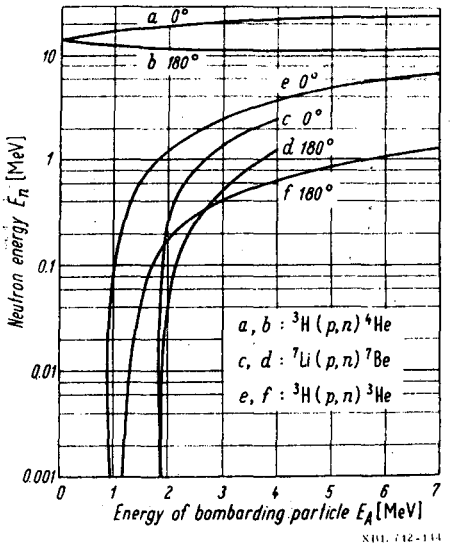

Fig. 3.12. Neutron energy in the forward (0 deg) and backward (180 deg) directions for the $^3H(p,n)\,^3He$, $^7Li(p,n)^7Be$, and $^3H(d,n)^4He$ reactions vs. energy of the bombarding particle. (From Madey, MAD R 68.)

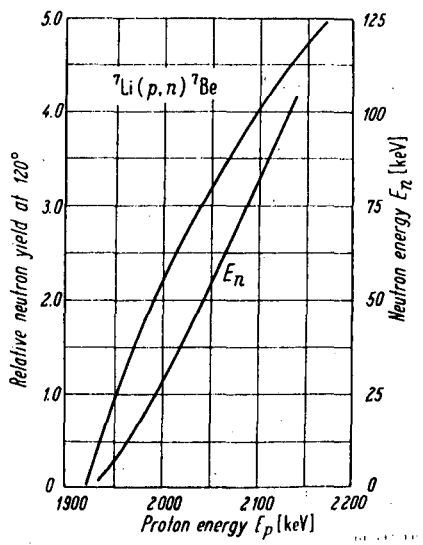

Fig. 3.13. Energy and relative yield at 120 deg of neutrons from the $^7Li(p,n)^7Be$ reactions vs proton bombarding energy (after Hanna, (HAN R 55; and Gibbons, GIB J 56). (From Madey, MAD R 68.)

Fig. 3.14 depicts the total cross section for the $^{7}Li(p,n)\,^{7}Be$ reaction as a function of proton energy from threshold to 5.5 MeV. The cross section rises steeply above threshold to a plateau which is interrupted by a strong resonance at a proton energy of 2.25 MeV. Macklin and Gibbons (MAC R 58b) measured a cross section of about 570 mb at the peak of this resonance. The cross section has another resonance at a proton energy of 5.4 MeV.

"The reaction $^{7}Li(p,n)\,^{7}Be^{*}$ produces a second group of neutrons when the proton energy bombarding the lithium target exceeds the threshold energy of 2.378 MeV for this excited state reaction. The excited state $^{7}Be^{*}$ decays to the ground state by the emission of a 430-keV γ ray.

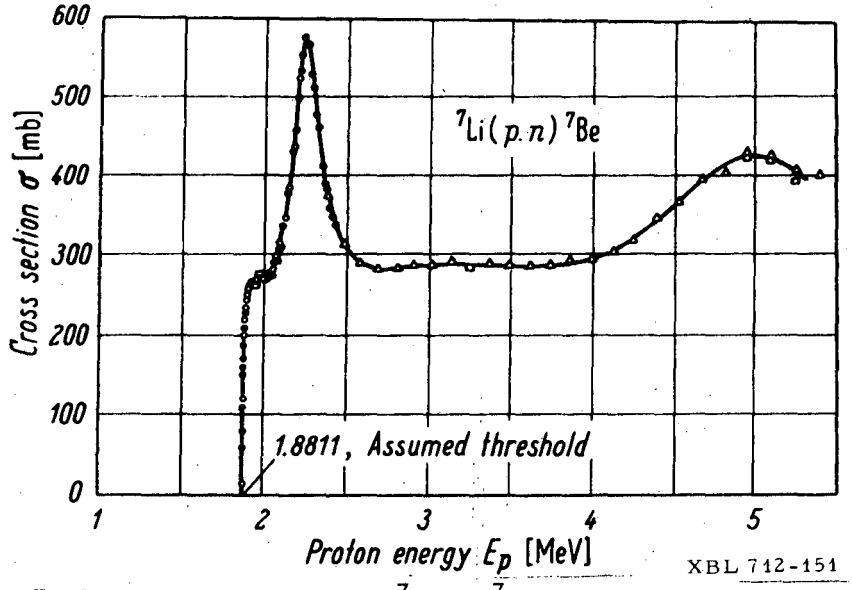

Fig. 3.14. Total cross section for $^{7}Li(p,n)\,^{7}Be$ reaction from threshold to 5.5 MeV vs. proton bombarding energy (after Gibbons and Macklin, GIB J 59). (From Madey, MAD R 68.)

"b. The $T(p,n)\,^{3}He$ Reaction.

"The total cross section for the $T(p,n)\,^{3}He$ reaction is shown in Fig. 3.15 as a function of bombarding proton energy from the threshold of 1.019 MeV to about 5 MeV. The yield of neutrons is substantial near the threshold energy. The absence of an excited state of ^{3}He in the observed energy region means that the $T(p,n)\,^{3}He$ reaction is not complicated by a second group of neutrons as arises in the $^{7}Li(p,n)\,^{7}Be^{*}$ reaction. The relativistic tables of Blumberg and Schlesinger (BLU L 56) give the energy and angle relationships for this reaction in both the laboratory and center-of-mass coordinate systems as a function of proton bombarding energy.

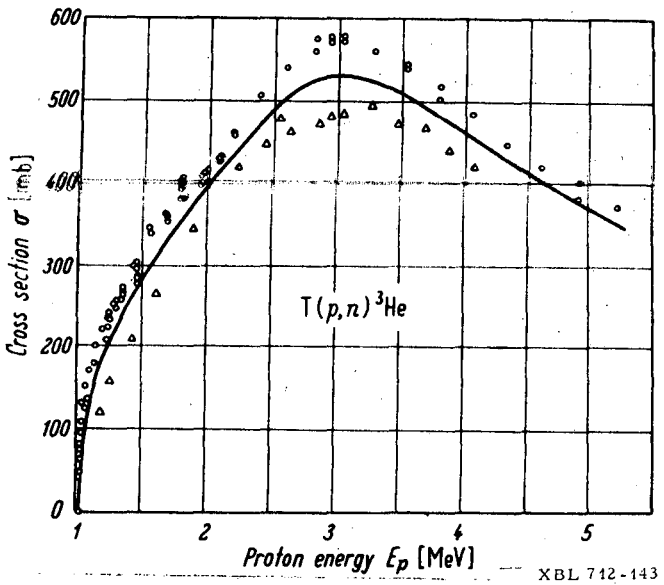

Fig. 3.15. Total cross section of $T(p,n)^3$ He reaction from threshold to 5 MeV vs. proton bombarding energy (after Macklin and Gibbons) (MAC R 58a,b GIB J 58); (and Jarvis) (JAR G 57). (From Madey, MAD R 68).

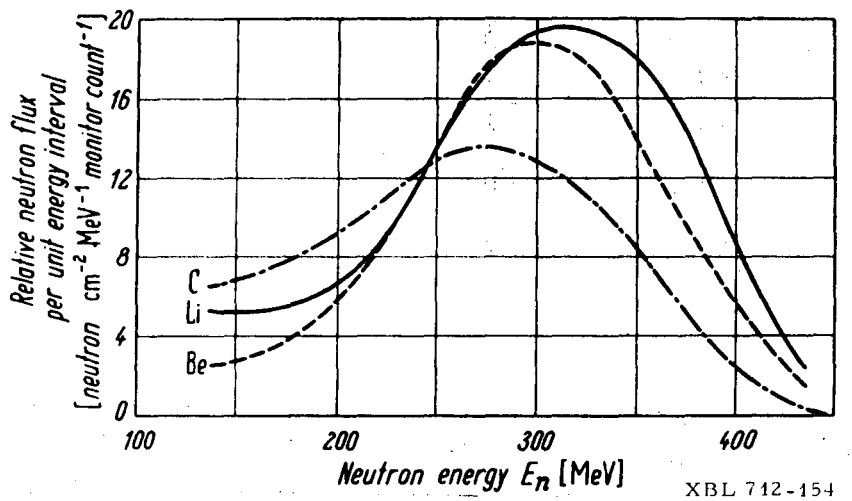

Fig. 3.16. Neutron energy distributions from the bombardment of beryllium, lithium and carbon targets with 375-MeV protons (after Goodell et al.), (GOO W 53). (From Madey, MAD R 68).

"*c. The (p,n) Reactions in Medium-Weight Nuclei.*

"Several (p,n) reactions with medium-weight nuclei are used as sources of monoenergetic neutrons in the low energy region from 5 to 150 keV in the forward direction. Table 3.IV lists the minimum energies of monoenergetic neutrons at 0 deg with a n energy below 120 keV (except exactly at threshold), reactions with medium-weight nuclei yield energies of a few keV.

"The cross sections for (p,n) reactions in medium-weight nuclei are smaller than the $^{7}Li(p,n)$ cross section; for example, in the energy region just above threshold, the cross sections for ^{45}Sc and ^{63}Cu targets average 1 to 3 millibarns per steradian in the forward direction, whereas those for ^{51}V and ^{65}C are somewhat smaller because of their lower threshold energy. The energy of the first excited state in the residual nucleus corresponds approximately to the maximum energy of monoenergetic neutrons that can be produced. As listed in Table 3.IV ^{65}Cu is limited in its ability to produce monoenergetic neutrons to a neutron energy of 50 keV, whereas ^{45}Sc, ^{51}V, and ^{63}C have much higher energy limitations.

"Table 3.IV. A comparison of energy characteristics of (p,n) reactions in medium- and light-weight nuclei.

Reaction	Minimum energy of neutrons at 0 deg [keV]	Threshold energy [MeV]	Required bombarding energy above threshold [keV]	Energy of 1st excited state [MeV]
$^{3}T(p,n)\,^{3}He$	288	1.019	128	—
$^{7}Li(p,n)\,^{7}Be$	120	1.882	39	0.478
$^{45}Sc(p,n)\,^{45}Ti$	5.60	2.908 + 0.004	1.46	0.743
$^{51}V(p,n)\,^{51}Cr$	2.36	1.5656 + 0.0015	0.61	0.775
$^{63}Cu(pn,)\,^{63}Zn$	4.20	4.214 + 0.005	1.08	0.191
$^{65}Cu(p,n)\,^{65}Zn$	2.03	2.1646 + 0.0009	0.52	0.054

"*d. The (p,n) Reaction at Synchrocyclotron Energies.*

Proton beams from synchrocyclotrons have been used to generate neutron beams with energies in the neighborhood of the bombarding energy. Fig. 3.16 shows the neutron energy distribution obtained by Goodell et al. (GOO W 53) from the bombardment of beryllium, lithium, and carbon targets by 375-MeV protons.

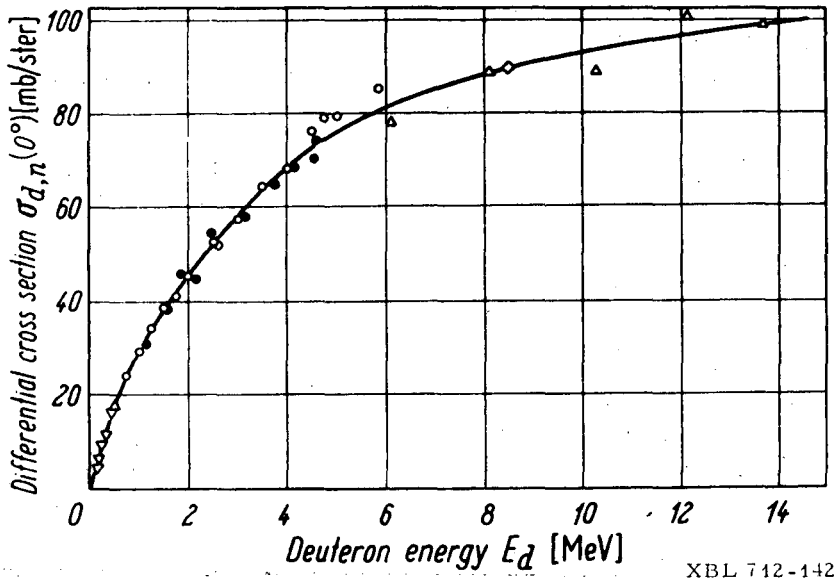

Fig. 3.17. Laboratory differential cross section for the production of neutrons in the forward (0 deg) direction from the D(d,n)^{3}He reaction vs. bombarding deuteron energy (after Brolley and Fowler, (BRO J 60). From Madey, MAD R 68.)

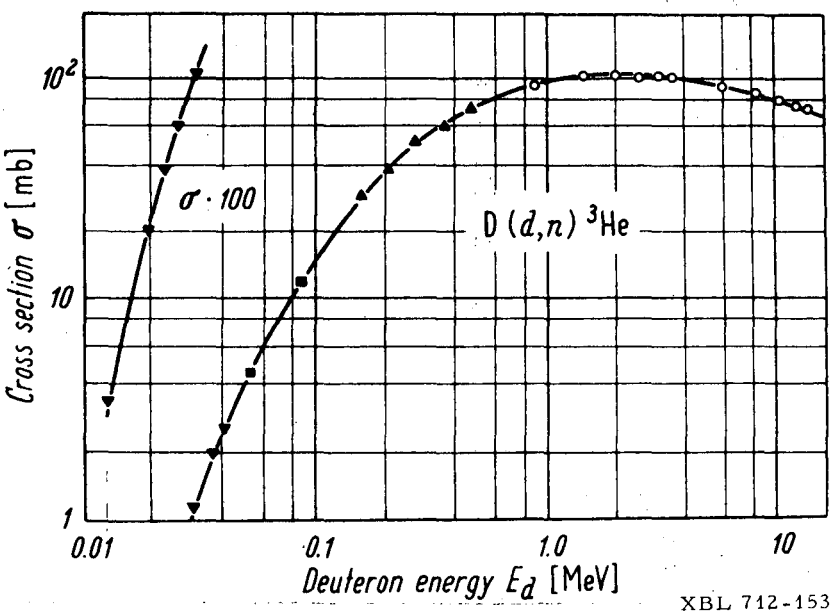

Fig. 3.18. Total cross section for D(d,n)^{3}He reaction vs. laboratory deuteron energy (after Brolley and Fowler), (BRO J 60). From Madey, MAD R 68.)

"II. THE (d,n) REACTIONS

"a. The D(d,n)^{3}He Reactions.

"The yield of forward (0 deg) neutrons from the D(d,n)^{3}He reaction increases with deuteron energy in the manner shown in Fig. 3.17, where the laboratory differential cross section for the production of neutrons in the forward (0 deg) direction is plotted as a function of laboratory deuteron energy. The total cross section for neutron production by the D(d,n) ^{3}He reaction is shown in Fig. 3.18 as a function of laboratory deuteron energy.

"b. The T(d,n)^{4}He Reaction.

"The T(d,n) ^{4}He reaction is characterized by its very high Q value of about 17.6 MeV and a total cross section that has a high peak value of 5 barns at a deuteron energy of 110 keV. Fig. 3.19 shows the energy dependence of the total cross section for neutron production by the T(d,n) ^{4}He reaction. As illustrated in Table 3.III, the high Q value makes possible the production of monoenergetic neutrons up to about 30 MeV with relatively low input energy. Below a deuteron energy of approximately 400 keV, the differential cross section is practically isotropic in the center-of-mass sytem. Because of the high Q value, the neutron energy is relatively insensitive to the angle of emission for low deuteron bombarding energies in the region of the peak total cross section; for example, at a deuteron energy of 200 keV, the neutron energy deviates from its value of 14.1 MeV at 90 deg by only about ± 7%. The energetics of this reaction are included in the tabulation of Blumberg and Schlesinger (BLU L 56).

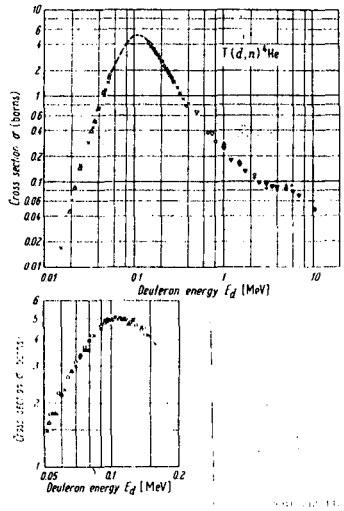

Fig. 3.19. Total cross section for T(d,n)^{4}He reaction vs. laboratory deuteron energy (after Brolley and Fowler). (BRO J 60).

"c. The $^{12}C(d,n)^{13}N$ Reaction.

"The $^{12}C(d,n)^{13}N$ reaction is endoergic with a Q value of 0.281 MeV and a threshold of 0.328 MeV. It produces monoenergetic neutrons from 2.76 to 3.4 keV for deuteron bombarding energies up to 3.09 MeV, which is the threshold energy for producing a second group of neutrons as a result of leaving ^{13}N in its first excited state at 2.37 MeV. Although the cross section for the $^{12}C(d,n)$ reaction is low compared with that for either the $^{7}Li(p,n)$ or the T(p,n) reaction, neutrons from this reaction often are produced as background from deuterons impinging on carbon deposited from pump oil or other organic contaminants.

"d. The Deuteron Stripping Process.

Acceleration of a deuteron imparts a kinetic energy to the neutron in the deuteron equal to one-half of the deuteron kinetic energy. In the deuteron stripping process, the target nucleus captures or "strips off" the proton in the deuteron and permits the neutron to continue in the forward direction. The energy distribution of the neutrons from the stripping process has a broad peak about an energy equal to approximately one-half of the energy of the incident deuteron; for example, a neutron beam produced by the stripping of 190-MeV deuterons has a maximum energy at about 85 MeV with an energy spread of the order of 20 MeV. The neutrons from the stripping reaction are concentrated in a narrow cone about the forward direction; for 190-MeV deuterons on carbon, the half-width of the neutron beam at half-maximum is of the order of 2 deg. Serber (SER R 47) has described the deuteron stripping process theoretically; whereas Schecter et al. (SCH L 55) have obtained confirming data on the energy and angular distributions, respectively, of neutron beams produced by the stripping of 190-MeV deuterons.

"III. THE (α,n) REACTIONS

"Possible target nuclei for the (α,n) reaction include all the elements when the bombarding α-particle energy exceeds about 20 MeV. The high intensity of α-particle beams in accelerators partially compensates for the usually small (α,n) reaction cross sections. The excitation curves shown in Fig. 3.20 for the $^{109}Ag(\alpha,n)$ and $^{109}Ag(\alpha,2n)$ reactions illustrate the magnitude of cross sections. The (α,n) reaction can be considered as leading to nuclei in highly excited states with many closely spaced levels. The decay of these nuclei results in a statistical energy distribution which can be characterized by a nuclear temperature. The reaction $^{109}Ag(\alpha,n)^{112}In$ discussed by Bleuler, Stebbins, and Tendam (BLE E 53) is a typical example.

"For a fixed α-particle beam energy, the neutron yield decreases rapidly with increasing atomic number of the target; for example, Fig. 3.21 shows the results of Allen et al (ALLA 51) on the fallingoff of the fast neutron flux in the forward direction for elements from beryllium to bismuth bombarded by 30-MeV α particles."

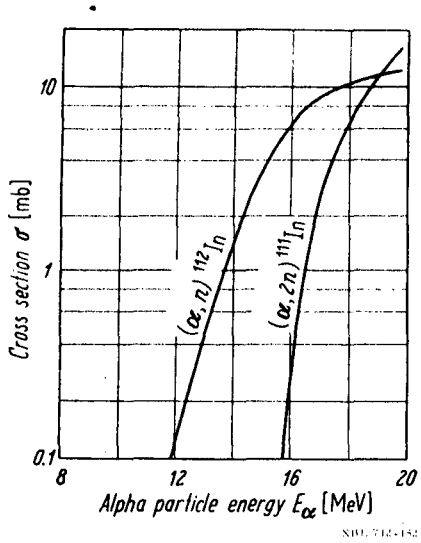

Fig. 3.20. Total cross section for the $^{100}Ag(\alpha,2n)$ reactions vs. alpha particle bombarding energy (after Tendam and Brady, TEN D 47). (From Madey, MAD R 68).

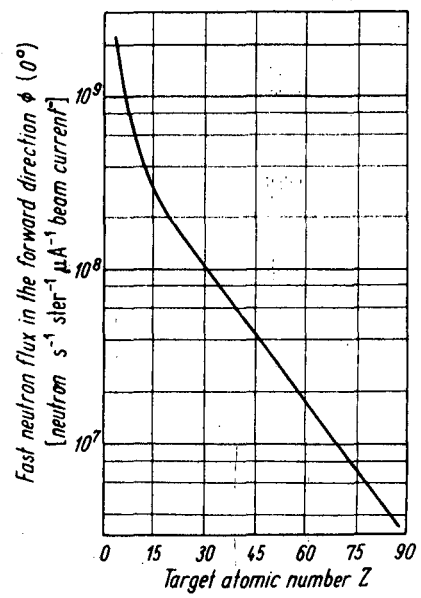

Fig. 3.21. Fast neutron flux produced in the forward (0 deg) direction by 30-MeV α particles vs. atomic number of target element (after Allen et al.) (ALL A 51). (From Madey, MAD R 68).

Proton Nucleus Reactions

Wallace (WAL R 62,65) has summarized neutron production from proton interaction in a variety of materials.

For protons striking an extended thick target, the total neutron production as a function of energy for carbon, aluminum, copper, and lead is shown in Fig. 3.22. This total neutron production consists of two parts, "cascade" and "evaporation" neutrons. There are also cascade protons. The particles that are knocked out during the immediate passage of the incident proton by direct interactions between the proton and the individual nucleons in a target nucleus have been extensively treated by Metropolis (MET N 58).

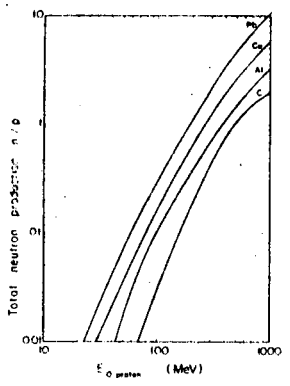

Fig. 3.22. Measured total neutron yields per proton stopping in a thick target for C, Al, Cu, and PB. (From Moyer, MOY B 61.)

Bertini (BER H 69) has extended the scope of the early intranuclear cascade calculation first performed by Metropolis. In a recent review article the current status of this work indicated excellent agreement with available experimental data. Total cross sections are predicted most accurately, within about 15% of experimental data, for proton and neutron nonelastic cross sections from energies between 30 and 3500 MeV for nuclei from carbon to lead.

Estimates of neutrons emitted per inelastic event for incident protons between 400 and 660 MeV are in good agreement with the values summarized by Wallace (WAL R 65) and with the experimental values of Vasilkov et al. (VAS R 68) (see Table 3.V).

Agreement between calculation and experiments is somewhat less exact when double-differential cross-section data are compared. Some qualitative differences are evident, and it is not yet completely clear whether these are due to deficiencies in the calculational models, experimental techniques, or both. Comparisons nevertheless are encouraging, and the difficulties should

be resolved within the next few years, when it seems reasonable that we might expect complete compilations of secondary-particle production, certainly more than adequate for the needs of the health physicist.

The cascade particles, because of momentum conservation, are strongly concentrated in the forward direction relative to the incident-proton direction. Because of their long mean free paths, only those cascade particles having energies above 150 MeV need be considered in shielding. Cascade particles do not contribute significantly to the secondaries produced by protons of less than 100 MeV.

The rest of the secondary particles are emitted isotropically, after the initial proton passage, by evaporation from the nucleus as a result of the excitation energy left behind in the nucleus. The cascade yields of neutrons and protons resulting from either neutron or proton bombardment are shown in Fig. 3.23 (the production from plural cascades within the nucleus is included).

Cascade Particles

The spectra of cascade particles computed by Metropolis (MET N 58) are shown in Fig. 3.24 for 460- and 1840-MeV protons incident on aluminum, and are in good agreement with each other except at the highest energies. These spectra multiplied by the appropriate normalization factors (given in Fig. 3.25) are shown in the energy region above 1 MeV in Fig. 3.26 for incident proton energies of 450, 600, and 850 MeV. It is seen that below about 100 MeV the cascade spectra are essentially the same.

The number of cascade neutrons per incident proton per inelastic collision as a function of proton energy is given in Fig. 3.25 for several target materials. It is seen that for energies above 200 MeV there is a monotonic increase in the number of cascade neutrons with target mass number, whereas for the energy region below 200 MeV the low-mass-number materials actually have a higher neutron production than the high-A materials. The inelastic cross sections for C, Al, Cu, and Pb are given in Fig. 3.27, from which, together with the data shown in Fig. 3.25, neutron yields from inelastic interactions may be calculated.

The number of cascade protons per incident proton per inelastic collision as a function of proton energy and target mass number is shown in Fig. 3.28. These curves bear a resemblance to those for neutron production in Fig. 3.25, and the same conclusion can be drawn with respect to production in the light elements. It should be noted that in the energy region near 500 MeV the Fig. 3.28 cascade-proton curves are in the reverse order, with the highest proton production coming from the low A's and the lowest proton production coming from the high A's, in contrast to Fig. 3.25 for cascade neutrons. Above 1000 MeV the low-A curve does cross over the others, but the others still remain in the inverted order. This particular

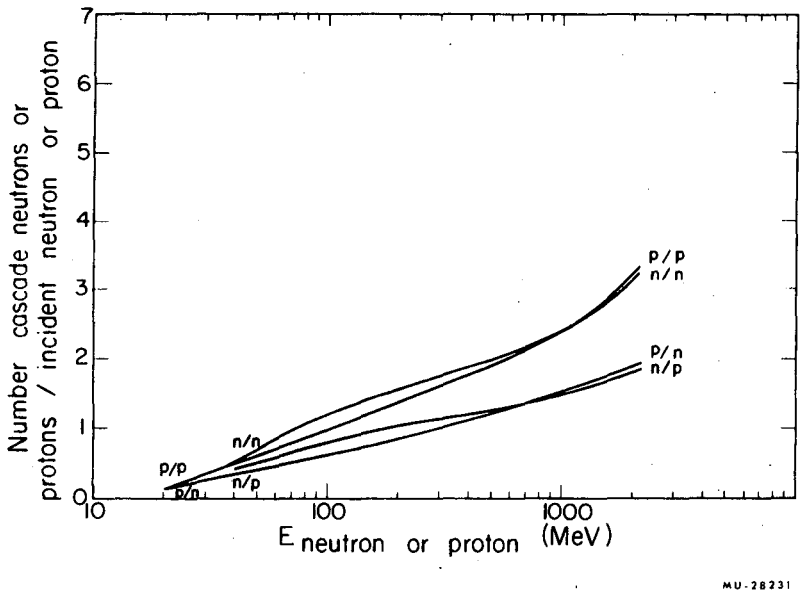

Fig. 3.23. Estimated cascade neutrons and cascade protons produced by incident neutrons or protons of energy E_n on nuclei near A = 20 per incident particle per inelastic collision. (After Metropolis et al. MET N 58.)

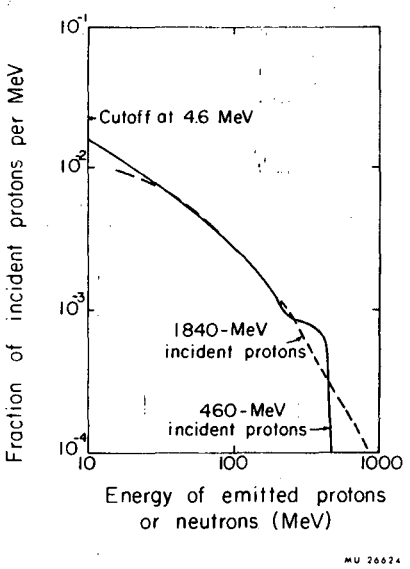

Fig. 3.24. Energy spectra of cascade nucleons emitted from aluminum. (After Metropolis et al., MET N 58.)

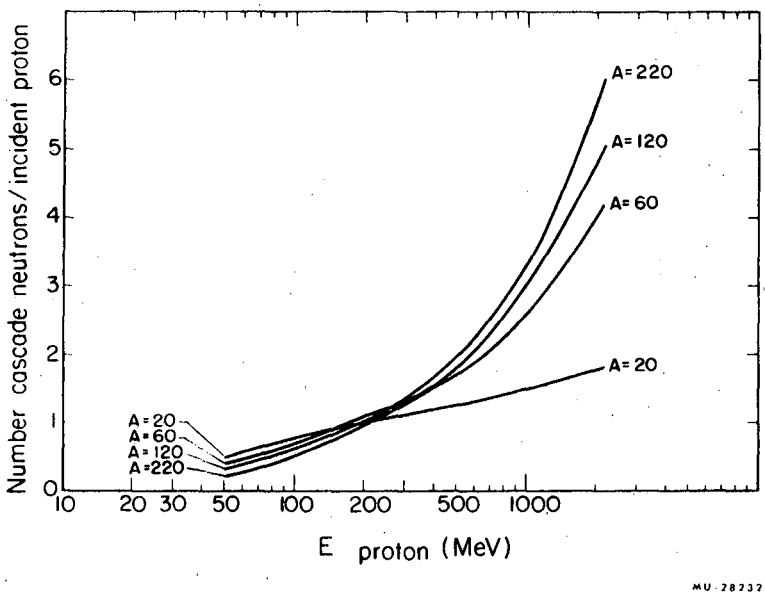

Fig. 3.25. Number of cascade neutrons per incident proton per inelastic collision as a function of proton energy and target A, (After Metropolis et al., MET N 58.)

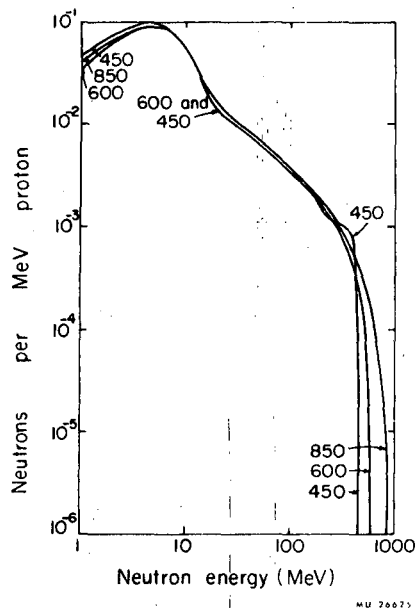

Fig. 3.26. Cascade and evaporation-neutron emission from 450-, 600-, and 850-MeV protons on aluminum, per incident proton.

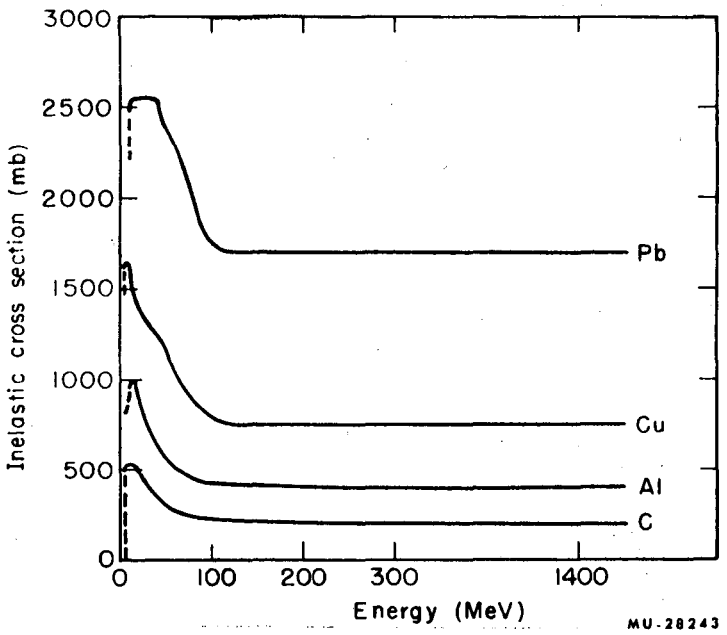

Fig. 3.27. Neutron or proton inelastic cross sections for C, Al, Cu, and Pb vs incident neutron or proton energy, (After Lindenbaum, LIN S 61.)

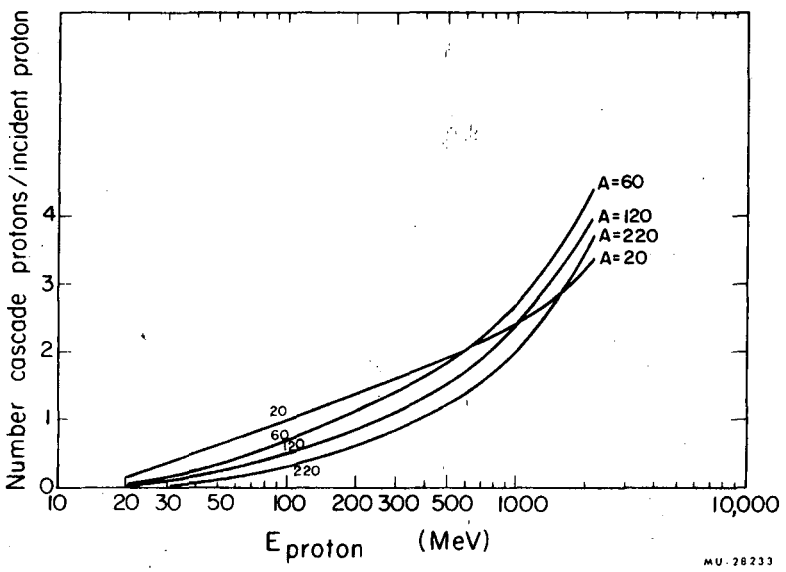

Fig. 3.28. Number of cascade protons per incident proton per inelastic collision as a function of proton energy for various values of target A. (After Metropolis et al., MET N 58.)

fact is of only minor importance to our present problem, since cascade protons have a very limited range and it is really the cascade neutrons that must be considered.

Evaporation Particles

Several authors (DOS I 58, LEC K 50, FUJ Y 50, DEU R 55) have treated the evaporation of nucleons from nuclei that have been excited by very-high-energy neutrons or protons. These evaporation neutrons provide the low-energy end of the spectrum. Nuclear evaporation is somewhat analogous to the evaporation of a liquid. The resulting particle spectra are obtained by estimating an excitation energy E_1 for the nucleus as a whole. This estimation, due to Moyer (MOY B 61), is shown in detail for A equals 20, 60, 120, and 220 in Fig. 3.29. This set of curves gives the "excitation" energy E_1 left behind in a nucleus by an incident proton or neutron of energy E. This energy is considered as a thermal kinetic-energy source which will eventually lead to evaporation.

The nuclear temperature produced in a nucleus by the deposition of energy E_1 by an incident neutron or proton is shown in Fig. 3.30. Note that nuclear temperatures for the light elements have plateaus in the region of several hundred MeV, therefore the change in temperature in this region with increasing incident proton energy is quite small.

The excitation energy is related to the nuclear "temperature" τ by an empirical equation (DOS I 58)

$$E_1 = (A/10)\tau^2, \qquad (4)$$

where E_1 is the nuclear excitation in MeV, and A is the atomic weight of the nucleus. This empirical equation is shown in Fig. 3.31 for four different values

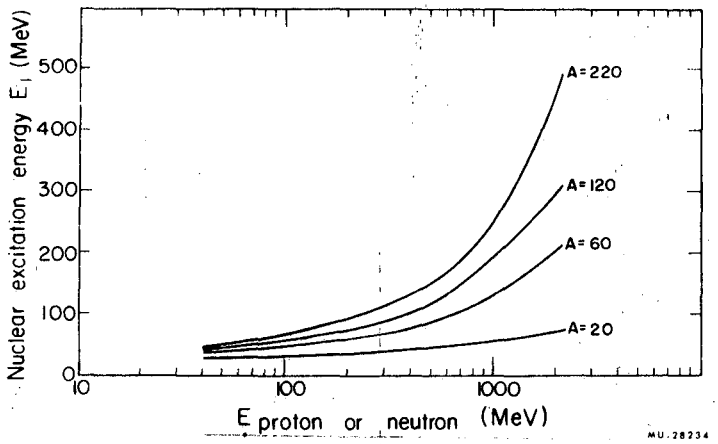

Fig. 3.29. Average nuclear excitation energy E_1 deposited in the nucleus by an incident neutron or proton of energy E in one inelastic collision. (After Moyer, MOY B 61.)

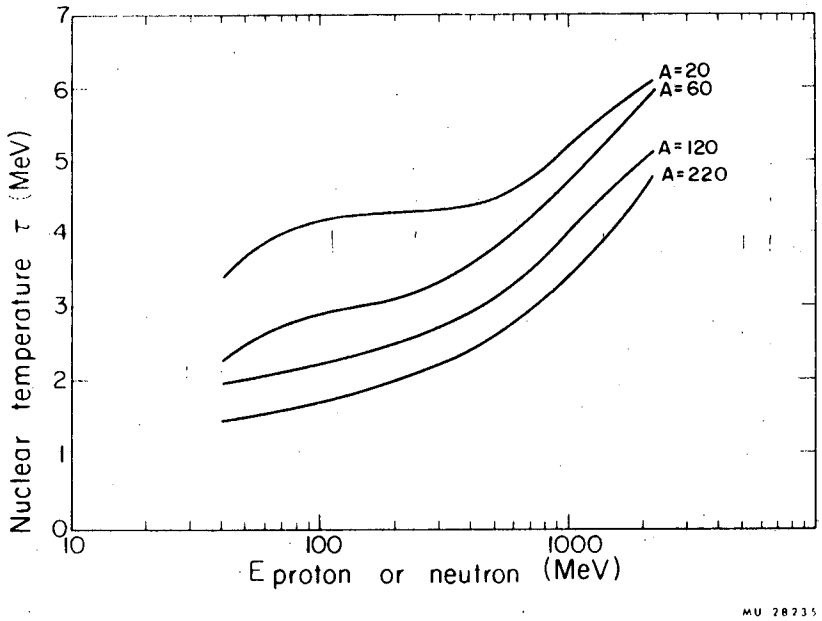

Fig. 3.30. Estimated residual nuclear temperature produced in the nucleus after excitation by a neutron or proton of energy E in one inelastic collision. (After Metropolis et al., MET N 58.)

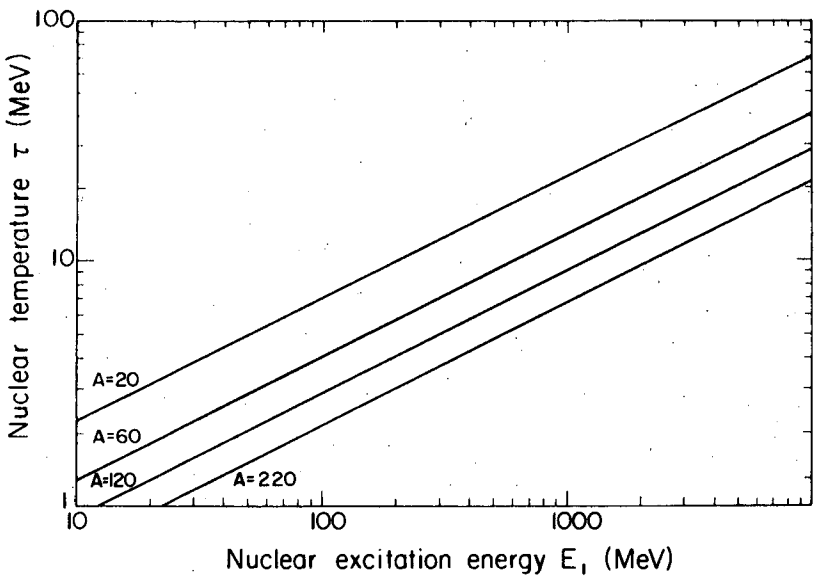

Fig. 3.31. Nuclear temperature τ vs nuclear excitation energy E_I for various A's.

of A. It is seen that the light elements have higher nuclear temperatures than heavy elements at a particular excitation energy. Figures 3.29 through 3.31 really represent a three-dimensional surface in a space whose coordinates are the total nuclear excitation energy, nuclear temperature, and bombarding-proton energy.

The evaporation spectrum itself is given by

$$N(E)\,dE = (E/\tau 2)e^{-(E/\tau)}dE, \qquad (5)$$

where N(E) dE gives the flux density, rather than the more familiar expression of the Maxwellian distribution items of number density. The presence of the factor E ahead of the exponential rather than the factor $E^{1/2}$ is thus explained.

Table 3.V summarizes the secondary cascade and evaporation particle production from a thick aluminum target bombarded by protons of 450, 600, and 850 MeV. Note that in this table it is appropriate for the sum of "cascade" and "evaporation" neutrons to not equal the "total" neutrons. The "total" production is given per incident particle on a thick target. The "cascade" and "evaporation" production given are per inelastic collision at the quoted energy. The sum of these two productions can be either less than or greater than the "total," depending on the ratio of proton removal by inelastic collision to proton energy loss by electromangetic dE/dx. The total neutron production per inelastic collision, and the ratio of the evaporation to the cascade process, as functions of both energy and A are given in detail in Figs. 3.32 and 3.33. The electromagnetic energy loss changes with proton energy, whereas the inelastic cross sections are quite constant with energy above 100 MeV, as seen in Fig. 3.27. It is seen that for the lightweight elements the number of evaporation neutrons is quite constant at about one neutron per proton over a wide energy range.

More details of this process are available, such as the suppression of the low-energy particles by the Coulomb barrier, as treated by Dostrovsky (DOS I 58) and Le Couteur (LEC K 50). Singly charged particles such as H, ^{2}H, and ^{3}H, as well as multiply charged particles such as ^{3}He and ^{4}He, can also be estimated as given in Figs. 3.34 through 3.39. The doubly charged particles have their evaporation spectrum peaks at about twice the energy of the proton spectrum peak for a nucleus of the same excitation. The angular distribution of the particles emitted in connection with nuclear evaporation is of course isotropic.

Evaporation particles are far more important for inducing radioactivity in accelerator components than are the cascade neutrons, since evaporation particles are considerably more numerous and their energy is more favorable for capture.

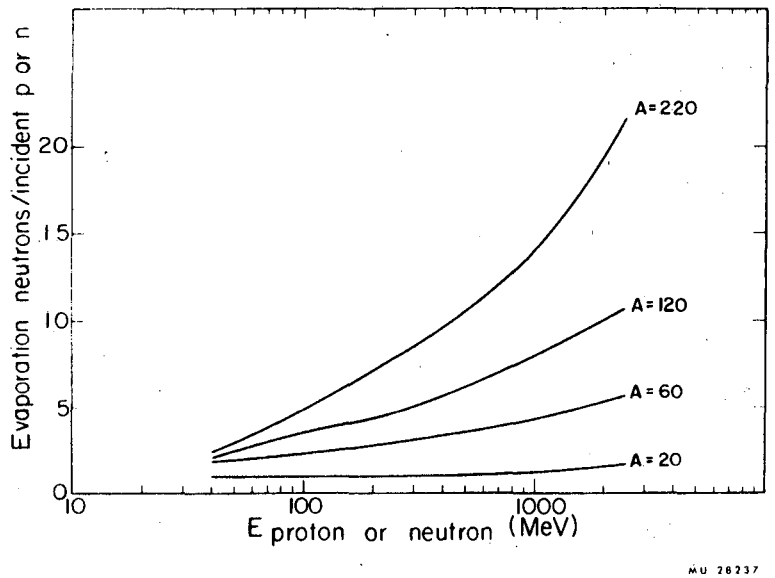

Fig. 3.32. Estimated number of evaporation neutrons produced per incident neutron or proton of energy E per inelastic collision. (After Metropolis et al., MET N 58.)

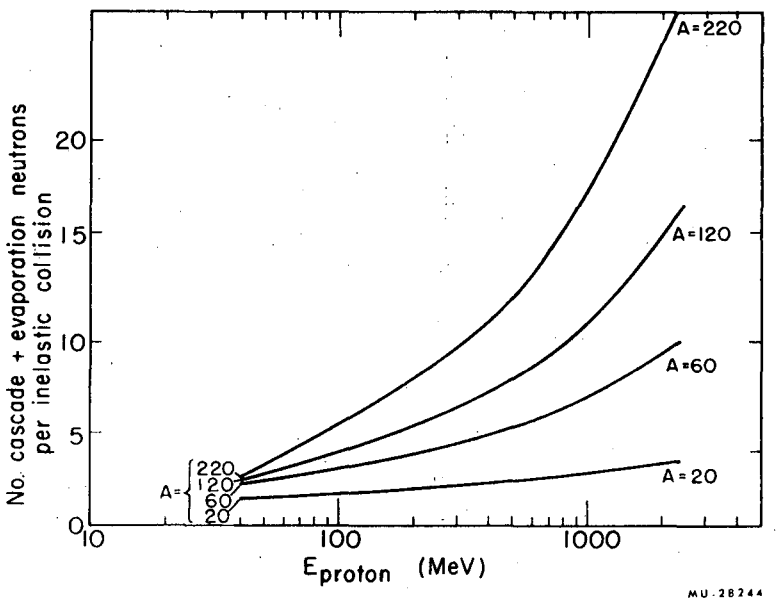

Fig. 3.33. Total neutron production per inelastic collision = cascade + evaporation as a function of the incident proton energy.

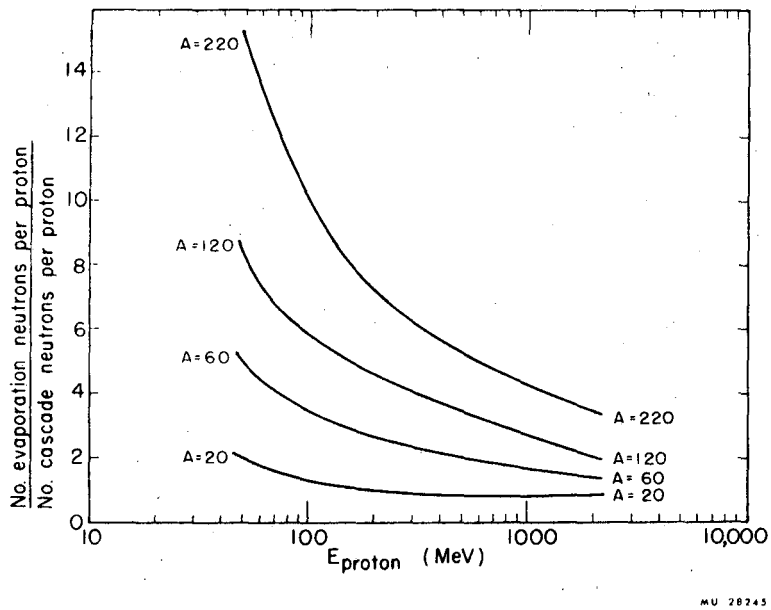

Fig. 3.34. Ratio of evaporation neutrons to cascade neutrons per inelastic collision as a function of the incident proton energy.

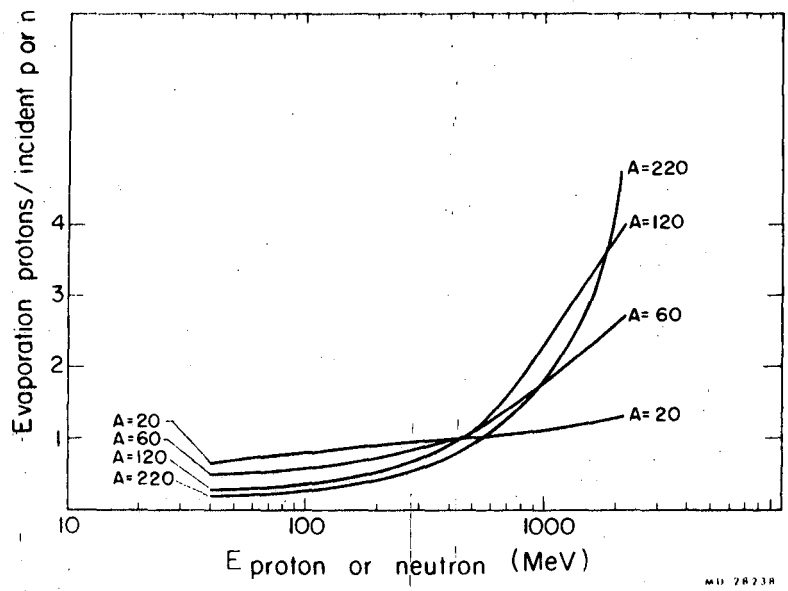

Fig. 3.35. Average number of evaporation protons per incident proton or neutron on various A's per inelastic collision vs energy of the incident particle. (After Metropolis et al., MET N 58.)

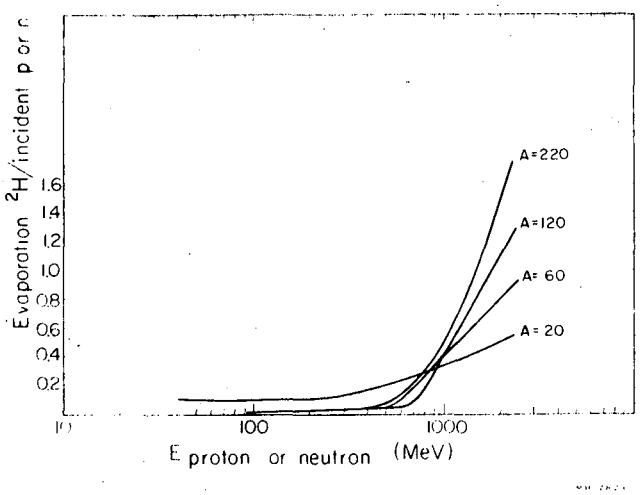

Fig. 3.36. Average number of evaporation ^2H per incident proton or neutron on various A's per inelastic collision vs energy of the incident particle. (After Metropolis et al., MET N 58.)

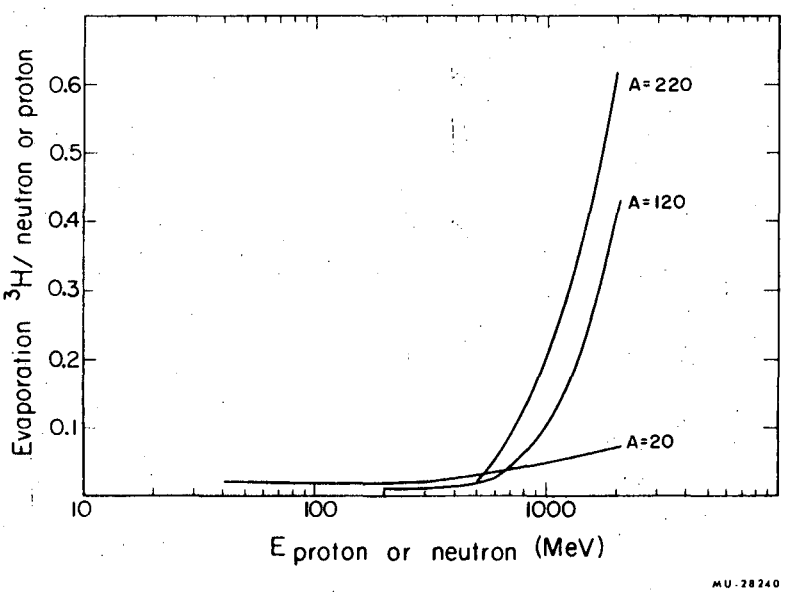

Fig. 3.37. Average number of evaporation ^3H per incident proton or neutron on various A's per inelastic collision vs energy of the incident particle. (After Metropolis et al., MET N 58.)

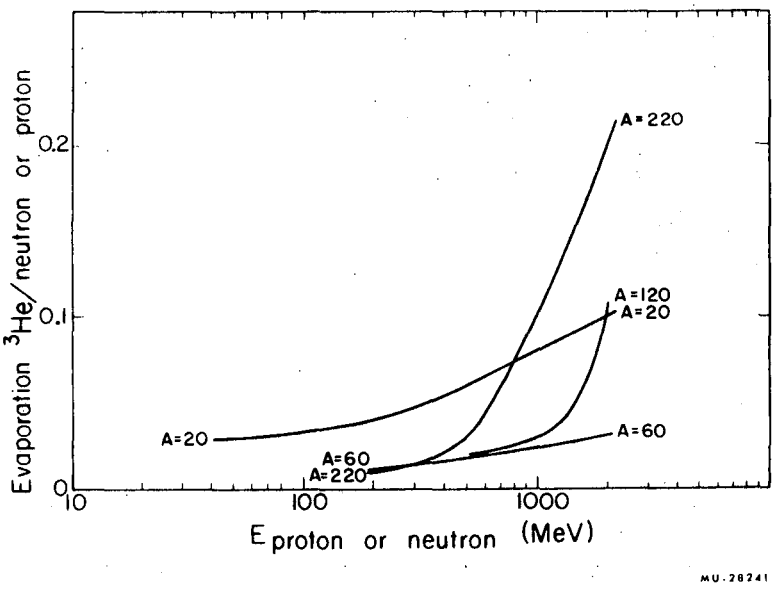

Fig. 3.38. Average number of evaporation ^{3}He per incident proton or neutron on various A's per inelastic collision vs energy of the incident particle. (After Metropolis et al., MET N 58.)

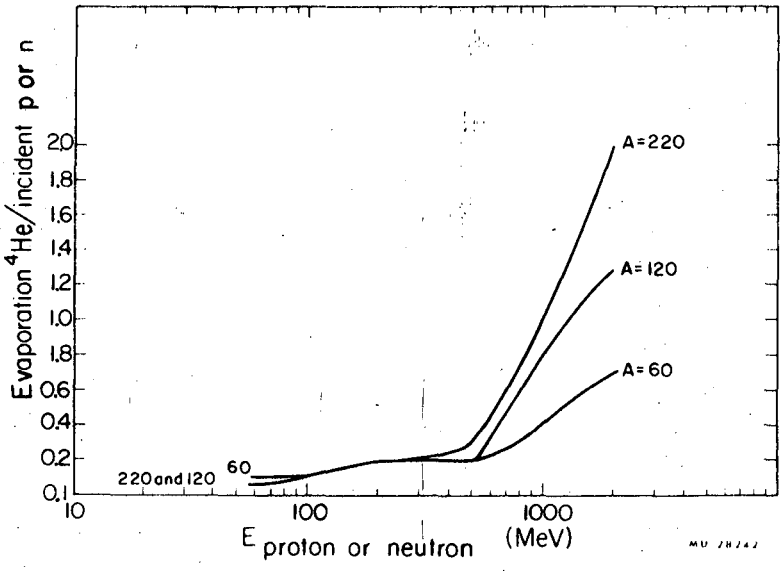

Fig. 3.39. Average number of evaporation ^{4}He per incident proton or neutron on various A's per inelastic collision vs energy of the incident particle. (After Metropolis et al., MET N 58.)

Table 3.V. Secondary cascade and evaporation-particle production, nuclear excitation energy, and temperature for aluminum targets in proton beams of three different energies.

	Proton energy (MeV)		
	450	600	850
Total neutron thick-target yield (n/p on Al	1.3	2.1	3.3
Number of particles per incident proton on Al per inelastic collision:[a]			
Neutrons	1.30	1.40	1.55
Protons	1.85	2.05	2.25
Total nucleons	3.15	3.45	3.80
Residual nuclear excitation E_1 (MeV)[a]	63	72	88
Residual nuclear temperature τ (MeV)[a]	4.3	4.5	4.9
Number of evaporation neutrons per incident or per inelastic collision	1.30	1.50	1.60

[a] See Refs. MAY B 61, LEC K 50, and BAI L 56.

Heavy-Ion Reactions: Neutron Production

Stephens and Miller (STE L 69) have summarized measured neutron yields for proton, deuteron, and α-particle reactions in a variety of target materials in the energy range 10 to 200 MeV, and their results are shown in Fig. 3.40.

Neutron production by heavy-ion bombardment has been investigated by Hubbard et al. (HUB E 60b). Neutron yeilds produced by ^{12}C, ^{14}N, and ^{20}Ne bombardment for a number of target materials were measured. The maximum bombarding energies were 10.4 MeV per nucleon of the bombarding ion. Table 3.VI summarizes their data for thick targets, which are shown graphically in Fig. 3.41.

Table 3.VI. Neutron yield from targets slightly more than one range thick, in units of neutrons per incident ion. The absolute standard errors are estimated to be about 6% except close to the Coulomb barrier, where they are about 50%.

Bombarding ion	Absorber (mg/cm^2 Be)	Calculated energy (MeV)	Neutron yields ($X10^4$)							
			C	Al	Cu	Ag	Ta	Pb	Th	U
^{13}C	0	122	8.0	14.1	17.6	19.6	18.5	18.9	24.7	25.1
	12.6	106				11.3	9.9			10.6
	20.9	92				6.9	4.8			5.2
	29.2	78				3.0	1.6			0.95
^{14}N	0	141	10.4			19.8	19.5			
^{20}Ne	0	201	4.83			16.2	17.1			20.2
	12.6	154	2.17			3.4	4.1			
	20.9	114				0.7	0.22			0.09

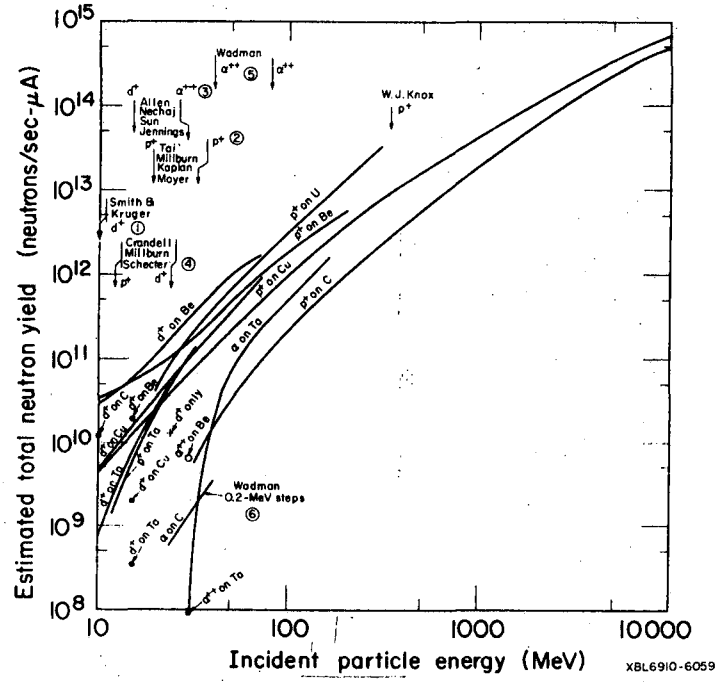

Fig. 3.40. Plot of neutron yields vs incident particle energy for several combinations of targets and ions. (1) Smith and Kruger, $MnSO_4$, (2) Tai, Millburn, Kaplan, and Moyer, Mn SO_4, (3) Allen, Nechaj, Sun, and Jennings, $^{32}S(n,p)^{32}P$, (4) Crandell, Millburn, and Schechter, Mn SO_4, (5) Wadman (40 and 80-MeV α^{++} on Ta), $^{58}Ni(n,p)^{58}Co$, (6) Wadman (23.2- to 40.8-MeV α on C). Moderated BF_3 curve shape accurate; yield value probably high. (From Stephens and Miller, STE L 69.)

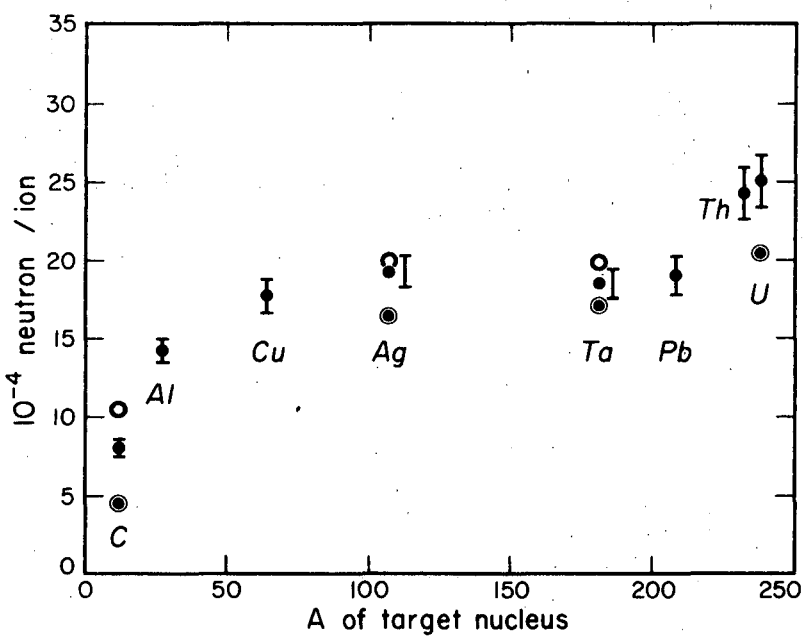

Fig. 3.41. Neutron yields from thick-target bombardments by heavy ions of approximately 10 MeV per nucleon. The points are ● for 122-MeV ^{12}C, O for 141-MeV ^{14}N, and △ for 201-MeV ^{20}Ne. (From Hubbard, HUB E 60b.)

High-Energy Reactions

Ranft has given a semiempirical formula for the proton (or neutron) yield in high-energy proton interactions (RAN J 67a). The double differential cross section is given by

$$\frac{d^2N}{d\Omega} = \left[\frac{A}{p_o} + \frac{Bp}{p_o^2}\left\{1+a\,(1-p_o/p)\right\}\right] X \left[1+a\,(1-\frac{pp_o}{m^2}\,)\right] p^2 \exp(-Cp^2\theta) \quad (6)$$

in units of protons-GeV per steradian per interacting proton, where A, B, and C are constants depending upon the target material; p is the secondary momentum in GeV/c; p_o is the primary proton momentum in GeV/c; $a=[1+(p_o/m)2]^{1/2}$; and m is the proton mass in GeV/c^2.

This formula agrees fairly well with experimental data for proton production from H_2, Be, and Pb targets for the following conditions:

(a) secondary momenta in the range $0.5 \leqslant p \leqslant p_o$,
(b) laboratory angle in the range $0 \leqslant \theta \leqslant 20$ deg,
(c) primary proton momenta in the range $10 \leqslant p_o \leqslant 20$ GeV/c.

Extrapolation of this formula to higher energies is probably reasonable, and it is a fair assumption that neutron and proton spectra are similar from targets other than hydrogen in this region of energy and angle (RAN J 67b).

The angular distribution predicted by the formula is nearly isotropic for low-energy secondaries, in agreement with observation. No account is taken in the formula for evaporation particles, however, and extrapolation to these very low (evaporation) energies is not reliable.

At large angles the simplifying assumption $p \sin\theta \approx p\theta$ breaks down. The exact behavior of the angular distribution is not known, and additional experimental data are needed to establish it precisely.

Equation (6) may be integrated to give the angular distribution of protons produced with momenta greater than some threshold p_{min},

$$\Theta(\theta)_{p>p_{min}} = \int_{p_{min}}^{p_o} \left(d^2N/dpd\Omega\right)dp. \quad (7)$$

Values of $\Theta(\theta)$ have been obtained by numerical integration of Eq. (7) for values of p_o between 1.7 and 300 GeV/c, with different values of p_{min} corresponding to proton energies of 0.1, 20, 150, and 600 MeV. This work is described fully elsewhere (ROU J 71), but a brief description of the results is given here for completeness.

At each threshold energy the family of curves for $\Theta(\theta)$ different incident proton energies is exponentially decreasing about 90 deg (Fig. 3.42). The slope of this exponential is insensitive to primary proton energy and target material, but is a strong function of threshold energy for thresholds above about 50 MeV. The region over which the angular distributions are

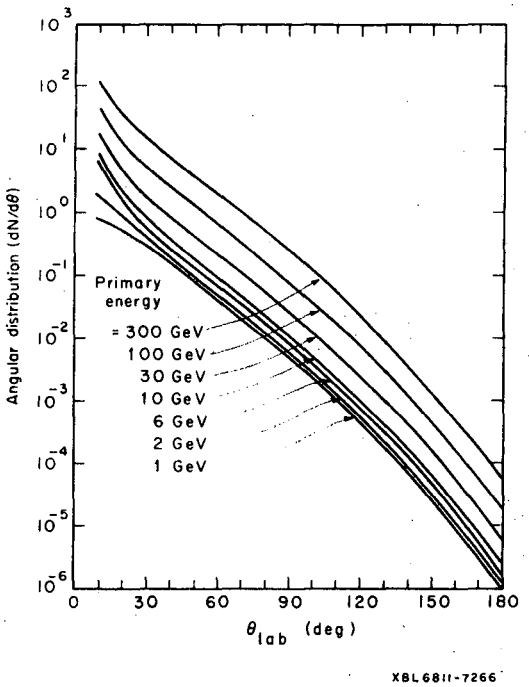

Fig. 3.42. Angular distribution of protons of energy greater than 150 MeV from a thin beryllium target, calculated from Ranft's equation. (After Gilbert et al., GIL W 68.)

exponential depends somewhat upon threshold and primary proton energy, but is always valid from 60 to 120 deg, the angular range which is important in determining the transverse shield thickness of a high-energy accelerator. In this energy range, and for 60 deg $\leqslant \Theta \leqslant$ 120 deg, the angular distribution may therefore be written

$$\Phi(\theta) \approx c\, e^{-a4\theta}. \tag{8}$$

At incident proton energies greater than about 10 GeV, the constant c is proportional to incident proton energy. This may be seen from Fig. 3.43, where $(dn/d\theta)_{90\ deg}$ is plotted as a function of primary proton energy for thresholds of 0, 20, 150, and 600 MeV. The family of curves shown are all asymptotic to unit slope at high incident energies. The lower the threshold energy, the sooner is unit slope achieved. Therefore, in extrapolations to higher energies it is a fairly good approximation to assume that, for energies greater than 10 to 20 GeV, the constant c of Eq. (8) is linearly proportional to incident proton energy. This may result in some small overestimate of

particle fluxes at higher energies if the experimental values of $\Theta(\theta)$ at 10 and 20 GeV are used to obtain value of the normalizing constant in

$$\Theta(\theta) \approx a_2 D\, e^{-a4\theta}. \tag{9}$$

To increase accuracy in the theoretical formula, evaporation-particle production should be considered, and at present no sound theoretical basis exists for any assumptions as to the form of the cross sections at laboratory angles as large as 90 deg. Also a highly accurate interpretation of the experimental data is difficult because of the interference from scattered particles and the finite source extension. A detailed interpretation of the available angular-distribution data is given elsewhere, (ROU J 69, 71).

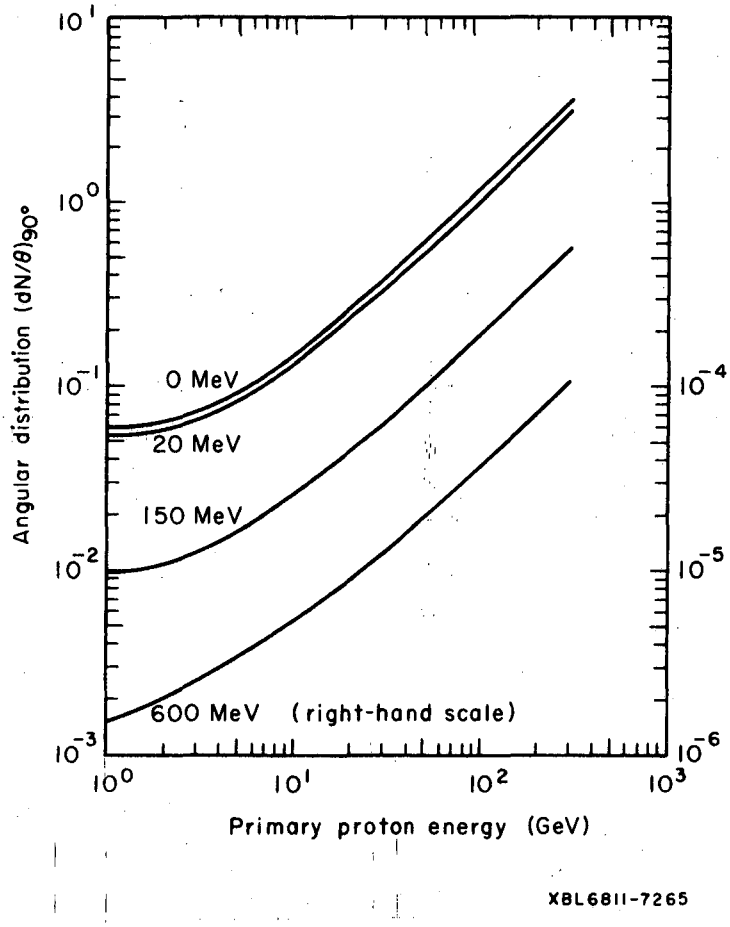

Fig. 3.43. Angular distribution, $(dn/d\theta)_{90°}$, as a function of primary proton energy. (After Gilbert et al., GIL W 68.)

Measurements of the angular distribution of neutrons from a thin beryllium target were made by using threshold detectors as a part of the CERN-LRL-RHEL shielding study (GIL W 68). Accurate measurements around targets inside the main accelerator vacuum chamber are difficult because of interference from adjacent beam losses. The results, however, when corrected for this interference, are supported by similar results from measurements made by Charalambus et al. (CHA S 67).

The results from activation detectors with thresholds of 20 and 600 MeV are in fair agreement with the angular distribution predicted from the production formula due to Ranft (RAN J 67a),based on the measurements of the pion and proton yields at small angles from thin targets. Figures 3.44 and 3.45 show the comparison of the CERN-LRL-RHEL measurements of the angular distributions made by using $^{12}C \rightarrow {}^{11}C$ (20 MeV threshold) and $Hg \rightarrow {}^{149}Tb$ (600 MeV threshold) activation detectors with values calculated from the Ranft formula (RAN J 67a).

μ-Meson Production at High-Energy Accelerators.

For accelerators below about 10 GeV, μ mesons produce few problens because the shield necessary to reduce radiation levels arising from nuclear cascade processes to tolerable levels is in excess of the ionization range of the μ mesons that could contribute to the radiation problems. The higher the intensity of machines below 10 GeV, the stronger is this effect. Lindenbaum (LIN S 61) pointed out that the Brookhaven AGS and CERN-PS were the first proton accelerators in which μ mesons would dominate some radiation problems. As previously discussed, Cowan (COW F 62) has reported the initial operational difficulties due to μ-meson production at the Brookhaven AGS.

The major source of μ mesons is π-meson and K-meson decay. Essentially all pions and about two-thirds of kaons decay into a muon and a neutrino. Once the μ meson is produced its only really significant mode of losing energy is by ionization, as its cross section for nuclear interactions is very small (a few microbarns). Thus the major difficulty that arises when μ mesons are produced is their effective removal. Since this is a health physics problem found at only a handful of accelerators, a complete discussion is not given here, but rather the pertinent literature is indicated for the interested reader.

Keefe (KEE D 64) has given a simple one-dimensional treatment that indicates the physical nature of the problem. Assuming π mesons to be produced in a target irradiated by high energy protons, Keefe writes the μ-meson spectrum, $n_\mu(E,\Delta)$, at the end of a drift space beyond the target as

$$n_\mu(E,\Delta) \approx \frac{1}{\Lambda(1-k)E} \int_E^{E_{max}} \Delta S_m(E',x_0) \frac{dE'}{E'^2} \quad ,$$

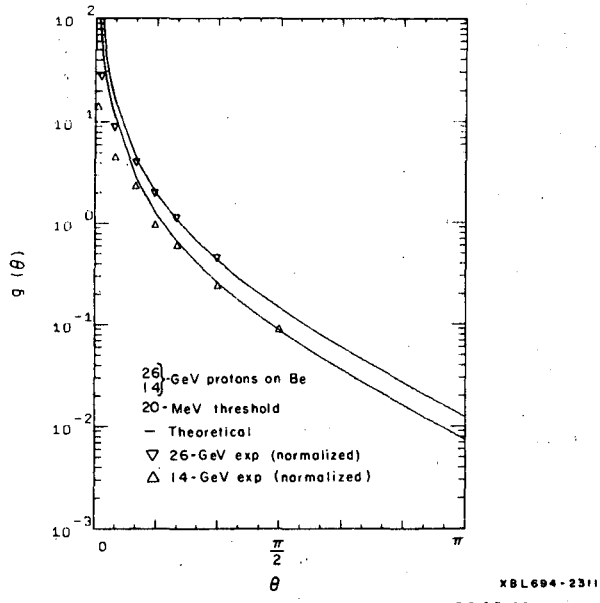

Fig. 3.44. The angular distribution of neutrons above 20 MeV energy produced by 26- and 14-GeV proton beams incident on a thin target, as measured by Gilbert et al. (GIL W 68.) and calculated from the Ranft formula.

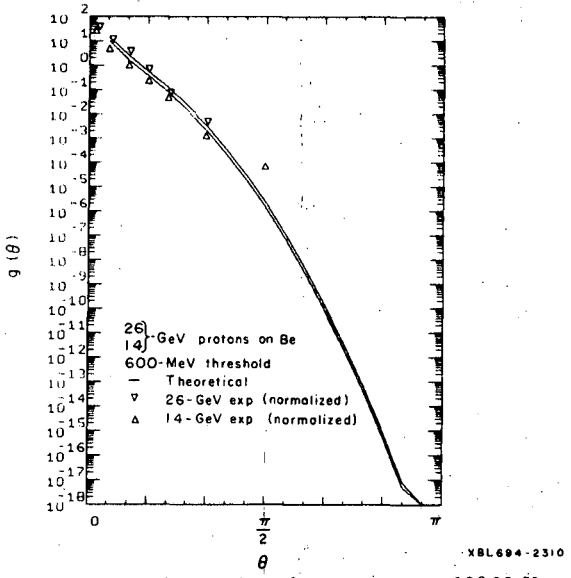

Fig. 3.45. The angular distribution of neutrons above 600 MeV energy produced by 26- and 14-GeV proton beam incident on a thin target, as measured by Gilbert et al. (GIL W 68.) and calculated from the Ranft formula.

where

Δ is the length of drift space,

$S_m(E',x)$ is the (differential) energy spectrum of the primary meson at depth x,

x_o is the target thickness,

$n_\mu(E,\Delta)$ is the primary meson of energy E'.

The primary meson of energy E' was assumed to produce a rectangular μ-decay spectrum between kE' and E'.

E_{max} is the smaller of E/k or E_o, the primary energy. By using the differential spectra proposed by Cocconi et al. (COC G 61), Keefe dervied the number of μ mesons transmitted by a shield. He showed that the effective attenuation length is about 4500 g/cm^2 (compared with 150 g/cm^2 for strongly interacting particles), increasing to about 6000 g/cm^2 at the highest energies (thick shields).

A full treatment of the transmission of the μ mesons through shielding must be performed in three dimensions and include multiple Coulomb scattering effects. Such calculations are reported in the LRL 200 BeV Accelerator Design Study (LRL 65), and have been extended by Nelson (NEL W 66a,b, 68) Keefe and Noble (KEE D 68), and Alsmiller et al. (ALS R 68,69). Operation of the 200 to 500 GeV proton synchrotron at the National Accelerator Laboratory, Batavia, will provide the first opportunity to study the health physics aspects of μ-meson production experimentally.

REFERENCES

A DA J 59 J. Adams, (Chairman), Status Reports on High-Energy Accelerators, Session 3A, in Proceedings of an International Conference on High Energy Accelerators and Instrumentation, CERN, 1959. (See Also CERN 60-4, 15 Feb. 1960.)

ALL A 51 A. J. Allen, J. F. Nechaj, K. H. Sun, and B. Jennings. Thick-Target Fast Neutron Yield from 15-MeV Deuteron and 30-MeV Alpha Bombardment, Phys. Rev. *81*, 536 (1951).

ALS R 68 R. G. Alsmiller et al., High Energy Muon Transport and the Muon Backstop for a 200 GeV Proton Accelerator, ORNL-4322, Nov. 1968.

ALS R 69 R. G. Alsmiller and J. Barish, High Energy Muon Transport and the Muon Backstop for a Multi-GeV Accelerator, ORNL-4386, March 1969.

ALV L 46 L. W. Alvarez, The Design of a Proton Linear Accelerator, Phys. Rev. *70*, 799 (1946).

AND R 69 R. A. Andrews et al., Design of the 200 GeV Slow Extracted Beam at NAL, National Accelerator Laboratory Internal Report C26, 1969.

AUS A 69 N. A. Austin et al., A Compact 4-MeV Linear Accelerator for Use in Cancer Therapy, in *Proceedings of the Second International Conference on Accelerator Dosimetry and Experience, Stanford, California,* Nov. 5-7, 1969, CONF-691101, p. 11.

BAA J 65 J. Baarli, and A. H. Sullivan, Radiation Dosimetry for Protection Purposes Near High Energy Particle Accelerators, Health Phys. *11*, 353 (1965).

BAI L 56 L. E. Bailey, Angle and Energy Distributions of Charged Particles from the High Energy Nuclear Bombardment of Various Elements (Ph.D. Thesis), UCRL-3334, March 1956.

BAL F 50 G. C. Baldwin, and F. R. Elder, Neutron Production in Various Substances by 50-MeV x Rays, Phys. Rev. *78*, 76 (1950).

BAN A 61 A. P. Banford and G. H. Stafford, The Feasibility of a Superconducting Proton Linear Accelerator, J. Nucl. Energy *C3*, 287 (1961).

BAR M 61 M. W. Barton, Catalog of High Energy Accelerators, Brookhaven National Laboratory Internal Report BNL-683, Sept. 6, 1961.

BAT G 67 G. Bathow, E. Freytag, and K. Tesch, Measurements on 6.3-GeV Electromagnetic Cascade and Cascade-Produced Neutrons, Nucl. Phys. *B2* 669 (1967).

BEN R 40 R. G. T. Bennet, U.S. Patent 2206558, 1940.

BER H 69 H. Bertini, Calculations of Nuclear Reactions for Incident Nucleons and π Mesons in the Energy Range 30 to 2700 MeV, in *Proceedings of the Second International Conference on Accelerator Dosimetry and Experience, Stanford, California, November 5-7, 1969.* CONF-691101, p. 42.

BET H 52 H. Bethe, and J. Atkin, Passage of Radiations Through Matter, Part II, in *Experimental Nuclear Physics* Ed. E. Segrè (John Wiley, New York, 1952).

BLU L 56 L. Blumberg and S. I. Schlesinger, Relativistic Tables of Energy and Angle Relationships for the T(p,n) He, D(d,n) He, and T(d,n) He Reactions, U.S. Atomic Energy Commission Report AECU-3118, 1956).

BLE E 53 E. Bleuler, A. K. Stebbins, and D. J. Tendam, The (α,n) and (α,2n) Cross Sections of ^{109}Ag, Phys. Rev. *90,* 460 (1953).

BOV C 64 C. Bovet, G. H. Lawrence, and K. H. Reich, Measurements on Slow Beam Ejection from the CPS, CERN 64-25, 1964.

BRA C 58 C. B. Braestrup, and H. O. Wyckoff, *Radiation Protection* (Charles Thomas, Springfield, Ill., 1958).

BRE G 28 G. Breit, O. Dahl, and M. A. Tuve, Magnetism and Atomic Physics, in Carnegie Institution of Washington Yearbook *27,* 209 (1928).

BRO J 60 J. E. Brolley, Jr., and J. L. Fowler, Monoenergetic Neutron Sources: Reactions with Light Nuclei, in *Fast Neutron Physics,* Ed. J. B. Marion and J. L. Fowler, Interscience Publishers, New York and London 1960, Chap. I.C.

BUR E 64 E. A. Burrill, Van de Graaff Accelerators for Radiation Research and Applications, in *Radiation Sources,* Ed. by A. Charlesby (Pergamon Press, London, 1964).

BUR E 68a E. A. Burrill, X-Ray Generators, Sect. 2.2.1.1 in *Engineering Compendium on Radiation Shielding,* Vol. 1 (Springer-Verlag, Berlin, 1968).

BUR E 68b E. A. Burrill, Van de Graaff and Other Direct Electron Accelerators, Sect. 2.2.1.2 in *Engineering Compendium on Radiation Shielding,* Vol. 1, (Springer-Verlag, Berlin, 1968).

BUR E 69 E. A. Burrill, The Expanding Use of Particle Accelerators in Research, Medicine, and Industry: A Statistical Review, in *Proceedings of the Second International Conference on Accelerator Dosimetry and Experience, Stanford, California, November 5-7, 1969,* CONF-691101, p. 1.

BUS D 69 D. D. Busick et al., Beam Safety Considerations of the Stanford Linear Accelerator Center, in *Proceedings of the Second International Conference on Accelerator Dosimetry and Experience, Stanford, California, November 5-7, 1969,* CONF-691101, p. 782.

CAR T 69a T. G. Carter et al., Radiation Surveys, High Energy Physics Laboratory, Mark III Electron Linac, Oct. 30-31, 1968, I. Film Badge Measurements, Stanford University Internal Report, RHT/TN/69-10, Sept. 20, 1969.

CAR T 69b T. G. Carter et al., Radiation Survey, High Energy Physics Laboratory, Mark III Electron Linac, Oct. 1-2, 1969, Stanford University Internal Report, RHT/TN/69-25, Oct. 27, 1969.

CHA S 67 S. Charalambus, K. Goebel, and D. Nachtigall, Angular Distribution of SEcondary Particles and Dose Rates Produced by 19.2 GeV/c Protons Bombarding Thin Be, Al, Cu, and U Targets, CERN DI/HP/97, March 14, 1967.

CHA V 69 V. M. Chakalian et al., Radiation Surveys, High Energy Physics Laboratory, Mark III Electron Linac, Oct. 30-31, 1968, II. Activation Detector Measurements, Stanford University Internal Report, RHT/TN/69-11, Sept. 30, 1969.

CLE M 65 M. Cleland, Dynamitrons of the Future, IEEE Trans. on Nucl. Sci. *12* [3], 227 (June 1963).

COC G 61 G. Cocconi, L. J. Koester, and D. H. Perkins, Calculation of Particle Fluxes from Proton Synchrotrons of Energy 10 GeV to 1000 GeV, in *Berkeley High Energy Physics Study Summer 1961*, UCRL-10011, 1961.

COC J 32 J. D. Cockcroft, and E. T. S. Walton, Experiments with High Velocity Positive Ions, Proc. Roy. Soc. (London) *A136*, 619 (1932).

COL F 69 F. J. Coleman et al., Studies of the Cascades Induced by 4-GeV Electrons in Concrete, in *Proceedings of the Second International Conference on Accelerator Dosimetry and Experience, Stanford, California, November 5-7, 1969*, CONF-691101, p. 209.

COW F 62 F. P. Cowan, A Preliminary Report on Health Physics Problems at the Brookhaven Alternating Gradient Synchrotron, in *Premier Colloque International sur la Protection Auprès des Grands Accélerateurs*, Presses Universitaires de France, Paris, 1962.

DEP J 69 J. De Pangher, and E. Tochlin, Neutrons from Accelerators and Radioactive Sources, Chapter 23 in *Radiation Dosimetry*, Vol. 3 Ed. F. H. Attix and E. Tochlin (Academic Press, New York, 1969).

DES H 62 H. De Staebler, Transverse Radiation Shielding for the Stanford Two-Mile Accelerator, USAEC Report SLAC-9, Stanford Linear Accelerator Center, Nov. 1962.

DES H 65 H. De Staebler, Similarity of Shielding Problems at Electron and Proton Accelerators, in *Proceedings of the First Symposium on Accelerator RAdiation Dosimetry and Experience, Brookhaven National Laboratory, November 3-5, 1965*, CONF 651109, p. 429.

DIS C 64 C. Distenfeld, (Brookhaven National Laboratory) private communication.

DEU R 55 R. W. Deutsch, Phys. Rev. *97*, Analysis of Secondary Particles Resulting from High-Energy Nuclear Bombardment, 1110 (1955).

DOS I 58 I. Dostrovsky, P. Rabinowitz, and R. Bivins, Monte Carlo Calculations of High-Energy Nuclear Reactions. I. Systematics of Nuclear Evaporation, Phys. Rev. *111* 1659 (1958).

EVA R 55 R. D. Evans, *The Atomic Nucleus* (McGraw-Hill, New York, 1955).

FAR F 64 F. J. M. Farley and B. S. Carter, Background Radiation in an Enclosure Following a Short Burst of Radiation from a Pulsed Accelerator, Nucl. Instr. Methods *28*, 279 (1964).

FES J 69 J. Festag, Comparisons Between Dose Rate Measurements with Protons, Deuterons, Helium, Ions and Heavy Ions at the Heidelberg Tandem and Emperor Van de Graaff Accelerators, in *Proceedings of the Second International C Conference on Accelerator Dosimetry and Experience, Stanford, November 5-7, 1969*, CONF-691101, p. 764.

FRY D 49 D. W. Fry, and W. Walkinshaw, Repts. Progr. in Phys. *12*, 102 (1949).

FUJ Y 50 Y. Fujimoto and Y. Yamaguchi, On the Nuclear Stars, Progr. Theoret. Phys. (Kyoto) *4*, 468 (1950); Note on Very Large Cosmic-Ray Stars, *ibid. 5*, 76 (1950); High Energy Nuclear Evaporation, *ibid*, *5*, 787 (1950).

GIB J 56 J. H. Gibbons, Neutron Resonances in the keV Region, Phys. Rev. *102*, 1574 (1956).

GIB J 58 J. H. Gibbons and R. L. Macklin, Total Cross Section for $T(t,n)^3He$, Bull. Am. Phys. Soc. *3, 365* (1958).

GIB J 59 J. H. Gibbons and R. L. Macklin, Total Neutron Yields from Light Elements Under Proton and Alpha Bombardment, Phys. Rev. *114*, 571 (1959).

GIB J 60 J. H. Gibbons and H. W. Newson: The $^7Li(p,n)^7Be$ Reaction, "*Fast Neutron Physics*," Ed. J. B. Marion and J. L. Fowler (Interscience Publishers, New York and London, 1960), Chap. I.E.

GIL W 68 W. S. Gilbert, et al., 1966 CERN-LRL-RHEL Shielding Experiment at CERN, UCRL-17941, Sept. 1968.

GIN E 48 E. L. Ginzton, W. W. Hansen, and W. R. Kennedy, A Linear Electron Accelerator, Rev. Sci. Instr. *19*, 89 (1948).

GLA O 61 D. Glasser, E. H. Quimby, L. S. Taylor, J. L. Weatherwax, and R. H. Morgan, *Physical Foundation of Radiology*, 3rd Ed. (Paul B. Hoeber, Inc., Medical Division of Harper and Brothers, New York 1961).

GOO W 53 W. F. Goodell, Jr., H. H. Loar, R. P. Durbin, and W. W. Havens, Jr., Neutron Energy Distribution from the Proton Bombardment of Li, Be, and C at 375 MeV, Phys. Rev. *89*, 724 (1953).

GOR H 63 H. S. Gordon and G. A. Behman, Particle Accelerators, Chapter 8 in *Nuclear Physics*, Ed. L. F. Curtiss American Inst. Physics Handbook (McGraw-Hill Book Co., New York 1963).

GOW F 46 F. K. Goward, and D. E. Barnes, Experimental 8-MeV Syn chrotron for Electron Acceleration, Nature *158*, 413 (1946).

GOW F 50 F. K. Goward, Betatrons and Synchrotrons, in *The Acceleration of Particles to High Energies* (Institute of Physics, London, 1950); p. 14.

GRU E 33 E. H. Grubbe, Priority in the Therapeutic Use of X Rays, Radiology *21*, 156 (1933).

HAN R 55 R. C. Hanna, Disintegration of ^{7}Be by Slow Neutrons. Phil. Mag. *46*, 381 (1955).

HEI W 36 W. Heiter, *The Quantum Theory of Radiation* (Oxford, London, 1936).

HER H 65 H. G. Hereward, J. Ranft, and W. Richter, Efficiency of Multi Traverse Targets, CERN Internal Report CERN 65-1, Jan. 6, 1965.

HOW F 67 F. T. Howard, High Energy Accelerators in 1967, in *Proceedings of the Sixth International Conference on High Energy Accelerators*, Cambridge, Mass., Sept. 11-15, 1967, CEAL-2000.

HUB E 60a E. L. Hubbard et al., Heavy-Ion Linear Accelerator, UCRL-9453, Nov. 1060.

HUB E 60b E. L. Hubbard et al., Neutron Production by Heavy-Ion Bombardments, Phys. Rev. *118*, 507 (1960).

IAEA 64 IAEA, Photonuclear Reactions, Bibliographical Series No. 10 Vienna (1964).

JAR G 57 G. A. Jarvis. Curves in Los Alamos Scientific Laboratory Report LA-2014, 1957.

KEE D 64 D. Keefe, μ-Meson Shielding Problems at 200 GeV--Approximate Calculations, LRL Internal Report UCID-10018, May 20, 1964.

KEE D 68 D. Keefe and C. M. Noble, Radiation Shielding for High Energy Muons--The Case of a Cylindrically Symmetric Shield and the Magnetic Field, Nucl. Instr. Methods *64*, 173, 1968).

KEE D 70 D. Keefe, Research on the Electron Ring Accelerator, Particle Accel. *1*, 1 (1970).

KER D 41 D. W. Kerst, The Acceleration of Electrons by Magnetic Induction, Phys. Rev. *60*, 47 (1941).

LAN L 51 L. H. Lanzl and A. O. Hanson, Z Dependence and Angular Distribution of Bremsstrahlung from 17-MeV Electrons, Phys. Rev. *83*, 959 (1951).

LAW E 30 E. O. Lawrence and N. E. Edlefsen, On the Production of High Speed Protons, Science *72*, 376 (1930)..

LAW E 31 E. O. Lawrence and M. S. Livingston, The Production of High Speed Protons Without the Use of High Voltages, Phys. Rev. *38*, 834 (1931).

LAW J 50 J. D. Lawson, Angular Distribution of Synchrotron Target Radiation--A Preliminary Experimental Study, Proc. Phys. Soc. (London) *A63*, 653 (1950).

LAW J 52 J. D. Lawson, Radiation Characteristics of High Energy Electron Accelerator Targets, Nucleonics *10* [11], 61 (1952).

LEC K 50 K. J. Le Couteur, The Evaporation Theory of Nuclear Disintegrations, Proc. Phys. Soc. (London) *A63*, 259 (1950).

LIN S 61 S. J. Lindenbaum, Shielding of High-Energy Accelerators, Ann. Rev. Nucl. Sci. *11*, 213 (1961).

LIV J 61 John J. Livingood, *Principles of Cyclic Particle Accelerators* D. Van Nostrand, (1961).

LIV M 49 M. S. Livingston, J. P. Blewitt, G. K. Green, and L. J. Haworth, Design Study for a 3-BeV Accelerator, Rev. Sci. Instr. *21*, 7 (1950).

LIV M 62 M. S. Livingston and J. P. Blewitt, *Particle Accelerators* (McGraw-Hill Book Company, New York 1962).

LRL-65 Lawrence Radiation Laboratory, 200 BeV Design Study, Chapter 12, UCRL-16500, June 1965.

MAC M 57a H. H. MacGregor, Production of Gamma Radiation with a Linear Electron Accelerator, Applied Radiation Co. Internal Report AM 100, March 1957.

MAC M 57b M. H. MacGregor, A Summary of Experimental Data on Neutron and Bremsstrahlung Production by Linear Electron Accelerators, Applied Radiation Co., Walnut Creek, Calif., Internal Report AM 102, March 6, 1957.

MAC R 58a R. L. Macklin and J. H. Gibbons, (p,n) Reactions in Light Nuclei, Bull. Am. Phys. Soc. *3*, 26 (1958).

MAC R 58b R. L. Macklin and J. H. Gibbons, Study of the $T(p,n)^3He$ and $^7Le(p,n)^7Be$ Reactions, Phys. Rev. *109*, 105 (1958).

MAD R 68 R. Madey, Nucleon Accelerators in General, Sect. 2.2.2.1 in *Engineering Compendium on Radiation Shielding*, Vol. I (Springer-Verlag, Berlin, 1968).

McM E 45 E. M. McMillan, The Synchrotron--A Proposed High Energy Particle Accelerator, Phys. Rev. *68*, 143 (1945).

McM E 59 E. M. McMillan, Particle Accelerators. Part XII in *Experimental Nuclear Physics* Vol. III, Ed. E. Segrè (John Wiley and Sons, Inc., New York, 1959).

MET N 58 N. Metropolis, R. Bivins, M. Storn, A. Turkevich, J. M. Miller, and G. Friedlander, Monte Carlo Calculations on Intranuclear Cascades. I. Low-Energy Studies. II. High-Energy Studies and Pion Processes, Phys. Rev. *110*, 185 (1958); *110*, 204 (1958).

MIL C 53 C. W. Miller, Metropolitan-Vickers Gazette, Dec. 1952.

MOR A 66 A. Morris et al., A Remote-Reading Integrating Radiation Dosimeter for the Range 10^4– 10^7 Rads, Rutherford Laboratory report RHEL/R132, Oct. 1966.

MOY B 61 B. J. Moyer (Lawrence Radiation Laboratory), Data related to nuclear star production by high-energy protons private communication, June 20, 1961.

MUI E 52 E. Muirhead, B. M. Spicer, and H. Lichtblau, The Angular Distribution of Synchrotron Target Radiation, Proc. Phys. Soc. (London) *A65*, 59 (1952).

NBS 54 National Bureau of Standards Handbook # 55, Protection Against Betatron-Synchrotron Radiations up to 100 Million Electron Volts, Feb. 26, 1954.

NBS 64 National Bureau of Standards Handbook # 97, Shielding for High Energy Electron Accelerator Installations, July 1, 1964.

NCRP 68 Medical X-Ray and γ-Ray Protection for Energies up to 10 MeV in Equipment Design and Use, Report No. 33, NCRP Washington, Feb. 1, 1968.

NCRP 70 Medical X-Ray and γ-Ray Protection for Energies up to 10 MeV-Shielding Design and Evaluation, Report No. 34, NCRP Washington, March 2, 1970.

NEL W 66a W. R. Nelson, Multiple Elastic Scattering of Muons with Energy Loss, SLAC Internal Report, SLAC-TN-66-41, Stanford Linear Accelerator Center, Stanford, 1966.

NEL W 66b W. R. Nelson, Muon Production Calculations for Muon Shielding, SLAC Internal Report SLAC-TN-66-37, Stanford Linear Accelerator Center, Stanford, California, 1966).

NEL W 68 W. R. Nelson, The Shielding of Muons Around High Energy Electron Accelerators--Theory and Measurements, Nucl. Instr. Methods *66*, 293 (1968).

PAT H 62 H. W. Patterson, The Effect of Shielding on Radiation Produced by the 730-MeV Synchrocyclotron and the 6.3-GeV Proton Synchrotron at the Lawrence Radiation Laboratory, in *Premier Colloque International sur la Protection Auprès des Grands Accelérateurs*, Presses Universitaires de France, Paris, 1962.

PER D 66 D. R. Perry, Neutron Dosimetry Methods and Experience on the 7-GeV Proton Synchrotron, "Nimrod," in *Proceedings IAEA Symposium on Neutron Monitoring for Radiological Protection, Vienna, August 1966.*

PRI G 50 G. A. Price and D. W. Kerst, Yields and Angular Distributions of Some Gamma-Neutron Processes, Phys. Rev. *77*, 806 (1950).

PRI W 58 William J. Price, *Nuclear Radiation Detection* (McGraw-Hill Book Co., New York, 1958).

RAN J 67a J. Ranft, Improved Monte Carlo Calculation of the Nucleon-Meson Cascade in Shielding Material. I. Description of the Method of Calculation, Nucl. Instr. Methods *48*, 133 (1967).

RAN J 67b J. Ranft (CERN), private communication, 1967.

RAN J 69 J. Ranft, Calculation of Beam Loss Distributions and Radiation Doses on Magnets in Proton Synchrotrons, in *Proceedings of the Second International Conference on Accelerator Dosimetry and Experience, Stanford, November 5-7, 1969,* CONF-691101, p. 416.

ROU J 69 J. Routti and R. H. Thomas, Moyer In tegrals for Estimating Shielding of High Energy Accelerators, Nucl. Instr. Methods *76*, 157 (1969).

ROU J 71 J. Routti and R. H. Thomas, Angular Distribution of Secondary Neutrons and Protons from High-Energy Interactions, in preparation.

SCH L 55 L. Schecter, W. E. Crandall, G. P. Millburn, and J. Ise, Jr., Cross Sections for producing High-Energy Neutrons from Carbon Targets Bombarded by Protons, Deuterons, and ^{3}He Particles, Phys. Rev. *97*, 184 (1955).

SER R 47 R. Serber, The Production of High Energy Neutrons by Stripping, Phys. Rev. *72*, 1008 (1947).

SHA K 67 K. B. Shaw and R. H. Thomas, Radiation Problems Associated With High Energy Extracted Proton Beam, Health Phys. *13*, 1127 (1967).

SLAC 69 SLAC, Feasibility Study for a Two-Mile Superconducting Accelerator, SLAC Internal Report, 1969.

SLE J 27 J. Slepian, U. S. Patent No. 1645304 (filed March 1922) (1927).

SLO D 31 D. H. Sloan and E. O. Lawrence, The Production of Heavy High Speed Ions Without the Use of High Voltage, Phys. Rev. *38*, 2021 (1931).

SMI A 65 A. R. Smith, Some Experimental Shielding Studies at the 6.2-BeV Berkeley Bevatron, in *Proceedings of the First Symposium on Accelerator Radiation and Experience, Brookhaven National Laboratory, Nov. 3-5, 1965,* CONF-651109, p. 365.

STE L 69 L. D. Stephens and A. J. Miller, Radiation Studies at a Medium Energy Accelerator, in *Proceedings of the Second International Conference on Accelerator Dosimetry and Experience, Stanford, California November 5-7, 1969*, CONF-691101, p. 459.

SZE A 68 A. Szeless and L. Ruby, Optimization Experiment Designed to Measure Experimental Decay Constants, Nucl. Instr. Methods *68*, 181 (1969).

TEN D 47 D. J. Tendam and H. L. Bradt, The Relative Yields of (α,n) and (α,2n) Reactions for Ag and Rb With 15-20 MeV α Particles, Phys. Rev. *72*, 1117 (1947(.

TER K 51 K. M. Terwilliger, L. W. Jones, and W. N. Jarmie, Relative Photo-Neutron Yield from 330-MeV Bremsstrahlung, Phys. Rev. *82*, 820 (1951).

TES K 69 K. Tesch, Radiation Problems Around the DESY 7-GeV Electron Accelerator, in *Proceedings of the Second International Conference on Accelerator Dosimetry and Experience, Stanford, California, November 5-7, 1969*, CONF-691101, pp. 252, 595.

THE D 70a D. Theriot, Muon dE/dx and Range Tables - Preliminary Results for Shielding Materials, National Accelerator Laboratory Internal Report TM-229, March 30, 1970.

THE D 70b D. Theriot, Muon dE/dx and Range Tables: Results for Shielding Materials National Accelerator Laboratory Internal Report TM-260 July 21, 1970.

THE D 70c D. Theriot and M. Awschalom, Muon Shielding Design Studies of Homogeneous Soil Shields at 200 GeV, National Accelerator Laboratory Internal Report TM-245, May 14, 1970.

THO R 62 R. H. Thomas, Skyshine Measurements Around the Rutherford Laboratory Proton Linear Accelerator, in *Premier Colloque International sur la Protection Auprés des Grands Accèlerateurs*, Presses Universitaires de France, Paris, 1962.

THO R 68 R. H. Thomas, The Proton Synchrotron as a Source of Radiation, in *Engineering Compendium on Radiation Shielding*, Sec. 2.2.22 Vol. 1 (Springer-Verlag, Berlin, 1968).

THO R 69 R. H. Thomas, Specification for a Heavy-Particle Accelerator, Stanford University Internal Report RHT/TN/69-13, July 15, 1969.

TOM M 65 M. E. Toms, Bibliography No. 24, U. S. Naval Research Laboratory, Washington, D. C., July 1965.

VON G 58 G. Von Dardel and N. G. Sjostrand, *Physics and Mathematics*, Vol. 2 (in Progress in Nuclear Energy Series I, 1958), p. 183.

VAN R 31 R. J. Van de Graaff, A 1 500 000-Volt Electrostatic Generator, Phys. Rev. *48*, 315 (1931).

VAS R 68 R. G. Vasilkov et al., Mean Number of Secondary Neutrons Evaporated from Nuclei Bombarded by High-Energy Protons, Soviet J. Nucl. Phys. *7*, 64 (1968).

VEK V 45 V. Veksler, A New Method of Acceleration of Relativistic Particles, J. Phys. USSR *9*, 153 (1945).

WAL E 29 E. T. S. Walton, Proc. Cambridge Phil. Soc. *25*, 469 (1929).

WAL R 62 R. Wallace, Shielding and Activation Considerations for a Meson Factory, Nucl. Instr. Methods *18 & 19*, 405 (1962).

WAL R 65 R. Wallace, Cyclotron Shielding, UCRL-11315, Aug. 11, 1965.

WAT A 57 A. Wattenberg, Nuclear Reactions at High Energy, in *Encyclopedia of Physics, Vol. 40* (Springer-Verlag, Berlin, 1957).

WID R 28 R. Wideröe, A New Principle for the Generation of High Voltage, Arch. Elektrotech. *21* (4), 387 (1928).

WID R 68a R. Wideröe, Betatrons and Synchrotrons, in *Engineering Compendium on Radiation Shielding* (Springer-Verlag, Berlin, 1968), Sect. 2.2.1.3, Vol. 1.

WID R 68b R. Wideröe, Linear Electron Accelerators, in *Engineering Compendium on Radiation Shielding*, Vol. 1 (Springer-Verlag, Berlin, 1968), Sect. 2.2.1.4.

CHAPTER 4.

HUMAN RESPONSE TO IONIZING RADIATION

TABLE OF CONTENTS

HUMAN RESPONSE TO IONIZING RADIATION

INTRODUCTION

Accelerator health physicists have two direct reasons for understanding the human response to ionizing radiations. Accelerator personnel is usually exposed chronically under well-controlled conditions to radiation at low levels of dose and dose rate. Guidelines, codes of practice, and legal requirements have been established to assist the health physicist in his duties of radiation protection, and it is well to understand the scientific basis for these radiation exposure limits. In addition, at particle accelerators there is the possibility of serious injury or death due to irradiation in accelerator beams. Familiarity on the part of the health physicist with the symptoms exhibited after acute radiation exposures may in some circumstances mitigate serious injury of prevent loss of life.

Table 4.I indicates the range of radiation exposures experienced in practice and the biological responses due to them.

Radiobiology has developed to the status of a separate discipline, and no brief review such as this can be comprehensive. However, many excellent review articles and texts have appeared in the past few years that can assist the accelerator health physicist in the performance of his duties. Some of these are indicated in the bibliography at the end of this chapter.

Table 4.I. Radiation exposure: human response and maximum permissible dose.

Dose equivalent (rem)	Response	Conditions of applicability
1000[a]	Certainty of death	
300[a]	50% probability of death within 30 days ($LD_{50/30}$)	
50	Changes in peripheral blood	
5		Maximum permissible annual dose equivalent for radiation workers over several years
0.5		Maximum permissible annual dose equivalent for members of general population in boundary of nuclear installations
0.17		Maximum permissible annual exposure to the critical segment of the population (based on genetic considerations) (5 rem/30 years)

a. Acute dose given in less than 24 hours.

GENETIC AND SOMATIC EFFECTS

Biological effects may conveniently be subdivided into two groups:

a. genetic effects, which occur in the reproductive cells and may be inherited.

b. somatic effects, which arise from damage to all cells in the body, and are observable in the individual affected

Thus the basic difference between genetic damage and somatic damage is that the latter may result in injury to the individual exposed to radiation, whereas genetic damage is observable in subsequent generations.

ACUTE AND LATENT SOMATIC EFFECTS

In discussing somatic effects it is convenient to further subdivide them into two groups,

a. short-term (or acute) effects, and

b. long-term (or latent) effects.

(genetic effects are of course always, in a sense, long term.)

Short-term effects arise from large acute exposures in excess of about 100 rads, and are observed in a few days or weeks after exposure. This division into short- and long-term effects is, of course, arbitrary, but symptoms occurring later than 60 days after the radiation insult are generally referred to as long term. Experience has shown that, in general, symptoms that do not appear within 2 months have latent periods of many months or years.

Studies of both short- and long-term effects of radiation are of immense importance in the establishment of guidelines for minimizing the risk inherent in the use of ionizing radiations. Thus the first radiation-protection standards were devised to protect workers from acute radiation effects. The radiation-protection standards currently recommended by ICRP for non-radiation workers are largely based upon estimates of the deleterious genetic effects resulting from the irradiation, at low levels, of large populations. Continuing studies are aimed at evaluating the risk, if any, of long-term somatic injury resulting from low-level chronic exposures.

SHORT-TERM SOMATIC EFFECTS

Short-term acute radiation effects may be characterized by the following features:

a. They are observed only after integrated doses of 50 rads or more delivered in a period of a few hours or less.

b. They exhibit a threshold, i.e., there is some dose below which they never occur.

c. They show dose-rate dependence, an effect that is greatest for low-LET radiation and smallest for high-LET radiation.

d. They exhibit, in general, a nonlinear response-dose relation.

These four characteristics are best identified by a discussion of specific examples, particularly of the acute radiation syndrome.

DEATH

The most serious manifestation of radiation injury following massive whole-body exposure to radiation is the ultimate death of the individual.

Study of the lethality of ionizing radiation toward experimental animals has facilitated a deeper understanding of acute radiation effects in man. Typical results obtained when mice are exposed to a single whole-body dose of radiation are shown in Fig. 4.1. The fraction of the irradiated population dying within 30 days is plotted as a function of radiation dose: the sigmoid curve is characteristic of all such experiments. Points to be noted are:

a. A distinct threshold is observed. Thus below $\approx$ 200 rads there is no possibility of death following acute radiation.

b. The dose-effect curve is nonlinear.

c. Beyond doses of $\approx$ 1000 rads there is no possibility of survival.

Experiments with different genetic strains of mice have shown the width of the sigmoid curve to depend strongly upon the intrinsic variability of the irradiated animals. Thus closely inbred strains of mice show much narrower dose-effect curves than do wild mice.

Experiments such as these allow measurements of $LD_{50/30}$ (the dose required to kill 50% of a population within 30 days) for different species, and typical data are summarized in Table 4.II, which is taken from a review article by Bond (BON V 68a).

Table 4.11. Radiation $LD_{50/30}$ values for different species. [After V.P. Bond (BON V 68a)]

Species	$LD_{50/30}$ (Midline absorbed dose, rads)
Sheep	155
Burro	155
Swine	195
Goat	230
Dog	265
Man	270
Man	243
Man	225
Rabbit	840
Mouse	900
Rat	900
Hamster	900
Gerbil	1059
Wild mice	1100-1200
Desert mice	
P. formosus	1300
P. longimembris	1520
Guinea pig	255
Monkey	398
Marmoset	200

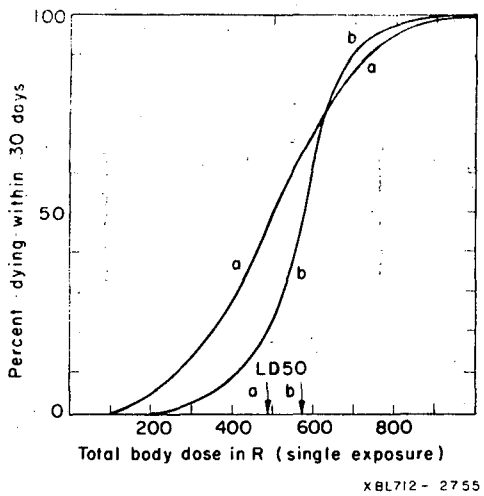

Fig. 4.1. Graph relating the number of mice killed by different doses of x rays. Curve a gives results with a "wild" strain in which there is a much wider variation between different animals than with a closely inbred strain, which is represented by curve b. (After Alexander.)

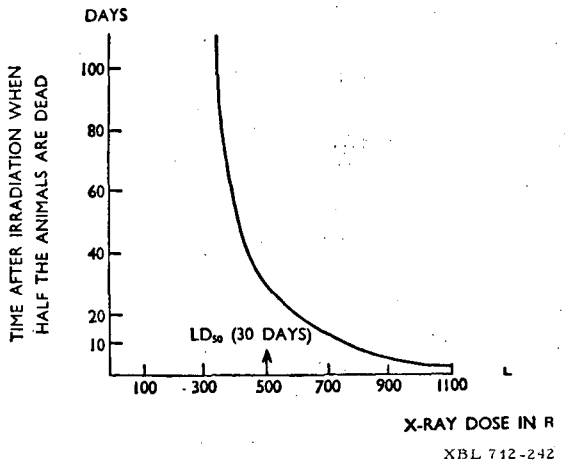

Fig. 4.2. Effect of different doses of radiation given at a single exposure on the survival time of mice. The value chosen is the time by which half the animals have died. From the curves the LD_{50} dose for different times of death is obtained. The LD_{50} in 30 days is about 500 R for these mice. (After Alexander.)

The presence of a threshold for early death may be demonstrated in a somewhat different manner. Thus if the time at which half of the population is dead after exposure is plotted as a function of absorbed dose, curves of the type shown in Fig. 4.2 are obtained. As the dose is reduced the wating time to death becomes very long--or, perhaps more accurately, the delay in death due to the exposure becomes longer than the normal life expectancy of the animal, and no effect due to irradiation is observed.

This demonstration of the existence of a threshold for death, as for all short-term radiation effects, is of great significance. Emphasis is given to the fact that a genuine threshold is observed, not merely an expression of low statistical probability. Thus, for example, the observation of death at doses of 500 rem does not signify any finite probability of death at doses of 1 rem. Ample proof of this assertion is that, from the billions of patients receiving a few rem in diagnostic radiology, no acute radiation effects have ever been observed.

RADIATION SICKNESS

Although death in itself might be thought of as an unambiguous biological end point in the study of radiation effects, the detailed reasons for death of an organism following irradiation are extremely complex.

Figure 4.3 shows how the time of death after whole-body irradiation is related to the magnitude of the exposure and to the major lethal modalities. In the radiation environments found at most accelerators, accidental whole-body exposures in excess of a few hundred rem are extremely unlikely--in most cases impossible. If accidental death should occur as a result of overexposure at an accelerator, it would therefore almost certainly be due directly or indirectly to failure of the blood-forming organs (hematopoietic death). Appropriate therapy may be effective in reducing human mortality from radiation exposures at this level, and studies of the phases of radiation sickness prior to death are therefore important because they permit conclusions of value in prognosis and subsequent treatment of accident victims.

Upton defines radiation sickness as "the term applied to the systemic manifestations of acute radiation injury. These manifestations vary, depending on the conditions of exposure. The signs predominating following high-level whole-body irradiation are referable to injury of the blood forming organs, gastrointestinal tract, cardiovascular system, brain, gonads, and skin. The associated symptoms and signs, known collectively as the *acute radiation syndrome*, constitute the earliest and most dramatic manifestations of radiation injury in man, some of them appearing almost immediately after intensive whole-body exposure in the lethal dose range."

The clinical course of radiation sickness encountered after an accidental exposure can be used to give a crude estimate of the whole-body dose absorbed by the individual. Even though experience with human radiation

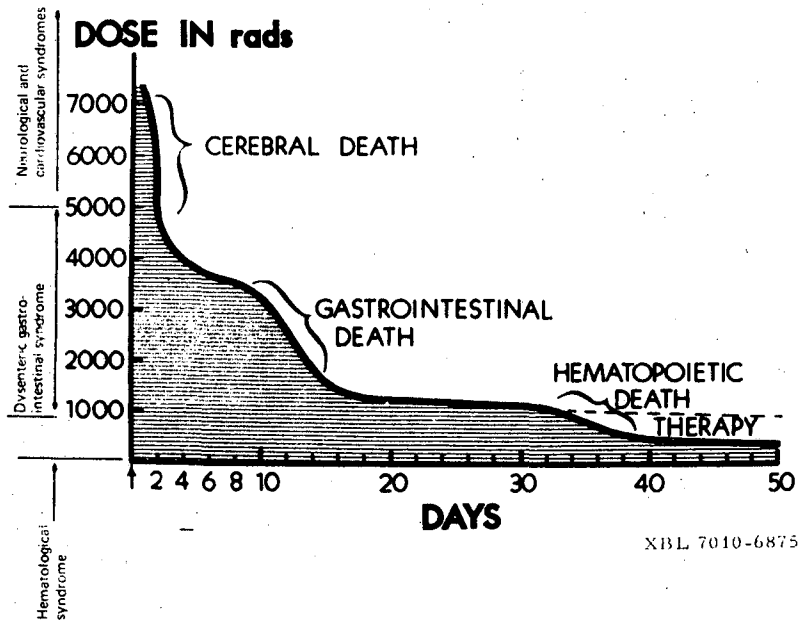

Fig. 4.3. The relation of time of death to whole-body radiation dose that defines the major lethal modalities. The dashed line over "therapy" defines the area in which symptomatic therapy of radiation damage is known to reduce human and animal mortality. (After SAENGER.)

sickness has been limited, enough cases have been observed to provide criteria that separate the injured into five groups, each identified by a range of whole-body doses, as shown in Fig. 4.4. Table 4.III summarizes the range of doses for each group estimated by Thoma and Wald (THO G 59) and by Gerstner (GER H 58). To understand these data it should be remembered that the variation in human response is very great. Thus the value of $LD_{50/30}$ for humans has been variously estimated by different authors in the range from less than 300 to more than 600 rads. From the classification in Table 4.III it can be seen that in going from 200 to 600 rads there is a very large change in the seriousness of the exposure. The first clinical manifestation of the radiation exposure is the prodomal phase.

Table 4.III. Clinical radiation injury groups. (After SAENGER)

Group No.	Clinical manifestations	Dose classification by—	
		Thoma and Wald[a]	Gerstner[b]
I	Mostly asymptomatic. Occasional minimal prodromal symptoms	10—160 rad-----	51—100 R 101—150 R
II	Mild form of Acute Radiation Syndrome. Transient prodromal nausea and vomiting. Mild laboratory and clinical evidence of hematopoietic derangement.	200—400 rad-----	150—400 R Hematopoietic
III	A serious course. Hematopoietic complications severe, and some evidence of gastroenteric damage present in upper portion of group.	400—600 rad (297+).	401—600 R Hematopoietic
IV	An accelerated version of Acute Radiation Syndrome. Gastroenteric complications dominate clinical picture. Severity of hematopoietic complications is related to survival time after exposure.	600—1400 rad---	Gastrointestinal
V.	A fulminating course with marked central nervous system impairment.	10,000 rad ±50 percent.	Cerebral

a. Doses in rad according to approximate ranges of Table III of Thoma and Wald.
b. Approximate doses in R from Table III and section on Dependency of Acute Radiation Syndrome on Air Dose by Gerstner. These doses are expressed as air dose, i.e., exposure dose, and are thus in terms of roentgens.

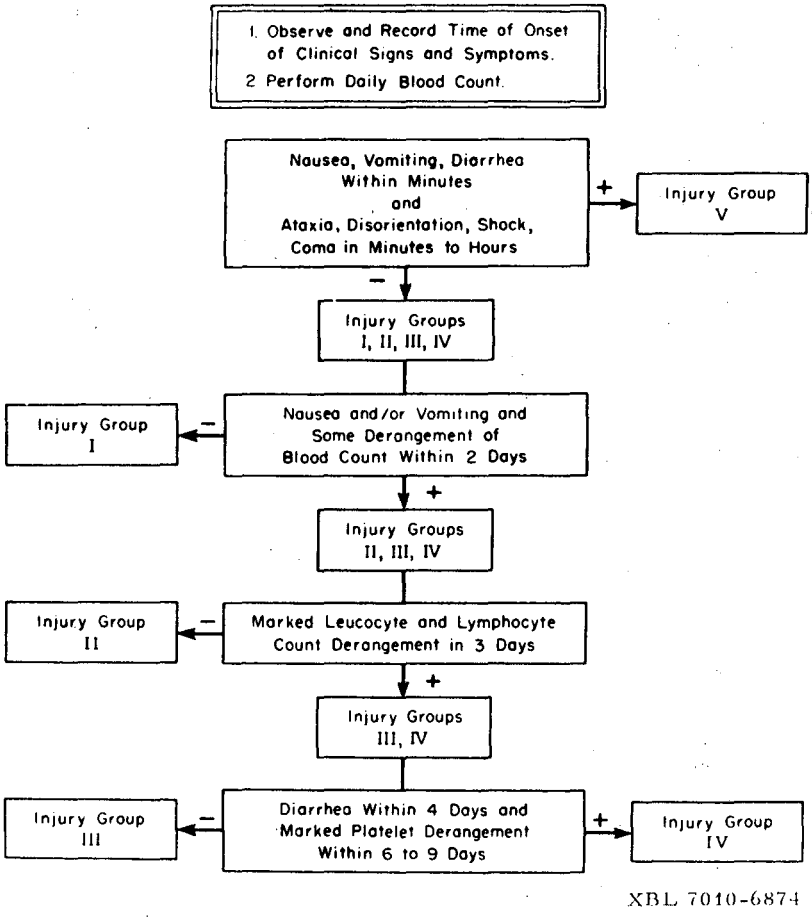

Fig. 4.4. Preliminary evaluation of clinical radiation injury following overexposure (After Saenger). To be read in conjunction with Table 4.III: + indicates manifestation observed; — indicates manifestation not observed.

Prodromal Response

The time of onset and the severity of the various prodromal responses are of great clinical value in prognosis. Thus it is important to study them and relate their incidence to the severity of the exposure. Lushbaugh (LUS C 67) has defined prodromal responses as "a prognostically useful group of symptoms that portend the severity of things to come."

When all, or the greater part, of the body is exposed to penetrating ionizing radiation, acute gastrointestinal and neuromuscular responses appear within a few hours after irradiation. Although nausea and fatigue are only the initial symptoms of the acute radiation syndrome, clinical studies have correlated their severity and duration with the subsequent progression of the radiation injury. Consequently early observation of persons exposed to high doses of radiation by a physician familiar with the prodromal response is an extremely important factor in determining the subsequent medical care of the patient.

The prodromal syndrome consists of a sequence of gastrointestinal and neuromuscular symptoms in order of increasing seriousness: anorexia (loss of appetite), nausea (without vomiting), fatigue, vomiting, diarrhea, and death. It begins within about 2 hours of exposure, except in very high doses, when it occurs within 5 to 15 minutes. Normally the prodromal syndrome lasts from 1 to 4 days, after which it subsides into the latent period—or, in severe exposures, leads directly into the fulminating stages of either the fatal neurological and cardiovascular syndrome (1000 to 5000 rads) or the fatal dysenteric gastrointestinal syndrome (500 to 1000 rads). The prodromal syndrome varies considerably with respect to time of onset, duration, maximum severity, and rate of recovery, depending upon the protraction of dose (distribution in time) and the region of the body irradiated; there is considerable variation in the sensitivity of individuals. Variations in the prodromal syndrome are reduced in massive single large acute doses.

When the dose is less than the median lethal value individual variation is so wide that it is impossible to predict a given patient's degree of prodromal response. There is strong evidence that in order for the prodromal response to be triggered the head, thorax, or abdomen must be directly irradiated.

Irradiation of the extremities alone does not produce the prodromal reaction. Exposure of the abdomen produced the syndrome following the smallest dose; partial-body exposure of the thorax or head is effective, also, although larger doses are required. The fact that abdominal shielding suppresses the response suggests that the autonomic nervous system is involved.

The prodromal syndromes fall into two groups, gastrointestinal and neuromuscular. In man the gastrointestinal symptoms predominate. The course of the syndrome can be seen as a function of time for a variety of doses in Fig. 4.5. Lushbaugh (LUS E 67) has reported comprehensive studies of therapeutic and accidental whole-body irradiation of more than 1600

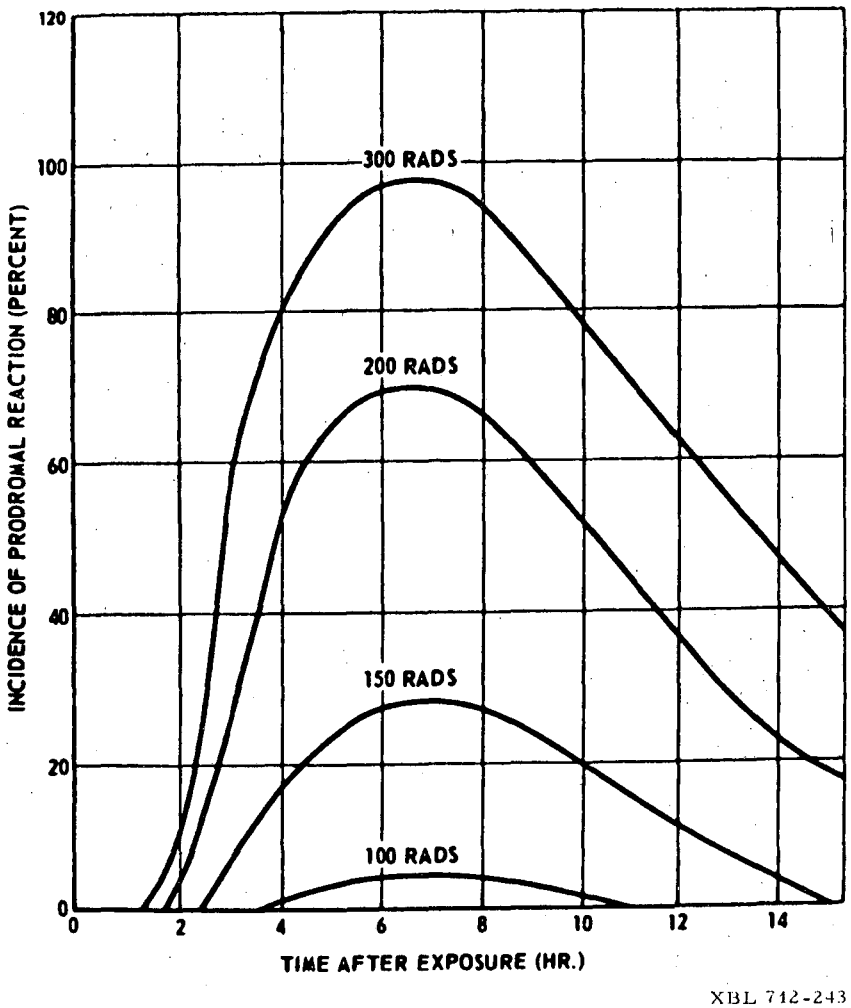

Fig. 4.5. Estimated incidence and timing of prodromal symptoms in man in relation to dose (modified from Langham) [after Upton (UPT A 69)]

patients. Figure 4.6 shows probit regression analyses (FIN D 64) of patients who vomited after exposure, and Fig. 4.7 shows a similar analysis for death occurring within 60 days of exposure.

Table 4.IV. summarizes the data relationships for single-dose response for five prodromal responses. Doses are expressed as equivalent absorbed dose (rads) in the human epigastrum for 50% incidence of the response, and an attempt was made in the statistical analysis to allow for the influence of the illness of patients included in the survey.

From the analyses reported by Lushbaugh, it is possible to calculate other levels of incidence of prodromal response. Table 4.V gives such data at the 10%, 50%, and 90% levels for nausea, diarrhea, and death.

The data of Lushbaugh presented here have low accuracy ($\approx \pm$ 50%) and are therefore of limited value in making precise predictions. They should be regarded as general guidelines based on presently inadequate human data, and probably are somewhat conservative. Furthermore, these data apply only for the x- and γ-ray energies used in conventional radiology. There is no information on the effect of LET on prodromal responses in man, but animal studies with fast neutrons suggest an RBE of 1 to 2 for the production of intestinal damage.

After the initial prodromal systems have subsided several days elapse in the *latent period.* The latent period is largely without symptoms, but silent changes are accurring due to the depletion of cells. Mitotically active tissues are most affected and highly differentiated tissues least affected (by radiation), because damage to stem cells may inhibit recovery. Thus if the population of stem cells has been seriously depleted the natural loss of cells during the latent period cannot be made good, and the irradiated patient is left with a serious deficiency in those cell systems that have a rapid turnover. The recovery of stem cells may be very slow or even lacking, and this severe shortage produces the *main phase* of the acute radiation sickness.

The severity of the main phase and the possibility of ultimate recovery from this phase depend entirely on the number of stem cells that survive in mitotically active tissues. These cells are the only source of the new cells needed for restoration of these tissues. If the acute dose has been greater than about 4000 rads, then (as seen in Fig. 4.3) death is due to brain damage and occurs too early for the main phase to appear. For dose values between several hundred and 4000 rads the main phase is reached, and death is due to bone-marrow damage or damage to the intestinal lining.

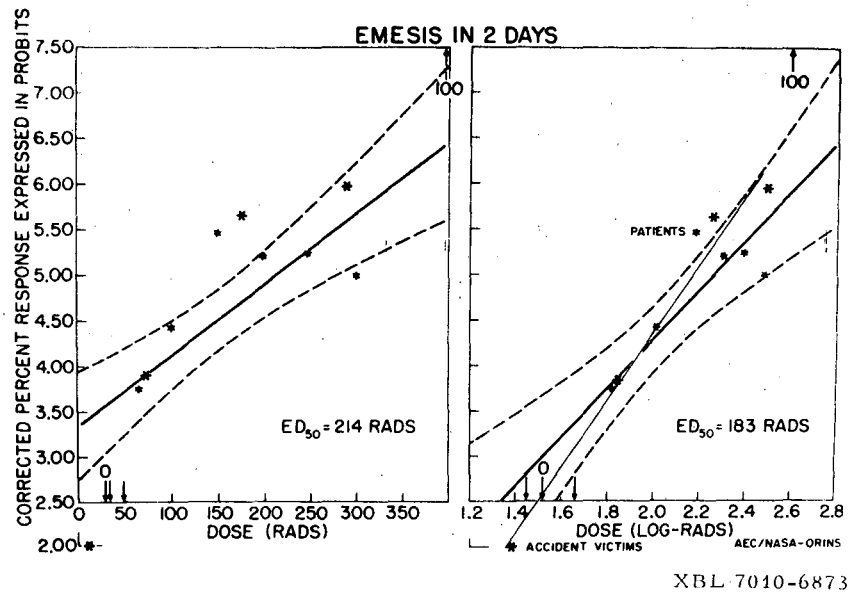

Fig. 4.6. Probit regression analyses of percent of exposed patients that vomited after radiation exposure in respect to dose in rads and log-rads. The resulting ED_{50}'s are shown. The thinnest line is the regression line obtained with data from studies made by others of 45 atomic accident victims.

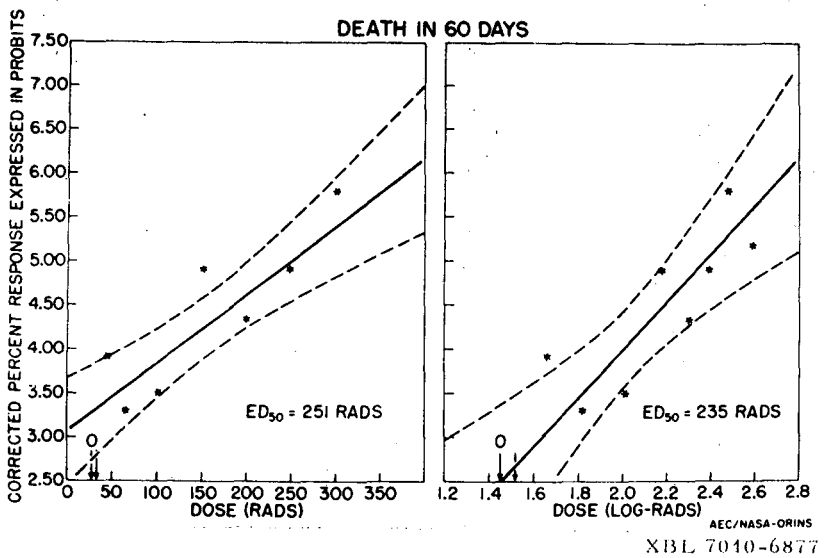

Fig. 4.7. Probit regression analyses of percent of exposed cases in which death from any cause occurred within 60 days of exposure, showing corrected estimates of lethal radiation dose using linear and logartithmic dosage scales.

Table 4.IV. Probit analysis of effective doses (50% incidence) for Gastrointestinal and systematic clinical responses to total-body irradiation in man (after Lushbaugh).

Clinical response	Response within (days)	Midline air exposure[a] (R)	Equivalent absorbed dose in epigastrum
Anorexia	2	124	82 ± 32
Nausea	2	209	138 ± 20
Vomiting	2	262	173 ± 18
Fatigue	42	206	136 ± 36
Diarrhea	42	294	194 ± 19
Death	60	425	281 ± 44

a. $^{137}C_s$ γ-ray equivalent (66 rads absorbed in tissue ≡ 100 R measured in air in absence of patient).

Table 4.V. Dose at different incidence levels for prodromal responses. (after Lushbaugh)

Clinical sign	Absorbed dose for probability of response (rads)		
	10%	50%	90%
Nausea within 2 days	50	170	320
Diarrhea within 60 days	90	240	390
Death within 60 days	220	285	350

Avoidance of Exposures That Produce the Prodromal Response

Although details of mechanisms causing prodromal response remain largely unknown, its appearance within the region of the body irradiated is fairly well known. The discussion in the preceding section leads one directly to conclude that serious injury may be prevented or mitigated at accelerators by either

a. locating beams above head height, or

b. providing at least partial local shielding around beams to avoid direct exposure of the abdomen.

It should further be borne in mind that many particle accelerators are not capable of delivering the high dose rates used in radiology, in most cases being lower by one or even two orders of magnitude.

Data obtained from the Rongelap fallout exposures (CON R 65) suggest a dose-rate-modifying effect upon the incidence of the prodromal responses. for example, the incidence of emesis was only 10% for an estimated absorbed dose of 175 rads, rather than the 50% to be expected from the data of Lushbaugh for single exposures of short duration. Experience gleaned from other accidental human exposures--notably the Mexican radiation accident (MAR G 64)--supports the view that an exposure delivered at low dose rate is less likely to produce the prodromal responses or hematologic death in man than the same total dose delivered either as a single acute dose or as a series of small doses at a high dose rate.

PHYSIOLOGICAL AND PSYCHOLOGICAL EFFECTS OF IRRADIATION ON THE CENTRAL NERVOUS SYSTEM

It is not likely that the accelerator health physicist will have the misfortune to observe the cerebral and cardiovascular form of the acute radiation syndrome in any victim of an accelerator accident. This form of the syndrome appears only after whole-body exposures exceed $\approx$ 5000 rem, and death follows in a few hours. A brief discussion is given for completeness.

Radiation effects on the central nervous system are complex, but intensive neurophysiological studies are under way.

The effect of radiation exposure on psychological functions and behavior is largely unknown. Experimental studies are complicated by the fact that many structures are simultaneously irradiated--thus, for example, in studies on the brain often the pituitary, thyroid, and sense organs are also irradiated. It is not yet clear whether behavioral changes following irradiation are a direct effect of the nervous system on other tissue or vice versa (or even some combination of these alternatives). In experimental studies the results of localized exposures may be more easily understood, since any resultant changes may be directly related to the exposed tissue.

Direct injury of nervous tissue requires a high radiation dose (WAS S 43, BAI O 62) to produce morphologic lesions. Animal experiments indicate that a single short dose of approximately 10 000 rem delivered to the brain can injure vital centers and cause death within minutes or hours. (BON V 65).

RESPONSE OF THE SKIN

Reddening of the skin was the first biological response to radiation noted in man; (GRU E 33) it still seems to be the most frequently observed injury in the sublethal range.

It is also of interest to note that the response of the skin to ionizing radiation was the first basis for an estimate of exposure. In the absence of any physical dosimeter the production of skin erythema was found to be so constant a postirradiation manifestation that exposure was estimated in units of skin erythema dose (SED). Radiation-protection standards, too, were defined in terms of erythema dose. Thus, in 1925 Mutscheller (MUT A 25) suggested a protection standard of exposures not to exceed 1/100 of a skin erythema dose in 30 days--slightly modified in the same year by Mutscheller and Sievert to 1/10 of an erythema dose per year (roughly corresponding to 25 R per year of 100-kV x rays).

Although the skin gives a full reaction to doses delivered to a depth of only 0.1 mm, it is such a major and important organ of the body that injury to only a rather small area causes serious discomfort. The biological response, in order of increasing severity, is:

a. erythema,

b. dry desquamation [loss of the squamous (--i.e., flat--) cells of the skin with no exudate or liquid loss],

c. moist desquamation,

d. sloughing of skin layers,

e. chronic ulceration.

Clinically evident permanent changes remain even after extended periods of recovery from all these injuries except erythema.

The response of human tissues to a radiation insult are complex, and in this the skin is no exception. Variables that influence the progression and severity of the injury are

a. total radiation exposure,

b. length of exposure time,

c. radiation quality and the consequent distribution of observed doses in the irradiated tissue,

d. region of the body exposed.

It is evident that generalization of the results of clinical observations may lead to half-truths inapplicable to particular situations. With this reservation in mind we may summarize clinical studies of skin erythema in man thus: (LUS C 67)

a. Erythema may appear within minutes to hours after exposure--in general the higher the exposures the quicker the appearance of reddening. As an example, two victims to accidental whole-body radiation exposures in excess of 4500 rads showed intense erythema only 15 minutes after exposure. (FAN H 67) Slow appearance of erythema within 4 weeks of exposure to a single radiation dose indicates an absorbed dose of 400 to 750 rads to the

skin. Most radiologists consider the skin erythema dose (SED) to be about 600 rads--i.e., there is 50% probability of observable erythema from a dose of 600 rads delivered to a depth of at least 0.1 mm (sometimes denoted by $ED_{0.5}$).

b. After doses of between 1600 and 2000 rads absorbed in the skin there is a more rapid appearance of erythema, followed by blisters, moist desquamation, and ulceration. Roughly speaking there is a 50% chance of moist desquamation following absorbed doses of 2000 rads. The skin of patients so exposed will heal in half the cases with the minimum of medical attention e.g., moist dressings). This observation is used to define the skin tolerance dose in man (TD_{50}) as approximately 2000 rads.

c. The severity of the skin response for a given dose increases with the area exposed up to areas of about 400 cm^2 and then becomes fairly constant.

d. Skin sensitivity varies, thus the face, trunk, arms, and legs are less sensitive than the backs of the hands, tops of the feet, scalp, eyelids, and perineum.

e. Temporary loss of hair from the scalp follows absorbed doses of about 300 rads at the hair follicle, and permanent baldness follows doses only 20 to 30% higher.

f. A dose of 500 rads to the hands or feet may result in loss of the nails.

g. Fractionation of the dose to the skin produces a marked change in the response of the skin. Thus Strandquist (STR M 44) has shown that the skin tolerance dose (TD_{50}) increases as the number of daily fractions administered is increased. He expresses his results as

$$TD_{50} = 2000\,(n)^{0.32},$$

where n = number of dose fractions given at daily intervals. Thus, for example, if n = 1, we obtain TD_{50} = 2000 rads, but TD_{50} increases to 4200 rads if the radiation is given in ten equal daily fractions.

Table 4.VI. Response of the skin.

Absorbed dose (rads)	Clinically observed effect	Comments
300	Temporary loss of scalp hair	
500	Loss of nails	Dose to hands or feet
600	Skin erythema, (50% probability	"erythema dose"
2 000	Moist desquamation, (50% probability	"skin tolerance dose"
10 000	Scarlet conjuctivae of the eye	"Welder's eyes"

EFFECTS ON THE BLOOD

For absorbed doses below values of the LD_{50} dose the principal cause of illness is the depletion of blood-forming stem cells in the bone marrow.

The change of several different components of the blood as a function of time after an acute exposure is seen in Fig. 4.8. The detailed effect that radiation has on the several cellular and noncellular components of the blood depends on the actual sensitivity of the component itself, the rate at which it is normally replaced, the sensitivity of the stem cells, if any, from which it is derived, and its mean survival time. For example, red blood cells are relatively radioresistant, but their stem cells or erythropoietic cells are quite sensitive, being directly killed by radiation. In fact less than 1% survive 500 rads.

In addition to being directly killed by radiation, cells may be mitotically inhibited, or morphological abnormalities such as chromosome bridges or binucleated cells may be induced. A good discussion of the specific effect of radiation on the several blood components is given by Upton (UPT A 69).

LATENT SOMATIC EFFECTS

Experiments on the lethality for mice of ionizing radiations indicated an effect that may have great significance in radiobiology: the period between irradiation and the observation of acute radiation effects increases as the radiation becomes more protracted. It is not yet known whether such an observation applies also to long-term somatic effects, although Evans (EVA R 69a,b) and his colleagues have presented strong evidence that such is the case for the radiogenic incidence of tumors subsequent to ingestion of radium.

Injuries normally identified under the category of late somatic effects are

induction of cancers,
induction of cataract,
nonspecific life-span shortening.

RADIATION CARCINOGENESIS IN HUMANS

Perhaps one of the greatest paradoxes revealed by the study of the effects of ionizing radiation on humans is that cancer may both be caused and cured by radiation exposure. Ionizing radiation thus reveals itself as, to use Alexander's apt phrase (ALE P 65) "a two-edged sword."

A complete study of such a complex topic as radiocarcinogenesis in man is, of course, beyond the scope of this chapter. The interested reader is referred to the textbooks in basic radiobiology and the publications of ICRP in the section on "background reading" at the end of this chapter. A brief review of available data on the production of leukemia and other cancers in humans, however, is given together with some discussion of the accuracy of extrapolation of these data, obtained at high doses, to the conditions of radiation protection.

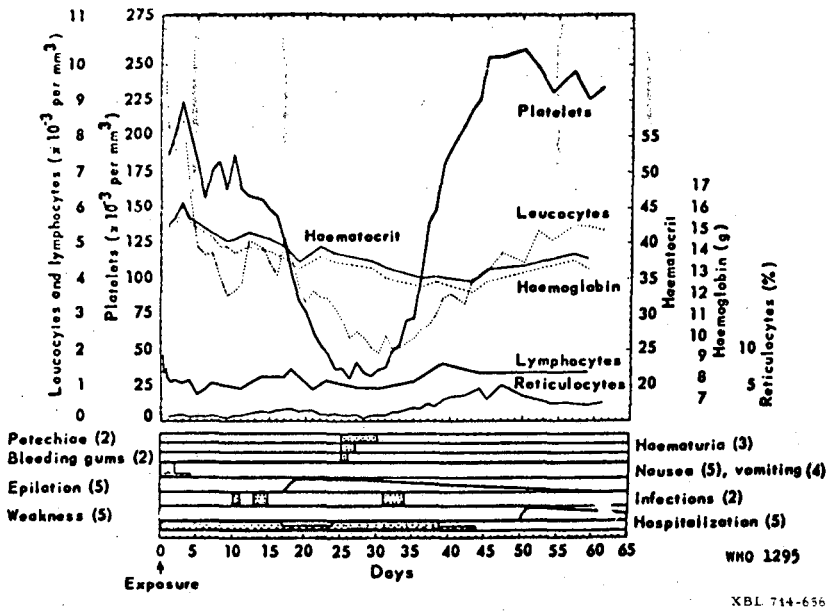

Fig. 4.8. Hematological values, symptons, and clinical signs in five men exposed in a criticality accident. (The blood counts are average values for the five men; the figures in parentheses denote the number showing the symptoms and signs indicated.) After Upton (UPT A 68).

Fortunately Man's experience of radiation-induced injury is nowadays quite infrequent. Nevertheless in the past 70 years a number of persons have been exposed to rather large doses of radiation, and the data obtained from epidemiological and cytogenic studies of them provide some measure of the incidence of radiation-induced diseases. In the main these persons fall into three main groups:

a. Medical patients undergoing radiotherapy--for example, ankylosing spondylitis patients treated by x-ray irradiations of the spine--radium-therapy and thorium-therapy patients, patients treated for hyperthyroidism, women treated for cervical cancer, or children irradiated for enlarged thymus and tinea capitis. A group of children exposed in utero for diagnostic purposes for the mother have also been studied.

b. Victims of nuclear warfare or testing, e.g., those exposed at Hiroshima, Nagasaki, and the Marshall Islands (CON R 65).

c. Occupationally exposed persons, e.g., radium dial painters, radiologists, and uranium miners.

From these three main groups the ankylosing patients, the Hiroshima and Nagasaki victims, and the radium dial painters have been most extensively studied. In the first two groups an increased incidence of leukemia was identified fairly rapidly because of its relatively short latent period. As studies have progressed, however, data on the incidence of other tumors have been collected. Table 4.VIII summarizes data due to Court Brown and Doll.

Table 4.VIII. Change in rate of induced malignant disease with duration of time since exposure in irradiated ankylosing spondylitics (data from Court Brown and Doll, 1965).

Years after irradiation	Cases per 10 000 man-years at risk	
	Leukaemia + aplastic anaemia	Cancers at heavily irradiated sites
0–2	2.5	3.0
3–5	6.0	0.7
6–8	5.2	3.6
9–11	3.6	13
12–14	4.0	17
15–27	0.4	20
Total of expected cases in 10 000 persons in 27 years calculated from the rates given	67	369

In discussing its most recent reexamination of the available data ICRP concluded (ICRP 69) "In essence this reexamination involved as detailed a subdivision as possible of the category of 'other fatal neoplasms' and the recognition that tissue dose was far from uniform in each of the three chief irradiated human populations—medical radiologists, ankylosing spondylitics and survivors of the atomic bomb explosions in Japan. It had also to be recognized that the time which has elapsed since exposure is still much too short for it to be possible to assess the full tumour incidence in the spondylitics and the Japanese: the following table shows that evidence collected during the first 15 years or so after exposure could be regarded as covering only the beginning of the period in which neoplasms other than leukemia might be expected to appear. If so, relatively small differences in the latent period of neoplasms arising in different tissues could lead to quite erroneous ideas about relative tissue susceptibility.

"The data in the table* may also suggest that malignant disease other than leukaemia will be 5–6 times more frequent than leukaemia plus aplastic anaemia when the yield is assessed after 27 years of observation. However, in this context the rates cited for 15–27 years after irradiation are quantitatively the most important and it should be stressed that these have a considerable statistical uncertainty."

Hiroshima and Nagasaki Victims

Perhaps the most thorough and extensive study of the incidence of disease in human populations exposed to ionizing radiations has been performed (and is still in progress) for the victims of the nuclear weapons attacks on Hiroshima and Nagasaki in 1945 (TOM M 59, HEY R 59, LAN R 54).

Within about 2 years from the exposure a significant increase in the incidence of leukemia was observed in the exposed population. Early studies showed the increased frequency of leukemia to be inversely related to distance from the hypocenter. This fact led Lewis (LEW E 57) to suggest that the incidence of leukemia was linearly related to dose. However, subsequent analyses of the dosimetry have revealed some uncertainties that make such a conclusion uncertain. In his analysis Lewis utilized dose distance curves (NEE J 56) known by their originators to have substantial errors, but the best available at that time.

Auxier et al. (AUX J 66), in a recent paper on dosimetry, have suggested the probable error in the *air dose* to be ±30% at Hiroshima and ±10% at Nagasaki. Problems of local shielding, spectral distribution, and relative proportions of neutron and γ dose make the assignment of *individual doses* a much more difficult problem. Moloney and Kastenbaum (MOL W 65) made this distinction when they showed that for persons exposed at the same dis tance the incidence of leukemia was higher in those who suffered radiation

*Table 4.VIII

Table 4.IX. Summary of Lewis's estimates of the probability of radiation-induced leukemia per individual per rad per year. Source: Lewis 1957.

Source of estimate	Type of radiation	Region irradiated	Types of leukemia produced	Probability of leukemia of specified type per individual per rad (or rem) to region irradiated per year		
				Estimated range		
				Lower limit	Upper limit	"Best" estimate
Atom-bomb survivors	γ Rays plus neutrons	Whole body	All	0.7×10^{-6}	3×10^{-6}	2×10^{-6}
Ankylosing spondylitis patients	x Rays	Spine	Granulocytic (only?)	0.6×10^{-6}	2×10^{-6}	1×10^{-6}
Thymic enlargement patients	x Rays	Chest	Lymphocytic (only?)	0.4×10^{-6}	6×10^{-6}	1×10^{-6}
Radiologists	x Rays, radium, etc.	Partial to whole body	All (?)	0.4×10^{-6}	11×10^{-6}	1×10^{-6}
Spontaneous incidence of leukemia (Brooklyn, N.Y.)	All natural background sources	Whole body	All (?)		10×10^{-6}	2×10^{-6}

(After Upton).

sickness in the few weeks immediately following the exposure. Milton and Shohoji (MIL R 68) have reviewed the dose estimates due to Auxier et al. and those made by Hashizume et al. (HAS T 67), based on measurements of residual induced activity and thermoluminescence in irradiated material, and concluded that "it is not possible at present to give a quantitative evaluation of either the accuracy or precision of the final (individual dose) estimates."

Inability to assign doses to individuals required that morbidity and mortality data be lumped on the basis of distance. When this is done, even with a distance interval as small as 50 meters, the uncertainty in dose is as large as 30%. And, if the data are lumped in large intervals, as is done in (ICRP 66), Publication 8, the dose uncertainty approaches two orders of magnitude. These considerations lead one to conclude that the Hiroshima-Nagasaki data are of insufficient accuracy to test any dose-exposure hypotheses. Lewis's analysis of several exposed groups summarized in Table 4.1X, assuming a linear dose-effect relationship, suggested the incidence of leukemia to be 1 to 2 cases per million person-years at risk per rem.

Recent studies suggest that different types of cancer do not have the same dose-incidence relationship (MAK H 68). These authors conclude: "It has been reconfirmed that in both sexes risk of leukemia mortality increases markedly with increase of dose. Also, in both sexes for all sites excluding leukemia, a slight trend is noted for the risk to increase with increase in dose. This increment is attributable chiefly to the increase of gastric cancer and lung cancer. Some, for example uterine cancer, show hardly any effect of exposure."

Studies made during autopsy indicated a slight tendency for higher mortality due to gastric cancer in females and lung cancer in females and lung cancer in both males and females, but the authors note these trends were not statistically significant. No significant relationship was noted between radiation exposure and *mortality* due to cancer of the liver and biliary ducts and cancer of the uterus (in women).

Studies of the incidence of cancer, however, showed that thyroid cancer, breast cancer, lung cancer, and leukemia all showed increased incidence with increasing exposure. "However, in Nagasaki, while incidence (for leukemia) increased with dose as in Hiroshima for the group exposed to 100 rad or more, no increase was noted under 100 rad." This latter conclusion by Maki et al. indicates the difficulties (and possible overestimates) in deriving estimates of cancer incidence in humans at chronic low doses and dose rates from these data on acute high doses.

Ankylosing Spondylitis Patients

Studies of the subsequent incidence of disease in patients treated with x rays for ankylosing spondylitis have revealed an elevation in the incidence of leukemia and other cancers (see Table 4.VIII).

Court Brown and Doll (COU W57) first suggested a correlation between the incidence of leukemia in these patients and radiation exposure. Furthermore, in the dose range studied, the data were consistent with a linear relationship. Court Brown and Doll, however excluded those cases in which extraspinal irradiation was given. Brues (BRU A 58) has noted that this exclusion resulted in a severe bias in the analysis because the cases excluded were predominantly in the high dose range. The complete Court Brown and Doll data thus indicate not only a curvilinear relationship, but perhaps also a threshold for leukemia induction in the range 50 to 100 R (BRU A 59), (see Fig. 4.9). Thus we infer that leukemia risk estimates based on linear extrapolations of these data may lead to overestimates at the dose levels found in radiation-protection work.

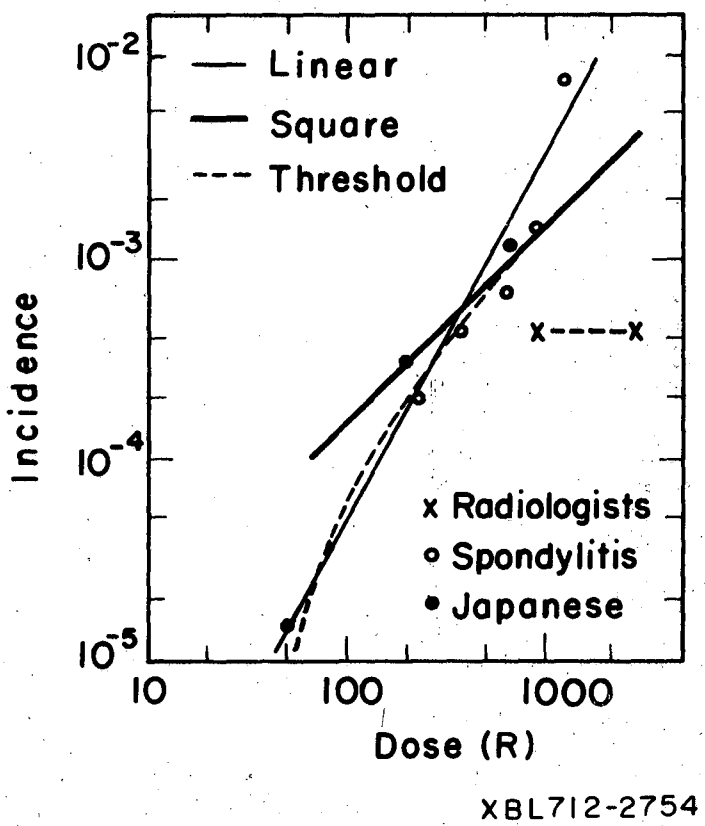

Fig. 4.9. Dose-response relationships for radiation leukemia in radiologists, irradiated spondylitic patients, and Japanese A-bomb survivors (from Brues 1959).

Incidence of Leukemia in U. S. Radiologists

Some additional data may be gleaned from a study of the incidence of leukemia in the early U. S. radiologists, who--it is estimated--received doses as high as 2000 rads over a period of many years (BRA C 57). Although this cumulative dose resulting from chronic exposure was far in excess of a lethal single dose in man, it resulted in an incidence of leukemia far lower than for either the nuclear bomb victims or the ankylosing spondylitis patients (see Fig. 4.9). This fact suggests that some substantial dose-rate effect may be important.

Internal Radiation Treatment of Hyperthyroidism

Although there is a clear association between increased incidence of leukemia in children who had received external irradiation for neck adenopathy and enlarged thymus glands (WIN T 61), no such association with ^{131}I isotope treatment of hyperthyroidism has been noted in the very careful studies recently reported by Saenger et al. (SAE E 68). Hyperthyroidism is the only major non malignant disease for which radioactive iodine has been given in relatively large doses to otherwise normal patients over a period of many years. Some early reports (POC E 60, POC E 66) indicated a possible causative relationship between ^{131}I therapy for thyrotoxicosis and leukemia. More extensive studies done by Werner et al. (WER S 61) and Saenger et al. (SAE E 60, SAE E 68) show no increased incidence of leukemia over that expected for untreated hyperthyroid patients. In the Cooperative Thyrotoxicosis Therapy Follow-Up Study initiated under the sponsorship of the National Center for Radiological Health of the Public Health Service (SAE E 60, SAE E 68), some 96% of 36 000 patients at some 26 medical clinics were followed. Of these, 22 000 were treated with ^{131}I and 14 000 were treated surgically. The incidence of leukemia in patients treated with ^{131}I, for whom the whole-body dose is about 10 rads, and the incidence of those treated surgically did not differ. Although these data show no statistically significant increase over that expected for the general population, they do not exclude the possibility of an increase in the incidence of leukemia at the level of 1% per rad.

To permit confidence at the 1% level a group of some 200 000 patients would have to be studied. This illustrates the difficulty in establishing an accurate measure of risk at acute whole-body exposures of 5 to 10 rads, and the problem is even more severe at long-term exposures at about 1 rad per year.

Gibson et al. (GIB R 68) have suggested that the probability of leukemia might be associated with a number of stressing situations. It is of interest in this respect to note that incidence of leukemia in hyperthyroid patients is 50% higher than that found in the U. S. population as a whole.

The Incidence of Lung Cancer in Uranium Miners

As early as 1500 the high incidence of lung disease amongst miners in the cobalt mines of Saxony and the pitchblende mines of Bohemia was recognized (MOR K 67). One component of this disease—colloquially referred to as "Bergkrankeit" — was finally identified, at the beginning of the twentieth century, as lung carcinoma. Sikl (SIK H 50) suggested in 1950 that the one common factor to these mines that seemed primarily responsible for the high incidence of lung cancer was the radiation exposure from the radioactive daughters of uranium, particularly radon and polonium. Several studies of the incidence of lung cancer showed the death rate from lung cancer in these mines to be about thirty times as great as normally expected (MOR K 67).

Studies of the relationship between the incidence of lung cancer and radiation exposure for uranium miners in the United States have recently been reported (JCAE 67, 69). The lowest exposure group studied in 1968 by a National Academy of Sciences Subcommittee (SCAE 69) had cumulative exposures roughly corresponding to lung doses from radon and its daughter products up to 250 rads. After careful study the subcommittee favored the hypothesis that radiation exposure had probably at least contributed to the higher incidence of lung cancer found in this group of workers than in the general population. However, they were careful to point out that a curvilinear relationship between dose and probability of cancer induction would be expected for lung cancer, which depends on localized tissue damage for its inception. Wagoner et al. (WAG J 65) did in fact find a curvilinear relation between working-level-months (a rough measure of radiation exposure) and annual incidence of respiratory cancer. Even after correction for the influence of age distribution in the working population, smoking habits, and number of years since onset of cancer, the relationship is still curvilinear. Cumulative exposure to the uranium miners was in the region of 100 rads or more and, in view of the curvilinear relation between exposure and incidence of cancer found by Wagoner et al., cancer risks based on linear extrapolations of these data will probably lead to overestimates.

Radium Dial Painters

The fate of radium dial painters who ingested toxic quantities of radium and radium daughters as a direct result of their occupation has been studied over the past 40 years. These painters absorbed radium through the mouth as a result of their practice of tipping their paint brushes with their lips. Radium and its daughters are deposited in bone and in time, if absorbed in sufficient quantities, can lead to skeletal damage, osteosarcoma, and other injury (MAR A 31). One of the most extensive and complete analyses of radium and mesothorium toxicity in human beings derives from the MIT group that has followed 604 cases of radium exposure over the past 40 years (EVA R 66, EVA R 67, EVA R 69a,b). Their data tend to show both a curvilinear dose-

effect response relationship and a practical threshold. They found the time for appearance of bone cancer is inversely related to the quantity of radium absorbed in bone. Thus at the point at which the latent period exceeds probable life span a practical threshold exists, and the MIT data put this at a few tenths of a microgram of radium deposited in bone. Statistical analysis of the data in which some incidence of bone cancer is observed (those cases in which the absorbed dose to the bone exceeds 1200 rads) indicates extreme improbability that the dose-response relationship is linear. Further the data suggest, but cannot yet prove, the existence of a threshold.

Other studies of radium dial painters, of patients treated therapeutically with radium, and of animals have shown essential agreement with the conclusions of the MIT group (FIN A 64a,b, FIN M 64b, HAS R 64 HAS R 65, SPI F 57, SPI H 51, SPI H 56, SPI H 69). Finkel et al. (FIN A 69), in a study of 293 patients treated with radium, found no person with a radium body burden below 1.2 μCi who had developed a malignant tumour ascribable to radium deposition.

CATARACT

Cataract induction is a possible risk for accelerator personnel, and it was indeed in cyclotron workers that dense opacities due to occupational irradiation were first noted (ABE P 49). Upton (UPT A 68) has reviewed the available data based on observations of accelerator workers, survivors of nuclear weapons attack, and victims of reactor accidents, as well as on clinical experience and animal experiments.

Low-LET Radiation

Upton (UPT A 68) summarizes the results of a survey of more than 500 radiotherapy patients exposed to low-LET radiation as follows:

a. An absorbed dose of 200 to 600 rads of low-LET radiation delivered in a single brief exposure is required to produce detectable changes in the lens of the human eye. A single acute exposure of 800 rads will almost certainly induce cataract.

b. Protraction of the irradiation increases this threshold. Thus if radiation is delivered fairly uniformly over a period of a few months the threshold may be 2 to 3 times as high as observed for single, acute exposures. However, this elevation of threshold does not continue indefinitely, and after total absorbed doses of 1100 to 1400 rads the formation of cataract is almost certain no matter how protracted the exposure.

c. Cataractogenesis is a function of the spatial as well as secular characteristics of exposure. Nonuniform or partial exposure of the lens of the eye is less likely to produce cataract.

d. No large differences in radiosensitivity of the lens of the eye as a function of age of the patient are evident.

e. The latent period between exposure and appearance of the cataract is a function of dose and dose rate, and varies from less than 1 year to more than 10 years. The average time of appearance is 2 to 3 years.

f. The probability of progression of the cataract after manifestation increases with the absorbed dose. Some cataracts remain stationary or even regress after appearance. It should further be noted that not all the lens opacifications detected by ophthalmological examination and designated "radiation cataracts" are necessarily so severe as to impair vision.

Exposure to low-LET radiation is of particular concern at electron accelerators or where direct access to high-energy photon beams is possible. Many potentially severe accidents may be avoided by locating particle beams well above head height.

High-LET Radiation

High-LET radiation is, however, much more effective in the production of cataract. Thus accelerators that produce secondary neutron beams or heavy charged particles may present a large potential hazard in this respect. Thus it has been estimated (HAN W 60) that the observation of cataract in the early cyclotron workers is consistent with a cataractogentic threshold of 75 to 100 rads of fast neutrons. Although this estimate is not completely consistent with all biological effects noted in the accident victims, particularly loss of hair, and may therefore be somewhat low, it appears to be consistent with data obtained from animal experiments (UPT A 68).

NONSPECIFIC LIFE-SPAN SHORTENING

Animal experiments have clearly demonstrated the influence of radiation exposure on life expectancy. Thus Blair (BLA H 56a,b) has reported measurements of life-span shortening of small rodents from single exposures to whole-body x and γ radiation. Even when death due to cancer is excluded there seems to be a real reduction of life span. However, experiments made with fractionated exposures indicate that life-span shortening is much less than with single exposures. Mole (MOL R 57) has reviewed chronic exposure data and shown that no significant effect can be detected with dose rates below 10 rads/week of γ rays or 1 rad/week of neutrons. Figure 4.10 shows Mole's summary of data relating to the survival time of mice exposed continuously to radiation throughout life. The data presented show a nonlinear relationship between life-span shortening and dose and tend to support the view that a threshold exists for this biological end point. The RBE of neutrons indicated is about 10.

Several experiments have reported the intriguing observation that at low-level chronic exposure, life span actually increased. Thus Mole reported that mice or guinea pigs irradiated at rates less than 1 rem per week lived longer than unirradiated animals. Carlson et al. (CAR L 57) have reported similar results with rats exposed to ^{60}Co γ rays at 0.8 r/day, but the number of experimental animals was small. Life-span extension has also been reported for the flour beetle (COR J 57).

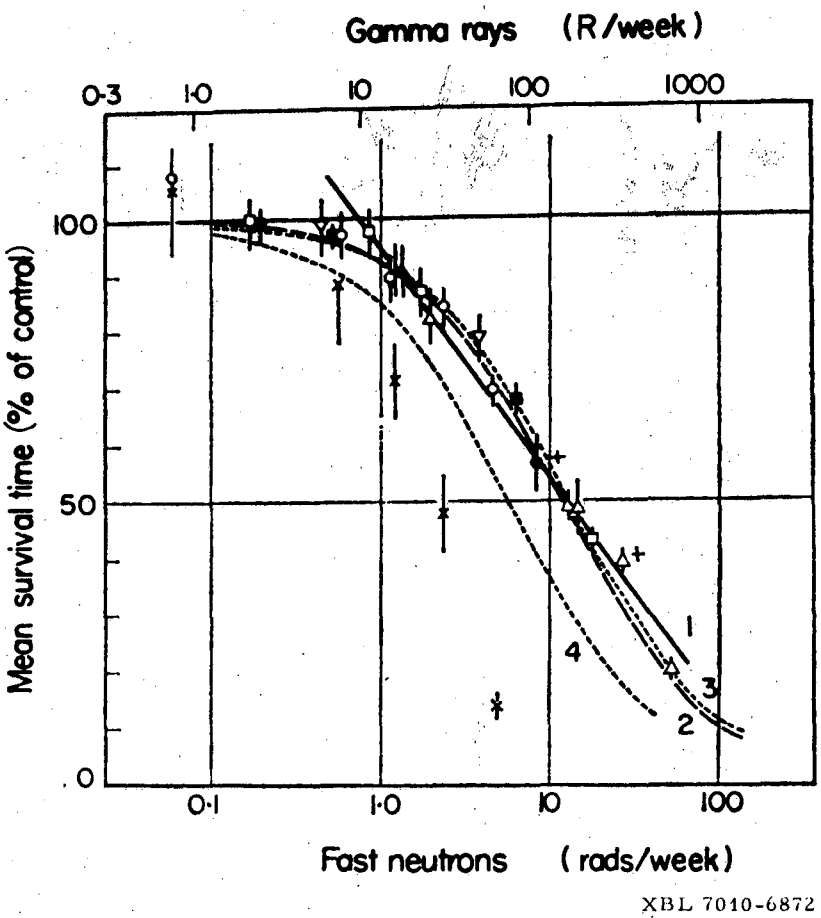

Fig. 4.10. Survival time (expressed as fraction of control) of mice exposed continuously to γ rays (top scale) and continuously to fast neutrons throughout life. Collected data suggest an RBE for life-span shortening by neutrons of about 10.

The observation of life-span shortening in animals led to suggestions that a comparable effect might exist in heavily irradiated human populations. Thus as early as 1948 Dublin and Spiegelman (DUB L 48) noted a relatively higher mortality rate in American radiologists than in other medical specialists, but unfortunately their data were not statistically significant. Warren (WAR S 56) reported similar findings in 1956, but his data were challenged because he had taken no account of the differing age distributions in the medical specialties studied. Subsequently, however, a more precise statistical study by Seltser and Sartwell (SEL R 65) essentially confirmed Warren's findings and reported a significantly higher age-specific mortality rate, both from non-neoplastic and neoplastic causes, for American radiologists than for other medical specialists. The excess mortality was found to be a function of age--no excess mortality was observed for radiologists under the age of 50 in the period of study, 1945 to 1958.

Similar studies in Britain reported by Court Brown and Doll (COU W 58) found no excess mortality in radiologists.

Warren (WAR S 66a,b) has amplified his earlier studies and reported findings similar to those of Seltser and Sartwell. Figure 4.11 shows the mean age at death for U. S. radiologists compared with the general population over the period of study. A remarkable change in life expectancy of radiologists is seen in the period from 1935–1963; the life span of the early radiologists was reduced 5 years or more. Warren has tentatively ascribed this effect to the increasing attention to radiation safety during the period.

Some additional evidence may be forthcoming from studies of the survivors of Nagasaki and Hiroshima and of the Marshall Islanders subjected to heavy radioactive fallout. In the latter group no life-span shortening has been observed to date (CON R 66), whereas in the former group interpretations of the increased mortality observed due to nonspecific causes is complicated by apparent inconsistencies in the data. (JAB S 65) In a recent review of the subject, Upton (UPT S 68) summarizes our present knowledge thus:

"Although the aforementioned data imply that high-level radiation may shorten the life span in human populations through mortality from late effects other than cancer, as in experimental animals, no quantitative dose-response relationship for such an effect can yet be formulated. The absence of an excess mortality from non-neoplastic causes in more distantly exposed Japanese atomic bomb survivors and in radiologists who may be presumed to have entered practice since 1940 suggests that life shortening is not a significant hazard of low level irradiation."

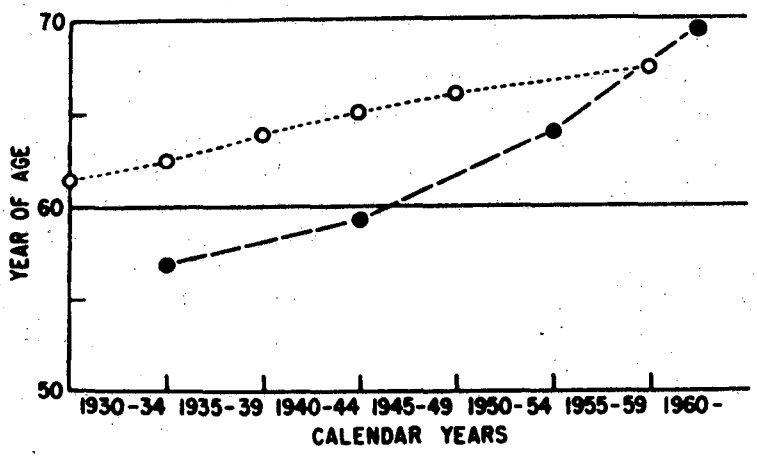

Fig. 4.11. Mean age at death by calendar years for radiologists (●—●) and for U.S. white males (○—○) over 25 years of age. After Warren, 66, (WAR S 66a).

SUMMARY

Fortunately, our experience of radiation exposures large enough to produce cancer in humans, at rates significantly higher than normal incidence, is limited to select groups and rather small numbers of people. We have seen, for example, that it is possible to observe a significant increase in the incidence of leukemia and other cancer in humans who have experienced whole-body radiation exposures of 100 rads or more. It is not yet clear what the effects, if any, of chronic radiation exposure at dose rates of the order of 1 rad per year might be. This topic will of necessity be an area of intensive study for many years to come, as it is vital in the setting of reliable radiation safety standards.

REFERENCES

ABE P 49 P. H. Abelson and P. G. Kruger, Cyclotron-Induced Radiation Cataracts, Science *110*, 655 (1949).

ALE P 65 P. Alexander, *Atomic Radiation and Life*, Rev. (Pelican Books, London, 1965).

AUX J 66 J. A. Auxier, J. S. Cheka, F. F. Haywood, T. D. Jones, and J. H. Thorngate, Free-Field Radiation-Dose Distributions from the Hiroshima and Nagasaki Bombings, Health Physics *12*, 425-429 (1966).

BAI O 62 O. T. Bailey, Basic Problems in the Histopathology of the Central Nervous System, in *Response of the Nervous System to Ionizing Radiation, Proc. Intern. Symp. Northwestern Univ. Med. School, Chicago, Illinois, Sept. 1960* (Academic Press, New York, 1962), p. 165.

BIZ O 66 O. J. Bizzozero, K. G. Johnson, and A. Chiocco, Radiation-Related Leukemia in Hiroshima and Nagasaki, 1946-1964, New Engl. J. Med. *274*, 1095-1101 (1966).

BLA H 56a H. A. Blair, Data Pertaining to Shortening of Life Span by Ionizing Radiation, University of Rochester Report 442, 1956.

BLA H 56b H. A. Blair, A Formulation of the Relation Between Radiation Dose and Shortening of Life Span. in *Proceedings of the First United Nations International Conference on the Peaceful Uses of Atomic Energy Geneva, Switzerland, 1955*, (UN, 1956), Vol. 11 p. 118.

BON V 65 V. P. Bond, T. M. Fliedner, and J. O. Archambeau, A Disturbance in Cellular Kinetics, in *Mammalian Radiation Lethality* (Academic Press, New York, 1965).

BON V 68b V. P. Bond, Radiation Mortality in Different Mammalian Species, in *Comparative Cellular and Species Radiosensitivity*, Ed. V. P. Bond and T. Sugahara (Williams and Wilkens Company, Baltimore, Maryland, 1969).

BRA C 57 C. B. Braestrup, Past and Present Radiation Exposure to Radiologists from the Point of View of Life Expectancy, Am J. Roentgenol., Rad. Therapy, and Nucl. Med. *78*, 988 (1957).

BRU A 58 A. M. Brues, Critique of the Linear Theory of Carcinogenesis, Science *128*, 693-699 (1958).

BRU A 59 A. M. Brues, Somatic Effects in Low Level Irradiation Ed. A. M. Brues. Amer. Assoc. Advan. Sci. Washington 1959 p. 75.

CAR L 57 L. D. Carlson, W. J. Scheyer, and B. H. Jackson, The Combined Effects of Ionizing Radiation and Low Temperature on the Metabolism, Longevity, and Soft Tissues of the White Rat, Radiation Res. 7,190 (1957).

CON R 65 R. A. Conard and A. Hicking, Medical Findings in Marshallese People Exposed to Fallout Radiation: Results from a Ten-Year Study, J. Am. Med. Assoc. *192*, 457 (1965).

CON R 66 R. A. Conard, A. Lowrey, M. Echer, K. Thompson and W. A. Scott, Ageing Studies in a Marshallese Population Exposed to Radioactive Fallout in 1954, in *Radiation and Ageing*, Eds. P. J. Lindop and G. A. Sacher (Taylor and Francis, London, England, 1966), p. 345.

COR J 57 J. M. Cork, Gamma Radiation and Longevity of the Flour Beetle, Radiation Res. *7*, 551 (1957).

COU W 57 W. M. Court Brown and R. Doll, Leukaemia and Aplastic Anaemia in Patients Irradiated for Ankylosing Spondylitis, Spec. Rept. Ser. Med. Res. Coun., No. 295 (H. M. Stationery Office, London, 1957).

COU W 58 W. M. Court Brown and R. Doll, The Expectation of Life and Cancer Mortality of British Radiologists, Brit. Med. J. *2*, 181 (1958).

COU W 65 W. M. Court Brown and R. Doll, Mortality from Cancer and Other Cuases After Radiotherapy for Ankylosing Spondylitis, Brit. Med. J. *2*, 1327-1332 (1965).

DUB L 48 L. I. Dublin and M. J. Spiegelman, Mortality of Medical Specialists, 1938-1942, J. Am. Med. Assoc. *137*, 1519 (1948).

EVA R 66 R. D. Evans, The Effect of Skeletally Deposited Alpha-Ray Emitters in Man, Brit. J. Radiol. *39*, 881-895 (1966).

EVA R 67 R. D. Evans, The Radium Standard for Bone Seekers--Evaluation of the Data on Radium Patients and Dial Painters, Health Phys. *13*, 267-278 (1967).

EVA R 69a R. D. Evans, A. T. Keane, R. J. Loenkow, W. R. Neal, and M. M. Shanahan, Radiogenic Tumor in the Radium and Mesothorium Cases Studied at MIT, in *Delayed Effects of Bone-Seeking Radionuclides*. Eds. C. W. Mays, W. S. S. Jee, R. D. Lloyd, B. J. Stover, J. H. Dougherty, and G. N. Taylor (University of Utah Press, Salt Lake City, Utah, 1969).

EVA R 69b R. D. Evans, Radium and Mesothorium Poisoning and Dosimetry and Instrumentation Techniques in Applied Radioactivity, Annual Progress Report, Physics Department, Massachusetts Institute of Technology, MIT 952-6 ppl-383, 1969.

FAN H 67 H. Fanger and C. C. Lushbaugh, Radiation Death from Cardiovascular shock Following a Criticality Accident, Arch. Path. *83*, 446 (1967).

FIN A 64 A. J. Finkel, C. E. Miller, and R. J. Hasterlik, Long Term Effects of Radium Deposition in Man, in Argonne National Laboratory Health Division, Gamma-Ray Spectroscopy Group Semiannual Report, Report ANL-6839, 1964, pp. 7-11.

FIN A 69 A. J. Finkel, C. E. Miller, and R. J. Hasterlik, Radium-Induced Malignant Tumors in Man, in *Delayed Effects of Bone-Seeking Radionuclides*, Eds. C. W. Mays, W. S. S. Jee, R. D. Lloyd, B. J. Stover, J. H. Dougherty, and G. N Taylor (University of Utah Press, Salt Lake City, Utah, 1969, pp. 195-225.

FIN D 64 D. J. Finney, Probit Analysis (Cambridge University Press, London, 1964).

FIN M 64 Finkel, M. P., P. B. Jinking, and B. O. Biskis, Parameters of Radiation Dosage that Influence Production of Osteogenic Sarcomas in Mice. National Cancer Institute Monograph No. 14, pp. 243-63, Washington.

FOL J 52 J. H. Folley, W. H. Borges, and T. Yamawaki, Incidence of Leukemia in Survivors of the Atomic Bomb in Hiroshima and Nagasaki, Am. J. Med. *13*, 311-321 (1952).

GER H 58 H. B. Gerstner, Acute Radiation Syndrome in Man: Military and Civil Defense Aspects, Armed Forces Med. J. *9*, 313-354 (1958).

GIB R 68 R. W. Gibson, I. D. J. Bross, S. Graham, A. M. Lilienfeld, L. M. Schuman, M. L. Levin, and J. E. Dowd, Leukemia in Children Exposed to Multiple Risk Factors, New England J. Med. *279*, 906-909 (1968).

GRU E 33 E. H. Grubbe, Priority in the Therapeutic use of X Rays, Radiology *21*, 156 (1933).

HAN W 60 W. T. Ham, Fast Neutron Radiation Hazards, in *Fast Neutron Physics*, Ed. J. B. Marion and J. L. Fowler (Interscience, N. Y. 1960), p. 841.

HAS R 64 R. J. Hasterlik, A. J. Finkel, and C. E. Miller, The Cancer Hazards of Industrial and Accidental Exposure to Radioactive Isotopes, Ann. N. Y. Acad. Sci. 114 [2], 832-837 (1964).

HAS R 65 R. J. Hasterlik and A. J. Finkel, Diseases of Bones and Joints Associated with Intoxication by Radioactive Substances, Principally Radium, Med. Clin. N. Am. *49*. 285-296 (1965).

HAS T 67 T. Hashizume, T. Maruyama, A. Shiragi, E. Tanaka, M. Izawa, S. Kawamura, and S. Nagaoka, Estimation of the Air Dose from the Atomic Bombs in Hiroshima and Nagasaki, Health Phys. *13*, 149-161 (1967).

HEY R 59 Robert Heyssel, A. B. Brill, L. A. Woodbury, E. T. Nishimura. T. Ghose, T. Hoshino, and M. Yamasaki, Leukemia in Hiroshima Atomic Bomb Survivors, Atomic Bomb Casualty Commission Rept. 02-59, Hiroshima and Nagasaki, 1959.

HEY R 60 R. Heyssel, Leukemia in Hiroshima Atomic Bomb Survivors, Blood *15*, 313-331 (1960).

HOL J 60 J. W. Hollingsworth, Delayed Radiation Effects in Survivors of the Atomic Bombings, Atomic Bomb Casualty Commission Rept. 01-60, Hiroshima and Nagasaki, 1960.

ICRP 66 International Commission on Radiological Protection, Committee I, The Evaluation of Risks from Radiation, Health Phys. *12*, 239-302 (1966).

ICRP 69 *Radiosensitivity and Spatial Distribution of Dose*, ICRP Publication 14 Pergamon Press, Oxford, 1969.

JAB S 65 S. Jablon, M. Ishida, and M. Yamasaki, Studies of the Mortality of A- Bomb Survivors, Radiation Res. *25*, 25 (1965).

JCAE 67 Radiation Exposure of Uranium Miners, Hearings before the Subcommittee on Research, Development, and Radiation of the Joint Committee on Atomic Energy, Congress of the United States, 90th Congress, first session on Radiation Exposure of Uranium Miners, Part 2. U.S. Government Printing Office. Washington, D. C. (1967).

JCAE 69 Radiation Standards for Uranium Mining, Hearings before the Subcommittee on Research, Development, and Radiation of the Joint Committee on Atomic Energy, Congress of the United States, 91st Congress, First Session on Radiation Standards for Uranium Mining March 17 and 18, 1969. U. S. Government Printing Office. Washington, D. C.

KAT H 63 H. Kato and S. Ueda, Influence of Concomitant Variables Upon Mortality Rate Comparison, Atomic Bomb Casualty Commission Rept. 08-63, Hiroshima and Nagasaki, 1963.

LAN R 54 R. E. Lange, W. C. Moloney, and T. Yamawaki, Leukemia in Atomic Bomb Survivors. I. General Observations, Blood *9*, 574-585 (1954).

LEW E 57 E. B. Lewis, 1957, Leukemia and Ionizing Radiation, Science *125*, 965-972 (1957).

LUS E 67 C. Lushbaugh, Some Biological End Points of Dosimetric Value, in *Proceedings of First International Symposium on the Biological Interpretation of Dose from Accelerator Produced Radiation Berkeley, March 13-16, 1967*, CONF-67035.

MAK H 68 H. Maki, T. Ishimaru, H. Kate, and T. Wakabayashi, Carcinogenesis in Atomic Bomb Survivors. Technical Report 24-68, Atomic Bomb Casuality Commission, 1968.

MAR A 31 A. S. Markland, The Occurrence of Malignancy in Radioactive Persons. A general view of data gathered in the study of the radium and dial painters, with special reference to the occurrence of osterogenic sarcoma and the interrelationship of certain blood diseases, Am. J. Cancer *15*, 2435 (1931).

LUS C 67 C. Lushbaugh, Some Biological End Points of Dosimetric Value Derived from Clinical Data, in Proceedings of the *First International Symposium in the Biological Interpretation of Dose from Accelerator-Produced Radiation, Berkeley, California March 13-16, 1967*, CONF-670305 Sect. III-3, p. 94.

MAR G. 64 G. R. Martinez, Accident from Radiation: Observations in the Accidental Exposure of a Family to a Source of Cobalt-60, Rev. Medica Inst. Med. Seguro Sociol. *3* Suppl. 1, 14-69 (1964).

MIL R 68 R. C. Milton and T. Shohoji, Tentative 1965 Radiation Dose Estimation for Atomic Bomb Survivors, Atomic Bomb casualty Commission Technical Report 1-68, 1968.

MOL R. 57 R. H. Mole, Shortening of Life by Chronic Irradiation: The Experimental Facts, Nature *180*, 456 (1957).

MOL W 55 W. C. Moloney and M. A. Kastenbaum, Leukemogenic Effects of Ionizing Radiation on Atomic Bomb Survivors in Hiroshima City, Science *121*, 308-309 (1955).

MOR K 67 K. Z. Morgan, Human Experience With Man-Made Sources of Ionizing Radiation, Section 1.3 in *Principles of Radiation Protection*, Ed. K. Z. Morgan and J. E. Turner (John Wiley and Sons, Inc., New York, 1967).

MUT A 25 A. Mutscheller, Physical Standards of Protection Against Roentgen-Ray Dangers, Am. J. Roentgenol. Rad. Therapy *13*, 65 (1925); see Stone, R. S., Radiology *58*, 639 (1952).

NEE J 56 J. V. Neel and W. J. Schull, The Effect of Exposure to the Atomic Bomb on Pregnancy Termination in Hiroshima and Nagasaki, National Academy of Science, National Research Council, Publication 461, Washington, D. C., 1956.

POC E 60 E. E. Pochin, Leukaemia Following Radioiodine Treatment of Thyrotoxicosis, Brit. Med. J. *2*, 1545-1550 (1960).

POC E 66 E. E. Pochin, Somatic Risks--Thyroid Carcinoma (the Evaluation of Risks from Radiation), International Commission on Radiation Protection, Publication 8 (Pergamon Press, Oxford, 1966, p. 9.

SAE E 60 E. L. Saenger, F. N. Silverman, T. D. Sterling, and M. E. Turner, Neoplasia Following Therapeutic Irradiation for Benign Conditions in Childhood, Radiology, *74*,889-904 (1960).

SAE E 63 E. L. Saenger, *Medical Aspects of Radiation Accidents*, USAEC, 1963.

SAE E 68 E. L. Saenger, G. E. Thoma, and E. A. Thompkins, Incidence of Leukemia Following Treatment of Hyperthyroidism, J. Am. Med. Assoc, *205*, 147-154 (1968).

SEL R 65 R. Seltser and P. E. Sartwell, The Influence of Occupational Exposure to Radiation on the Mortality of American Radiologists and other Medical Specialists, Am. J. Epidemiol. *81*, 2 (1965).

SIK H 50 H. Sikl, Acta Unio Intern. Contra Cancrum *6*, (1950).

SPI F 57 F. W. Spiers and P. R. J. Burch, Measurements of Body Radioactivity in a Radium Worker, Brit. J. Radiol. Suppl. *7*, 81-89 (1957).

SPI H 51 H. Spiess, Uber Anwendung and Wirkung des Peteosthor bei pulmonaler und extrapulmonaler Tuberkulose in Kindersalter, Augleich eine allgemeine Stellungnahme zur Thorium X- and Peteosthor-Therapie. Z. Kinderheilk. *70*, 213-252 (1951).

SPI H 56 H. Spiess, Schwere Strahlenschäden nach der Peteosthorbehandlung von Kindern, Deut. med. Wochschr *81*, 1053-1054 (1956).

SPI H 69 H. Spiess, ^{224}Ra-Induced Tumor in Children and Adults, in *Delayed Effects of Bone-Seeking Radionuclides*, Eds. C. W. Mays, W. S. S. Jee, R. D. Lloyd, B. J. Stover, J. H. Dougherty, and G. N. Taylor (University of Utah Press, Salt Lake City, Utah, 1969, pp227-247.

STO R 52 R. S. Stone, The Concept of a Maximum Permissible Exposure. Carman Lecture, Radiology *58*, 639 (1952).

STR M 44 M. Strandquist, A Study of the Cumulative Effects of Fractionated x-Ray Treatment Based on the Experience Gained at the Radiumhemmet With the Treatment of 280 Cases of Carcinoma of the Skin and Lip, Acta Radiol. *55*, 300 (1944).

SUT W 59 W. W. Sutow and E. West, Studies on Nagasaki (Japan) Children Exposed in Utero to the Atomic Bomb, Atomic Bomb Casualty Commission Rept. 31-59, Hiroshima and Nagasaki.

THO G 59 G. E. Thoma, Jr., and N. Wald, The Diagnosis and Management of Accidental Radiation Injury, J. Occupational Med. *1*. 421-447 (1959).

TOM M 59 T. Tomonaga, M. A. Brill, I. Itoga, and R. Heyssel, Leukemia in Nagasaki Atomic Bomb Survivors, Atomic Bomb Casualty Commission Rept. 11-59, Hiroshima and Nagasaki.

UPT A 68 A. C. Upton, Effects of Radiation on Man, Ann. Rev. Nucl. Sci. *18*, 495 (1968).

UPT A 69 A. C. Upton, *Radiation Injury* (University of Chicago Press, Chicago, 1969).

WAG J 65 J. K. Wagoner, V. E. Archer, F. E. Lundin, D. A. Holaday, and J. W. Lloyd, Radiation as the Cause of Lung Cancer Among Uranium Miners, New Engl. J. Med. *273*, 181-188 (1965).

WAR S 43 S. J. Warren, Effects of Radiation on Normal Tissues: VIII. Effects on the Gonads, Arch. Pathol. *35*, 121-139 (1943).

WAR S 56 S. J. Warren, Longevity and Causes of Death from Irradiation in Physicians, J. Am. Med. Assoc. *162*, 464 (1956).

WAR S 66a S. J. Warren and O. M. Lombard, New Data on the Effect of Ionizing Radiation on Radiologists, Arch Environ. Health *13*, 415 (1966).

WAR S 66b S. J. Warren, The Basis for the Limit of Whole-Body Exposure -- Experience of Radiologists, Health Phy. *12*, 737 (1966).

WER S 61 S. C. Werner, A. M. Geittelshon, and A. B. Brill, Leukemia Following Radio-iodine Therapy of Hyperthyroidism, International Atomic Energy Agency, Vienna, 1961.

WIN T 61 T. Winship, and R. V. Rosvoll, Childhood Thyroid Carcinoma, Cancer *14*, 734-743 (1961).

BIBLIOGRAPHY

P. Alexander, *Atomic Radiation and Life*, (Pelican Book Co., London, 1965).

Z. M. Baq and P. Alexander, *Fundamentals of Radiobiology* (Pergamon Press, Oxford, 1961).

A. P. Casarett, *Radiation Biology* (Prentice Hall, New York, 1968).

D. E. Lea, *Actions of Radiations on Living Cells* (Cambridge University Press, 1962).

K. Z. Morgan and J. E. Turner, eds., *Principles of Radiation Protection* (John Wiley and Sons, Inc., New York, 1967).

R. Wallace, ed., *Proceedings of the First International Symposium on the Biological Interpretation of Dose from Accelerator-Produced Radiation, Berkeley, California, March 13-16, 1967, CONF-670305.*

A. C. Upton, *Radiation Injury* (University of Chicago Press, Chicago, 1969).

CHAPTER 5

THE MEASUREMENT OF RADIATION FIELDS - RADIATION DETECTORS

RADIATION DETECTORS

TABLE OF CONTENTS

CHAPTER 5 (cont.)

THE MEASUREMENT OF RADIATION FIELDS-- RADIATION DETECTORS

INTRODUCTION

THE PHILOSOPHY OF ACCELERATOR RADIATION MEASUREMENTS

The challenge presented to the health physicist is nowhere greater than at accelerator installations, where the radiation environments may be extremely complex (Chapter 3). In consequence the investigation of radiation fields at accelerators has led to the development of many sophisticated instruments and techniques of measurement.

In a discussion of radiation detectors appropriate for use in particle-accelerator radiation environments, it will be helpful first to define the goals of radiation measurements. It has been the experience at most accelerator laboratories known to the authors that an accelerator radiation safety program has six primary goals:

(a) Personnel protection.
(b) Study of accelerator operating characteristics.
(c) Radiation shielding studies.
(d) Accelerator and equipment protection.
(e) Program support.
(f) Public relations.

Personnel protection is demanded by the moral obligations an employer has for his employees' safety; but, in any event, certain mandatory requirements must be satisfied. These are discussed briefly in Chapter 8. It is certainly true that an excellent radiation-protection program contributes to good employee morale.

The need to provide radiation protection naturally leads to studies of accelerator operating conditions and radiation shielding, but the information obtained is of great value in supporting the general program of the accelerator. Accelerator operation and utilization may be made more efficient and the accelerator and its associated equipment protected from damage.

Last, but not least, good public relations between the accelerator operator and his neighbors may be maintained only if the former is prepared to give solid evidence of his good faith in providing good radiation protection, not only for his employees, but for the general public as well.

Because of the diversity of applications to which accelerator radiation measurements are put, it is worth taking a little trouble to ensure that appropriate instruments and techniques are used. An accelerator radiation measurement should

(a) Be capable of general application to the varied problems of accelerator operation and utilization. Which, in turn, demands that it should

(b) Be of high precision and as accurate as is reasonably possible. The errors inherent in the measurement should be thoroughly analyzed and well understood.

(c) Describe the radiation field in fundamental physical terms such as particle type, flux density, energy spectrum, and angular distribution.

(d) Be a complete and thorough description of all significant components of the radiation field.

(e) Be usable for deriving quantities appropriate to radiation protection (absorbed dose, dose equivalent). (See Chapter 2.)

SPECIAL PROBLEMS OF RADIATION MEASUREMENTS AT ACCELERATORS

The measurement of the radiation fields produced by an accelerator presents some special problems. Two major areas which may be unfamiliar are dosimetry in mixed radiation fields, in which high–LET particles are extremely important, and in fields which are often produced with unusual duty cycles.

Mixed Radiation Fields

In principle the radiation fields of accelerators, particularly those of high energy, may be extremely complex. Two basic types of radiation measurement are, however, usually required:

(a) Dosimetry of the primary beam and its reaction products from irradiated targets, and

(b) dosimetry of the general radiation environment outside thick shielding.

Beam dosimetry often requires specialized techniques (discussed in greater detail later in this chapter). The production of secondary particles by interaction of the primary beam with targets is described in Chapter 3, and the transport of these particles through shielding is discussed in Chapter 6. As we have suggested (Chapters 2 and 3), despite the potential complexity of accelerator radiation environments, in many cases the principal contributions to dose equivalent are due to photons and neutrons. As an example, Perry and Shaw (PER D 65, PER D 67) have reported measurements of the composition of the radiation field outside thick concrete shielding above a 7-GeV proton beam; their data are given in Table 5.I. Although Perry and Shaw find 70% of the neutron flux density in the energy range 1 eV to 0.7 MeV, 60% of the estimated dose equivalent is due to neutrons of energy greater than 0.7 MeV.

Baarli et al (BAA J 64) have reported similar findings outside thick shields of the 28-GeV CPS. These findings, typical of proton accelerators, show that $\approx$ 90% of the dose equivalent is due to neutrons and energetic fast particles. More recently, additional studies have been reported of neutron spectra outside thick shielding (TAR P 67, THO R 67, GIL W 68, SHA K 68,

69). Those reported by Gilbert et al. outside thick concrete shielding at the 28-GeV CPS (shown in Table 5.II) are typical.

Table 5.I. Approximate radiation spectrum 5 m above extracted-beam roof shielding. (From Perry, PER D 67.)

Type of radiation	Energy range	Estimated portion of neutron (%)	Estimated portion of total (%)
Neutrons	< 1 eV	< 7	< 1
Neutrons	1 eV - 0.7 MeV	70	20
Neutrons	0.7 - 3 MeV	15	35
Neutrons	3 - 7 MeV	7	25
Neutrons	7 - 20 MeV	1.5	5
Neutrons + protons	20 - 100 MeV	1	5
Neutrons + charged particles	> 100 MeV	0.5	4
Other particles + gamma rays	–	–	< 2

Table 5.II. Neutron dose-equivalent spectrum outside concrete shielding at the 28-GeV CPS.

Neutron energy interval	Neutron DE rate in energy interval (mrem/h)
< 1 eV	–
< 0.1 MeV	1
0.1 to 15 MeV	19
15 to 20 MeV	2
> 20 MeV	37
Total	59

From data such as these it may be concluded that the principal problem outside the shielding of proton accelerators is evaluation of the dose equivalent contributed by neutrons between 0.1 and 100 MeV. Only at the very

highest energy accelerators is it necessary to consider the contribution from neutrons above about 20 MeV.

The contribution to the dose equivalent by charged particles is not often significant. Although there are always some protons in equilibrium with the dominant flux of neutrons, at low energies ionization losses deplete the protons and at high energies (where they are present at densities similar to those of neutrons) their absolute flux density is small and consequently their contribution to the dose equivalent is also small. Good shield design should eliminate charged-particle leakage from cracks or small holes. Such leakage is extremely difficult to monitor. Some attempts using scintillation-counter telescopes (PEN J 68) have been reported, but the technique has not been widely used.

Duty Cycle

The time structure of accelerator beams, described in Chapter 3, can impose severe limitations on radiation-monitoring equipment. Duty cycle is defined as the fraction of time during which an accelerator delivers a useful beam. Low energy accelerators such as the Van de Graaff or Cockcroft-Walton generator supply beam continuously, in which case the duty cycle is 100%. On the other hand, high energy accelerators often have rather poor duty cycles. Thus, for example, the 22-GeV electron linac of the Stanford Linear Accelerator produces beams in pulses of 1- to 2-μsec duration at a repetition rate of 360 pulses per second. The duty cycle is then $< 0.1\%$! High energy proton synchrotrons typically have duty cycles of $\approx 5\%$. An additional difficulty with synchronous accelerators is that the accelerating radiofrequency supply imposes a fine structure on the periodic structure of the accelerated beam. Current in each rf bunch occurs for only a fraction (about 5 to 30%) of the rf cycle, and the beam pulses therefore contain several bunches of particles at time intervals (determined by the rf supply) which may typically have a frequency of a few to several hundred megahertz.

The "prompt" radiation field, with the exception of thermal neutrons, even outside accelerator shielding, is closely correlated (within a few nanoseconds) with time structure of the primary beam (Chapter 3). Readings of pulse counters, described later in this chapter, are particularly influenced by the time structure of the radiation environment, since they may have dead times of several μsec (even longer for Geiger-Müller counters). Ionization chambers are less influenced, but in the more severe duty cycles columnar recombination may occur. Whenever possible the chamber should be operated with adequate voltage to overcome this problem. Should this be impracticable it is important that the chamber be calibrated in the pulsed field in which it is to be used.

An extremely helpful analysis of the impact of duty cycle on the readings of several instruments in the environment of the 20-GeV Stanford electron linac has been given by Jenkins (JEN T 69).

The actual counting rate, R, of an instrument of resolving time τ is given by

$$R/R_0 = f\Delta t/(f\Delta t - R_0\tau),$$

where R_0 is the observed counting rate in counts/sec,
Δ_t is the pulse duration,
f is the pulse repitition frequency,
and τ is the counter dead time,
provided that $\Delta_t >> R_0\,\tau/f$.

Figure 5.1 shows the factor, η, by which the observed counting rate, R_0, of a typical proton recoil proportional counter should be multiplied to obtain the true counting rate. In this case the pulse width of the accelerator, Δ_t, has been taken as 1.5 μsec. We see that at an accelerator pulse-repetition rate of 10 pps the correction factor is about 1.5 at a counting rate of only 2 counts/sec.

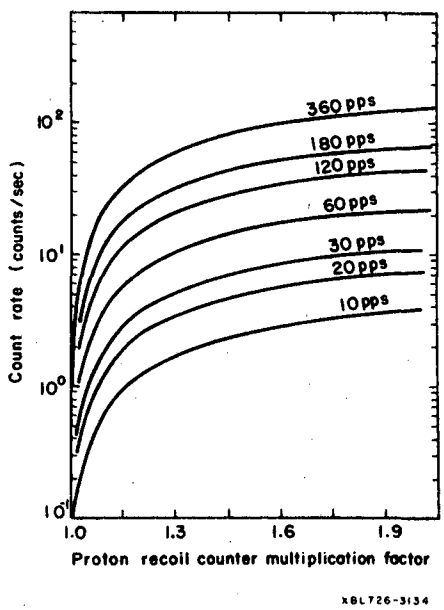

Fig. 5.1. Factor by which the observed counting rate of proton recoil counter of dead time 2 μsec, must be multiplied to obtain the true counting rate, when operated in a pulsed radiation field. (Pulse width-1.5 μsec) as a function of observed counting rate and pulse repetition rate (after T. M. Jenkins.)

When a moderated BF_3 counter is used, the spread in time necessary for neutron thermalization results in a smaller count-loss correction. Jenkins (JEN T 69) has studied the arrival of neutrons at a BF_3 counter surrounded by a 6.3-cm paraffin moderator as a function of time after the beam pulse. Figure 5.2 shows the fraction of total counts arriving in 20-μsec-wide intervals. At the maximum count rate (which in this case occurs at 90 μsec) less than 10% of the total counts occur within the 20-μsec-wide interval. Figure 5.3 shows that 50% of all the counts have arrived by 135 μsec and 80% by 270 μsec. Figure 5.4 shows the correction factor for a BF_3 counter with a dead time of 300 μsec used under these conditions. The dramatic influence of the moderator may be seen by comparing Figs. 5.1 and 5.4. The correction factor of 1.5 now occurs at a counting rate of ≈ 500 counts/sec for an accelerator repetition rate of 10 pps.

Rather than correct instrument readings for the effect of duty cycle, it is sometimes more convenient to circumvent the problem by using a detector which integrates the effects produced by prolonged radiation exposure. Photographic emulsion or thermoluminescent dosimeters readily come to mind as examples of such detectors. Ionization chambers may be operated in a current-integration mode rather than the pulsed mode. Activation detectors too may be used under conditions that minimize or eliminate duty-cycle effects.

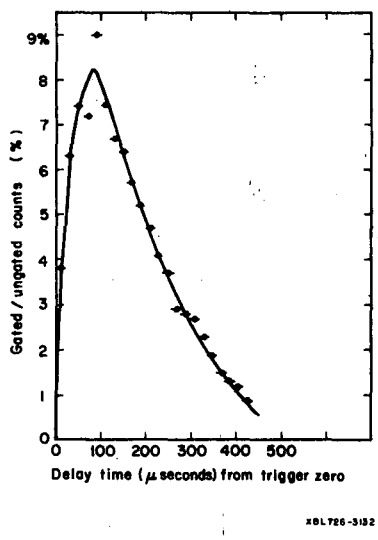

Fig. 5.2. The number of neutrons detected by a BF_3 counter surrounded by 6.3 cm of paraffin in a time interval of 20 μsec, as a function of time following a beam pulse. The ratio of counts in each 20 μsec interval to the total number of observed counts is plotted. (after T. M. Jenkins).

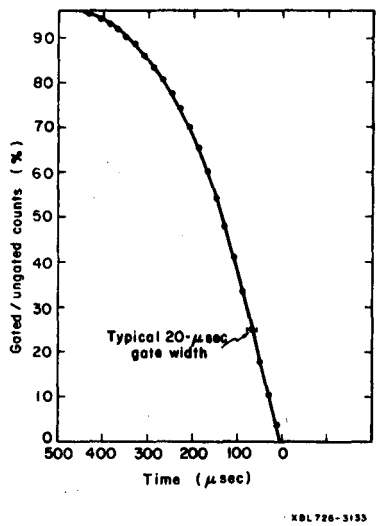

Fig. 5.3. The fraction of neutrons detected by the BF_3 counter as a function of time after the beam pulse (see Fig. 5.2) (after T. M. Jenkins).

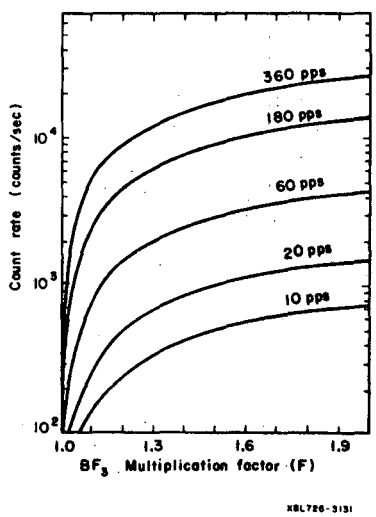

Fig. 5.4. Factor by which the observed counting rate of moderated BF_3 counter must be multiplied to obtain the true counting rate, when operated in a pulsed radiation field (pulse width-1.5 μsec) (after T. M. Jenkins).

SCOPE OF THE CHAPTER

Many of the techniques of radiation measurement used in accelerator environments have wide general application, and are therefore familiar to the health physicist. In this chapter, therefore, we emphasize the techniques and instruments developed to meet some of the special needs at particle accelerators. Familiarity with general practicies in health physics is assumed.

The chapter is divided into two major sections, the first dealing with the techniques of environmental monitoring and the second with personal dosimetry.

In the section on environmental monitors, the use of ionization chambers (often thought by some to be the "conventional" method of radiation measurement) to measure absorbed dose and to determine LET spectra and quality factor is described. This is followed by a description of the alternative techniques of particle spectrometry with nuclear emulsions (and other visual techniques), activation detectors, particle counters, and Bonner spheres. The application of some of these techniques to the design of rem-meters is discussed in considerable detail.

In the second principal section both routine and accident personal dosimetry is discussed.

ENVIRONMENT MONITORING

IONIZATION CHAMBERS

Of the physical techniques available for the quantification of x rays, their production of ionization in gases has been found to be one of the most reliable and convenient. As early as 1928 the International Commission on Radiation Units and Measurements (ICRU) adopted the roentgen as the unit of radiation exposure (ICRU 28) (see Chapter 2). Roesch (ROE W 65) has reviewed the evolution of the definition of "exposure" and its unit, "roentgen", as evidenced in the publications of the ICRU (ICRU 38, ICRU 57, ICRU 62). It seems clear, that foremost in the minds of the early pioneers of radiation protection was the idea that biological effects were quantitatively related to the "amount of radiation" (now called exposure) incident upon the irradiated person.

In this regard it is of interest to note that one of the earliest radiation-protection standards directly related biological effects to the roentgen. Mutscheller (MUT A 25) proposed a maximum annual permissible limit to exposure from x rays of one-tenth of an erythema dose, corresponding to 25 to 50 R per year, depending upon the voltage of the x-ray tube used. Characterization of a field of x-rays incident on the body by a measurement of ionization in air was believed sufficient to predict biological effects.

The desirable simplicity of this view was due in part to the rather low voltage ranges of the x-rays then available to the early radiologists. As the energy of the x-ray sources increased and the radiations emitted by radioactive

substances discovered by Becquerel (at about the same time as Roentgen first observed x-rays) were investigated, it soon became clear that a simple measurement of ionization in gas alone was insufficient; it became common practice to specify, in addition to exposure, information related to photon spectrum, such as the voltage of the x-ray tube or the filtration used.

This additional information then permitted better prediction of biological effects, and to this day such a technique is used in radiotherapy (JOH H 69), for which the distribution of energy absorption in patients exposed to x rays is calculated from a measurement of exposure and from knowledge of the incident photon spectrum.

The determination of dose equivalent in photon fields is simplified because the quality factor is unity in all practical cases (Chapter 2). All that is required, therefore, is a determination of the exposure in air, from which the absorbed dose in tissue. may be calculated.

Consideration must be given to the photon energy spectrum in selecting an appropriate instrument (or instruments). Although the ion chamber is the most commonly used instrument in x- and γ-ray fields for energies in the range from about 50 keV to about 3 MeV, its use outside this range can lead to large errors. At low-energy, wall absorption can be a problem; at high energies it is inconvenient to make chamber walls thick enough to establish particle equilibrium. In practice, however, ion chambers are often used where photon energies extend beyond these ranges. This often produces little error, provided equilibrium has been achieved, which is usually the case outside the shielding of particle accelerators (Chapter 6). Once radiation equilibrium in a shield has been achieved the transmission is governed by the higher energy photons, despite the fact that the dominant-particle flux density (and hence the absorbed dose) is due to low-energy particles. If it is suspected that radiation equilibrium has not been achieved, a convenient check may be made by measuring the ion-chamber response as a function of added absorber around the chamber, up to thicknesses of about 30 g/cm^2. Between 150 keV and 3 MeV the interactions of photons in air and tissue are similar enough to permit the estimation of absorbed dose in tissue by calculation following a measurement of exposure with an air-equivalent chamber. Above 3 MeV pair production becomes increasingly important, and, since the cross section for this process is dependent upon Z^2, it is necessary for any ionization detector to more closely match the composition of tissue. This has led to the development of the so-called tissue-equivalent ionization chambers, particularly for measurements at high energies.

Many aspects of the use of ionization chambers are well understood, and have been discussed with great competence elsewhere. Boag (BOA J 66) has reviewed the entire use of ionization chambers. ICRU Report 17 (ICRU 70) discusses in detail the use of free-air ionization chambers for photon energies below 150 keV. ICRU Report 14 (ICRU 69) considers the dosimetry of photons up to energiew of 50 MeV. Burlin (BUR T 68,

BUR T 70) has described cavity-chamber theory and the determination of absorbed dose with these instruments in some detail. Rather than attempt to review the entire field of ionization chambers, therefore, we limit our remarks to a few topics of special interest with respect to accelerators.

The Measurement of Absorbed Dose with Ionization Chambers

We have discussed how the quantification of x and γ radiation (below energies of about 2 MeV) is conveniently achieved by the use of an air-equivalent ionization chamber to determine the exposure.

In the late thirties and forties it increasingly became the opinion of radiobiologists that the quantity of energy absorbed by biological systems was a better measure of their biological response than was exposure. Moreover, severe difficulties were met in measuring exposure due to neutrons formed by ionization in air. However, the first approaches to evaluation of absorbed energy were made through the measurement of exposure. We quote from D. E. Lea (LEA D 56):

"The roentgen is a unit of dose internationally accepted for γ-rays and x-rays, and capable ofobvious extension to cover most of the other ionizing radiations. It is a unit chosen primarily for convenience in physical measurement, and while 1 R of any radiation represents the same amount of ionization in air it does not always represent the same ionization or energy deposition in tissue. It is necessary therefore in comparing the efficiencies of different radiation to be able to convert roentgens into ionization in tissue or into energy dissipation in tissue. There is no difficulty in principle in converting roentgens into energy dissipation in tissue, and if the elementary analysis of the tissue is known the conversion can probably be made with an error of less than 10%.

"The most obvious unit of energy to employ is the erg. One R of γ rays or x rays involves the dissipation of about 90 ergs/g of tissue."

Contrary to Lea's opinion, however, attempts to extend the use of the roentgen to the measurement of neutrons through the "n unit" (AEB P 42) in the United States or the "v unit" (GRA L 44) in the United Kingdom proved abortive. Conceptually, the idea of energy absorption represents a radical departure from the earlier idea of relating biological effects directly to the external radiation field in which the body is irradiated.

The concept of radiation protection via a determination of exposure is philosophically rather close to the idea of determining the properties of the radiation field independently of its interaction with tissue.

The idea of energy absorption in tissue, however, led to the development of instruments designed to determine absorbed dose. The low dose rates normally experienced in health physics preclude use of the only direct absolute instrument, the calorimeter, which is too insensitive. However, measurement of ionization in a gas provides an indirect means of absolute

determination of energy deposited in the gas. Cavity-chamber theory makes it possible to relate this energy absorption in gas to the energy absorption in dense material.

Cavity Chamber Theory

In principle the absorbed dose rate in any medium may be determined by inspecting the radiation field in a small cavity in the medium. (The cavity is assumed to be so small as not to perturb the radiation field being investigated.) It is possible to relate the ionization produced in the cavity to the ionization in the medium by theoretical means. This relation has led to development of the so-called cavity chamber, often used to measure absorbed dose in a variety of media.

In general the insertion of a cavity chamber into a medium produces a discontinuity in the radiation field, since the cavity differs slightly from the medium with respect to atomic number and electron density.

In the following treatment we consider inserting an infinitesimal gas-filled cavity of mass Δm and density ρ_g into a solid medium. (The suffices g and s are used to refer to appropriate parameters in the gas and solid, respectively.)

The number of ion pairs per gram produced in the gas, $J_g(T)\,dT$, is given by

$$J_g(T)\,dT = n_g(T)\,\ell_g(T)\left(\frac{dT}{dx}\right)_g dT / W\,\Delta m_g \qquad (1)$$

where $n_g(T)\,dT$ is the number of electrons crossing the cavity with kinetic energy between T and $T + dT$,

$\ell_g(T)$ is the average path length traversed by these electrons in the cavity,

$\left(\frac{dT}{dx}\right)$ is the average energy dissipated per unit distance along the track. (This quantity is a function of the kinetic energy of the electron, and under many conditions is different from the stopping power of the electron. Stopping power measures energy removal from the electron rather than energy absorption. If the energy lost by the electron is deposited some distance away from the particle path--as for δ-ray emission, for example-- the stopping power can be larger than dT/dx),

and W is the average energy required to produce an ion pair.

The energy deposited in the cavity is then

$$W\,J_g(T)\,dT = n_g(T)\,\ell_g(T)\left(\frac{dT}{dx}\right)_g dT / \Delta m_g \qquad (2)$$

We are, however, interested in energy absorption in the solid medium rather than in the gas. Consider, then, the deposition of energy in a volume of the solid medium having the same shape as the air cavity but with linear dimensions scaled according to the relation

$$\ell_g(T)\left(\frac{dT}{dx}\right)_g = \ell_s(T)\left(\frac{dT}{dx}\right)_s. \tag{3}$$

The number of electrons $n_s(T)\,dT$ in the energy group T, T+dT crossing the solid volume under the same irradiation conditions is proportional to the relative projected area of the solid volume.

Thus
$$n_s(T)\,dT = \left[\frac{\ell_s(T)}{\ell_g(T)}\right]^2 n_g(T)\,dT. \tag{4}$$

The mass of the solid volume Δm_s is then

$$\Delta m_s = \left[\frac{\ell_s(T)}{\ell_g(T)}\right]^3 \frac{\rho_s}{\rho_g}\,\Delta m_g. \tag{5}$$

The energy absorbed in the solid volume is

$$J_s(T)\,dT = n_s(T)\,\ell_s(T)\left(\frac{dT}{dx}\right)_s dT/\Delta m_s. \tag{6}$$

Substituting for $n_s(T)\,dT$ from Eq. 4 and for Δm_s from Eq. 5 into Eq. 6, we obtain

$$J_s(T)\,dT = [\ell_g(T)]^2\left(\frac{dT}{dx}\right)_g \rho_g\, n_g(T)\,dT/\ell_s(T)\,\rho_s\,\Delta m_g \quad . \tag{7}$$

Now we define a relative mass absorption ratio R(T) by

$$R(T)\,dT = \rho_g\left(\frac{dT}{dx}\right)_s / \rho_s\left(\frac{dT}{dx}\right)_g \quad , \tag{8}$$

whence, combining Eqs. 2, 3, 7, and 8, we obtain

$$J_s(T)\,dT = R(T)\,W\,J_g(T)\,dT. \tag{9}$$

Now, considering the entire energy distribution, we see that we have

$$J_s = \int_0^{T_{max}} J_s(T)\,dT = \int_0^{T_{max}} R(T)\,W\,J_g(T)\,dT. \tag{10}$$

$$\text{But} \qquad J_g = \int_0^{T_{max}} J_g(T)\,dT = \int_0^{T_{max}} \frac{J_g(T)}{R(T)\,W}\,dT, \tag{11}$$

$$\text{whence} \qquad J_s = \int_0^{T_{max}} R(T)\,W\,J_g(T)\,dT$$

$$= \frac{\int_0^{T_{max}} R(T)W J_g(T)dT \int_0^{T_{max}} J_g(T)\,dt}{\int_0^{T_{max}} J_g(T)\,dT} = W\langle R\rangle J_g, \tag{12}$$

where the definition of $\langle R\rangle$ is self-evidently

$$\langle R\rangle = \int_0^{T_{max}} R(T)\,J_g(T)\,dT \Big/ \int_0^{T_{max}} J_s(T)\,dT. \tag{13}$$

The final expression, Eq. 12, is the general cavity-chamber formula, for a gas-filled cavity. The number of ion pairs produced in the gas, J_g, may therefore be related to the energy absorbed in the material if W and $\langle R\rangle$ are known. Throughout the years several theories of cavity chamber operations have been developed—all basically differing in their treatment of the quantity $\langle R\rangle$.

Equation 12 is the general expression that gives the theoretical basis for the cavity chamber.

Several detailed theories have been developed over the past several years to evaluate the parameter $\langle R\rangle$, which appears in Eq. 12.

Bragg-Gray Theory

First suggested by Bragg (BRA W 12) in 1912, this treatment has been developed somewhat (GRA L 29, GRA L 36). In its final form it may be summarized in Gray's *Principle of Equivalence*, which may be stated as:

"The energy lost per unit volume by electrons in a cavity in a solid material is $1/\langle R\rangle$ times the energy lost by γ-rays per unit volume of the solid."

In arriving at this conclusion $\langle R \rangle$ was defined by

$$\langle R \rangle = \left(\frac{dT}{dx}\right)_s \Big/ \left(\frac{dT}{dx}\right)_g , \tag{14}$$

the ratio of the linear stopping powers in the two media.

Two assumptions were implied in the development of the principle:

Assumption 1: Charged particles produced by the interaction of uncharged particles (e.g. neutrons, photons) are assumed to deposit their entire energy locally. This constraint is equivalent to the requirement of absolute charged-particle equilibrium. At higher energies this constraint can lead to inaccuracies, as, for example, when a significant fraction of particle energy loss occurs in the form of δ-rays.

Assumption 2: $\langle R \rangle$ is assumed to be constant with energy. This assumption results in significant errors only when the solid medium and the gas differ in atomic number.

Both these assumptions have subsequently been found not to be entirely true, particularly for photons with energy greater than about 3 MeV. Subsequent theoretical treatments due to Spencer and Attix (SPE L 55.) and Burch (BUR P 55, BUR P 57) have taken δ-ray production into account. Spencer-Attix theory also included the variation of $\langle R \rangle$ with energy.

Both the original Bragg-Gray theory and the Spencer-Attix theory assume that the electron spectrum set up in the medium is undisturbed by the presence of the cavity. Photon or neutron interactions (or both) that produce electrons are assumed to be negligible. These assumptions are equivalent to considering that the medium (chamber wall) surrounding the cavity is the source of all the electrons in the cavity, and that the range of these electrons is much larger than the size of the cavity.

Large Cavities

In a cavity that is large in comparison with the range of electrons generated in the chamber wall, wall electrons make a negligible contribution to the absorbed dose in the cavity. Furthermore, if the cavity and wall are irradiated by photons, the source of electrons is no longer the chamber wall, but the gas in the cavity.

If the cavity is large enough the energy absorbed in the gas is close to that transferred from photons to electrons. Thus, for a large cavity, we can write

$$\langle R \rangle \approx (\mu_s/\rho_s)/(\mu_g/\rho_g), \tag{15}$$

where μ is the mass-energy transfer coefficient.

Equation 15 should be compared with Eq. 8, obtained for a small cavity,

$$\langle R \rangle \approx \rho_g \left(\frac{dT}{dx}\right)_s \Big/ \rho_s \left(\frac{dT}{dx}\right)_g .$$

General Cavity Theory

Burlin (BUR T 70) has developed a more general theory relating the energy absorption per gram of material in a cavity, E_1 to the energy absorption per gram in the surrounding material, E_2. In a simplified form this gives

$$E_2 = A \frac{E_1}{[1-d]\ [\mu_1/\rho_1 \times \rho_2/\mu_2] + d\left[\rho_2\left(\frac{dT}{dx}\right)_1 \Big/ \rho_1\left(\frac{dT}{dx}\right)_2\right]}, \quad (16)$$

where the suffices 1 and 2 refer to the cavity and surrounding material, respectively.

In Eq. 16 the factor A takes account of the disturbance of the photon flux by the presence of the cavity. (For small cavities A approaches unity.) The weighting factor d varies between unity and zero, and expresses the attenuation of the electron spectrum emerging from the wall material, averaged throught the cavity; it is given by (BUR T 70) as

$$d = (1 - e^{-\beta g})/\beta g, \quad (17)$$

where g is the average path length of electrons in the cavity material,

β is the effective mass-attenuation coefficient of the electrons in the cavity material.

As a practical illustration of the use of Eqs. 16, and 17, Svenson (SVE G 69) has described the high pressure ionization chambers used at the Stanford Linear Accelerator Center. These chambers have aluminum walls 1 mm thick, and are filled with air at a pressure of 60 psi. The average path length in the gas (g in Eq. 17) is 5 cm (or 3.2×10^{-2} g/cm^2).

Table 5.III summarizes values of effective mass-attenuation coefficients for the electrons produced by several isotopic sources. These may be derived from the observations (EVA R 55) that

(a) the shape of the electron distribution is essentially unchanged during absorption,

(b) the electrons are absorbed exponentially with a mass attenuation coefficient, β, given by

$$\beta = 17/E_{max}^{1.14}, \qquad (18)$$

and E_{max} is the maximum electron energy in the β spectrum. From these values of β, Eq. 17 may be used to calculate d as a function of energy.

In the last columns of Table 5.III the energy absorption in an air cavity relative to that in aluminum and lead is given. The similarity in atomic number between air and aluminum leads to good agreement between E_{air} and E_{Al}. As expected, however, the variations are considerable for lead.

Table 5.III. Parameters for SLAC high-pressure air-filled ionization chamber. (After Svensson.)

Radionuclide	E_{max} (MeV)	β (cm^2/g)	d	$\frac{E_{air}}{E_{Al}}$		$\frac{E_{air}}{E_{Pb}}$
^{198}Au	0.28	72.9	0.38	1.07		0.79
^{137}Cs	0.48	39.2	0.57	1.09		1.22
^{60}Co	1.04	16.3	0.78	1.02		1.38
—	7.7	1.64	0.98	1.00	≈	1.62

The use of cavity-chamber theory therefore makes it possible for the absorbed dose in tissue to be determined by using an ionization chamber of suitable design. It has to be realized, however, that in practice it can be difficult to obtain the conditions required for the application of the Bragg-Gray principle unless the radiation environment is known. The composition of the walls of the chamber, the thickness of the walls, and the composition of the gas are very critical parameters and are related to the type of radiation to be measured. There are also some practical difficulties in the direct measurement of absorbed dose in the human body. Extensive development of ionization chambers whose walls and gas filling approximate the composition of tissue has been reported in the literature (ROS H 56). Such chambers have been widely used around some high energy accelerators (BAA J 65), but severe practical limitations make their use at low dose rates inconvenient in routine health physics. In unknown radiation fields, a single measurement of absorbed dose is not enough: depth-dose distributions are required for providing the information needed for a correct evaluation. (See Chapter 2.) The rather large volume of adequately sensitive tissue-equivalent chambers makes depth-dose studies in phantoms difficult, with the result that measurements are often made outside the body. *In such a case, of course, depth-dose distributions must be calculated from a physical knowledge of the incident radiation field.*

Tissue-Equivalent Chambers

Tissue-equivalent chambers are essentially a specialized development of the cavity chamber, in which the energy-absorption processes are now related to tissue. We have seen how generalized cavity-chamber theory shows that for small cavities the chamber wall effectively acts as the source of all the electrons in the cavity. In large cavities the gas filling determines the electron spectrum. It is therefore possible in principle to design chambers in which, if either the wall material or gas filling (or both) has an atomic composition similar to that of human tissue, the absorbed dose in tissue due to all types of radiation may be measured.

Rossi and Failla (ROS H 56) have described the design of tissue-equivalent chambers used extensively by the Columbia group. Figures 5.5 and 5.6 show two typical designs. In practice true tissue equivalence may only be approximated. Thus, for example, chambers constructed with walls of polyethylene impregnated with carbon may be adequate for many purposes, but they are not recommended for measurement of thermal neutrons even if they are adequate in the energy range 0.2 to 20 MeV. Chambers constructed of this material, however, give an approximately correct response to thermal neutrons if they have a volume greater than approximately 1 liter and are filled with a tissue-equivalent gas (under these conditions most of the electrons measured will originate in the gas) (ICRU 71). For most applications tissue may be approximated with plastic material having the relative proportions by weight of hydrogen : nitrogen : carbon of 10.1% : 3.5% : 86.4% (FAI G 50). This material differs from tissue principally in that the oxygen in human tissue is replaced in the plastic by carbon. A tissue-equivalent gas mixture is composed of 64.4% methane, 32.4% carbon dioxide, and 3.2% nitrogen (where the percentages refer to the partial pressures). It is possible to use other plastic materials to more closely match the chemical composition of tissue ($C_5 H_{40} O_{18} N$), but their use is often inconvenient (ICRU 71). Particular care in the use of tissue-equivalent chambers must be exercised when neutrons in the energy range from $\approx$ 0.1 to 10 MeV are measured; in this range the hydrogen content of the tissue-equivalent chamber materials is quite critical. Use of the material described by Failla (FAI G 50) can produce errors up to 6% in this energy region.

Further, it has not yet been shown that TE chambers perform reliably under all possible radiation conditions (BAA J 69b). For example it remains to be shown that the energy required to produce an ion pair is the same for energetic heavy ions as for electrons. Nevertheless these detectors have found wide use in many of the radiation environments around accelerators.

At CERN, for example, the reading of a tissue-equivalent chamber has been adopted as a measurement of absorbed dose independent of radiation type and energy (BAA J 65, BAA J 69a), and has even been used in beam dosimetry.

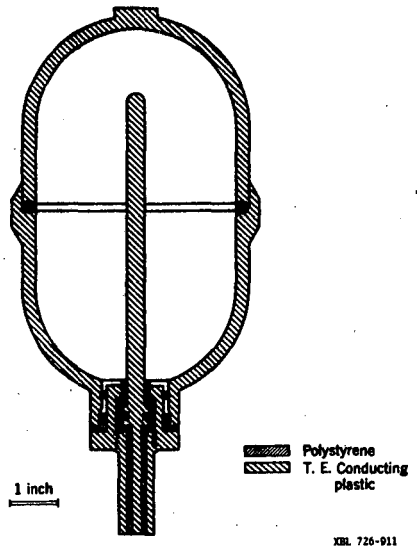

Fig. 5.5. Cross section of a large tissue-equivalent chamber (after G. S. Hurst).

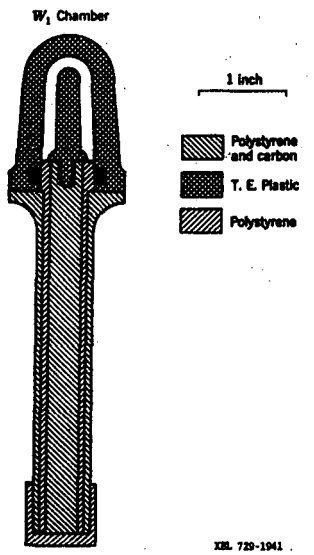

Fig. 5.6. Cross section of a small tissue-equivalent chamber (after G. S. Hurst).

LET Spectrometers

In Chapter 2, determination of the LET spectrum of charged particles produced by the interaction of radiation with matter was shown to be one method of determining dose equivalent.

The dose equivalent, DE, is given by

$$DE = \int_{L_{min}}^{L_{max}} QF(L)\, d(L)\, dL, \tag{19}$$

where D(L) is the distribution of absorbed dose as a function of linear energy transfer, L, and QF(L) is the quality factor at L; L_{min} and L_{max} represent the range of L in the spectrum. Thus dose equivalent may be determined by measuring the distribution of absorbed dose as a function of L This concept is the basis of all LET spectrometers. Rossi and Rosenzweig (ROS H 55a, ROS H 55b) proposed that this distribution could be inferred from a measurement of the pulse-height distribution in a spherical tissue-equivalent proportional counter.

A rough theoretical basis for operation of an LET spectrometer may be found by considering a simple special case. Consider a point source of radiation, S, placed at some distance a from the center of a sphere of radius r (see Fig. 5.7a). Assume that the source emits charged particles of uniform energy isotropically.

The number of particles $N(\theta)\, d\theta$ emitted into the solid angle $d\Omega$, defined by the angles θ and $\theta+d\theta$, is proportional to $\sin\theta\, d\theta$:

$$N(\theta)\, d\theta \propto \sin\theta\, d\theta.$$

Now from Fig. 5.7 it is apparent that

$$\cos\theta = \left\{1 - (r/a)^2 \left[1 - \left(\frac{x}{2r}\right)\right]^2\right\}^{1/2}. \tag{20}$$

Differentiating Eq. 20 gives

$$\sin\theta\, d\theta = \left(\frac{1}{2a}\right)^2 \left\{1 - \left(\frac{r}{a}\right)^2 \left[1 - \left(\frac{x}{2r}\right)\right]^2\right\}^{-1/2} x\, dx. \tag{21}$$

This expression for $\sin\theta\, d\theta$ is proportional to the probability of a particle's having a path length in the spherical volume between x and x+dx. If it is assumed that the linear energy transfer of particles crossing the volume does not significantly change, this so-called path-length distribution may be used to infer the pulse-height distribution directly.

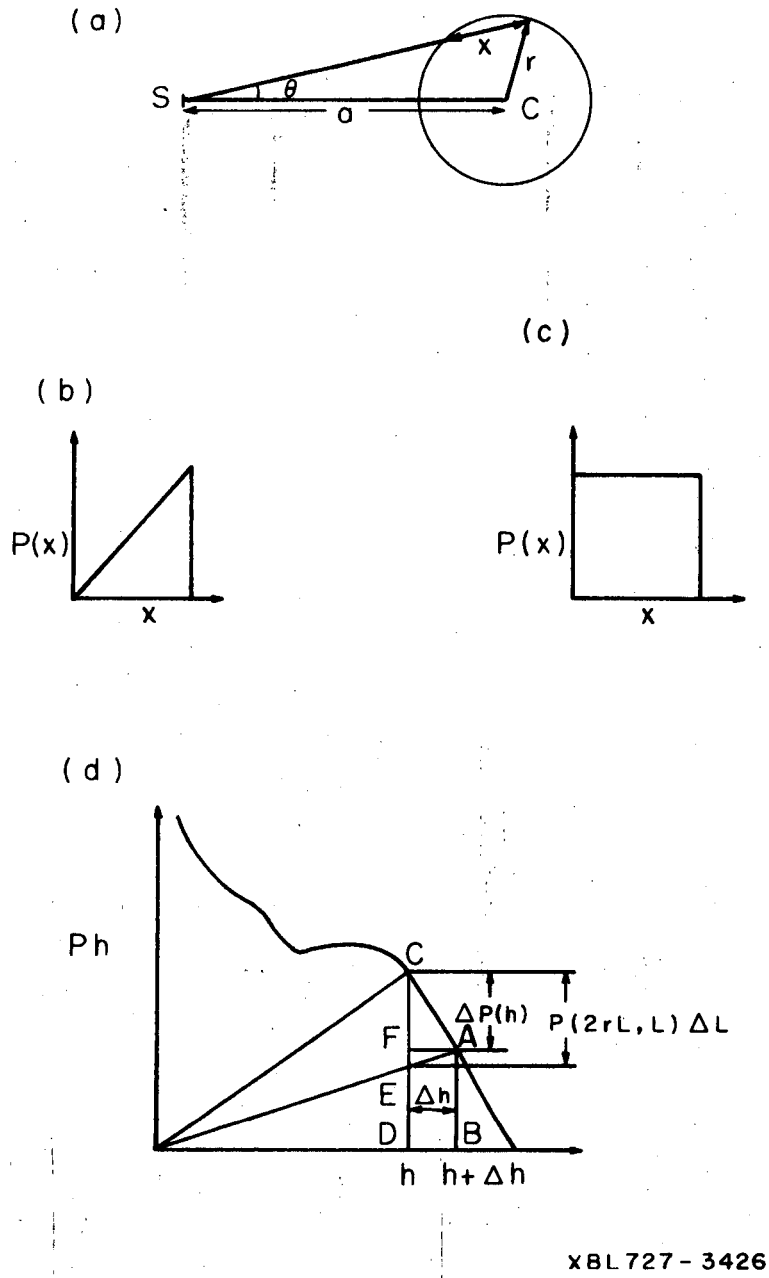

Fig. 5.7. Pulse height distribution in an LET spectrometer (see text).

A particle crosses the spherical volume only in the angular range corresponding to values of x between 0 and 2 r. Thus the normalized path-length distribution, P(x) dx, can be written

$$P(x)dx = \frac{\left\{1 - \left(\frac{r}{a}\right)^2 \left[1 - \left(\frac{x}{2r}\right)^2\right]\right\}^{-1/2} x\,dx}{\int_0^{2r} \frac{x\,dx}{\left\{1 - (r/a)^2 \left[1 - \left(\frac{x}{2r}\right)^2\right]\right\}^{1/2}}} . \qquad (22)$$

Two limiting cases are of particular interest:

(a) when the source is at an extremely large distance from the sphere, i.e. $a \gg r$:

$(r/a) \rightarrow 0$;

(b) when the source is on the surface of the sphere, i.e. $a = r$:

$(r/a) = 1$.

Case a reduces to

$$P(x)\,dx = \frac{x\,dx}{\int_0^{2r} x\,dx} = \frac{1}{2r^2}\,x\,dx, \qquad (23)$$

which gives a triangular path-length distribution (Fig. 5.7b).

Case b reduces to

$$P(x)\,dx = \frac{x\,dx}{\frac{x}{2r}\int_0^{2r} 2r\,dx} = \frac{1}{2r}\,dx, \qquad (24)$$

giving a rectangular spectrum (Fig. 5.7c).

In the measurement of radiation fields at accelerators the detector is in general irradiated uniformly, and thus Eq. 23 is appropriate.

If it is assumed that the energy losses produced in the volume are sufficiently small that we may also assume the linear energy transfer, L, to be constant, the pulse height h, observed from a particle with linear energy transfer L, having a path length x across the volume, is then

$$h = Lx.$$

If the number of particles crossing the volume with linear energy transfer between L and L+dL is N(L)dL, then it is easy to show that the number of pulses between h and h+dh, due to these particles P(h,L) dh dL, is given by

$$P(h,L)\,dL\,dh = \frac{h}{2r^2 L^2}\,N(L)\,dL\,dh \quad \text{for} \quad 0 < h \leq 2rL \tag{25a}$$

$$= 0 \qquad \text{for} \quad (h > 2rL,) \tag{25b}$$

and the absorbed dose D(h,L) is given by

$$D(h,L)\,dL\,dh = K\,h\,P(h,L)\,dL\,dh, \tag{26}$$

where K relates pulse height to absorbed dose.
Integrating over all pulses, we obtain

$$D(L)\,dL = K\,dL \int_0^{2rL} \frac{h^2}{2r^2 L^2}\,N(L)\,dL\,dh$$

$$= \frac{4}{3} K\,r\,L\,N(L)\,dL, \tag{27}$$

which gives the absorbed dose as delivered by particles with linear energy transfer between L and L+dL.

The experimental information most easily obtained is the pulse-height spectrum P(h), which is due to a number of particles N(L) of varying linear energy transfer. Let P (h) dh be the number of pulses in the pulse-height interval (h, h + dh) due to the particle spectrum N(L) (Fig. 5.7d). We see that we have

$$-[P(h) - P(h+\Delta h)] + P(2rl,L)\,\Delta L = P(h+\Delta h)\,\frac{\Delta h}{h} \tag{28}$$

or

$$\Delta P(h) + \frac{N(L)}{rL}\,\Delta L = P(h)\,\frac{\Delta h}{h}\,, \tag{29}$$

and since

$$\frac{\Delta h}{h} = \frac{\Delta L}{L}\,, \tag{30}$$

Eq. 29 becomes

$$\frac{N(L)}{rL}\,\Delta L = -\,\Delta P(h) + \frac{P(h)}{h}\,h\,\frac{\Delta L}{L}\,. \tag{31}$$

Substituting for N(L) dL into Eq. 27 we obtain

$$D(L)\,\Delta L = \frac{4}{3} K r^2 \left[-L^2 \Delta P(h) - LP(h)\,\Delta L\right], \qquad (32)$$

which may be rewritten

$$D(L) = \frac{2}{3} Kr \left[-h^3 \frac{d}{dh}\left(\frac{P}{h}\right)\right]. \qquad (33)$$

By definition, we have

$$k = 1/\frac{4}{3}\pi r^3 \rho_g, \qquad (34)$$

where ρ_g is the density of the gas filling; then, finally,

$$D(L) = \frac{1.6 \times 10^{-7}}{2\pi r^2}\left[-h^3 \frac{d}{dh}\left(\frac{P}{h}\right)\right] \text{ in rads/keV/}\mu,$$

where D(L) = absorbed dose per LET interval, in rads/kev/μ

r = radius of spherical proportional counter (cm),

h = pulse height (in keV/μ),

P = total counts in a given pulse-height interval.

(Compare with Eq. 9, Chapter 2.)

In Chapter 2 we have described how Eq. 35 may be used to evaluate dose equivalent from a pulse-height spectrum. Dvorak (DVO R 66) has described a pulse-analysis system and computer program suitable for reducing Rossi's LET spectrometer data.

Considerable experience of the use of these instruments in accelerator environments has been reported in the literature (ROS H 62, PHI L 65, DVO R 66, OVE T 66). Measurements utilizing this technique require considerable time and equipment. The simple theory of operation described here requires that the particles crossing the chamber suffer no large changes in linear energy transfer. Interactions in the chamber wall or gas filling, and large-angle elastic scattering in the gas, may all produce significant perturbations in the measurements. For this reason these instruments are of little value in radiation fields where neutrons in the intermediate energy region are dominant (ROS H 62). Another limitation is that the proportional counter has a finite recovery time, which limits the particle flux density that may be measured (ICR U 71).

Dvorak (DVO R 66) has pointed out that because the pulse-height spectra obtained are typically exponential, extremely long data-collection

times are required to achieve good statistical accuracy at large pulse heights. This is somewhat unfortunate, of course, in that the large pulse heights are mostly due to particles with high linear energy transfer, which can contribute significantly to the dose equivalent because of their large quality factors. Furthermore certain instrumental difficulties have been noted. Overton (OVE T 66) has described difficulties experienced due to gas leakage, outgassing, and electronic pickup. It is perhaps not surprising to learn that this detector, although promoted by the ICRP/ICRU RBE committee (ICRP 63) has not found general favor at high energy accelerators. A recent survey by Freytag and Nachtigall (FRE E 70) of the experimental techniques used to determine dose equivalent at 23 accelerator centers showed that only one reported an LET spectrometer in common use, and only three others reported such instruments in occasional use. All the laboratories, on the other hand, had found it necessary to use activation detectors in their routine operations. Nevertheless, where the radiation field is constant in composition for several hours, measurements with an LET spectrometer can provide a helpful comparison with dose-equivalent estimates obtained by the routine systems in use. Interpretation of the LET spectra obtained is greatly facilitated if the radiation environment in which measurements are made is well understood (OVE T 66).

Universal Dose-Equivalent Instruments

A single instrument that can measure total dose-equivalent rates in mixed radiation fields has some advantages in radiation protection work, particularly at high energy accelerators. The distribution of dose with LET may be determined by means of the spherical LET spectrometer just discussed. As we have seen, however, this instrument is difficult to use and the interpretation of its readings complicated. Baum and his colleagues have described how some of these difficulties may be overcome (BAU J 67, BAU J 70). The use of multichannel analyzer and complex data-reduction techniques may be avoided by means of specially designed operational amplifier circuits. Baum et al. (BAU J 70) have discussed the alternative methods of operating such a system and the limitations of each system. In tests in mixed radiation fields with effective quality factors between 1.0 and 6.5 the error in QF determination was consistently less than 10%. At small source-to-detector distances the pulse-height spectrum can be distorted, with the effect of producing decrease in apparent QF. (Fortunately this is not the situation in which the instrument is normally operated.)

Baum (BAU J 70) tells us: "A number of other errors should be considered. Changes in the detector gas composition due to outgassing of the sphere wall result in errors in QF of 1 to 2% per month for a well-conditioned sphere. (BAU J 69). Therefore, periodic changes of the gas are needed. Tests indicate that lack of proportionality in the gas gain for large pulses can result

in 7 to 10% errors in apparent QF." [This may be effectively compensated]. 'Particles' starting or stopping within the chamber can result in large errors. For low energy neutrons the problem is particularly acute. (DVO R 69). This effect can be reduced to negligible levels by operation of the detector at submicron equivalent sphere sizes. However, at the low pressures needed to simulate these sizes it is difficult to maintain gas purity for extended periods.

"Several approaches were considered for possible development of mixed-radiation dose-equivalent instruments based on tissue-equivalent detectors with internal gas gain. The most promising approach employs a combination of current measurements and two or more biased amplifiers operating on pulses to achieve the desired output. By suitable choice of bias and gain it is possible to achieve a dose-equivalent output from a single detector followed by two amplifiers and an electrometer. Weighting errors of approximately 24% could occur in fields consisting of particles having a mono-LET energy-loss characteristic (if such fields exist). However, in typical radiation environments the response errors tend to average out and actual errors are more apt to be caused by statistics, depth-dose variations, and errors due to the finite size of the detector cavity. The latter caused particles to change LET as they cross the cavity. If these changes are large, weighting will be incorrect. This may cause errors as large as a factor of 2 for 50-keV neutrons unless simulated sphere diameters can be reduced to about 0.2 μ (DVO R 69). Output in dose rate (mrads/hr) or dose-equivalent rate (mrem/hr) can be obtained from the same instrument by simple switching arrangements. Errors due to divergent field conditions can be limited to less than 10% by maintaining a source-to-detector distance of greater than 3 or 4 detector diameters." (BAU J 70)

Cowan (COW F 72) has described the use of the instrument to measure radiation levels in flight, as part of the program of studying passenger exposure levels in the SST. He reports that useful data are being accumulated, but the instrument is at present critically sensitive to amplifier settings, temperature, pressure, and humidity.

Quality-Factor Determination By Use of Ionization Chambers

In Chapter 2 the determination of quality factors (QF's) by use of the recombination chamber was briefly mentioned. When absorbed doses are measured, as we have previously noted, some estimate of the QF must be obtained to permit dose-equivalent evaluation.

In normal use ionization chambers are designed to avoid ion recombination so that they operate under conditions of saturation. Two types of ion recombination must be considered in the design of ionization chambers.

(a) General or intercolumnar recombination (ions from several particle tracks recombine before they are collected at the chamber electrodes). Boag (BOA J 66) has described the phenomenon in some detail. Because it is dose-rate-dependent it can be of importance in radiation-protection measurements in pulsed radiation fields having short duty cycles (as, for example, at many particle accelerators).

(b) Columnar recombination along a single particle track. Columnar (or initial) recombination is never significant in ionization chambers operated at atmospheric or lower pressure with lightly ionizing radiation. Chambers operated at high gas pressures or irradiated with high LET particles (or both) can,however, exhibit the phenomenon. Jaffé and others have studied the effect both theoretically and experimentally (JAF G 13 a, JAF G 13 b, JAF G 29 a, JAF G 29 b, JAF G 40).

Columnar recombination can be significant when ionization chambers are used to determine absorbed dose due to high LET radiations (e.g., proton recoils produced by neutrons). Zanstra (ZAN H 35) has described how the best value of saturation current may be obtained when initial recombination is significant.

The phenomenon of columnar recombination is not, however, always an inconvenience. Thus Zielczynski (ZIE M 63) and Sullivan and Baarli (SUL A 63) have used the effect "to obtain an indication of effective quality factor for an unknown mixture of radiation" (ICR U 71). A parallel-plate chamber was designed that operates at gas pressure up to 6 atmospheres and with field strengths up to 2000 V/cm. Over a considerable range of field strengths the collected ionization current, i, of such chambers is given by

$$i = K V^n \qquad (36)$$

where K is a function of dose rate and type of radiation,
V is the electrostatic field strength,
and n is a function of LET only.

Figure 2.6 shows the calculated and experimentally determined response of such a chamber as a function of QF. It has been reported that under typical operational conditions the accuracy of QF determination is about 20%. Alternative approaches have been reported that use two chambers with widely differing collection potentials (SUL A 64, DIS C 65) or multiplate chambers (ZIE M 64).

PARTICLE SPECTROMETRY

Activation Detectors

Measurement of radiation environments from a determination of the radioactivity induced in a sample placed in the environment is a long-established technique. Following the discovery by Amaldi et al. (AMA E 35) of the moderation of fast neutrons in hydrogenous materials, slow-neutron capture, and the consequent induction of radioactivity, it has been possible to measure neutron flux densities by activation techniques.

THERMAL-NEUTRON DETECTION

The capture of a thermal neutron by a stable nucleus usually leads to the production of an unstable, neutron-rich nucleus which will decay by the emission of a β particle or the capture of an orbital electron (most frequently from the K shell) into the nucleus. Beta-particle emission is also often associated with emission of one or more γ rays, whereas electron capture is always accompanied by the emission of characteristic x rays, produced during rearrangement of orbital electrons following the occurrence of a vacancy in one of the inner electron shells. Internal-conversion transitions may also result in the production of x-ray emission spectra (EVA R 55). Typical examples are

$$n + {}^{23}Na \rightarrow {}^{24}Na \xrightarrow[15\text{-h half life}]{} \beta + \gamma + {}^{24}Mg$$

and $$n + {}^{108}Cd \rightarrow {}^{109}Cd \xrightarrow{EC} {}^{109}Ag + \text{Ag x rays.}$$

Determination of thermal-neutron flux densities is therefore possible from an absolute determination of the radioactivity induced in a sample placed in the radiation field.

It is sufficiently accurate for our purposes here to write the thermal neutron capture rate, R, as

$$R = N \sigma \phi,$$

where ϕ = is the thermal neutron flux density,

N is the number of atoms per cm^2,

and σ is the thermal neutron absorption cross section.

The activity, A, produced in an infinitely thin sample is, then,

$$A = N\sigma\phi(1 - e^{-T/\tau}),$$

where T is the irradiation time

and τ is the radioactive mean life.

Thus the accurate determination of thermal neutron flux by the use of activation techniques requires accurate knowledge of thermal neutron cross sections and of the nuclear decay parameters of the radioactive species

produced. In addition, techniques for the absolute determination of the induced activity are needed.

In the 30 years since development of the first nuclear reactor the characteristics of slow-neutron interactions have been extensively studied, and comprehensive compilations of thermal-neutron capture cross sections are available.

In addition Lederer et al. (LED C 67) have compiled the nuclear decay parameters (half lives, decay schemes, branching ratios, etc.) of all known radionuclides, and it is therefore possible to select many materials suitable for thermal-neutron detection.

Techniques for absolute determination of activity are now well established and are discussed in many excellent text books. The absolute activity of many radionuclides can be determined to an accuracy within ±1% or less. The accuracy of thermal-neutron flux-density determination by activation techniques usually depends on two factors. Depression of thermal-neutron flux density by the presence of the sample used to detect it can become significant if samples of large mass or absorption cross section (or both) are used. The magnitude of the flux depression has been discussed by several authors (BOT W 43, RIT R 60, SKY T 43, TIT C 51). In certain circumstances (e.g., certain rare earths) a significant contribution to the measured activity may arise from the resonance capture of neutrons in the eV energy region. This difficulty can be avoided by choice of a suitable detector or by enclosing the detector with cadmium.

In summary (NCRP 60), "In a careful thermal-neutron flux measurement, several important factors to be considered are: (1) whether or not the flux is depressed by the detector and by the cadmium wrapper, if used; (2) whether activation may be produced by resonance or fast neutrons; (3) if beta rays are counted, self-absorption in the source must be considered; (4) unwanted activities may be produced as well as the desired activity; (5) a foil thick to the neutron radiation is *not* an isotropic detector; (6) the outer layers of the foil may shield the inner foil from the neutron flux." There should be little difficulty, if these points are considered, in determining thermal-neutron flux densities with an accuracy adequate for helath physics purposes. (At accelerators thermal neutrons rarely present a significant problem.)

Materials which in practice have been found convenient are usually readily available in convenient and pure chemical form, produce only one readily identifiable radionuclide, and have a high thermal-neutron capture cross section but no large resonances in the cross section at neutron energies in the eV energy range. In accelerator environments indium and gold foils have been found to be convenient and are widely used. In addition sodium is often used in suitable chemical compounds. Table 5.IV summarizes the typical sensitivity of thermal-neutron activation detectors used by the Berkeley Health Physics Group (GIL W 68).

Table 5.IV. Activation reactions commonly used in the determination of thermal neutron flux densities.

Reaction	Decay products	Half life	Detector	
$^{115}In(n, \gamma)\ ^{116m}In$	β^- γ : 0.47 MeV (36%) 1.09 MeV (53%) 1.25 MeV (80%)	54 min	γ spectrometer β-particle detector	Four foils 7.6 X 15.2 cm, total mass 46 g, have a sensitivity of 300 cpm/unit flux density.
$^{197}Au(n,\gamma)\ ^{198}Au$	β^- γ : 0.42 MeV (95%)	64.8 h	γ spectrometer β-particle detector	(a) 2.54-cm-diam foil, mass 0.5 g, has a sensitivity of 1.8 cm/unit flux density (Typical G-M counter background: 10 cpm.) (b) 5.08-cm-diam foil, mass 2.0 g, has a sensitivity of 13.4 cpm/unit flux density. [NaI (Tl) crystal background: 48 cpm].
$^{23}Na(n,\gamma)\ ^{24}Na$	β^- γ: 1.37 MeV (100%)* 2.75 MeV (100%)	15 h	γ spectrometer	Used in form of Na_2CO_3 cylinder 4.5 cm diam X 2 cm high, mass 11 g.

*^{24}Na γ-rays in cascade.

MODERATED ACTIVATION DETECTORS

Just as a moderated BF_3 counter may be used to measure fast neutrons ($0 < E < 15$ MeV)--as for example in the long counter (HAN A 47)--so may any activation technique normally used to detect thermal neutrons be used to measure fast neutrons.

Stephens and Smith (STE L 58) first described such a technique, in which the activation of indium foils placed at the center of 6-in.-diameter paraffin spheres encased in cadmium (Fig. 5.8) was used to determine fast-neutron flux densities.

The thermal-neutron capture cross section of gold, the convenient half life (2.7 d) LED C 67), and β emission of the reaction product ^{198}Au make this also a useful and sensitive detector of fast neutrons when appropriate moderators are used (STE L 58). Some neutrons that penetrate the cadmium jacket become thermalized near the centrally located foil and are captured by it; the thermal-neutron flux detected by the gold foil is also (nearly) directly proportional to the incident fast-neutron flux in the energy range from about 0.02 to 20 MeV.

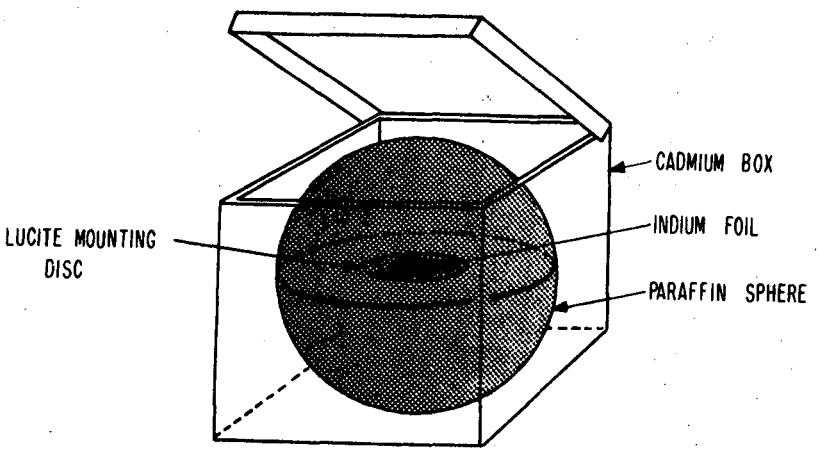

Fig. 5.8. Phantom view showing indium foil placed inside a paraffin sphere inside cadmium base. (from Stephens and Smith).

At LBL the β activity in these 2.54-cm-diam 0.5-g foils is conveniently measured with a thin-window methane flow proportional counter. If a 0.50-g foil were irradiated to saturation in unit flux and counted immediately afterwards, we would observe 2.1 counts/min at the zero bias point of the electronic counting system. For typical counter operation, we observe about 90% of this zero-bias count rate and maintain close check on the operating point through frequent use of the β activity from a ^{137}Cs source. Calibration of the detector with various neutron sources showed it to be fairly insensitive to neutron energy in the range 20 keV to 20 MeV (Fig. 5.9).

Since issuance of the original paper many accounts have been published describing the use of moderated thermal-neutron activation detectors (now colloquially referred to as "moderators"). Simpson (SIM P 64) has reported very careful studies of the angular and energy-response characteristics of both spherical and cylindrical moderators using indium, gold, and cobalt foils. Similar studies have been reported by a group from DESY (BOT G 67). Figure 5.10 summarizes the most recent measurements of energy sensitivity of these detectors in which indium is used.

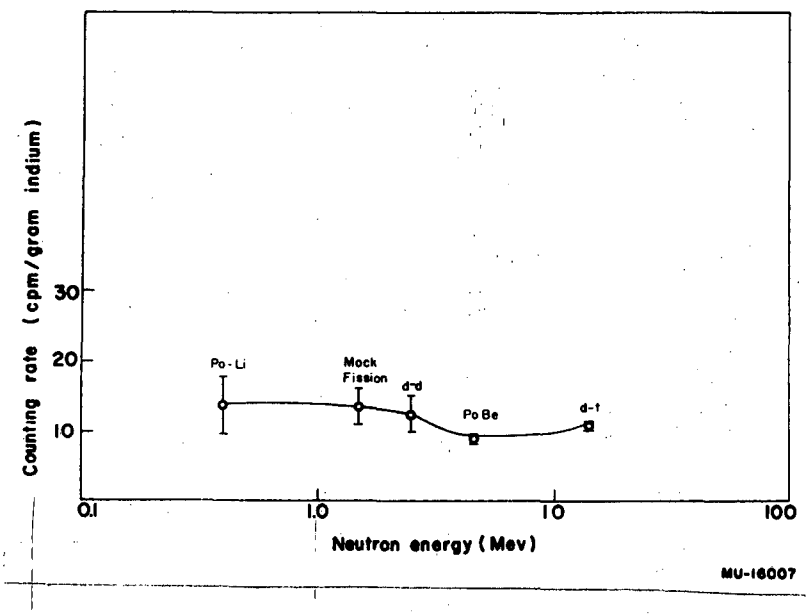

Fig. 5.9. Variation of sensitivity with average neutron energy of 6 in. diam. paraffin moderator (from Stephens and Smith).

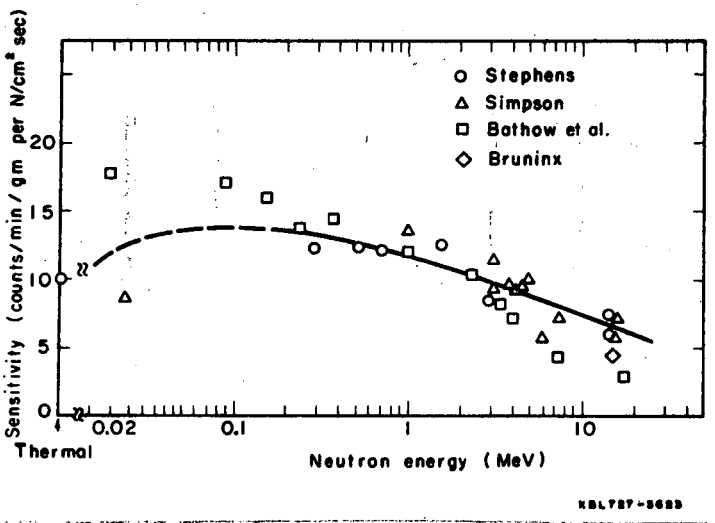

Fig. 5.10. Comparison of several measurements of sensitivity of moderators as a function of neutron energy.

That these detectors are insensitive to γ rays and also able to cope with the pulsed nature of many accelerator environments makes it likely that they will remain in wide use. Many thermal-neutron detectors may be used, giving them wide applicability. Thus Smith has used both cobalt (^{60}Co half life 5.2 y) and tantalum (^{182}Ta half life 115 d) to measure flux densities, integrated over many years (SMI A 61, SMI A 66, CAR T 70).

NEUTRONS OF ENERGY GREATER THAN 2.5 MeV— THE SULFUR TECHNIQUE

The ^{32}S (n,p) ^{32}P reaction is frequently used for the measurement of fast-neutron flux around high-energy particle accelerators. This technique has several advantages:

(a) The resultant ^{32}P is a beta emitter and can easily be separated from most of the sulfur by a simple burning technique if necessary (REI P 58).

(b) The cross section for the reaction has been thoroughly investigated from 1 to 20 MeV (LIS H 62).

(c) ^{32}P half life is 14.3 d; samples can therefore be recounted when required.

(d) Samples are readily available commercially in disk form and are of low cost. The long half-life of ^{32}P does have the disadvantage that the technique is insensitive for short irradiations. At the Rutherford Laboratory the technique is usually limited to the use of convenient 4-g samples (2.54 cm-diam,

0.64 cm thick). The lowest detectable flux for such samples, determined by a count rate equal to the background of the detection equipment, is 10^3 n/cm^2-sec for a 12-h irradiation, and 10^2 n/cm^2-sec if the sample is irradiated to saturation.

Shaw has described the sulfur technique and calibration used at the Rutherford Laboratory (SHA K 63). Calibrations using several monoenergetic neutron sources have been performed, and a calibration constant has been obtained relating sample count rate to neutron flux. For a typical high-energy-accelerator radiation environment, the effective value of the (n,p) reaction cross section is estimated to be 300 mb, with an effective threshold of 3 MeV (SHA K 63).

The count rate at saturation activity, C_{sat}, of a 4-g 1-in.-diam disk is given by

$$C_{sat} = 0.049\,\phi \tag{37}$$

where C_{sat} is in counts/min and ϕ is the neutron flux density in n/cm^2 sec.

Counting is usually performed on either an end-window Geiger counter, a thin plastic scintillator, or a gas-flow proportional counter, the choice of counter depending on the activity of the sample.

If one assumes that the measured activity is due entirely to neutrons, the saturated activity is given by

$$C_{sat} = K \int_{E_{min}}^{E_{max}} \phi_n(E)\,\sigma_n(E)\,dE, \tag{38}$$

where

K is a constant,
$\phi_n(E)\,dE$ is the differential neutron spectrum,
$\sigma_n(E)$ is the cross section at energy E,
E_{min} is the threshold energy for the reaction, and
E_{max} is the upper energy limit of the spectrum.

The integral of Eq. 38 may be expressed as

$$\langle\phi_n\rangle\,(E,E_0)\,\langle\sigma_n\rangle\,(E,E_0), \tag{39}$$

where

$\langle\phi_n\rangle(E,E_0)$ is the number of neutrons greater than E_0m
and $\langle\sigma_n\rangle(E,E_0)$ is an appropriately chosen cross section.

Shaw (SHA K 63) shows that, provided E_0 is chosen greater than E_{min} (the reaction threshold, 2.3 MeV), then a corresponding value of $\langle\sigma_n\rangle(E,E_0)$ may be selected which gives the value of $\langle\phi_n\rangle(E,E_0)$ to within less than 30% for spectra typically found outside thick accelerator shields.

THE ALUMINUM TECHNIQUES—$^{27}Al\left(^{n}_{p,3pn}{}^{\alpha}\right)^{24}Na$— (NEUTRONS GREATER THAN ABOUT 6 MeV

The reaction $^{27}Al(n,\alpha)\,^{24}Na$ is often used to measure neutrons with energy greater than about 6.5 MeV (SMI A 65). The reaction product ^{24}Na decays with a 15-h half life (LOC E 53), emitting two photons of energy 1.37 and 2.75 MeV respectively. The relative transparency of aluminum to these high-energy γ rays makes it possible to use large amounts of material with a consequent high sensitivity.

Gilbert et al. (GIL W 68) have described in some detail the use of this reaction for the measurement of neutrons. The excitation function of the (n,α) reaction is well understood (see Fig. 5.11), and detection systems are conveniently calibrated by using the (d,t) reaction, which produces 14-MeV neutrons. Using large samples (6600 g), Smith has reported that the determination of unit flux density is "not difficult" (SMI A 68).

Gilbert et al. discuss the problems presented by the production of activities other than ^{24}Na in the aluminum detectors. ^{56}Mn is found to be the principal activity due to the presence of impurities (slow neutron capture in ^{55}Mn). This radionuclide is a serious problem only in extremely high thermal-neutron flux densities.

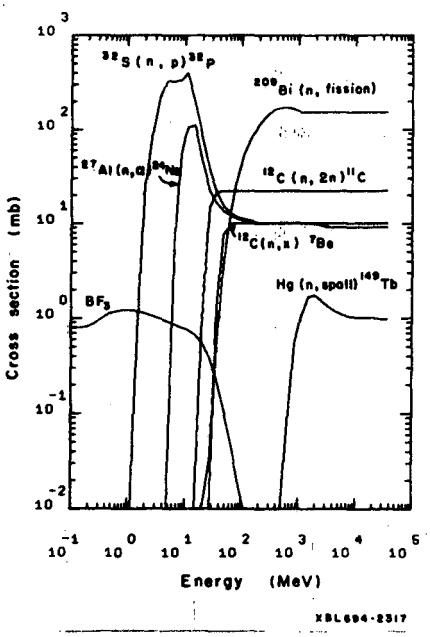

Fig. 5.11. Response functions of high-energy neutron detectors.

The $^{27}Al \rightarrow {}^{22}Na$ reaction

One of the competing reactions in aluminum is the production of ^{22}Na, which may be used as a threshold detector in its own right. The threshold of this reaction is about 30 MeV for incident neutrons, and beyond 60 MeV the production cross section is constant at approximately 10 mb. The half life of ^{22}Na is 2.6 y, and so the sensitivity is low for short irradiations. A 17-g disk is capable of detecting flux densities of $\approx 3X10^2$ particles/cm^2 sec when irradiated to saturation.

NEUTRONS OF ENERGY GREATER THAN 20 MeV—THE $^{12}C \rightarrow {}^{11}C$ REACTION

Carbon-11 is a positron emitter with E_{max} = 0.98 MeV and a half life of 20.34 min. It can be produced from ^{12}C by (p,pn), (n,2n), and (γ,n) reactions, and by other charged particles. The excitation functions for these reactions have been studied experimentally, most information being available for the (p,pn) reaction, for which measurements have been made from the threshold energy (20.6 MeV) to about 28 GeV (CUM J 63).

Beyond threshold the reaction cross section increases rapidly to a peak value of about 92 mb at 35 MeV, then falls to 61 mb at 100 MeV and to 49 mb at 142 MeV, finally reaching a fairly constant value around 27 mb at higher energies.

Fewer experimental data are available for the (n,2n) reaction. The (n,2n) cross section is lower than that for (p,pn) partly because (p,n) exchange collisions can produce ^{11}C but (n,p) exchanges cannot. An effective (n,2n) cross section of 22 mb is used (McC J 60).

The determination of ^{11}C produced from ^{12}C is therefore a practical means of measuring the flux densities of particles with energies greater than 20 MeV in accelerator radiation enivronments. In typical situations outside shielding, the radiation field is such that the only significant ^{11}C activity is produced by neutrons. However, inside accelerator shielding both energetic photons and energetic protons may be present, and careful assessment of the data is necessary.

An extremely convenient technique is to irradiate plastic scintillator in the area to be monitored, and then count the sample on a vertically mounted photomultiplier employing a mineral oil optical coupling (McC J 60, SHA K 62). In practice scintillator sizes used typically range from 2.54 cm long X 2.54 cm diam to 20.3 cm long X 12.7 cm diam, although other sizes may, of course, be used, depending upon the sensitivity required. The entire positron energy is absorbed in the scintillator, and in the larger scintillators a significant portion of the annihilation γ-ray energy is also contained. Special care in selection of the energy interval for counting, the counting-room location, and shielding materials around the photomultiplier is repaid with high sensitivity and reproducibility. This

technique, described in some detail in the Appendix (Section 8), is of very high sensitivity, unit flux densities being easily measurable with the largest scintillators.

When less sensitivity is required (for example in beam-calibration measurements) the ^{11}C produced in graphite, polyethylene, or polystyrene (or any other convenient hydrocarbon) may be measured. In this case the ^{11}C may be assayed by using a NaI spectrometer. Recent comparisons between the plastic scintillator and NaI spectrometer techniques indicate agreement within less than 2% in ^{11}C determination.

^{7}Be PRODUCTION—NEUTRONS ABOVE 30 MeV

A second reaction in carbon samples may often be utilized. The reaction $^{12}C \rightarrow {}^{7}Be$ has a threshold close to 30 MeV for neutrons (actually somewhat higher than the ^{27}Al reaction) and a production cross section which is constant, above 60 MeV, at approximately 10 mb.

^{7}Be decays with emission of 477-keV γ rays in 10% of the events, with a half life of 53.6 d, and may be conveniently counted on a NaI γ spectrometer. The unfavorable γ-ray branching ratio coupled with the long half life of ^{7}Be make this reaction rather insensitive for short irradiations.

The similarity of the nuclear reactions of neutrons and protons with oxygen and carbon has led several authors (McC J 68, CHA V 69, GIL W 69) to suggest and use the measurement of the production of ^{7}Be in water to provide a convenient and economic monitor of protons and neutrons of energy greater than about 40 MeV in the environment of high energy accelerators. This is particularly convenient for irradiations of long duration ($\geqslant$ 150 d) or at high intensities (e.g., in the beam of high intensity accelerators).

NEUTRONS AND PROTONS ABOVE 600 MeV—^{149}Tb PRODUCTION

Above particle energies of 50 MeV there are few nuclear reactions that may be conveniently used to monitor radiation environments. Use of activation detectors having low thresholds can, under some circumstances, lead to significant errors in the calibration of high-energy particle beam intensities. There is some interest, therefore, in developing suitable techniques with high effective thresholds.

Duffield and Friedlander (DUF R 54) first reported the production of ^{149}Tb from gold irradiated by high energy protons. This reaction has a threshold at about 600 MeV and is therefore of some interest in high-energy dosimetry. Furthermore, the decay of ^{149}Tb is effected by the emission of an energetic α particle (3.95 MeV) with a half life of 4.1 h, which facilitates its easy measurement.

The excitation function for the production of ^{149}Tb from gold is now quite well known for proton irradiation. In addition to data of Duffield and Friedlander from 600 MeV to 3 GeV, Winsberg (WIN L 59) has reported

measurements up to 6.2 GeV, Bruninx (BRU E 65) has reported measurements between 7 and 26 GeV, and Franz and Friedlander (FRA E 66) have covered the entire region between 600 MeV and 30 GeV. There are some discrepancies between the earlier data and these more recent measurements. The latter data are preferred for beam calibration purposes. No measurements of ^{149}Tb production cross sections for neutrons have yet been reported in the literature, but it is assumed that at these energies protons and neutrons are equally effective.

Beam calibration is conveniently achieved by irradiating thin gold foils and counting the induced ^{149}Tb activity with a methane gas-flow proportional counter. Typically for a 1-in.-diam disk weighing 0.5 g, a saturated counting rate immediately after irradiation is 2.7×10^{-6} cpm per unit flux (to be compared with a background counting rate in the detector of 0.1 cpm)—thus flux densities of $\approx 10^6$ particles/cm^2 sec and greater may readily be measured.

Thin gold is clearly too insensitive to use for monitoring the relatively small high energy particle flux densities found in the general environment outside the shielding of high energy accelerators (where flux densities of particles above 600 MeV are a few tenths particles/cm^2 sec or less). The range of the α particles emitted by ^{149}Tb in gold is only 11 mg/cm^2, and sensitivity cannot therefore be achieved by increasing the thickness of the gold sample irradiated. The counting of large areas of thin gold foil presents severe technical problems and still lacks adequate sensitivity for any reasonable-sized detector.

In order to increase sensitivity it is therefore necessary to separate the ^{149}Tb produced in large quantities of target material so that detection efficiency may be increased.

The most successful technique of separation so far has been a physical one (McC J 67). It has been observed that the ^{149}Tb produced in mercury (a target nucleus similar to gold) diffuses slowly to the top surface of the liquid. This ^{149}Tb floating on the surface may then be removed by adhesive tape. The process is very slow under normal conditions but may be accelerated by centrifuging the mercury sample. McCaslin and Stephens report that a reproducible fraction ($\approx$ 60%) of the ^{149}Tb is extracted from a sample of $\approx$ 500 g of mercury by centrifuging the sample for 1 hour at an acceleration corresponding to 1700 g. Calibration of the technique with 6.2-GeV protons indicates that the sensitivity of the gold foil technique may be improved by a factor of more than 10^4. At present particle flux densities of $\approx 10^2$ particles/cm^2 sec may be measured. Further efforts are continuing; an obvious improvement may be made simply by more efficient centrifuging. Some success in using chemical separation of the ^{149}Tb from

mercury has also been reported by workers at the Rutherford High Energy Laboratory (SHA J 70).

FUTURE POSSIBILITIES

The detection of spallation products in medium-heavy targets offers some interesting possibilities for a new type of high-energy threshold detector system. Routti (ROU J 69) has reported preliminary studies of the feasibility of direct γ spectrometry of a large number of reactions in one target. As an example, the γ rays resulting from more than 20 nuclear reactions may be observed in copper with a high-resolution Ge-Li detector. Figure 5.12 shows the excitation function for some 11 neutron interactions in copper calculated by use of Rudstam's formalism (RUD G 66). Observation of all these reactions simultaneously would allow use of one target to determine the neutron spectrum in which it is irradiated. The small cross sections of some of the reactions and the low detection efficiency of some of the products may limit such techniques to regions of high flux density.

Table 5.V summarizes important characteristics of currently available activation detectors.

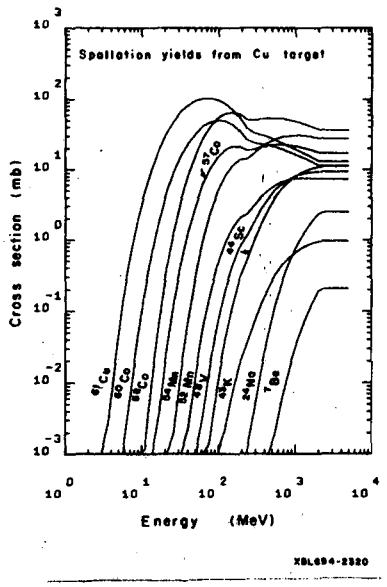

Fig. 5.12. Spallation yields for different reaction products from Cu targets calculated from Rudstam formula. (from Routti)

Table 5.V. Important characteristics of various activation-detector techniques.

Detector	Reaction	Energy range (MeV)	Detector size	Response to unit flux	Background response
sulphur	$^{32}S(n,p)\ ^{32}P$	> 3	1-in. diam 4 g disk	0.049 cpm[a]	10 cpm
plastic scintillator	$^{12}C(n,2n)\ ^{11}C$	> 20	13 to 2700 g	88 cpm[a] at 85% efficiency 1700 g scint	165 cpm 1700 g scint
mercury	Hg(Spal.) ^{149}Tb	> 600	up to 500 g	0.03 cpm[b]	0.1 cpm
gold foils	^{197}Au (Spal.) ^{149}Tb	> 600	1-in. diam 0.5 g	2.7×10^{-6} cpm[b]	0.1 cpm
aluminum	^{27}Al (n,α) ^{24}Na	> 6	16.9 to 6600 g	101 cpm[a] 6600 g E_n = 14 MeV	111 cpm, 16.9 g 118 cpm, 6600 g NaI(Tl)
aluminum	^{27}Al (Spal.) ^{22}Na	> 25	16.9 g	0.21 cpm[a]	67 cpm NaI(tl)
plastic scintillator	^{12}C (Spal.) ^{7}Be	> 30	1 in. diam by 1 in. high	0.0114 cpm[a]	59 cpm NaI(Tl)

a. At saturation and zero time.
c. At saturation zero time and zero bias.

INFLUENCE OF INTENSITY VARIATIONS IN RADIATION FIELD

The particular choice of any nuclear reaction is, in part, determined by the length of the irradiation to be monitored. If the radioactive half life of the measured radioactive specimen is very much longer than the irradiation time the reaction may be too insensitive. If, on the other hand, the irradiation time is very much longer than the half life of reaction product, the result obtained may be quite inaccurate. (The induced activity of the sample reflects only the flux density conditions that prevailed during the latter part of the irradiation.) These considerations are special cases of the more general one of the influence of flux-density variations on the results of measurements using activation detectors.

One of the frequently quoted advantages of activation detectors is that they are not influenced by the pulsed character of the radiation field, as are some counters. However, activation detectors reflect changes in radiation intensity over periods comparable in magnitude with the radioactive half life of the reaction product.

The formation of radioactive atoms is governed according to

$$\frac{dn}{dt} = N\sigma\phi(t) - \lambda n, \tag{40}$$

where n = number of radioactive nuclei present in sample,

N = number of target nuclei present in sample,

σ = effective reaction cross section,

$\phi(t)$ = effective neutron flux density at time t,

λ = radioactive decay constant.

This equation may be rewritten

$$\frac{d}{dt}\left(ne^{\lambda t}\right) = N\sigma\phi e^{\lambda t}, \tag{41}$$

which on integration over the irradiation time, T, gives

$$n = N\sigma\, e^{-\lambda T}\int_0^T \phi(t)\, e^{\lambda t}dt\,. \tag{42}$$

The quantities most often required from activation-detector measurements are the neutron fluence, Φ, given by

$$\Phi = \int_0^T \phi(t)\, dt, \tag{43}$$

and the average flux density $\langle\phi\rangle$, given by

$$\langle\phi\rangle = \frac{\Phi}{T} \quad \frac{1}{T} \quad \int_0^T \phi(t)\, dt \,. \tag{44}$$

Using Eqs. 42 and 43, we may write (LIT D 52)

$$\Phi = \int_0^T \phi(t)\, dt = \frac{e^{-\lambda T} \int_0^T \phi(t)\, e^{\lambda t}\, dt \;\; X \;\; e^{\lambda t} \int_0^T \phi(t)\, dt}{\int_0^T \phi(t)\, e^{\lambda t}\, dt} \tag{45}$$

$$= \frac{n}{N\sigma} \quad \frac{e^{\lambda T} \int_0^T \phi(t)\, dt}{\int_0^T \phi(t)\, e^{\lambda t}\, dt} \tag{45a}$$

Now, because $\phi(t)$ appears in both numerator and denominator, we need determine only some quantity proportional to flux density and not, of course, the absolute value of $\phi(t)$. Thus some suitable record of accelerator intensity or equivalent parameter as a function of time, I(t), may be substituted:

$$\Phi = \frac{n}{N\sigma} \; X \; \frac{e^{\lambda T} \int_0^T I(t)\, dt}{\int_0^T I(t)\, e^{\lambda t}\, dt} \,. \tag{46}$$

NEUTRON SPECTROMETRY USING THRESHOLD DETECTORS

We have described elsewhere in this volume the characteristics of the complex radiation environments around particle accelerators (Chapters 2, 3, and 6). In general the neutron spectra to be measured are characterized by energies and intensities extending over several orders of magnitude, and the flux densities are often small. In the subsequent discussion we draw heavily upon the review by Routti. (ROU J 69)

The use of activation detectors has been proved to be one of the better techniques to measure such neutron fields, but their use does not directly yield the neutron spectrum. A mathematical unfolding procedure is required to obtain the spectrum from a set of measured data.

Formulation of the Problem

The measurement of the radioactivity induced by neutrons yields information on flux density. In principle, simultaneous measurements with several activation detectors, whose excitation functions are known in sufficient detail, can give information on the variation of flux density with neutron energy. The saturation activity of the j th detector A_j is given by

$$A_j = C_j \int_{E_{min}}^{E_{max}} \sigma_j(E)\, \phi(E)\, dE, \quad \text{for } j = 1,2\cdots m\ , \tag{47}$$

where $\sigma_j(E)$ is the corresponding excitation function (cross section as a function of energy),

C_j is a normalizing constant which relates counting rate to neutron flux density,

E_{min}, E_{max} define the energy range of the spectrum,

and m determines the number of detectors.

Equation 47 is a degenerate case of a Fredholm integral equation of the first kind,

$$A(E') = \int_{E_{min}}^{E_{max}} K(E',E)\, \phi(E)\, dE, \tag{48}$$

which arises in many unfolding problems of this nature (MOR P 55).

The composition of the kernel K(E',E) of this integral equation is of great significance in many methods of solution. In practical applications accurate knowledge of the excitation function is necessary, experimental information clearly being preferred. When precise measurements are scant they may have to be supplemented by calculated values. Figure 5.11 shows the excitation functions for several threshold detectors in frequent use at high energy accelerators. These reactions have been discussed in some detail and, in most cases, if suitable samples are used, are capable of measuring flux densities as low as 1 n/cm^2 sec.

Solution of the Fredholm Integral Equation

Several methods exist for the formal solution of first-order Fredholm Integral equations. These formal methods may not be applied, however, when neither the measured distribution A(E') nor the kernel K(E',E) is known analytically. In practice, of course, values of A(E') are obtained as a set of discrete points, when the solution to the Fredholm equation may be obtained by numerical techniques. In most numerical methods of solution the integral equation is approximated by a set of linear equations of sufficiently high order, and the well-known methods of solution for such sets of equations are utilized. Activation-detector spectroscopy presents a severe test of such techniques and special procedures are required to yield an adequate solution. We now discuss in some detail the special problems that arise.

Nonuniqueness of the Solution

When the number of activation detectors, m, is smaller than the number of points needed to adequately define the neutron spectrum, no unique solution to the integral equation may be obtained. In the limiting case in which only one detector is used its response may be matched by a spectrum of any shape, provided it is properly normalized and has some neutrons above the detector threshold. If no restrictions are placed on the shape of the solution, the homogeneous system--the system with zero responses--has also nonzero solutions. Such solutions may appear as unwanted oscillations in the solution of the nonhomogeneous system. This is exemplified by a calculation by Burrus (BUR W 65), which shows that for any integrable kernel the attenuation of a sinusoid increases. In any practical measurement neither the responses nor the kernel are known exactly. These uncertainties add to the uncertainty of the solution.

Solution Classes

The terms "exact," "approximate," and "appropriate" are often used to characterize the solution obtained. An exact solution satisfies accurately

the activation equations but often has unacceptable oscillatory character. An approximate solution matches the responses only within reasonable error limits. Selection of a physically acceptable approximate solution yields an appropriate solution, which is generally not unique. The remaining ambiguity reflects the accuracy and the number of responses and the composition and accuracy of the kernel.

Prior Information on the Solution

The selection of an appropriate solution among the nonunique solutions requires the use of prior information on the solution. Such information is almost always available on physical grounds. In neutron spectroscopy the solution is known to be nonnegative, and zero beyond certain maximum energy. Beyond some thickness of shielding the neutron spectrum can also be assumed to be relatively smooth. Additional information on its intensity or shape may be available at some energies.

In the solution technique it is important to properly weigh the prior knowledge and the information contained in the measured responses. The additional constraints applied to the solution should not prevent it from matching the measured responses, nor should they prevent the solution from assuming any physically acceptable shape.

Requirements for a Solution Method

Any appropriate solution method for the determination of a neutron spectrum from activation measurements has to meet two basic requirements.

The first requirement is that the neutron spectrum found be a solution to the activation equations if such a solution exists. This means that the method has to be able to find a solution that accurately matches the responses due to any reasonable spectrum.

The second requirement is that if there be many solutions to the activation equations, then an appropriate solution must be found. In other words there must be a flexible way to apply physical prior information on the solution, such as nonnegativity conditions and requirements of smoothness and general shape of the solution.

In determining neutron spectra from measured data some difficulties are likely to arise. Because of measurement errors and large uncertainties in the response functions one often encounters inconsistent sets of responses, that is, responses for which no appropriate solution exists. In such a case a compromise has to be made between the requirement of matching measured responses and satisfying the prior information on the solution. But here again, with such cases, we can have confidence only if the solution method is known to be able to find a reasonable solution if such exists. The flexibility in applying the constraining information to the solution is also of major importance with these cases.

Testing Solution Methods

It is important to make sure that the solution method employed meets the requirements discussed above. This can be done conveniently by simulating the experiment by specifying test spectra and computing the responses of different detectors for these given test spectra. Uncertainties in the response functions and in the measurement are simulated by introducing random errors in the synthesized responses or in the response functions. the solution is then obtained from the synthesized responses without using any other information.

The testing procedures are much easier to perform in this manner than with actual measurement. Furthermore "the true solution" is known and can be compared with the spectrum obtained.

To illustrate the testing procedure we use the block diagram shown in Fig. 5.13. A test spectrum, ϕ^{test} which has a reasonable shape for a high-energy neutron spectrum is first specified. The responses due to this are obtained by simply integrating the activation equations. The errors and uncertainties in the measurement and in the cross sections can be simulated by perturbing these responses by random deviations. We thus get the input responses A^{input}. In a measurement we of course obtain these input responses without knowledge of the true spectrum and true errors.

In determining the solution spectrum ϕ^{sol} one combines the information contained in the input responses with the prior information. And finally, or usually in the course of finding the solution ϕ^{sol}, we also compute the responses A^{sol} corresponding to ϕ^{sol}.

The requirement of ability to satisfy the activation equations can be restated now in the following words. If we start with a reasonable test spectrum and do not use any perturbation--that is, $A^{input} = A^{test}$--then the method employed has to find such a solution that $A^{sol} = A^{input} = A^{test}$. For this to be true it is generally not necessary that $\phi^{sol} = \phi^{test}$, although such a conditon would also satisfy the requirement.

It is very instructive to use the test procedures in studying the importance of the a priori conditions as well. With many response kernels a synthesized response may be easily matched with an appropriate solution that may be quite different from the test spectrum. In such cases we need to estimate the amount of prior information required for a close match between the two spectra. This is closely related to what could be called the inherent resolution of the kernel. That determines how exactly the solution is defined without using any prior information on the solution. In many cases specific prior knowledge of the solution must be applied to obtain an appropriate solution that is less ambiguous.

To estimate the success obtained in a test case we check the match between the test and the solution responses and the closeness of the solution to the test spectrum. We also evaluate the agreement of integral quantities such as the flux, the dose rate, and the mean energy.

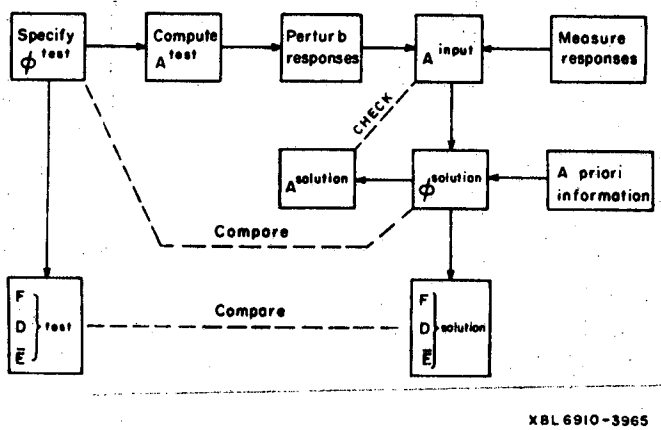

Fig. 5.13. Block diagram of the procedures used in testing the solution methods and analyzing measured data. (from Routti)

Review of Existing Solution Methods

Several numerical techniques have been applied to the solution of neutron spectra from activation-detector measurements. Most such studies have been directed towards the determination of epithermal and fast-neutron spectra in nuclear reactors. The extension of these techniques to high-energy neutron spectroscopy has not always been successful, because of lack of suitable detectors and reliable cross-section data, inadequate prior knowledge of the solution, and the wide energy and intensity ranges encountered.

The utilization of prior information on the solution is essential to obtain a physically acceptable solution. This is done either by smoothing procedures, by nonnegativity constraints, or by a choice of suitable expansion functions. In the following some of the methods employed for fast-neutron spectroscopy and their applicability to high-energy neutron spectrometry are discussed.

Parametric Representation

If there is available a functional representation of the neutron spectrum, based either on theoretical considerations or on previous experimental results, then the parameters in such a representation can be determined by

matching the measured responses. For instance, in reactor experiments both thermal-neutron and fission spectra can be approximated by such formulae. Functional representation of neutron spectra has been applied to high-energy neutron spectroscopy as well (OMB R 67, SKL L 67, PAT H 69). The formula often used assumes a spectral shape of E^{-n} form, or a spectrum composed of several such sections of different slopes on a logarithmic scale, with possibly a smooth extension to zero at cutoff energy. The slope of the spectrum, the parameter n, and possible other parameters can be easily determined by matching the measured responses in the least-squares sense.

Parametric representations of this kind severely restrict the form which the neutron spectrum may assume. Consequently they should be used only when such restrictions are well founded, or more often, when not enough experimental information is available for other approaches. On the other hand this approach avoids most mathematical complications peculiar to other methods, and in some cases allows determination of neutron spectra directly from calculated tables, as described by Patterson et al. (PAT H 69).

Orthonormal Expansions

Several numerical techniques used for the solution of neutron spectra from the activation equations can be classified as series-expansion methods. The neutron spectrum is expressed as a sum of linearly independent functions $\psi_k(E)$,

$$\phi(E) = W(E) \sum_{k=1}^{m} \beta_k \psi_k (E) , \qquad (49)$$

where $W(\gamma)$ is a weighting function and m, the number of terms, is equal to the number of response functions. In the selection of the expansion functions one may try to satisfy boundary conditions of the solution, and use orthonormal functions to simplify the calculations. Orthogonal functions can be obtained also from the cross sections through the Gram-Schmidt procedure. The formalism of the orthonormalization and the determination of the coefficients β_k in the expansion through known techniques of linear algebra have been discussed in detail by Ringle (RIN J 63) and Di Cola and Rota DIC G 65). With such techniques the linear independence of the response functions is of great importance; this requirement often limits the choice of activation detectors.

The application of orthonormal expansion techniques to neutron spectroscopy have been studied by several authors. Ringle investigated their use with threshold detectors in the energy range of 2.5 to 30 MeV, and Gold (GOL R 64) and Di Cola and Rota in the determination of reactor fast-neutron spectra with activation foils. Severe limitations in the reliability and accuracy of the method were found in the studies. The

convergence rate of the expansion is often not adequate to provide good accuracy and physically acceptable boundary conditions in the solution with a limited number of terms. Proper choice of the functions can improve the convergence; the necessity of such choice limits the flexibility of the method. Unfortunate choice of detectors may result in an ill-conditioned system in which small changes in known terms result in large variations in the solution. The solution often assumes negative values, and it is not possible to easily use nonegativity or other prior information of the solution. The deficiencies of the expansion methods are likely to be amplified when a larger energy range is covered by few detectors.

Least-Squares Expansion Methods

In the least-squares expansion or relative-deviation-minimization method the neutron spectrum is again expressed as a sum of expansion functions, as in Eq. 49. The coefficients β_k are determined by minimizing the quadratic form

$$Q = \sum_{j=1}^{m} \left[\frac{A_j - \sum_{k=1}^{n} \beta_k \int_0^{E_{max}} W(E)\, \psi_k(E)\, \sigma_j(E)\, dE}{A_j} \right]^2 \qquad (50)$$

with respect to β_k.

This minimization can be performed for $1 \leqslant n \leqslant m$. The optimal value of n corresponds to smallest Q and a physically acceptable solution; in most cases this is found when $n < m$. The case $n = m$ is equivalent to the formal expansion method discussed in the preceding section. The details of the procedures are discussed by Di Cola and Rota.

The success in the least-squares expansion method depends strongly on the choice of the basis functions. A proper choice gives an opportunity to satisfy the boundary conditions and reflect the expected behavior of the solution.

Least-squares techniques have been applied to the study of reactor fast-neutron spectra with activation detectors. Chebyshev and Laguerre polynomials have been used as expansion functions; both were found to give physically acceptable results (RIN J 63, COL G 65). The method has generally been found superior to the orthonormal expansion method. Di Cola et al. found the method to be more sensitive to the effects of experimental errors, but the results were still better than those from orthonormal expansions.

The minimum-relative-deviation method has been applied to high-energy neutron spectroscopy in the range of 2.5 to 30 MeV by Kohler

(KOH A 64). Step-function and polygonal approximations were used for the solution. An iterative technique was employed to minimize the sum of the squares of the deviations with respect to parameters defining the amplitude of each step. These parameters were squared to impose the nonnegativity.

Although least-squares expansion methods have shown good success in the determination of the reactor fast-neutron spectrum, their use is less profitable with high-energy spectra. Since both the shape and the energy range of the spectrum may vary widely, it is difficult to find generally applicable basis functions. The step-function and polygonal approximations provide flexibility in this respect; however, the resolution, which is dictated by the small number of the expansion terms, remains very poor. Furthermore it is not possible to use prior information on the neutron spectrum in a flexible manner.

Iterative Unfolding Method for Response Matrices

An iterative unfolding method has been described by Scofield (SCO N 62) and Gold (GOL R 64). The method finds nonegative solution by minimizing through an iterative procedure the deviation between the measured and computed responses. The procedure is terminated after a certain number of iterations or when the deviations pass through a minimum.

This iterative method has been applied to proton-recoil spectroscopy by O'Brien et al. (O'BR K 67) in the study of high-energy accelerator leakage spectra, to multisphere spectroscopy by Awschalom (AWS M 66), and to multisphere and threshold-detector spectroscopy by Stevenson. (STE G 67). The procedure was compared to least-squares techniques by Su (SU Y 67).

The studies indicate that the method compares favorably to the others discussed above. The studies of multisphere technique by Awschalom and Stevenson indicated good success in the computation of integral quantities, such as flux and dose, in unfolding given test spectra. The determination of differential spectra indicated larger deviations from test spectra. In application to threshold detectors the method failed to match some of the responses, and consequently there was significant discrepancy between the solution and the test spectra (STE G 67). The method imposes a nonnegativity condition on the solution, and it is possible to use also smoothness constraints. The application of specific prior knowledge, such as cutoff energy or preferred spectral shape, has not been incorporated in the method.

Iterative Perturbation Methods

An iterative technique which employs the on-line facilities of the CDC-6600 computer has been developed at LBL and used for the analysis of high-energy neutron spectroscopy with few threshold detectors (GIL W 68). A cathode-ray-tube display is used with light-pen input. The user draws a spectrum with the light pen on the screen, after which the responses are computed for each detector. The solution is then perturbed in order to get a better match between the computed and the measured responses. After a number of trials the responses are matched, with an accuracy reflecting the experimental errors. The procedure also allows the user to apply any prior knowledge of the solution.

With an increasing number of detectors with overlapping response curves it becomes increasingly difficult to make decisions on the direction of the next iteration. This and the slow speed restrict the applicability of this method to the study of systems with relatively few response functions. In such cases, however, it performs quite well and avoids all the numerical difficulties that are common with all the other methods mentioned.

An iterative method in which the subsequent perturbations to the initial trial spectrum are automatically computed by using energy-dependent sensitivity functions has been reported by McElroy et al. (McE W 67). This method has been successfully applied to the determination of neutron spectra, mainly reactor spectra in the energy range 10^{-8} to 18 MeV. Hargreaves and Stevenson (HAR D 68) have employed a simpler iterative technique based on regions of maximum response defined for each detector. The results reported from such calculations applied to high-energy neutron spectroscopy are still somewhat inconclusive. The iterative procedure used imposes the nonegativity condition, but ill-conditioned cases may still result in diverging solution. The results obtained with the simpler method, however, indicate that as good results can be expected as with the more complex procedures mentioned (HAR D 68).

Constrained Least-Squares Methods With Matrix Inversion

A numerical technique for the solution of first-order Fredholm integral equations incorporating a controlled degree of smoothness or closeness to a given approximative solution has been proposed by Phillips (PHI D 62) and further developed by Twomey (TWO S 63). More recently extensions of these techniques have been reported by Greer et al. (FRE C 67) and Strand and Westwater (STR O 68). A generalized formalism was introduced by Routti (ROU J 69) and is discussed below.

The integral equation

$$\int_{E_{min}}^{E_{max}} K(E',E)\,\phi(E)\,dE = A(E') + \epsilon(E') , \qquad (51)$$

where $\epsilon(E')$ reflects the uncertainties and error, is first replaced by a quadrature form

$$K\phi = A + \epsilon . \tag{52}$$

Here A is the measured spectrum with components A_j and errors ϵ_j, $j=1, \cdots, m$; ϕ is the solution vector with components ϕ_i, $i= 1 \cdots n$; and K is the response matrix of dimensions n X m. In the derivation of the quadrature form we approximate the solution by a piecewise linear continuous function. With an adequate number of steps this approximation provides an arbitrary closeness to any real continuous function without prescribing the shape of the solution.

The solution of the integral equation is obtained by minimizing the quadratic form

$$Q = Q_0 + \gamma (W_1 Q_1 + W_2 Q_2). \tag{53}$$

where

$$Q_0 = \sum_{j=1}^{m} r_j^{\epsilon} \epsilon_j^2,$$

$$Q_1 = \sum_{i=1}^{n} r_i^{\phi 0} (\phi_i - \phi_i^0)^2,$$

$$Q_2 = \sum_{i=2}^{n-1} r_i^{d} (\phi_{i=1} - 2\phi_i + \phi_{i+1})^2.$$

The term Q_0 is related to the matching of the responses, which can be weighted by r_j^{ϵ}. The term Q_1 requires closeness to a given approximate solution ϕ^0; this criterion may be weighted with an energy-dependent function specified by weights $r_i^{\phi 0}$. The term Q_2 imposes a smoothness requirement by including the numerical second derivative of the solution in the sum to be minimized; this also can be weighted with energy-dependent terms r_i^d.

The auxiliary conditions included in terms Q_1 and Q_2 are weighted relatively by W_1 and W_2, and finally γ specifies the overall importance of the a priori conditions. The solution is obtained by minimizing Q with respect to ϕ_i by setting

$$\frac{\partial Q}{\partial \phi_i} = 0, \text{ for } i = 1, \cdots, n. \tag{54}$$

The resulting equations can be written in matrix form and solved in a single matrix inversion (ROU J 69).

Somewhat similar techniques are used in the method reported by Tikhonov (TIK A 63). In this case the sum to be minimized includes the norm of the solution and its first derivative. The application of that method to the multisphere spectroscopy has been proposed by Buxerolle et al. (BUX M 67).

The statistical aspects of the numerical solution techniques have been discussed by Burrus (BUR W 65) and Strand and Westwater (STR O 68). The latter treat the problem where the covariance matrices of both the observed vector A and the solution ϕ are known, and derive an optimal smoothing criterion based on maximum-likelihood method.

Greer et al. (GRE C 67) have discussed in detail the case in which the function to be minimized may be written as

$$Q = \sum_{j=1}^{m} e_j^2 E \sum_{i=1}^{n} \left(\frac{\phi_i - \phi_i^0}{\phi_i^0} \right)^2 . \qquad (55)$$

An iterative procedure was derived in which the problem is solved in several steps by replacing the approximate solution ϕ^0 by the solution ϕ of the preceding step. The limiting solution, which except for numerical difficulties may be obtained directly, is shown to converge to the solution that is closest to the original trial solution in the least-squares sense. The iterative procedure has been applied by Greer et al. to the determination of reactor fast-neutron spectra from activation-detector measurements. Generally a fission-neutron spectrum was used as initial trial solution. Good results for both integral and differential quantities were obtained in test cases and with actual data.

The methods described provide convenient means to apply prior information on both the smoothness and the shape of the solution. However, the nonnegativity of the solution is not guaranteed. This leads into difficulties with large uncertainties in the measured responses and the cross sections, where a compromise must be made between matching the responses and satisfying the prior information. It is also difficult to properly weigh the auxiliary conditions in cases in which the neutron spectrum extends over very many orders of magnitude. On the other hand, the computation is quite fast even in cases with many response functions, such as proton recoil spectroscopy.

Generalized Least-Squares Method With Nonnegative Solution

To overcome the difficulties of the above matrix-inversion methods Routti has developed a formalism in which the solution is forced to be nonnegative and the auxiliary conditions can be used on several different scales (ROU J 68). The neutron spectrum is again approximated by a piece wise linear continuous function defined at energy points E_i by intensity values ϕ_i, which are taken

to be squares of real numbers, ϕ_i^2, to eliminate negative values. The requirements of matching the measured responses as well as satisfying the a priori conditions are combined by defining a quadratic form as in Eq. 53. Because of computation-economy requirements the neutron spectrum may be defined at fewer points than the cross sections. The constraints about the smoothness and approximative shape of the spectrum are now expressed either on a linear, a relative, or a logarithmic scale--for instance, on a logarithmic scale, as

$$Q_1^{\log} = \sum_{i=1}^{n} r_i (\log X_i^2 - \log \phi_i^0)^2, \tag{56}$$

$$Q_2^{\log} \sum_{i=2}^{n-1} r_i^d (\log X_{i-1}^2 - 2 \log X_i^2 + \log X_{i+1}^2)^2.$$

The solution can no longer be obtained through matrix inversion, but rather by minimizing Q with respect to the parameters X_i through iterative techniques. A gradient minimization technique with variable metric to be well suited for this computation was found (ROU J 69).

The formalism described above allows us the combination of prior information of the neutron spectrum with the information contained in the measurement of the responses in a very flexible form. The method and the computer program LOUHI (ROU J 69), written to perform the analysis, have been subjected to mathematical tests, discussed in the section of Testing Solution Methods. These results indicate that the method meets all the requirements set therein for a solution method. The technique is best suited for a large computer. In most cases the solution obtained is not a sensitive function of the weighting parameters used in the expression of Q. However, when largely perturbed test responses or inconsistent sets of measured data are used, the analysis benefits greatly from the possibility of running LOUHI on-line with cathode-ray-tube display on intermediate results and the option of choosing optimal weighting parameters while solving the problem.

Examples and Comments

To illustrate some of the points made of testing and analysis procedures we next consider a few examples. These computations have been performed with the program LOUHI. All the cases discussed have been run by using a uniform logarithmic smoothing criterion and no other prior information on the solution.

Figure 5.14 shows a test case run with a simulated neutron spectrum having a 14-MeV peak and the emulsion kernel. Excellent agreement is

obtained between simulated and calculated spectra, for both protons and neutrons. In this case the very good agreement between the solution and the test spectra is due to an unrealistically close match between the two proton spectra. If the proton spectrum had realistic uncertainties, then such a close match would result in an oscillatory solution spectrum. Figure 5.15 shows a case in which such oscillations have been avoided by using the smoothing criteria; however, the agreement between the test and solution spectrum is no longer so good.

With kernels of lower resolution than that of the emulsion kernel the statistical uncertainties of the responses often are not recognizable. In such cases even the perturbed responses may be matched arbitrarily accurately without introducing unacceptable oscillations in the solution spectrum. And often it is difficult to say whether the structure in the solution spectrum necessitated by a close match of the input responses is due to errors in the data or to real structure of the neutron spectrum. For example, in Fig. 5.16 we show a neutron spectrum obtained from a set of detectors exposed inside the beam tunnel of the CERN PS. (GIL W 68). Requiring a 5% match between the measured and computed responses necessitates the structure shown in the spectrum. If only four of the seven detectors exposed were used, or if 50% descrepancies between the measured and the computed responses were accepted for the other three detectors, then the smoother solution shown could be obtained. In this case it is difficult to know whether the structure is real or only a reflection of experimental uncertainties.

Kernels of lower resolution often leave some ambiguity in the results even when there are no errors in the input data. For example, in Fig. 5.17 there is considerable discrepancy at low energies between the test and the solution spectra despite an excellent match between the unperturbed input responses and the solution responses. In this case it is obviously caused by the lack of any response of the detectors at low energies. But often such discrepancy is more subtle, and can be best explained by the limited inherent resolution of the kernel. This quantity unfortunately cannot be easily characterized by any single number, but rather has to be determined in each case by using the testing procedures.

The limited inherent resolution also explains the apparent inconsistency that different solution spectra are obtained when different initial guesses are used in iterative methods. Once the responses have been matched accurately then the remaining ambiguity of the neutron spectrum depends on the a priori information specified or built into the program, rather than indicates any inadequacy of the method. For the same reason it is quite difficult to obtain reliable estimates of the accuracy of the spectral shape, or confidence limits of the solution, from a single computation. Rather this has to be estimated through multiple trials with different starting values and perturbed input responses.

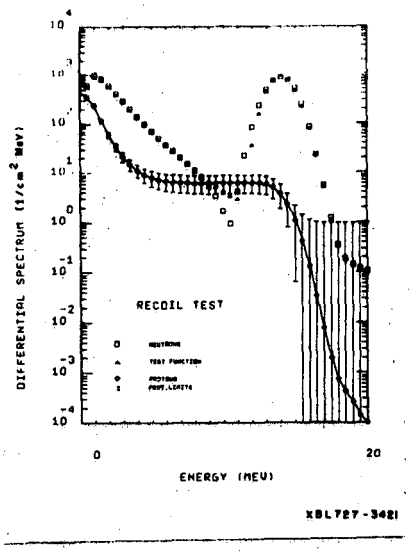

Fig. 5.14. Results from a test case with the proton-recoil scattering kernel. (from Routti)

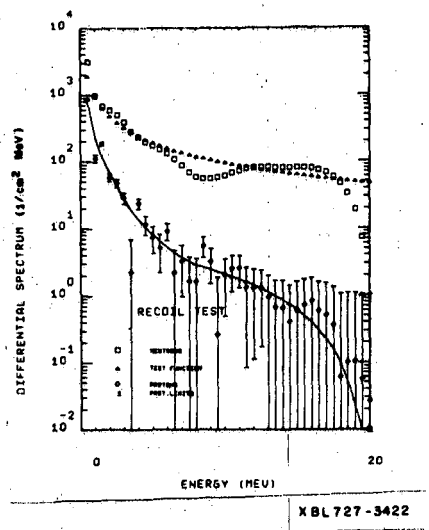

Fig. 5.15. Results from a test case with the proton-recoil scattering kernel. (from Routti)

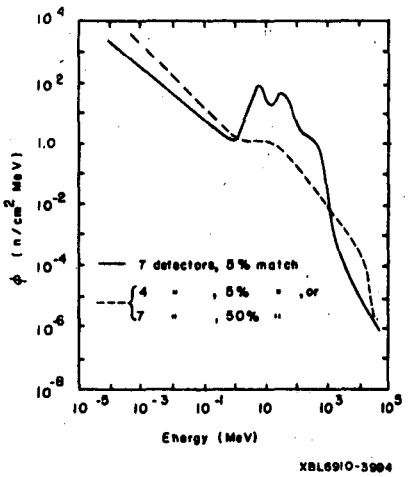

Fig. 5.16. Neutron spectra unfolded from measurements with four detectors (BF_3, $Al \rightarrow {}^{24}Na$, $C \rightarrow {}^{11}C$, Bi-fission) and with seven (the above plus $S \rightarrow {}^{32}P$, $C \rightarrow {}^{7}Be$, $Hg \rightarrow {}^{149}Tb$)) exposed in the beam tunnel of the CERN 28-GeV proton synchrotron. (from Routti)

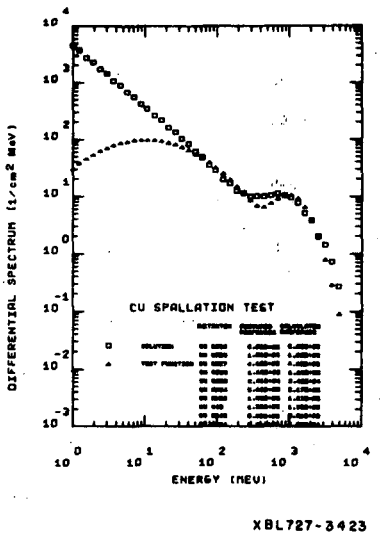

Fig. 5.17. Results from a test case with Cu-spallation kernel and program LOUHI. Excellent agreement is obtained between the unperturbed input responses and the calculated responses. The deviation of the solution from the test spectrum can be explained by the absence of all response functions at low energies. (from Routti)

Because of the mathematical nature of the problem the resolution obtained in neutron spectroscopy with activation detectors remains limited even in ideal cases. The detailed structure introduced in the test spectra or possibly existing in the real spectrum is difficult or impossible to recover. For the specification of accelerator shields the resolution obtained is, however, quite adequate. And although spectral shapes may be sensitive functions of errors in the input data, these errors affect integrated quantities, such as flux and dose rates, much less severely. Knowledge of the energy distribution of the neutrons can also be used to obtain appropriate conversion factors to justify the use of a single detector or a few detectors to measure such integrated quantities (RIN A 68). This information can also be used to justify simplified models in shielding calculations and dose estimations (ROU J 69).

Moderated Thermal Neutron Detectors and Their Application to the Measurement of Fast Neutrons

BUILDUP

Elastic scattering of neutrons on protons or very light nuclei is an extremely efficient means of slowing down (or moderating) neutrons with energies of only a few MeV. Thus if a thermal neutron detector is surrounded by increasing thicknesses of an efficient moderator (e.g., paraffin), its response in a fast neutron field steadily increases as moderator is added. Its response increases to some optimum value at which the production of thermal neutrons is a maximum. Beyond this optimum thickness the response declines because of increasing attenuation of the incident fast neutrons in the moderator. This "buildup" and subsequent reduction in response depends upon the average energy of the incident neutron spectrum. Wallace et al. (WAL R 61) have reported the measurements of the response of a paraffin-moderated BF_3 counter as a function of moderator thickness, for several neutron sources. Figure 5.18 summarizes their results. The average energies of the neutron sources used were either measured or calculated from the neutron spectra reported by Hess (HES W 59a) for several isotopic sources.

These data may also be presented in the form of Fig. 5.19, which shows the counting efficiency of two thermal neutron detectors as a function of incident neutron energy. The upper curve shows the response of an indium foil, surrounded by 7.5 cm of paraffin; the lower set of curves is for a BF_3 proportional counter surrounded by various thicknesses of moderator. It may be seen that the response of a thermal neutron detector surrounded by 5 to 7.5 cm of paraffin is fairly independent of incident neutron energy in the energy range from 20 keV to 14 MeV. This fact has given rise to a host of closely related techniques for the determination of neutron flux densities and dose-equivalent rates, many of which are discussed in this volume. The use of moderated activation detectors is more fully discussed under the related sections are those dealing with Bonner spheres and Neutron Rem-Meters.

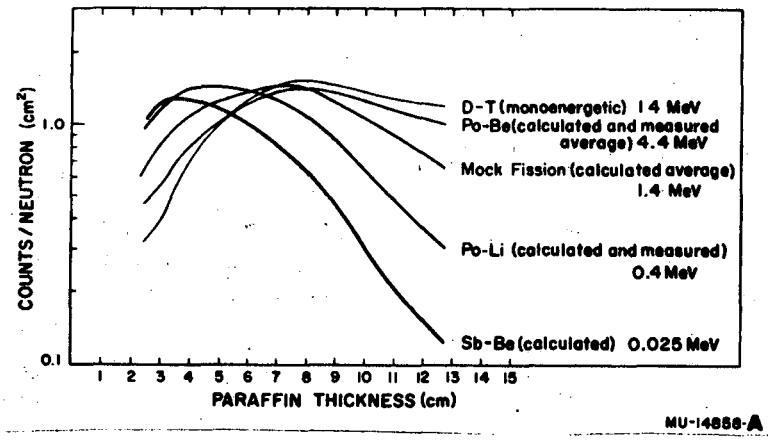

Fig. 5.18. Counting rate in a BF_3 counter surrounded by a paraffin moderator as a function of paraffin thickness for various neutron sources (corrected for non-isotropy of irradiation). The entire assembly was covered by cadmium. (from Wallace et al.)

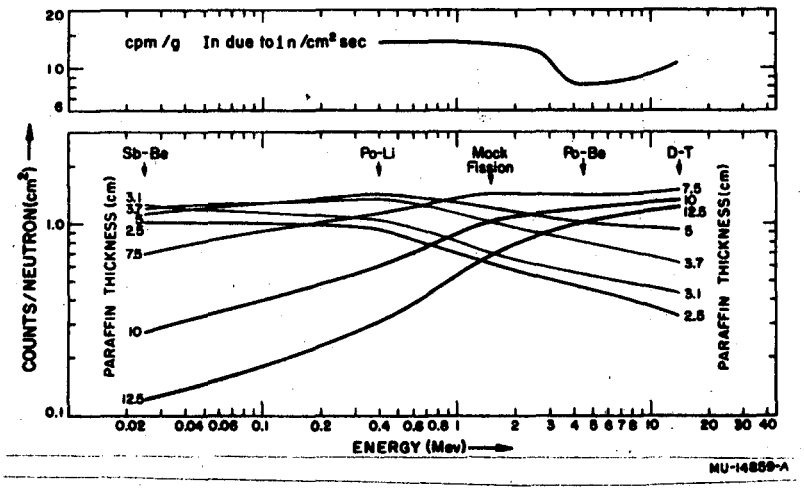

Fig. 5.19. The average efficiency of two moderated thermal neutron detectors as a function of average neutron energy for various thicknesses of paraffin moderator (corrected for non isotropic irradiation). The top curve is for an Indium activation detector surrounded by 7.5 cm of paraffin. The lower curves are for a BF_3 counter. (from Wallace et al.)

Experiment 3 in the appendix discusses in some detail the practical use of a moderated BF_3 counter.

BONNER SPHERES

Following the suggestion by Stephens and Smith (STE L 58) that a thermal neutron detector surrounded by a 6-in.-diameter paraffin sphere could be usefully employed to measure neutrons in the energy range from a few keV to about 15 MeV, a sophisticated technique of neutron dosimetry has been developed.

Bramblett et al. (BRA L 60) suggested the use of several moderating spheres of varying size to measure neutron radiation fields. These workers used a small cylindrical (4 mm high, 4 mm dia.) lithium iodide scintillator (Eu activated) placed in the centers of polyethylene moderators of various diameters. Thermal neutrons arriving at the center of moderator interacted in the scintillator predominantly via the $^6Li\ (n,\alpha)^3H$ reaction, producing a 4.79-MeV α particle which is stopped in the crystal. The scintillator was coupled to a photomultiplier tube by a 0.5-in.-diam polystyrene light pipe, and the output of the photomultiplier therefore gave a measure of the thermal neutron flux density at the center of the moderator assembly.

Bramblett et al. calculated the response of polyethylene spheres of diameter 2, 3, 5, 8, and 12 in. at some discrete energies to neutrons in the energy range 50 keV to 15 MeV. (Such spheres have subsequently been generally referred to as "Bonner Spheres," after the senior author of the original paper.) The largest of these moderators has a diameter comparable with that of the human trunk, and the variation with energy of its response to neutrons is therefore similar to that of the human body. This has led to the development of a family of rem meters described somewhat later. Since, as we have already discussed, it is often necessary to obtain detailed information of the neutron spectrum, these detectors have also been used for spectroscopy.

Neutron Spectroscopy With Bonner Spheres

In principle the determination of neutron spectra by use of Bonner spheres is very similar to that with activation detectors, and many of the unfolding procedures are also similar. For a detailed account the reader is referred to the previous section, discussing neutron spectrometry with use of threshold detectors.

The appropriate Fredholm integral equation may now be written

$$A_j = C_j \int_{E_{min}}^{E_{max}} R_j(E)\,\phi(E)\,dE, \quad \text{for } j = 1 \cdots m, \tag{57}$$

where A_j is the counting rate observed in the j th detector,

$R_j(E)$ is the response function of the j the detector as a function of energy.

The response functions $R_j(E)$ have not been measured in sifficient detail (BRA R 60), and one has to make use of calculated values. Other calculated values of the response functions for spheres 2, 3, 5, 8, and 12 in. in diam, and also for 18-in.-diam spheres, have been reported; the adjoint neutron transport method by Hansen and Sandmeyer (HAN G 65) and by McGuire (McG S 66) were used. Several tabulations of these response functions have been given in the literature (O'BR K 65, AWS M 66, WAT G 68). See Table 5.VI.

Figure 5.20 shows these response functions graphically. These calculated response functions have been used by McLaughlin et al. (McL. J 66), Awschalom (AWS M 66), and Stevenson (STE G 67) in studies including both mathematical tests of unfolding routines and practical measurements.

A successful use of multisphere technique requires accurate knowledge of the response functions and an appropriate method for unfolding the neutron spectrum. Among the nonunique solutions to the integral equations relating the measured response to the unknown spectrum, an appropriate solution is to be sought. Such a solution matches the measured responses within reasonable experimental errors and has a physically acceptable nonnegative and nonoscillatory shape. The solution method should be stable enough to accommodate probable uncertainties in the response functions. In the studies mentioned above the iterative unfolding method by Scofield (SCO N 62) and Gold (GOL R 64) was used. The results by Awschalom indicated that significant disagreements were common between a given differential test spectrum and the one synthesized from calculated responses. Introduction of errors in response functions was shown by Stevenson to enhance these discrepancies. Fortunately, however, the computed values of integrated quantities such as flux and dose indicate acceptable agreement. For practical measurements an experimental verification of the calculated response functions is necessary.

When the multisphere method is compared with the threshold detector spectroscopy the following points should be noted. The size and cost factors favor the threshold detectors, which can be conveniently exposed in many locations simultaneously. The response of a threshold detector gives directly an approximation to a quantity of physical interest, the integrated flux above the threshold energy. The determination of the differential neutron spectrum by use of either sytem requires careful experimental techniques and critical use of mathematical unfolding methods.

Table 5.VI. Response matrix for Bonner-sphere counting system

Neutron energy (eV)	Counting efficiency (counts per neutron per square centimeter)						
	Bare detector	Cd covered detector	2 in. sphere	3 in. sphere	5 in. sphere	8 in. sphere	12 in. sphere
1.0 (−2)†	0.1220	0.0000	0.1372	0.1059	0.0540	0.0156	0.0024
1.6 (−2)	0.1220	0.0000	0.1401	0.1087	0.0560	0.0162	0.0025
2.5 (−2)	0.1220	0.0000	0.1457	0.1140	0.0588	0.0171	0.0026
4.0 (−2)	0.1180	0.0000	0.1513	0.1225	0.0639	0.0185	0.0029
6.3 (−2)	0.1160	0.0000	0.1620	0.1446	0.0712	0.0207	0.0032
1.0 (−1)	0.1140	0.0000	0.1760	0.1530	0.0824	0.0240	0.0037
1.6 (−1)	0.1100	0.0000	0.1977	0.1787	0.0975	0.0285	0.0044
2.5 (−1)	0.1020	0.0000	0.2207	0.2050	0.1141	0.0333	0.0051
4.0 (−1)	0.1160	0.1160	0.2410	0.2326	0.1327	0.0386	0.0059
6.3 (−1)	0.1100	0.1100	0.2553	0.2560	0.1480	0.0433	0.0065
1.0 (0)	0.0840	0.0840	0.2560	0.2701	0.1605	0.0479	0.0071
1.6 (0)	0.0760	0.0760	0.2532	0.2809	0.1710	0.0517	0.0080
2.5 (0)	0.0680	0.0680	0.2480	0.2853	0.1818	0.0541	0.0082
4.0 (0)	0.0600	0.0600	0.2382	0.2872	0.1897	0.0572	0.0088
6.3 (0)	0.0520	0.0520	0.2257	0.2880	0.1971	0.0598	0.0091
1.0 (1)	0.0420	0.0420	0.2121	0.2877	0.2033	0.0617	0.0096
1.6 (1)	0.0360	0.0360	0.1991	0.2847	0.2094	0.0647	0.0100
2.5 (1)	0.0280	0.0280	0.1890	0.2800	0.2150	0.0675	0.0105
4.0 (1)	0.0200	0.0200	0.1767	0.2743	0.2203	0.0707	0.0111
6.3 (1)	0.0100	0.0100	0.1630	0.2672	0.2252	0.0732	0.0113
1.0 (2)	0.0020	0.0020	0.1528	0.2608	0.2292	0.0763	0.0117
1.6 (2)	0.0000	0.0000	0.1427	0.2535	0.2236	0.0789	0.0122
2.5 (2)	0.0000	0.0000	0.1318	0.2451	0.2349	0.0816	0.0127
4.0 (2)	0.0000	0.0000	0.1201	0.2362	0.2357	0.0829	0.0129
6.3 (2)	0.0000	0.0000	0.1106	0.2227	0.2363	0.0842	0.0130
1.0 (3)	0.0000	0.0000	0.1013	0.2187	0.2375	0.0865	0.0132
1.6 (3)	0.0000	0.0000	0.0935	0.2107	0.2392	0.0901	0.0142
2.5 (3)	0.0000	0.0000	0.0860	0.2050	0.2409	0.0935	0.0150
4.0 (3)	0.0000	0.0000	0.0785	0.1915	0.2412	0.0956	0.0153
6.3 (3)	0.0000	0.0000	0.0703	0.1850	0.2418	0.0983	0.0158
1.0 (4)	0.0000	0.0000	0.0655	0.1780	0.2423	0.1023	0.0167
1.6 (4)	0.0000	0.0000	0.0594	0.1707	0.2445	0.1069	0.0171
2.5 (4)	0.0000	0.0000	0.0535	0.1625	0.2453	0.1106	0.0181
4.0 (4)	0.0000	0.0000	0.0470	0.1532	0.2474	0.1178	0.0197
6.3 (4)	0.0000	0.0000	0.0421	0.1457	0.2499	0.1266	0.0220
1.0 (5)	0.0000	0.0000	0.0380	0.1372	0.2536	0.1402	0.0256
1.6 (5)	0.0000	0.0000	0.0322	0.1258	0.2591	0.1582	0.0312
2.5 (5)	0.0000	0.0000	0.0257	0.1120	0.2644	0.1792	0.0396
4.0 (5)	0.0000	0.0000	0.0178	0.0950	0.2641	0.2063	0.0533
6.3 (5)	0.0000	0.0000	0.0127	0.0788	0.2520	0.2356	0.0745
1.0 (6)	0.0000	0.0000	0.0085	0.0600	0.2310	0.2705	0.1040
1.6 (6)	0.0000	0.0000	0.0060	0.0390	0.2050	0.2720	0.1500
2.5 (6)	0.0000	0.0000	0.0038	0.0287	0.1550	0.2640	0.1856
4.0 (6)	0.0000	0.0000	0.0024	0.0191	0.1153	0.2380	0.2067
6.3 (6)	0.0000	0.0000	0.0013	0.0130	0.0685	0.1950	0.1995
1.0 (7)	0.0000	0.0000	0.0010	0.0074	0.0563	0.1415	0.1742
1.6 (7)	0.0000	0.0000	0.0003	0.0041	0.0337	0.0992	0.1420
2.5 (7)	0.0000	0.0000	0.0002	0.0020	0.0205	0.0737	0.1141
4.0 (7)	0.0000	0.0000	0.0001	0.0010	0.0130	0.0476	0.0853
6.3 (7)	0.0000	0.0000	0.0000	0.0004	0.0056	0.0265	0.0543
1.0 (8)	0.0000	0.0000	0.0000	0.0003	0.0037	0.0152	0.0266
1.6 (8)	0.0000	0.0000	0.0000	0.0001	0.0001	0.0035	0.0150

†Digit in parentheses denotes power-of-ten multiplier. (from O'Brien et al.)

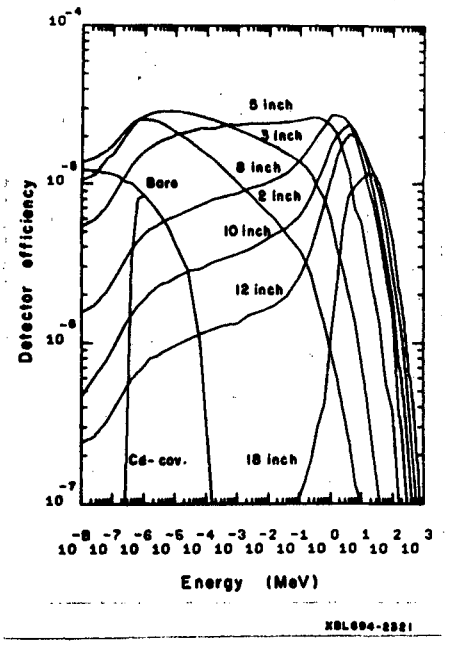

Fig. 5.20. The response function of Bonner spheres of different diameters.

Many unfolding methods fail to perform well with either technique. With Bonner spheres the response matrix is close to an ill-conditioned linearly dependent system; the threshold-detector method often suffers from the small number of detectors used to cover a wide energy range. Employment of unfolding techniques allowing flexible use of a priori information should benefit both multisphere and threshold-detector methods.

Different unfolding routines have been compared (reported by THO R 69). Bonner spheres of different sizes were exposed at 90 deg to a well-shielded thick target bombarded by 500-MeV electrons at the Mark III electron linac at Stanford. Routti (ROU J 69) has used the computer program LOUHI to determine the neutron spectrum from these data. Figure 5.21 shows the spectrum obtained and the measured and computed responses for the spheres. There is good agreement between these calculated and measured responses, and the neutron spectrum is acceptable.

Comparison of the dose-equivalent rates calculated by using the three unfolding routines LOUHI, ENDIM, and ALFIE (HAR D 68, HAR D 69) showed good agreement (± 15%). Comparison of these dose-equivalent

rates with those determined by using NTA films and activation detectors, however, showed a discrepancy of a factor of two (THO R 69). (See Table 5. VIII) Further intercomparison of this nature are clearly desirable.

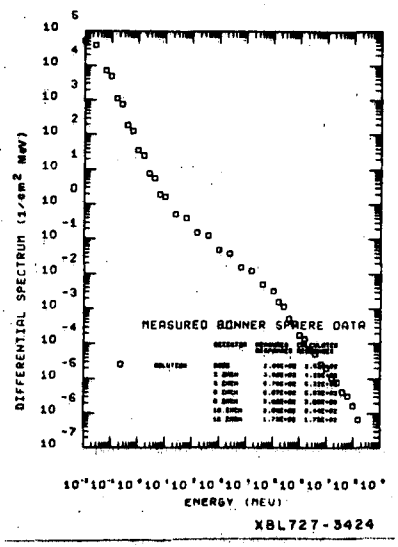

Fig. 5.21. A neutron spectrum determined with the computer program LOUHI from Bonner sphere data measured at the Mark III linear accelerator outside thick shielding. (from Routti)

Table 5.VII. Summary of dose-equivalent rate estimates. Measured at the Mark III electron linear (after Thomas).

Method	Dose-equivalent rate (mrem/hr)
NTA films	106 ± 2
Activation detectors	95 ± 19
Bonner spheres	47 (LOUHI)
	56 (ENDIM)
	58 (ALFIE)

NEUTRON REM METERS

In the discussion on Bonner spheres it was noted that response of larger spheres to neutrons would be expected to be similar to that of the human body.

Bonner suggested that a single 12-in.-diam sphere need be calibrated at only one energy to give a roughly dose-equivalent response over a wide neutron energy range (thermal to 15 MeV). The advantages of such a detector are quite clear (see Chapter 2). It gives an approximately dose-equivalent response over a wide energy range, can measure low dose-equivalent rates ($\approx$ 0.5 mrem/h), has little or no geometrical dependence, and can be used as a portable instrument with a minimum of training in its use.

These desirable features have led to the development of a whole family of closely related instruments collectively known as "Rem Meters."

The term rem meter is normally used for neutron-measuring instruments whose sensitivity per unit neutron fluence is proportional to appropriate ICRP values. The readings of such instruments are taken to be proportional to the maximum dose rate equivalent in a human body, regardless of the neutron energy spectrum in the range of practical interest, i.e. thermal energy to about 10 MeV. Such instruments are all based upon the principle already discussed many times in this volume, that fast neutrons may be conveniently monitored if they are first thermalized in the moderator that surrounds a thermal-neutron detector.

Rem meters are particularly valuable when maximum neutron energies are less than 14 MeV or when there are large numbers of intermediate-energy neutrons. Obviously, if one wishes to understand the physical details of the radiation field, additional detectors must be used. However, when prior knowledge of the neutron spectrum is available, a rem meter is very useful for on-the-spot radiation surveys.

Nachtigall (NAC D 67) has published an excellent review of rem meters and classified and compared the different types of instruments.

Rem Meter Design

All existing rem meters are fitted with at least one thermal neutron detector. The reactions most frequently used are $^{10}B(n,\alpha)$ in BF_3 proportional counters, $^{6}Li(n,\alpha)$ in LiI scintillation counters; activation and solid-state detectors are used occasionally.

The detector is always surrounded by moderator material, usually polyethylene or paraffin wax. They are portable or movable but fairly heavy. In each the basic principle is that the moderator surrounding the thermal neutron detector is chosen in such a way that by means of suitable dimensions and judicious combinations of additional absorbers, the response is as far as possible proportional to the dose equivalent.

Rem meters may be classified as follows:

Type 1: Rem Meter Without Internal Absorber.

A typical instrument in this category consists of a LiI(Eu) crystal, 4 mm in diam. and 4 mm thick, which is more than 80% "black" to thermal neutrons. The crystal is coupled to a photomultiplier tube by a 0.5-in.- diam quartz or polystyrene light pipe and is mounted in the center of a 10 or 12-in.-diam polyethylene moderator. The first such detector, utilizing a 12-in. moderator, was reported by Bramblett et al. (BRA R 60).

Subsequent improvements (HAN D 62, HAN D 63, NAC D 62) have led to an improved rem response. Hankins (HAN D 62, HAN D 63) has described an instrument with a 10-in.-diam sphere, represented in Fig. 5.22.

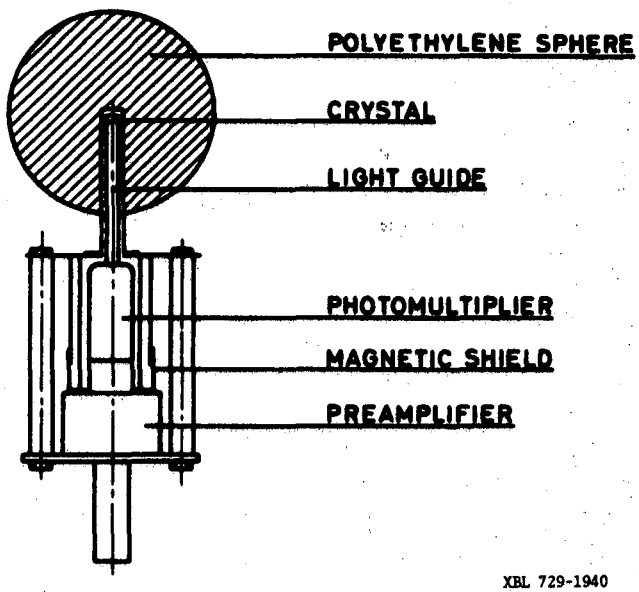

Fig. 5.22. Diagram of a single sphere rem-meter without an internal absorber (Type 1) (from Nachtigall)

Figures 5.23 and 5.24 show the measured and calculated response of this instrument compared with the desired response (based on the exact NBS and ICRP recommendations). As may be seen from Fig. 5.24, although the response of the 10-in. sphere is quite good for thermal neutrons ($\approx \pm 4\%$) and fast neutrons in the range 0.2 to 7 MeV ($\pm$ 15%), some serious discrepancies can occur. In the intermediate energy region the instrument can overrespond by as much as a factor of five. At energies above 7 MeV the instrument can considerably underestimate the neutron dose equivalent.

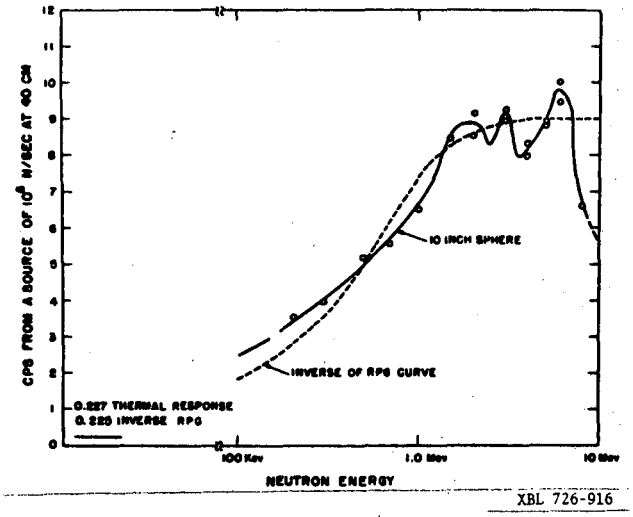

Fig. 5.23. Estimated response of a 10 in. diam. single sphere rem-meter as a function of neutron energy. The open circles show calibration points. The dashed line indicates values derived from NBS handbook 63. (from Hankins)

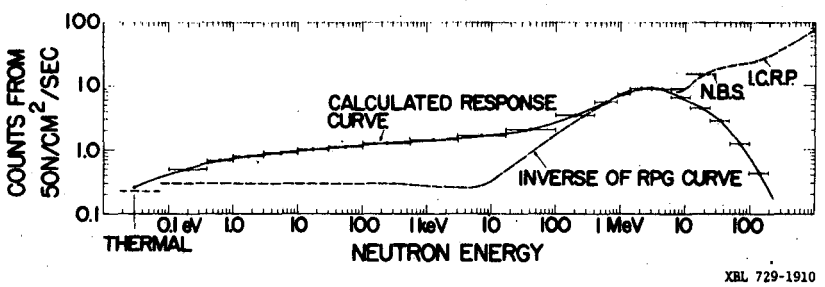

Fig. 5.24. Calculated response of a 10 in. diam. single-sphere rem-meter as a function of neutron energy. The dashed line shows values derived from NCRP and ICRP recommendations extant in 1965. (from Hankins)

Type 2: Rem Meter With Internal Absorber

In an attempt to improve the response of Type 1 rem meters to intermediate-energy neutrons, Andersson and Braun (AND I 63) developed a counter similar in geometry to the long counter. A BF_3 counter placed along the axis of a cylindrical polyethylene moderator detects thermal neutrons. The number of low energy neutrons reaching the BF_3 counter is reduced by surrounding the tube with a cylinder of boron-impregnated plastic (see Fig. 5.25) in which holes have been drilled to allow some slow neutrons to pass. By a judicious balancing of the distance of the boron-plastic from the tube, the outer diameter of the moderator, and the quantity of boron plastic in the cylinder, Andersson and Braun devised an instrument with much improved energy response. With a polyethylene moderator of 21.6 cm and with a well-dimensioned internal absorber, 22% of whose surface contains holes, greater absorption of the intermediate neutrons occurs; this ensures that the sensitivity curve of the rem meter follows the dose-equivalent curve occurs again in the intermediate range at 5 keV and is about a factor of 1.7. (See Fig. 5.26)

Such an instrument weighs about 15 kg, and--although portable--is inconveniently heavy.

An instrument similar to that of Andersson and Braun and based upon the long counter has been described by Frid et al. (FRI E 64).

Leake (LEA J 67) has described a spherical version of the Andersson-Braun counter which has the advantage of weighing only 6.2 kg but has somewhat less favorable energy response. In the Leake rem meter the LiI (Eu) crystal (16 mm in diam and 2 mm thick) is centered in a moderator 8.2 in. in diameter. The crystal is surrounded by a cadmium dome $\approx$ 2 in. in diam in which there is a hole through which the crystal and light guide are inserted. Fig. 5.27 This instrument will overread by a factor of 3.5 at 5 keV but underread by a factor of 3 at 15 MeV. (Fig.5.28)

Keirim-Markus and Kraitov (KEI I 67) have described a spherical rem meter having an internal absorber and utilizing boron-loaded ZnS as a scintillator.

Type 3: Multi-sphere Rem Meter

Here several moderating spheres are used in conjunction with one scintillation counter, measurements being taken sequentially (see the section on Bonner spheres). Such a technique is limited to radiation fields that are not changing with time. Several authors have described practical systems (NAC D 64, BAR A 64, McG S 66, NAC D 67b).

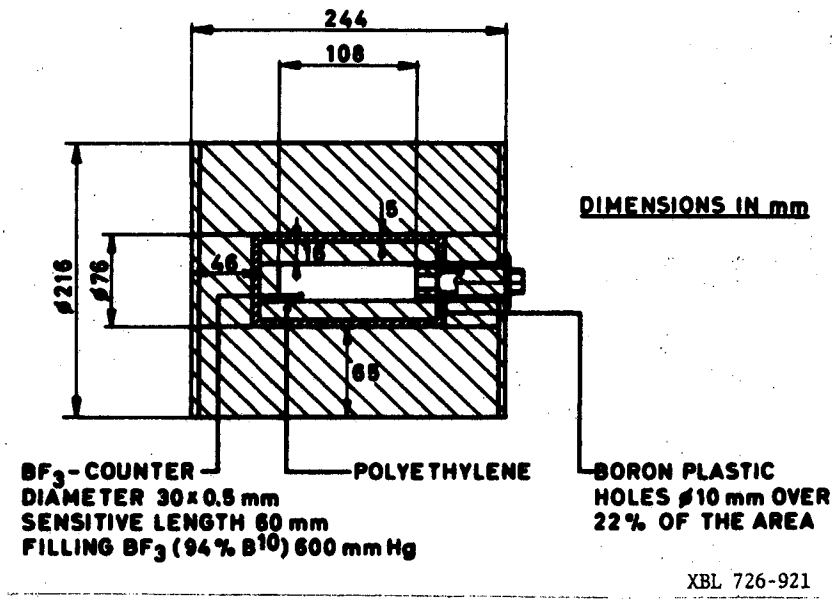

Fig. 5.25. Diagram of a cylindrical rem-meter with an internal absorber (Type 2) (from Nachtigall).

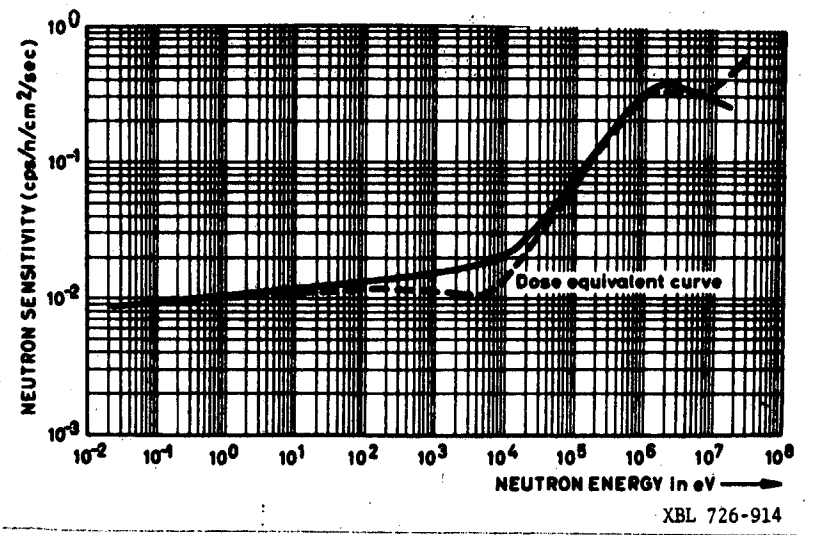

Fig. 5.26. Response curve of a cylindrical rem meter with an internal absorber (from Nachtigall).

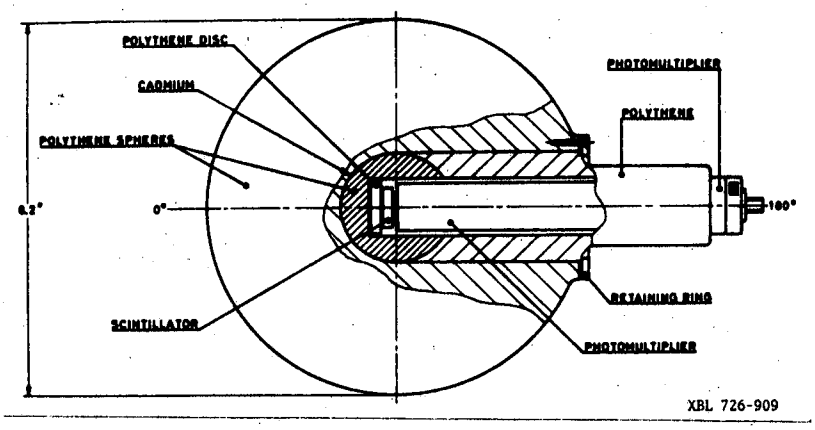

Fig. 5.27. Spherical rem-meter with an internal absorber (after Leake).

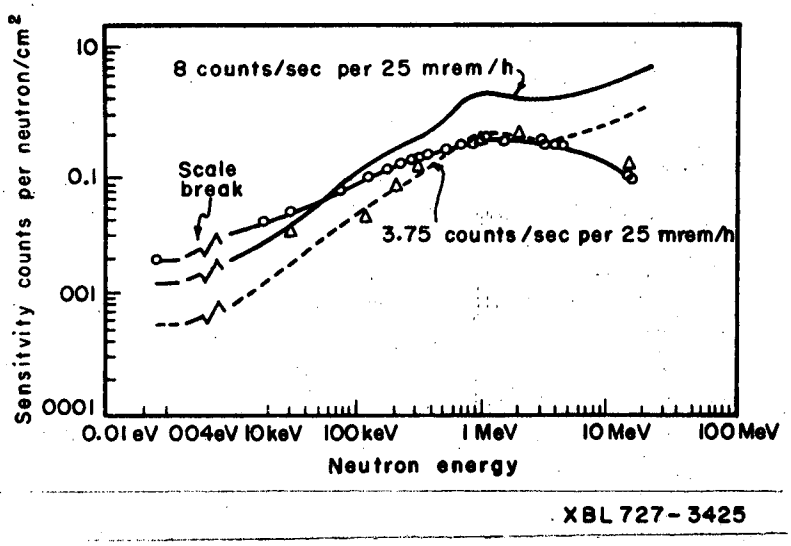

Fig. 5.28. Energy response characteristics of the Leake rem-meter
x response of 9 in. diam. assembly
0 response of Harwell monitor 0072 (8.2 in. diam. moderator) using a 16 mm diam X 2 mm thick Li I (Eu) crystal.
—— required response characteristics to meet the recommendations
- - - of the ICRP (1963). (after Leake)

Type 4: Multidetector Rem Meter

Rather than use one detector and several moderators, one can obtain equivalent results by placing several detectors in one moderator. This technique is based on the suggestion by Mandl (MAN M 52) that the thermal flux distribution inside a moderator may be used to determine both the incident neutron flux density and its spectrum.

Tatsuta et al. (TAT H 67) have described the use of four BF_3 counters in a cylindrical moderator. One counter is placed along the central axis of the cylinder and the three others are placed parallel to it, equispaced on the circumference of a circle (Fig. 5.29).

Dvorak and Dyer (DVO R 65) have described an instrument using activation detectors. The moderator consists of a 12-in.-diam paraffin sphere encased in aluminum. Nine thermal activation foils located within the moderator are used to determine neutron fluence and dose equivalent. The activation of six of these foils, located 1 in. below the surface of the moderator, is used to determine neutron fluence to better than 10% in the energy range 20 keV to 2.3 MeV. The neutron dose equivalent is determined from the activation of the three remaining foils, which are placed at the center of the moderator. Dose equivalent may be determined within 75% over the same energy ranges. Figure 5.30 shows the response of the Dvorak-Dyer detector as a function of energy.

A spherical rem meter using solid-state detectors (GAR G 53) has been discussed. It should be no surprise to the reader that rem meters of types 3 and 4 show much smaller deviation from the dose-equivalent curve than is shown by types 1 and 2. A larger number of parameters may be adjusted in the more complex instruments, and better agreement inevitably results. Thus, for example, Nachtigall and Rohloff (NAC D 67b) have reported that four moderators are capable of determining the dose equivalent to within less than 10% in the energy range 0.025 eV to 50 MeV.

However, it must be emphasized that all the sensitivity curves in the intermediate energy region are calculated.

Several of the instruments of types 1 through 4 are commercially available (see Ref. LBL 71).

Determination of the Dose-Equivalent Rate By Using Rem Meters

In practice rem meters are usually calibrated with Po-Be, Ra-Be, Am-Be, or Pu-Be neutron sources after a suitable discriminator threshold has been determined.

In rem meters types 1 and 2 the indication of the reading device is given directly in mrem/h. These instruments have a sensitivity to neutrons of about 1 count/sec per millirem/h, their γ sensitivity is lower by a factor of more than 1000. These devices may be used for neutrons between thermal energies and 7 to 10 MeV.

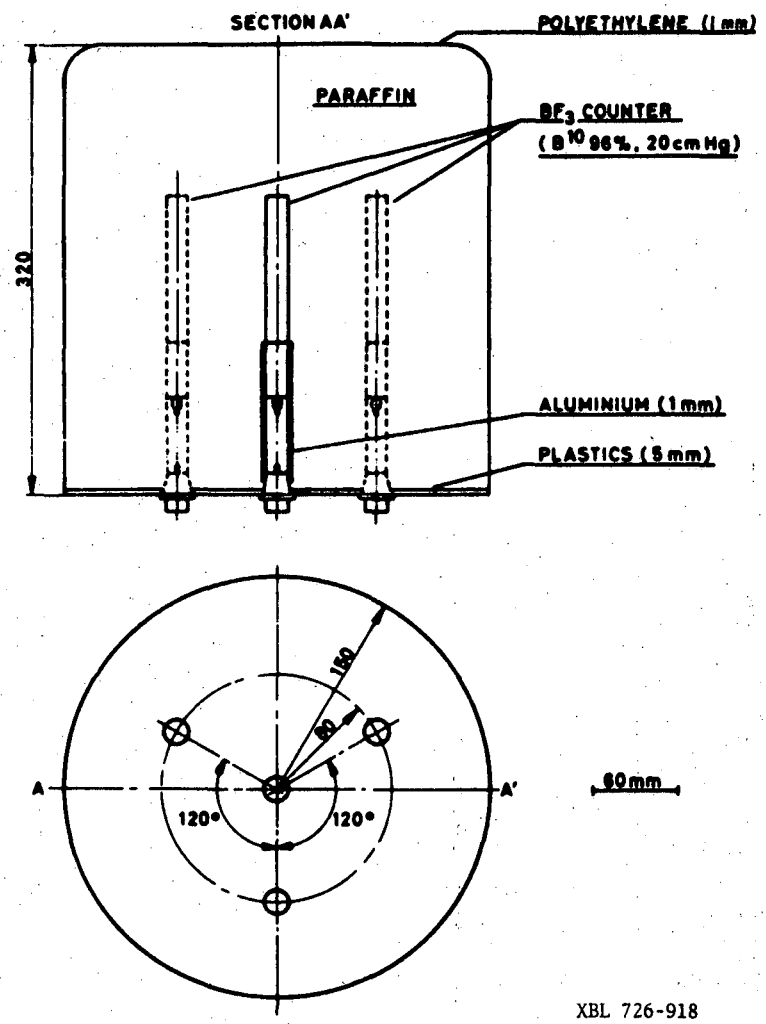

Fig. 5.29. Diagram of a multi-detector rem-meter (from Nachtigall).

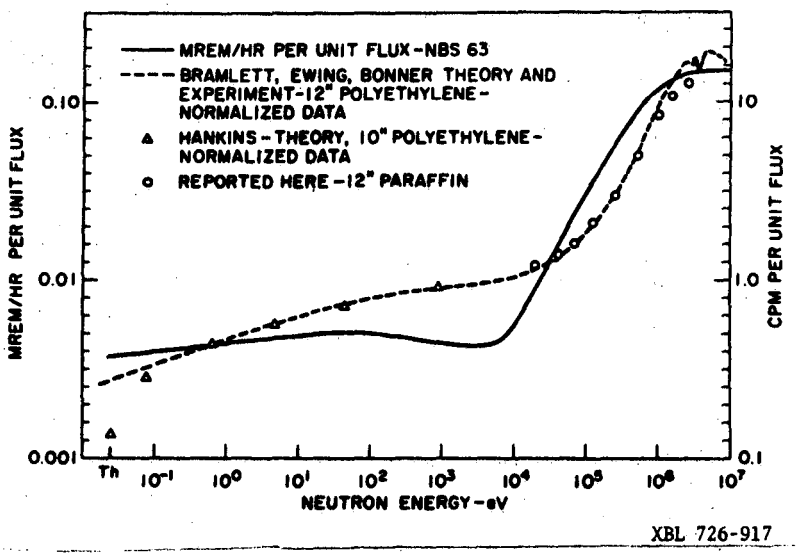

Fig. 5.30. Comparison of response characteristics of three spherical neutron detectors (from Dvorak and Dyer).

When several spheres are used (type 3 rem meter) the dose-equivalent rate DE may be written

$$DE = K \sum_i f_i C_i, \tag{58}$$

where K is a factor dependent upon the size and shape of the crystal, the optical coupling to the photomultiplier and the discriminator setting,

f_i is a weighting factor for the i th moderator,

and C_i is the counting rate of the detector in the i th moderator.

Thus, for example, Nachtigall and Rohloff (NAC D 67b) show that, for moderators of 2, 5, 11, and 18 in. in diameter, the equation

$$DE = K(0.3\,C_2 + 9\,C_{11} + 10\,C_{18} - 0.8\,C_5) \tag{59}$$

gives the DE rate in the region from thermal energies to 50 MeV in the region from thermal energies to 50 MeV. In this equation C_i refers to the counting rate in the sphere of diameter i. The dose-rate equivalent is obtained in a similar way with the multidetector rem counters.

For the cylindrical type of rem meter described by Tatsuta et al. (TAT H 67) with BF_3 counter, (DE) is given by

$$(DE) = (1.15N_1 - 0.0639N_2) \times 10^{-2}\ 9\text{mrem/h}). \qquad (60)$$

Here N_i is the counting rate of the central BF_3 counter and N_2 the sum of the three BF_3 counters (TAT H 67). A common feature of the multisphere and multidetector types is that any change in the dose-equivalent curve for neutrons recommended by advisory authorities can be allowed for by altering the moderator diameters and the position of the detectors and the weighing factors (or both).

Calculated Sensitivity Curves

All the rem meters described here (Type 1-4) use either spherical or cylindrical moderators.

Fräki et al. (FRÄ R 62) have made calculations of the variation of sensitivity of rem meters as a function of energy in cylindrical geometry. As previously mentioned, Bramblett et al. (BRA R 60), Hansen and Sandmeir (HAN G 65, ORNL 63) and McGuire (McG S 66) have calculated the response of spheres of various sizes up to energies as high as 200 MeV. Unfortunately these calculations are not in good agreement, especially in the intermediate energy region (see Fig. 31).

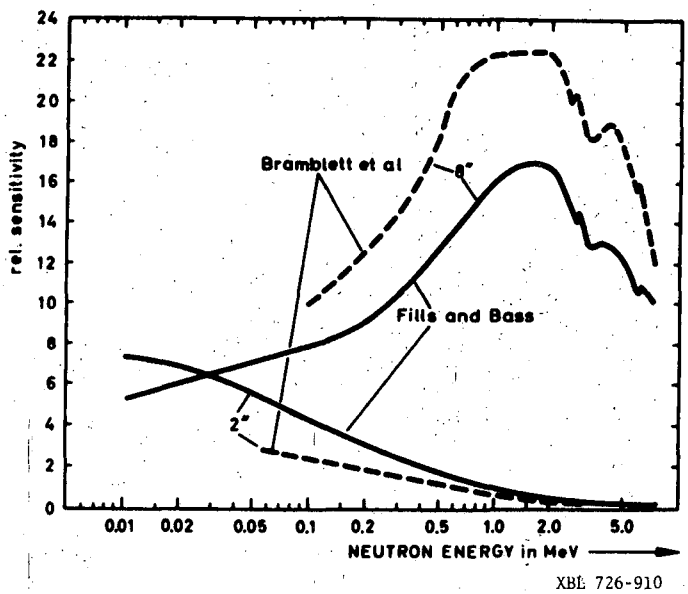

Fig. 5.31. Calculated (- - -) and measured (——) energy response for 2 in. and 8 in. diam. Bonner spheres (from Nachtigall).

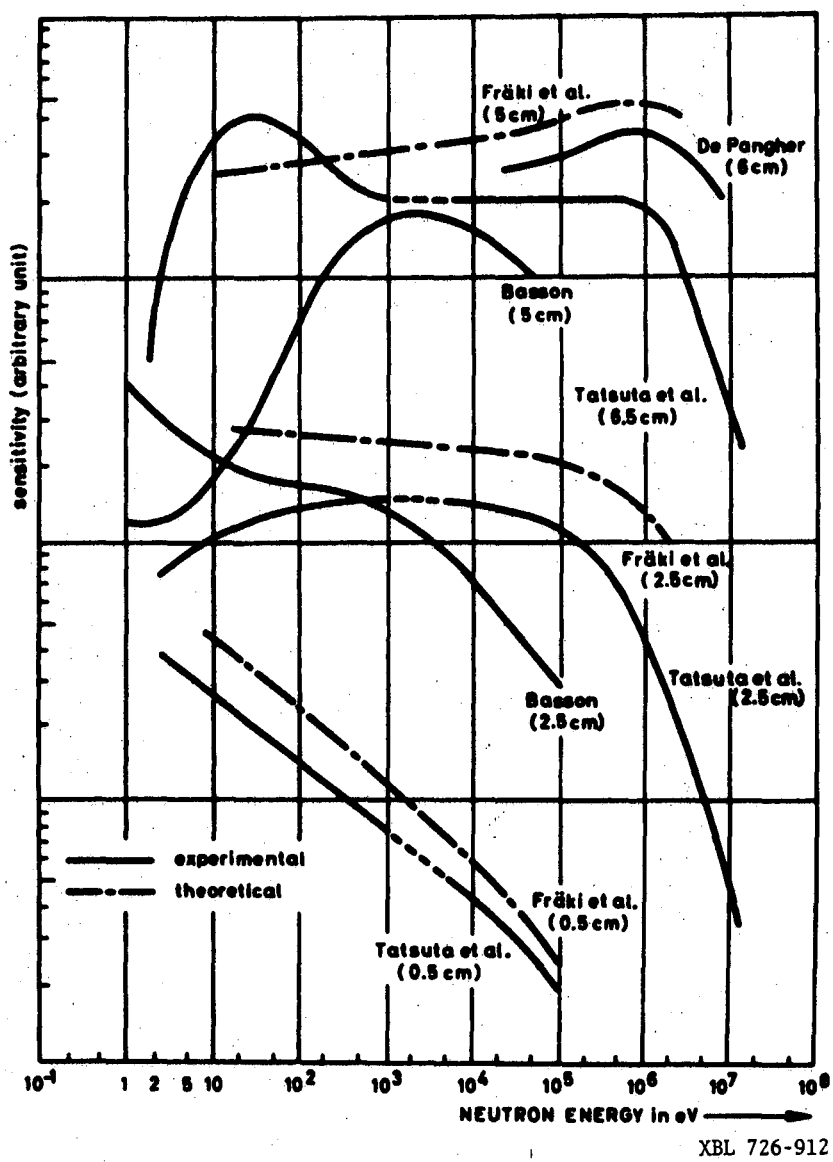

Fig. 5.32. Calculated and experimental sensitivity curves for $^{10}B(n, \alpha)$ detectors in paraffin moderators (from Nachtigall).

Experimental Studies of Response Functions

These discrepancies will have to be resolved experimentally, but this has not yet been done completely for several reasons. Convenient monoenergetic sources of neutrons in the intermediate energy region are not available. Neutron scattering from floors, walls, and even air present a difficult background problem at these energies. Finally, the directional dependence of the instruments (particularly those using cylindrical geometry) may present added difficulties in making accurate calibrations.

Experimental studies made to date are not unequivocal. Nachtigall (NAC D 64) has reported good agreement with the sensitivity curves for spherical moderators originally calculated by Bramblett et al. (BRA R 60). Fillis and Bass (FIL P 65), on the other hand, have reported discrepancies up to a factor of 1.7 (see Fig. 31).

Nachtigall (NAC D 67) has reviewed experimental studies in a variety of paraffin and polyethylene moderators. Figure 5.32 shows his comparison between the experimental and theoretical values. Fairly large discrepancies are seen.

Conclusions

The conclusions to be drawn from this discussion of rem meters are brought into focus by a practical example. Nachtigall (NAC D 67) has reported a radiation survey around a medium-energy proton accelerator with four rem meters, each calibrated under identical conditions with the same Am-Be source. Table 5.VIII shows that the worst discrepancy between the different instruments is by as much as a factor of five. This large divergence occurred where the average neutron energy was the lowest observed ($\approx$ 40 keV). Nachtigall summarizes his experience with rem meters thus:

"Rem meters consist of detectors for thermal neutrons and more or less complicated moderator covereings. Therefore, the calculation and experimental determination of sensitivity curves of such measuring arrangements in the energy range from thermal up to some 10^7 eV is of high interest to Health Physicists. A comparison of published calculations, curves, experimental results, and estimations on this subject shows large deviations.

"The deviations of the sensitivity curves of rem counters from the dose-equivalent curve amount to up to a factor of 5 in the intermediate region. Calculated sensitivity curves of LiI crystals with sphere moderators differ by a factor of 1.5. Experiments with fast neutrons and LiI crystals with sphere moderators yielded differences up to a factor of 1.7 compared with other experiments and calculations. Long counter measurements for calibration purposes are only correct within the factors 1.1 to 1.2. The factor 1.2 must also be applied when uncertainties of energies of Van de Graaff neutrons in the 10-keV region are estimated. Between calculated and measured sensitivity curves in the intermediate energy range there

Table 5.VIII. Dose equivalent evaluations by means of different rem-counters.

Location	Multisphere [22]	Single sphere without internal absorber	Cylindrical type with internal absorber	Spherical type with internal absorber Dia Cd-sphere	
				55 mm	59 mm
	mrem/h	mrem/h	mrem/h	mrem/h	mrem/h
Linac, flight path 2	1.4	2.5	1.5		
Linac, flight path 4	2.7	4.2	2.0		
Linac, flight path 6	2.4	5.0	3.0		
BR2, tube R2, 45°	1.4	3.0	2.0	5	4.5
BR2, tube R2, 0°	3.0	5.8	6.9	8	8.8
BR2, tube R3 0°	3.4	7.7	4.9	9.2	9.4
BR2, tube R1,	2.5	4.2	2.1	5.5	6.0
BR2, above tube R2	1.1	4.2	4.0	5	5.5

are differences of a factor of 3. Errors due to directional dependence, inexactly known fluence-dose conversion curves, and unisotropic calibration sources can be represented by factors in the order of 1.2.

"Under adverse conditions and when small moderators are used, the appearance of scattered neutrons may cause errors up to a factor of 2.3. Finally, dose-equivalent measurement in the same neutron field with different rem counters, which are calibrated under the same conditions, show deviations up to a factor of 5.

"Therefore, measurements of the dose rate equivalent obtained by means of different rem counter types are not comparable. Even results obtained with the same rem counter inside one laboratory show varying degrees of error. In order to overcome these uncertainties research work in this field of dosimetry must be intensified. Especially more investigations of sensitivity curves, mainly in the intermediate energy range, are necessary. As long as this has not been done and provided that no other information such as flux density, absorbed dose, information on spectra, etc. are used for corrections, "[it is probably unsafe]" to assume that the error of a rem counter measurement is smaller than a factor of 2. In most cases the error will be larger."

Rem meters should be used with caution, and always with an understanding of their response to radiation and the radiation field in which they make measurements.

PULSE COUNTERS

Pulse counters operating in the ion-chamber, proportional, or Geiger-Müller modes (as well as other radiation detectors) use, in some way, the phenomenon of ionization. Radiation detectors may be categorized according to the mechanisms used to detect this ionization. One such grouping might then be:

a. Ion-chamber, proportional counters, and Geiger-Müller counters.
b. Scintillation counters.
c. Cloud chambers and bubble chambers.
d. Photographic emulsions.

Of these, detectors in category a have found wide application in the immediate detection and analysis of accelerator radiation fields; scintillation counters (category b) are used to detect both prompt and residual radiation fields produced by accelerators.

Detectors in categories c and d are discussed in the section on Visual Techniques.

We have already discussed the use of ionization chambers in the current mode. In this section is discussed the operation of counters in categories a and b in the pulse mode. Basic texts in dosimetry and instrumentation should be consulted for detailed information about these detectors, their

principles of operatiion, their design and application. Among these are books by Rossi and Staub (ROS B 49), Price (PRI W 58), Handloser (HAN J 59), and Attix, Roesch, and Tochilin (ATT F 68). In the simple and elementary discussion that follows, we try to emphasize particular features and qualities of these detectors that are of importance in accelerator monitoring.

The detectors in category a produce an electrical signal or pulse as a direct consequence of the production of ionization. Figure 5.33 shows how pulse size depends on applied voltage in such detectors. Curve A in Fig. 5.33 represents a case in which a larger number of primary ion pairs is produced than for curve B. It is evident that these curves can be divided into six regions. In region I the pulse height increases with an increase in the applied voltage. In region II the pulse height is unaffected by an increase in the applied voltage. It is in this region of about 100 to 300 volts that an ionization chamber operates. An example of such a pulse-ion counter is the bismuth fission counter.

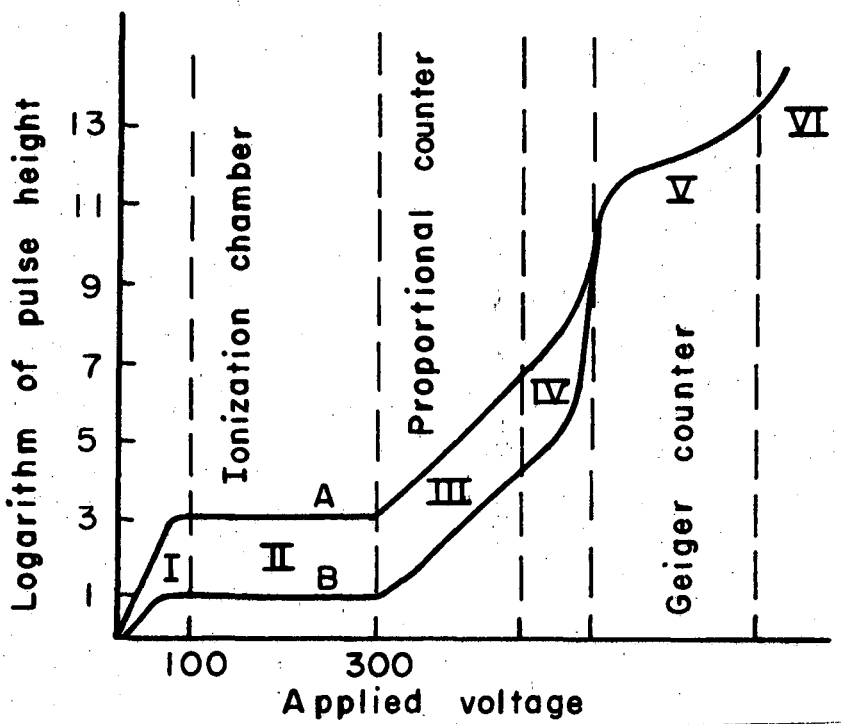

Fig. 5.33. Dependence of pulse height on applied voltage in an ionization chamber.

Fission Counters

Fission of the bismuth nucleus by high energy neutrons or protons sets in at about 50 MeV and rises slowly, reaching a constant value at about 1 GeV. The Bi fission cross section for protons is well known from threshold up to about 30 GeV (see Fig. 5.34) (DeCH 63), and what few measurements are available indicate that the neutron and proton cross sections are similar (MOY B 52, HES W 57).

The fragments resulting from fission of bismuth may be detected in a suitably designed ion chamber. Several papers in the literature have described features of such instruments (KEL E 48, WIE C 49, BEA J 59, McC J 68, and HES W 57). Small chambers have proved extremely useful for measurements in accelerator beams, but the rather small flux densities that must be measured in accelerator surveys make it necessary to develop an extremely sensitive chamber. Operation of the chamber in the pulse mode discriminates strongly against γ rays and low energy reactions, because the ratio of the pulse height obtained from fission to that obtained from other particles is roughly of the order of the ratio of their energies. Because the range of the fission fragments is typically ≈ 4 mg/cm^2 it is necessary to develop a fission chamber with a large bismuth surface area to give the required sensitivity. Hess et al. (HES W 57) have described the construction of a parallel-plate chamber with an effective surface area 65 000 cm^2 of bismuth. Such a chamber with 42 plates 30 cm in diam coated with bismuth to a thickness of 1 mg/cm^2 and operated at 300 V has a sensitivity of about 1 count/min in unit flux density. The background count rate in this counter is less than 1 count/hr. The counter is sensitive to charged particles (protons and pions) above 50 MeV, but relatively few of these are ordinarily present in the equilibrium spectrum outside a thick shield. If necessary, they may be discriminated against by means of an anticoincidence shield. In their paper Hess et al. (HES W 57) describe how the difficulties due to large capacitance were overcome by means of a delay line. More recently McCaslin (McC 68) has shown how p-n junction field-effect transistors may be used to improve the signal-to-noise ratio. Other elements may be used in fission ionization chambers. At low energies thorium and uranium have been used, but in using a uranium fission chamber one should be aware that the presence of ^{235}U makes a U fission chamber sensitive to thermal neutrons in addition to fast neutrons. The fission cross sections of Th and U are shown in Fig. 5.34.

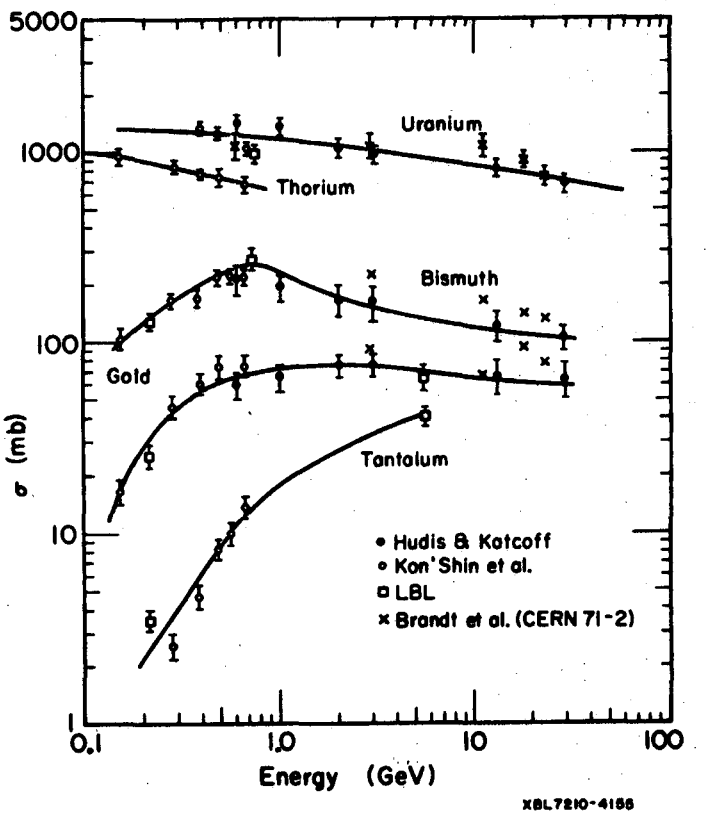

Fig. 5.34. Fission cross sections of a function of neutron or proton energy.

Proportional Counters

In region III of Fig. 5.33 the pulse height again increases with an increase in the applied voltage, owing to an effect at the central wire called multiplication. The field gradient near the wire is sufficiently high so that an electron can acquire enough energy in the intervals between successive collisions with the gas to ionize many molecules. This results in the release of additional electrons, which in turn cause the release of even more electrons. For a given voltage, the multiplication is constant. This is evidenced by the fact that the vertical separation between curves A and B of Fig. 5.33 is constant in region III. Thus, for a given voltage, the pulse height is proportional to the number of primary ion pairs formed. The proportional counter operates in this region;

Typical examples of proportional counters are the BF_3-filled counter and the polyethylene-lined counter, which are described in the Appendix (Laboratory Manual). The theory of operation of this latter counter and details of its use are described in Section 4 of the Appendix. Another type of proportional counter is used in the LET spectrometer, which has already been described in this chapter.

Geiger Counters

In region IV of Fig. 5.33 the curves again rise with increased voltage, but at different rates. This is the region of limited proportionality, and counters should not ordinarily be operated in this region because of possible instability. Operation in region VI is not possible because of continuous discharge or arcing.

In region V of Fig. 5.33 curves A and B coincide, indicating that for a given voltage the pulse height is independent of the number of primary ion pairs formed; the Geiger counter operates in this region. What is occurring is that the multiplication process has become so energetic at these higher voltages that photons of light are released, and they ionize other gas atoms near the wire as they proceed down the bessel. This causes a cascade all along the wire—a phenomenon known as a corona discharge.

The great advantage of the Geiger-Müller counter is its simplicity. For example, one does not have to control its voltage very closely. Its chief limitation is that its dead time is of the order of 100 microseconds, owing to the time required for the discharge to be quenched. Any particle entering during that time is not recorded. If one particle entered every microsecond, the Geiger counter would record only 1% of the incoming particles, since it can produce only one count every 100 μsec.

With suitable techniques this limitation can be overcome or minimized, however, thus permitting GM counters to be used in areas of high instantaneous radiation fields. One such technique involves gating the counter off during the pulse of radiation from the accelerator and then on immediately afterward. A foil which captures neutrons is wrapped around the counter and the assembly is imbedded in a moderator. The activity induced in the foil and then detected can be made to be proportional to either the instantaneous or the average neutron fluence. The use of Geiger counters surrounded with silver foil in an accelerator radiation survey is described in Experiment 7 of the Appendix.

Scintillation Counters

Detectors in category b—scintillation counters—do not directly produce an electrical signal as a result of ionization, but rather depend upon the conversion of light emitted, as a result of ionization in a scintillating medium, to an electrical signal by a phototube.

Section 10 in the Appendix discusses in some detail the use of a NaI(Tl) scintillation counter for γ spectrometry. Such a detector is of great value in accelerator radiation measurements, for example, in determining the radioactivity induced in threshold activation detectors (see section on Particle Spectrometry).

Section 8 of the Appendix describes the use of irradiated plastic scintillator to detect neutrons with energy greater than 20 MeV.

VISUAL TECHNIQUES

This section describes techniques by which the passage of an ionizing particle is "visualized." This may be conveniently done in solids, liquids, or gases. In dense materials passage of an ionizing particle may lead to chemical changes or radiation damage, along the path of the particle, which may be detected and permanently recorded by photographic emulsion, mica, or various plastics. The passage of an ionizing particle may trigger the production of liquid droplets in a supersaturated gas (cloud chamber) or of sparks (spark chamber) along the path of the particle. A permanent record may be obtained by photographing the track consisting of drops of sparks.

Neutron Spectroscopy with Nuclear Emulsion

INTRODUCTION

Nuclear emulsion has been used extensively for neutron spectroscopy. Neutrons that pass through emulsion may be scattered by a hydrogen nucleus in the emulsion. Some fraction of the neutron energy is then imparted to the ionized hydrogen atom, which moves through the emulsion and leaves behind itself a trail of silver bromide crystals in such a state that, upon action by a chemical developer, they will be changed to colloidal silver particles. These grains of silver can be observed with a microscope. The more highly ionizing the particle, the greater the density of silver grains per unit track length, and the greater the energy of the ionizing particle the longer the track. Any ionizing particle can, in principle, produce these effects, and under suitable circumstances, the particle may be uniquely identified by the relationships between grain density and track length.

Excellent discussions of the process and techniques of nuclear emulsion are found in the text by Yagoda (YAG H 49) and in a survey article by Beiser (BEI A 52). The monograph by Barkas (BAR W 63) should be consulted when detailed information is necessary. For those wishing to learn something of the technique of the microscope, the text by Shillaber is also excellent (SHI C 44).

The techniques described here are limited to neutrons of energy between approximately 0.5 and 15 MeV. Protons of energy less than $\approx$ 0.5 MeV produce tracks too short to observe, whereas above $\approx$ 15 MeV few tracks are observed in emulsion exposed to the neutron spectra that typically prevail outside accelerator shielding. This is because both the neutron flux density and the n,p cross section decrease with increasing energy. Over this energy interval 0.5 to 15 MeV, n,p scattering is essentially isotropic. Consequently monoenergetic neutrons that interact with the hydrogen in a volume of emulsion produce (with equal probability) proton recoils having an energy from zero up to that of the incident neutron. This is illustrated in Fig. 5.35. It follows that if the neutrons are not monoenergetic, the resulting proton recoil spectrum will be formed by the superposition of individual proton spectra from each increment of neutron energy (as illustrated in Fig. 5.36).

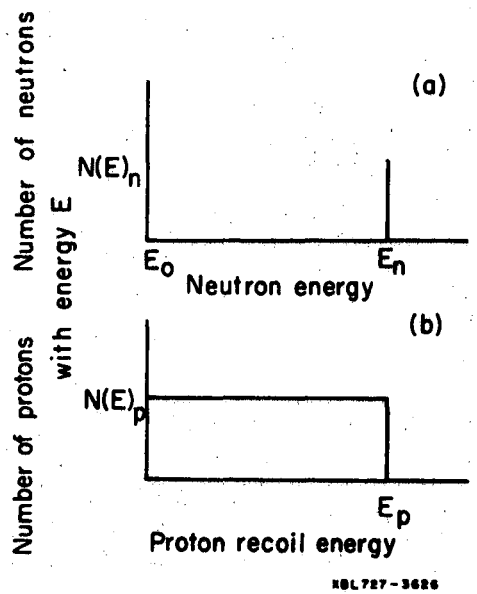

Fig. 5.35. An idealized proton recoil spectrum produced in emulsion (b) by a mono-energetic source of neutrons (a).

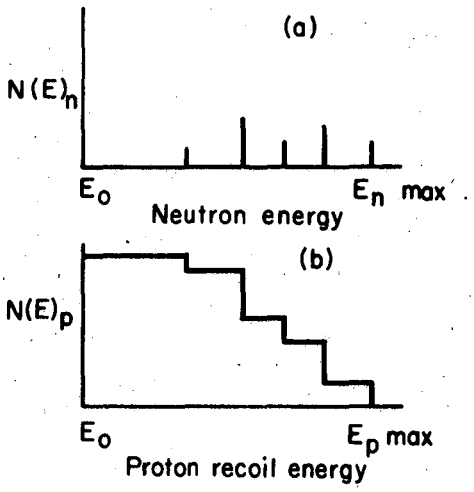

Fig. 5.36. An idealized proton recoil spectrum produced in emulsion (b) by a neutron source with several discrete energies.

Idealized proton spectra like these are not observed in practice, owing to such effects as statistical fluctuations in proton ranges because of straggling, and finite thickness of emulsion. Later we shall see how these and other effects operate to produce the spectra we observe. However, Figs. 5.35 and 5.36 indicate that once a proton recoil spectrum has been determined, it is then possible by differentiation of the proton spectrum to derive the neutron spectrum to which the emulsion was exposed.

METHODS AND TECHNIQUES

The methods and techniques to be described are those in use at our Laboratory and have proved satisfactory. Many of them were developed by Lehman and have been described in the literature (AKA H 63, LEH R 64a, LEH R 64b, LEH R 64c, LEH R 64d).

The emulsion used is type L4, manufactured by Ilford Ltd. (U.K). This type is chosen because it is sensitive to ionizing particles of any energy and because of its small grain size, $\approx 0.14\ \mu$, which permits heavy tracks to be registered by individual grains rather than by a continuous filament of silver.

Emulsion pellicles, 1X1 in., 600 μ thick, have been found most convenient. That the emulsion is unsupported aids processing by allowing

the developer and fixer to penetrate from both sides. Thicker emulsions take longer to process, and in thinner ones the probability that proton recoil tracks will be contained is smaller. Before use each pellicle is numbered, wrapped in a single thickness of black paper, and sealed with black tape. An emulsion history chart is kept (AKA H 63). After exposure, the pellicles each have their thickness measured, so that shrinkage after processing may be determined, and are then processed, with Amidol as the developer, by the following prescription.

Table 5.IX Processing of 600-μ L4 Ilford emulsions.

Procedure	Temperature (°C)	Time
Water presoak	5	1 hr
Developer presoak	5	2.5 hr
Warm development	24	50 min
Short stop	5	1 hr
Fixer	5	approx 24 hr
Dilution and Wash	5	approx 24 hr
5% Glycerine in 50% ETOH	5	1 hr
5% Glycerine in 75% ETOH	5	1 hr
Ethanol saturated with rosin	5	24 hr
Silk screen drying	20-25	24 hr

After processing, the pellicles are again measured and the shrinkage (ordinarily about 15%) is determined. Next they are mounted on 1 in. X 3 in. glass microscope slides with clear epoxy cement and are then ready for scanning.

A microscope fitted with 10X wide-field eye pieces and a 65X oil-immersion objective, whose working distance is adequate for the emulsion thickness, should be used in scanning.

The coordinate readout microscope used at the Lawrence Berkeley Laboratory for scanning track emulsions is one of a series designed and constructed by James C. Hodges of our Laboratory. It is fitted with a special moving stage. Two handwheels drive the precision lead screws that control the horizontal motion of the stage (x and y axes). The vertical (z-axis) motion of the microscope barrel is controlled by standard coarse- and fine-focus knobs. Shaft position encoders are mechanically coupled to the precision lead screw shaft and to the shaft of the fine-focus knob. These encoders "sense" minute rotation increments as electrical impulses that can be

translated and amplified. The encoders resolve 1000 units per turn, or 0.36 deg of shaft rotation. The x- and y-axis encoders permit a digital readout over the range of 100 turns. Suitable gearing and intermediate binary-to-decimal electronic translating enable the encoder to read out to a card-punch machine translation of the stage or motion of the barrel in units of microns. Thus, at a fixed-focus setting, every point in the working volume has a unique set (x_i, y_i, z_i) of rectangular space coordinates. A point of interest is located by cross hairs in the field of view and by the fine-focus setting.

When the scanner pushes the "punch button" on the control box, the three shaft encoder positions are sensed and three five-digit numbers--the track end-point coordinates in emulsion space--are punched into IBM cards. This is repeated for the other end point of the track. Although in principle one should measure the length of every track in the volume of emulsion considered, it has been shown by Lehman (LEH R 64e) that this is not necessary. We therefore use the more rapid random-walk method of sampling. In this method, the track to be measured next is the one whose end point lies nearest to the last end point of the track previously measured. However, only tracks that have both end points within the emulsion are selected.

For each track a correct length in microns is computed,

$$l = (f_1^2 \Delta x^2 + f_1^2 \Delta y^2 + f_2^2 \Delta z^2)^{1/2} \qquad (61)$$

where l is the length of the track, f_1 is the correction factor for the lateral (x,y) shrinkage, and f_2 is a correction containing the thickness (z) shrinkage factor. The Δx—i.e $(x_1 - x_2)$ — and Δ_y —i.e. $(y_1 - y_2)$— are in units of microns, but Δ_z is expressed in units of 0.60 μ. Therefore the correction f_2 is the product of 0.60 X the z shrinkage factor. Our program compares the computed length with a range-energy table (BAR W 63) for protons in nuclear emulsion (Fig. 5.37), and the track is assigned to one of 85 energy intervals. Several hundred tracks or more thus generate the points of a raw proton-recoil energy spectrum.

Next, our program corrects the raw proton spectrum by a function based on geometry. This function gives the probability that a track of a given length originating in the emulsion will end in the emulsion. This function is derived in by Akagi and Lehman (AKA H 63) and is shown in Fig. 5.38.

Each point on the spectrum is also corrected by its energy interval. The program thus computes 85 proton-recoil spectrum points $\Delta N/P\Delta E$ and the standard deviation $\sqrt{\Delta N/P\Delta E}$ for each point, where ΔN is the number of tracks in energy interval ΔE and P is the appropriate geometry correction.

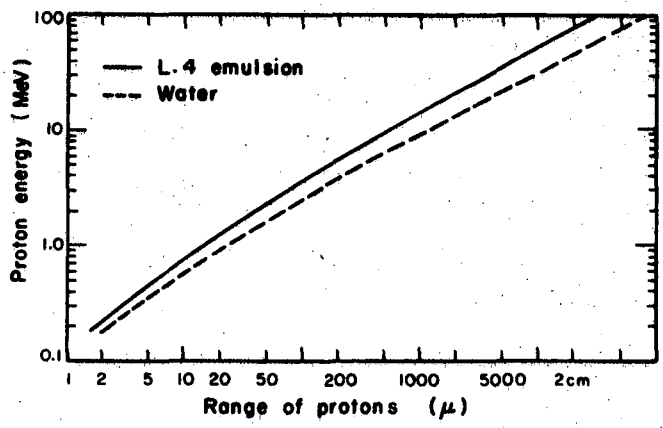

Fig. 5.37. The range-energy relation for protons in standard nuclear emulsion and in water. (after Barkas)

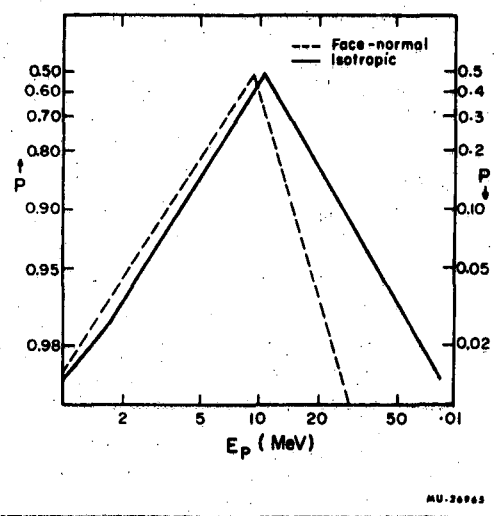

Fig. 5.38. A graph showing the geometric correction factors for isotropic and face-normal exposure of 625 μ emulsion. (from Akagi and Lehman)

Figure 5.39 shows a typical proton recoil spectrum derived by this method. Several features are worthy of comment. First, there are essentially no tracks of protons of energy < 0.5 MeV. This is because these have only a few grains and consequently are hard to see, especially when their axes are at large angles to the horizontal plane of the emulsion. Second, there are peaks in the proton recoil spectrum at energies of ≈ 0.7 and ≈ 1.25 MeV. The 0.7-MeV peak is due to thermal neutron capture in nitrogen in the emulsion, which gives rise to a proton by the reaction $^{14}N(n,p)^{14}C$. The 1.25-MeV peak is from α particles emitted from naturally occurring isotopes in the emulsion; chief among these are U, Th, and Rn. Occasionally "stars" are observed where two or more α particles have been emitted by the same nucleus. These can be distinguished from stars caused when a high energy nucleon interacts inelastically with a nucleus in the emulsion because stars formed by alpha decay have tracks with the same heavy grain density and (nearly) the same length, whereas stars resulting from inelastic interactions have tracks with differing lengths and grain densities. These qualities can be used to gain information about the shape of the neutron spectrum at high energies, as is discussed subsequently. Third, as expected, the proton recoil spectrum exhibits a more or less smooth decrease with increasing energy, marred somewhat by poor statistics. This is a consequence of the principle illustrated in Fig. 5.36. Finally, there are a few proton tracks with energies above 15 MeV. We attribute these to cosmic-ray neutrons if the accelerator neutrons are known to have energies below this. However, even when emulsions are exposed to continuous neutron spectra extending to the GeV region, there are still so few tracks above 15 MeV that poor statistics prevent acquisition of any information about the neutron spectrum. Emulsions exposed to monoenergetic neutrons exhibit the same features except that the proton spectrum does not decrease monotonically with energy. Rather, it is more or less flat up to the energy corresponding to the neutron energy, at which it undergoes a precipitous decrease. A proton recoil spectrum formed from exposure to a (D,T) neutron source is shown in Fig. 5.40.

We have used two methods to find the neutron spectrum from such data. Method I involves drawing or plotting a smooth curve through the proton recoil data points. The artificial peaks at 0.7 and 1.25 MeV are ignored and a smooth curve is constructed. This curve is made to monotonically decrease with energy (in the case of distributed neutron spectra) and to take into account the statistical error of the points making up the proton recoil spectrum. A second computer program then determines points along the smooth curve at 0.1-MeV intervals from 0.4 to 1 MeV, at 0.2-MeV intervals from 1 to 3 MeV, at 0.3-MeV intervals from 3 to 6 MeV, and at 0.4-MeV intervals beyond 6 MeV. This program finds these points by successively fitting a second-order polynomial curve to three adjacent input values and differentiating the curve at the point of interest. For instance,

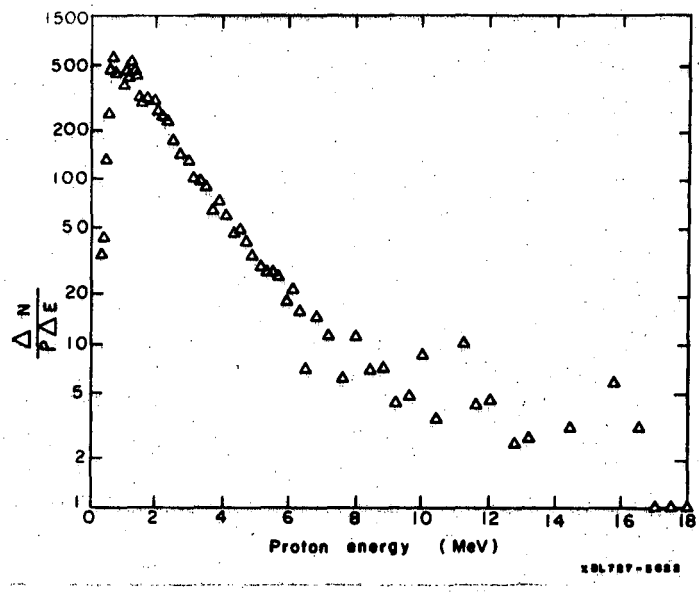

Fig. 5.39. Typical recoil proton spectrum procedure. Obtained by Lawrence Berkeley Laboratory scanning procedure. Emulsion scanned was exposed outside the shield of the 184" synchrocyclotron.

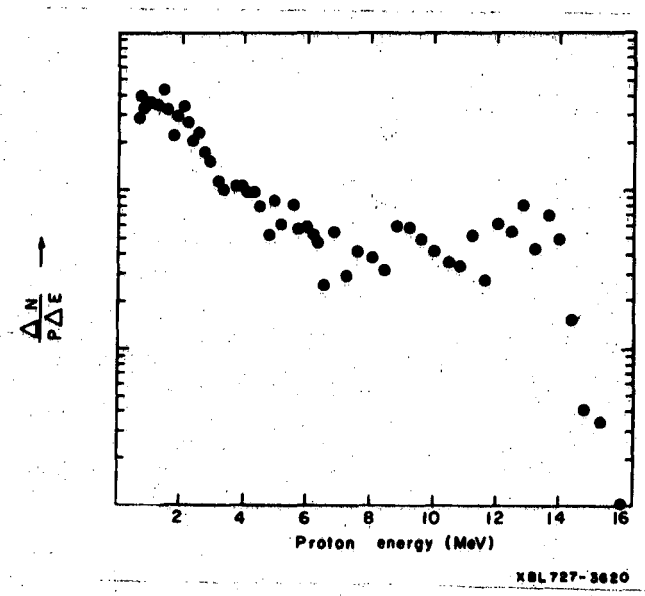

Fig. 5.40. Proton spectrum measured in an emulsion exposed to D,T (14 MeV) neutrons.

if $f(E) = a + bE + cE^2$ is the polynomial curve based on the input points at 0.4, 0.5, and 0.6 MeV, then $f(0.5)[0.5/\sigma(0.5)]$ is the relative value of the neutron spectrum at 0.5 MeV if $\sigma(0.5)$ is the elastic-scattering cross section for hydrogen at 0.5 MeV. This process is illustrated in Fig. 5.41 by use of the proton recoil data generated by 14.7-MeV neutrons as shown in Fig. 5.40. Note that the neutron spectrum also has a peak at 2.2 MeV. This is due to (D,D) neutrons formed by deuteron buildup on the target.

Method II involves the computer program LOUHI (discussed in the section on Particle Spectrometry in this chapter). When this program is used it is not necessary to generate a smooth curve through the proton recoil data points but nevertheless, a subjective element remains in the analysis in the choices of various smoothing and fitting functions.

Irrespective of the method of spectrum analysis utilized, it should be capable of a resolution comparable to that shown in Figs. 5.39 through 5.41. The resolution of the system should be tested and demonstrated before the method is accepted.

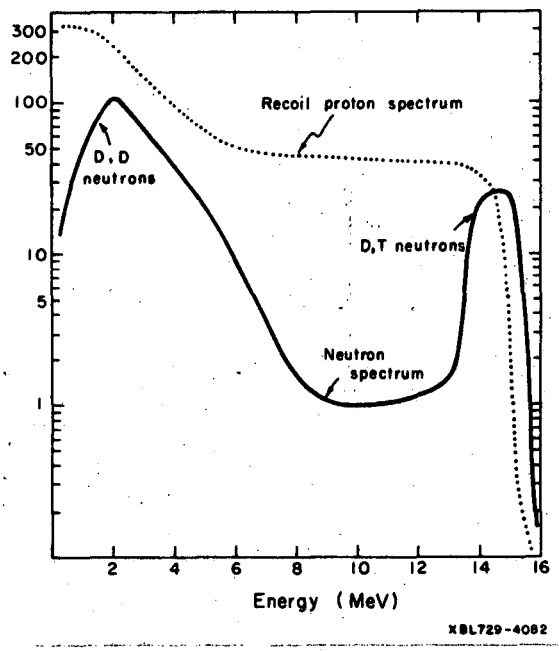

Fig. 5.41. Generation of a neutron spectrum from the proton recoil data shown in Fig. 5.40. The dotted line shows the smoothed curve fitted to the proton recoil scanning data while the solid line shows the (derived) neutron spectrum.

APPLICATIONS OF STAR PRODUCTION IN EMULSION

When stars are produced in nuclear emulsion by high-energy neutrons there is a strong dependence of the average number of grey prongs per star on the incident neutron energy (REM R 65). Omberg and Patterson have shown how this relationship could be used to estimate the slope of a neutron spectrum at energies above ≈ 50 MeV (OMB E 67). Subsequently, Patterson, Heckman, and Routti reported on extensions of and improvements on this earlier work (PAT H 69). They found the relationship shown in Fig. 5.42. They also showed that under the assumption that the cross section for producing a star is independent of energy, the average number of grey prongs per star can be computed for any given neutron spectrum. For a number of simple idealized spectra their results are given in Fig. 5.43.

Table 5.X gives results found by Patterson et al. for a number of actual neutron exposures, including one very hard spectrum from the 184-inch synchrocyclotron. They conclude that "The study of stars in nuclear emulsions extends the usefulness of emulsion methods in neutron spectroscopy to energies much higher than the upper limits of recoil proton techniques. Although it is not possible to reveal any detailed structure in the spectra, the information obtainable from stars is adequate in many applications of Health Physics and shielding design."

Table 5.X Spectral indices obtained from measured values of the average number of grey prongs per star. (ANG P.)

Location	E_{max} (MeV)	Measured ANGP	Neutron spectrum slope
184-inch cyclotron between Bays 10 and 11	730	0.442	0.75
Bevatron west tangent tank shielding wall (WTT)	6200	0.500	1.50
Bevatron Col. 7, main floor	6200	0.321	1.68
Bevatron mezzanine	6200	0.272	1.78
CERN PS	14000	0.291	1.80
CERN PS	14000	0.214	1.95
CERN PS	28000	0.447	1.68
White Mountain, 12000 ft altitude	(50000)	1.071	1.32
White Mountain, 14000 ft altitude	(50000)	1.038	1.35

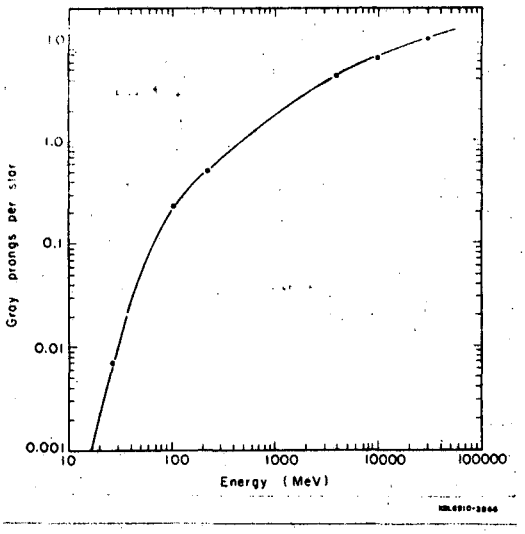

Fig. 5.42. Average number of grey prongs per star as a function of neutron energy. (after Patterson et al.)

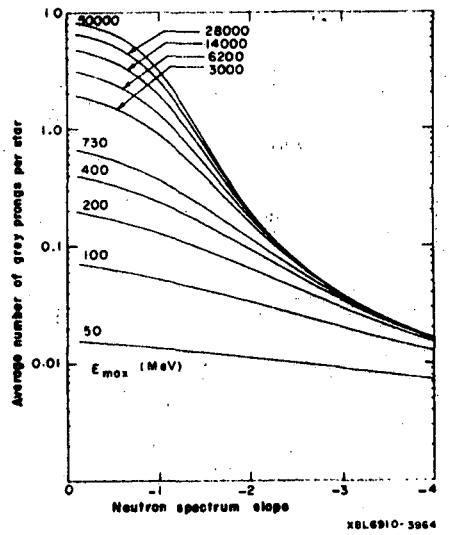

Fig. 5.43. A graph relating the average number of grey prongs per star to the spectrum shape (characterized by the logarithmic slope γ) and the maximum neutron energy in the spectrum. (from Patterson et al.)

Track Registration in Solids

Track registration in nuclear emulsion has been used extensively in health physics to provide a permanent record of neutron exposures. Limitations of nuclear emulsion such as fading and fogging, which can be controlled, and others such as limited energy response and the necessity of microscopy for evaluation have led to a search for other techniques. One such technique is the production of pits or holes in insulators irradiated with heavily ionizing charged particles and then etched with a suitable acid or base. Early studies of their technique have been described by Fleischer, Price, and Walker (FLE R 63, FLE R 65, PRI B 62, PRI B 63) (see also the Appendix–Experiment 12).

The response of a substance to charged particles depends on their specific ionization, dJ/dx, a function of β; the effective charge of the ionizing particle; the ionization energy of the outer electrons of the substance; and the electron's mass. For a given substance there is a critical value of dJ/dx above which tracks form and below which there is no preferential etching of the solid.

Many insulating solids are suitable, and among those investigated are cellulose nitrate, Lexan, and high-grade muscovite mica. Mica has an advantage in some circumstances in that the etch pits are diamond-shaped and are easy to identify under the microscope. The others have the advantage that they can be read automatically by use of the spark-through method, described by Cross and Tommasino (CRO W 72). The spark counting technique depends on having a thin film that has been etched until its tracks have become holes all the way through, or nearly so. The etched film is placed on the center electrode (positive polarity); then, a strip of aluminized Mylar is placed over both the film and the outer electrode (grounded) and held firmly in place by a plastic or rubber lid. When high voltage is applied, sparks occur through the etched holes. The heat of the spark causes localized evaporation of aluminum from the aluminized Mylar in an area much larger than that of the detector hole; it is therefore impossible to get any more sparks through individual holes.

The counter can be coupled to a scaler through a simple, GM-type quenching circuit so that each spark can be counted automatically. This permits rapid, automatic counting of tracks in a detector film which might otherwise require hours or days of microscope work.

Variables that affect reproducibility are foil thickness, diameter of the etched tracks, voltage applied and its polarity, air pressure, and length of time between sparks. These variables, as well as the use of other sparking atmospheres such as He, have been investigated by Cross and Tommasino. (CRO W 72).

They report that "The length and slope of the plateau in the curve of counts vs voltage was improved by varying the air pressure during counting

in such a way that all sparks occur at nearly the same voltage, by using positive polarity for the thin Al electrode and by controlling the time between sparks. For insulators 10 μ thick, slopes of 1% per 100 V, from 400 to 800 V, were obtained and the reproducibility of repeated counts with the same insulator was about 0.5 % (standard deviation for 10 measurements).

The relations found between minimum sparking voltage and air pressure x distance, and between spark energy and the amount of aluminum evaporated, can explain the length of the plateau obtained under varying conditions. Improved track resolution and higher maximum hole densities were obtained in a sparking atmosphere of He. Percentage counting losses were proportional to hole density up to 5000 tracks/cm^2, when 10% of the holes were missed. The main cause of nonreproducible track counting was found to be double sparking in a track rather than failure of some tracks to pass a spark."

The method is not in routine use in accelerator health physics, but Table 5.XI summarizes data obtained at LBL in exposing fission-foil track-detector assembly under a variety of conditions. The configuration of the assembly is generally a target foil or glass whose thickness is infinite with respect to the range of fission fragments ($\approx$ 10 mg/cm in the target foils we use). Detectors of high-grade muscovite mica or Lexan plastic are attached directly to the target. After exposure the detectors are removed and etched (the mica in 48% HF at room temperature, the Lexan in 28% KOH at 70° C) to enhance the damage pits caused by the nucleon-induced fission fragments. We prefer to use mica because its diamond-shaped pits are easy to identify and it is more durable than Lexan.

The flux is determined by the equation $\phi = \rho/n\sigma e$, where ϕ is the flux in nucleons/cm^2, ρ is the track density, n is the number of nucleii per cm^2 of target material within fission fragment range of the detector, and e is the efficiency (0.5 for our detector-target configuration). Assemblies have been exposed to thermal and low-energy neutrons in reactors, to intermediate-energy neutrons from a PuBe source and a 14-MeV generator, and to neutron and proton beams of several hundred MeV and a few GeV at LBL accelerators. Data for in-beam exposures are from detectors placed on the downstream face of the target foils. For a given target material the sensitivity (number of tracks per nucleon) varies directly with the effective fission cross section of the target material.

The effective energy of the nucleons above 50 MeV is determined by comparing ratios of track densities of various targets (the ratios U/Au, U/Ta, and Bi/Au, for example) with calibration curves of energy versus track density ratio,. Knowing the effective energy, one can get an effective cross section from experimentally determined cross-section curves, and can then determine an effective nucleon flux for the exposure conditions (see Fig. 5.34).

Table 5.XI. Sensitivities of foil-detector assemblages for nucleons of varying energies.

Target	Detector	Nucleon	Energy	Sensitivity (tracks/nucleon)	Exposure conditions
U glasses, 20, 50 500 ppm (natural U)	mica and Lexan	neutrons	thermal	9×10^{-9} for 500 ppm glass	LPTR, thermal column
U foil, Cd covered	mica	neutrons	epi-Cadmium	4.0×10^{-6}	exposure room, TRIGA reactor, UC campus
U foils	mica and Lexan	neutrons	$E \approx 4$ MeV	4.5×10^{-6}	PuBe source
Th foils	mica and Lexan	neutrons	$E \approx 4$ MeV	1.2×10^{-6}	PuBe source
U foil, Cd covered	mica	neutrons	14 MeV	1.4×10^{-5}	HENRE, N.T.S.
Th foil	mica	neutrons	14 MeV	4.5×10^{-6}	HENRE, N.T.S.
Ta foil	mica	neutrons	230 MeV	5.0×10^{-8}	184-Inch Cyclotron external beam
Bi foil	mica	neutrons	230 MeV	2.0×10^{-6}	184-Inch Cyclotron external beam
Au foil	mica	neutrons	230 MeV	4.5×10^{-7}	184-Inch Cyclotron external beam
Bi foil	mica	protons	740 MeV	3.6×10^{-6}	184-Inch Cyclotron beam
Au foil	mica	protons	740 MeV	1.3×10^{-6}	184-Inch Cyclotron beam
U foil	mica	protons	740 MeV	1.25×10^{-5}	184-Inch Cyclotron beam
Ta foil	mica	neutrons	5.5 GeV	6.1×10^{-7}	Bevatron external beam
Bi foil	mica	neutrons	5.5 GeV	1.1×10^{-6}	Bevatron external beam
Au foil	mica	neutrons	5.5 GeV	0.3×10^{-7}	Bevatron external beam
U foil	mica	neutrons	5.5 GeV	3.6×10^{-6}	Bevatron external beam

When the flux is great enough, or the exposure long enough, the fission-track method is a reliable, accurate means of determining a parameter of a neutron or proton exposure. With proper care the fission-track detectors furnish quickly developed, permanent records of an exposure. The practical use of fission-track detectors is described in Section 12 of the Appendix.

Other Visual Techniques

CLOUD CHAMBERS

Cloud chambers, although used extensively in the past in nuclear physics applications, have not found much application to practical accelerator health physics, because of their complexity and high cost of operation. They do continue to serve a useful function in studies of the details of the track structure of ionizing particles (DEL H 70). Similar comments apply to bubble chambers.

SPARK CHAMBERS

Spark chambers are detectors commonly used in nuclear physics and high-energy physics research to locate the tracks of ionizing particles. In their primitive form they consist of two parallel metal plates separated by a gap filled with a suitable gas. If ions due to the passage of a charged particle are present in the gap when a high voltage pulse is applied across the gap, break-down can occur so that a spark is produced. By arranging a stack of many of these two-plate modules with an appropriate high voltage supply and with suitable photography it is possible to record the passage and interaction of charged particle very efficiently (WEN W 64).

For similar reasons to those that obtain for cloud chambers, spark chambers have not found general application to the problems of accelerator health physics. They are being increasingly applied, however, in radiation physics and medicine, and Rindi has described their possible use for neutron spectrometry (RIN A 69).

ADDENDUM: INSTRUMENT CALIBRATION

The complexity of accelerator radiation environments necessitates special care in the calibration of radiation detectors. Both neutrons and γ rays must be measured. The calibration of instruments used to measure γ rays is well understood and is not discussed further here (the interested reader is referred to ICRU Reports 14 and 17 for a comprehensive bibliography and to IAEA Handbook 133 -- ICRU 69, ICRU 70, IAEA 71.)

Neutrons often control the radiation field to be measured (Chapters 2, 3, and 6), and consequently all radiation detectors to be used at accelerators must have their response to neutrons tested. Moreover, the response of all neutron detectors to neutrons of different energies must be determined.

Consequently we describe neutron calibration in some detail. Two types of measurements are made with neutron detectors. Measurements that we can call "experimental" need to be done only once for each type of detector, and thereafter can be relied on until some change is made in the detector. Such a measurement is the determination of the angular response to neutrons of a particular configuration of a BF_3 counter in a moderator. Measurements that we can call "calibration" might check the response of the instrument as a function of previously determined instrumental parameters such as sensitivity, energy response, and background counting rate. An example of this type of measurement would be taking a bias or discriminator curve for a moderated BF_3 counter under conditions of fixed voltage and amplifier gain. Such measurements should be repeated frequently.

A variety of neutron sources should therefore be available for these measurements--sources having different energy spectra (and different average energies) as well as a range of source strengths or neutron emission rates. Under some circumstances accelerator-produced neutrons may be used for calibration purposes (Chapter 3), but in general isotropic neutron sources are most widely used.

Photoneutron Sources

Gamma rays can "knock out" neutrons from nuclei if the energy of the γ ray is greater than the binding energy of the neutron in the nucleus (Chapter 3). For all elements other than deuterium and beryllium, however, the neutron binding energy is high—between 6 and 8 MeV. This in practice restricts the fabrication of photoneutron sources to some combination of D or Be (which have low binding energy) with some suitable radionuclide. Since the threshold energy in beryllium is 1.67 MeV and in deuterium 2.23 MeV, the list of isotopes with suitable half-lives is not long.

Wattenbert (WAT A 49) gives the energy of photoneutrons as

$$E_n = \frac{A-1}{A}\left[E_\gamma - Q - \frac{E_\gamma^2}{1862(A-1)}\right] + \delta\cos\theta, \qquad (62)$$

where E_n is the neutron energy (in MeV), A is the mass number of the target nucleus, E_γ is the gamma energy (in MeV), Q is the threshold energy in MeV for the γ-n reaction for a nucleus of mass A, and δ is a spread in energy (in MeV) that is a function of the angle θ between the directions in which the γ ray travels and the neutron is emitted,

$$\delta \approx E_\gamma\left(\frac{2(A-1)(E_\gamma-Q)}{931\,A^3}\right)^{1/2} \qquad (63)$$

As Feld (FEL B 53) points out, the inherent energy spread in photoneutrons sources is not large. In most sources, where the γ-ray source is surrounded by deuterium in some form or by beryllium, the energy spread ΔE_n is given by

$$\Delta E_n = 2\delta. \qquad (64)$$

The relative spread decreases with increasing neutron energy and is usually less than 25%. A larger source of energy spread is caused by neutron scattering in the deuterium or beryllium shell surrounding the gamma source—particularly when deuterium is used in the form of heavy water, deuterated wax or polyethylene.

A further source of neutron energy spread is the production of neutrons by γ rays that have been degraded in energy by Compton scattering. This energy spread is enhanced by the large quantities of Be or D necessary to obtain adequate neutron yields. Even when optimum quantities of these elements are used to maximize neutron production, the ratio of γ rays to neutrons is $\approx 10^3$ (about the same as the ratio of the Compton scattering cross section to that for photodisintegration).

This problem of gamma intensity is a bothersome one, with respect to both personnel exposure and detector response. Careful attention must be given especially to safe handling and storage of the γ-ray source and to making sure that the response of the detector is not to the γ rays but only to the neutrons.

Although spherical geometry produces the most efficient neutron yield, cylindrical geometry is often used for convenience in handling.

Several laboratories provide an absolute neutron calibration service (e.g., National Bureau of Standards, Washington, D. C.; Mound Laboratory, Ohio). The high γ-ray output of such sources does have one advantage: once an absolute calibration is obtained the neutron output may be followed and checked by measurements with a gamma-ionization chamber. Table 5.XII summarizes the data for some of the important photoneutron sources.

Whereas the spectrum of neutrons from photoneutron sources tends to be quite simple, it is nevertheless extremely difficult to measure, because the neutrons produced are low in energy (< 1 MeV). This low energy, in addition to the extremely high gamma background, has militated against experimental neutron spectroscopy.

Alpha-neutron Sources

The classic reaction which led to the discovery of the neutron is

$$^{9}Be_{4} + {}^{4}He_{2} \rightarrow {}^{12}C_{6} + {}^{1}n_{0},$$

and to this day most isotopic neutron sources are made with beryllium because the absolute neutron yield is greatest when beryllium is used. However, other light elements are also frequently used.

The neutron spectra from α,n sources, through easier to measure, tend to be complex for the following reasons:

a. The presence of excited levels in the final nucleus can lead to neutron production in several energy groups, even with incident monoenergetic α particles.

b. The relatively large quantities of target material (e.g., Be) required for good neutron yield efficiency produce an energy spread in the incident α-particle energies.

c. Neutron scattering in the source mixture and in the protective container also introduces some spread in energy.

d. The inherent energy spread depends on the direction of the emergent neutron with respect to the incoming α particle.

e. More than one isotope of the target material or impurities may be present (e.g., Am is a contaminant of Pu-Be neutron sources).

Although the neutron spectrum of α,n sources may be complex it may be determined experimentally in many cases. The γ background is low and the neutron energies may extend up to 13 MeV. Neutron spectroscopy can therefore be carried out in nuclear emulsions and with other proton-recoil detectors.

Figures 5.44 and 5.45 show some experimentally determined neutron spectra for Po-Be and Pu-Be sources. It is probable that these differences are due in part to the different construction of the particular sources measured. In general the spectra differ most at low energies, where measurement is greatest. The absorbed dose and dose equivalent per unit neutron fluence are

Table 5.XII. Photoneutron sources.

Source	$T_{1/2}$	E_γ (MeV)	E_n (MeV)	Yield (10^6 n/sec per curie)
$^{24}Na + Be$	15 h	2.76	0.83	1.9
$^{24}Na + D_2O$		2.76	0.22	4.0
$^{88}Y + Be$	87 d	1.9, 2.8	0.158 ± 0.005	1.5
$^{88}Y + D$		2.8	(0.31)[a]	0.044
$^{124}Sb + Be$	60 d	1.7	0.024 ± 0.003	2.8
$^{140}La + Be$	40 d	2.50	0.62	0.044
$^{140}La + D_2O$		2.50	0.151 ± 0.008	0.18
$^{228}Ra + Be$	6.7	1.80, 2.62	0.827 ± 0.030	0.52
$^{228}Ra + D_2O$		2.62(ThC'')	0.197 ± 0.010	1.4
Ra + Be	1620 y	1.69, 1.75, 1.82, 2.09, 2.20, 2.42	many	0.44
$Ra + D_2O$		2.42	0.12	0.015

a. Values in parentheses are estimates.

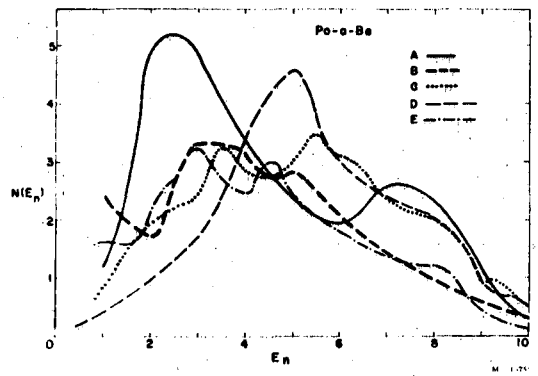

Fig. 5.44. Summary of several experimental determination of the spectrum emitted by a Po-Be source.

Curve A. Data of Perlman, Richards, and Speck
Curve B. Data of Cochran and Henry.
Curve C. Data of Elliott, McGarry, and Faust.
Curve D. Data of P. Demers.
Curve E. Data of Whitmore and Baker.

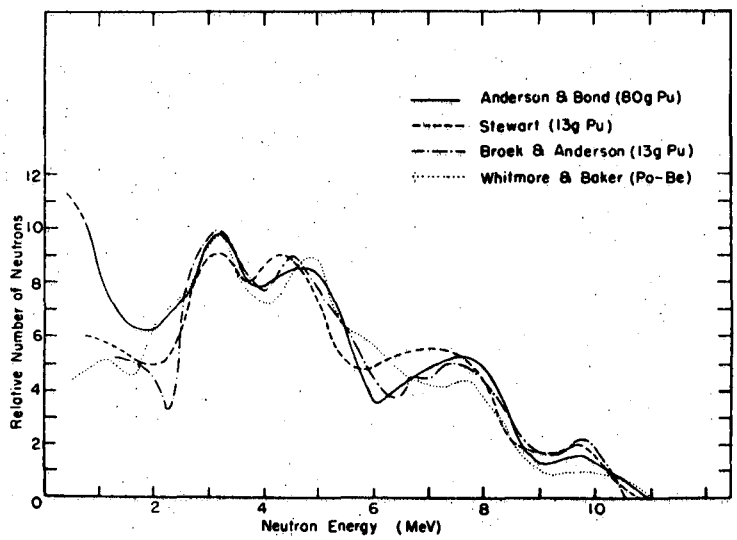

Fig. 5.45. Comparison of several Pu-Be and Po-Be sources. (from Anderson and Bond)

relatively insensitive to the neutron spectrum. Hess(HES W 59a) has calculated the spectra from some other α,n sources and compared them with various experimental data. These are shown in Figs. 5.46, 5.47, and 5.48.

Table 5.XIII gives some yields calculated by Hess (HES W 59a) for these same sources.

Hess and Smith (HES W 59b) have also measured the effective energy or average energy of a number of α,n sources, and their data are summarized in Table 5.XIV.

The specific activity of ^{239}Pu is low, which necessitates the use of large masses of material for high yields, resulting in problems of self-absorption and neutron scattering. In addition, Am and other isotopes of Pu frequently are contaminants that influence the neutron output of such sources (^{241}Am, the daughter, by β decay, of ^{241}Pu, is particularly important in this regard.) Of the other alpha emitters listed in Table 5.XIII, ^{226}Ra has an intense γ-ray background, and ^{210}Po has an inconveniently short half-life. Two other isotopes which are better on all these counts are ^{238}Pu ($T_{1/2}$= 86 years) and ^{241}Am ($T_{1/2}$=458 years). Both these isotopes are now available from commerical sources in combination with a number of different target materials. The yield of neutrons per 10^6 α particles is comparable to that from Po, and the spectra are substantially the same (see Fig. 5.45).

Caution is needed in evaluating the emission calibration of these sources. There may be axial asymmetry in emission, especially in sources of large physical size. For example, in an 80-g PuBe source, Anderson and Bond (AND M 63) report the relative neutron flux parallel to the axis of cylindrical symmetry at 0 and 180 deg was respectively 76% and 69% of that at 90 deg. If boron is the target material in the source, it competes for the available slow neutrons in a $MnSO_4$ bath, and for this reason such a calibration may be in error. $MnSO_4$ bath results should be compared with a long-counter measurement for any neutron standard; this is especially true for sources containing boron.

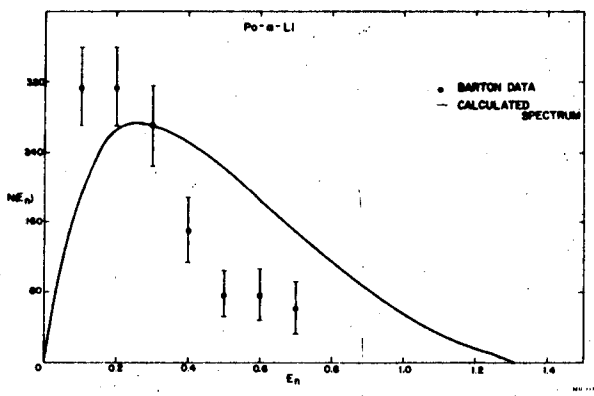

Fig. 5.46. Calculated and Measured Neutron Energy Spectra of a Po-Li neutron source. (from Hess)

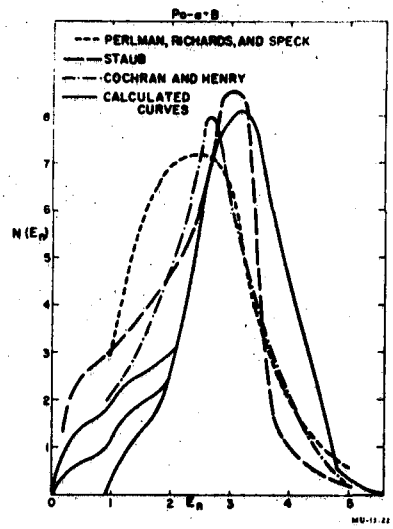

Fig. 5.47. Neutron energy spectrum calculated for a Po- natural B neutron source compared with several experimental spectra. (from Hess)

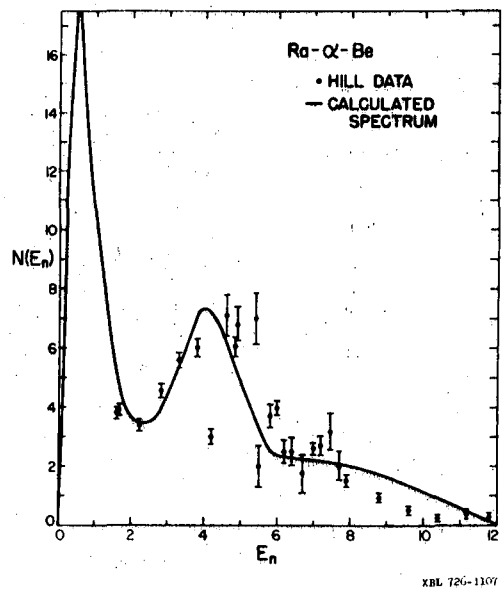

Fig. 5.48. Calculated neutron energy spectrum for a Ra-Be source. The experiments of Hill are shown for comparison. (from Hess)

Table 5.XIII Yields of α,n neutron sources.

Source	Calculated yield (neutrons per 10^6 α particles)
Po-α-Li	2.5
Po-α-Be	58
Po-α-B	24
Po-αBF_3	15.4
Po-α-F	
^{239}Pu-α-Be	35
^{226}Ra-α-Be	1.35×10^7 neutrons/sec per g Ra (new source)
	1.56×10^7 neutrons/sec per g Ra (old source)

Table 5.XIV. Average energies for various α,n neutron sources.

Source	Calculated	Energy (MeV) Experimental values	
		a	b
Po-Li	0.460	0.480	
Po-Be	4.08	4.2	4.5
^{239}Pu-Be	4.05	4.1	4.2
Ra-Be	3.50	3.7	4.1

(a) Measured by attenuation in polyethylene.

(b) From use of proton recoil counter (see Appendix in Experiment 4).

Spontaneous Fission Sources

A number of the transuranic elements decay (partially) by spontaneous fission and could be used as neturon sources. The spectrum of these transuranic spontaneous fission neutrons is not known to us, but a suitable close empirical approximation is given by Goldstein (GOL H 59):

$$(N(E) = 0.453\, e^{-E/0.965} \sinh \sqrt{2.29\, E}, \qquad (65)$$

N(E) being the fraction of neutrons per unit energy interval emitted per fission. A graph of this equation is given in Fig. 5.49. The neutron yields of various spontaneous sources have been tabulated by Denham (DEN D 68) and are given in Table 5.XV.

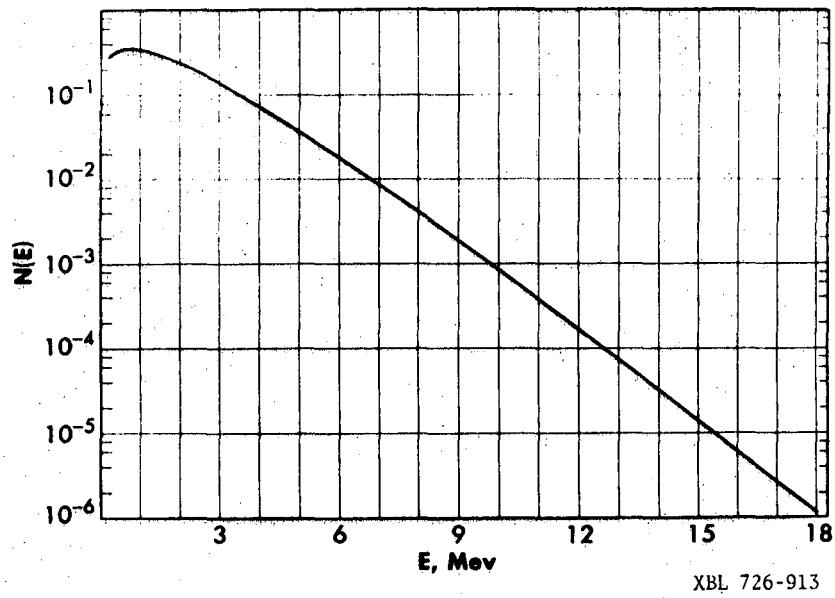

Fig. 5.49. The fraction of neutrons per MeV interval emitted at energy E, N(E) from thermal fission of ^{235}U. (from Goldstein)

Table 5.XI. Radioactive and spontaneous fission half-lives of selected isotopes (from Denham).

Isotope	Radioactive half-life (years)	Specific activity (Ci/g)	Spontaneous fission half-life (years)	Calculated neutron emission rate (n/sec/g)
^{239}Pu	24,400	0.062	$5.5X10^{15}$	0.03
^{243}Am	7950	0.185	--	--
^{241}Am	458	3.24	$2X10^{14}$	0.6
^{244}Cm	17.6	83.3	$1.3X10^{7}$	$1.2X10^{7}$
^{252}Cf	2.646	536	85	$2.3X10^{12}$
^{249}Bk[a]	0.86	1680	$6X10^{8}$	$2.7X10^{5}$
^{254}Es	0.756	1870	$7X10^{5}$	$2.9X10^{8}$

(a) Beta emitter; all other decay by alpha emission.

Since all these sources except ^{252}Cf decay largely by alpha emission, there will also be (α,n) neutrons accompanying the fission neutrons. Detailed studies of the spectra and practical use must await widespread availability of the isotopes ^{241}Am, ^{241}Cm, ^{250}Cm, and ^{252}CfO.

Slow-Neutron Sources

It is often most desirable in accelerator health physics to be able to calibrate and test thermal- and slow-neutron detectors. Seldom in our experience have slow and thermal neutrons contributed much to the dose received outside accelerator shields, but measurements of the contribution, even though small, should be made. For this reason it is necessary to test and calibrate detectors in thermal (or slow) neutron fluxes. A slow-neutron flux can be generated by immersing a fast-neutron source in water, but the flux gradient as a function of distance from the source is steep. This fact plus the problems arising from the water itself make this technique difficult to use. Much easier in practice is the device first described by Patterson and Wallace (PAT H 58). This is a cavity in concrete with walls that are thick compared with the mean depth of thermalization of neutrons of a few MeV energy. When a fast neutron source is introduced into the cavity, fast neutrons leaving the source are slowed down in the walls, and some diffuse back into the cavity, producing a slow- and thermal-neutron fluence. The largely empirical equation which describes this is

$$nv = K\,(Q/X), \tag{66}$$

where K is a constant, slightly greater than unity, Q is the emission of the fast neutron source in n/sec, and S is the surface area of the cavity in cm^2. The thermal flux is independent (within 10%) of position in the cavity. Such a device has been used at LBL for many years to calibrate BF_3 counters and foils.

Source Storage

Although most isotopic neutron sources are already doubly encapsulated, an additional thin-walled stainless steel container fastened to a light chain has the following advantages. First, if the source should leak, the screw-top stainless container would tend to confine the activity. Second, handling is simplified. Fastened to a chain, the source cannot fall down a hole or crack, and it is not so likely to be picked up inadvertently by a passerby. Third, the other end of the chain is a convenient place to fasten a radiation warning sign which gives the number of the source, the type, the curie content, the neutron emission, the safe working distance and time, and the date of calibration. When necessary the tertiary capsule can be removed, but this is seldom done in our experience.

The IAEA has prepared a useful handbook which discusses the sources of radiation, associated apparatus, and calibration techniques. A comprehensive bibliography is included (IAEA 71).

PERSONNEL MONITORING

INTRODUCTION

Perhaps no other aspect of radiation protection has received so much attention and had so much effort put into it as personnel monitoring. The reason for this is that--at least with respect to accelerator health physics--other techniques of radiation protection such as area monitoring, radiation surveys, and shielding studies make it possible to derive the dose equivalent received by an individual only indirectly. Personnel monitoring, at least in theory, gives this directly, and in addition personnel monitoring data form the primary record of exposures required by law and regulation. However, the actual role of personnel monitoring in accelerator health physics is being one part of a system. Because of the complexity of accelerator radiation fields no single instrument, device, or monitor is capable of indicating dose equivalent, and consequently personnel monitors must be interpreted by using information from other detectors and systems. In other words, proper interpretation of personnel monitors requires a priori knowledge of the radiation field and of accelerator operating parameters, and also requires proper calibration. Not only is such knowledge required for interpretation but also for selection of a dosimeter system that will be adequately sensitive to every component of the radiation field that can contribute substantially to total dose equivalent. In what follows we present a general discussion of these aspects of personnel monitors from the standpoint of accelerator radiation protection.

SELECTION OF SUITABLE PERSONNEL MONITORS

As we have seen in Chapter 3, the radiation fields produced by accelerators are both prompt (electromagnetic, or neutron, or a mixture) and permanent (mixed beta and gamma, due to induced activity).

When neutrons contribute an insignificant fraction of the dose equivalent, many choices of personnel monitoring devices present themselves. Of the dosimetry systems which have been increasingly used in the past decade, thermoluminescent materials, radiophotoluminescent materials, and thermally stimulated exo-electron-emitting materials come to mind. (Of these, only the first--TLD--have passed beyond the stage of research and development, and we confine our discussion to them.)

In addition, photographic film and small ionization chambers, which have been used for the past 20 years to monitor x and γ radiation, continue to play an important role. Pocket ionization chambers are typically used for

short-term exposure control in high-radiation-level areas, and data from them do not usually appear in personnel monitoring records. (Specifications for such dosimeters are given in American National Standards Institute Standard N 13.5, ANSI 72.) We see that in practice there are really only two choices for a personnel monitor, thermoluminescent material (TLD) and film. The use, application, and limitation of film in personnel monitoring has been authoritatively discussed in reviews by Ehrlich (EHR M 62), Barber (BAR D 66) Becker (BEC K 66) and the IAEA (IAEA 62) . Similarly TLD, in many applications, some of which are suitable to the interests of accelerator health physicists has been discussed by Cameron (CAM J 68), by Cusimano and Cipperley (CUS J 68), and in the proceedings of several international conferences on luminescence dosimetry (STAN 67, ORNL 69, and RISO 71). Attix (ATT F 71) has evaluated the use of possible systems of personal dosimetry. (See also LIN F 68.)

For accelerator personnel monitoring a comparison shows that TLD has the following advantages over film:

1. Accuracy and precision are somewhat better.
2. The range of measurement is greater.
3. Fading is less.

Film provides some advantages, however:

1. Its nonuniform energy and directional response is occasionally useful in the interpretation of exposures.
2. The cost is lower.

When the radiation field in which personnel monitors are to be used contains a large dose-equivalent component due to fast and high energy neutrons, then photographic film is the only choice presently available. The limitations of film which must be overcome are well-known, and in brief they are:

1. Response is influenced by energy and angular dependence.
2. Latent tracks fade at high temperatures and humidity.
3. Neutrons below $\approx$ 0.5 MeV are not detected.
4. Track counting by eye is necessary.

That they can be overcome in practice is borne out by the authors' personal experience at various accelerators and by Schimmerling and Sass (SCH W 65), who describe a 3-year study of a commercial film badge service which included monitoring of accelerator neutrons.

Alternatives to film for fast-neutron personnel monitoring have been discussed by Cross (CRO W 71). There are two possibilities, albedo dosimeters and fission-track detectors. Albedo dosimeters have been described by Harvey et al., (HAR J 69), Hoy (HOY J 72) and Hankins (HAN D 72). They are designed to measure neutrons reflected from the body of the wearer, and consist of a thermal neutron detector, usually ^{6}LiF, a polyethylene or other moderator, and, in some cases, an outer Cd absorber. Empirical

calibration shows them to be very useful for monitoring intermediate-energy neutrons. Although it has been suggested by Awschalom (AWS M 71) that they would be useful around accelerators where there are high energy neutrons, this seems unlikely. On the other hand, fission-track detectors may be, although their sensitivity is less and the most convenient fissile material to use, ^{232}Th, has a fission threshold of 1.5 MeV. ^{237}Np has a lower threshold but is not significantly different from film in this respect. Figure 5.50, after Cross (CRO W 71) compares relative responses of NTA film with fission-track detector using ^{237}Np and ^{232}Th.

Hack (HAC R 71) has reported an interesting empirical solution to the problem of accurate personal fast-neutron dosimetry in the spectra encountered around Nimrod (the 7-GeV proton synchrotron of the Rutherford Laboratory). The standard fast-neutron personal dosimeter used in the United Kingdom (various types of film pack all based on NTA emulsion) gives an estimate of dose equivalent that is strongly dependent upon neutron spectrum. The film response (defined by Hack to be reported rem per true rem) increases with increasing spectrum hardness, giving unacceptable underestimates of personal exposure in soft spectra and unacceptable overestimates in hard spectra (See Fig. 5.51). The response of a ^{6}LiF thermal neutron detector worn on the body, however, decreases with increasing spectrum hardness (Fig. 5.52). This suggests that if both detectors are worn a linear combination of their readings may be used to improve dose-equivalent estimates over a wide range of neutron spectra. Hack suggests that the expression True DE = 0.1 reported Film DE + 0.05 reported ^{6}LeF DE(67) gives a good fit to his data. By using such a prescription Hack has significantly improved the accuracy of his personal dose-equivalent estimates. To date no detailed explanation of the mechanisms responsible for the observed responses of the two detectors comprising this system has been proposed.

SELECTION OF DOSIMETER CALIBRATION FACTORS

Although the response of personnel monitors to radiation sources of various energies or energy distributions can (and should be) determined, it is not likely that a particular source will provide a calibration satisfactory for use in typical radiation fields. In most cases what is required is the response of the personnel monitor to the accelerator radiation field. This is best determined by exposing the monitor for various periods of time, with and without a phantom, in a variety of geometrical and physical conditions to the accelerator field in question, whose dose-equivalent rate has been previously measured or estimated by other methods. Such a study will yield data giving detection response vs dose equivalent for a number of situations. From these a suitable choice of the appropriate

calibration factor (or factors) to use in actual practice can be made. Such a study has recently been reported by Oshino (OSH M 71), who tested the response of NTA film pockets to the various sources of neutrons given in Table 5.XVI below.

Table 5.XVI. Neutron sources.

Neutron source	Average neutron energy[a] (MeV)
^{238}PuF	0.7
^{252}Cf with 15-cm lead shield	1.0
^{252}Cf with 5-cm lead shield	1.4
^{252}Cf bare	1.8
Combination of ^{252}Cf and $^{238}PuBe$ I	2.7
Combination of ^{252}Cf and $^{238}PuBe$ II	3.5
$^{238}PuBe$	4.4
Bevatron neutron I	3.3
Bevatron neutron II	4.2

a. Average neutron energies were measured by PE and BF_3 counters by the technique described in the appendix (Exp. 4). For the Bevatron there results do not include neutrons of energy > 20 MeV.

To each of these sources, Oshino exposed NTA film packets in free air, in a fixed position (front normal exposure) and rotated (isotropic exposure), and on a rotating tissue-equivalent phantom. His results for the phantom exposure only are given in Table 5.XVII.

It can be seen from the table that the selection of a valid calibration factor for NTA film requires knowledge of the incident neutron spectrum and the application of considerable judgment in making the selection. Factors to be considered in making such a judgment include the possibility of fading during the period of wearing the films, efficiency of the person doing the track counting, interference with track observation by beta-gamma fogging, and the statistical accuracy desired.

Table 5.XVII. The response of NTA films worn on the phantom, isotropic exposure (phantom rotated).

Neutron source	Dose equivalent (mrem)[a]	Tracks / Field	Net track density (t/f)	Track density per DE (t/cm^2 mrem)
^{238}PuF	$6.98X10^2$	292/200	1.43	3.40±0.22
^{252}Cf + 15cm Pb	$1.52X10^3$	252/100	2.49	2.73±0.19
^{252}Cf + 5 cm Pb	$7.86X10^2$	238/150	1.55	3.30±0.22
^{252}Cf	$3.83X10^2$	187/200	0.89	3.87±0.30
^{252}Cf + $^{238}PuBe$ I	$4.94X10^2$	304/200	1.46	4.92±0.30
^{252}Cf + $^{238}PuBe$ II	$2.61X10^2$	255/200	1.22	7.77±0.30
$^{238}PuBe$	$1.50X10^2$	263/300	0.83	9.23±0.62
Bevatron I	$1.20X10^3$	352/40	8.70	12.1 ±0.7
Bevatron II	$9.38X10^2$	333/50	6.56	11.7 ±0.7

a. Determined by folding the differential neutron into the relation between neutron fluence and dose equivalent.

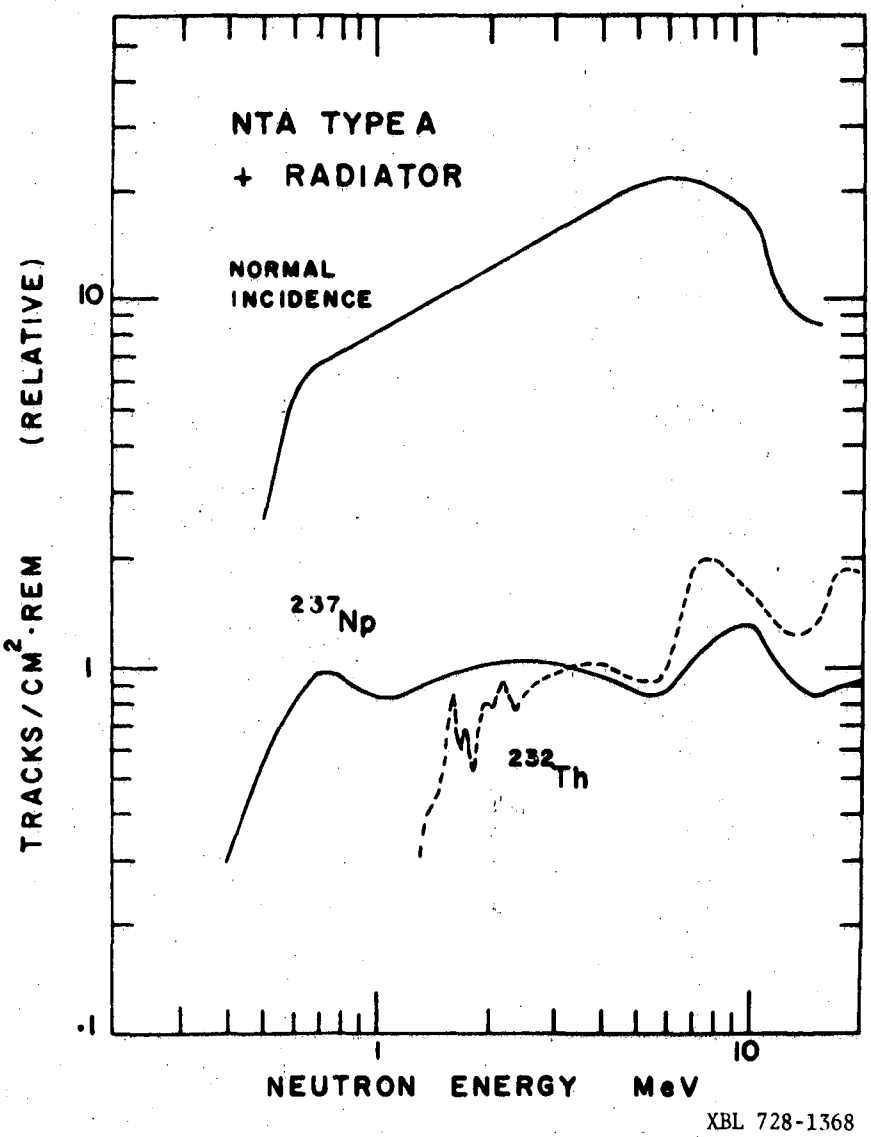

Fig. 5.50. A comparison of the relative response of NTA film with fission track detectors using ^{237}Np and ^{232}Th. (from Cross)

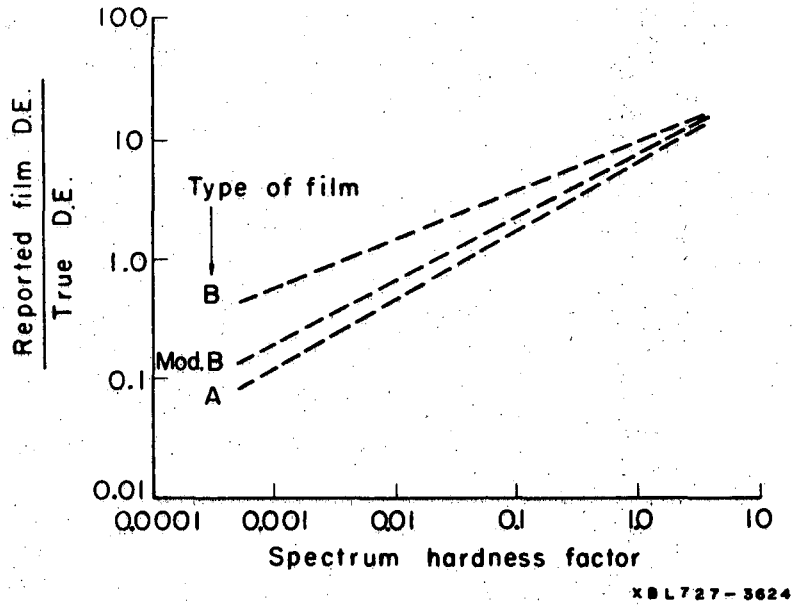

Fig. 5.51. Variation of NTA film response with spectrum hardnes factor for bilateral irradiation). (The spectrum hardness factor is defined to be the ratio of flux density measured by C rpoduction to that measured with a moderated thermal neutron detector) [from Hack]

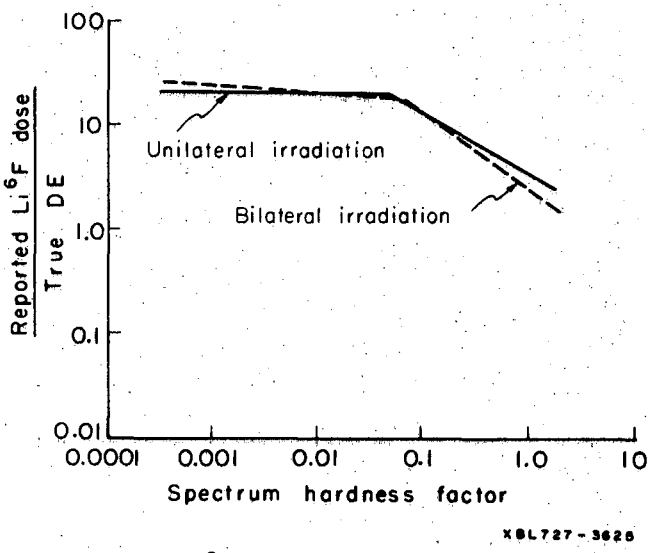

Fig. 5.52. Variation of ^6LiF response with spectrum hardness factor. (from Hack)

REFERENCES

AEB P 42 P. C. Aebersold and J. H. Lawrence, Physiological Effects of Neutron Rays, Ann. Rev. Physio. *4*, 25 (1942).

AKA H 63 H. Akagi and R. L. Lehman, Neutron Dosimetry in and Around Human Phantoms by Use of Nuclear Track Emulsions, Health Phys. *9*, 207 (1963).

AMA E 35 E. Amaldi, O. D'Agostino, E. Fermi, B. Pontecorvo, F. Rasetti, and E. Segrè, Artificial Radioactivity Produced by Neutron Bombardment, Proc. Roy. Soc. (London) *A 149*, 522 (1935).

AND I 63 I. O. Andersson and J. Braun, A Neutron Rem-Counter with Uniform Sensitivity from 0.025 eV to 10 MeV, in *Neutron Dosimetry*, Vol. 2 (IAEA, Vienna, 1963), p. 87.

AND M 63 M. E. Anderson and W. H. Bond, Neutron Spectrum of a Plutonium Beryllium Source, Nucl. Phys. *43*, 330 (1963).

ANSI 72 ANSI Standard N 13.5 , Performance Specifications for Direct Reading and Indirect Reading Pocket Dosimeters for X and Gamma Radiation (American National Standards Institute, New York, 1972).

ATT F 66 F. H. Attix, W. C. Roesch, and E. Tochilin, *Radiation Dosimetry*, Vol. 2, *Instrumentation* (Academic Press, New York, 1966).

ATT F 71 F. H. Attix, A Current Look at TLD in Personnel Monitoring, Health Phys. *22*, 287 (1971).

AWS M 67 M. Awschalom, The use of the Multisphere Neutron Detector for Dosimetry of Mixed Radiation Fields, in *Neutron Monitoring* (IAEA, Vienna, 1967).

AWS M 71 M. Awschalom, The Radiation Safety Philosophy and Its Implementation at NAL, in *Proceedings of International Congress on Protection Against Accelerator and Space Radiation, Geneva, 1971*, CERN 71-16, Vol. 2, p. 1050.

BAA J 64 J. Baarli, private communication to W. C. Middelkoop, CERN AR/INT/SG 64-6, 1964.

BAA J 65 J. Baarli and A. H. Sullivan, Radiation Dosimetry for Protection Purposes Near High Energy Particle Accelerators, Health Phys. *11*, 353 (1965).

BAA J 69a J. Baarli, Dosimetry of Very High Energy Radiation, in *Health Physics*, Vol. *2*, Ed. A.M.F. Duhamel (Pergamon Press, Oxford 1969).

BAA J 69b J. Baarli, Dosimetry of Very High Energy Radiation, *Health Physics*, Vol. 2, Ed. A .M.F. Duhamel (Pergamon Press, Oxford, 1969), p. 297.

BAR D 66 D. E. Barber, Standards of Performance for Film Badge Services, PHS Publication 99-RH-20, Environmental Health Series (USDHEW, Public Health Service, Washington, D.C., 1966).

BAR W 63 Walter H. Barkas, *Nuclear Research Emulsions*, Vol. I. *Techniques and Theory* (Academic Press, New York and London, 1963).

BAR A 64 A. Barthoux, G. Benezech, and H. Zaborowski, Dosimetrie des neutrons—technique multisphere, Commissariat a L'Energie Atomique report PAS 64/53, 1964.

BAT G 67 G. Bathow, E. Freytag, and K. Tesch, Measurement on 6.3-GeV Electromagnetic Cascades, Nucl. Phys. *B2*, 669 (1967).

BAU J 67 J. Baum, Nonlinear Amplifier for Use in Mixed Radiation Rem-Responding Radiation Meters, Health Phys. *13*, 775 (1967).

BAU J 69 J. W. Baum, R. C. Woodcock, and A. V. Kuehner, Factors Affecting Pulse Size in Sealed Tissue-Equivalent Counters, in *Proceedings of the USAEC Second International Conference on Accelerator Radiation Dosimetry and Experience, held at Stanford, 1969*, CONF-691101, p. 625.

BAU J 70 J. W. Baum, A. V. Kuehner, and R. L. Chase, Dose-Equivalent Meter Designs, Based on Tissue-Equivalent Proportional Counters, Health Phys. *19*, 813 (1970).

BEA J 59 J. W. Beasley, The Mean Fission-Fragment Range in Bismuth As Applied to Pulse-Type Ion Chambers, Lawrence Radiation Laboratory report UCRL-8760, May 15, 1959.

BEC K 66 K. Becker, *Photographic Film Dosimetry*, (The Focal Press, London and New York, 1961 in German, 1966 in English).

BEI A 52 A. Beiser, Nuclear Emulsion Technique, Rev. Mod. Phys. *24* [4] 273 (1952).

BOA J 66 J. W. Boag, Ionization Chambers, in *Radiation Dosimetry*, Vol. 2, Ed. F. H. Attix and W. C. Roesch (Academic Press, New York, (1966).

BOT W 43 W. Bothe, Zur Methodik der Neutronensonden, Z. Angew. Phys. *120*. 437 (1943).

BRA R 60 R. L. Bramblett, R. I. Ewing, and T. W. Bonner, A New Type of Neutron Spectrometer, Nucl. Instr. Meth. *2*, 1 (1960).

BRA W 12 W. H. Bragg, *Studies in Radioactivity*, (Macmillan, New York, 1912).

BRU E 65 E. Brunninx, The Production of ^{149}Tb from gold in the GeV Region, Nucl. Phys. *64*, 481 (1965).

BRU E 70 E. Brunninx, Simple Method for Measuring Fast Neutron Fluxes, in *Proceedings International Conference on the Use of Cyclotrons in Chemistry, Metallurgy, and Biology, Oxford, England*, (Butterworths, London, 1970), p. 250.

BUR P 55 P. R. J. Burch, Cavity Ion Chamber Theory, Radiation Res. *4*, 361 (1955).

BUR P 57 P. R. J. Burch, Comment on Recent Cavity Ionization Theories, Radiation Res. *6*, 79 (1957).

BUR T 68 T. E. Burlin, Cavity-Chamber Theory, in *Radiation Dosimetry*, Vol. 1, Ed. E. H. Attix and W. C. Roesch (Academic Press, New York 1968).

BUR T 70 T. E. Burlin, The Theory of Dosimeter Response With particular Reference to Ionization Chambers, in *Manual on Radiation Dosimetry*, Ed. N. W. Holm and R. J. Berry (M. Dekker Inc., New York, 1970), Section B.I.

BUR W 65 W. R. Burrus, Utilization of A Priori Information by Means of Mathematical Programming in the Statistical Interpretation of Measured Distributions (Ph.D. thesis), Oak Ridge National Laboratory report ORNL-3743, June 1965.

BUX M 67 M. Buxerolle and J. Lamberieux, Applications de la Méthode de Tikhonov à la spectrometrie des neutrons intermédiaires au moyen du détecteur polysphere Radioprotection *2*, 201 (1967).

CAM J 68 J. R. Cameron, N. Suntharalingam, and G. N. Kenney, *Thermoluminescent Dosimetry* (University of Wisconsin Press, Madison, 1968).

CAR T 70 T. G. Carter, V. M. Chakalian, and R. H. Thomas, Stanford Mark I Moderator Calibration Using Tantalum, Stanford University internal report RHT/TN/70-2 1970.

CHA V 69 V. M. Chakalian and R. H. Thomas, On the Possibility of Using Water to Monitor High-Energy Neutrons, Stanford University internal report RHT/TN69-16, Sept. 10, 1969.

COW F 72 F. P. Cowan, Units and Measurements, unpublished lecture delivered at the Symposium on Radiation Standards and Regulations, Oak Ridge, Tennessee, April 28, 1972.

CRO W 71 W. G. Cross, Alternatives to Nuclear Track Emulsions for Fast Neutron Personal Dosimeters, paper presented at Symposium on Personnel Dosimetry, Health Physics Society annual meeting, New York, July 12-16, 1971.

CRO W 72 W. G. Cross and L. Tommasino, Improvements in the Spark Counting Technique for Damage Track Neutron Dosimeters, paper presented at Symposium on Neutron Dosimetry in Biology and Medicine, Munich, May 15-19 1972.

CUM J 63 J. B. Cummings, Monitor Reactions for High-Energy Proton Beams, Ann. Rev. Nucl. Sci. *131*, 261 (1963).

CUS J 68 J. Cusimano and F. Cipperley, Personnel Dosimetry Using Thermoluminescent Dosimeters, Health Phys. *14*, 339 (1968).

DeC H 63 H. G. De-Carvalho, G. Cortini, M. Muchnik, G. G. Potenza, R. Rinzivillo, and W. O. Lock, Fission of Uranium, Thorium, and Bismuth by 20-GeV Protons, Nuovo Cimento *27* [2], 468 (1963).

DEL H 70 H. J. Delafield and P. D. Holt, An Assessment of a Low-Pressure Cloud Chamber for Measuring the Spatial Distribution of Ions Producted by High-LET Particles, in *Charged-Particle Tracks in Solids and Liquids*, Conference Series No. 8 (Institute of Physics, London, 1970), p. 35.

DEN H 68 D. H. Denham, Health Physics Considerations in Processing Transplutonium Elements, Battelle Memorial Institute report BNWL-SA-1397, June 1968.

DIC G 65 G. Di Cola and A. Rota, Calculation of Differential Fast-Neutron Spectra from threshold-Foil Activation Data by Least-Squares Series Expansion Methods, Nucl. Sci. Eng. *23*, 344 (1965).

DeP J 59 J. De Pangher, Double Moderator Neutron Dosimeter, Nucl. Instr. Meth. *5*, 61 (1959).

DIS C 65 C. H. Distenfeld and A. M. Markoe, Determination of Quality Factor Through the Utilization of a Balanced Tissue-Equivalent Ionization Chamber, in *Proceedings of the First Symposium on Accelerator Radiation Dosimetry and Experience, held at Brookhaven National Laboratory, Nov. 1965,* CONF-651109, p. 181.

DUF R 54 R. B. Duffield and G. Friedlander, Brookhaven National Laboratory Annual Report, Chemistry Section, Nuclear Chemistry Sub-section, BNL -303, July 1954, p. 27.

DVO R 65 R. F. Dvorak and N. C. Dyer, A Neutron Monitor for Simultaneous Measurement of Fluence and Dose Equivalent, Argonne National Laboratory report ANL-7085, 1965.

DVO R 66 R. F. Dvorak, A Pulse Analysis System and Computer Program for the Rossi LET Counter, in *Proceedings of the First International Congress of Radiation Protection.* Pergamon, Press, Oxford, 1968, p. 295.

DVO R 69 R. F. Dvorak, Calculation of dE/dx and Energy Loss Distributions in Spherical Cavities for Monoenergetic Neutron Fields, Health Phys. *17*, 279 (1969).

EHR M 62 M. Ehrlich, The Use of Film Badges for Personnel Monitoring, IAEA Safety Series No. 8 (IAEA, Vienna, 1962).

EVA R 55 R. D. Evans, *The Atomic Nucleus* (McGraw-Hill, New York, 1955).

FAI G 50 G. Failla and H. H. Rossi, Tissue Equivalent Ionization Chambers, Am. J. Roent. Radium Therapy Nucl. Med. *64*, 489 (1950).

FEL B 53 B. Feld, The Neutron, in *Experimental Nuclear Physics*, Vol. III, Ed. E. Segrè (John Wiley, New York, 1953), p. 368.

FIL P 65 P. Fills and R. Bass, Untersuchungen an einem Kugelzähler-Neutronen Spektrometer, Nukleonik *7*, 109 (1965).

FLE R 63 R. L. Fleischer, P. B. Price, and R. M. Walker, Method of Forming Fine Holes of Near Atomic Dimensions, Rev. Sci. Instr. *34*, 510 (1963).

FLE R 65 R. L. Fleischer, P. B. Price, and R. M. Walker, Tracks of Charged Particles in Solids, Science *149*, 383 (1965).

FRA E 66 E. M. Franz and G. Friedlander, Cross Sections for Production of ^{149}Tb from Au by High-Energy Protons, Nucl. Phys. *76*, 123 (1966).

FRÄ R 62 R. Fräki, M. Leimdörfer, and S. Malmskog, The Energy Variation of the Sensitivity of a Polyethylene-Moderated BF_3 Proportional Counter, Aktiebolaget Atomenergi, Sweden, Report AE-91, 1962.

FRE E 70 E. Freytag and D. Nachtigall, A Comparison of Health Physics Measuring Procedures at Accelerators, Deutsches Elektronen-Synchrotron internal report DESY/70, 1970.

FRI E 64 E. S. Frid, E. W. Miroschnikow, N. J. Sloschenikin, and W. W. Barzigow, Neutron Dosimetry Based on a "Long Counter," Atomnaya Energija *16*, 365 (1964).

GAR G 53 G. F. Garlick, Experimental Method for Measurement of Neutron Dose, Hanford Works, Richland, Washington, report HW-81746 5.46-53 (1953).

GIL W 68 W. S. Gilbert et al., (1966 CERN-LRL-RHEL Shielding Experiment, Lawrence Radiation Laboratory report UCRL-17941, Sept. 1968.

GIL W 69 W. S. Gilbert, K. Goebel, H. W. Patterson, and A. R. Smith, Concrete Activation Experiment at the Bevatron, Lawrence Radiation Laboratory report UCRL-19368, Dec. 1969.

GOL H 59 H. Goldstein, *Fundamental Aspects of Reactor Shielding* (Addison-Wesley, Reading, Mass., 1959).

GOL R 64a R. Gold, An Iterative Unfolding Method for Response Matrices, Argonne National Laboratory report ANL-6984, 1964.

GOL R 64b R. Gold, Limitations in the Orthonormal Expansion of Neutron Spectra with Activation Measurements, Nucl. Sci. Eng. *20*, 493 (1964).

GRA L 29 L. H. Gray, The Absorption of Penetrating Radiation, Proc. Roy Soc. (London) *A 122*, 647 (1929).

GRA L 36 L. H. Gray, Radiation Dosimetry, Brit. J. Radiol. *10*, 600 and 721 (1936).

GRA L 44 L. H. Gray, The Ionization Method of Measuring Neutron Energy, Proc. Cambridge Phil. Soc. *40*, 72 (1944).

GRE C 67 C. R. Greer, J. A. Halbleib, and J. V. Walker, A Technique for Unfolding Neutron Spectra from Activation Measurements, Sandia Laboratories report SC-RR-67-746, Dec. 1967.

HAC R 71 R. C. Hack, Personal Fast-Neutron Dosimetry around Nimrod, Rutherford Laboratory report RHEL/M R8, Nov. 1971.

HAN A 47 A. O. Hansen and J. L. McKibben, A Neutron Detector Having Uniform Sensitivity from 10 keV to 3 MeV, Phys. Rev. *72*, 673 (1947).

HAN D 62 D. E. Hankins, A Neutron Monitoring Instrument Having a Response Approximately Proportional to the Dose Rate from Thermal to 7 MeV, Los Alamos Scientific Laboratory report LA-2717, 1962.

HAN D 63 D. E. Hankins, New Methods of Neutron-Dose-Rate Evaluation, in *Neutron Dosimetry* Vol. 2 (IAEA, Vienna 1963), p. 123.

HAN D 72 D. E. Hankins, Factors Affecting the Design of Albedo-Neutron Dosimeters Containing Lithium Fluoride Thermoluminescent Dosimeters, Los Alamos Scientific Laboratory report LA-4832, Jan. 1972.

HAN G 65 G. E. Hansen and H. A. Sandmeier, Neutron Penetration Factors Obtained by Using Adjoint Transport Calculations, Nucl. Sci. Eng. *22*, 315 (1965).

HAN J 59 J. S. Handloser, *Health Physics Instrumentation*, (Pergamon Press, New York, 1959).

HAR D 68 D. M. Hargreaves and G. R. Stevenson, Unfolding Neutron Energy Spectra Using the ALFIE Routine, Rutherford High Energy Laboratory report RHEL/M 147, July 1968.

HAR D 69 D. M. Hargreaves and G. R. Stevenson, Rutherford Laboratory, private communication to R. H. Thomas Feb. 1969. (See THO R 69.)

HAR J 69. J. R. Harvey, W. H. R. Judd, and S. Townsend, A Personal Dosimeter Which Measures Dose from Thermal and Intermediate - Energy Neutrons and from Gamma and Beta Radiation, Central Electricity Generating Board (UK) report RD/B/N/1547, Dec. 1969.

HES W 57 W. N. Hess, H. W. Patterson, and R. Wallace, Delay-Line Chamber Has Large Area, Low Capacitance, Nucleonics *15*, 74 (1957).

HES W 59a W. N. Hess, Neutrons from (α,n) Sources, Ann. Phys. *6*, |2|, 115 (1959).

HES W 59b W. N. Hess and A. R. Smith, Measurement of Average Neutron Energies for (α,n) Neutron Sources, Lawrence Radiation Laboratory report UCRL-8617, April 1959.

HOY J 72 J. E. Hoy, Personnel Albedo-Neutron Dosimeter with Thermoluminescent ^{6}LiF and ^{7}LiF, Savanannah River Laboratory report DP-1277, Jan. 1972.

IAEA 62 International Atomic Energy Agency, The Basic Requirements for Personnel Monitoring, IAEA Safety Series No. 14 ((AEA, Vienna, 1962).

IAEA 71 International Atomic Energy Agency, *Handbook on Calibration of Radiation Protection Monitoring Instruments*, Technical Report Series No. 133 (IAEA, Vienna, 1971).

ICRP 63 ICRP, Report of the RBE Committee to the ICRP on Radiological Units and Measurements, Health Phys. *9* [4], 357 (1963).

ICRU 38 ICRU, Recommendations of the ICRU, Chicago, 1937, Am. J. Roent. Radium Therap. Nucl. Med. *39*, 295 (1938).

ICRU 57 ICRU, *Report of the International Commission on Radiological Units and Measurement, 1956*, National Bureau of Standards Handbook NBS #62, 1957.

ICRU 62 ICRU, Radiation Quantities and Units, Report 10a of the International Commission on Radiological Units and Measurements, in *National Bureau of Standards Handbook* NBS #84, 1962.

ICRU 69 ICRU, Radiation Dosimetry: X Rays and Gamma Rays with Maximum Photon Energies Between 0.6 and 50 MeV, ICRU report 17, 1969.

ICRU 70 ICRU, Radiation Dosimetry: X Rays Generated at Potentials of 5 to 150 kV, ICRU report 17, 1970.

ICRU 71 ICRU, Radiation Protection Instrumentation and Its Application, ICRU report 20, 1971.

JAF G 13a G. Jaffé, Zur Theorie der Ionisation in Kolonnen. I, Ann. Physik *4*, 42, 303 (1913).

JAF G 13b G. Jaffé, Columnar Ionization, Radium *10*, 126 (1913).

JAF G 29a G. Jaffé, Zur Theorie der Ionisation in Kolonnen. II, Ann. Physik *5*, 1, 977 (1929).

JAF G 29b G. Jaffé, Kolonnenionisation in Gasen bei erhöhtem Druck, Physik Z. *30*, 849 (1929).

JAF G 40 G. Jaffé, On the Theory of Recombination, Phys. Rev. *58*, 968 (1940).

JEN T 69 T. H. Jenkins (Stanford Linear Accelerator Center), private communication, 1969.

JOH H 69 H. E. Johns, Use of X and Gamma Rays in Radiotherapy, in *Radiation Dosimetry* Vol. 3, Ed. F. H. Attix and E. Tochlin (Academic Press, New York, (1969), Chap. 30.

KEI I 67 I. B. Keirim-Markus and S. N. Kraitov, Use of Fissionable Substances in Neutron Dosimetry, in Neutron Monitoring: Proceedings of Symposium on Neutron Monitoring for Radiological Protection; held in Vienna, Aug. - Sept. 1966 (IAEA, Vienna, 1967), p. 425.

KEL E 48 E. L. Kelly and C. Wiegand, Fission of Elements from Pt to Bi By High-Energy Neutrons, Phys. Rev. *73*, 1135 (1948).

KOH A 64 A. D. Kohler, Jr., An Improved Method of Neutron Spectroscopy Using Threshold Detectors (M.S. thesis), Lawrence Radiation Laboratory report UCRL-11760, Dec. 1964.

LBL 71 Lawrence Berkeley Laboratory, Instrumentation for Environmental Monitoring, LBL-1 Vol. *3*, Dec. 1971.

LEA D 56 D. E. Lea, Actions of Radiation on Living Cells, (University of Cambridge Press, London, 1956), p. 21.

LEA J 67 J. W. Leake, Portable Instruments for the Measurements of the Neutron Dose-Equivalent Rate in Steady-State and Pulsed Neutron Fields, in *Neutron Monitoring: Proceedings of Symposium on Neutron Monitoring for Radiological Protection, held in Vienna, Aug.-Sept. 1966* (IAEA, Vienna, 1967), p. 313.

LED C 67 C. M. Lederer, J. M. Hollander, and I. Perlman, *Table of Isotopes* (John Wiley, New York, 1967).

LEH R 64a R. L. Lehman, H. Akagi, and O. M. Fekula, Neutron Dosimetry Near a Bare Pulsed Reactor, Health Phys. *10*, 517 (1964).

LEH R 64b R. L. Lehman and J. R. Wayland, Jr., Geometry Correction Factors for Proton-Recoil Track Samples Taken from Nuclear Emulsions, Lawrence Radiation Laboratory report UCRL-11296, Feb. 1964.

LEH R 64c R. L. Lehman and O. M. Fekula, Semiautomatic Scanning of Proton Recoil Tracks in Nuclear Emulsion, Lawrence Radiation Laboratory report UCRL-11321, March, 1964.

LEH R 64d R. L. Lehman and O. M. Fekula, Energy Spectra of Stray Neutrons from the Bevatron, Nucleonics *22* [11], 35 (1964).

LEH R 64e R. L. Lehman, O. M. Fekula, and J. R. Wayland, Jr., Sampling Bias in Scanning Proton-Recoil Tracks in Nuclear Emulsion, Lawrence Radiation Laboratory report UCRL-11703, Oct. 1964.

LIN F 68 F. M. Lin and J. R. Cameron, A Bibliography of Thermoluminescent Dosimetry, Health Phys. *14*, 495 (1968).

LIS H 62 H. Liskien and A. Paulsen, Compilation of Cross Sections for Some Neutron-Induced Threshold Reactions, Euratom report EUR-119e, July 1962.

LIT D 52 D. J. Littler and R. H. Thomas, Absolute Neutron Density Determinations Using Cobalt, Atomic Energy Research Establishment, Harwell report AERE-R/R-1019, Sept. 1952.

LOC E 53 E. E. Lockett and R. H. Thomas, The Half Lives of Several Radioisotopes, Nucleonics *11*, 14 (1953).

MAN M 52 M. E. Mandl, A Method of Measuring the Average Energy of a Neutron Spectrum in the Range 0.3 to 3.0 MeV, Atomic Energy Research Establishment, Harwell report AERE-TR-1008, Aug. 1952.

McC J 60 J. B. McCaslin, A High-Energy Neutron-Flux Detector, Health Phys. *2*, 399 (1960).

McC J 67 J. B. McCaslin and L. D. Stephens, High-Sensitivity Neutron and Proton Flux Detector with a Practical Threshold Near 600 MeV, Using Hg (spallation) ^{149}Tb, Lawrence Radiation Laboratory report UCRL-17505, April 1967.

McC J 68 J. B. McCaslin, H. W. Patterson, A. R. Smith, and L. D. Stephens, Some Recent Developments in Technique for Monitoring High-Energy Accelerator Radiation, in *Proceedings of First International Radiation Protection Association, Rome, Italy, September 5-10, 1966* (Pergamon Press, New York, 1968), p. 1131.

McE W 67 W. N. McElroy, S. Berg, and G. Gigas, Neutron-Flux Spectral Determination by Foil Activation, Nucl. Sci. Eng. *27*, 533 (1967).

McG S 66 S. A. McGuire, A Dose Instrument for Neutrons from Thermal to 100 MeV, Los Alamos Scientific Laboratory report LA-3435, 1966.

McL J 67 J. E. McLaughlin and K. O'Brien, Accelerator Stray-Neutron Dosimetry: Spectra of Low- and Intermediate-Energy Neutrons, in *Neutron Monitoring: Proceedings of Symposium on Neutron Monitoring for Radiological Protection, held in Vienna, Aug.-Sept. 1966* (IAEA, Vienna, 1967), p. 335

MOR P P. M. Morse and H. Feshbach, *Methods of Theoretical Physics* (McGraw-Hill, New York, 1953).

MOY B 52 B. J. Moyer, Survey Methods for Fast and High-Energy Neutrons, Nucleonics *10* [5], 14 (1952).

MUT A 25 A. Mutscheller, Physical Standards of Protection Against Roentgen Ray Dangers, Am. J. Roent. Radium Therapy *13*, 65 (1925).

NAC D 62 D. Nachtigall, Der gegenwärtige Stand der praktischen Neutronen-dosimetrie, Kernforschungsanlage, Jülich, W. Germany report JUL-69-ST, 1962.

NAC D 64 D. Nachtigall and F. Rohloff, Neue Verfahren zur Messung von Neutronenflussdichten und Neutronendosisleistungen mit Szintillationszähler und Kugelmoderatoren, Nukleonik *6*, 330 (1964).

NAC D 67a D. Nachtigall, Determination and Accuracy of Results of Rem-Counter Measurements, in *Conference on Radiation Dose Measurements, Their Purpose, Interpretation, and Required Accuracy in Radiological Protection* (European Nuclear Energy Agency, Stockholm, 1967), pp. 391-415.

NAC D 67b D. Nachtigall and R. Rohloff, Verfahren zur Messung der Flussdichten und Dosisleistungsäquivalenz von Neutronen im Energiebereich zwischen thermischer Energie und 50 MeV, Nucl. Instr. Meth. *50*, 137 (1967).

NCR P 60 NCRP, Measurement of Neutron Flux and Spectra for Physical and Biological Applications, NBS Handbook 72, 1960.

O'BR K 65 K. O'Brien, R. Sanna, and J. McLaughlin, Inference of Accelerator Stray Neutron Spectra from Various Measurements, in *Proceedings of the First Symposium on Accelerator Radiation Dosimetry and Experience, held at Brookhaven National Laboratory, Nov. 1965*, CONF-651109, p. 346.

O'BR K 67 K. O'Brien, R. Sanna, M. Alberg, J. E. McLaughlin, and S. A. Rothenberg, High-Energy Accelerator Shield Leakage Neutron Spectra, Nucl. Sci. Eng. *27*, 338 (1967).

OMB R 67 R. P. Omberg and H. W. Patterson, Application of the Stars Produced in a Nuclear Emulsion to the Determination of a High Energy Neutron Spectrum, Lawrence Radiation Laboratory report UCRL-17063, Feb. 1967.

ORNL 63 Oak Ridge National Laboratory, Neutron Physics Division, Annual Progress Report for Period Ending Sept. 1, 1962, ORNL-3360, 1963, p. 297.

ORNL 69 *Proceedings of the Second International Conference on Luminescence Dosimetry, held at Gatlinburg, Tenn. Sept. 23, 1968*, Ed. J. A. Auxier, K. Becker, and E. Robinson, CONF-680920, 1969.

OSH M 71 M. Oshino, Response of NTA Personnel Neutron Monitoring Film Worn on a Human Phantom, Lawrence Berkeley Laboratory report LBL-342, Sept. 1971.

OVE T 66 T. R. Overton, Experience with a Linear Energy Transfer (LET) chamber at CERN, CERN internal report CERN 66/33, 1966.

PAT H 58 H. W. Patterson and R. W. Wallace, A Method of Calibrating Slow-Neutron Detectors, Lawrence Radiation Laboratory report UCRL-8358, July 1958.

PAT H 69 H. Patterson, H. Heckman, and J. T. Routti, New Measurements of Star Production in Nuclear Emulsions and Applications to High-Energy Neutron Spectroscopy, in *Proceedings of the Second International Conference on Accelerator Dosimetry and Experience, held at Stanford, Calif., Nov. 1969*, CONF-691101, 1969, p. 750.

PEN J 68 J. Penfold and G. R. Stevenson, Preliminary Measurements of the Angular Distribution of the Stray Radiation Field, Rutherford Laboratory Radiation Protection Group internal note RP/PN/23, Sept. 1968.

PER D 65 D. R. Perry and K. B. Shaw, Radiation Levels in and Around Nimrod, in *Proceedings of the First Symposium on Accelerator Radiation Dosimetry and Experience, held at Brookhaven National Laboratory, Nov. 1965*, CONF-651109.

PER D 67 D. R. Perry, Neutron Dosimetry Methods and Experience on the 7-GeV Proton Synchrotron Nimrod, in *Neutron Monitoring: Proceedings of Symposium on Neutron Monitoring for Radiological Protection, held in Vienna, Aug.-Sept. 1966* (IAEA, Vienna, 1967), p. 355.

PHI D 62 D. L. Phillips, A Technique for the Numerical Solution of Certain Integral Equations of the First Kind, J. Assoc. Comput. Mach. *9*, 84 (1962).

PHI L 65 L. F. Phillips et al., Linear Energy Transfer Spectra and Effective Quality Factors in Stray Radiation Areas of the Brookhaven National Laboratory Proton Synchrotron, in *Proceedings of the First Symposium on Accelerator Radiation Dosimetry and Experience, held at Brookhaven National Laboratory, Nov. 1965*, CONF-651109.

PHI L 67 L. F. Phillips, E. D. Scalsky, and R. J. Champagne, Dose Distributions as a Function of LET and Measurements of QF Around the BNL Medical Research Reactor, Health Phys. *13*, 1175 (1967).

PRI P 62 P. B. Price and R. M. Walker, Observations of Charged-Particle Tracks in Solids, J. Appl. Phys. *33* [12] 3400 (1962).

PRI P 63 P. B. Price and R. M. Walker, A Simple Method of Measuring Low Uranium Concentrations in Natural Crystals, Appl. Phys. Letters *2*, 23 (1963).

PRI W 58 W. J. Price, *Nuclear Radiation Detection*, (McGraw Hill, New York, 1958).

REI P 58 P. W. Reinhardt and F. J. Davis, Improvements in the Threshold Detector Method of Fast Neutron Dosimetry, Health Phys. *1-2*, 169 (1958).

REM R 65 R. Remy, Neutron Spectroscopy by the Use of Nuclear Stars from 20 to 300 MeV (M.S. thesis), Lawrence Radiation Laboratory report UCRL-16325, Aug. 1965.

RIN A 68 A. Rindi, Evaluation of Fluxes and Dose-Equivalent Rates in Neutron Fields Around High-Energy Proton Accelerators, Lawrence Radiation Laboratory report UCRL-18424, Aug. 1968.

RIN A 69 A. Rindi, Present and Projected Uses of Multiwire Spark Chambers in Health Physics, in *Proceedings of the Second International Conference on Accelerator Dosimetry and Experience, held at Stanford, Calif., Nov. 1969*, CONF-691101, 1969, p. 660.

RIN J 63 J. C. Ringle, A Technique for Measuring Neutron Spectra in the Range 2.5 to 30 MeV Using Threshold Detectors (Ph.D. thesis), Lawrence Radiation Laboratory report UCRL-10732, Oct. 1963.

RISO 71 *Proceedings of the Third International Conference on Luminescence Dosimetry, held in Risö, Denmark, 1971*, Danish Atomic Energy Commission report RISO-249, 1971.

RIT R 60 R. H. Ritchie and H. B. Eldridge, Thermal Neutron Flux Depression by Absorbing Foils, Nucl. Sci. Eng. *8*, 300 (1960).

ROE W 65 W. C. Roesch and F. H. Attix, Eds., Basic Concepts of Dosimetry, in *Radiation Dosimetry*, Vol. 1 (Academic Press, New York, 1968), Chap. 1.

ROS B 49 B. B. Rossi and H. H. Staub, *Ionization Chambers and Counters--Experimental Techniques* (McGraw-Hill, New York, 1949).

ROS H 55a H. H. Rossi and W. Rosenzweig, A Device for the Measurement of Dose as a Function of Specific Ionization, Radiology *64*, 404 (1955).

ROS H 55b H. H. Rossi and W. Rosenzweig, Measurement of Neutron Dose as a Function of Linear Energy Transfer, Radiation Res. *2*, 417 (1955).

ROS H 56 H. H. Rossi and G. Failla, Tissue Equivalent Ionization Chambers, Nucleonics *14* [2], 32 (1956).

ROS H 62 H. H. Rossi, W. Rosenzweig, M. H. Biaviati, L. Goodman, and L. Phillips, Radiation Protection Surveys at Heavy Particle Accelerators Operating at Energies Beyond Several Hundred Million Electron Volts, Health Phys. *8*, 331 (1962).

ROU J 69a J. T. Routti, High-Energy Neutron Spectroscopy With Activation Detectors, Incorporating New Methods for the Analysis of Ge(Li) Gamma-Ray Spectra and the Solution of Fredholm Integral Equations (Ph.D. thesis), Lawrence Radiation Laboratory report UCRL-18514, April 1969.

ROU J 69b J. T. Routti and R. H. Thomas, Moyer Integrals for Estimating Shielding of High-Energy Accelerators, Nucl. Instr. Meth. *76*, 157 (1969).

RUD G 66 G. Rudstam, Systematics of Spallation Yields, Z. Naturforschung *21a*, 1027 (1966).

SCH W 68 W. Schimmerling and F. Sass, Experience with a Commercial Film Badge Service, Health Phys. *15*, 73 (1968).

SCO N 62 N. E. Scofield, Iterative Unfolding, in *Proceedings of Symposium on Applications of Computers to Nuclear and Radiochemistry, held at Gatlinburg, Tennessee, 1962*, NAS-NS-3107.

SHA A 70 A. J. Shaw, The Extraction of Terbium from Mercury by a Chemical Method, Rutherford Laboratory Internal Report RP/PN/43, Jan. 1970.

SHA K 62 K. Shaw, High Energy Flux Measurement Using Plastic Scintillators, CERN Health Physics Internal report DI/HP/6 1962.

SHA K 63 K. Shaw, The Measurement of Accelerator-Produced Neutron Flux Using the $^{32}S(n,p)^{32}P$ Reaction, Rutherford Laboratory report NIRL/R/31, March 1963.

SHA K 68 K. B. Shaw, G. R. Stevenson, and R. Thomas, Depth Dose and Depth-Dose Equivalent Data as Functions of Neutron Energy, Rutherford High Energy Laboratory report RHEL/M149, 1968.

SHA K 69 K. B. Shaw, G. R. Stevenson, and R. Thomas, Evaluation of Dose Equivalent from Neutron Energy Spectra, Health Phys. *17*, 459 (1969).

SHI C 44 C. P. Shillaber, *Photomicrography in Theory and Practice* (John Wiley, New York, 1944).

SIM P 64 P. W. Simpson, The Measurement of Accelerator-Produced Neutron Flux by Activation of Indium, Gold, and Cobalt, Rutherford Laboratory internal report NIRL/M/70, Nov. 1964.

SKL L 67 L. Sklavenitis, Sur la mésure et l'analyse des rayonnements, de haute energie par detecteurs à activation, application à la dosimetrie (Ph.D. thesis), Commissariat a l'Energie Atomique, Saclay report CEA-R-3376, Oct. 1967.

SKY T 43 T. H. R. Skyrme, Reduction in Neutron Density Caused by an Absorbing Disc, TRE Malvern, England, report MR-91, 1943.

SMI A 61 A. R. Smith, A Cobalt Neutron Flux Integrator, Health Phys. *7*, 40 (1961).

SMI A 65 A. R. Smith, Threshold Detector Application to Neutron Spectroscopy at the Berkeley Accelerators, in *Proceedings of the First Symposium on Accelerator Radiation Dosimetry and Experience, held at Brookhaven National Laboratory, Nov. 1965*, CONF-651109, p. 365.

SMI A 66 A. R. Smith, A Tantalum Fast Neutron Integrator, Lawrence Radiation Laboratory report UCRL-17051, 1966.

SMI A 68 A. R. Smith (Lawrence Radiation Laboratory Berkeley), private communication, 1968. (See also GIL W 68).

SPR L 55 L. V. Spencer and F. H. Attix, A Theory of Cavity Ionization, Radiation Res. *3*, 239 (1955).

STAN 67 *Luminescence Dosimetry: Proceedings of International Conference on Luminescent Dosimetry, held at Stanford, Calif., June 21-22, 1965*, Ed. F. H. Attix, CONF-650637, 1967.

STE G 67 G. Stevenson, Neutron Spectrometry from 0.025 eV to 25 GeV, Rutherford High-Energy Laboratory report RHEL/R154, Nov. 1967.

STE L 58 L. D. Stephens and A. R. Smith, Fast Neutron Surveys Using Indium Foil Activation, Lawrence Radiation Laboratory report UCRL-8418, Aug. 1958.

STR O 68 O. N. Strand and E. R. Westwater, Statistical Estimation of the Numerical Solution of a Fredholm Integral Equation of the First Kind, J. Assoc. Comput. Mach. *15*, 100 (1968).

SU Y 67 Y. S. Su, Study of Scintillation Spectrometry: Unfolding Methods, Nucl. Inst. Methods *54*, 109 (1967).

SUL A 63 A. H. Sullivan and J. Baarli, An Ionization Chamber for the Estimation of the Biological Effectiveness of Radiation, CERN report 63-17, 1963.

SUL A 64 A. H. Sullivan, An Approach to Rem Dosimetry Using Ionization Chambers, CERN Report DI/HP/29, 1964.

SVE G 69 G. Svensson, Lecture Notes on Cavity Chamber Theory, lecture given to Third Annual Accelerator Health Physics Training Course held at Lawrence Berkeley Laboratory, University of California, Berkeley, California, March 1969.

TAT H 67 H. Tatsuta, H. Ryufuku, and T. Shirotani, A New Rem-Counter for Neutrons, Health Phys. *13*, 559 (1967).

THO R 67 R. Thomas, Radiation Field Observed Around High Energy Accelerators, in *Progress in Radiology, Vol. 2 (Proceedings XI International Congress of Radiology, held at Rome, 1965)* (Excerpta Medica Foundation, Amsterdam, 1967).

THO R 69 R. H. Thomas, Radiation Surveys--High Energy Physics Laboratory Mark III Electron Linac: III,—Bonner Sphere Measurements, Stanford University internal report RHT/TN/69-18, Sept. 1969.

TIK A 63 A. N. Tikhonov, Solution of Incorrectly Formulated Problems and the Regularization Method, Doklady Akad. Nauk. SSSR *151*, 501 (1963); English Transl.: Soviet Mathematics *4*, 1035 (1963).

TIT C 51 C. W. Tittle, Slow Neutron Detection by Foils, Nucleonics *8* [6], 5 and *9* [1], 60 (1951).

TWO S 63 S. Twomey, On the Numerical Solution of Fredholm Integral Equations of the First Kind by the Inversion of the Linear System Produced by Quadrature, J. Assoc. Comput. Mach. *10*, 97 (1963).

WAL R 61 R. Wallace, B. J. Moyer, H. W. Patterson, A. R. Smith, and L. D. Stephens, The Dosimetry of High-Energy Neutrons Produced by 6.2-GeV Protons Accelerated in the Bevatron, in *Proceedings of Selected Topics in Radiation Dosimetry* (IAEA, Vienna, 1961).

WAT A 49 A. Wattenberg, Photo-Neutron Sources, National Research Council Preliminary Report No. 6, July 1949.

WAT G 68 G. L. Watkins and G. R. Holeman, Evaluation of an Iterative Technique's Use in Unfolding Neutron Spectra Data, Health Phys. *15*, 535 (1968).

WEN W 64 W. A. Wenzel, Spark Chambers, Ann. Rev. Nucl. Sci. *14*, 105 (1964).

WIE C 49 C. Wiegand, High-Energy Neutron Detector, Rev. Sci. Instr. *19*, 790 (1949).

WIN L 59 L. Winsberg, The Production of ^{149}Tb From the Bombardment of Tantalum, Gold and Bismuth by High-Energy Protons, in Chemistry Division Semiannual Report, UCRL-8618, 1959, p. 52.

YAG H 49 H. Yagoda, *Radioactive Measurements With Nuclear Emulsions* (John Wiley, New York; Chapman and Hall, London; 1949).

ZAN H 35 H. Zanstra, Determination of the Saturation Current on Jáffe's Theory of Positive-Column Ionization, Physica *2*, 817 (1935).

ZEL M 63 M. Zel'chinskii, Recombination Method for Determination of Linear Energy Transfer (LET) of Mixed Radiation, in *Neutron Dosimetry*, Vol. 2 (IAEA, Vienna 1963).

ZEL M 64 M. Zel'chinskii, V. N. Lebedev, and M. I. Salatskaya, Instrument for Determination of Recommended Relative Biological Effectiveness of Radiation, Pribory i Tekhn. Eksperim. *1964*, 73 (English Transl.: Instruments and Experimental Techniques, *1964*, 1217.

CHAPTER 6

ACCELERATOR SHIELDING

TABLE OF CONTENTS

CHAPTER 6 (cont.)

ECCELERATOR SHIELDING

INTRODUCTION

As recently as 1960 Thomas Jaeger (JAE T 60) was able to write "Currently, the design of shielding for high energy accelerators is more an art than a science," and it is an unfortunate fact that most people would have had to agree with him! It is gratifying that today, about 10 years later, our knowledge of the radiation environment of high energy accelerators is on a reasonably secure footing and that most of the obscurities extant in 1960 have been clarified. In consequence most of the technical radiation problems met in the design studies of proton synchrotrons of several hundred GeV are being confidently handled. It is no longer necessary to rely on what are euphemistically called "safety factors" but what should more properly be called "factors of ignorance."

This rapid change in our understanding has been brought about largely as a result of the design, construction, and operation of several large research accelerators around the world in the late fifties and early sixties.

WHY SHIELD?

There are two reasons why accelerators must be shielded--the first (legal) applicable in all cases, the second (experimental) of concern only in specialized research applications.

LEGAL REQUIREMENTS

There is a legal (and moral) necessity to protect not only workers at the accelerator but also the general population from the harmful effects of radiation. The limits of exposure are derived from recommendations made by the International Commission on Radiological Protection (ICRP), which serves as the basis for national and local legislation. A detailed discussion of the appropriate legal regulations will be found in Chapter 8, and it is assumed in what follows that the reader is familiar with these requirements.

EXPERIMENTAL NEEDS

At research institutions, personnel safety is not necessarily the limiting factor in determining radiation levels. Often the working environment is well below limits, because many radiation detectors are so sensitive that they operate only in radiation levels one or two orders of magnitude below those allowed for personnel safety.

ECONOMY

These problems are not of great fundamental scientific interest, and great effort is applied to their resolution only when economic pressures

become intense. For many years shielding of accelerators was not studied seriously because their use was largely limited to research. Accelerators were unlike nuclear reactors, used in power production, in that there was no need to consider competitive economic alternatives. For accelerators whose shielding costs only tens of thousands of dollars the problem may be solved by gross overshielding. For large research accelerators, however, and for accelerators used in industry and medicine, this is no longer acceptable, and the value of precise estimates of shielding requirements in large projects cannot be overemphasized. With the increasing use of smaller accelerators in industry and medicine, economic arguments weigh more heavily than for a research instrument.

Besides the obvious economic advantages, the increased confidence that results from precise estimates is invaluable. Thus, for example, architects are given much greater flexibility in siting buildings adjacent to the accelerator, maintenance programs for heavy equipment may be planned ahead, access roads can be built. All the many decisions necessary in the design and construction of a large accelerator are much more easily made if the radiation environment is well understood.

HISTORICAL RESUMÉ OF SHIELDING STUDIES

The beam intensities accelerated by heavy-particle accelerators in the thirties and early forties were too low to produce severe radiation problems, except possibly directly in the accelerated beam.

Shortly after World War II, when extensive nuclear physics research was resumed, several new accelerators were designed and constructed. Rotblat (ROT J 50), in reviewing the progress of the 350-MeV synchrocyclotron at Liverpool, England, has described the fundamental lack of knowledge of the radiation fields produced by these instruments. He stated that this lack of basic knowledge, of both the biological effects and the nuclear interactions of high energy particles, made it impossible at that time to design effective radiation shields. Two alternative solutions to this dilemma were adopted, each having its own advantages and disadvantages. Several synchrocyclotrons were constructed underground with substantial earth shielding overhead, both for the accelerator proper and for its associated experimental areas. Examples of underground accelerators are the 350-MeV synchrocyclotron at Chicago and the 110-inch synchrocyclotron at Harwell (LIV M 52b). Such a solution had the advantage of eliminating any problems of excessive radiation external to the shield, and although costly, was not excessively so, because of the rather small physical size of the machines. However, such a solution was only short term—it could not be adopted indefinitely as accelerators grew in physical size, energy, and intensity. Furthermore, the absence of any radiation problem tended to inhibit undertaking fundamental studies leading toward efficient shield design.

By 1952 seven synchrocyclotrons were in operation around the world and four more were under construction. At Columbia proton energies of 385 MeV with an average beam current of 0.1 μA had been achieved. At lower particle energies even higher currents were possible; typical proton currents of 1 μA were available, and a current of 25 μA of deuterons at 28 MeV had been achieved at Amsterdam. As Livingston wrote (LIV M 52a):

"A useful contribution at this time (1952) would be a careful study of the shielding problem by one or more of the laboratories which have instruments in operation; at present information is incomplete on the attenuation of high energy radiations, the intensity of scattered radiation, and the effects of cracks or apertures in shields."

The era of high energy accelerators ($>$ 1 GeV) opened in 1952 with the operation at 3 GeV of the Cosmotron at Brookhaven National Laboratory. This was shortly followed by the successful acceleration of protons to almost 1 GeV at Birmingham.

Other accelerators rapidly followed, and with the successful operation of the Stanford Mk III electron linac at 700 MeV and the Cornell Synchrotron at 1.4 GeV in 1954, both proton and electron energies in the multi-GeV region became possible.

To some extent the accelerator physicists were too successful! Predictions of beam intensity of these early accelerators were difficult and in all cases were too modest. People talked hopefully of accelerating 10^9 particles per beam pulse in the Bevatron. They were delighted to find that the available beam intensity increased steadily as the operators learned the "tricks of their trade." Both the Cosmotron and Bevatron were planned with essentially no shielding; consequently, as the experimenters demanded higher and higher beam intensities, the operators sat with increasing apprehension; keeping one eye on the radiation monitors and the other on the beam current!

At some laboratories--as, for example, at the Lawrence Berkeley Laboratory (PAT H 57)--accelerators were built above ground level with minimal shielding in place. It was fully expected that as these accelerators were developed, beam energy and intensity would increase, although inadequate information initially precluded the design of an economical and efficient radiation shield. At such laboratories it was intended that radiation studies would form an integral part of the accelerator development program. Although the presence of continuing and increasing radiation problems at many of the first-generation accelerators has been a great stimulus for the improvement in our knowledge of shielding, such a policy also has considerable disadvantages. They are perhaps best summarized by Lofgren (LOF E 57) at a symposium at New York, organized by the USAEC in 1957 to discuss the mounting radiation problem at accelerators, thus:

"I hope that the Cosmotron and the Bevatron are the last two large accelerators to be designed without shielding. I might mention a few of the varied problems from our experience when shielding is left as an afterthought.

"1. Shielding foundation had to be put in after the machine was completed, and this resulted in a serious interference with operation.
"2. Financing was inadequate because it was not planned long enough in advance.
"3. Many components that were installed in areas of high radiation level requiring shutdown for servicing might otherwise have been installed in low-level areas.
"4. In some areas it was nearly impossible to design a really good shield and also have access holes in the shield.
"5. It was necessary to abandon an appreciable area in the building which might have been used for laboratories and offices."

From the moment of their first operation both the Cosmotron and Bevatron were essentially radiation-limited accelerators. The reduction in radiation levels achieved by the addition of shielding was often more than compensated by increases in operating intensity. Lindenbaum (LIN S 57a) described the situation at the Cosmotron in the following terms:

"The shielding problem has always been with us at the Cosmotron. As a matter of fact our maximum average intensity has been limited since the beginning of machine operations. We have made attempts to improve the shielding a step at a time and have gained a factor approximately 20 to 50 for most internal-beam experiments; however, the maximum available beam intensity has increased by a factor of several hundred; thus we have been fighting a losing battle. Furthermore, the recent development and considerable use of external proton beams have further increased the general radiation problem because of the introduction of new, less adequately shielded target areas."

Smith, too, has described the operational difficulties that resulted for the addition of shielding around the Cosmotron (SMI L 56).

The economic and operational inefficiencies resulting from incomplete consideration of radiation problems were documented at the New York symposium, and this documentation paved the way for extensive studies of accelerator radiation fields in a more fundamental sense than hitherto. It was realized that the mere technical solution of particular problems did not facilitate extrapolation to new and unfamiliar situations. Falk (FAL C 57), in his introduction to the New York symposium, suggested that if shielding design were handicapped by the lack of available high-energy particle interaction data then experiments should be performed to remedy this. He also drew attention to the fact that much available data failed to find its way into the technical literature. Both the deficiencies exposed by Falk have been remedied in the sixties, and it is indeed fortunate that the rather gloomy prediction by Green (GRE K 57), who said at the New York Conference: ". . . .I am a confirmed pessimist. I doubt if any accelerator builder will put enough money in the shielding. If he has extra money, he will use it to build a larger machine" has been proved false by the successful operation of several high energy accelerators around the world with few serious radiation problems.

The radiation environment of an accelerator is initially determined by its beam characteristics. Beam losses during acceleration or beam transport to experiments, as well as use of beam for experiments, all generate nuclear cascades in accelerator components and shielding. This results in the "prompt" radiation field that is present only when the accelerator is operating. (See Chapter 3.)

Physical understanding of the production of this nuclear cascade and its transmission through the accelerator shield provides the key to successful solution of accelerator radiation problems. The attenuation of the nuclear cascade determines the quantity of shielding needed, and the composition of the nuclear cascade at large depths determines the biological potency of the leakage radiation.

Our earliest understanding of the development of the nuclear cascade came from studies of neutrons produced in the atmosphere by cosmic radiation. The attenuation length of about 110 to 120 g/cm^2 found for the strongly interacting component of cosmic rays was found also in the early shielding experiments done in poor geometry. These results were interpreted by Lindenbaum (LIN S 61) in terms of the particle-nucleus inelastic cross sections and a simple nuclear cascade model which explained the approximately exponential attenuations (and the cascade equilibrium) observed at large depths in the shield.

By 1960 Lindenbaum (LIN S 61) and Moyer (MOY B 57) had suggested the "lines of attack" on the problem of shielding proton accelerators from several hundred MeV to several GeV. The qualitative features of the nuclear cascade induced by high energy nucleons were understood and the concepts of particle buildup and equilibrium developed, and by utilizing data from several sources (cosmic ray data, nucleon-nucleus cross-section data, the Metropolis (MET N 58) intranuclear cascade calculations, and shielding data), it was possible to make quantitative estimates of shielding.

This qualitative understanding of the nuclear cascade was obtained in terms of the high-energy neutron interaction lengths and low-energy particle buildup. High-energy neutrons regenerate the cascade but are present in relatively small numbers. The radiation field observed at the outerface of a shield consists of these high-energy "propagators" born deep in the shield, accompanied by a train of "camp followers" of much lower energy produced close to the shield surface. These lower-energy particles are directly produced in the intranuclear cascade or in the subsequent de-excitation of the struck nucleus by evaporation. Moyer (MOY B 57) estimated the radiation accompanying each surviving 6-GeV nucleus in his calculation of Bevatron shielding—his results are given in Table 6.I.

Although pions (and kaons, which are produced only about one tenth as frequently) have little influence on the propagation of the nuclear cascade, their decay products, the muons, which have no strong interaction, form a

very penetrating radiation—which will be of great importance at future high energy accelerators (KEE D 64).

Table 6.1. Estimated number of particles accompanying each surviving 6-BeV nucleon. (After Moyer.)

Protons (from cascade and evaporation)	4
Charged pions	3
Muons	0.3
Neutrons (from cascade and evaporation in original star plus equal number from secondary collisions)	7
Slow neutrons	70
Electrons (from π^0 decay and Compton scattering of capture γ rays and nuclear γ rays)	10 (?)
γ Rays	Enough to yield ionization dose of $3X10^{-4}$ mrem

Increasing beam intensities at the Lawrence Berkeley Laboratory's 6-GeV synchrotron, the Bevatron, necessitated design of an improved shield. This necessity led to the invention, by Moyer in 1961, of a semiphenomenological model used in may subsequent shield designs, and first referred to as "the Moyer Model" by De Staebler (DeS H 62). Subsequent experience at the Bevatron has shown this model to be extremely valuable in shield design (SMI A 64, SMI A 65, THO R 70). The subsequent development of this model in the past 10 years is discussed later in some detail.

Radiation problems were heightened not only by the operational experience described at New York, but also by the fact that several large accelerators around the world were either in the advanced design stage or under construction and would be operating at increased beam intensities or energies (or both) in the early sixties.

As might be expected by a reader with historical perspective, this concern shown over the experience with the first high energy accelerators initially resulted in an overreaction, and the second-generation accelerators were in general over-shielded at great expense and often at great inconvenience. (PIC T 59, CRE A 59, CRO E 57, WHI M 56) Thus, for example, accelerators like Nimrod (UK) and the ZGS (Argonne) were buried under large mounds of earth. Extension of experimental facilities for Nimrod was therefore made quite expensive because of additional excavation required. However, even the second-generation machine design groups gave little attention, in detail, to the general radiation

problems due to these accelerators. At most accelerator laboratories the problems presented by induced radioactivity, radiation damage, transmission of radiation along tunnels, and the composition of the radiation field outside shielding were little studied. It was not until the mid-sixties that these problems were extensively investigated.

The sixties represent a decade of steady and significant progress in the study and understanding of radiation shielding phenomena at high energy accelerators. The first half of the period was one of consolidation of the foundation begun in the fifties. The first accelerator to incorporate in its design the results of the studies by a physicist working full time on radiation problems was the Stanford 20-GeV electron linear accelerator.

Its successful operation since 1966, free of severe radiation problems, must be attributed to the careful investigation during the design study of all radiation problems. (DES H 62, DES H 65). The interest of the Stanford group had been stimulated by experience at the Mark III accelerator (NEA R 56, PAN W 57). The SLAC design study provided a wealth of information. DeStaebler (DES H 65) showed the similarities between the shielding problems at large-intensity high-energy electron accelerators and high-energy proton accelerators. In calculating transverse shielding (DES H 62), he was able to use the technique developed by Moyer and his colleagues and applied to the 184-Inch Berkeley Synchrocyclotron and the Bevatron (MOY B 61, MOY B 62, WAL R 62). Theoretical calculations were generated to check the empirical methods used by DeStaebler, and experimental check of these calculations, measuring the transmission through concrete of dose due to fast neutrons produced by a 5-GeV photon beam at the Cambridge Electron Accelerator, gave agreement within a factor of two of the calculation (KAO S 63).

The first fruits of the general concern exhibited at New York were presented at the First International Conference on Accelerator Shielding organized in Paris early in 1962 (PARIS 62).

In the early and middle sixties there were design studies for proton synchrotrons in the several-hundred-GeV region at Berkeley (LRL 65) and CERN (CERN 64), the Stanford 20-GeV electron linac already mentioned, and high intensity proton accelerators intended for use as meson factories; (WAL R 62)--particularly two high-intensity proton linear accelerators close to 1 GeV in energy at Yale (YALE 64) and Los Alamos (LASL 64). Also, there were improvement programs at the Brookhaven AGS (BNL 64) and CERN PS. All these led to important advances in our knowledge of accelerator radiation phenomena. The successful operation of the 70-GeV proton synchrotron at Serpukhov is already yielding new information (CHI M 69, GOL V 69, GOL V 70), and we now look forward to the experience to be gained at the National Accelerator Laboratory, Batavia, with operation at 200 GeV.

Although the buildup factors estimated by Moyer permitted crude estimates of dose rate at a shield surface, precise details of particle spectra

were of course of much greater value. Tardy-Joubert (TAR P 65) and Thomas (THO R 67) made estimates of neutron spectra developed in accelerator shielding, assuming similarity at higher energies to the Hess cosmic-ray spectrum (HES W 59, PAT H 59). Experimental techniques have been developed capable of measuring such spectra (ROU J 69a), and their conversion to dose rate is now well understood (GIL W 68, SHA K 69). These developments in the past 5 years have led to extremely important improvements in the accuracy of shield design.

In the sixties several large-scale shielding experiments mounted at high energy accelerators contributed greatly to our understanding of shielding phenomena and the development of the electromagnetic and nuclear cascades in matter.

In this decade the physical intuition of Moyer and Lindenbaum was essentially verified by these experiments, which, because of their importance, are described in some detail later in this chapter.

The early (1960-63) CERN experiments distinguished between attenuation on beam axis and "lateral integrated" attenuation, but did not completely succeed in identifying the attenuation length appropriate to accelerator shield design. Nuclear emulsions proved to be an invaluable visual technique facilitating a description of the cascade development. In 1964 the development of extracted proton beams at the Bevatron facilitated studies of the low-energy neutrons produced in the cascade and led to neutron spectrum measurements. As yet no formal analysis of these straight-ahead shielding measurements has been attempted in terms of a phenomenological model such as that due to Moyer, although both series of experiments can be interpreted to confirm its basic assumption. Measurements at great depths in the shield at Berkeley indicated the presence of an equilibrium spectrum at low energies and much lower attenuation lengths than had previously been reported--close to those predicted by use of high energy inelastic cross sections.

As the very large 200- to 500-GeV proton accelerators were designed, the emphasis and interest shifted from straight-ahead to transverse shielding, because transverse shielding is a substantial capital investment for such large machines. At present (1971) interest has reverted to straight-ahead experiments because of the need to design adequate beam backstops for disposal of the intense beams extracted from the strong-focusing synchrotrons. Levine and Moore (LEV G 69a, LEV G 69b) have reported studies in a composite assembly of tungsten, uranium, steel, and concrete; most recently Bennett et al (BEN B 71a, BEN B 71b) have carried out both transverse and straight-ahead shielding measurements in steel to hitherto unprecendented depths to provide shield design data for 30-GeV proton beams at intensities up to 10^{13} protons/sec.

Finally, any historical resume, no matter how brief, would be incomplete without an acknowledgement of progress in the past 10 years in the computation of particle transport through accelerator shields. A brief review

is given in the section on the Physics of Shielding, but more detailed information is given by Zerby (ZER C 62a, ZER C 62b, ZER C 62c), Alsmiller (ALS R 65, ALS R 69), and most recently by Ranft (RAN J 72).

A recent comparison between experimental and theoretical data by Goebel and Ranft (GOE K 69) indicates agreement to about a factor of two.

The advances in our understanding of the development and transmission of the nuclear cascade in matter summarized here have made it possible to design accelerator shields with fair precision. This will facilitate economies in the shielding construction, and reduce the investment in static blocks of steel and concrete! This is of course to be lauded and encouraged, but some words of caution are needed. All is not yet perfect in our understanding, and it would be ironic if the mistakes of the fifties were repeated in the seventies in a display of overconfidence. To check the accuracy of existing calculational models it would be desirable to plan future "shielding measurements" so that the experimental results obtained are in a form susceptible of calculation. Conversely, theoreticians might be persuaded to make calculations in terms of the radiation detectors available to the experimenter, and of realistic shielding materials.

The advances in our understanding of particle accelerator shielding briefly described here have been principally documented in the proceedings of several international conferences —the first organized in Paris in January 1962 (PAR 62), followed by others at Brookhaven, 1965 (BNL 65), Chilton (Harwell), 1969 (HAR 69), and most recently Stanford, 1969 (STAN 69). Reviews by Lindenbaum (LIN S 61), Livingston and Blewett (LIV M 62), Shaw (SHA K 68), Hargreaves (HAR D 68), Ladu (LAD M 69) and Patterson and Thomas (PAT H 71), and those contained in the Engineering Compendium on Radiation Shielding (JAE R 68, JAE R 70) fill in many specific details.

THE PHYSICS OF SHIELDING

INTRODUCTION

Much of the early formulation of our ideas concerning accelerator radiation shielding, particularly at higher energies, was derived from studies of fundamental particle interactions in the cosmic radiation, as we have already described in our historical resume'. From these studies we conclude that shielding theory must be firmly based on an understanding of particle production and transport in the electromagnetic and nuclear cascades.

For nucleon accelerators up to about 10 GeV, neutrons largely determine the shield configuration. Above proton energies of 10 GeV the production of muons in the forward direction may have to be taken in account, and above 100 GeV muons become an extremely important factor. The shielding of electron accelerators below 100 MeV in energy is usually determined by the electromagnetic cascade attenuation, although in particular circumstances (e.g., production of neutrons by photofission) neutrons may be an important, if not

major, problem. As the energy and intensity of electron accelerators increase the more similar their radiation environments become to those of proton accelerators (DES H 65).

Electromagnetic shower propagation is now well understood, both analytical and Monte Carlo calculations having been successfully tested by experiment.

Our knowledge of the propagation of the nuclear cascade is not on such a firm footing; empirical shielding techniques have been developed from several experimental studies. Recently both analytical and Monte-Carlo techniques have been developed that are in fair agreement with the experimental data.

COSMIC RAY STUDIES

Outer space is irradiated by cosmic radiation of galactic origin. This radiation consists of stripped nuclei in the energy range from $\approx 10^8$ to $\approx 10^{19}$ eV, having a mass distribution similar to that of the universe (Table 6.II). In free space these particles are distributed isotropically and are present at an intensity of about 4 particles/cm^2 sec. Table 6.II summarizes the intensity of and mass distribution of these nuclei. From Table 6.II we see that the principal component of galactic (cosmic) radiation is due to protons. Alpha particles are present at only 10% of the proton intensity, and all other heavier nuclei contribute only 10% of the α-particle intensity. Photons and electrons are present at an intensity comparable to that of the heavy nuclei ($\approx$ 1% of the proton intensity).

Table 6.II. Comparison of charge distributions in galactic radiation and galactic matter (estimated).

Element group	Intensity[a] (particles/cm^2-sec)	Atomic abundance (% by number)	Universal abundance (% by number)
Hydrogen (protons)	3.6	88	90
Helium (α particles)	4×10^{-1}	9.8	9
Light nuclei (Li, Be, B)	8×10^{-3}	0.2	10^{-4}
Medium nuclei (C, N, O, F)	3×10^{-2}	0.75	0.3
Heavy nuclei ($10 \leqslant Z \leqslant 30$)	6×10^{-3}	0.15	0.01
Very heavy nuclei ($Z \geqslant 31$)	5×10^{-4}	0.01	10^{-5}
Electrons and photons ($E > 4$ Bev)	4×10^{-2}	1	–

[a]At solar minimum

The energy spectrum of these charged particles, particularly that for protons, has been extensively studied. Close to the earth these charged particles are strongly influenced by the geomagnetic field, the earth acting

as a magnetic spectrometer. Protons of energy less than 15 GeV cannot reach the magnetic equator and the proton energy spectrum between 0 and 15 GeV is therefore a function of latitude. Figure 6.1 summarizes measurements of the integral proton spectrum by a variety of experimental techniques up to $\approx 10^{10}$ GeV. Above about 10 GeV the integral spectrum in monotonically decreasing and has the form

$$N(>E) \propto E^{-1.5}.$$

Measurements of the integral spectra of heavier charged particles up to energies of 10 GeV/nucleon reveal spectra similar to that obtained for protons (Fig. 6.2).

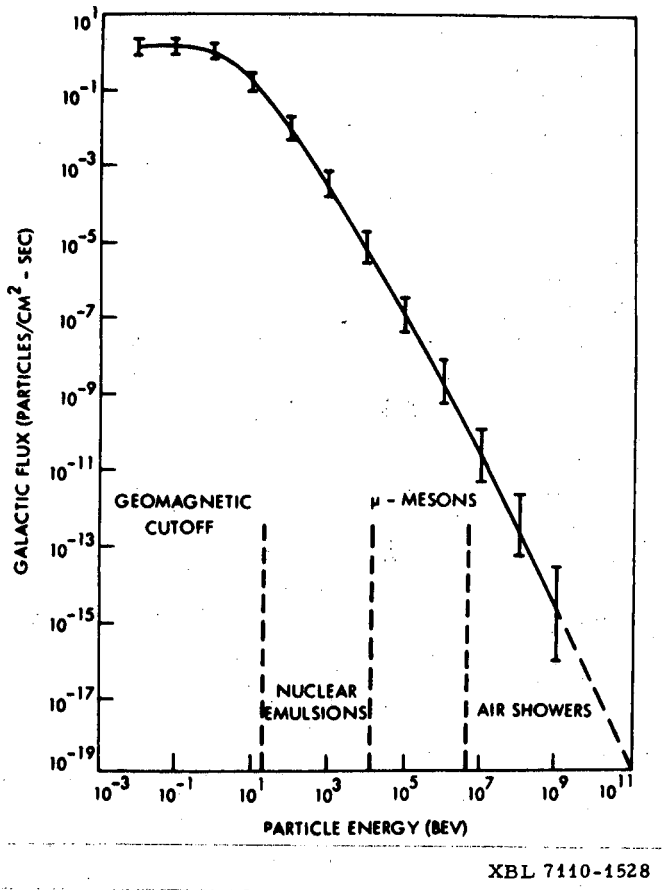

Fig. 6.1. Integral energy spectrum for total galactic radiation. (From Haffner.)

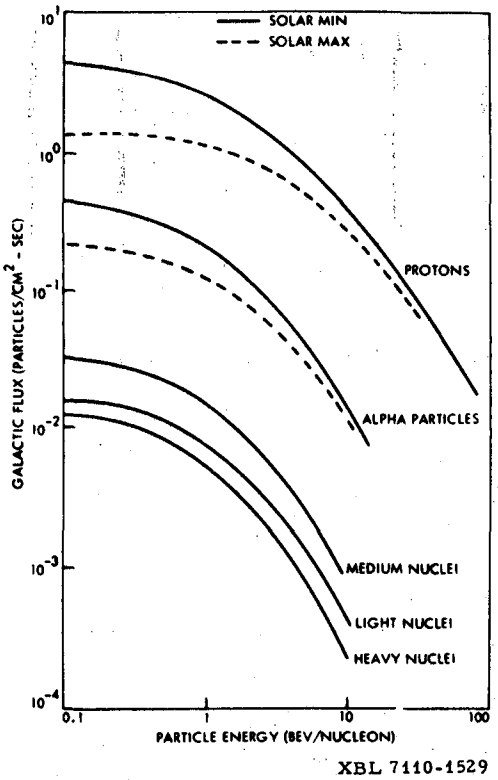

Fig. 6.2. Integral energy spectra for the various components of the galactic radiation. (From Haffner.)

It is from study of the interaction of these charged particles (principally protons) with the atomosphere that we might expect to learn about the interaction of energetic particles in an accelerator shield.

Figure 6.3 schematically illustrates the physical processes of interaction of the cosmic radiation with the earth's atmosphere. Protons are the principal component at the top of the atmosphere (neutrons are radioactive and have decayed by β-particle emission during their journey across the galaxy). The diagram shows one nucleus entering the atmosphere (this would most probably be an α particle). The earth's atmosphere is about 1030 g/cm^2 thick, or approximately 12 interaction lengths; there is therefore an extremely high probability for the incident protons to interact in the atmosphere.

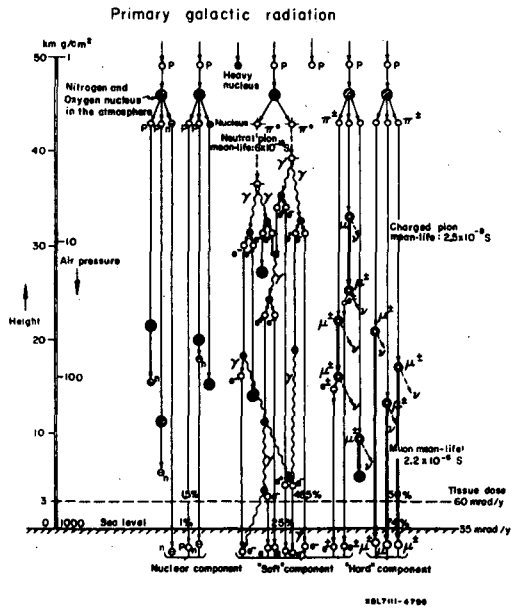

Fig. 6.3. Schematic representation of the interaction of galactic cosmic rays with the atmosphere.

Nucleons produced in these interactions subsequently reinteract in their passage down through the atmosphere. Ionization selectively removes low energy protons or charged fragments and prevents their reaching ground level. Proton interactions with nitrogen or oxygen nuclei also generate charged and uncharged π mesons ($\pi^{\pm}, \pi^{0}$). The lifetime of the π^{0} mesons is 6×10^{-15} sec, and they promptly decay into two energetic photons, which then, in passing through the atmosphere, generate an electromagnetic cascade often referred as to the "soft component."

Charged pions may interact, but have a longer lifetime than π^{0} mesons (2.5×10^{-8} sec), and thus have a decay length given by

$$\Lambda = 55 \text{ p meters}, \qquad (6.1)$$

where p is the pion momentum in units of GeV/c. Charged pions produced in the atmosphere therefore have a high probability of decaying to give a μ meson:

$$\pi^{\pm} \rightarrow \mu^{\pm} + \bar{\nu}/\nu.$$

The mean life of a μ meson is very long ($\tau = 2.2 \times 10^{-6}$ sec), corresponding to a decay length of 484 meters/(GeV/c). Once produced, therefore, μ mesons reach ground level suffering only ionization energy losses because they have only a weak interaction with matter. The μ mesons

form an extremely penetrating component of the cosmic radiation at sea level, often referred to as the "hard component."

The very energetic galactic radiation then, interacts with the atmosphere to produce nucleons, pions, muons, electrons, and photons. Particles of high energy can generate secondaries, known as Extensive Air Showers, which are very widely spread at ground level (GRE K 56, GRE K 60).

Measurements of the attenuation length, λ, of the shower-producing component (principally nucleons and pions) have shown a remarkably constant value of λ over a wide energy range, from 20 GeV to 10^7 GeV (PER D 61), as can be seen in Fig. 6.4.

Measurements of the interaction length of pions and protons in nuclear emulsion also show constant values over a wide energy range. Many measurements in the energy range 5 to 20 GeV for the interaction length of protons have been reported in the literature, all in close agreement between 36 and 38 cm (RAJ V 60, WIN H 60, BOG N 58, JAI P 61, BAR A 61a, CVI G 61). Measurements made with cosmic rays at energies above 100 GeV give values in essential agreement; for example, Perkins (PER D 60) reports a value of 32 ± 3 cm based on 100 interactions for primaries over an extended energy range of 300 GeV to 10^5 GeV. Lohrmann et al. (LOH E 61), for example, obtained a value of 41 ± 10 cm at 250 GeV for protons produced by fragmentation of heavy primary nuclei in the cosmic radiation, Barkow et al. (BAR A 61b)reported 41 ± 8 cm at 100 GeV for pions, and Farrow et al. (FAR E 63) have given a value of 41 ± 5.6 cm (based on 55 events) for the energy range 1 to 100 GeV.

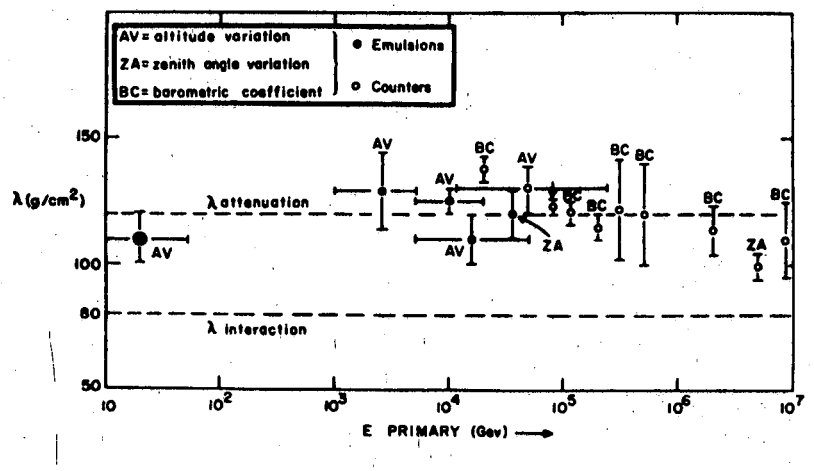

XBL 7110-1530

Fig. 6.4. Attenuation length in air measured in cosmic-ray studies. (From Perkins.)

It seems clear from these cosmic ray studies that

a. The attenuation length for the strongly interacting particles produced in Extensive Air Showers is independent of energy from 20 GeV to very high energies at about 120 g/cm^2 air.

b. The interaction length of these strongly interacting particles in nuclear emulsion, also constant over a wide energy range above 5 GeV, is about 38 cm or about 137 g/cm^2 in emulsions.

These results suggest that the attenuation length of the secondary particles produced in the air showers is determined by the interaction length (the difference between the value of 120 g/cm^2 observed in air and the value of 137 g/cm^2 observed in emulsion being due to the different chemical compositions of air and emulsion). Under these conditions some degree of particle equilibrium would be expected. Hess et al. (HAS W 59) studied the spectrum of neutrons in the energy range from about 100 keV to about 100 MeV and indeed found the spectrum to be invariant at depths below about 300 g/cm^2 (Fig. 6.5).

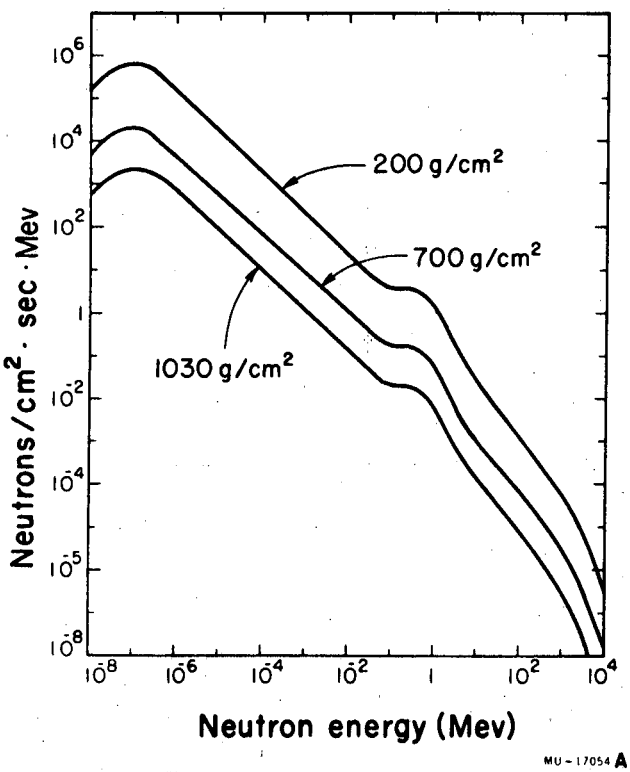

Fig. 6.5. The cosmic-ray neutron spectrum at different altitudes. (From Hess et al.)

It was not clear for many years whether the shape of this equilibrium spectrum was determined by the incident spectrum of the cosmic rays or by the nature of the cascade interactions. As theoretical calculations for monoenergetic high energy protons become available (RID R 65), however, their similarity to the cosmic ray spectrum was evident (THO R 65), and it became clear that the equilibrium spectrum shape is determined by the features of interaction processes and is fairly insensitive to the shape of the incident nucleon energy spectrum.

This capsule summary of cosmic ray studies is of course far from comprehensive. The interested reader is referred to the many excellent texts, review articles, and the extensive literature dealing with this subject. A good starting point would be the texts by Hooper and Scharff (HOO J 58), Janossy (JAN L 48), LePrince-Ringuet (LeP L 50), Rossi (ROS B 52, ROS B), and Wolfendale (WOL J).

The results summarized here are of importance to the accelerator physicist because in a nuclear sense air is quite similar to the lighter materials commonly used to shield accelerators (earth, concrete). Thus the attenuation length, about 120 g/cm^2, measured for the shower-producing component in the atmosphere would be expected to be applicable to the attenuation of dose or flux density through an accelerator shield. The equilibrium spectrum of neutrons measured in the atmosphere by Hess et al. was used to estimate the relative contribution to dose equivalent of neutrons of differing energy by Patterson et al. (PAT H 59), several years before measurements of neutron spectra outside high energy accelerator shields had been obtained.

At sea level we might reasonable expect to observe a radiation environment very similar to that generated outside an accelerator shield. In one important respect, however, the atmosphere differs from an accelerator shield—it is much less dense. There is therefore a much higher probability of decay into a muon in air than in a dense concrete or earth shield. We might therefore expect the μ-meson penetration of an accelerator shield to be substantially less. Only at high incident proton energies could they be expected to be a troublesome component. Neutrons produced in the nuclear cascade and protons produced in the electromagnetic cascade therefore appear to be the major source of radiation outside an accelerator shield.

THE NUCLEAR CASCADE

The nuclear cascade is of major importance in determining the shielding of both high-energy nucleon and high-energy high-intensity electron accelerators (DES H 65). In either case the nuclear cascade is the most important means of transporting radiation initiated by the accelerator through matter (viz., the shield).

In proton accelerators the cascade is initiated when the beam interacts with components of the accelerator or the extraction system. High energy

electrons produce energetic hadrons, principally by photodisintegration of psuedodeuterons within the nucleus or by photoproduction of energetic pions, which are then reabsorbed within the nucleus. The resultant high energy neutrons and protons also can then generate a nuclear cascade.

Since knowledge of the characteristics of nuclear interactions in the laboratory is limited to energies below 70 GeV for incident protons and 20 GeV for electrons, our only available source of information at very high energies is obtained from cosmic-ray studies. These data, coupled with the more precise data obtained at high energy accelerators, have allowed assembly of a fairly detailed description of the nuclear cascade.

QUALITATIVE DESCRIPTION OF THE NUCLEAR CASCADE

The collision of a high energy nucleon with a nucleus gives rise to a large number of particles, principally nucleons, pions, and kaons. In Chapter 3 we discussed the production of these particles of most importance for radiation studies. A substantial fraction of the incident energy may be vested in a single nucleon, which in crude terms may be thought of as propagating the cascade. At high energies, about 1 GeV, something like 20 to 30% of the primary energy is radiated as pions (PER D 61), but since their production spectra fall steeply with increasing energy, they do not play an important part in the cascade penetration. The production of rare particles at high energies is unimportant in the propagation of the cascade.

Thus the main means of energy transfer is due to the interaction of high energy nucleons, and it is those particles whose energies are above about 150 MeV that serve to propagate the cascade. Nucleons in the energy range 20 to 150 MeV also transfer their energy predominantly by nuclear interactions, but at these incident energies the energy is transferred to a large number of nucleons, each receiving on the average a small fraction of the total energy and thus having a rather low kinetic energy (below about 10 MeV). In general, charged particles at these energies are rapidly stopped by ionization, and thus neutrons predominate at low energies, but charged π mesons (and K mesons, which are produced only about one-tenth as frequently as π mesons [DEK 65, JOR 65]) decay into μ mesons:

$$\pi^{\pm} \rightarrow \mu^{\pm} + \bar{\nu}, \nu.$$

The μ mesons have no strong interaction and can be stopped only by ionization energy losses. The effective attenuation length of these muons depends upon the energy spectrum of the parent pion and kaons (and thus upon the energy of the incident nucleus). Keefe (KEE D 64) indicated in 1964 that muons would represent an increasing problem as the intensity of existing 30-GeV accelerators increased and at the new accelerators at Serpukhov (70 GeV), Batavia (200 GeV) and CERN (300 GeV).

Energetic γ rays produced in the decay of π^0 mesons initiate electromagnetic cascades, but the attenuation length of these cascades is in general

much shorter than the absorption length for the strongly interacting particles. Hence they contribute little to the energy transport.

Deep in the shield, therefore, neutrons take on the dominant role in cascade propagation, because energy loss is significant for protons and pions below about 450 MeV (where the ionization range becomes roughly equal to the interaction length). Production of evaporation and low-energy cascade particles (Chapter 3) is then controlled by the most penetrating particles.

Figure 6.6 schematically represents the development of the nuclear cascade and indicates the interrelationship between its separate components.

At present there is not sufficient information about the various production and interaction cross sections of the many particles involved in the nuclear cascade to permit complete calculation of the radiation emerging from a shield. However, the problem can be simplified by neglecting all those components which are produced in relatively small numbers, have short lifetimes, or are rapidly attenuated. Of the last, only components produced in the outermost layer of a thick shield actually emerge; these are fewer in variety and number than in the early stages of the cascade, since the average energy of the cascade particle is reduced to a fraction of that they initially possessed.

ONE-DIMENSIONAL INFINITE-SLAB MODEL

Lindenbaum (LIN S 61) has given a qualitative but instructive analytical treatment of the development of the nuclear cascade in a shield. Although of limited value for a practical application, this model (described below) is of great value in understanding the main features observed in shielding experiments.

Consider a parallel monoenergetic beam of neutrons of infinite extent incident upon a perpendicular plane shield of infinite width and breadth, and further assume that when the energy of a neutron is reduced below some cutoff value, E_c, it may be ignored.

At some depth, x, in the shield the number of remaining neutrons above the cutoff energy, $\phi(x)$, that undergo removal in the next thickness element, dx, is given by

$$d[\phi(x)] = \phi(x)\,\frac{dx}{\lambda_{rem}} \tag{6.2}$$

(provided backscattering is insignificant),
which has the solution

$$\phi(x) = \phi(0)\, e^{-x/\lambda_{rem}}, \tag{6.3}$$

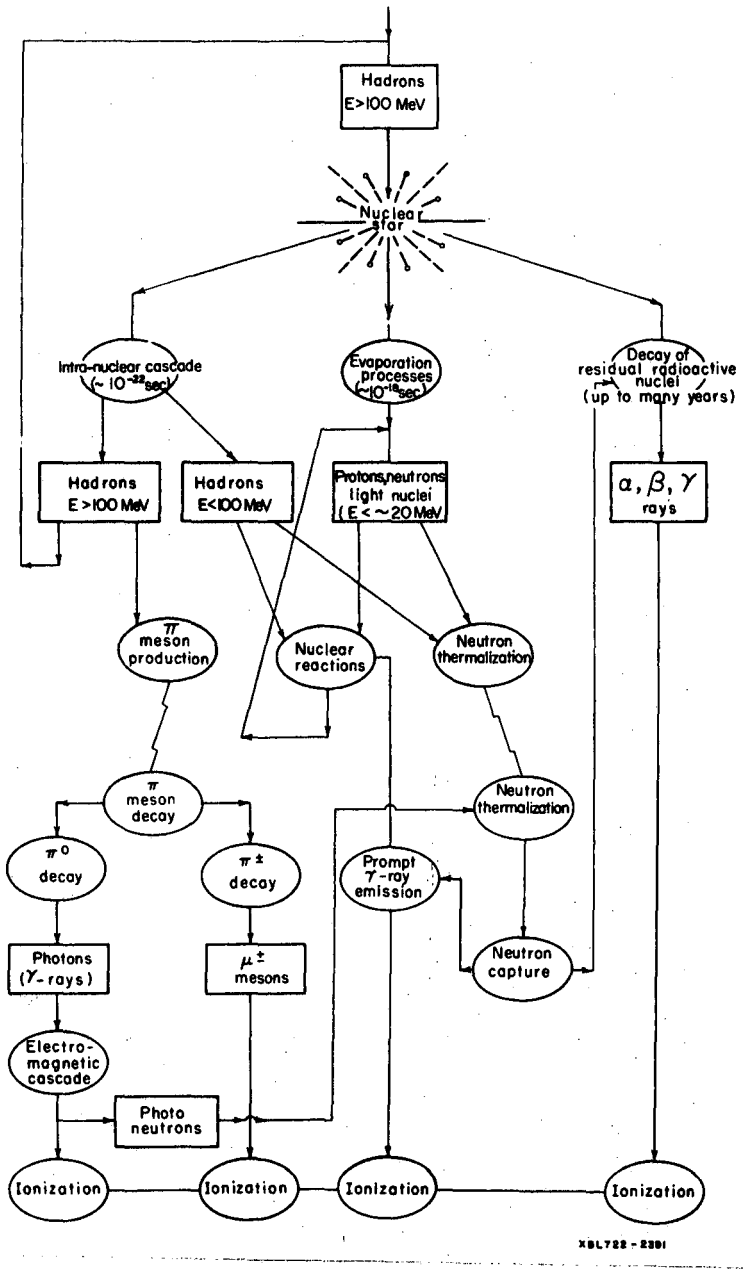

Fig. 6.6. Schematic representation of the development of the nuclear cascade. (After Hargreave.)

where

λ_{rem} is the mean free path for effective removal of the neutrons,

$\phi(0)$ is the incident primary flux density above the cutoff energy, E_c.

Primary neutron interactions produce secondary particles below the energy cutoff which build up in the shield as the nuclear cascade is developed. It is usual practice to describe this production of secondary particles by a buildup factor B(x), which may represent ionization density, absorbed dose, dose equivalent, flux density, or any other required parameter. Thus, for example, the dose-equivalent rate at depth x, is given by

$$DE(x) = B(x)\,\phi(0)e^{-x/\lambda_{rem}}, \qquad (6.4)$$

where

B(x) is a buildup factor which in this case converts primary particle flux density to dose-equivalent rate.

The buildup factor at x = 0 converts primary neutron flux density to dose-equivalent rate, but in the shield also takes account of the production of low-energy secondary particles.

Now consider a simple model in which the primary neutrons (designated as the "0th" generation) interact and produce m_1 secondaries of effective removal mean free path λ_1. These first generation secondaries interact and produce m_2 secondaries of removal mean free path λ_2, and so on. Then the differential equations which describe the production of secondary, tertiary, . . . etc. particles are

$$\begin{aligned}
\frac{d[\phi_0(x)]}{dx} &= \frac{\phi_0}{\lambda_0}\,, \\
\frac{d[\phi_1(x)]}{dx} &= \frac{m_1\phi_0(x)}{\lambda_0} - \frac{\phi_1(x)}{\lambda_1}\,, \\
\frac{d[\phi_2(x)]}{dx} &= \frac{m_2\phi_1(x)}{\lambda_1} - \frac{\phi_2(x)}{\lambda_2}\,, \\
&\cdots\cdots\cdots\cdots\cdots\cdots\cdots\cdots \\
\frac{d[\phi_i(x)]}{dx} &= \frac{m_i\phi_{i-1}(x)}{\lambda_{i-1}} - \frac{\phi_i(x)}{\lambda_i}\,.
\end{aligned} \qquad (6.5)$$

These equations are very similar to those which describe the production of radionuclides in the radioactive series (EVA R 55), and the general solution has been given by Bateman (BAT H 10). The appropriate value of the multiplicities m_1, $m_2 \cdots m_i$ depends upon the value chosen for the energy cutoff.

Three cases are of general interest in shielding problems.

Case 1. The removal mean free path of all reaction products is much smaller than that of the primary neutrons,

$$\text{i.e., } \lambda_0 >> \lambda_1, \lambda_2, \cdots \lambda_i.$$

In this case it can be shown that the total flux at depth x, $\Phi(x)$, is given by

$$\Phi(x) = B \cdot \phi_0 e^{-x/\lambda_0}, \quad x \geqslant \lambda_1, \lambda_2 \cdots \lambda_i, \tag{6.6}$$

where B is a buildup factor that is almost independent of depth x. It follows that particle flux density, absorbed dose, dose equivalent and other parameters of interest are all attenuated experimentally with a relaxation length determined by that of the primary particles.

Case 2. The removal mean free path of one reaction product is much greater than that of the primary particles, i.e., for some particular value of f,

$$\lambda_f >> \lambda_0 .$$

Then it can be shown that at depths large compared with λ_f we have

$$\Phi(x) = B\, \phi_0 e^{-x/\lambda_f} \quad x >> \lambda_f \tag{6.7}$$

where B is a buildup factor that remains approximately constant.

This particular case is of practical interest in high energy electron or photon shielding, when the high energy neutrons generated in the shield have a larger interaction mean free path.

Case 3. All interaction products and the primary neutrons have the same interaction length.

Since the removal mean free path for neutrons is constant down to about 150 MeV, we would expect this case to correspond to that found for high energy neutron beams. Upon interaction such neutrons produce one or more secondary particles with roughly the same removal mean free path and in the same approximate direction as the incident particle (see Chapter 3). When a secondary particle is produced with energy below 150 MeV it is disregarded. Thus we may write

$$\lambda_0 = \lambda_1 = \lambda_2 = \ldots = \lambda_i = \lambda \text{ (Say)}.$$

The general differential equations now take the form

$$\frac{d\phi_0(x)}{dx} = \frac{\phi_0}{\lambda},$$

$$\frac{d\phi_1(x)}{dx} = \frac{m_1 \phi_0(x)}{\lambda} - \frac{\phi_1(x)}{\lambda},$$

$$\frac{d\phi_2(x)}{dx} = \frac{m_2\phi_1(x)}{\lambda} - \frac{\phi_2(x)}{\lambda} \quad , \qquad (6.8)$$

cont.

$$\frac{d\phi_3(x)}{dx} = \frac{m_3\phi_2(x)}{\lambda} - \frac{\phi_3(x)}{\lambda} \quad ,$$

$$\frac{d\phi_i(x)}{dx} = \frac{m_i\phi_{i-1}(x)}{\lambda} - \frac{\phi_i(x)}{\lambda} \quad ,$$

with the respective solutions

$$\phi_1(x) = m_i(x/\lambda)\,\Phi_0\,e^{-x/\lambda}$$

$$\phi_2(x) = \frac{m_1 m_2}{2}(x/\lambda)^2\,\Phi_0\,e^{-x/\lambda} \quad ,$$

$$\phi_3(x) = \frac{m_1 m_2 m_3}{3}(x/\lambda)^3\,\Phi_0\,e^{-x/\lambda} \quad , \qquad (6.9)$$

$$\phi_i(x) = \frac{m_1 m_2 \cdots m_i}{i}(x/\lambda)^i\,\Phi_0\,e^{-x/\lambda} \quad .$$

The total number of particles at depth x with energy greater than the cutoff energy, E_c,: $\Phi(E > E_c, x)$ is given by

$$\Phi(E > E_c x) = \sum_{i=1}^{i=n} \phi_i(x)$$

$$= \left[1 + m_1(x/\lambda) + \frac{m_1 m_2}{2}(x/\lambda)^2 + \frac{m_1 m_2 m_3}{3}(x/\lambda)^3 + \ldots\right]\Phi_0\,e^{-x/\lambda} \quad . \qquad (6.10)$$

Thus in sufficiently thick shields we will observe an exponential attenuation. The extent of the initial buildup is of course determined by the magnitude of the multiplicities $m_1\ m_2 \cdots m_n$.

Although this simple model cannot be expected to give an accurate quantitative account of nuclear cascade development, it does reveal its main features and is extremely useful in understanding the main principles of accelerator shielding.

THEORETICAL SOLUTIONS TO THE NUCLEAR CASCADE DIFFUSION EQUATIONS.

The simple one-dimensional model of the nuclear cascade cannot reveal more than the qualitative features of nuclear cascade development. More sophisticated analytical models (PAS C 62, ALS R 63a, FIS C 63, ALS F 65) yield approximate solutions to the Boltzman transport equations describing the cascade growth.

As an example of the form these analyses take, we describe the approach taken by Fisher (FIS C 63). Although the calculations by Fisher are no longer the most rigorous published in the literature, their study is of great value because of their clarity and because, along with the calculations by Passow (PAS C 62), they represent the earliest attempts to develop an analytical solution to the problem of nuclear cascade development in matter.

In his treatment, Fisher acknowledges his indebtedness to similar treatments of the development of electromagnetic cascades at high energies by Nishimura and Kamata (KAM K 58, NIS J 67) and Pinkau (PIN). Fisher writes the diffusion equations for the generation of nucleons and pions (which follow from the conservation of particles) as

$$\frac{\partial n(E,x)}{\partial x} = -\frac{n(E,x)}{\lambda_n} - \frac{1}{\lambda_n}\int_{E'}^{E_0} R_{nn}(E',E)\, n(E',x)\, dE'$$

$$+ \frac{1}{\lambda_\pi}\int_{E'}^{E_0} R_{n\pi}(E,E')\, \pi(E',x)\, dE', \qquad (6.11)$$

$$\frac{\partial \pi(E,x)}{\partial x} = -\pi(E,x)\frac{mc}{\tau_\pi E} - \frac{\pi(E,x)}{\lambda_\pi} + \frac{1}{\lambda_n}\int_{E'}^{E_0} R_{\pi n}(E,E')\, n(E',x)\, dE'$$

$$+ \frac{1}{\lambda_\pi}\int_{E'}^{E_0} R_{\pi\pi}(E,E')\, \pi(E',x)\, dE', \qquad (6.12)$$

where $n(E,x)$ and $\pi(E,x)$ are the number of nucleons and pions respectively between depths x and $x+dx$ in the energy range E to $E+dE$,

λ_n = nucleon interaction length,

λ_π = pion interaction length,

R_{nn} = probability of a nucleon of energy E' producing a secondary nucleon of energy E,

$R_{n\pi}$ = probability of a pion of energy E' producing a secondary nucleon of energy E.

In these equation the terms $\frac{n(E,x)}{\lambda_n}$ and $\frac{-\pi(E,x)}{\lambda_\pi}$ represent the loss of particles in the energy range E to $E+dE$ due to nuclear interaction. The integral terms represent particles that enter the energy range E to $E+dE$ from interactions that occur between depths x and $x+dx$. The first term of Eq. 6.12 is due to the loss of pions by decay. Similar equations could be set up for k mesons, hyperons, and other rarer particles, but their small production cross sections make them of little consequence in cascade generation and they have been ignored in Fisher's treatment. Of more importance is the neglect of energy loss of charged particles due to ionization. At higher energies this is relatively unimportant, the energy loss of energetic particles being about 300 MeV in one interaction length (comparable to the total energy given to charged particles of low and moderate energy in a nuclear interaction). At lower energies (say below 1 GeV), however, ionization losses cannot be ignored, and in the particular case of μ mesons, which interact only weakly in matter, proper account must be taken of ionization energy loss if reliable conclusions are to be reached.

Fisher solves these diffusion equations by making the substitutions

$$n(E,x) = \exp(-x/\lambda_n) \sum_{k=0}^{\infty} n_k(E)\,(x/\lambda_n)^k \qquad (6.13)$$

$$\pi(E,x) = \exp(-x/\lambda_\pi) \sum_{k=0}^{\infty} \pi_k(E)\,(x/\lambda_\pi)^k \qquad (6.14)$$

and obtains for the quantities $n_k(E)$ and $\pi_k(E)$ the recurrence relations

$$(k+1)n_{k+1}(E) = \int_E^{E_0} R_{nn}(E',E)\, n_k(E')\, dE'$$

$$+\left(\frac{\lambda_n}{\lambda_\pi}\right)^{k-1} \exp(-x/\lambda) \int_E^{E_0} R_{n\pi}(E',E)\pi_k(E')\, dE', \quad (6.15)$$

where $$\frac{1}{\lambda} = \frac{1}{\lambda_\pi} - \frac{1}{\lambda_n}, \quad (6.16)$$

and

$$(k+1)\,\pi_{k+1}(E) = -\frac{\lambda_\pi}{E}\,\pi_k(E)$$

$$+\int_E^{E_0} R_{\pi\pi}(E',E)\,\pi_k(E')\,dE' + \left(\frac{\lambda_\pi}{\lambda_n}\right)^{K+1} \exp(x/\lambda)$$

$$+\int_E^{E_0} R_{\pi n}(E',E)\, n_k(E')\, dE'. \quad (6.17)$$

To proceed further analytic expressions for the differential production functions would be required, but—as Fisher pointed out—the functions $R_{n\pi}$, $R_{\pi\pi}$, were largely unknown. Two choices were available:

a. To use simple functions, which describe only those particles emitted in the "forward direction" (at very small angles to the primary particle direction) and which therefore contribute directly to the Longitudinal development of the cascade along its axis, or

b. to use functions that represent all the secondary particles produced by interactions, attempting to compute a three-dimensional model of the cascade. In such a treatment it is not sufficient merely to substitute functions representing total particle production into a one-dimensional equation—the so-called "straight-ahead approximation"—because the cascade is a three-dimensional phenomenon, and secondary-particle trajectories with respect to the primary-particle direction and the variation of interaction lengths with particle energy must properly be taken into account.

Fisher attempted to develop a description only of the axial development of the nuclear cascade, and so considered the simpler alternative (a). On the basis of available evidence from nuclear emulsion experiments and

cosmic-ray data, Fisher writes

$$R_{nn}(E,E')\,dE = \frac{dE}{E'}, \tag{6.18}$$

$$R_{\pi n}(E', E)\,dE = 0 \tag{6.19}$$

(i.e. the production of fast nucleons by pions is neglected),

$$R_{\pi\pi}(E,E') = R_n(E,E') = E'/E^2. \tag{6.20}$$

For justification for these assumptions the reader is referred to the original paper by Fisher.

Substituting these production functions into the recurrence relations (Eqs. 6.15 and 6.17) and assuming a monoenergetic incident beam of energy E_0, Fisher obtains, for the nucleon spectrum at depth x, the expression

$$n(E,x) = \exp(-x/\lambda)\,\frac{N_0}{E_0}\,\frac{1}{i}\left(\frac{x}{\lambda}\right)^{1/2}\frac{1}{\sqrt{\log\left(\frac{E_0}{E}\right)}}\,J_1\left(\frac{1}{i}\sqrt{\frac{x}{\lambda}\log\frac{E_0}{E}}\right)$$

$$+ N_0\,e^{-x/\lambda}\,\delta(E-E_0), \tag{6.21}$$

where $J_1(\quad)$ is a first-order Bessel Function,

and for the pion spectrum

$$\pi(E,x) = e^{-x/\lambda}\,\frac{N_0E_0}{E^2}\,\frac{x}{\lambda}\left\{\frac{1}{i\sqrt{\xi}}\,J_1\left(\frac{1}{i}\sqrt{\xi}\right) - \frac{E_0^2-E^2}{2E_0^2}\left(\frac{x}{\lambda}\right)J_2\left(\frac{1}{i}\sqrt{\xi}\right)\right\} \tag{6.22}$$

when pion decay is neglected, and ξ has been substituted for $\frac{x}{\lambda}\left(\frac{E_0}{E}\right)$.

J_1 and J_2 are first-and second-order Bessel Functions.

By integrating the expressions for the nucleon and pion densities with respect to energy and adding, Fisher shows that the total number of nuclear active particles at depth x with energy greater than E, $N(>E,x)$ is given by

$$\frac{N(>E,x)}{N_0} = \delta(E-E_0)e^{-x/\lambda} + \sum_{j=1}^{\infty}\left(\frac{x}{\lambda}\right)^j\frac{1}{j!}\left\{(-1)^{j-1}\,\frac{E_0}{E}\sum_{k=0}^{j-1}\frac{\log^k\left(\frac{E_0}{E}\right)}{k!}(-1)^k\right.$$

$$+\frac{E}{(E_0)}\sum_{k=0}^{j-1}\frac{\log^k\left(\frac{E_0}{E}\right)}{k!}\Bigg\}$$

$$+\frac{e^{-x/\lambda}}{2}\sum_{j=2}^{\infty}\left(\frac{x}{\lambda}\right)^j\frac{1}{j!}\left\{(-1)^{j-2}\frac{E_0}{E}\sum_{k=0}^{j-2}\frac{\log^k\left(\frac{E_0}{(E)}\right)}{k!}(-1)^k\right.$$

$$\left.+\frac{E}{E_0}\sum_{k=0}^{j-2}\frac{\log^k\left(\frac{E_0}{(E)}\right)}{K!}\right\}. \qquad (6.23)$$

This function gives the peak track density as a function of depth if the production functions $R_{n\pi}$, $R_{\pi\pi}$ etc. are reasonable, and Fig. 6.7 shows its general form.

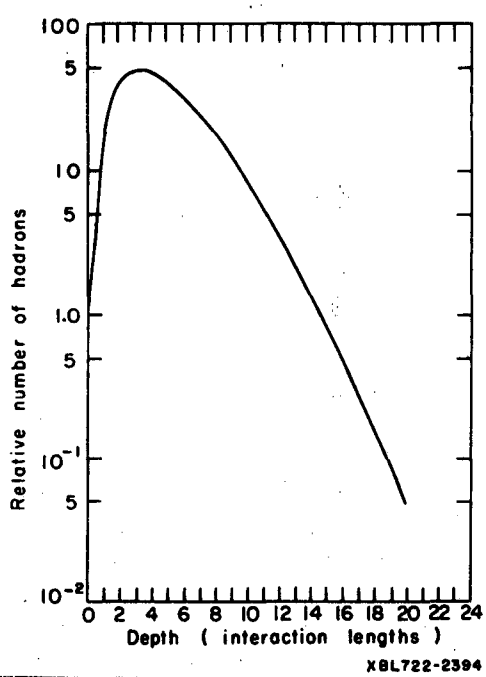

Fig. 6.7. Calculation of the number of nuclear active particles on the beam axis with energy greater than 500 MeV. (From Fisher.)

The familiar buildup followed by an approximately exponential attenuation of the nuclear active particles (E> 500 MeV) is clearly seen. We may define an attenuation length, λ_a, by the relations

$$-\frac{1}{\lambda_a} = \frac{1}{N(>E)} \frac{\partial N(>E)}{\partial x} . \tag{6.24}$$

Substituting for $N(>E)$ from Eq. 6.23, we find

$$-\frac{1}{\lambda_a} = -\frac{1}{\lambda_{int}} + \frac{1}{\lambda_{int}} \frac{\left\{ \sum_{j=1}^{\infty} \left(\frac{x}{\lambda}\right)^{j-1} \frac{1}{(j-1)!} F_j^1(E) + \frac{1}{2} \sum_{j=2}^{\infty} \left(\frac{x}{\lambda}\right)^{j-1} \frac{1}{(j-1)!} F_j^2(E) \right\}}{\left\{ \sum_{j=1}^{\infty} \left(\frac{x}{\lambda}\right)^{j} \frac{1}{j!} F_j^1(E) + \frac{1}{2} \sum_{j=2}^{\infty} \left(\frac{x}{\lambda}\right)^{j} \frac{1}{j!} F_j^2(E) \right\}} , \tag{6.25}$$

where

$$F_j^1(E) = \left\{ (-1)^{j-1} \frac{E_0}{E} \sum_{k=0}^{j-1} \frac{\log^k \left(\frac{E_0}{E}\right)}{k!} (-1)^k + \frac{E}{E_0} \sum_{k=0}^{j-1} \frac{\log^k \left(\frac{E_0}{E}\right)}{k!} \right\} \tag{6.26}$$

$$F_j^2(E) = \left\{ (-1)^{j-2} \frac{E_0}{E} \sum_{k=0}^{j-2} \frac{\log^k \left(\frac{E_0}{E}\right)}{k!} (-1)^k + \frac{E}{E_0} \sum_{k=0}^{j-2} \frac{\log^k \frac{E_0}{E}}{k!} \right\} . \tag{6.27}$$

Comparisons of the results of this type of calculation with experimental data are extremely difficult. The very large buildup factor suggested by the calculation was not observed in experimental cascade studies with 10- and

and 20-GeV incident protons (THO R 63). Fisher suggests that this difference is due to

a. an overestimate in the number of low-energy particles, due to the choice of a production function of the form dE/E^2 in the theoretical calculations,

b. the dependence of the experimental buildup factor on the lateral width of the cascade inspected.

The value of the attenuation length derived from Eq. 6.25 is

$$\lambda_{att}\,(\text{calc}) \approx 1.7\,\lambda_{int},$$

but again depends strongly on the choice of production functions. Fisher suggests that an analytic calculation is in principle probably susceptible of an exact solution if approximations are made to the kernel functions used. However, the three-dimensional development of the cascade must be studied if comparisons with experimental data are to prove enlightening.

As we have already discussed, Fisher's calculations would not be expected to give reliable estimates of the μ-meson transmission in matter because of the neglect of ionization energy loss. Furthermore, many assumptions have been made in developing the analytical expression for nucleons and pions as a function of depth in matter. These assumptions were necessitated partly by the lack of physical information concerning nuclear interactions and partly by mathematical considerations to permit relatively simple mathematical expressions for the final solutions.

In the early 1960's several similar analytical solutions to the cascade transport equations were obtained (PAS C 62, ALS R 63a, ALS R 65) but all are limited in the same way as the solutions obtained by Fisher. The description given indicates the relative complexity of solutions that describe only the one-dimensional development of the nuclear cascade.

A solution of the coupled cascade transport equation, using the straight-ahead approximation, for 24-GeV protons in concrete was compared, in 1963, with experimental data (ALS R 63a). Although qualitative agreement was obtained, it was obvious that substantial improvements were needed in cascade calculation before they could be reliably used in shield design. Since that time substantial efforts have been directed toward application of Monte Carlo techniques to the calculation of nuclear cascade development. The successful interpretation of experimental data by use of this technique was reported by Geibel and Ranft (GEI J 65a), and the development of this technique has been reported in review articles by Alsmiller (ALS R 65, ALS R 69) and Ranft (RAN J 72). Goebel and Ranft (GOE K 69) have reported a comparison between neutron flux densities of energy greater than 100 MeV calculated by Monte Carlo techniques and measurements with threshold detectors outside a 3-meter-long beam stop. Agreement was obtained in general within a factor of 2.

In investigating the radiation problems of a 300-GeV proton synchrotron, substantial progress has been made in comparing experimental and theoretical cascade data. Thus, for example, predicted values of radiation heating, radiation doses, induced radioactivity, particle flux densities, and star densities all agree reasonably with experimental data obtained at Nimrod (the British 7-GeV proton synchrotron) or the CERN 25-GeV proton synchrotron. Van Ginnikin (VAN A 71) has recently reported fair agreement between calculations using the computer program TRANSK and experimental shielding data obtained at the 30-GeV Brookhaven AGS (BEN G 70B).

Additional confidence in the theoretical models is given by the recent comparisons by Freytag and Ranft (FRE E 71) of calculations with measurements by Hofstadter et al., using their TANC detector (HUG E 69) and by Pilcher and Rubbia (PIL J 70), with their SANC detector.

Concurrent with the successful application of Monte Carlo techniques to shielding calculations has been a continuing interest in analytical solutions to the problem, principally because of their relative simplicity. O'Brien (OBR K 68a, OBR K 68b, OBR K 69) has discussed the extension of neutron transport theory to the solution of transverse shielding problems. Comparison of these calculations with experimental data obtained at the AGS and CPS is discussed later. This technique, although relatively simple, is essentially one-dimensional and does not have the power and versatility of Monte Carlo Methods, nevertheless it has proved useful in the design of linear accelerator shielding (see section on Shield Design Examples).

Experimental data available are insufficient to determine the absolute accuracy of such calculations under the conditions at particle accelerators. However, a great many comparisons of calculated and measured data have been made in an essentially one-dimensional problem, cosmic ray propagation in the atmosphere, to which the method is well suited. The experimental data needed most urgently in shield design are details of particle production in hadron-nucleus collisions, transmitted neutron flux density, and dose-equivalent rate. Comparisons of these calculated parameters with experimental cosmic-ray data at different altitudes indicate agreement to within about a factor of 3 (OBR K 70, OBR K 71).

The results of calculations will be best improved by providing reliable input data on particle production in hadron-nucleus collisions. Extensive experimental studies are being made at CERN (GOE K 71) to provide such information. In addition, theoretical calculations of the intranuclear cascade, such as those due to Bertini (BER H 69), will provide increasingly reliable input information for the Monte Carlo routines, which have been developed to calculate the cascade transport with good accuracy.

EXPERIMENTAL STUDIES OF THE NUCLEAR CASCADE

We have seen from a discussion of the galactic cosmic radiation that neutrons, because they have no charge, play an extremely important role in transporting the nuclear cascade. Neutrons are attenuated by two mechanisms, elastic and inelastic scattering. In accelerator shield design the influence of both these mechanisms must be understood.

Elastic scattering is not really an effective means of absorbing high energy nucleons: the higher the incident energy the more forward peaked is the elastic scattering, and beyond about 150 MeV it is to all practical purposes actually in the forward direction. Since the incident particle retains *at least* a fraction (A-1/A+1) of the incident particle energy, it is readily seen that at high energies, in shield materials with moderate mass numbers, little change in either energy or direction results from elastic scattering.

As we shall show later, even at energies as low as 20 MeV the inelastic cross section plays a dominant role in neutron attenuation. However, the presence of hydrogen in shielding material can have an important influence in the transmitted neutron spectrum, with important consequences on the effectiveness of the shield. Shields with no hydrogen content (for example, iron) depend upon inelastic interactions for neutron attenuation. When neutrons have been reduced in energy to that of the lowest inelastic level of the target nuclei there is then no efficient mechanism for energy reduction. In consequence neutrons at this energy build up and penetrate the shield in large numbers. Perry and Shaw (PER D 65) have observed this effect along the shielding of a transported 7-GeV proton beam. The shielding along this beam was constructed principally of concrete (5 ft thick, 366 g/cm^2), but one short length was made of steel (2 ft thick, 475 g/cm^2). Outside the steel shielding radiation levels were higher by a factor of six than outside the concrete shield, despite the greater thickness of the former. Gilbert et al. (GIL W 68) have observed the depletion of low energy neutrons in the equilibrium spectrum transmitted by wet earth below the level in that transmitted by concrete.

The presence of hydrogen in a shield can therefore have an extremely important influence. Earth and concrete are commonly used shielding materials, and usually contain sufficient hydrogen to efficiently moderate neutrons of a few MeV. Earth in all but arid regions contains between 5 and 15% of water by weight. Table 6.III gives the composition of typical concrete.

Table 6.III. Elemental composition of concrete (after Wallace).

Element	Atoms/cm^3 (X 10^{22})
O	4.73
H	1.73
Si	1.57
Ca	0.26
Al	0.17
Fe	0.053
Na	0.028
K	0.028
Mg	0.013

NEUTRON ATTENUATION MEASUREMENTS

With the foregoing in mind, consider the attenuation of a monoenergetic neutron beam. In a good-geometry experiment the total removal of neutrons from the beam, by both elastic and inelastic processes, is measured. The beam is attenuated exponentially according to the relation

$$I_x = I_0 e^{-N\sigma_{tot}x}, \tag{6.28}$$

where I_x = neutron intensity at depth x,

I_0 = initial neutron intensity,

N = number per unit volume of absorber,

$\sigma_{tot} = \sigma_{el} + \sigma_{in}$,

σ_{el} = elastic cross section,

σ_{in} = inelastic cross section.

The effective "removal" of a neutron is often defined, for shielding purposes, to be transfer to an energy below the threshold of the radiation detector used to measure transmission of radiation by the shield. Measurements of shielding characteristics often utilize a neutron detector that responds to a wide range of neutron energies.

Thus, in practice, removal from the beam (defined as a failure to detect a particle) depends upon the geometry of the experiment and the energy threshold of the detector. A better description of a shielding experiment might therefore be to write

$$R_x = R_0 e^{-N\sigma_{rem}x}, \tag{6.29}$$

where R_x, R_0 represent the detector response at shield depths, x and 0 respectively,

σ_{rem} is a "removal cross section,"

and it is assumed that the detector responds only to neutrons close in energy to those of the primary beam. De Staebler (DES H 62) has qualitatively described what is observed as this restriction is relaxed.

As the energy threshold of the detector, E_{th}, is lowered so that $E_{th} \ll E_0$ (the primary beam energy), then the response of the detector depends on the shield thickness compared with the interaction length, λ, of the primary neutron.

a. For $x < \lambda$ there are few interactions and the response is constant.

b. For $x \approx \lambda$, one or two interactions of the primary neutron have occurred, which produce one or more secondaries, and each secondary has sufficient energy to trigger the detector, so the response rises.

c. For x greater than a few λ some of the secondaries (or tertiaries, quaternaries, etc.) have energies below the detector threshold and the response starts to fall.

d. For x much greater than a few λ the primaries (which are the most penetrating) are in complete equilibrium with secondaries, and the observed attenuation results from the interaction of the primaries followed by rapid absorption of the interaction products.

The detector response curve would therefore be expected to show the classic buildup curve, ultimately reducing to an exponential transmission with slope $1/N\sigma_{rem}$. We would therefore expect an experimental transmission curve similar to that predicted by the simple analytical one-dimensional cascade model previously described.

For extension to higher energies the removal cross section, σ_{rem}, may be written, as a function of energy, as

$$\sigma_{rem}(E) = a(E)\,\sigma_{el} + \sigma_{in}, \tag{6.30}$$

where $a(E) \to 0$ as the energy increases (PAT H 57, THO R 61).

Removal Cross Section Measurements for Neutron Energies Between 0.5 and 15 MeV

It has been necessary for physicists concerned with the calculation of nuclear reactor shields to devote special attention to neutrons in the energy region 0.5 to 15 MeV. The processes by which neutrons in this energy region are transmitted through matter are extremely complex, since this region coincides with the resonances in the cross section for the formation of compound nuclei. Consequently mathematical formulation and solution of neutron transport problems is difficult.

The empirical approach to this problem suggested by the definition of an effective removal cross section, which represents an average cross section over the energy region from about 0.5 MeV to 15 MeV for removal of those neutrons responsible for transmitting dose (or dose equivalent) through thick shields) has proved extremely valuable.

To quote Clark (CLA F 71): "Removal cross section theory permits estimation of shielding in a simple one-velocity model. The requirements that must be met for removal cross section theory to apply are:

"1. The shield must be sufficiently thick and the neutrons so distributed in energy that only a narrow band of the most penetrating source neutrons give any appreciable ultimate contribution to the dose outside the shield.

"2. There must be sufficient hydrogen in the shield, intimately mixed or in the final shield region, to assure a very short characteristic transport length from about 1 MeV to absorption at or near thermal energy.

"3. The source energy distribution and the shield material (nonhydrogenous) properties must be such as to assure a short transport distance for slowing down from the most penetrating energies to 1 MeV.

"Requirements 2 and 3 assure that spatial equilibrium of all other components with the most penetrating component will be rapidly approximated. Requirement 1 assures that the purely material attenuation of the dose will be exponential." Several tabulations of total and partial cross sections are available for neutron energies up to about 15 MeV (UCRL-5351, BNL-325). Neutron total cross sections averaged over many adjacent resonances do, in general, decrease with increasing neutron energy, and a broad description, for shielding purposes, of the behavior of these neutrons may be obtained by defining the cross section for removal to an energy below about 0.5 MeV.

In principle such a cross section could be measured by carrying out a neutron-transmission experiment with a neutron detector with its threshold energy set to 0.5 MeV. However, since in many practical cases the outer regions of the shield contain hydrogen (indeed hydrogen must be there if condition 2 above is to be fulfilled), an alternative procedure is possible. In practice measurements may be made by a difference technique. A wide neutron beam (i.e., bad geometry) passes through a large water tank and

the dose equivalent transmitted is measured. Then the shielding whose removal cross section is to be measured is placed between the neutron source and the tank (i.e., with water between the shield and the detector), and the transmitted dose equivalent is measured. In this way the detection of thermal neutrons transmitted by the composite shield may be used to determine the removal of resonance neutrons. The transmission or resonance neutrons is found to be exponential, and is given by

$$DE = \text{constant} \exp(-\Sigma_{rem} t), \tag{6.31}$$

where DE is the neutron dose equivalent transmitted,

Σ_{rem} is the macroscopic removal cross section,

t is the thickness of shield material.

The constant appearing in the equation is the dose equivalent transmitted by the water tank assembly without the shield in place. Price, Horton, and Spinney (PRI B 57) have summarized some typical results. Particularly the data of Chapman and Storrs (CHA G 55) are of interest, since their work covered a wide range of shield materials. Figure 6.8 shows the results obtained plotted as a function of mass number.

For all but the very light nuclei the removal cross sections are about 2/3 of the total cross section. Furthermore, the variation of removal cross section with mass number is monotonically decreasing, and beyond nuclei of mass 10 approaches the form

$$\Sigma_{rem} \approx 0.21 A^{-0.58}$$

(very close to the variation expected at higher energies of $\sigma \propto A^{2/3}$). Price, Horton, and Spinney quote values for 15 elements and 6 chemical compounds for neutrons having a fission spectrum. It is probably accurate enough to assume these measurements to be valid at the mean energy of the fission spectrum ($\approx$ 2 MeV).

The macroscopic removal cross section, Σ_r, is given by

$$\Sigma_r = \frac{0.602 \sigma_r \rho}{A} \text{ cm}^{-1} \tag{6.32}$$

where σ_r = microscopic removal cross section in barns,

ρ = density (g/cm^3),

and A = mass number.

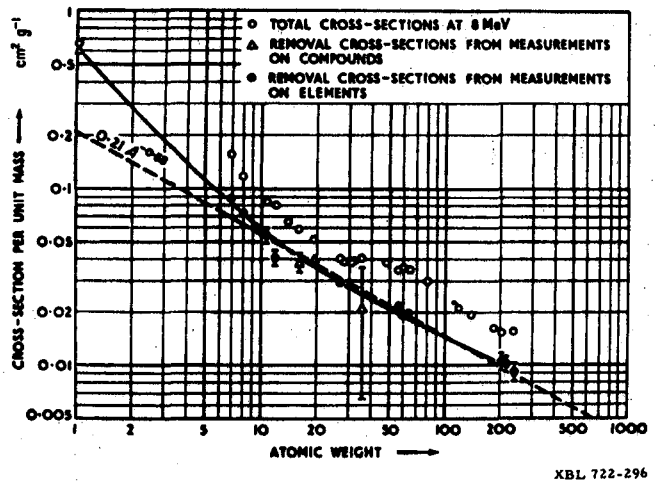

Fig. 6.8. Removal cross sections per unit mass for fission neutrons as a function of mass number (over the range $8 \leq A \leq 240$ the values are well fitted by the function $0.21\ A^{-0.58}$). (From Price, Horton, and Spinney.)

For a shielding material consisting of several elements the macroscopic removal cross section is given by

$$\Sigma_r = \sum_{i=1}^{n} \left(\frac{\Sigma_r}{\rho}\right)_i \rho_i, \tag{6.33}$$

where $\sum$ represents summation over the n elemental constituents,

$\left(\frac{\Sigma_r}{\rho}\right)$ is removal cross section per unit mass of the ith constituent,

ρ_i is the density of the ith constituent (see Figs. 9 through 13).

Equation 6.31 may be generalized to other geometries by incorporating a geometric form factor, G:

$$DE = \text{constant } G \exp(-\Sigma_{rem}\, t). \tag{6.34}$$

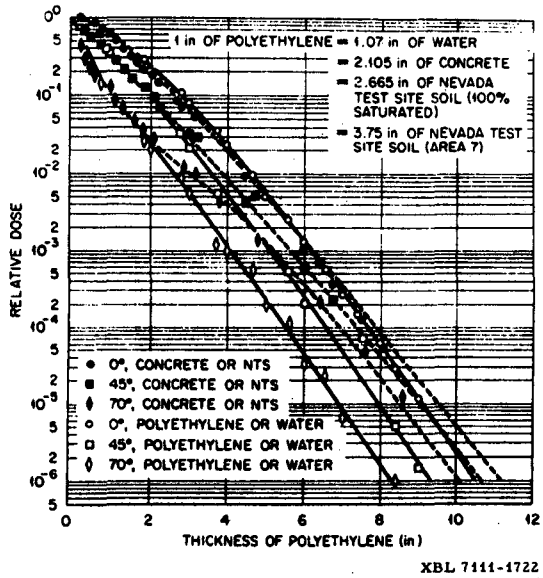

Fig. 6.9. Attenuation of absorbed dose by 0.5-MeV incident neutrons penetrating various materials at various angles. (From NCRP Report 38.)

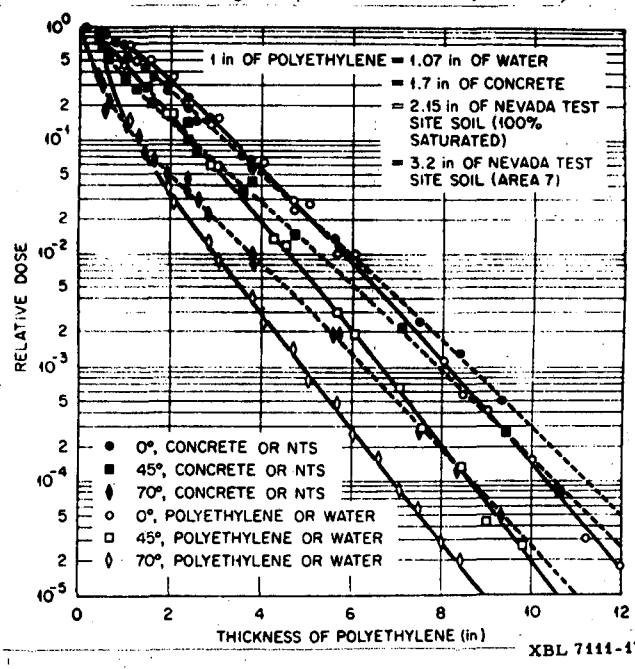

Fig. 6.10. Attenuation of absorbed dose produced by 1-MeV incident neutrons penetrating various materials at various angles. (From NCRP Report 38.)

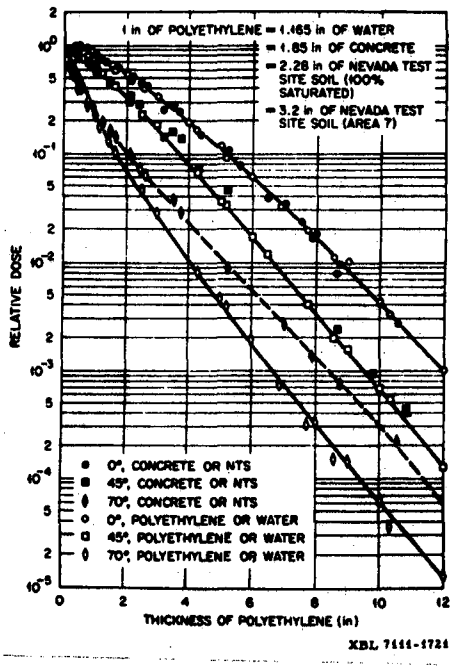

Fig. 6.11. Attenuation of absorbed dose produced by 2-MeV incident neutrons penetrating various materials at various angles. (From NCRP Report 38.)

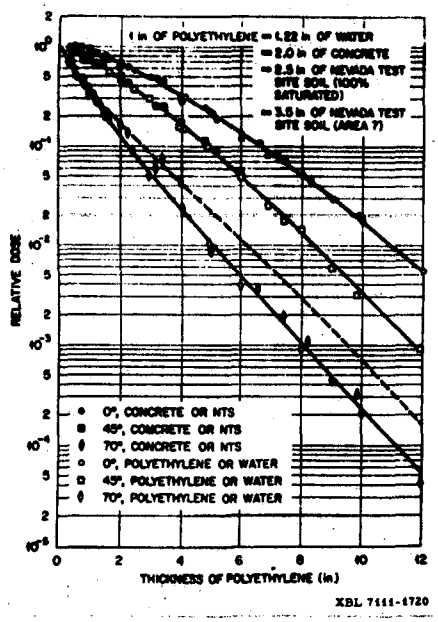

Fig. 6.12. Attenuation of absorbed dose produced by 3-MeV incident neutrons penetrating various materials at various angles. (From NCRP Report 38.)

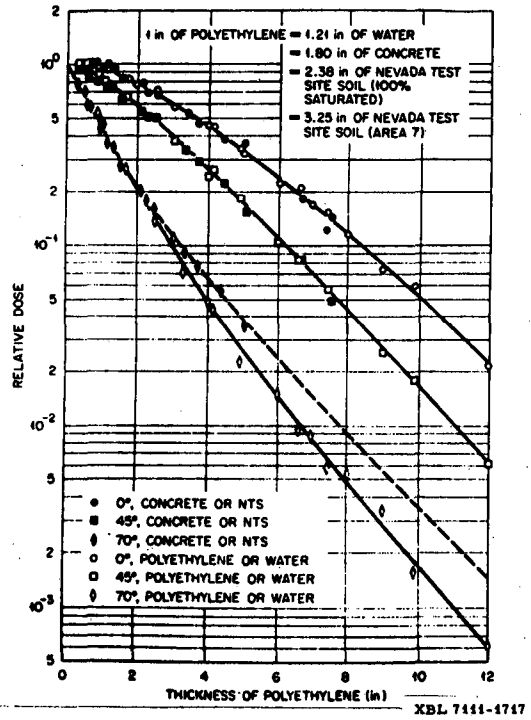

Fig. 6.13. Attenuation of absorbed dose produced by 5-MeV incident neutrons penetrating various materials at various angles. (From NCRP Report 38.)

For a parallel beam G = 1, whereas for a point source $G = 1/4\pi r^2$. Various form factors applicable to other geometries may be found in the literature (PRI B 57, ROC T 56). Few measurements of removal cross section have been reported in the literature for neutrons of varying incident energy. Broder et al. (BRO D 59) have reported transmission measurements for 4-MeV and 14.7-MeV neutrons and have summarized other data at 2.9 MeV, 6.7 MeV, and 14.9 MeV, and for fission spectrum neutrons. The materials considered include water, graphite, iron, and lead. Their data are summarized in Table 6.IV.

Table 6.IV. Removal cross-section data, σ_{rem} (in barns) (Broder et al.). Typical accuracy quoted, ± 5%.

Element	1 MeV	Fission spectrum	2.9 MeV	4 MeV	6.7 MeV	14.9 MeV
Carbon		0.90	1.58	1.05	0.83	0.50
Aluminum		1.31				
Iron	1.1	1.96	1.94	1.98	2.26	1.60
Copper		2.04				
Lead		3.28	3.70	3.44	3.77	2.95

Because of the paucity of experimental data one frequently must depend upon calculations. Allen and Futterer (ALL F 63) have calculated the transmission of absorbed dose through slabs of various materials, for beams of neutrons of incident energy between 0.5 and 5 MeV incident at angles from 0° to 70° from normal. Table 6.5 summarizes the chemical composition of the shielding materials studied and Table 6.VI summarizes their equivalence to polyethylene. Until recently measurements of the transmission of 14-MeV neutrons published in the literature were in poor agreement. Thus Hacke (HAC J 67) pointed out that reported dose transmission factors of 1.5 m of concrete varied by as much as a factor of 200. Although part of this difference may be explained by experimental technique and by chemical composition of the concrete, such a large difference highlights the surprising lack of reliable experimental data in this neutron energy range. Marshall has recently reported a careful measurement of the attenuation of 14-MeV neutrons through water under approximately broad beam conditions. Figure 6.14 shows the vairation of neutron dose equivalent with water thickness. The dose equivalent is clearly attenuated exponentially with a relaxation length of 16.3 cm (± 4%). Of particular interest is the variation of the composition of the total DE rate. Neutrons in the energy range 0.15 to 20 MeV always dominate the neutron contribution to the dose equivalent, the total contribution from neutrons below 0.15 MeV never exceeding 22%. However, the contribution of γ rays increased from 10% of the total at the front of the shield to about 60% through 125 cm of water, as may be seen in Fig. 6.15.

Table 6.V. Chemical composition of materials used in shielding calculations by Allen and Futterer. (From NCRP Report 38.)

Material	Density (g/cm3)	Elements contained	Atoms/cm3 (X 10^{-21})
Borated polyethylene (8% B_4C by weight)[a]	0.97	H	76.80
		C	39.20
		^{10}B	0.658
		^{11}B	2.67
Water	1.00	H	66.90
		O	33.45
Concrete	2.26	H	13.75
		O	45.87
		Al	1.743
		Si	20.15
NTS[b] soil (dry)	1.15	H	8.553
		O	22.68
		Al	2.014
		Si	9.533
NTS[b] soil (100% sat.)	1.25	H	16.87
		O	27.00
		Al	1.976
		Si	8.963

[a]Several calculations were made for pure polyethylene slabs of density 0.925 g/cm^3 up to 6 inches thick. Results differ negligibly from corresponding results for 8% borated polyethylene.
[b]Nevada test site.

Table 6.VI. Thickness of shielding materials equivalent to 1 inch of borated polyethylene as a function of neutron energy (Allen and Futterer).

Neutron energy (MeV)	Shield material			
	Water	Concrete	Dry soil	Saturated soil
0.5	1.07	2.10	3.75	2.66
1	1.07	1.70	3.20	2.15
2	1.16	1.85	3.20	2.28
3	1.22	2.00	3.50	2.50
5	1.21	1.80	3.25	2.38

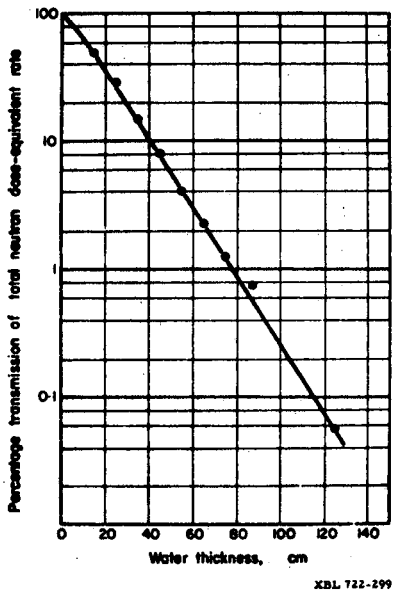

Fig. 6.14. Variation of the total transmitted neutron dose-equivalent rate with water thickness. Incident neutron energy 14-MeV. (From Marshall.)

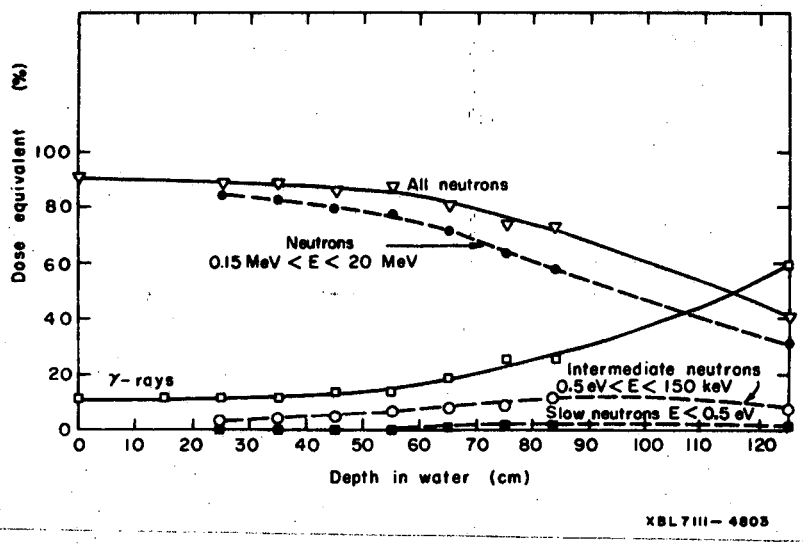

Fig. 6.15. Relative contribution to the transmitted dose-equivalent rate as a function of water thickness. Incident neutron energy 14 MeV. (From data by Marshall.)

Early Accelerator Shielding Studies

Early experimental studies of neutron attenuation at 90 and 270 MeV in a variety of materials and for poor-geometry conditions have been reported by Moyer and his colleagues (MOY B 57, PAT H 57, PAT H 62). Patterson, who also reported a measurement in concrete alone at 4.5 GeV (PAT H 62), has interpreted the Berkeley experimental data in terms of an energy-dependent attenuation cross section, analogous to the "removal cross section" used in reactor physics, and defined by

$$\sigma_{rem}(E) = \alpha(E)\sigma_{e\ell} + \sigma_{in}. \qquad (6.30)$$

Table 6.VII shows values of $\alpha(E)$ suggested from Patterson's data (PAT H 62), and Fig. 6.16 shows attenuation mean free path, calculated by using this prescription, compared with measurements at 90 MeV, 270 MeV, and 4.5 GeV in concrete. The general agreement between calculated and measured values is seen to be quite good, but the basic experimental technique was limited in these measurements to poor-geometry conditions. These early measurements at 270 were also supported by one of the first Monte Carlo calculations of cascade development due to Tsao et al. (TSA C 58). At an incident neutron energy of 300 MeV these workers calculated an attenuation length in concrete of 145 ± 10 g/cm^2 (to be compared with the experimental value of 152 5/cm^2 at 270 MeV).

Table 6.VII. Values of $\alpha(E)$ for concrete (after Patterson).

Neutron energy (MeV)	$\alpha(E)$	σ_{rem}
1	1.00	$\sigma_{e\ell} + \sigma_{in}$
5	0.30	$0.30\ \sigma_{e\ell} + \sigma_{in}$
14	0.10	$0.10\ \sigma_{e\ell} + \sigma_{in}$
$\geqslant$ 150	0	σ_{in}

Lindenbaum has described attenuation measurements of a 3-GeV proton beam in heavy concrete (ρ = 4.0 to 4.3 g/cm^3), at depths between 3 ft (90 cm) and 13.5 ft (430 cm). The incident beam was contained within a square 6.6 in. (15.15 cm) and had a divergence less than 3 deg. Ionization density and the proton and pion flux ($E_p > 50$ MeV, $E_\pi > 25$ MeV) were measured as functions of depth and distance from the beam axis. After transition, the primary component, ionization density and the absorbed dose rate were all attenuated exponentially with mean free path of ± 15 g/cm^2 at ≈ 1.5 GeV, and 169 ± 32 g/cm^2 at ≈ 2.5 GeV.

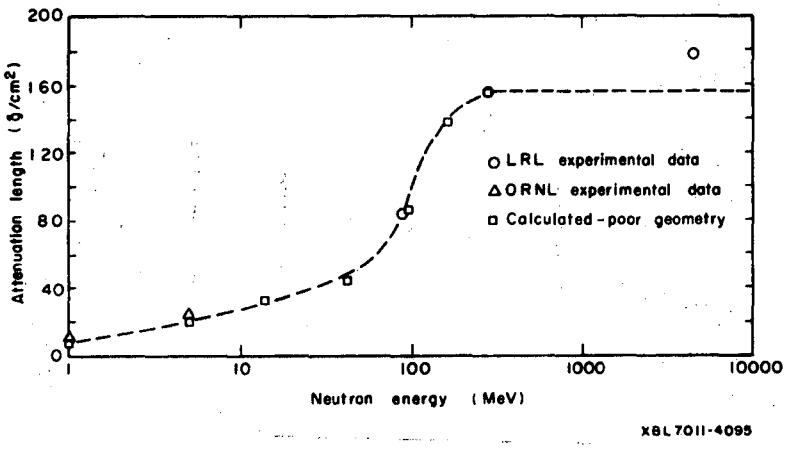

Fig. 6.16. Comparison between calculated and measured values of attenuation lengths in concrete for neutrons. (After Patterson.)

Measurements of the attenuation of 4-, 5-, 6-, and 9-GeV pions, made by Tinlot et al. (TIN H 64) using counters, gave values of λ_{atten} independent of energy: an average of 123 g/cm^2 for concrete (ρ = 2.3 g/cm^2) and 163 g/cm^2 for steel. Errors in these measurements are hard to assess, particularly in the case of steel because of the thin shield [only 2 feet (60 cm) at 9 GeV] (THO R 68).

Limiting Attenuation Length at High Energies

Lindenbaum (LIN S 61) has explained these early experiments in terms of the variation of the inelastic cross sections with energy: "... Below 100 MeV the neutron inelastic cross section increases rapidly with decreasing energy until $E < 25$ MeV were in most cases the neutron inelastic cross sections level off and then decrease suddenly as shown in [Fig. 6.17.] The increasing inelastic neutron cross section with decreasing energy in the region 25 MeV $< E_n <$ 100 MeV means that neutron secondaries of high-energy primaries in this energy range reach an equilibrium buildup factor relative to the long-range primary component which controls the attenuation. For $E > 100$ MeV the secondary neutrons may still have an effectively shorter mean free path than a higher-energy secondary, even though the inelastic cross sections are about the same, because of the increasing angular divergence with decreasing energy of the secondaries. It is these facts which tend to make high-energy ($E <$ several hundred MeV to several BeV) nucleon beams attenuate approximately exponentially (after a sufficient transition region) with a mean free path which is not very sensitive to the initial energy and is not much longer than the geometric mean free path calculated from the inelastic cross sections of the elements in the shield."

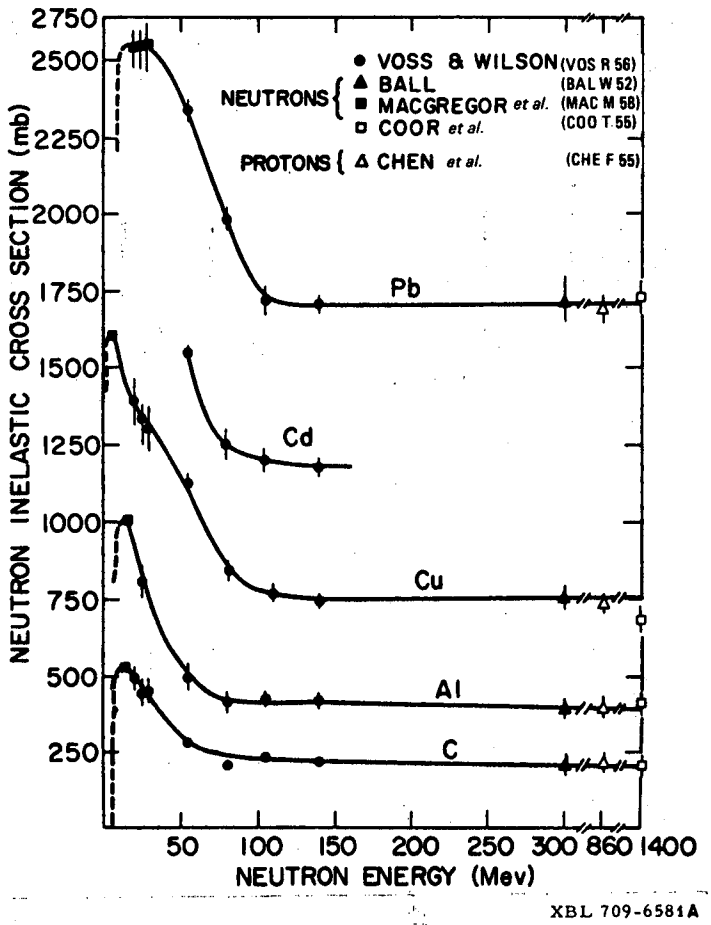

Fig. 6.17. Inelastic neutron cross sections as a function of energy in the range 0 to 1.4 GeV. (After Lindenbaum.)

Thus we might expect at high energies that the attenuation length, λ_{atten}, would be given by

$$\lambda_{atten} \approx \frac{1}{N\sigma_{in}} \text{ cm}, \tag{6.31}$$

where N is the number of atoms/cm^3,

σ_{in} is the inelastic cross section,

from which it follows that

$$\rho\lambda_{atten} = 38\,A^{1/3} \text{ g/cm}^2, \tag{6.32}$$

if the inelastic cross section is assumed to be geometric and the nucleon radius is taken as 1.2×10^{-13} cm.

Keefe and Scolnick (KEE D 66) have reviewed experimental measurements of absorption cross sections. The cross section for interaction of strongly interacting particles in the GeV range with nuclei is relatively insensitive to the individual nuclear-nucleon cross section because of the small probability of penetration of the nucleus without an interaction. Several measurements have been made of the absorption cross section, σ_a, of high energy strongly interacting particles with several nuclei (ASH A 60, ATK J 61, CHE F 55, COO T 55, CRO K 57). The results (see Fig. 6.18) are well represented by the formula

$$\sigma_a = 43\, A^{0.69} \text{ mb}, \tag{6.33}$$

where A is the mass number (WIL R 64). [It should be noted that this formula is not valid for hydrogen. Rarita (RAR W 64) has discussed the expected behavior of the individual particle cross sections on hydrogen as a function of energy.]

Results from cosmic ray experiments suggest Eq. 6.33 should be valid up to energies of several hundred GeV.

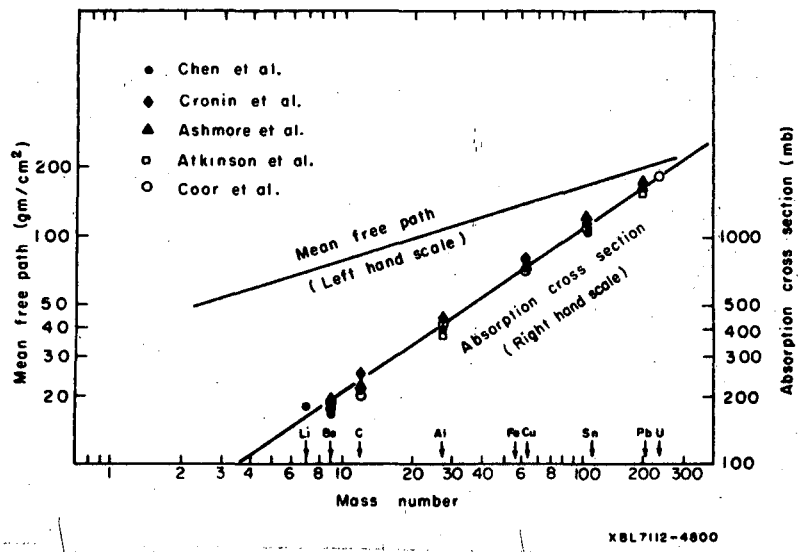

Fig. 6.18. Mean free path and atomic cross section as a function of mass number. (From Keefe and Scolnick.)

The absorption mean free path, λ_a, measured in g/cm^2, is given by

$$\lambda_a = \rho/N\sigma_a, \tag{6.34}$$

where ρ is the density of g/cm^3.

Thus, using Eq. 6.31, we obtain

$$\lambda_a = 38.5\ A^{0.31}\ \text{g/cm}^2 \tag{6.35}$$

(not significantly different from the simple approximation given in Eq. 6.34). The attenuation length, λ_a, is a monotonic function of mass number (see Fig. 6.18) when measured in units of g/cm^2, but not when measured in cm (see Table 6.VIII which gives values of λ_a for a variety of materials), since density is an erratic function of mass number.

An examination of the experimental data indicates no strong dependence, upon either energy or mass number, of the ratio of the elastic cross section (σ_e) to the absorption cross section (σ_a). The best value for this ratio is

$$\sigma_e/\sigma_a = 0.57.$$

The mean free path appropriate to the total cross section, σ_{tot}, may therefore be obtained from the value of λ_a in Table 6.VIII divided by 1.57.

Many of the early high energy shielding experiments were of insufficient precision to confirm the limiting value of attenuation length predicted in Table 6.VIII. Thus attenuation length in steel has been reported in the literature as ranging from 119 to 179 g/cm^2 (cf 134 g/cm^2 in Table 6.VIII), whereas in concrete the values range from 108 to 172 g/cm^2 (THO R 68) (see Table 6.IX). The wide variations are due principally to differences in experimental technique, but also in part to different interpretations of the term "attenuation length." In many cases, too, the density of the shielding materials was not accurately known.

The evaluation of a precise attenuation length is of course a matter of great importance, since it is this parameter, above all others, that influences the radiation field transmitted by an accelerator shield. Considerable economies may be achieved at the larger accelerators if shielding need not be overdesigned. De Staebler (DeS H 62), in justifying his use of a large value of attenuation length in earth (170 g/cm^2), summarized the situation thus:

"It may appear that we are being unnecessarily conservative in taking the largest values of λ which have been measured, but the specter which haunts us in this connection is the unknown contribution to the attenuation from scattering out."

By similar reasoning shield designs for the 200- and 300-GeV accelerators at Berkeley (LRL 65) and CERN (CERN 64) were based on attenuation lengths that were perhaps longer than necessary, because of the uncertainty in available data in the early 1960's,

Table 6.VIII. High energy removal mean free paths and radiation lengths.

Element	A	ρ (g/cm^3)	σ_a (mb)	Removal free path (g/cm^2)	Mean free path (cm)	Radiation length (g/cm^2)
Li	6.94	0.534	164	70	131.0	77.5
Be	9.01	1.84	196	76	41.4	62.2
B	10.82	2.5	222	80.5	32.2	52
C	12.01	2.25	240	83.2	37.2	42.5
Mg	24.32	1.74	389	99.5	57	24.6
Al	26.98	2.7	417	107	39.7	23.9
Cr	52.01	7.0	655	131	18.7	14.9
Mn	54.94	7.42	680	133	18.4	14.6
Fe	55.85	7.7	688	134	17.4	13.8
Co	58.94	8.7	718	136	15.7	13.55
Ni	58.71	8.7	714	136	15.7	12.6
Cu	63.54	8.9	752	139	15.6	12.8
Zn	65.37	7.0	770	140	20	12.35
Ag	107.87	10.5	1085	164	15.6	8.6
Sn	118.69	7.0	1160	168	24	8.54
Ba	137.34	3.78	1285	177	47	7.85
Ta	180.95	16.6	1555	192	11.6	6.35
W	183.85	18.8	1565	193	10.2	6.28
Ir	192.2	22.42	1610	196	8.8	6.15
Pt	195.1	21.37	1638	197	9.25	6.05
Au	196.96	19.0	1640	198	10.4	6.0
Hg	200.59	13.5	1655	198	14.6	6.10
Pb	207.19	11.0	1710	202	18.4	5.8
U	238.03	18.7	1870	210	11.2	5.5

Table 6.IX. Summary of high-energy shielding measurements (up to 1965). After Thomas (THO R 68).

	Incident particle	Beam energy [GeV]	Shield material	Shield density [g/cm^3]	De-tector	λ_{atten} [g/cm^2]
LBL	n	0.09	concrete	2.3	BF	81
LBL	n	0.27	concrete	2.3	BF	152
Princeton	n	0.30	concrete	3.85	MC	145 ±10
BNL	p	1.5	concrete	4.0–4.3	CT	130 ±15
BNL	p	2.5	concrete	4.0–4.3	CT	169 ±32
LBL	n	4.5	concrete	2.3	BF	172
BNL	π	4.5	concrete	2.3	CT	118 ±8[a]
BNL	π	4.5	steel	7.8	CT	155 ±11[a]
BNL	π	6	concrete	2.3	CT	121 ±8[a]
BNL	π	6	steel	7.8	CT	155 ±11[a]
LBL	p	6.2	concrete	2.4	^{11}C	108 ±20[b]
LBL	p	6.2	concrete	2.4	^{27}Al	112 ±20[b]
LBL	p	6.2	concrete	2.4	^{198}Au	116 ±20
R.L.	p	6.2	concrete	2.4	^{32}S	123 ±10
LBL	p	6.2	concrete	2.4	G5	160 ±20[c]
BNL	π	9	concrete	2.3	CT	129 ±9[a]
BNL	π	9	steel	7.8	CT	179 ±12[a]
RL, ORNL	P	10	concrete	3.65	G5	164 ±20
RL, ORNL	p	10	steel	7.8	G5	119 ±10
CERN	p	10	steel	7.8	^{11}C	145 ±15
CERN	p	10	steel	7.8	IC	155 ±16
DESY, SLAC, CERN, etc.	p	20	concrete	3.65	G5	132 ±5[d]
DESY, CERN, SLAC	p	20	steel	7.8	G5	137 ±10
CERN	P	20	steel	7.8	^{11}C	170 ±17[b]
CERN	p	20	steel	7.8	IC	155 ±16
CERN	p	24	concrete	2.4	G5	145 ±10
			concrete and earth	3.65 1.5		

Key:
BF Bismuth fission chamber
CT Counter telescope
MC Monte Carlo calculation
^{11}C
^{32}S
^{37}Al
Activation detectors,
G5 Nuclear emulsion,
IC Ionization chamber.

a DeStaebler's estimate of error
b Thomas's estimate of error
c Unpublished data.
d Weighted mean of results from DESY, CERN, RL, and Stanford

Recent Shielding Experiments at High Energy Proton Accelerators

As we have described in the historical resumé, little information pertinent to the problems of accelerator shielding was available in the 1950's. This was in part due to the fact that radiation problems were avoided in the shielding design. Thus Livingston (LIV M 52b) has described the typical design of cyclotron shielding in the following words: "The completely closed vault with a minimum of apertures has become standard design for cyclotron laboratories. Movable doors with overlapping side panels have displaced the labyrinth entry used in early designs; a baffled entry through the shielding walls must be long and tortuous to result in as efficient shielding as a solid door. Water tanks have been completely displaced, in favor of solid construction. The most satisfactory material in use is concrete loaded with iron ore or scrap iron to increase density for γ-ray absorption and at the same time provide material with large cross section for inelastic scattering of neutrons. Typical of recent designs is the vault for the Brookhaven 60-in. cyclotron. This vault has 5-ft walls and 4-ft roof of limonite-loaded concrete; two 5-ft-thick concrete doors are raised or lowered into pits below floor level by electric motor drive, one of 8 by 8 ft for large apparatus and one 3 by 7 ft for personnel access. Ports are provided for handling radioactive targets through the walls and for bringing an emergent beam through into an auxiliary vault for experiments. This amount of shielding will reduce fast neutron intensity, by a factor of about 10^{-5}, and slow neutrons or γ rays by about 10^{-6}. To keep leakage through apertures down to an equivalent small fraction of incident intensity, the area of such apertures is kept less than 10^{-5} of the total area, and apertures are designed to eliminate direct radiation leakage. Conduits of ventilation or electrical leads have double bends, and doors are overlapped to prevent straight channels through the shield."

Ironically this type of solution, developed for relatively low energy accelerators, may have delayed our full understanding of accelerator radiation problems and consequently our ability to design an efficient shield.

Although the construction of these standard cyclotrons in vaults adequately reduced radiation levels for the purposes of radiation protection, little attempt was made at optimum design. In most cases gross overshielding minimized the problems and in consequence no studies of radiation fields around the accelerator or of the shielding properties of various materials were necessary, or, in fact, made. This latter omission was to prove increasingly embarrassing as available particle energies increased. Speaking of the newer synchrocyclotrons, Livingston wrote in 1952 (LIV M 52a):

"The shielding requirements for a synchrocyclotron do not differ in principle from those for the standard cyclotron. The higher energy radiations do require greater thickness of shield for attenuation; on the other hand, the lower duty cycle and the correspondingly lower average beam make the scattered radiation intensity much smaller. As a consequence the shield must be thicker in the

horizontal plane of the primary, high energy radiations, but can have a thinner roof. This has been carried to an extreme at the University of Rochester, where there is no overhead shielding, and it is admitted to result in undesirably high intensities of scattered radiation. A structure of overlapping concrete blocks is used at Berkeley, forming a wall 15 ft thick and with a 4-ft layer overhead. A completely closed vault with movable doors 8 ft thick is the answer at Harvard. At Harwell and at the University of Chicago the cyclotron is located in a pit below ground level with heavy overhead concrete slab shielding."

However, the increasing energy, intensity, and physical size of particle accelerators, the cost of the "classical solution" to the radiation, and the inefficiencies it led to produced an acute situation described at the New York Symposium held in 1957.

THE "MOYER MODEL"

The increasing capability of Monte Carlo calculations and other computational techniques is encouraging—it might eventually be possible to simulate the precise operational details in the computer and obtain exact estimates of radiation levels. Such calculations, however, are difficult, expensive, and perhaps several years into the future. Furthermore, we must not fall into the trap of leaning too heavily on the results of calculations unsupported by experimental data. There still remains a large amount of painstaking work to be done before we can depend entirely upon such predictions. Indeed, even when extremely accurate calculations are feasible, it seems likely that the perturbations due to operational uncertainties will not permit full advantage to be taken of their precision.

There will continue to be a need for methods capable of estimating shields reliably, cheaply, and quickly (albeit not with the precision possible with the use of a computer); such methods will facilitate rapid decisions in the preliminary stages of planning experiments or modifications to the accelerator. There will continue to be a demand, too, for methods that give sufficient physical insight into the problem of shielding to permit full utilization of the more sophisticated calculational methods.

Based on experience at the Berkeley accelerators, Moyer developed a phenomenological model capable of estimating the additional shielding to be required as part of the Bevatron improvement program during 1962-63 (MOY B 61, MOY B 62).

Point Source (Target Problem)

Consider a high-energy proton beam incident upon a target (see Fig. 6.19a). Secondary particles are emitted from the target as a result of nuclear interactions. The basic problem is to estimate the total number and energy spectrum of those neutrons that penetrate the accelerator shielding. The number of neutrons with energy between E and E+dE emitted into solid angle $d\Omega$ is given by

$$N\left(\frac{d^2n}{dE\,d\Omega}\right), \tag{6.36}$$

where N protons/sec interact in the traget.

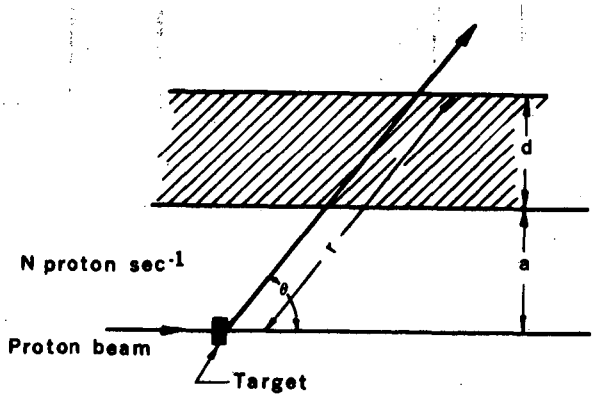

fig VIII-1

XBL 689 4916

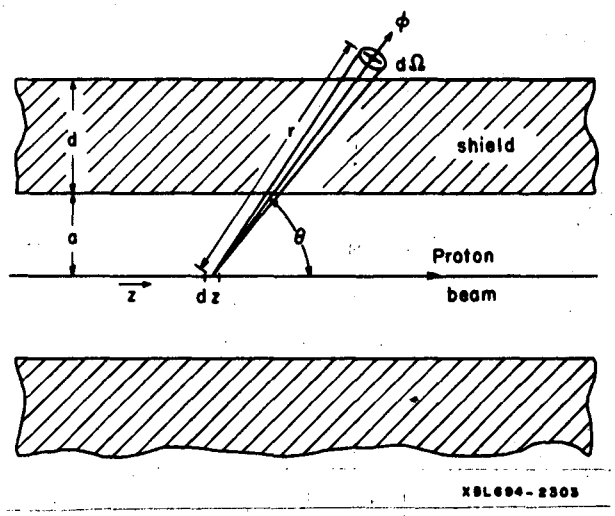

XBL694-2303

Fig. 6.19. Two-dimensional representation of shielding geometry for a large proton accelerator. (After Routti and Thomas.)

For the shield configuration shown in Fig. 6.19a the path length through the overhead shielding is given by d cosec θ. Thus if the removal mean free path of neutrons of energy E is $\lambda(E)$, an attenuation factor of $\exp[-d \csc\theta/\lambda(E)]$ must be applied. In addition, a buildup factor should be applied which takes account of "scattering in" and, in a gross way, of particles that are produced by interactions of higher-energy particles and which arrive at the shield surface in the energy interval E+dE. The flux of particles of energy between E and E+dE leaving the shield surface at angle 0 to the target is given by

$$\frac{dn}{dE} = N\left(\frac{d^2n}{dE\,d\Omega}\right) d\Omega\, B(E) \exp[-d \csc\theta/\lambda(E)], \tag{6.37}$$

where the solid angle $d\Omega$ is given by

$$4\pi d\Omega = \frac{1}{r^2} = \frac{1}{(a+d)^2 \csc^2\theta} \tag{6.38}$$

The integral flux at point p is

$$\Phi_p = \int_{E_{min}}^{E_{max}} \frac{dn}{dE}\, dE$$

$$= \int_{E_{min}}^{E_{max}} N\left(\frac{d^2n}{dE\,d\Omega}\right) d\Omega\, B(E) \exp[-d \csc\theta/\lambda(E)]\, dE, \tag{6.39}$$

where E_{min} and E_{max} represent reasonable energy limits for the integral.

Moyer used a simplified form of Eq. 6.39 for prediction of additional shielding required at the Bevatron. Because at the time of his calculations experimental data were limited, he proceeded by making several reasonable physical assumptions. They were:

a. Because the neutron inelastic cross section is essentially constant above 150 MeV, Moyer wrote

$$\lambda(E) = \lambda(\text{const}) \text{ for } E < 150 \text{ MeV}$$

and (6.40)

$$\lambda(E) = 0 \text{ for } E < 150 \text{ MeV}.$$

This is equivalent to ignoring the lower-energy neutrons produced, i.e., to setting $E_{min} = 150$ MeV in the integral of Eq. 6.39. Thus Φ_p now

becomes Φ_p (E_n>150 MeV). However, for the typical shield thickness around high-energy accelerators, the larger intensity of low-energy neutrons produced at the source inside the shield is more than compensated for by the considerably larger attenuation cross sections appropriate to these energies. Thus the flux at the point p can be written as

$$\Phi_p (E_n > 150 \text{ MeV}) =$$

$$N \exp\left(\frac{-d \operatorname{scs} \theta}{\lambda}\right) d\Omega \int_{150 \text{ MeV}}^{E_{max}} B(E) \left(\frac{d^2 n}{dE d\Omega}\right) dE. \qquad (6.41)$$

b. The integral in Eq. 6.44 is simplified by writing it as the product of a multiplicity factor, $m(E_{max})$, which is the number of neutrons emitted at all angles from the target with energy greater than 150 MeV with a relative angular distribution $f(\theta)$. Thus we can write

$$\int_{150 \text{ MeV}}^{E_{max}} B(E) \left(\frac{d^2 n}{dE d\Omega}\right) dE = m(E_{max})\, f(\theta) = g(\theta). \qquad (6.42)$$

(It should be noted that $m(E_{max})$ is a constant for given E_{max} and a given target.) Equation 6.39 is further simplified to

$$\Phi_p (E_n > 150 \text{ MeV}) = \frac{N\, m(E_{max})\, f(\theta)}{(a+d)^2 \csc^2 \theta} \exp\left(\frac{-d \csc \theta}{\lambda}\right). \qquad (6.43)$$

Moyer estimated $m(E_{max})$ and $f(\theta)$ in the particular case for 6-GeV protons incident upon a thick (≈ 100 g-cm^2) copper target. In obtaining suitable values he utilized cosmic-ray data, the Monte Carlo calculations by Metropolis et al. (MET N 58), and experimental data taken at the Bevatron.

c. The dose equivalent DE_p produced by neutrons with energies greater than 150 MeV was then estimated by assuming a constant dose equivalent per unit fluence, F:

$$DE_p (E_n > 150 \text{ MeV}) = F\, \Phi_p (E_n > 150 \text{ MeV}), \qquad (6.44)$$

and the total DE evaluated by writing

$$DE \text{ (total)} = k\, DE_p (E_n > 150 \text{ MeV}), \qquad (6.45)$$

where k is a constant greater than 1. This last approximation is made plausible by considering that the low-energy neutrons are in equilibrium with neutrons greater than 150 MeV at shielding depths greater than a few mean free paths.

Thus Moyer's final simplification of Eq. 6.37 becomes:

$$DE_p\,(\text{total}) = \frac{kF\ Nm(E_{max})\ f(\theta)}{(a+d)^2\ \text{cosec}^2\,\theta}\ \exp\left(\frac{-d\ \text{cosec}\ \theta}{\lambda}\right) \qquad (6.46)$$

Solution of Eq. 6.49 was obtained by calculating $(DE)_p$ as a function of d and then fixing d at the required $(DE)_p$.

Moyer's shield calculation was predicted on an increase by a factor of 50 in proton intensity of the Bevatron beam and removal of temporary wooden shielding that afforded a neutron-flux attenuation factor of 2. The effective design neutron attenuation (or reduction in transmission) was therefore a factor of 100. Extensive neutron-flux measurements were made before and after the imrpovement program. The overall effect of the recommended shield was to reduce the neutron flux levels by 90 to 100, the exact value depending on the neutron detector and detector lovation (SMI A 65, THO R 70).

Generalization of the Moyer Model

Although the approximations used by Moyer produce satisfactory results at the Bevatron (see Shield Design Examples), the model needs to be generalized to permit its wider use.

A proton accelerator may be considered, for the purpose of calculating shielding, as a source of neutrons. In the high-energy strong-focusing proton synchrotrons it is sufficiently accurate to ignore the radial curvature of the accelerator. Figure 6.19b shows a typical two- dimensional representation of the accelerator as a line source of neutrons of variable intensity.

The neutron flux density, ϕ, in n/cm^2 sec, at a point outside the shield and greater than some energy E_{min}, is now expressed as

$$\phi = \int_{-\infty}^{\infty} \int_{E_{min}}^{E_{max}} S(z)\ f(E,\theta) r^{-2}$$

$$X \exp[-d\,\text{cosec}\,\theta/\lambda\,(E)]\ B(E,\theta)\ dE dz, \qquad (6.47)$$

where d,r, and θ are explained by Fig. 6.19b.

$S(z)dz$ is the number of neutrons emitted in unit time by the line element between z and z+dz,

$f(E,\theta)$ is the distribution of the neutrons emitted as a function of the energy and the angle, per steradian,

and the symbols have previously been explained. Using the Moyer approximations leads to

$$\lambda(E) = \lambda$$

$$\int_{E_{min}}^{E_{max}} B(E,\theta)dE \approx g(\theta),$$

and Eq. 6.47 becomes

$$\phi(E_n > 150\ \text{MeV}) = \int_{-\infty}^{+\infty} S(z)\, g(\theta) r^{-2} \exp(-d \operatorname{cosec} \theta/\lambda)dz. \quad (6.48)$$

The integral is evaluated over the appropriate limits of z.

For more general use the geometrical configurations of different accelerators need to be considered, together with the variation of buildup factors and angular distributions with proton energy.

During the past ten years several carefully designed experiments have been performed; they merit discussion in some detail, since they resulted in an understanding of the physical phenomena of importance to shield design at all energies. As shielding experiments progressed through the decade they became more sophisticated in design and ambitious in scope. Development of understanding reveals the sources of confusion in earlier radiation studies. Later in the decade, measurements of attenuation length were in good agreement with those predicted; particle spectra were measured and their conversion to dose rate studied. In consequence particle accelerator shields may now be designed to give an accuracy within about a factor of two in radiation field at the shield surface.

CERN SHIELDING EXPERIMENTS, 1960-1963

Increasing pressure, from groups actively engaged in accelerator design or construction, for a resolution of the early uncertainties discussed above led to the performance of a series of shielding experiments at the CERN PS during the period 1960-1963 (CIT A 61, HOF L 63, THO R 63). It had become clear that two alternative approaches to solving the problem of scattering out were possible. First was to use a very wide incident particle beam with large angular divergences and assume that "scattering in" and "scattering out" were balanced. The second approach was to use a narrow, parallel incident beam and to count all the particles reaching a given depth in

the absorber, either by using a large detector or by making particle-density profile scans. The latter alternative was adopted in the CERN experiments, primarily because a narrow beam was more readily available, but also because inherently more information is available from such an experiment.

The four series of experiments carried out at CERN in the period 1960-1963 are summarized in Table 6.X.

Table 6.X. CERN shielding experiment, 1960-1963.

Experiment	Date	Incident proton energy (GeV)	Absorber density (g/cm^3)	Beam size[a]	Neutron contamination of primary beam	Attenuation length (g/cm^2)
1	1960	20-24	Concrete $\rho = 2.5, 3.6$ Earth $\rho = 2$	H: 25 cm[b] V: 8 cm[c]	48±5%	145±10
2	1960	20	Concrete $\rho = 3.6$	H: 1.7 cm V: 6.2cm	29±4%	132±5
3	1962	10	Concrete $\rho = 3.6$	H: 6 cm V: very wide	20±3%	164±20
4(a)	1962	10	Steel $\rho = 7.8$	H: 1 cm V: 1 cm	25±5%	119±20
4(B)		20			10±3%	137±10

a. Width at half intensity.

b. H means horizontal.

c. V means vertical.

Ilford G.5 nuclear emulsions were the principal detectors used throughout the entire CERN series of experiments. Scanning was carried out for both minimum-ionizing tracks and stars, providing the possibility of discriminating between nuclear active particles and muons at large depths in the shield.

The final experiment in steel with 10- and 20-GeV/c protons (whose design is shown in Fig. 6.20) incorporated all the experience gleaned from its predecessors (GEI J 65). Neutron contamination of the primary proton beam was reduced by large bending of the secondary proton beam scattered from an internal target in the accelerator. Beam size (which at incidence was 1.2X1.2 cm) and divergence (±2.1 milliradians) were limited by two collimators in the beam transport system. Unwanted "halo" around the incident beam and side scattering were reduced by concrete shielding around the steel assembly, which itself was sufficiently large in comparison with the beam dimensions to be regarded essentially as an infinite steel slab. Cavities in the steel, in which detectors were placed, were made as small as possible to reduce any perturbation of the nuclear cascade. Although not entirely successful in achieving

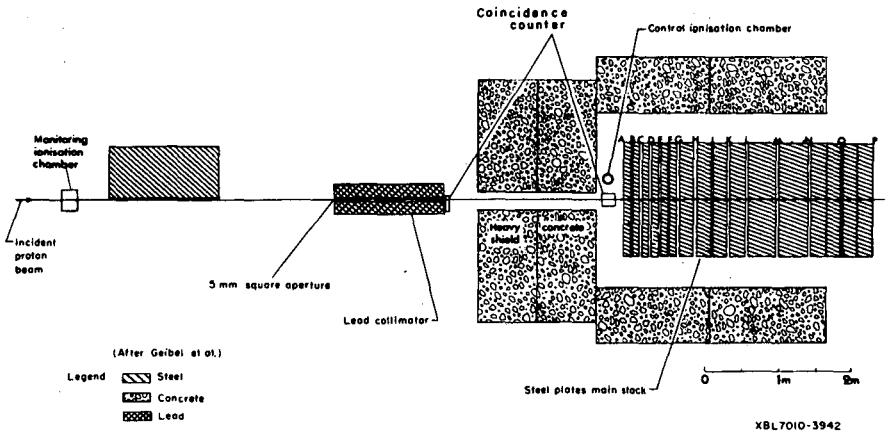

Fig. 6.20. Detailed experimental layout of CERN shielding experiment in steel. (After Geibel et al.)

all these goals, this final experiment in steel represented a great step forward in the design of shielding experiments and went a long way toward eliminating many of the extraneous factors that had influenced previous experiments and made their interpretation difficult.

Since the measurements in steel are the most accurate of the series, we describe in detail the results obtained. Figure 6.21 shows typical beam-profile scans as a function of depth in steel, made with protons of incident momentum 10 GeV/c (CHI R 65). Similar results were obtained at 20 GeV (CIT A 65); they are summarized in Fig. 6.22, which shows the full width at half intensity of such lateral distributions obtained from both track and star scanning. The linear increase in particle distribution with penetration is a qualitative indication that Moyer's concept of "ray tracing" high-energy particles through the absorber, described in the preceding section, is realistic. From such profiles the total number of particles crossing a plane perpendicular to the beam direction may be obtained by integration. Figure 6.23 shows such an integrated track intensity compared with the track intensity on the beam axis measured at 10 GeV/c. The slope of the peak intensity curve obtained was 119±5 G/cm^2, compared with an estimate of 165 (±30%) g/cm^2 for the slope of integrated intensity. The difference between these two estimates of slope gives an indication of the influence of geometry on the results of attenuation measurements, and—in large measure—explains the wide range reported in the literature. Although at 10 GeV/c no buildup on beam axis for either stars or tracks was observed in steel, at 20 GeV/c some small buildup was measured (CIT A 65). Integration of star and track profiles gave an asymptotic relaxation length of 185±20 g/cm^2. Figure 6.24 shows star densities measured on and parallel to the beam axis (as a function of depth) (CIT A 65) at 20 GeV/c. The difficulty in defining a unique relaxation length is clearly demonstrated!

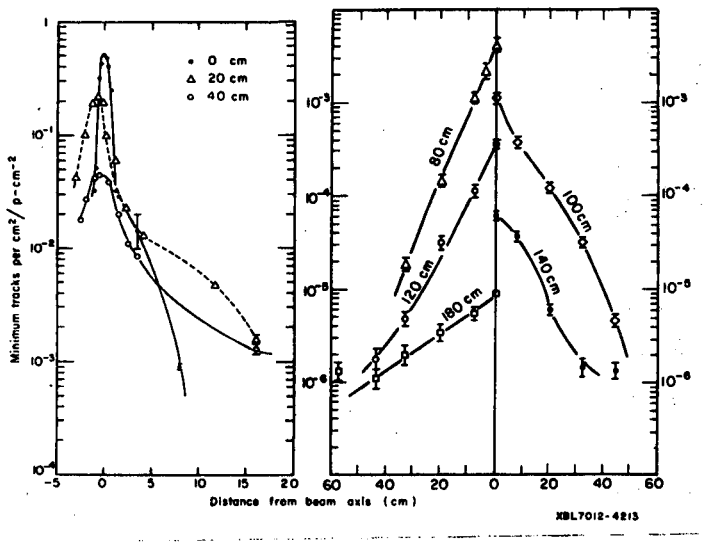

Fig. 6.21 a, b. Typical horizontal scans at beam height in steel as a function of depth (incident proton momentum 10 GeV/c). (After Childers et al.)

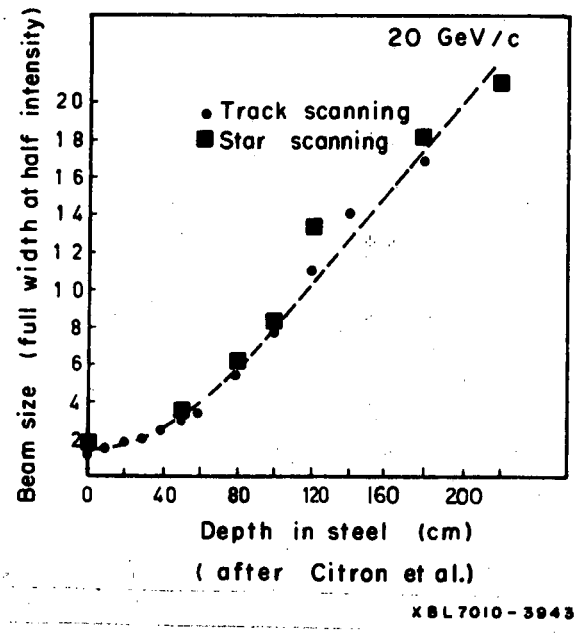

Fig. 6.22. Increase in width of high-energy particle distribution in steel. Incident proton momentum 20 GeV/c. (After Citron et al.)

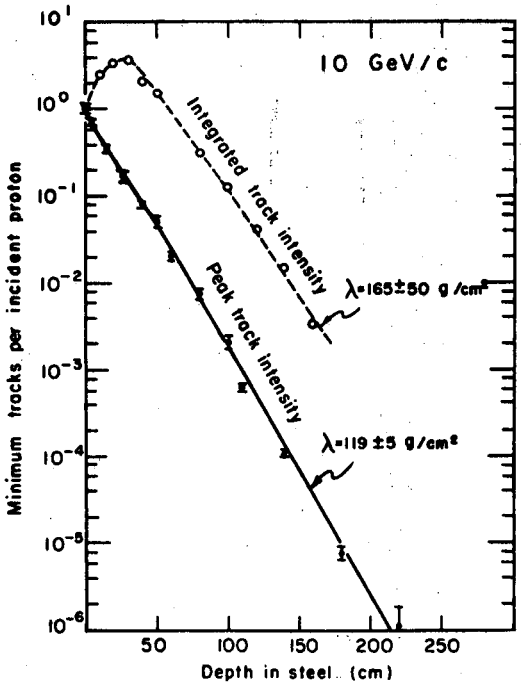

Fig. 6.23. Maximum and integrated track intensity as a function of depth in steel. Incident proton momentum 10 GeV/c. (After Childers et al.)

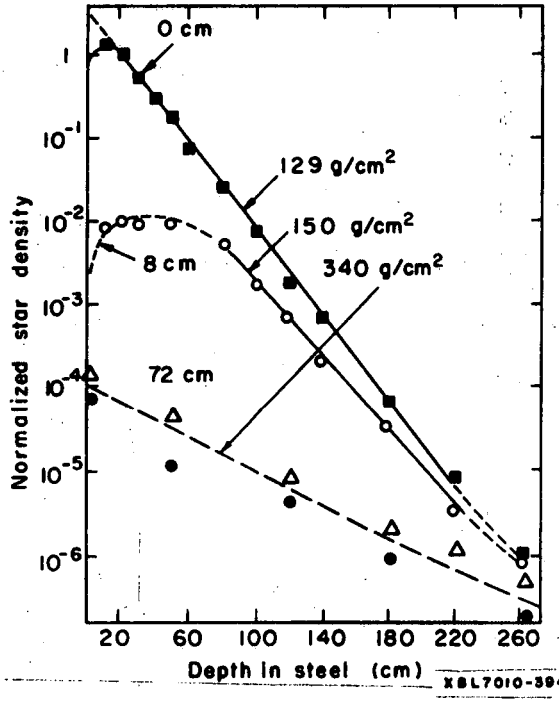

Fig. 6.24. Variation of star density as a function of depth in steel measured along the beam axis and along parallel lines 8 cm and 72 cm from the axis. Incident proton momentum 20 GeV/c. (After Citron et al.)

The use of nuclear emulsion permitted visual inspection of stars and hence a rough determination of whether they were produced by an uncharged or charged incident particle. Figure 6.25 shows the fraction of stars with no charged primary (judged by the absence of a minimum-ionizing particle in the backward hemisphere) measured for 20-GeV/c primary protons. The increasing fraction of stars created by neutrons is clearly seen; its steady increase probably indicates that an equilibrium ratio of high energy protons to neutrons has not been completely established. Measurements at 10 GeV/c indicate a somewhat more rapid approach to equilibrium (CHI R 65).

Measurement of the average multiplicity of minimum-ionizing particles emitted from stars gives a rough indication of the average energy of the incident particles. Figure 6.26 shows that the average shower track number, n_s, of stars produced by the interaction of charged primaries decreases rapidly with penetration into the steel. Thus at a depth of 100 cm in steel, n_s is about 2.6 corresponding to an average energy of 6 GeV. The energy loss of 20-GeV protons in 100 cm of steel is about 1.6 GeV, therefore at this depth the uninteracted primary proton beam would have an energy of 18.4 GeV. This difference of about 12 GeV is of course due to energy transfer by nuclear interaction and indicates that the charged particles initiating the stars deep in the steel have themselves originated from nuclear interactions.

In addition to nuclear emulsion, carbon threshold detectors and ionization chambers were used. Although limited by sensitivity and large detector size, these measurements confirmed a relaxation length of about 160 g/cm^2, both for absorbed dose and for particles greater than 20 MeV. Because of the large detector size relative to the beam, information of particle buildup is limited, but Baarli et al. (BAA J 65) estimate a total of nine particles of greater than 20 MeV produced by an incoming 20-GeV proton, which they consider to be in good agreement with the value of nine cascade nucleons per inelastic interaction at 3 GeV listed by Lindenbaum (LIN S 65). It is not completely clear, however, to what extent charged pions were detected in the experiment by Baarli et al.

Two groups have attempted to compare the experimental data obtained in the CERN series of shielding measurements.

The earlier experiments have been studied by Alsmiller et al. (ALS R 62, ALS R 63a, ALS R 63b), who solved the coupled cascade transport equations in "straight-ahead" approximation and applied these results to the calculation of the components of a cascade generated in heavy concrete by 24-GeV protons (ALS R 63a). Comparison of these calculations with the measurements at 20 and 24 GeV reported by Citron et al. (CIT A 61) is difficult for several reasons. Citron et al. measured the nuclear star density on beam axis, whereas the one-dimensional Oak Ridge calculations should be compared to an integration over a plane transverse to the beam direction. Furthermore, the effective energy threshold of a star is somewhat ambiguous,

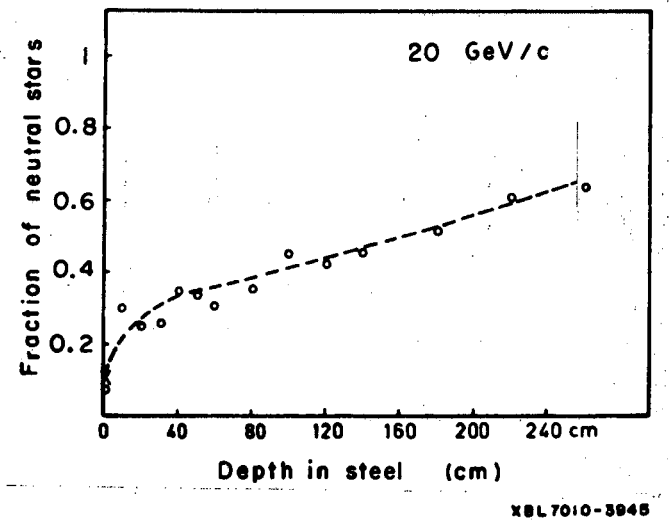

Fig. 6.25. Fraction of "neutral" stars (i.e., with no charged primary in the backward hemisphere) as a function of depth in steel. Incident proton momentum 20 GeV/c. (After Citron et al.)

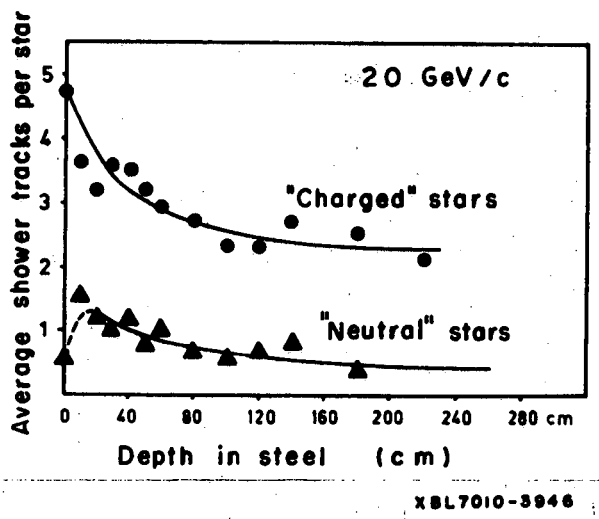

Fig. 6.26. Average number of shower (minimum ionizing) tracks emitted per star as a function of depth in steel. Incident proton momentum 20 GeV/c. (After Citron et al.)

depending upon scanning technique and efficiency, but is of the order of 100 MeV. Figure 6.27 shows a comparison between measured star density in the broad- and narrow-beam experiments and the calculated values for different production energy thresholds. The measured star densities are attenuated more rapidly than the calculations predict, as expected. Figure 6.28 compares the measured and calculated fractions of all stars produced by neutrons. Neutron contamination of the beam influences the experimental results.

Geibel and Ranft (GEI J 65a) used a Monte Carlo method to estimate the three-dimensional development of the nuclear cascade induced in steel, and obtained good agreement with the experimental data reported by Citron et al. (CIT A 65) and Childers et al. (CHI R 65). These early calculations were, however, limited by the secondary-particle production input data. Ranft (RAN J 67a) has now improved these data and repeated the calculations more precisely with improved secondary-particle production information. Figures 6.29 and 6.30 show typical results obtained, indicating excellent agreement. Unfortunately, good as this agreement is, neither experimental nor theoretical techniques have yet reached the stage where direct overlap is possible. Numerical solutions of the coupled cascade transport equations in straight-ahead approximation, although accurate at high energies became less and less reliable at low energies. Similarly, particle-production information adequate for input into Monte Carlo calculations is not yet available, and the results of such computations become increasingly suspect at lower secondary particle energies.

BERKELEY SHIELDING EXPERIMENT, 1964

The beam intensity available for the CERN experiments was limited to $\approx 10^5$ protons/sec. Measurements with nuclear emulsions were made down to relative transmissions of between 10^{-5} and 10^{-6}, but measurements with activation detectors and ionization chambers were limited to relative transmission of only 10^{-3}. Since secondary particles below 50 MeV in general produce the largest components to the dose equivalent outside shielding (THO R 67), it is necessary to study their production and transmission through thick shields.

The development of an extracted proton beam of much higher intensity at the Bevatron made it possible to design an experiment to fill in some of the unresolved details in the CERN series of experiments.

In 1964 an experiment was mounted at the Bevatron that used a 6.2-GeV proton beam of maximum intensity 10^{11} protons/sec. At the front face of the experimental array of concrete blocks the beam spot was circular and approximately 5 cm in diam. The high incident beam intensity permitted measurements by several threshold detectors to depths of 24 ft in ordinary concrete (1760 g/cm^2), or transmission of $\approx 10^{-6}$.

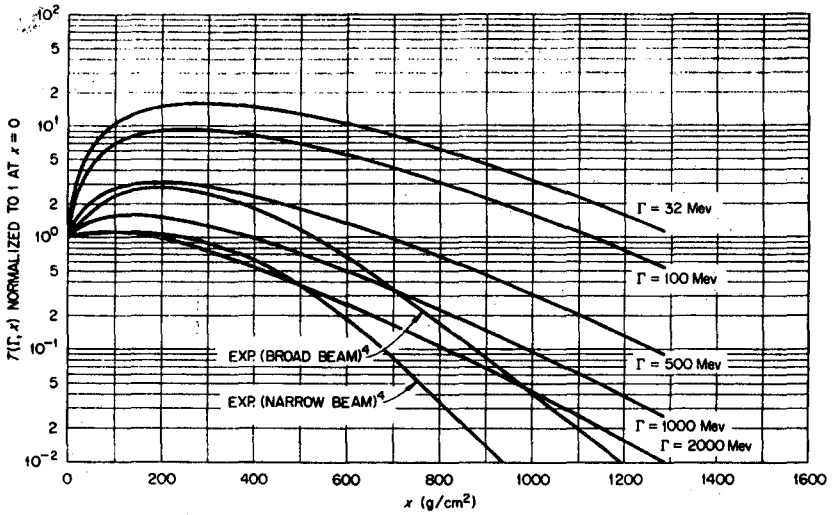

Fig. 6.27. Comparison of star densities calculated by a "straight-ahead" model with experimental data in concrete. Incident proton energy 24 GeV. (After Alsmiller and Murphy.)

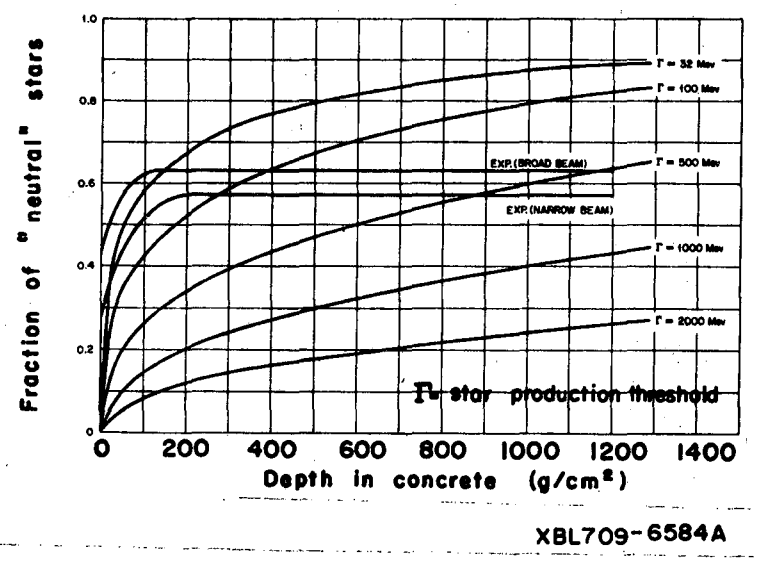

Fig. 6.28. The fraction of stars produced by neutrons as a function of depth in concrete—a comparison between experimental and calculated data. Incident proton energy 24 GeV. (After Alsmiller and Murphy.)

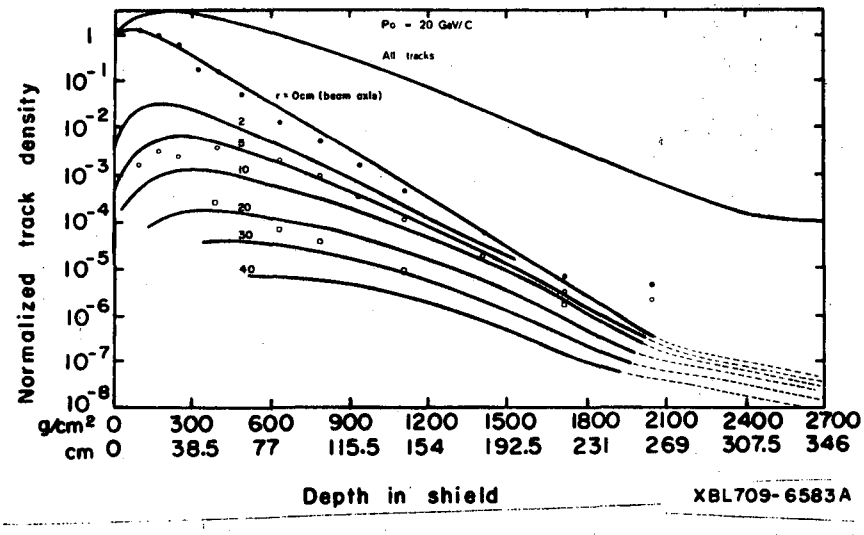

Fig. 6.29. The longitudinal development of the nuclear cascade—a comparison between experimental and calculated data. The curves show the calculated total track density (sum of proton, pion, and muon track densities) for a cascade initiated by a well-collimated proton beam of cross section 1 X 1 cm and initial momentum 20 GeV/c. The curves are normalized to unit proton track density at r = 0. Z = 0. The points represent the track densities measured along the beam axis (r = 0) (●) and at distances from the axis of 8 (o) and 32 cm (□). By Citron et al. The change in slope of the curves near a depth of z = 2000 g/cm² arises from the muon track density. (After Ranft.)

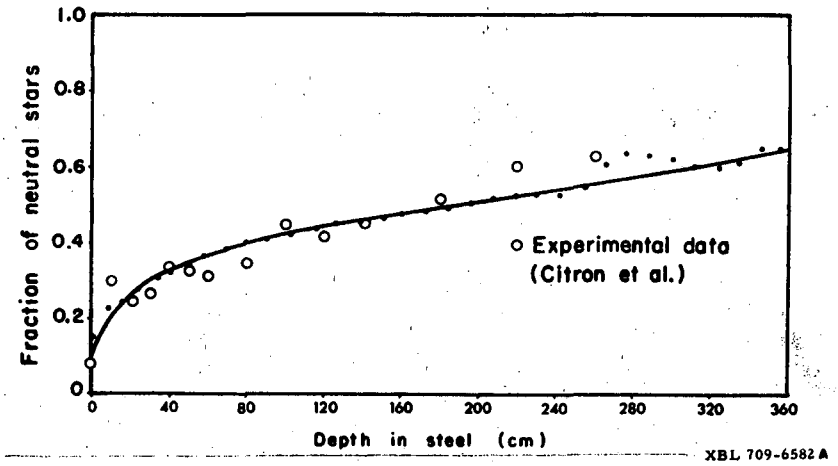

Fig. 6.30. Fraction of neutral stars as a function of depth in steel—comparison between calculated and measured values. Incident proton momentum 20 GeV/c. (After Ranft.)

Figure 6.31 shows a general view of the shielding array and gives an impression of the size of the structure, which was designed to be large enough to prevent interference from stray radiation scattered in from the sides. The assembly consisted of ordinary concrete in block form, and was 24 ft thick along the beam direction, 22 ft wide, and 18 ft high. Several special thin blocks were placed at the front of the array (not visible in Fig. 6.31); deeper in the stack, slots provide access to the beam line at intervals of 4 feet. Rows of blocks were separated by 3-in.-wide gaps to allow insertion of detectors, but all portions of these gaps are filled with gypsum (approximately the same density as concrete) to prevent neutron diffusion along the slots.

Two principal goals were set for the experiment. The first was to extend the information obtained at CERN to neutrons of much lower energy. This was achieved by the use of various activation detectors with thresholds between 3 and 20 MeV. Secondly, the experiment was designed to test in a systematic way some of the predictions of the "Moyer Model." This phenomenological model had met with some success in extrapolating shielding for the Bevatron, and it will be recalled that it might usefully be generalized. Since the Moyer model posits that the transmission of the nuclear cascade is controlled by high-energy neutrons and that an equilibrium cascade is rapidly created, measurements of low-energy neutrons forms a sensitive test of the model.

Details of the experimental data obtained have been given by Smith, McCaslin, and Pick (SMI A 64) and Smith (SMI A 65), who described data obtained with activation detectors, and by Thomas (THO R 64), who described data obtained by using nuclear emulsions and measurements of the activity induced in sulfur measured by Shaw (SHA K 64) of the Rutherford Laboratory.

Figure 6.32 shows typical lateral flux-density profiles measured in the assembly—in this case by using the 6-MeV threshold reaction $^{24}Al(n,\alpha)\,^{24}Na$. Similar data were obtained for thermal neutrons and by using the $^{32}S(n,p)\,^{32}P$ and $^{12}C(n,2n)\,^{11}C$ reactions. From such traverses, the transmission of flux density from the front of the shield assembly, at a given angle to beam direction, was obtained. Figure 6.33 shows such data for the Al activation detector for angles up to 60 deg. These transmission curves are seen to be exponential and essentially parallel within the experimental accuracy. (The errors were no larger than point size indicated.) Similar results were obtained with ^{12}C threshold detectors.

Figure 6.34 shows transmission measurements along the beam direction made with gold, aluminum, and carbon detectors. A steady progression in slopes of the transmission curves is eveident—the slopes tend to become similar at great depths but the curves are not identical. The data have been normalized at a depth of 8 ft in the assembly to show this effect clearly. At deep depths the carbon detector gives an effective attenuation length of

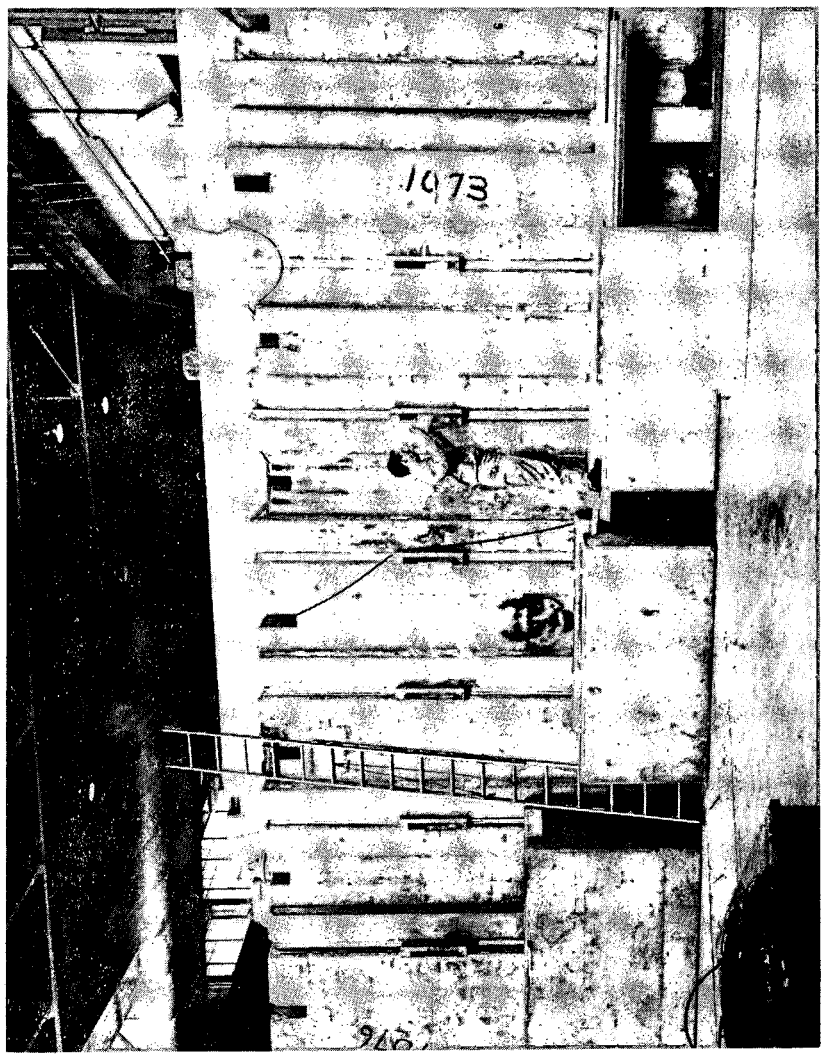

Fig. 6.31. Shielding experiment at the Bevatron. The proton beam is incident from the left. Radiation detectors are being placed in position.

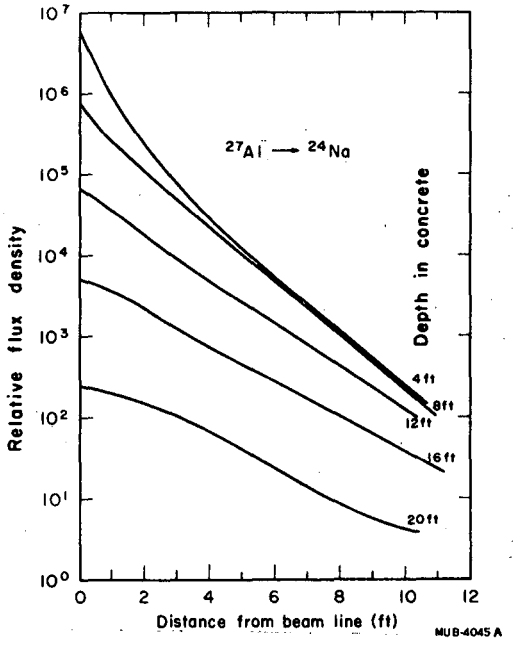

Fig. 6.32. Relative flux-density distributions normal to the incident beam direction measured in concrete by using the $^{27}Al \rightarrow {}^{24}Na$ reaction. Incident proton energy 6 GeV. (After Smith et al.)

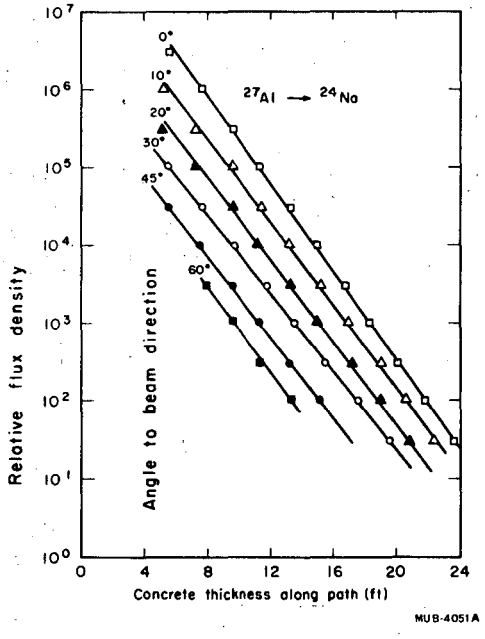

Fig 6.33. Relative flux-density distribution measurements along paths drawn at several angles to the point of incidence of the proton beam on the concrete shield. Measurements made with the ^{27}Al $^{27}Al \rightarrow {}^{24}Na$ reaction. Incident proton energy 6 GeV. (after Smith et al.)

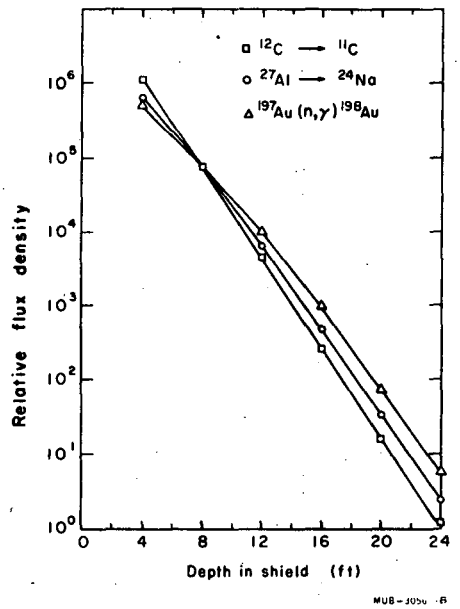

Fig. 6.34. Relative flux density along beam axis. Measurements made with $^{197}Au\ (n,\gamma)\ ^{198}Au$, $^{27}Au \rightarrow {}^{24}Na$, and $^{12}C \rightarrow {}^{11}C$ reactions. Data normalized at a depth of 8 ft in concrete. Incident proton energy 6 GeV. (After Smith et al.)

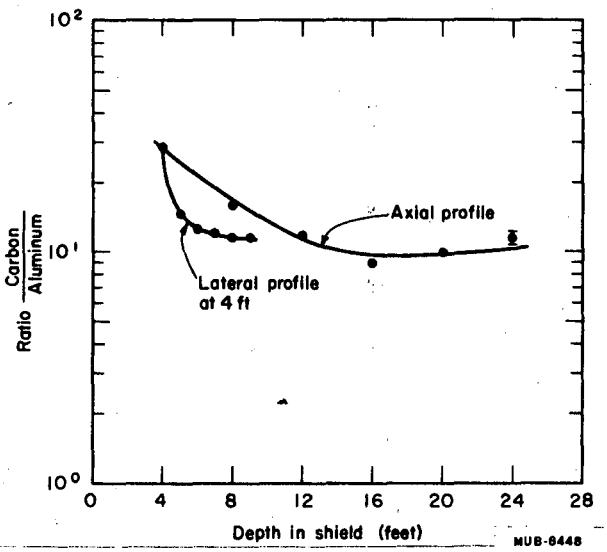

Fig. 6.35. Typical example of the ratio of detector response as a function of distance from the point of incidence to the proton beam on the shield. The curve labeled "axial profile" was obtained in the beam direction; that labeled "lateral profile" was obtained at a depth of 4 ft into the shield in a direction normal to the beam direction. Incident proton energy 6 GeV. (After Smith).

108 g/cm^2; the Al and Au detectors give 114 and 120 g/cm^2 respectively. Smith interprets this result as evidence that complete equilibrium is not established until rather deep depths in the concrete are reached—say, 12 to 16 ft. In support of this view Fig. 6.35 shows that the ratio of activity measured by carbon and aluminum detectors becomes constant at deep depths in the beam direction. In the transverse direction, however, equilibrium is more rapidly attained. In further support of his hypothesis that equilibrium is not reached at shallow depths, Smith reports measurements made with the same detector but with varying initial proton energy—between 2.2 and 6.2 GeV. The lower the primary beam energy, the lower the apparent attenuation length, values ranging from 99 to 114 g/cm^2 being obtained (see Fig. 6.36).

Unfortunately the data obtained in this experiment were not numerically analyzed by a technique similar to that described by Gilbert et al. (GIL W 68). The successful use of the Moyer model in interpreting the latter experiment may now encourage this step. It is clear, however, that the data give strong support for the basic premises of the Moyer model, namely:

1. The transmission of particle fluxes with an attenuation length independent of angle to the radiation source, and
2. the establishment of an equilibrium spectrum at sufficiently deep depths in the shield.

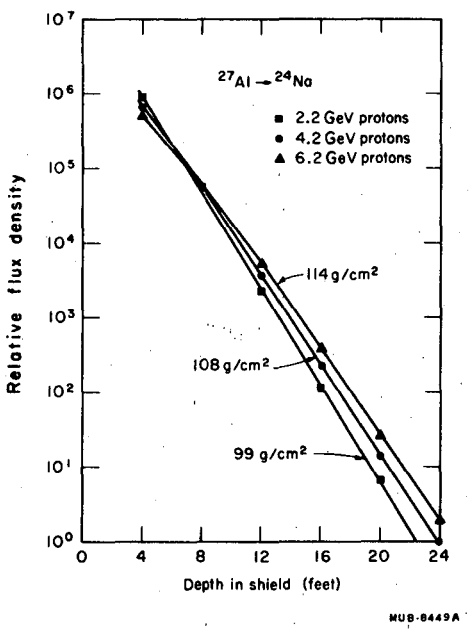

Fig. 6.36. Flux-density transmission along the beam axis measured by aluminum threshold detectors for protons of 2.2, 4.2, and 6.2 GeV. (After Smith.)

BROOKHAVEN AGS EXPERIMENT, 1965

Significant though the CERN and Berkeley experiments were in the development of our understanding of the nuclear cascade, they left many questions unanswered. They were primarily concerned with the development of the nuclear cascade in the forward direction; but in the design of the permanent shielding of a large high-energy accelerator, knowledge of the transverse development of the nuclear cascade is also needed as well as the spectrum of radiation field produced.

In planning for an increase in intensity of the Brookhaven AGS, measurements of particle attenuation transverse to the beam in both the accelerator room and the shield were made. Circulating 30-GeV protons struck an internal Be target, and readiation measurements were made by activation detectors and photographic film. In the accelerator room, flux densities were measured around the beam axis downstream from the target, giving the isoflux contours shown in Fig. 6.37. The approximately cylindrical nature of these contours (FRI W 65) led Moore (MOO W 66) to interpret the flux density from the target by the equation

$$\phi(r,\theta) = \frac{k}{r^2\theta^2} \quad \text{for } 20 \text{ deg} \leqslant \theta \leqslant 90 \text{ deg}, \tag{6.52}$$

where $\phi(r,\theta)$ is the flux density of particles greater than 20 MeV,

r is the distance from the target,

and θ is the angle from the beam direction.

With r measured in feet and θ in degrees, Moore found a value of k of 1.5 per circulating 30-GeV proton. In commenting upon the $1/\theta^2$ from the angular distribution, Moore drew attention to the similar result reported by Hoffman and Sullivan (HOF L 65) of measurement around a thin beryllium target. More recent angular distribution measurements by Charalambus et al. (CHA S 67) at 20 GeV and by Gilbert et al. (GIL W 68) at 15 and 25 GeV show the suggested $1/\theta^2$ form to be a fair approximation. From Eq. 6.52 Moore deduces that 24 particles having energy greater than 20 MeV are produced per 30-GeV proton incident upon a Be target.

To study the transmission of radiation through the AGS shielding, vertical holes were drilled through the sand above accelerator magnets and in the side shielding. These holes allowed measurements to be made through 10 feet of sand vertically above the accelerator and through 20 feet of sand to the side.

Typical transmission data obtained vertically above the accelerator are shown in Fig. 6.38 (CAS N 67). Over a limited range possible (≈ 50 in attenuation) the relaxation length of flux density was evaluated to be 83 g/cm^2. Toextend data to greater depth, measurements were made in the median plane, and typical results are shown in Fig. 6.39. The strong influence of

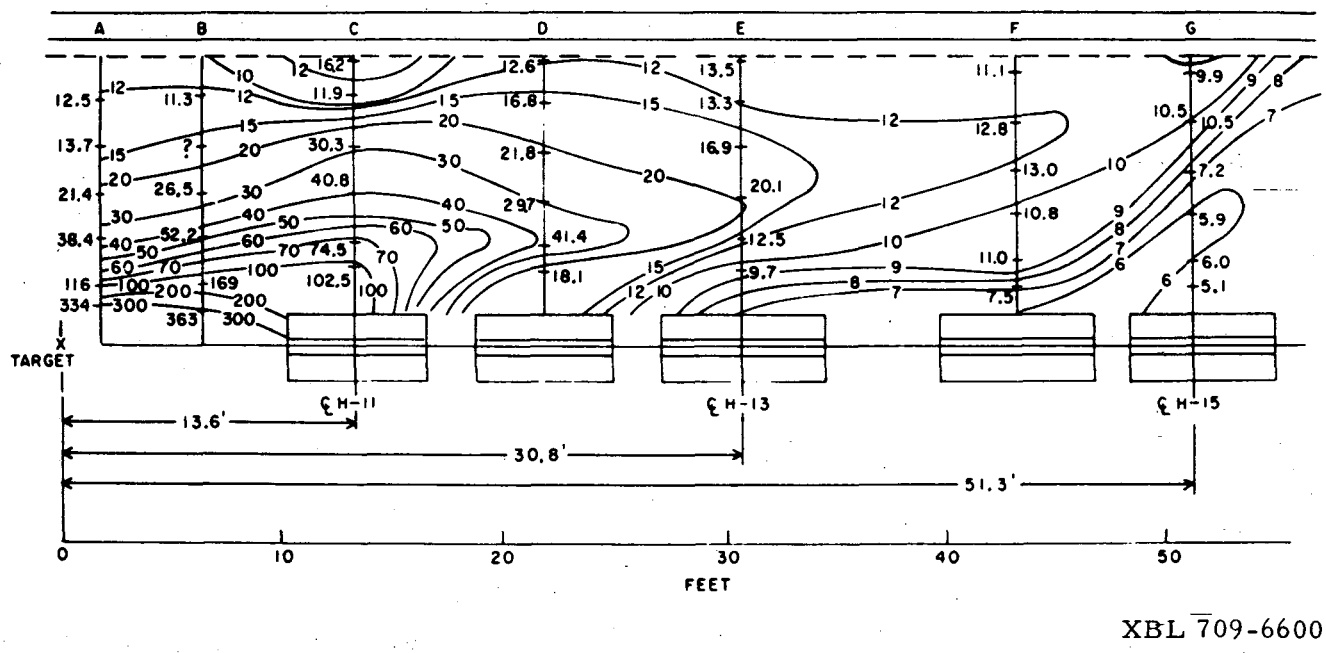

Fig. 6.37. Flux-density distribution in the AGS accelerator tunnel around an internal target. Measurements made with polyethylene foils and 2.78 X 10^{11} protons incident upon a thin Be target. The relative accuracy of contours is ≈ 10%. (After Casey et al.)

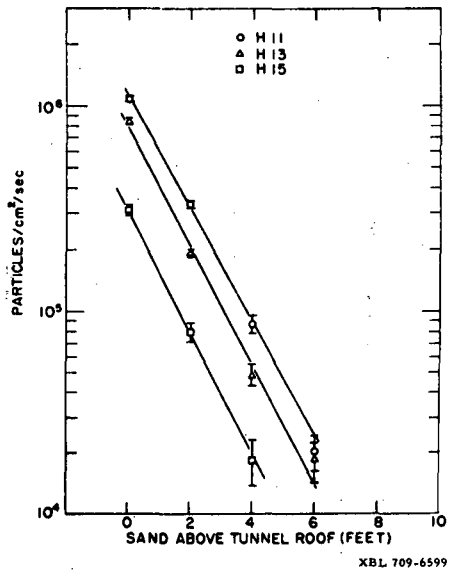

Fig. 6.38. Variation of flux density in sand shield of the AGS. Measurement with carbon activation detectors. Beam intensity 2.8 X 10^{11} protons/sec on target in straight section H 10. Measurements made in vertical direction at mid-magnet positions H 11, H 13, and H 15. (After Casey et al.)

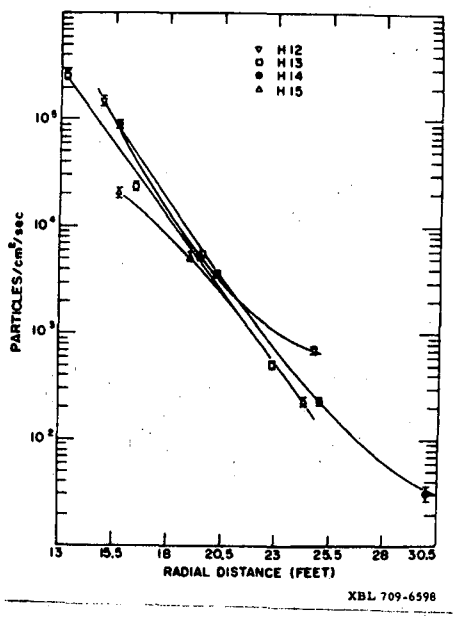

Fig. 6.39. Variation of flux density in sand shield of the AGS—horizontal direction. Other conditions as for Fig. 6.38. Measurements made at mid-magnet positions H 12, H 13, H 14, and H 15. (After Casey et al.)

geometrical factors on the data is clearly seen, making a simple interpretation difficult. Casey et al. (CAS N 67) summarize their results by an exponential transmission of flux density (or dose rate) with relaxation length 83 g/cm^2 (using a measured value of 1.82 g/cm^3 for the density of earth). They suggest, however, that the exponential character is fortuitous, resulting from a special combination of geometry, angular distribution of secondaries from the target, and change in interaction length at various inclinations to the beam direction

O'Brien and McLaughlin (O'BR K 68a, O'BR 68 b) have applied polynomial neutron transport theory (DAVB 58) to neutrons of 500 MeV and below, generated in a nuclear cascade, and compared their calculations with measurements reported by Distenfeld and Colvett (DIS C 66). Figure 6.40 shows a comparison between calculated and measured attenuation of neutrons having an energy greater than 20 MeV. Agreement between the normalized data is seen to be good.

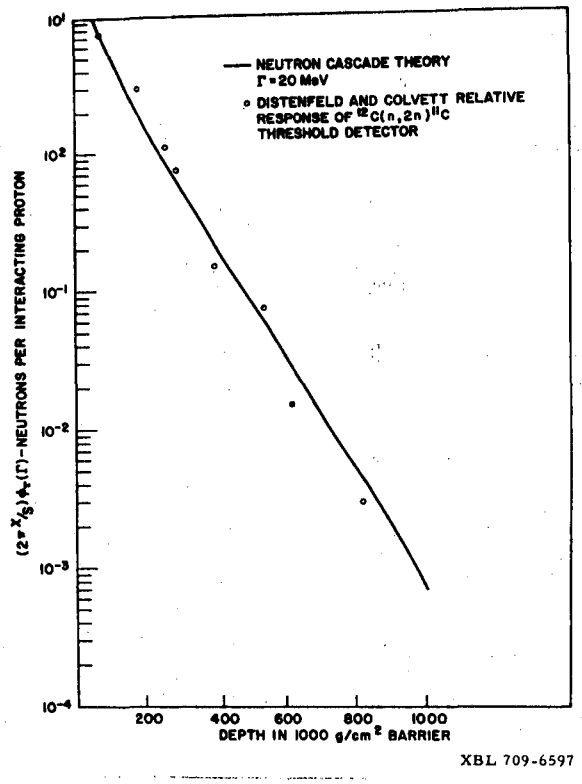

Fig. 6.40. A comparison between calculated and measured relative neutron transmission through the sand shield of the Brookhaven AGS. (After O'Brien and McLaughlin.)

Although these techniques have been successful in describing relative neutron transmission through accelerator shields, it has not yet been possible to make an absolute comparison of theoretically predicted and measured neutron flux densities. Recent calculations of neutron dose-equivalent rates from galactic cosmic rays by such techniques has revealed only fair agreement with measured values, however (O'BR K 70).

Casey et al. concluded that particle attenuation transverse to the beam direction was much more rapid than would be concluded from calculations based on strongly interacting particle interaction lengths. This suggestion is in conflict with the Moyer model, and was of such interest as to stimulate further studies.

CERN-LRL-RHEL SHIELDING EXPERIMENT, 1966

Following the work at Brookhaven, another experiment was planned at the CERN PS by groups drawn from CERN, the Lawrence Berkeley Laboratory, and the Rutherford Laboratory, all of whom were actively engaged in the design of accelerators in the several-hundred-GeV range. The goals of this experiment, designed to answer many of the questions posed by the Brookhaven measurements, were:

1. Study of the transmission of particles through earth shielding, principally at 90 deg to an internal target in the accelerator.
2. Measurement of neutron spectra at different depths in the earth shield.
3. Measurement of the angular distribution of high energy particles from and internal target.

As at the AGS, vertical holes were drilled in the earth shield above and to the side of the accelerator. Figure 6.41 shows a vertical cross section of the CPS tunnel, indicating hole locations; Fig. 6.42 shows a plan view of the area in which radiation measurements were made in the dhielding.

Extensive discussions of the experimental data obtained have been published (FOR R 67, GIL W 67a, GIL W 67b, GIL W 68, GIL W 69), and it is possible to give only a brief discussion here.

Figure 6.43 shows some details of actual measurements of beam losses made with aluminum foils on the accelerator vacuum chamber close to an internal target. Fine structure due to the presence of accelerator magnets may be seen. Subsequent analysis of these data showed the beam-loss distribution about the target to be sufficiently accurately represented by a base level, a, representing the average low-level losses on which is superposed a target contribution that decreased in intensity downstream from the target. Thus the beam loss s(z) may be represented by

$$s(z) = a \qquad \text{for } z < 0, \qquad (6.48)$$

$$s(z) = a(1 + \beta e^{-z/\mu}) \qquad \text{for } z > 0, \qquad (6.48a)$$

where z is measured from the target position.

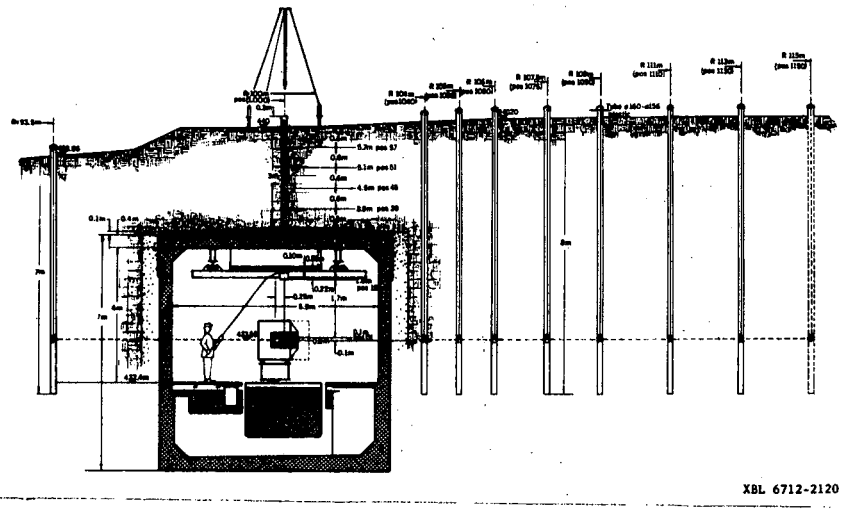

Fig. 6.41. Vertical cross section of the 25-GeV CERN proton synchrotron tunnel, showing the disposition of detector holeds in the earth shield. (After Gilbert et al.)

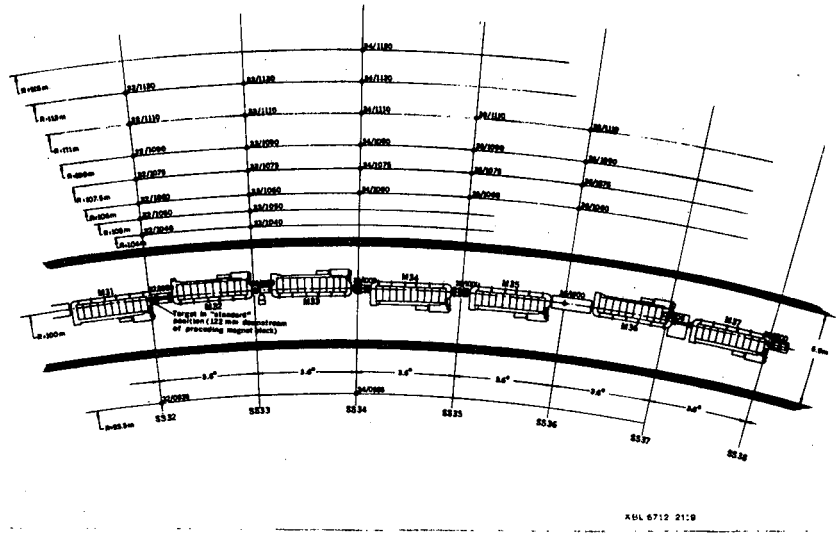

Fig. 6.42. Plan view of the CPS, showing the disposition of detector holes in the earth shield. (After Gilbert et al.)

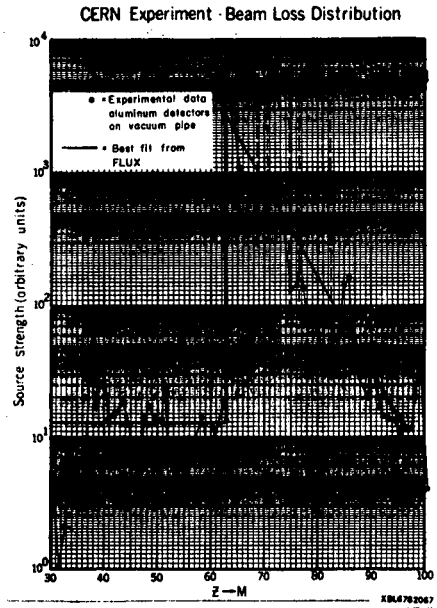

Fig. 6.43. Fine-structure details of the beam-loss distribution measured in the vacuum chamber of the CPS close to an internal target. (After Gilbert et al.)

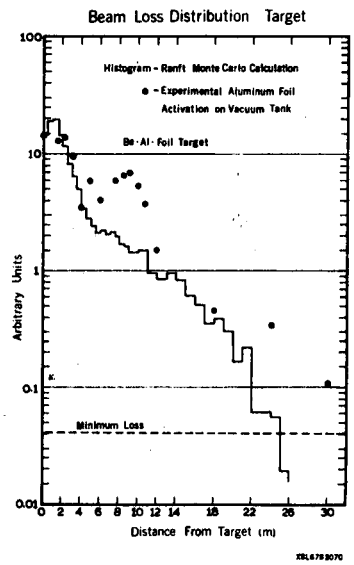

Fig. 6.44. Comparison of measured beam-loss distribution with Monte Carlo calculations due to Ranft. (After Gilbert et al.)

More sophisticated analytical representation of the data (AWS M 68, AWS M 70a) or even use of the actual numerical data, does not produce any significant improvement in the quality of fit to measured fluxes in the earth shield (GIL W 68), and it may therefore be inferred that Eq. (6.53) is an adequate representation of the source term for the CPS. It might quite correctly be objected that the relative activities of aluminum foils (which are sensitive to rather low energy particles) only indirectly reflect the high-energy proton source structure. It would have been preferable to use detectors with a much higher energy threshold, but this was technically not feasible at the time measurements were made. However, measurements with other low energy detectors gave the same results and support the view that no serious error is involved, as also do Monte Carlo estimates of beam loss by Ranft (RAN T 67b) (Fig. 6.42). At large distances from internal targets such a simple prescription as Eq. 6.53 fails at the CPS, the beam loss at levels $\approx$ 1% of the maximum being somewhat random (GIL W 68). The approximately exponential reduction of target contribution to the beam losses with distance from the target that was observed at the CPS will not necessarily be observed at other accelerators. A somewhat different distribution was observed, for example, at the AGS (CAS R 67). The precise details of the beam-loss distribution is of course a complex function of target dimensions, magnet spacing, and physical size, accelerator magnetic field configuration, and other accelerator characteristics. It is nevertheless important to have good estimates of the beam-loss distribution pattern if the distribution of secondary particles through the shield is to be understood. Awschalom (AWS M 70a) has indicated that large errors (as much as a factor of 10) can result in estimates of flux densities if no account is taken of source distribution.

It is important to understand not only spatial distribution of beam losses but also the angular distribution of neutrons emitted from the primary beam interactions.

Figures 6.45 and 6.46 show measurements of the angular distribution of neutrons from a thin Be target made with activation detectors having thresholds of 20 and 600 MeV respectively. A comparison with the angular distribution predicted by Ranft (RAN J 67a) is surprisingly good, giving confidence in Ranft's semi-empirical formula. Routti and Thomas (ROU J 69b) have used Ranft's formula to calculate the angular distribution of protons greater than 150 MeV from a thin Be target, and have shown that the shape of the distribution about 90 deg is nearly independent of primary proton energy between 1 and 300 Gev. For angles around 90 deg, the angular distribution may be expressed (ROU J 69b) by a simple exponential form,

$$\Theta(\theta) = ae^{-\beta\theta} .$$

Figure 6.47 shows a comparison of the function exp(-4θ) with the angular distribution of neutrons of more than 150 MeV produced by 14-GeV protons incident upon beryllium and iron targets. Routti and Thomas (ROU J 69b) conclude such an angular distribution should be used in the estimation of transverse shielding when Eq. 6.51 is used.

Preliminary results of the CERN shielding experiment reported by Gilbert et al. indicated that a simple exponential model of transmission was inadequate, because the attenuation length inferred is a function of the assumed geometry, and also of position relative to the target at which the measurement was made. Figure 6.48 shows the result of expressing identical flux measurements in terms of different geometrical models. Although of high accuracy ($\approx$ 3%), the data are nevertheless inadequate of themselves to permit any objective choice as to the preferred geometrical model. Additional information is therefore required if the relaxation lengths obtained from shielding experiments are to be related to particle-attenuation lengths. The influence of source distribution on relaxation length is indicated in Fib. 6.49, which shows the vertical attenuation of neutron flux as measured with aluminum activation detectors in three locations. Although the experimental data are well fitted by straight lines (exponentials), it is incorrect to assume, without incorporating geometrical effects and the influence of source shape, that the slopes of these lines yield the attenuation mean free path in earth.

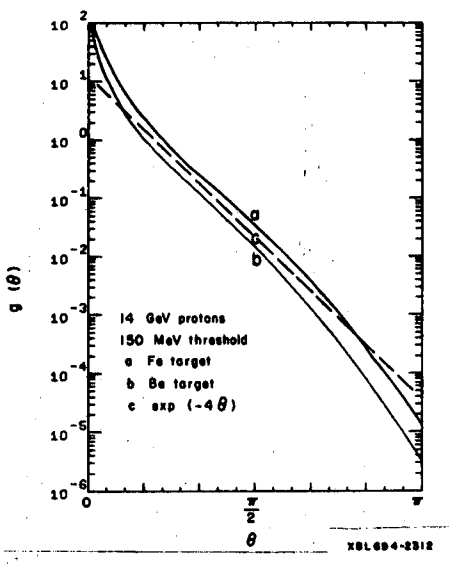

Fig. 6.47. The angular distribution of neutrons above 150 MeV energy produced by 14-GeV protons incident on thin Fe and Be targets, as calculated from Ranft's semiempirical formula. (After Routti and Thomas.)

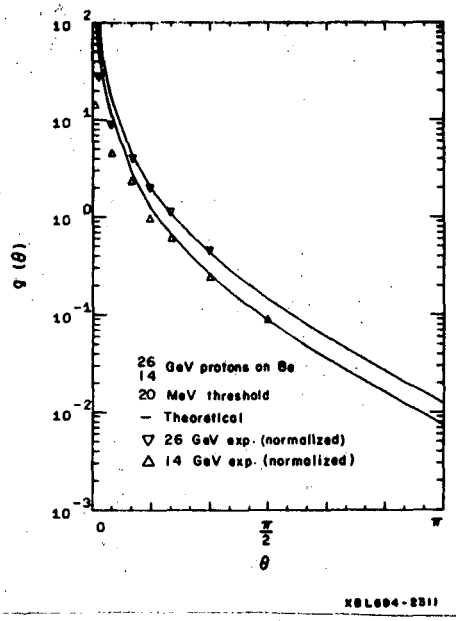

Fig. 6.45. The angular distribution of neutrons above 20 MeV energy produced by 26- and 14-GeV proton beam incident on a thin target, as measured by Gilbert et al., and calculated from Ranft's semiempirical formula. (After Routti and Thomas.)

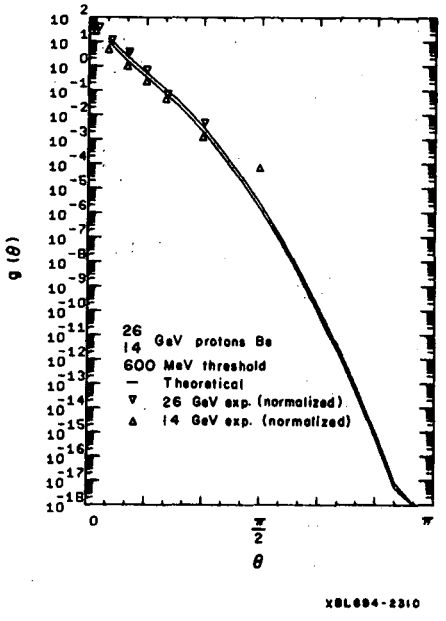

Fig. 6.46. The angular distribution of neutrons above 600 MeV energy produced by 26- and 14-GeV proton beam incident on a thin target, as measured by Gilbert et al., and calculated from Ranft's semiempirical formula. (After Routti and Thomas.)

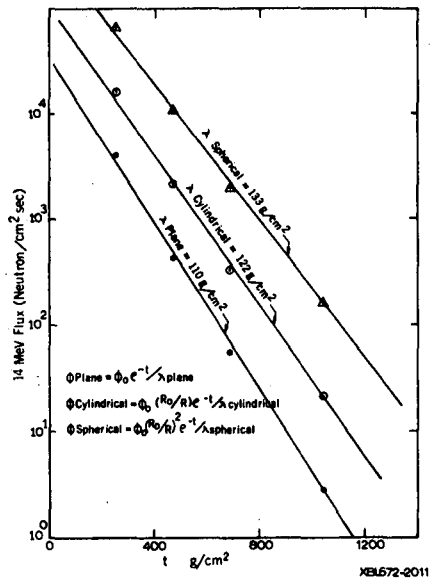

Fig. 6.48. The influence of geometrical models on apparent attenuation length. (After Gilbert et al.)

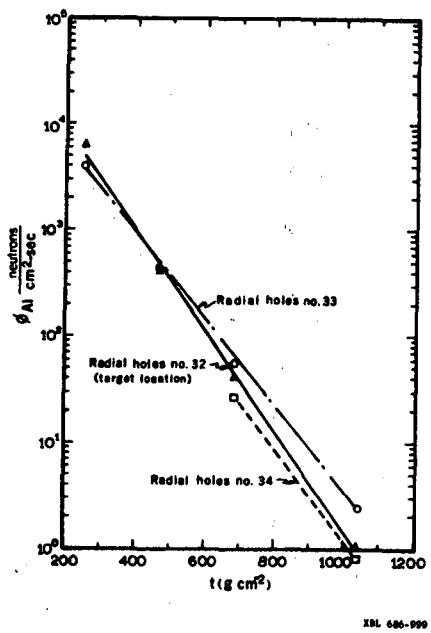

Fig. 6.49. The influence of source distribution on relaxation length (From Gilbert et al.)

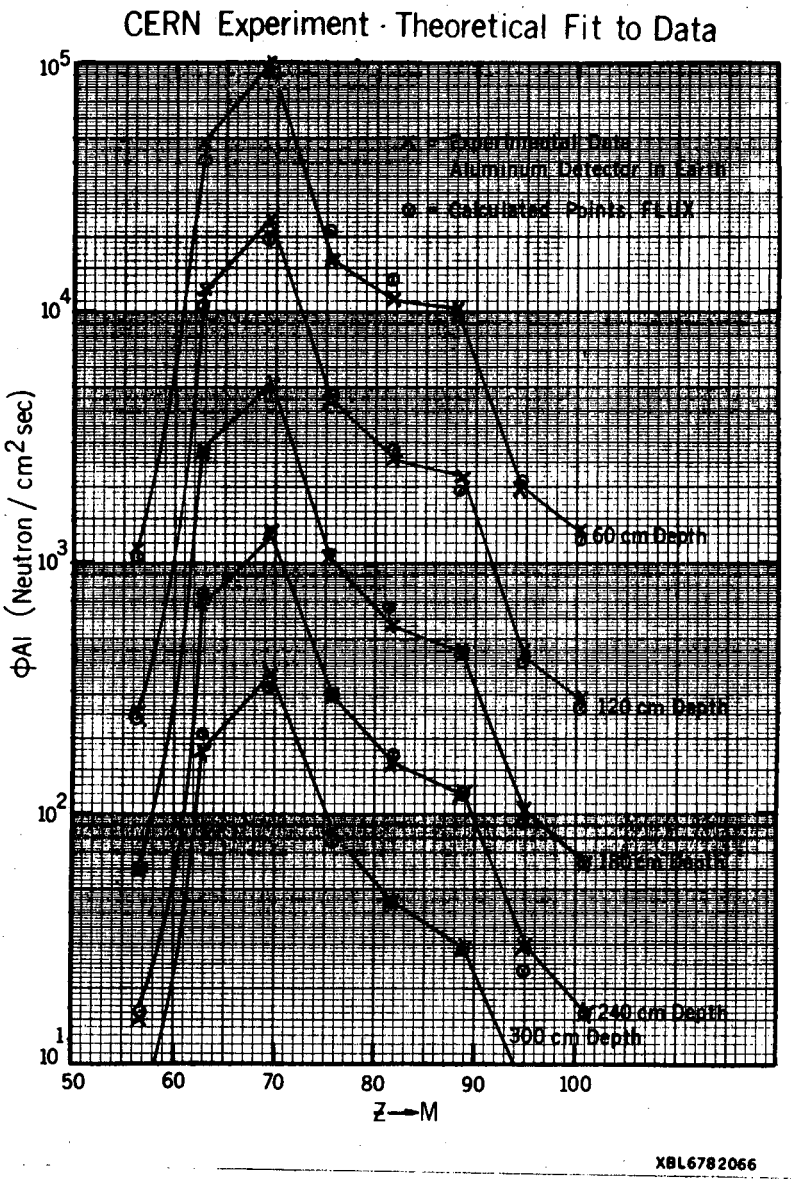

Fig. 6.50. Examples of typical fits to experimental data obtained at CERN when FLUXFT is used. (After Gilbert et al.)

Because the CERN experimental data in the earth shield were so extensive, analysis was attempted in terms of the simple phenomenological model first derived by Moyer. The flux at a point in the shield was written as

$$\phi_p = \int S(z)\,\Theta(\theta)\,e^{-x/\lambda}\,d\Omega\,dz\,, \qquad (6.49)$$

where $S(z)$ is the number of protons interacting in a line element dz,
$\Theta(\theta)$ is the angular distribution of particles at the target,
x is the total shield thickness traversed,
λ is the attenuation length.

The practical problem of analysis consisted of two parts—the first of defining realistic physical functions for $S(z)$ and $\Theta(\theta)$ (appropriate functional forms have already been discussed), and the second of obtaining the "best fit values" for the parameters of the functions.

A computer program—FLUXFT—developed by Close (CLO E 67), incorporates an appropriate geometry subroutine and a minimization procedure that may operate with up to eight parameters. It was used to analyze the data and to describe experimental flux measurements ranging over distances of nearly 100 meters from the target and over a flux range of $\approx 10^5$ by only five independent parameters (mean free path, angular distribution coefficient, source relaxation length, and two normalization constants). Typical results (Fig. 6.50) showed that this single set of parameters could fit measured data to within less than 20% over an attenuation range of 10^5. As might be expected, the attenuation length in earth was quite well constrained to 117±2 g/cm^2. The angular distribution coefficient, β, is not so well constrained, but has a value between 2 and 2.5 for flux densities of energy greater than 20 MeV. The quality of the fit finally obtained by using these best-fit parameters is indicative of the excellence of the phenomenological model.

Moyer Integrals

The experimental data obtained during the CERN experiment just described permitted development of a convenient formula for shielding calculation.

The Moyer Model shows that the flux of high energy neutrons of energy greater than some energy E_t is given by

$$\phi(E_n > E_t) = \frac{S}{a+d} \int_0^{\pi} g(\theta) \exp\left(\frac{-d\ \mathrm{cosec}\ \theta}{\lambda}\right) d\theta \qquad (6.50)$$

The combined effect of the angular distribution of the neutrons produced and the attenuation geometry means that the transverse shield thickness needed for a high energy accelerator is largely determined by the number of neutrons emitted around 90 deg to the incident proton beam. The CERN experiments

just described show that in the region of $0 \approx 90$ deg the angular distribution is well approximated by the simple exponential function

$$g(\theta) \approx a \exp(-\beta\theta).$$

When the exponential approximation for $g(\theta)$ is substituted, the angular distribution in Eq. 6.50 yields

$$\phi(E_n > E_t) = \frac{a\,S}{(a+d)} \int_0^{\pi} \exp(-\beta\theta) \exp\left(-\frac{d \operatorname{cosec} \theta}{\lambda}\right) d\theta . \qquad (6.51)$$

Routti and Thomas (ROU J 69) define the Moyer Integral

$$M(\beta, \ell) = \int_0^{\pi} \exp(-\beta\theta) \exp(-\ell \operatorname{cosec} \theta)\, d\theta , \qquad (6.52)$$

which is a function of the angular distribution coefficient β and the number of mean free paths in the shield ℓ, where $\ell = d/\lambda$. The solution of shielding problems is often facilitated by the use of these integrals. Routti and Thomas have evaluated Moyer integrals for values of ℓ up to 40 and β up to 15 to within 0.1%. Table 6.XI gives the values of $M(\beta,\ell)$.

The general form of the Moyer Integrals is shown in Fig. 6.51. It is seen that with an increasingly forward-peaked angular distribution—that is, increasing β—the transmission of the shield is reduced. At larger depths the curves may be approximated, for most practical purposes, by simple exponentials.

This approximation becomes better the smaller the value of β or the larger the value of ℓ. At very large depths the effective slope of the Moyer Integral corresponds to the mean free path in the shield, but at values of practical interest—that is, 10 to 15 mean free paths—the effective slope is somewhat steeper. For example, at $\beta \approx 4$, corresponding to 150 MeV threshold energy, the slope is about 7% steeper.

USE OF MOYER INTEGRALS TO ESTIMATE SHIELDING THICKNESS

The flux of high energy neutrons at the sruface of the shield may now be expressed as

$$\phi(E_n > E_t) = \frac{a\,S}{a+d}\, M(\beta,\ell). \qquad (6.53)$$

The term S is proportional to the incident beam loss, B, and also to the energy, E_0, above 10 GeV. It follows from the properties of the nuclear cascade that the dose-equivalent rate, DE, is proportional to $\phi(E_n)$ where $E_n > 150$ MeV, and is expressed as

$$DE = \text{constant} \times \frac{BE_0}{a+d}\, M(\beta,\ell) \qquad (6.54)$$

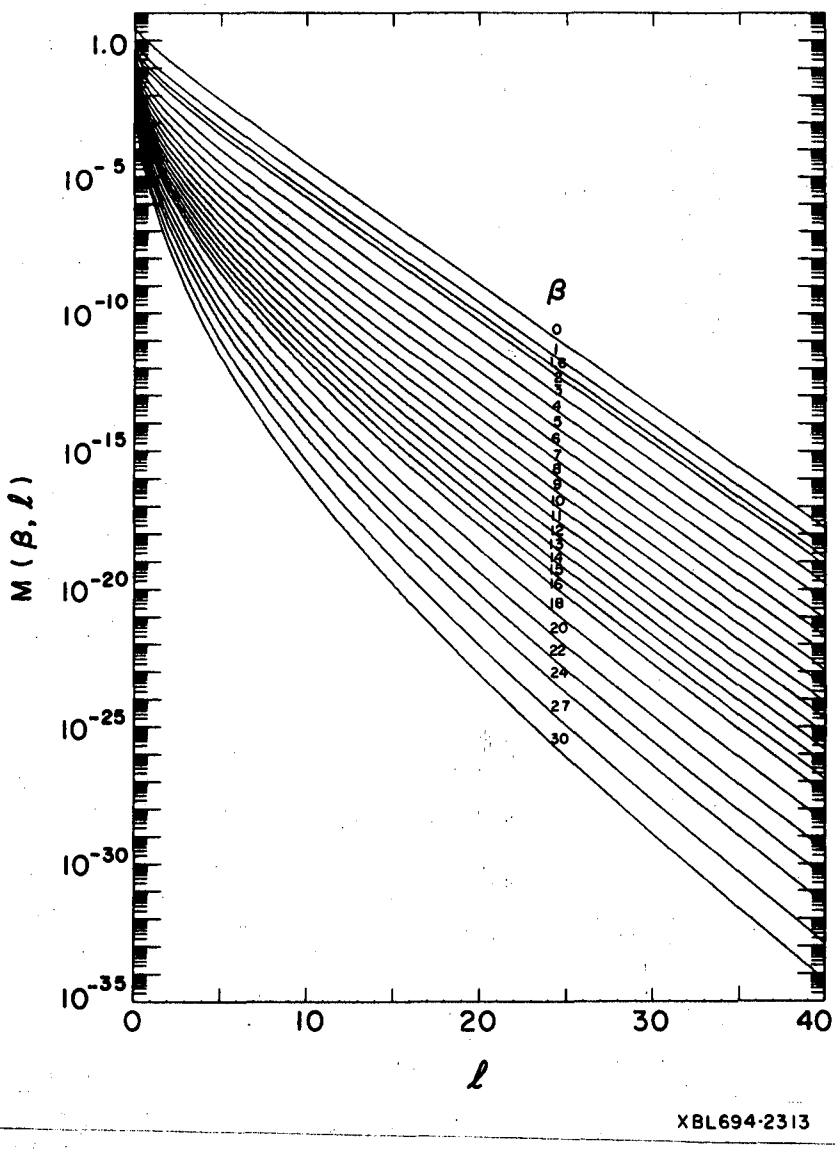

Fig. 6.51. Plot of Moyer Integrals over a wide range of β and ℓ. (From Routti and Thomas.)

Table 6.XI. Tabulated values of Moyer Integrals $M(\beta, \varrho) = \int_0^{\pi} \exp(-\beta\theta) \exp(-\varrho \operatorname{cosec}\theta)\, d\theta$

ϱ \ β	0	1	1.6	2	3	4	5	6	7	8	9	10
0.	3.14E+00	9.56E-01	6.20E-01	4.98E-01	3.32E-01	2.49E-01	1.99E-01	1.66E-01	1.42E-01	1.24E-01	1.10E-01	9.90E-02
.25	1.88E+00	5.11E-01	2.90E-01	2.12E-01	1.13E-01	6.85E-02	4.53E-02	3.17E-02	2.30E-02	1.73E-02	1.32E-02	1.04E-02
.50	1.29E+00	3.34E-01	1.80E-01	1.26E-01	6.02E-02	3.32E-02	2.01E-02	1.29E-02	8.69E-03	6.06E-03	4.34E-03	3.18E-03
1.00	6.57E-01	1.62E-01	8.17E-02	5.44E-02	2.27E-02	1.10E-02	5.87E-03	3.36E-03	2.03E-03	1.28E-03	8.34E-04	5.58E-04
1.50	3.52E-01	8.46E-02	4.09E-02	2.66E-02	1.00E-02	4.42E-03	2.16E-03	1.14E-03	6.34E-04	3.70E-04	2.24E-04	1.40E-04
2.00	1.94E-01	4.57E-02	2.15E-02	1.35E-02	4.81E-03	1.97E-03	8.96E-04	4.40E-04	2.30E-04	1.26E-04	7.20E-05	4.25E-05
3.00	6.17E-02	1.41E-02	6.39E-03	3.90E-03	1.26E-03	4.64E-04	1.89E-04	8.33E-05	3.92E-05	1.94E-05	1.01E-05	5.41E-06
4.00	2.03E-02	4.57E-03	2.02E-03	1.20E-03	3.64E-04	1.24E-04	4.65E-05	1.89E-05	8.18E-06	3.75E-06	1.80E-06	8.96E-07
5.00	6.82E-03	1.52E-03	6.58E-04	3.87E-04	1.11E-04	3.58E-05	1.26E-05	4.78E-06	1.94E-06	8.30E-07	3.73E-07	1.75E-07
6.00	2.32E-03	5.13E-04	2.20E-04	1.28E-04	3.54E-05	1.08E-06	3.62E-06	1.30E-06	4.99E-07	2.02E-07	8.60E-08	3.81E-08
7.00	8.00E-04	1.76E-04	7.43E-05	4.28E-05	1.15E-05	3.40E-06	1.09E-06	3.74E-07	1.37E-07	5.28E-08	2.14E-08	9.03E-09
8.00	2.78E-04	6.06E-05	2.55E-05	1.45E-05	3.83E-06	1.09E-06	3.38E-07	1.12E-07	3.91E-08	1.45E-08	5.62E-09	2.28E-09
9.00	9.70E-05	2.11E-05	8.79E-06	4.99E-06	1.29E-06	3.59E-07	1.07E-07	3.43E-08	1.16E-08	4.14E-09	1.55E-09	6.04E-10
10.00	3.40E-05	7.37E-06	3.06E-06	1.73E-06	4.38E-07	1.19E-07	3.48E-08	1.08E-08	3.54E-09	1.22E-09	4.42E-10	1.67E-10
12.00	4.24E-06	9.13E-07	3.75E-07	2.11E-07	5.19E-08	1.37E-08	3.81E-09	1.13E-09	3.51E-10	1.15E-10	3.91E-11	1.39E-11
14.00	5.35E-07	1.15E-07	4.68E-08	2.61E-08	6.31E-09	1.61E-09	4.36E-10	1.24E-10	3.70E-11	1.16E-11	3.76E-12	1.27E-12
16.00	6.80E-08	1.45E-08	5.91E-09	3.28E-09	7.79E-10	1.95E-10	5.13E-11	1.42E-11	4.08E-12	1.23E-12	3.84E-13	1.25E-13
18.00	8.71E-09	1.86E-09	7.51E-10	4.15-10	9.75E-11	2.40E-11	6.17E-12	1.66E-12	4.65E-13	1.36E-13	4.10E-14	1.29E-14
20.00	1.12E-09	2.38E-10	9.52E-11	5.30E-11	1.23E-11	2.98E-12	7.54E-13	1.98E-13	5.43E-14	1.54E-14	4.53E-15	1.38E-15
22.00	1.45E-10	3.08E-11	1.24E-11	6.81E-12	1.57E-12	3.75E-13	9.33E-14	2.41E-14	6.46E-15	1.79E-15	5.15E-16	1.53E-16
24.00	1.88E-11	3.99E-12	1.60E-12	8.78E-13	2.01E-13	4.75E-14	1.17E-14	2.97E-15	7.82E-16	2.13E-16	5.97E-17	1.73E-17
25.00	6.80E-12	1.44E-12	5.77E-13	3.16E-13	7.19E-14	1.70E-14	4.14E-15	1.05E-15	2.78E-16	7.37E-17	2.05E-17	5.87E-18
26.00	2.45E-12	5.19E-13	2.08E-13	1.14E-13	2.58E-14	6.06E-15	1.47E-15	3.70E-16	9.58E-17	2.56E-17	7.06E-18	2.00E-18
28.00	3.21E-13	6.78E-14	2.71E-14	1.48E-14	3.34E-15	7.78E-16	1.87E-17	4.64E-17	1.19E-17	3.12E-18	8.46E-19	2.36E-19
30.00	4.20E-14	8.86E-15	3.54E-15	1.93E-15	4.33E-16	1.00E-16	2.39E-17	5.86E-18	1.48E-18	3.85E-19	1.08E-19	2.81E-20
32.00	5.51E-15	1.16E-15	4.63E-16	2.52E-16	5.64E-17	1.30E-17	3.07E-18	7.45E-19	1.86E-19	4.78E-20	1.28E-20	3.40E-21
34.00	7.24E-16	1.53E-16	6.07E-17	3.30E-17	7.36E-18	1.68E-18	3.95E-19	9.53E-20	2.36E-20	5.98E-21	1.56E-21	4.15E-22
35.00	2.63E-16	5.53E-17	2.20E-17	1.20E-17	8.66E-18	6.07E-19	1.42E-19	3.41E-20	8.41E-21	2.12E-21	5.48E-22	1.46E-22
36.00	9.53E-17	2.01E-17	7.98E-18	4.34E-18	9.62E-19	2.19E-19	5.11E-20	1.22E-20	3.00E-21	7.54E-22	1.94E-22	5.11E-23
38.00	1.26E-17	2.64E-18	1.05E-18	5.70E-19	1.26E-19	2.86E-20	6.63E-21	1.58E-21	3.84E-22	9.56E-23	2.44E-23	6.35E-24
40.00	1.66E-18	3.49E-19	1.38E-19	7.51E-20	1.66E-20	3.74E-21	8.63E-22	2.04E-22	4.93E-23	1.22E-23	3.07E-24	7.93E-25

ℓ \ β	11	12	13	14	15	16	18	20	22	24	27	30
0.	8.99E-02	8.23E-02	7.59E-02	7.04E-02	6.57E-02	6.15E-02	5.46E-02	4.90E-02	4.45E-02	4.07E-02	3.61E-02	3.23E-02
.25	8.24E-03	6.64E-03	5.41E-03	4.45E-03	3.70E-03	3.10E-03	2.22E-03	1.62E-03	1.21E-03	9.19E-04	6.23E-04	4.33E-04
.50	2.38E-03	1.81E-03	1.39E-03	1.08E-03	8.54E-04	6.79E-04	4.40E-04	2.94E-04	2.00E-04	1.40E-04	8.38E-05	5.20E-05
1.00	3.82E-04	2.67E-04	1.90E-04	1.37E-04	9.99E-05	7.39E-05	4.17E-05	2.44E-05	1.47E-05	9.05E-06	4.58E-06	2.41E-06
1.50	8.98E-05	5.89E-05	3.93E-05	2.67E-05	1.85E-05	1.29E-05	6.55E-06	3.46E-06	1.89E-06	1.07E-06	4.73E-07	2.20E-07
2.00	2.58E-05	1.60E-05	1.02E-05	6.59E-06	4.34E-06	2.90E-06	1.34E-06	6.53E-07	3.30E-07	1.72E-08	6.83E-08	2.86E-08
3.00	3.00E-06	1.71E-06	1.00E-06	5.97E-07	3.63E-07	2.25E-07	9.00E-08	3.80E-08	1.68E-08	7.71E-09	2.55E-09	9.98E-10
4.00	4.62E-07	2.45E-07	1.34E-07	7.48E-08	4.26E-08	2.48E-08	8.79E-09	3.81E-09	1.31E-09	5.39E-10	1.53E-10	4.67E-11
5.00	8.47E-08	4.24E-08	2.18E-08	1.15E-08	6.20E-09	3.41E-09	1.09E-09	3.71E-10	1.33E-10	5.01E-11	1.25E-11	3.35E-12
6.00	1.75E-08	8.31E-09	4.06E-09	2.04E-09	1.05E-09	5.49E-10	1.60E-10	4.98E-11	1.64E-11	5.69E-12	1.26E-12	3.01E-13
7.00	3.96E=09	1.79E-09	8.38E-10	4.02E-10	1.98E-10	9.88E-11	2.66E-11	7.65E-12	2.33E-12	7.50E-13	1.49E-13	3.22E-14
8.00	9.57E-10	4.16E-10	1.87E-10	8.60E-11	4.06E-11	1.96E-11	4.88E-12	1.30E-12	3.70E-13	1.11E-13	2.00E-14	3.93E-15
9.00	2.44E-10	1.02E-10	4.42E-11	1.96E-11	8.95E-12	4.17E-12	9.67E-13	2.41E-13	6.43E-14	1.81E-14	2.97E-15	5.35E-16
10.00	6.52E-11	2.64E-11	1.10E-11	4.73E-12	2.08E-12	9.41E-13	2.05E-13	4.80E-14	1.20E-15	3.19E-15	4.80E-16	7.98E-17
12.00	5.13E-12	1.96E-12	7.69E-13	3.11E-13	1.29E-13	5.51E-14	1.07E-14	2.23E-15	5.02E-16	1.20E-16	1.54E-17	2.21E-18
14.00	4.47E-13	1.62E-13	6.05E-14	2.33E-14	9.19E-15	3.72E-15	6.51E-16	1.24E-16	2.52E-17	5.47E-18	6.13E-19	7.67E-20
16.00	4.19E-14	1.46E-14	5.21E-15	1.92E-15	7.24E-16	2.80E-16	4.49E-17	7.80E-18	1.46E-18	2.90E-19	2.87E-20	3.18E-21
18.00	4.17E-15	1.39E-15	4.94E-16	1.70E-16	6.17E-17	2.29E-17	3.40E-18	5.45E-19	9.42E-20	1.74E-20	1.53E-21	1.52E-22
20.00	4.33E-16	1.40E-16	4.66E-17	1.59E-17	5.59E-18	2.01E-18	2.77E-19	4.14E-20	6.67E-21	1.15E-21	8.18E-23	8.17E-24
22.00	4.66E-17	1.46E-17	4.73E-18	1.57E-18	5.33E-19	1.86E-19	2.40E-20	3.37E-21	5.08E-22	8.19E-23	5.92E-24	4.88E-25
24.00	5.15E-18	1.58E-18	4.97E-19	1.60E-19	5.30E-20	1.79E-20	2.19E-21	2.90E-22	4.12E-23	6.26E-24	4.14E-25	3.09E-26
25.00	1.73E-18	5.24E-19	1.63E-19	5.19E-20	1.68E-20	5.66E-21	6.73E-22	8.66E-23	1.20E-23	1.77E-24	1.12E-25	8.04E-27
26.00	5.84E-19	1.75E-19	5.37E-20	1.69E-20	5.46E-21	1.80E-21	2.09E-22	2.61E-23	3.52E-24	5.06E-25	3.09E-26	8.18E-27
28.00	6.74E-20	1.98E-20	5.95E-21	1.83E-21	5.78E-22	1.96E-22	2.06E-23	2.45E-24	3.14E-25	4.30E-26	2.43E-27	1.55E-28
30.00	7.91E-21	2.28E-21	6.73E-22	2.03E-22	6.27E-23	1.98E-23	2.09E-24	2.39E-26	2.92E-26	3.81E-27	2.01E-28	1.19E-29
32.00	9.41E-22	2.67E-22	7.74E-23	2.29E-23	6.95E-24	2.15E-24	2.18E-25	2.39E-26	2.80E-27	3.50E-28	1.72E-29	9.59E-31
34.00	1.13E-22	3.16E-23	9.03E-24	2.63E-24	7.85E-25	2.38E-25	2.33E-26	2.46E-27	2.77E-28	3.32E-29	1.54E-30	8.08E-32
35.00	3.95E-23	1.09E-23	3.10E-24	8.97E-25	2.65E-25	7.99E-26	7.68E-27	7.94E-28	8.78E-29	1.03E-29	4.65E-31	8.36E-32
36.00	1.38E-23	3.79E-24	1.07E-24	3.07E-25	8.99E-26	2.69E-26	2.54E-27	2.58E-28	2.80E-29	3.24E-30	1.42E-31	6.97E-33
38.00	1.69E-24	4.60E-25	1.28E-25	3.62E-26	1.04E-26	3.08E-27	2.82E-28	2.77E-29	2.90E-30	3.24E-31	1.34E-32	6.25E-34
40.00	2.99E-25	5.62E-26	1.54E-26	4.31E-27	1.23E-27	3.57E-28	3.18E-29	3.02E-30	3.07E-31	3.31E-32	1.30E-33	5.76E-35

or $$DE = C \frac{L}{a+d} M(\beta, \ell) , \qquad (6.55)$$

where $L = BE_0$ is the energy loss from the accelerator vacuum chamber.

The value of the normalizing constant C appearing in Eq. 6.55 may be obtained from the data of the CERN-LRL-RHEL experiment.

On substituting experimental data, Routti and Thomas show that the value of C is unity when the Moyer integral of order 4 is used.

The dose-equivalent rate can thus be expressed as

$$D\ [\text{mrem/h}] = \frac{L\ [\text{GeV/cm sec}]}{(a+d)\ [\text{m}]} M(4, \ell). \qquad (6.56)$$

This equation is of great value in estimating shielding for high energy proton synchrotrons. Table 6.XII compares values of shield thickness for a 200-GeV synchrotron calculated by using Moyer Integrals with values obtained by extrapolating experimental data from Gilbert et al. (GIL W 68). The results are seen to be in good agreement. An even simpler representation of these latter data is obtained by writing the total shielding thickness, t, as a function of L/D, in the simple expression

$$t\ [\text{g/cm}^2] = 230 \log_{10} \frac{L\ [\text{GeV/cm sec}]}{D\ [\text{mrem/h}]} - 610 \qquad (6.57)$$

This simple formula, however, applies only to regions of fairly uniform beam loss.

Above the internal targets the use of this simple formula is not very precise. Typically the value of L/D above the targets is some two orders of magnitude higher than in the regions of low beam loss. Such an assumption with the Moyer Integrals leads to a conservative estimate. For precise shield configurations detailed beam-loss distribution should be used.

In summary, the use of the Moyer Integrals allows rapid and accurate estimates of the high energy neutron flux above different threshold energies as well as allowing the dose-equivalent rate to be found at the surface of the shield for a proton accelerator operating in the energy region 5 to 500 GeV.

The flux and dose-rate may be estimated in regions of uniform beam loss to within a factor of 2, and even in target regions the dose-rate estimates are fairly reliable.

Table 6.XII. Calculated shield thicknesses for high energy proton synchrotrons (from Routti and Thomas).

Accelerator	Energy (GeV)	Beam loss (p/sec)	Radius (m)	L (GeV per cm sec)	(mrem/h)	L/D	Magnet thickness (g/cm^2)	Total shield thickness including magnet (g/cm^2) Gilbert et al.	Routti and Thomas
CPS	25.5	$2X10^{11}$	100	$1.8X10^{7}$	0.8[a]	$2.3X10^{7}$[b]	400	1085[c]	1085[c]
CPS	25.5	10^{12}	100	$9.0X10^{7}$	0.8	$1.1X10^{8}$[b]	400	1240	1240
CPS	25.5	10^{13}	100	$9.0X10^{8}$	0.8	$1.1X10^{9}$[b]	400	1455	1470
LBL design study	200	$2X10^{12}$	693	$9.2X10^{8}$	1.25	$7.4X10^{8}$	280	1440	1430
	200	$2X10^{12}$	693	$9.2X10^{8}$	0.25	$3.7X10^{9}$	280	1600	1590
CERN design study	300	$6X10^{12}$	1200	$2.4X10^{9}$	0.8	$3.0X10^{9}$	300	1585	1570

a. Experimental value.

b. Effective value due to beam clipper.

c. Normalized to the same value.

The Electromagnetic Cascade

Charged particles passing through matter lose energy by two mechanisms, by collision and by radiation.

"Most of the energy lost by collision is spent in exciting atoms or ejecting from the atoms electrons of small energy, and is thus dissipated" (ROS B 52). "The energy lost by radiation, instead, is fairly uniformly distributed among secondary photons of all energies from zero up to the energy of the primary particle itself.

"For electrons of small energy and for heavier particles of practically all energies, collision losses are more important than radiation losses. Thus the electromagnetic interactions of heavy particles and of low-energy electrons result mainly in an energy dissipation. Electrons of large energy, however, lose most of their energy by radiation. Hence in the interactions of high-energy electrons with matter only a small fraction of the energy is dissipated, while a large fraction is spent in the production of high-energy photons. The secondary photons, in turn, undergo materialization or Compton collision. Either process gives rise to electrons of energy comparable with that of the photons. These new electrons radiate more photons, which again materialize into electron pairs or produce Compton electrons. At each new step the number of particles increases and their average energy decreases. As the process goes on, more and more electrons fall into an energy range where radiation losses cannot compete with collision losses, until eventually the energy of the primary electron is completely dissipated in excitation and ionization of atoms.

"The phenomenon outlined is called a *multiplicative shower,* or a *cascade shower.* It is clear that a shower can be initiated by a high-energy photon as well as by a high-energy electron. Occasionally a meson or a proton, too, can give rise to a shower by producing a secondary electron or photon of high energy."

Figure 6.52 shows a multiplate cloud-chamber photograph of such an electromagnetic shower initiated by a particle of several tens of GeV.

In discussing radiation phenomena two terms, *radiation length* and *critical energy,* are frequently used. It is convenient to express the thickness of matter traversed in units of *radiation length,* X_0 (Chap. 3), defined to be that thickness of material that will reduce the energy of an electron of high energy by a factor of e when radiative losses only are considered. X_0 is given approximately by

$$\frac{1}{X_0} = 4\alpha \frac{L}{A} Z^2 r_e^2 \ln(183\, Z^{-1/3}), \qquad (6.58)$$

where α is the fine-structure constant,
r_e is the classical electron radius,
Z and A are the atomic and mass numbers,
and L is Avogadro's number.

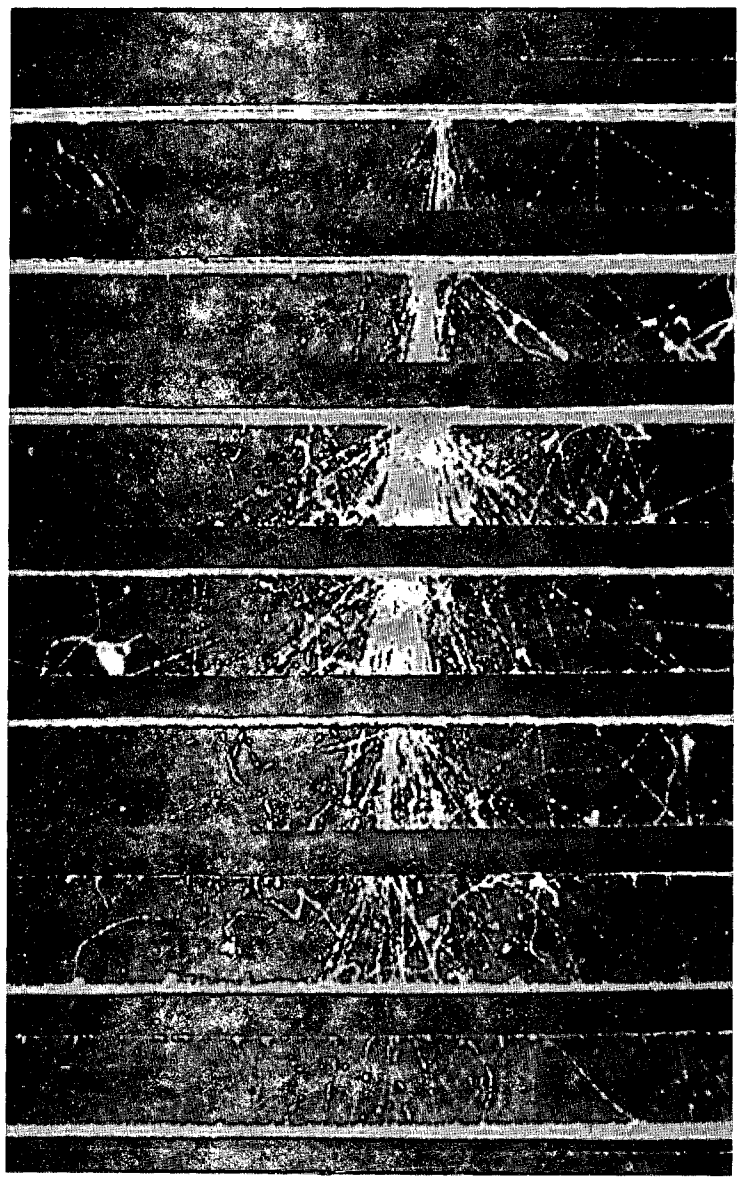

XBB 711-564

Fig. 6.52. Cloud-chamber picture of a large electromagnetic cascade shower. The thickness of the lead plates is 1.27 cm. (From C. Y. Chao.)

More precise considerations show that X_0 is better given by

$$\frac{1}{X_0} = 4\,a\,L\,\frac{Z}{A}\,(Z+1)\,r_e^2 \ln\left(183\,Z^{-1/3}\right) / \left[1 + 0.12\left(\frac{Z}{82}\right)^2\right] \qquad (6.59)$$

which attempts to make corrections for electron screening and inaccuracies in Born's approximation (ROS B 52). However, the exact corrections for screening effects are still under investigation. Dovzhenko and Pomanskii (DOV O 63) have shown that discrepancies of 10 to 20% in calculated values of radiation length are evident from the literature. The values of X_0 calculated by Dovzhenko and Pomanskii are given in Table 6.XIII. They should be compared with those given in Tables 3.II and 6.VIII.

Table 6.XIII. Values of radiation lengths and critical energies for various materials.

Material	Radiation length X_0 (g/cm^2)	Critical energy ϵ_0 (MeV) (with denisty effect)
Lead	6.4	7.4
Copper	13.0	18.8
Air	37.1	81[a]

a. The correction for the density effect is negligibly small for gases and is not accounted for in this value.

The *critical energy*, ϵ_0, is defined as that electron energy at which the separate contributions to energy loss due to radioactive and collision processes are equal. An approximate value for the critical energy may be obtained from

$$\epsilon_0 = \left(\frac{800}{Z + 1.2}\right) \quad \text{MeV.} \qquad (6.60)$$

At very high energies (greater than 1 GeV), where virtually all the energy losses are due to radiative processes, it may be shown the fractional energy loss per radiation length is independent of absorbing material and particle energy and very close to unity (KAS K 72).

Although the basic interactions of electrons and photons are well understood, the solution of the transport equations that describe the development of the cascade is extremely difficult.

THEORETICAL TREATMENTS OF THE ELECTROMAGNETIC CASCADE

Analytical shower theory gives a good account of the main features of the development of the electromagnetic cascade. Rossi and Greisen (ROS B 41, 52) developed descriptions of the longitudinal development, and the lateral and angular spread have been treated by Kamata and Nishimura (KAM K 58) and by Belenkii and Ivanenko (BEL S 59).

The difficulty of solving the diffusion equations of the shower have led to use of various assumptions, which may result in some errors at great depths in matter. DeStaebler (DES H 65) pointed out that although, at the time of writing, few experiments went deeper than 15 to 20 radiation lengths (MUR Y 65, BAC G 63, BLO W 50), they agreed with simple theory in showing that "the shower decreased exponentially with an absorption mean free path of several radiation lengths. This agreement may be accidental, however, because the most penetrating component, which one would expect to control the shower at great depths, consists of photons near the minimum in the interaction cross section . . .and in most analytic shower theory there are approximations that eliminate this minimum in the photon cross section" (DES H 65).

Nevertheless, the general behavior of the longitudinal behavior may be represented by an attenuation length, Λ, which is shown in Fig. 6.54. Λ varies from about $2X_0$ at low Z to about $4X_0$ at high Z.

Monte Carlo methods are of most value in obtaining numerical descriptions of the three-dimensional growth of the cascade.

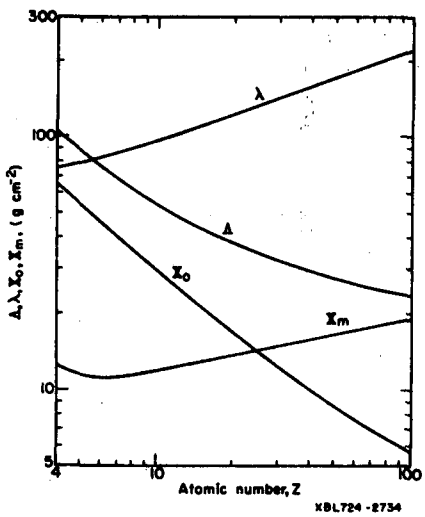

Fig. 6.53. Variations with atomic number of nuclear mean free path λ, radiation length x_0, radial distribution parameter x_m, and the maximum photon mean free path Λ. (After De Staebler and Nelson.)

DeStaebler has summarized Monte Carlo data by considering the energy, W, absorbed per unit volume (dw/dv). Assuming cylindrical symmetry, he defines the fraction of energy absorbed beyond radius a by

$$U(a) = \frac{1}{E_0} \int_{r=a}^{\infty} \int_{z=0}^{\infty} \left(\frac{dw}{dv}\right) 2\pi r \, dr \, dz. \qquad (6.61)$$

It is convenient to measure the transverse spread of the cascade in terms of the Molière unit of length, X_m, which is the characteristic measure for the radial distributions in analytical theory (GRE K 56). X_m is given by

$$X_m = X_0 \left(\frac{E_s}{E_0}\right) , \qquad (6.62)$$

where E_s is a constant equal to 21.2 MeV. DeStaebler has summarized data from Monte Carlo calculations in water, aluminum, copper, and lead. Empirical values of X_m are given in Fig. 6.53; Fig. 6.54 shows that the fraction of energy observed beyond radius a is independent of material when measured in units of X_m. Nelson et al. (NEL W 66) have collated more recent data extending out to radii of 4 Molière units (Fig. 6.55).

The early calculations by Wilson (WIL R 52), Messel and his colleagues MES H 62, CRA D 62, CRA D 65), and the Oak Ridge Group (ZER C 62b, ZER C 62c, ZER C 63) have recently been improved (in the case of lead) by Nagel (NAG H 65) and Völkel (VOL J 65), both of whom lowered the cutoff energy used in the earlier calculations.

Figure 6.56 compares the results of three Monte Carlo calculations of an electromagnetic cascade shower initiated in lead by 1-GeV electrons. All the calculations used a cutoff energy of 10 MeV and a radiation length in lead of 5 g/cm^2. Excellent agreement is obtained between the various calculations. The choice of the cutoff energy used in such calculations has a significant influence on the shape of the transition curve obtained, whether particle denisty or energy deposition be calculated. A reduction in cutoff energy has been found to shift the maximum to larger depths in the absorber and to decrease the slope of the tail (ZER C 62b, ZER C 62c, ZER C 63, NAG H 65, VÖL U 65). Great care should therefore be taken in the comparison of theoretical and experimental data.

The position of the cascade maximum, t_{max}, may be obtained from

$$t_{max} = \ell n \left(\frac{E_0}{E_C}\right) - K, \qquad (6.63)$$

where $E_C = E_0/2.3$ and t_{max} is measured in radiation lengths. Ott (OTT K 54) gives values for K of 1.6 for copper and 1.3 for lead.

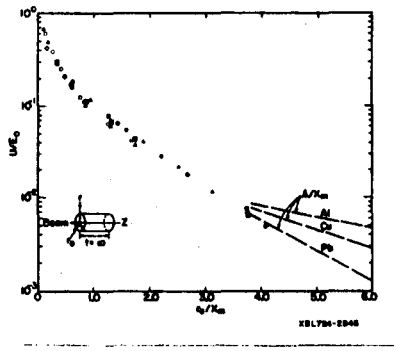

Fig. 6.54. Fraction of energy absorbed beyond radius as a function of radius approximate Mollère units. The points are taken from Monte Carlo calculations for the energies and materials indicated. The solid line is taken from Air Shower Theory. (After De Staebler.)

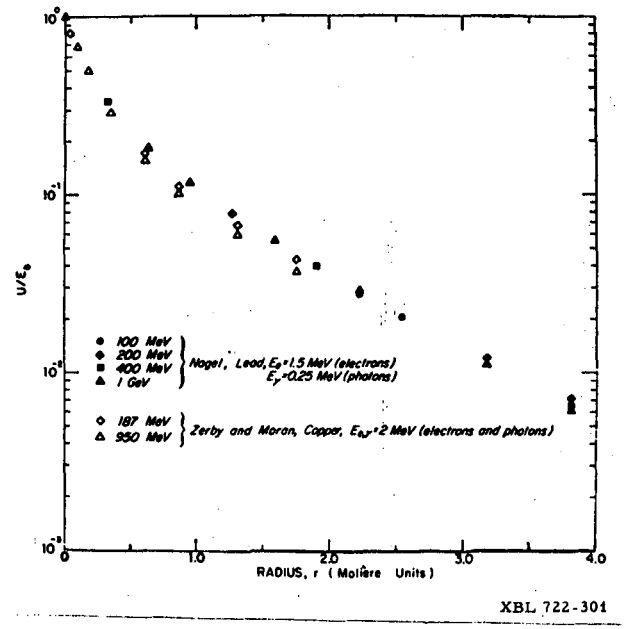

Fig. 6.55. Fraction of the incident energy that escapes various cylindrical volumes. A comparison of Monte Carlo results showing the independence of the choice of absorber and of incident energy. (From Nelson et al.)

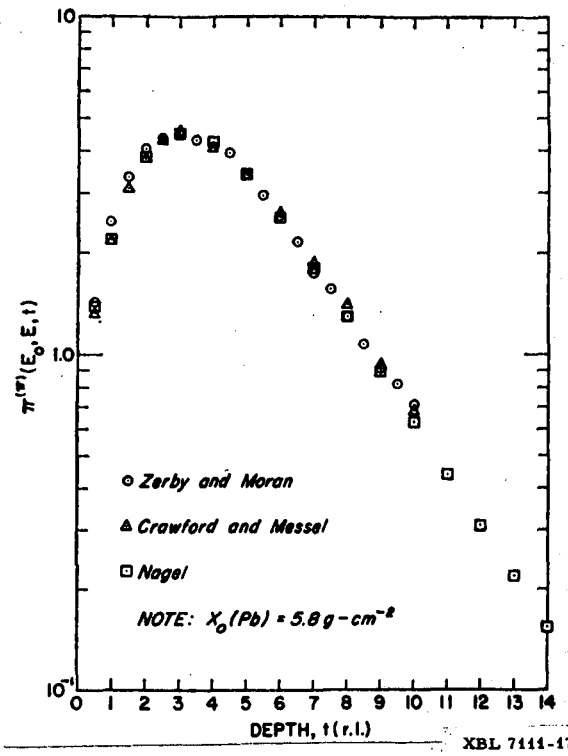

Fig. 6.56. A comparison of three Monte Carlo calculations for an electromagnetic cascade shower initiated by a 1-GeV electron in lead. A cutoff energy of 10 MeV and a radiation length of 5/8 g/cm^2 was used. (From Nelson et al.)

Several experimental measurements of shower propagation have been reported in the literature. A variety of experimental techniques have been employed, ranging from ionization chambers (BLO W 50), scintillation counters (KAN A 53), and photographic film (MUR Y 65) through spark chambers (CRO J 62, KAJ R 63), cloud chambers (WIL M 62, LAL S 62, BEC E 64, THO H 64, ZAI O 67), and bubble chambers (LEN H 63) to nuclear emulsions (AKA M 62) and Cerenkov counters (HEU C 64).

The most recent experiments have compared experimental data with the Monte Carlo calculations already discussed. Nelson et al. (NEL W 66) have reported good agreement with their measurements (with thermoluminescent dosimeters) of longitudinal and radial development of electromagnetic cascades induced by 1-GeV electrons in copper and lead. Figures 6.57 and 6.58 show energy transition curves obtained by these workers in copper and lead compared with Monte Carlo calculations. In the case of copper the experimental data indicates a somewhat deeper shower maximum than calculated. In the calculation a cutoff energy of 2 MeV was applied, and one would expect better agreement if the cutoff were lower (ZER C 62b).

After the shower maximum the measured and theoretical slopes are in good agreement. For lead, agreement is not quite so good (but still good!)—probably because of the influence of the air gaps between the plates of lead necessary to position detectors.

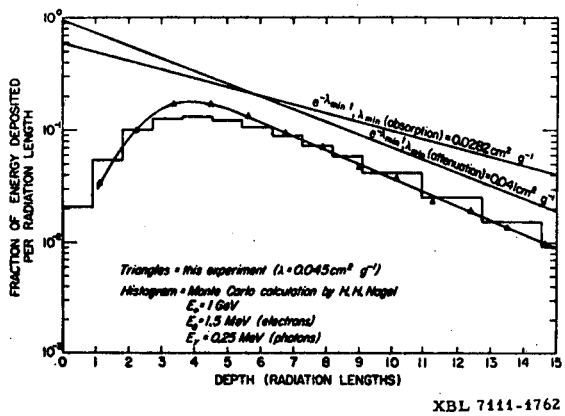

Fig. 6.57. Longitudinal energy deposition in copper. Comparison of this experiment with a Monte Carlo calculation; X_0 = 13.0 g/cm^2, ρ = 8.89 g/cm^3. (From Nelson et al.)

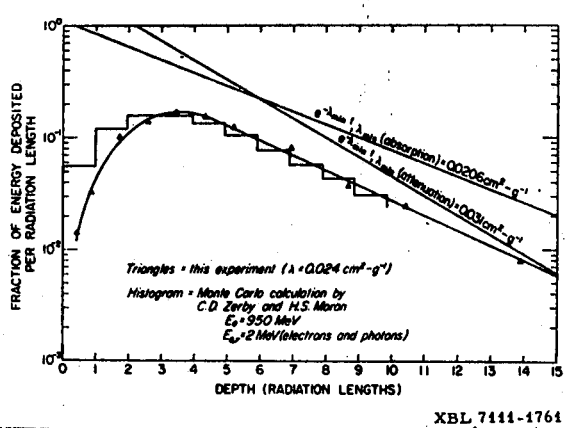

Fig. 6.58. Longitudinal energy deposition in lead. A comparison of this experiment with a Monte Carlo calculation; X_0 = 6.4 g/cm^2, ρ = 11.35 g/cm^3. (From Nelson et al.)

Figures 6.57 and 6.58 also show the slopes corresponding to the minimum attenuation coefficient λ_{min} (attenuation) and the energy-absorption coefficient λ_{min} (absorption). Nelson et al. conclude that such a model is probably too simple to permit precise calculations of energy deposition. Bathow et al. (BAT G 67) have reported experimental studies of the electromagnetic cascades produced by 6.3-GeV electrons in heavy concrete, copper, and lead. Measurements were made with a tissue-equivalent ionization chamber and compared with Monte Carlo calculations due to Völkel (VÖL U 65) for copper and lead. Excellent agreement was obtained between calculated and measured transition curves. Figure 6.59 shows the absorbed-dose measurement on axis as a function of depth in matter. Table 6.XIV gives values of the attenuation length calculated from the maximum absorption coefficients λ_{min}, the characteristic attenuation length measured for the experimental region of the transition curve, λ_{exp}, and the attenuation length measured on the beam axis, λ_0.

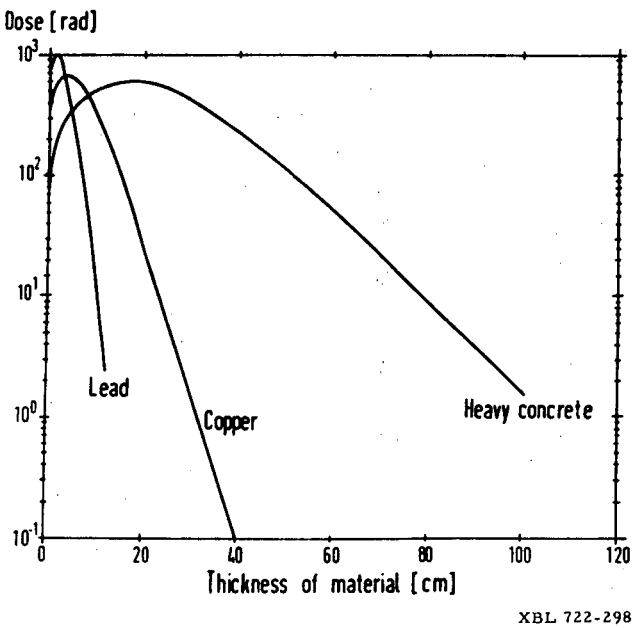

Fig. 6.59. The dose on the axis of a 6-GeV cascade as a result of an incident beam of 5 x 10^9 equivalent quanta plotted against the thickness of material. (From Bathow et al.)

Table 6.XIV. Attenuation lengths for an electromagnetic cascade initiated by 6.3-GeV electrons (after Bathow et al.).

Material	ρ(g/cm^3)	X_0(g/cm^2)	λ_{min}	λ_{exp}	λ_0
Lead	11.35	6.4	24.1	23.2	16.2
Copper	8.94	13.0	33.1	35.8	33.1
Heavy concrete	3.7	18.5	40.7	52.9	40.7

After the shower maximum in copper and lead the transition curve decays exponentially, with slope equal (within the limits of experimental error) to that determined by the minimum absorption coefficients. In heavy concrete, however, the measured attenuation length is much larger than would be expected from the minimum absorption coefficients. The measured value in heavy concrete had been observed earlier in an experiment using a 4.8-GeV bremsstrahlung beam (BAT G 65), and probably differs from the expected value because low-Z materials have a broad absorption minimum in which forward-scattered Compton photons have an appreciable mean free path. It is, of course, to be expected that λ_0 will be somewhat smaller than λ_{exp} because of "scattering out" from the beam. Figure 6.60 shows the distribution of absorbed dose measured behind heavy concrete shielding.

More recently Bathow et al. (BAT G 69) have performed some very precise measurements of both the longitudinal and lateral development of 6-GeV electromagnetic cascades in aluminum, copper, and lead. They report excellent agreement with Völkel's Monte Carlo calculations for depths up to 40 radiation lengths. The longitudinal development agrees with theory to about 5%. Good agreement is found at lateral distances out to 4 cm, in which distance the dose decreases by three orders of magnitude, but at larger distances the measured energy deposition is somewhat higher than that calculated. The extreme discrepancy, roughly a factor of two, occurs in lead at small shower depths (see Fig. 6.61).

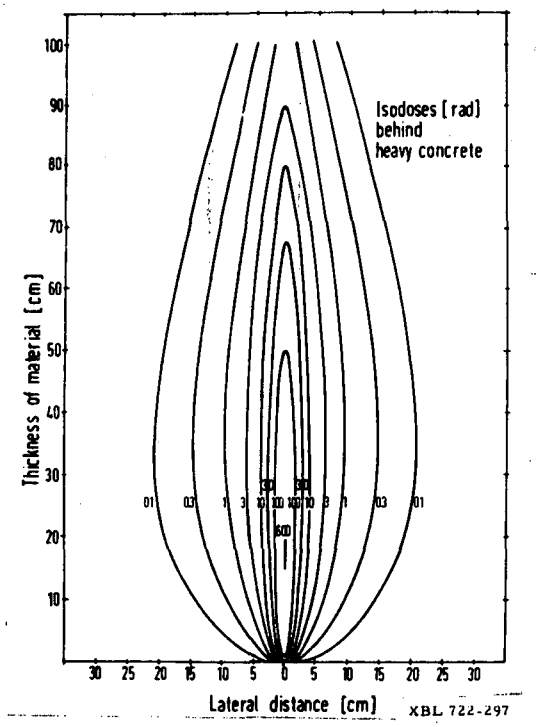

Fig. 6.60. Curves of equal dose behind heavy concrete for incident 5×10^9 equivalent quanta. Doses are measured in rads at 6 GeV. (From Bathow et al.)

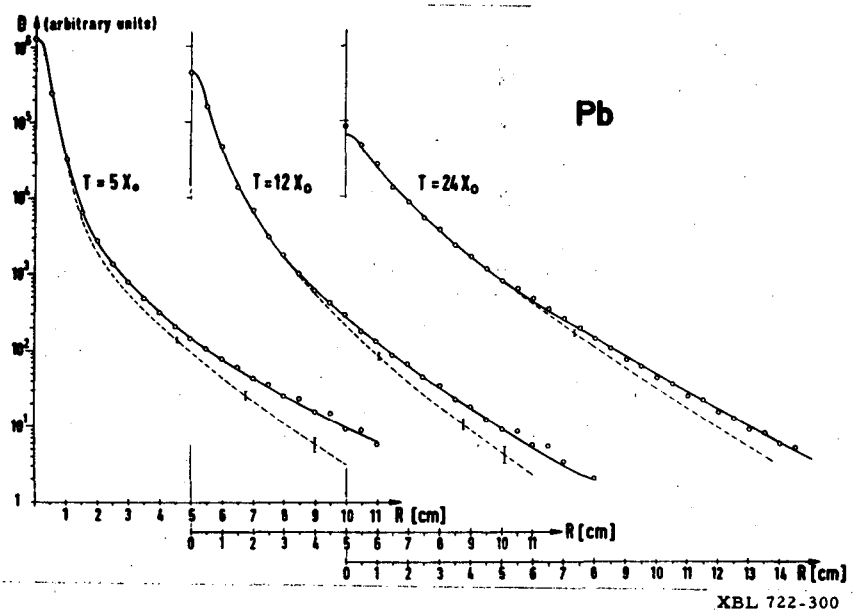

Fig. 6.61. Measured lateral distribution of the electromagnetic cascade initiated in lead by 6-GeV electrons (circles) compared with Monte Carlo data (dotted line with error bars). (From Bathow et al.)

HADRON PRODUCTION BY THE ELECTROMAGNETIC CASCADE

Photoproduction of nucleons from complex nuclei is largely due to three processes (Chapter 3).

a. Dipole interaction. In the energy region 10 to 20 MeV, photons are absorbed through the dipole interaction to form a compound nucleus which then decays to produce low energy nucleons. The neutrons so produced are often referred to as "Giant Resonance" neutrons. The cross section for such interactions decreases rapidly with energy.

b. Photodisintegration. Photodisintegration of quasi deuterons within the nucleus can produce n-p pairs. Above 150 MeV this cross section may be written (LEV J 51, LEV J 60) as

$$\sigma\ (\gamma,np) = L\ \frac{NZ}{A}\sigma_d\,, \qquad (6.64)$$

where A is the mass number,
N and Z are the numbers of neutrons and protons in the nucleus,
L is a constant,
and σ_d is the photodisintegration cross section of the deuteron.
The cross section for photodisintegration of the deuteron, σ_d, of kinetic energy T may be approximated by the three equations:

$$\sigma_d = \frac{7 \times 10^3}{T}\ \mu b \qquad \text{for } 50 < T < 125 \text{ MeV}, \qquad (6.65a)$$

$$= 57 \mu b \qquad \text{for } 125 \text{ MeV} < T < 300 \text{ MeV}, \qquad (6.65b)$$

$$= \frac{1.3 \times 10^9}{T^3}\ \mu b \qquad \text{for } T < 300 \text{ MeV} \qquad (6.65c)$$

(ALL L 55, KEC K 56, MEY H 61).

Levinger (LEV J 51, LEV J 60), on theoretical considerations, gives the value of L appearing in Eq. 6.64 as 6.4; experimental data are contradictory, but appear to indicate a value of L=3 (BAT G 67a). As may be seen from Eq. 6.65c, the cross section for this reaction falls off approximately as the third power of the photon energy, and so may be neglected above 500 MeV.

c. Absorption of photo pions. At high energies pions may be produced, and in complex nuclei most of these are reabsorbed in the nucleus in which they were created. This leads to the development of an intranuclear cascade and the subsequent production of energetic and low energy nucleons.

SHIELDING EXPERIMENTS AT HIGH ENERGY ELECTRON ACCELERATORS

Bathow et al. (BAT G 65) have described some of the earliest shielding measurements made at high energy electron accelerators. Figure 6.62 shows their general layout. A 4.8-GeV bremsstrahlung beam was stopped in a quantameter shielded on all sides by heavy concrete. The thickness of this shielding could be varied, and radiation measurements were made with a variety of detectors in the regions A---A shown in Fig. 6.62. In this, attenuation curves and angular distributions for various components of the radiation field could be measured.

The radiation detectors used included a tissue-equivalent ionization chamber, Jordan ionization chamber, and several activation detectors. These early measurements were beset by difficulties due to large backgrounds, but several conclusions were possible. Two components of the neutron production were identified, one isotropic ("giant resonance neutrons"), the other forward peaked due to the photodisintegration of quasideuterons. The estimated production of quasi-resonance neutrons was 0.5 ± 0.15 neutron per 1-GeV photon. The authors conclude that dose rates measured with the TE chamber are accurate to ±30%. Figure 6.63 shows the measured attenuation of absorbed dose at different angles through the shield. The attenuation of absorbed dose is seen to be exponential at all angles down to dose rates of about 1 mrad/h, which was thought to be the general background level due to scattering. In the forward direction the contribution to the dose rate by neutrons is small, and the electromagnetic cascade dominates in this region of the shield. This domination is indicated by the attenuation measured length of 44 g/cm^2 at 0 deg, which should be compared with a value of 41 g/cm^2 for the most penetrating component of the electromagnetic cascade in heavy concrete. In the transverse direction neutrons contribute the major fraction of dose equivalent because of their higher quality factor (see Chapter 2) Thermal neutrons were found to be negligible under all conditions. Fig. 6.64 shows the angular distribution of absorbed dose about the incident beam direction measured with a TE chamber.

With the increase in available intensity at the DESY synchrotron, these studies were extended to thicknesses between 2 and 4 m in heavy concrete for incident 4-GeV and 6-GeV electron beams (BAT G 67b). Figure 6.65 shows the neutron flux densities measured with bare indium foils, moderated indium foils, and neutron films. For the films, measurements were made along the beam axis parallel to the beam at distances of 40 and 90 cm. In this case the transmission curves are seen to be parallel, with an attenuation length of about 185 g/cm^2 independent of subtended angle with the beam direction—a result also observed in a 6-GeV proton shielding experiment at the Bevatron (SMI A 65)— suggesting that the neutron flux densities at these large depths are controlled by neutrons of energies greater than 150 MeV.

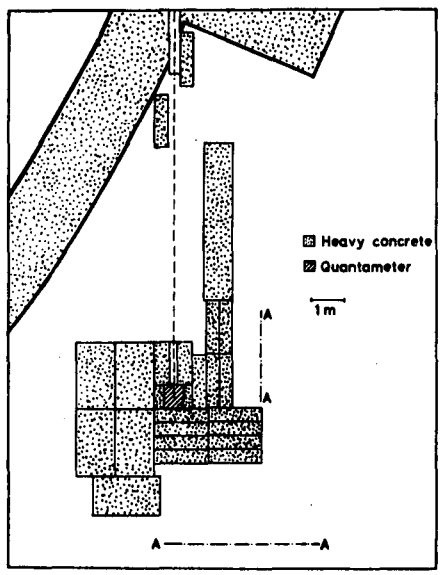

Fig. 6.62. Experimental arrangement of quantameter shielding.

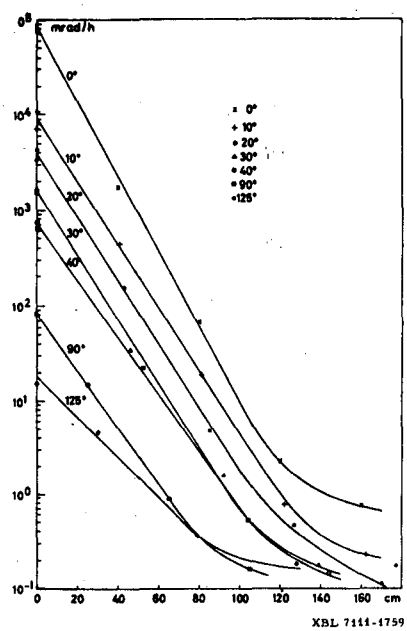

Fig. 6.63. Attenuation curves at various angles to the beam direction as measured with a TE chamber. (From Bathow et al.)

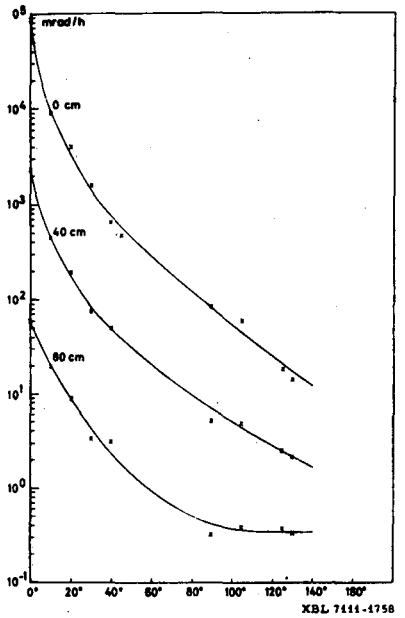

Fig. 6.64. Angular distribution of absorbed dose with respect to the incident beam direction, at various depths in the shielding, as measured by a TE chamber. (From Bathow et al.)

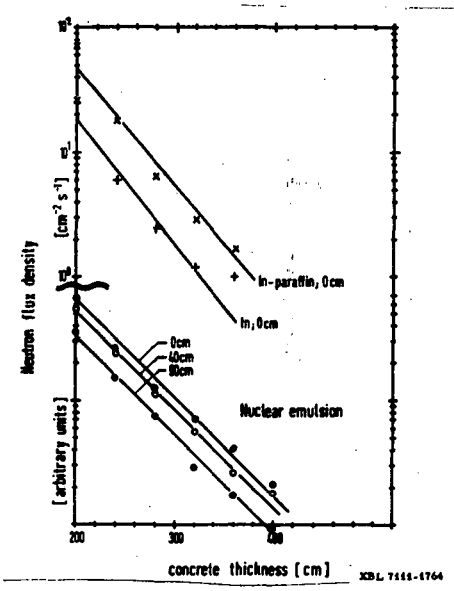

Fig. 6.65. The variation of neutron flux density with depth in concrete. Data shown for bare indium foils, moderated indium foils, and nuclear emulsions (NTA), taken along the beam direction and parallel to the beam direction at distances of 40 cm and 90 cm. Electron beam energy 4 GeV. (From Bathow et al.)

(The concrete used in this experiment was of high density—3.7 g/cm^3—and contained 50% iron by weight; a large attenuation length is therefore to be expected, although the quoted value of 185 g/cm^2 seems a little too high, possibly due to an error in the estimation of average density of the concrete).

The influence of the electromagnetic cascade is, however, still important even at these large depths. Figure 6.66 shows lateral profiles of dose rate measured with an ionization chamber and with neutron track films. The pronounced peak measured by the ionization chamber is attributed by Bathow et al. to muons produced by photoproduction. This suggestion is supported by estimates of muon production from the work of Clement and Kessler (CLE G 65). Bathow et al. show that photoproduction of muons would lead to change in the slope of the measured absorbed-dose transmission curve with incident electron energy. Figure 6.67 shows this to be experimentally observed, and the measured attenuation lengths are in good agreement with those calculated (205 g/cm^2 at 4 GeV, 340 g/cm^2 at 6 GeV).

It has been a long-lived superstition at many high energy electron accelerator laboratories that the dominant irradiation problems is due to photons and electrons. However, as we have seen, the early measurements by Bathow et al. showed (BAT G 65, BAT G 67a, BAT C 67c) that there is significant neutron production, and it is dometimes a complex matter to decide whether neutrons or photons are the major concern outside shielded electron accelerators. Recent investigations have found an increasing number of conditions under which neutrons are dominant.

Thus, for example, measurements outside concrete shielding normal to the electron beam direction at the Mark III accelerator showed that less than 10% of the total DE rate was due to γ rays, and also showed the presence of a significant flux of neutrons with energy greater than 20 MeV (CAR T 69, CHA V 69, THO R 69a). Measurements around a 6-foot-thick concrete beam dump showed great variations in the relative contribution of neutrons to the total DE rate, varying from 50 to 90% depending upon location. Perhaps even clearer evidence of this variability has been presented in radiation surveys atound an unessentially unshielded target bombarded by 1-GeV electrons.

The most recent evidence that neutrons must not be neglected in shielding considerations has been given by Coleman et al. (COL F 71). These authors performed a series of radiation measurements in the shielding surrounding the 4-GeV electron synchrotron NINA and associated beam lines, in a manner rather similar to that described by Gilbert et al. (GIL W 68) for the 24-GeV CPS.

A 4-GeV bremsstrahlung beam was impinged on the outer concrete wall of the accelerator room, effectively passing through 1.5 m concrete and then dissipating in the surrounding earth shield. The fraction of total DE rate contributed by photons decreased with depth in the earth and with angle with the beam direction subtended. Values ranged from (a) 0.90 in the beam

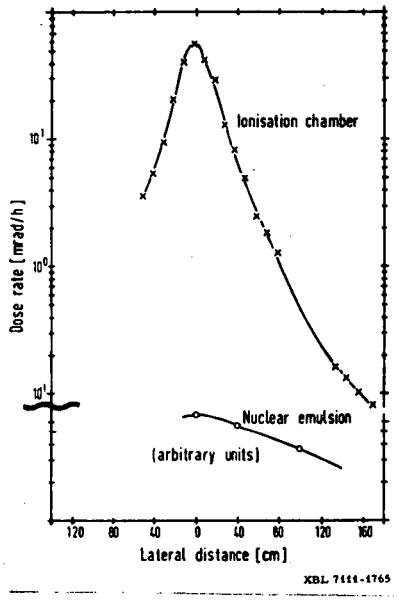

Fig. 6.66. Comparison of the lateral distribution of dose rate measured with an ionization chamber and with nuclear track films. Electron beam energy 6 GeV. (From Bathow et al.)

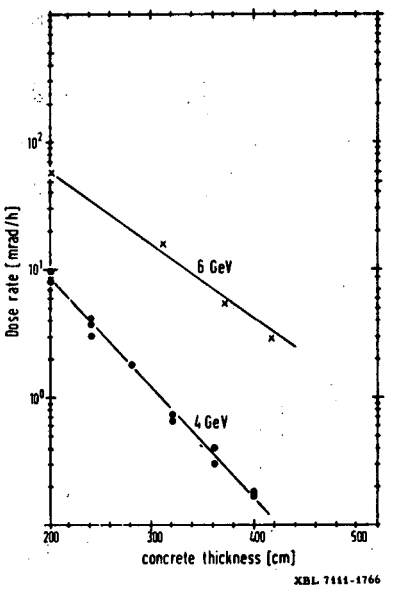

Fig. 6.67. The variation in dose rate in the beam direction for two different beam energies. (From Bathow et al.)

direction close to the shield wall to (b) 0.13 at 53 deg to the beam direction and 2 m deep in the earth. Similar measurements were made on top of the concrete roof of the accelerator room close to the target. The contribution of photons was about 20% whereas measurements made on the side of the accelerator room gave values of about 45%. Surprisingly, in all cases quoted, the contribution to the neutron DE of neutrons of energy greater than 10 MeV exceeded 80%.

NEUTRON TRANSMISSION THROUGH THE ATMOSPHERE –"SKYSHINE"– AND THROUGH THE GROUND–"GROUNDSHINE"

Introduction

The term "skyshine" was coined when high radiation levels were observed around accelerators with little or no roof shielding. Such background is largely due to the backscattering of radiation from the atmosphere–hence, the name. However, the effect of ground absorption for accelerators, where the sources of radiation are close to the ground, is significant. Thus the term "skyshine" as commonly used is something of a misnomer, since it usually describes all the radiation reaching points close to the accelerator, whether unscattered or scattered by the ground, air, or neighboring buildings, and often including "groundshine."

Skyshine has not been a serious problem at those high-energy accelerators provided with adequate roof shielding. However, it can present a limitation to the operation of accelerators with minimal or no roof shielding. Experience suggests that some overhead shielding is required for essentially all accelerators that produce neutron intensities greater than about 10^9 n/sec. Maximum permissible radiation levels at laboratory perimeters often dictate the limits on "skyshine." Members of the general population should not be exposed to radiation levels exceeding 0.5 rem per year, correstponding to 0.06 mrem/h (if permanent occupancy at the laboratory perimeter is assumed). In a climate of increasing public concern with radiation safety it is prudent, therefore, to document the radiation field around accelerators. Such surveys, in any case, are sound health physics practice; they will prove invaluable in determining frequency and type of radiation surveys, and will be helpful in siting nearby laboratories, workshops, and offices.

PROPAGATION OF NEUTRONS THROUGH THE ATMOSPHERE

Following the finding of high neutron background levels around the Cosmotron, Lindenbaum (LIN S 57a, LIN S 57b, LIN S 61) formulated a theoretical treatment of the propagation of low energy neutrons (few MeV) through the atmosphere. Essentially, he used the expression for the neutron flux produced by a point source in an infinite isotropic scattering medium that was derived by Case et al. (CAS K 53), using diffusion theory. They write the neutron flux density, $\phi(r)$, in the form

$$\frac{4\pi r^2 \phi(r)}{Q} = e^{-\Sigma_t(r)}\, \epsilon(c,r) + \frac{k(c)}{D}\, e^{-k_0 r}, \tag{6.66}$$

with Σ_t = macroscopic total cross section,

D = diffusion coefficient,

k_0 = diffusion length,

$\epsilon(c,r)$ = and K(c) are fuctions of c (ratio of scattering to total cross section),

Q = neutron source strength (n/S).

Experience at the Cosmotron showed the major radiation field to consist of neutrons of a few MeV; for neutrons of 1 to 5 MeV Lindenbaum derived the expression

$$\phi(r) = \left[\frac{8.5 \times 10^{-5}}{r^2} \exp(-r/450)\, \epsilon(c,r) + \frac{4.7 \times 10^{-7}}{r} \exp(-r/830)\right] Q, \tag{6.67}$$

with ϕ in n/cm^2 sec,

Q in n/sec,

r in feet.

It is clear from Eq. 6.67 that the second term will dominate after distances of about 100 ft (30 meters). Lindenbaum approximated the influence of ground absorption by putting c = 0.8 to 0.9 (c for air is 0.97), based on values for the albedo of earth ranging from 0.5 to 0.8. Figure 6.68 shows values of $4\pi r^2 \phi(r)/Q$ calculated from Eq. 6.67 for values of c = 0.5 and 0.9.

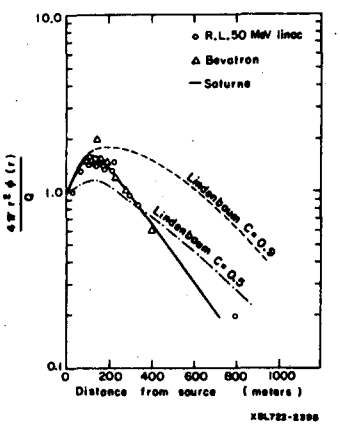

Fig. 6.68. Comparison of measurements of skyshine at three proton accelerators (50-MeV proton linear accelerator and 3-GeV and 6-GeV proton synchrotrons) with theoretical values calculated from Lindenbaum equation. (After Thomas.)

Lindenbaum's equation was readily shown to predict neutron fluxes observed around accelerators to within a factor of 2 or 3 (LIN S 57b, LIN S 61) (THO R 60), and experience over the past 10 years has shown this factor to hold true for a large variety of particle accelerators. In many cases this accuracy is adequate for health physics purposes. More accurate determinations are difficult for a variety of reasons. The available intensity of most accelerators has limited the range of measurements to about 300 m; in many cases the effects of scattering and the intercalibration of different neutron detectors together with the uncertain effects of a changing neutron spectrum add to the confusion. Nevertheless, several careful measurements have been reported. Cowan and Handloser (COW F 53) made measurements with an ionization chamber of the radiation levels between 250 and 1000 ft (75 and 300 m) from the Cosmotron at Brookhaven. Although not specifically stated, it seems likely that the exposure rate was almost entirely due to neutrons. Assuming a variation of the form $\phi(r) = \phi_0 r^{-n}$, they report $n = 2.3 \pm 0.2$.

Dakin (DAK H 61) measured neutron fluxes between 350 and 1650 ft (107 and 500 m) around the Bevatron by using a BF_3 counter shielded at the back and sides with concrete. Concrete was placed in front of the detector, and crude estimates were made of the fast-neutron energy spectrum. Dakin interprets his results by assuming the neturon spectrum consists of two groups, the first having an average energy between 1.3 and 4 MeV and the second between 100 and 260 MeV. For both groups, the radial variation of neutron flux was similar and, within the experimental accuracy, did not differ greatly from an inverse square. More recent and more precise measurements of the low-energy neutron group were made with a moderated BF_3 counter, 300 to 1200 feet from the center of the Bevatron (DAK H 62). It is apparent from these latest observations that the neutron flux falls off faster than inverse square and could be better represented by an equation of the form

$$\phi(r) = \frac{a}{4\pi r^2} e^{-r/\lambda} \qquad (6.68)$$

over the range of measurements.

Moyer has explained (MOY B 62) the surprising observation by Dakin that the radial dependences of both the high-energy and low-energy neutrons are almost indistinguishable in the range 100 to 500 meters.

Measurements of the propagation of low-energy neutrons have been reported by a group from the Rutherford Laboratory. (THO R 62a, THO R 62b, SIM P 62). This group was fortunate in that downstream from the neutron source there was a flat area completely free of buildings. Neutrons were produced by stopping a 30-MeV proton beam in a thick aluminum target, giving a well-defined "point" source about 5 ft (1.3 m) above the ground. Measurements of the mean neutron energy indicated a value close to

to 0.75 MeV. Absolute measurements of the neutron flux at distances between 100 and 2500 ft were made with a calibrated long counter, whereas fluxes between 3 and 100 ft were measured with sulfur capsules and moderated indium foils. It was also possible to make an accurate estimate of the neutron source strength, which permitted an absolute comparison with Lindenbaum's prediction. Measurements at distances up to 980 ft indicated that Eq. 6.66 predicts fluxes considerably higher than those observed (a factor of 3 at 1000 ft); from these measurements it was not possible to obtain a good fit to an equation by the form of Eq. 6.66. Later measurements by Simpson and Laws (SIM P 62) at distances out to 2500 ft even further accentuate the divergence.

Tardy-Joubert and De Kerviler (TAR P 63) have reported measureements made around "Saturne." Unfortunately, they do not give numerical data or errors, but show a smooth curve between 37 and 700 m from the machine.

By 1966 measurements of the variations of neutron background with distance had been made at several accelerators. Thus Ladu et al. (LAD M 65) and Bathow et al. (BAT G 67c) had reported measurements at 1-GeV and 4-GeV electron synchrotrons. Further measurements at proton accelerators included those at the CERN 650-MeV synchrocyclotron (RIN A 63), the 24-GeV proton synchrotron (BAA J 64), the Dubna 10-GeV synchrophasotron (LEB V 65), and the BNL 30-GeV AGS (DIS C 65).

Bathow et al. (BAT G 67c) analyzed those early measurements for which mean neutron energy measurements were also reported, and found best values for the parameters of the Lindenbaum equation, which are summarized in Table 6.XV.

The paramters found are quite similar, with the exception of those for the CERN cyclotron. For this accelerator the mean neutron energy reported ($\approx$ 10 MeV) was considerably higher than for the other accelerators ($\approx$ 1 MeV), which may account for the considerably greater value of relaxation length ($1/k_0$) (300 meters, to be compared with 100 to 140 meters for the other machines). It is questionable, however, whether such an analysis based merely upon the shape of neutron flux distribution can uniquely determine the four paramteres of the Lindenbaum equation. In a strict test of the Lindenbaum equation it is necessary to determine the source strength, Q, and it is desirable to extend measurements out to as great a distance as possible.

Thomas (THO R 68) has summarized the experimental results obtained at Berkeley, Harwell, and Saturne. Figure 6.68 shows the parameter

$$f(r) = \frac{4\pi r^2 \phi(r)}{Q} \tag{6.69}$$

as a function of distance from the accelerator. Such a procedure removes the $1/r^2$ dependence and permits a study of the residual variations. Only the Harwell data included a precise estimate of the source strength Q. For the

Table 6.XV. Summary of Lindenbaum's equation parameters obtained from skyshine measurements at several accelerators.

Laboratory	Primary beam energy	Range of measurements (meters)	$1/k_0$ (meters)	Σ_t ($m^{-1}X10^{-2}$)	$\bar{C}$	D (meters)	Mean neutron energy (MeV)	Reference
CERN	600-MeV protons	80-1500	300	0.68	0.91	53	10	RIN A 63
Frascati	1.1-GeV electrons	50-200	100	1.7	0.86	22	0.25-0.4	LAD M 65
DESY	4-GeV electrons	50-550	140	1.3	0.88	28	0.5	BAT G 67c
Harwell	30-MeV protons	30-300	140	1.2	0.86	31	0.71	THO R 62
Dubna	10-GeV protons	100-500	140	1.0	0.81	37	0.7-3.0	LEB V 65
Saclay	3-GeV protons	50-600	135	1.0	0.77	39	0.9-4.0	TAR P 63

Berkeley data, an arbitrary normalization was chosen so that $4\pi r^2\phi(r)/Q=1.0$ at r = 280 m. The source strength taken for the Saclay data was obtained by extrapolating the smooth curve back to r = 0.

The main features of the curve are the buildup to a maximum of 1.6 at 110 m, return to 1.0 at 280 m, and exponential decrease thereafter with slope 267 m. The experimental results of all three laboratories are seen to be in fair agreement (discrepancies $\approx$ 6%).

An empirical expression that fits the experimental data well is

$$f(r) = a(1-e^{-r/\mu})\, e^{-r/\lambda} \quad \text{for } r \geq 50 \text{ m}, \tag{6.70}$$

with

$$a = 2.8,$$

$$\mu = 56 \text{ m},$$

$$\lambda = 267 \text{ m}.$$

Table 6.XVI compares the measured and calculated values of f(r) and shows good agreement. A very convenient representation of the variation of neutron flux as a function of distance from a point source is, then,

$$\phi(r) = \frac{Q}{4\pi r^2} f(r) = \frac{aQ}{4\pi r^2} (1 - e^{-r/\mu})\, e^{-r/\lambda} \text{ for } r \geq 50 \text{ m}. \tag{6.71}$$

Table 6XVI. Comparison of measured and calculated values of f(r)

r (m)	f(r) (measured)	f(r) (calculated from Eq. 6.70)
50	1.30	1.29
75	1.55	1.56
100	1.61	1.60
150	1.56	1.49
200	1.36	1.28
400	0.63	0.62
500	0.42	0.43

Kompochkov (KOM M 70) has reported from measurements at the Dubna Synchrophasotron that Eq. 6.71 expresses the dependence of neutron flux density with distance better than the Lindenbaum equation out to a distance of 440 meters from the accelerator.

It is of interest to note that the value of attenuation mean free path for the skyshine neutrons obtained from measurements around accelerators

is in fair agreement with that found around reactors. Stephens et al. (STE L 64), using reactor facilities at the Nevada Test Site, found $\lambda \approx 245$ yards (224 m). There are, of course, differences in the neutron spectra in the two cases.

The measurements reported by Rindi and Baarli at the CERN synchro-cyclotron (RIN A 63), however, would suggest a much larger value of attenuation length, λ. Distenfeld and Colvett (DIS C 65), too, have reported measurements that indicate a somewhat longer attenuation length. Data taken at distances up to 900 meters from the Brookhaven 30-GeV AGS were interpreted in the form of Eq. 6.71, with values of μ of 47 m and λ of 600 m. The attenuation length of 600 m (72 g/cm^2) would correspond to the transport of quite energetic neutrons (about 70 to 80 MeV).

These apparent discrepancies are almost certainly due to the inability of simple empirical models to describe the physical situation precisely. Neutrons emerging from the accelerator shield are distributed in a continuous energy spectrum up to very high energies. The interaction length of neutrons of energy greater than bout 150 MeV in air is about 1000 meters, but the interaction length of 10-MeV neutrons is about 30 g/cm^2 (250 m).

Thus all the measurements of skyshine reported have been made in the region in which the neutron spectrum is in transition at the shield-air interface. The attenuation observed in air therefore depends crucially upon the energy spectrum of neutrons emerging from the accelerator shield.

It seems clear from experience at a variety of accelerators that calculations of neutron flux density by use of Eq. 6.67 or 6.71 is sufficient for prediction of dose rates and design of roof shielding. In certain special cases it may be necessary to make measurements to check the performance of the shield.

When the accelerator becomes physically very large, as in the case of high energy strong-focusing accelerators, it is no longer reasonable to consider the radiation to originate at a point source. The accelerator itself and its experimental beams must be treated as extended radiation sources. This somewhat specialized case has been briefly discussed in a design study for a 200-GeV proton accelerator (LRL 65.)

Groundshine

The phenomemon known as "groundshine," the leakage of radiation underneath heavy-density shielding, was first observed at the Brookhaven AGS around target shielding (BNL 64). Knowles has discussed the problem in the Yale Meson Factory Design Study Report, (YALE 64), and its solution lies in reducing the scattered radiation by extending the high-density shielding into the lighter-density foundation (LRL 65).

Alsmiller et al. (ALS R 70) have recently made calculations of "groundshine" for a target bombarded by high-energy protons shielded by iron above an earth foundation. The calculations indicate that, close to the shield wall, roughly half the observed radiation level may be due to groundshine.

RADIATION TRANSMISSION ALONG TUNNELS AND LABYRINTHS

Efficient shield design must take account of the contribution to external radiation levels due to transmission through the inevitable holes and voids necessary for access to the accelerator.

The major theoretical and experimental studies of the transmission of radiation by tunnels have concentrated on neutron fluxes produced by reactors. An excellent summary of the pioneer work is given by Price, Horton, and Spinney (PRI B 57). More recent studies have been reviewed by several authors in the Engineering Compendium on Radiation Shielding (JAE R 68). Substantial progress is reported in our under standing of the transmission of relatively low-energy neutrons along straight, empty cylindrical ducts. In most cases experimental data agree with theoretical predictions to within about 25% (BER B 68a). (However, almost all the published experimental work reports studies in ducts that penetrate water shields.) Substantial work on penetrations of other shapes and types of interest in reactor shield design is also reported: multisectional cylindrical ducts, straight cylindrical ducts filled with material differing from the main shield material (BER B 68b), liquid-filled cylindrical ducts (AAL E 68), and annular ducts (NIL J 68, VES W 68).

Of most interest to the accelerator shield designer, however, are the studies of neutron attenuation along rectangular ducts reported by Maerker et al. (MAE R 68). The geometrical complexities of such ducts have led to the development of computational methods that are capable of extension to the problems of high energy accelerators. The most successful of these has been a combination of a Monte Carlo technique to follow the progress of a neutron along the duct together with a treatment of multiple scattering by the albedo method. Calculations by use of these techniques can, in general, estimate flux densities through multilegged labyrinths over attenuation of five orders of magnitude to an accuracy within $\approx 25\%$.

Unfortunately, these calculations have until recently been limited to neutron energies below a few MeV. We are, of course, concerned around high-energy accelerators with the dose transmitted by neutrons of considerably higher energy than found around a nuclear reactor. Furthermore, transmissions of only approximately 10^{-5} or less are necessary for tunnels penetrating future high-energy accelerator shields, and until recently few pertinent experimental data were available.

DeStaebler has reported γ-ray dose level and fast-neutron flux as a function of position in a labyrinth at the Cambridge Electron Accelerator (DeS H 63). He concludes that the measurements compare fairly well with calculations although the dose transmission was only approximately 10^{-2}. Doty has made a duct transmission measurement using d-D and d-T neutrons as the source (DOT D 64), and obtained results not incompatible with theoretical calculations for similar transmissions.

Shaw (SHA K 66), has reported transmission measurements for γ rays and neutrons along a curved tunnel leaving the Nimrod accelerator room. He found that at a sufficient depth in the tunnel, where there was no direct contribution from the accelerator, intermediate and thermal neutrons were the major components of flux. The larger weighting of fast neutrons in dose-rate assessments, however, made the fast-neutron contribution to the dose roughly equivalent to that due to intermediate and thermal neutrons. The transmission of the tunnel for low-energy neutrons may be estimated by using the semi-empirical relationship described by Price, Horton, and Spinney (PRI B 57).

STRAIGHT TUNNELS

In the last 5 years additional experimental data have been obtained, and the computational methods developed for reactor problems have been modified for use at higher energies. Gilbert et al. (GIL W 68) have reported measurements of the attenuation of neutron flux density and γ-ray dose along tunnels of large cross section at depths up to 100 meters. Figure 6.69 shows relative transmission data obtained with activation detectors, β,γ film, and TLD (see Chapter 5) whose characteristics are given in Table 6.XVII.

Table 6.XVII. Detectors and their characteristics. Used by Gilbert et al. in their tunnel movements.

Detector	Reaction	Energy range (MeV)
Bare gold foils	$^{197}Au\ (n,\gamma)\ ^{198}Au$	thermal
Large bare indium foil	$^{115}In\ (n,\gamma)\ ^{116m}In$	thermal
Moderated gold foils	$^{197}Au\ (n,\gamma)\ ^{198}Au$	0.02 to 20
Kodak Type-B neutron film	proton recoil	0.5 to 25
Sulfur	$^{32}S\ (n,p)\ ^{32}P$	>3
Aluminum	$^{27}Al\ (n,\alpha)\ ^{24}Na$	>6
Plastic scintillator	$^{12}C\ (n,2n)\ ^{11}C$	>20
$\beta\gamma$ film LiF TLD	γ rays + charged particles	

Figure 6.69 summarizes the transmission data obtained by using different detectors. For convenience, the data are presented graphically by normalizing all the transmission curves to unity at a depth of 0 m. A systematic trend is immediately obvious in that the higher the threshold of the neutron detector, the larger the flux transmission. Thus the difference in overall transmission for thermal and ^{11}C neutrons is more than a factor of 10 at 80 m. Gilbert et al. concluded that the flux transmission T_1 of a tunnel expressed as a function of length z along the tunnel, the effective tunnel radius a, and the energy response E of the detector is

$$T(z,a,E) = \Gamma\left(\frac{z}{a}, E\right)e^{-z/\lambda(E)}, \qquad (6.72)$$

where $T(z,a,E)$ is the overall transmission, $\Gamma(z/a, E)$ is the transmission of the tunnel uncorrected for neutron-absorption processes, and $e^{-z/\lambda(E)}$ is a correction factor which takes account of neutron interactions in the air along the tunnel. The mean free path $\lambda(E)$ is determined by the neutron total cross section in air. At large values of (z/a) we expect

$$\Gamma\left(\frac{z}{a}, E\right) \rightarrow \left(\frac{a}{z}\right)^2 \qquad (6.73)$$

For $z/a \geq 10$, and thus a semilog plot of $z^2\,T(z,a,E)$ should give a straight line with negative slope $\lambda(E)$.

Figure 6.70 shows semilog plots of $z^2\phi$ [proportional to $z^2T(z,a,E)$] against z (in meters) for badges and TLD, aluminum, and carbon. For penetrations greater than 20 m in large tunnels, the attenuations were found to be nearly exponential. Table 6.XVIII lists the estimated removal mean free paths (attenuation length) and the corresponding removal cross sections, assuming an atmosphere of nitrogen. At neutron energies between 1 and 20 MeV, the inelastic cross section for nitrogen is 200 mb, and the total cross section 2b.

Table 6.XVIII Attenuation lengths and removal cross sections for tunnel transmission.

Detectors	Attenuation length (meters)	Removal cross section (barns)
Plastic scintillator	100	1.9
Aluminum	60	3.2
Film and TLD	55	3.3
Bare gold	30	6.2

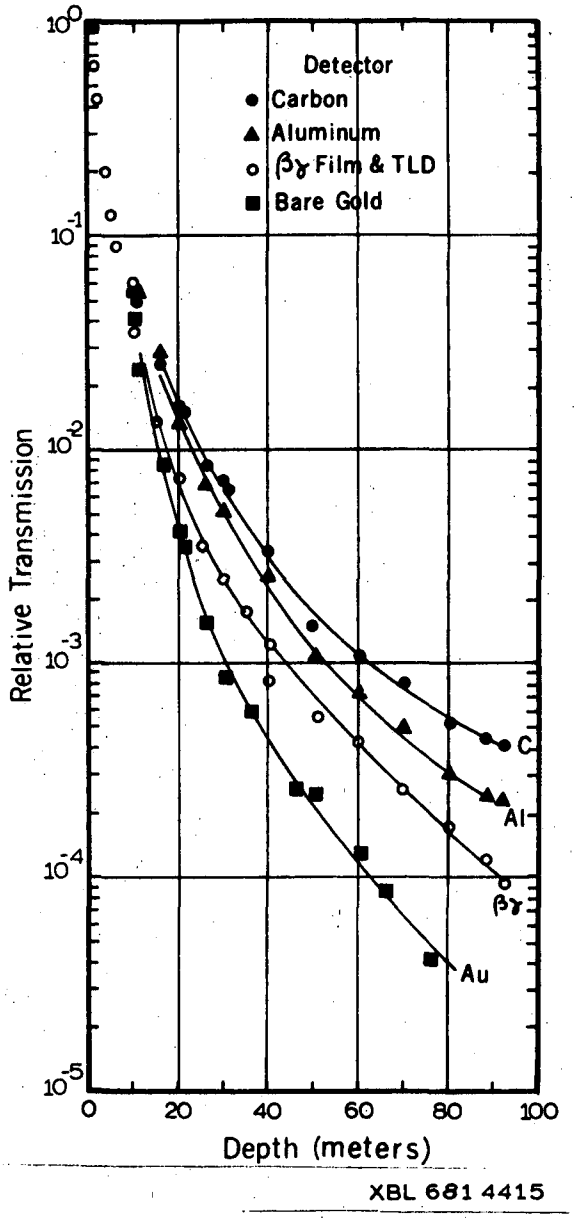

Fig. 6.69. The relative transmission of neutron flux density and γ dose rate along large straight tunnels. (From Gilbert et al.)

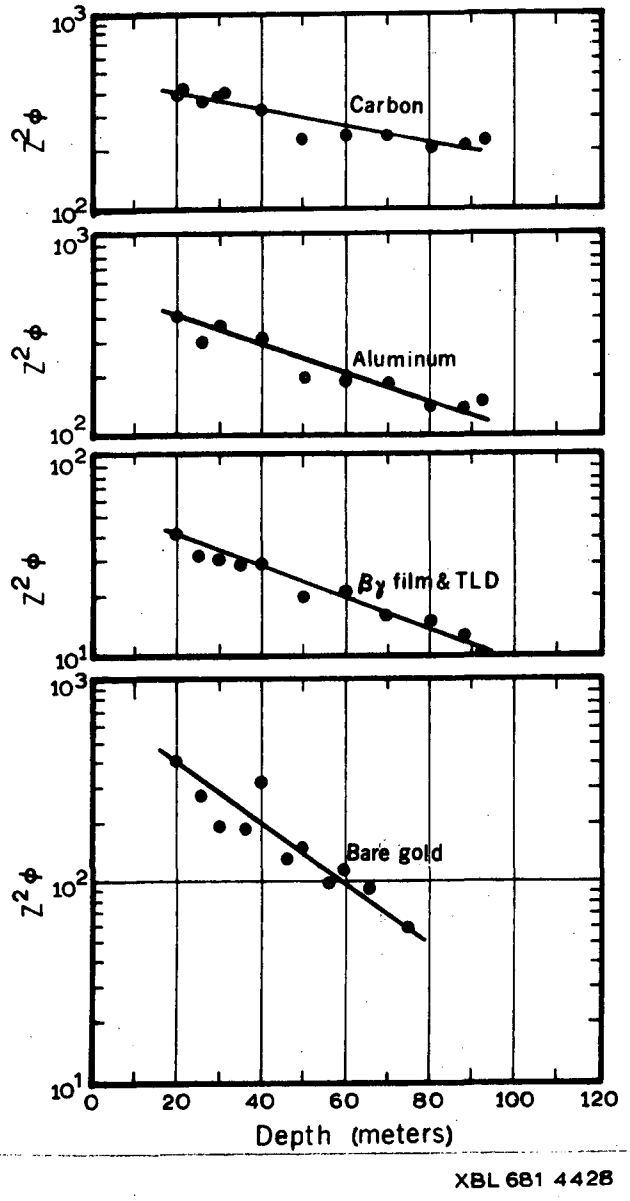

Fig. 7.70. Approximate exponential absorption of neutron flux density and γ dose rate along large straight tunnels for a variety of detectors. (From Gilbert et al.)

A similar variation in transmission with energy threshold of the detector was reported in transmission studies through the shield of the CERN 600-MeV Synchrocyclotron by Rindi and Tardy-Joubert (RIN A 67), who have also reported measurements of absorbed dose and neutron flux densities with counters along long straight tunnels.

Throughout the series of measurements reported by Gilbert et al. there was some uncertainty as to the effective location of the radiation source with respect to the tunnel mouth, due to the geometrical configuration of the tunnel and the accelerator (see Gilbert et al.). Schimmerling and Awschalom (SCH W 69) have reported some studies of the influence of moving a point source (accelerator target bombarded by 3-GeV protons) across the opening of a four-legged labyrinth in concrete. They show that the epi-cadmium neutron flux density may vary by as much as a factor of two at great distances along the labyrinth as the source moves across the opening.

In a recent carefully designed experiment, Stevenson and Squier (STE G 71) made measurements of neutron transmission along a tunnel of moderate length (18 m) but with the position of the radiation source well defined: 7-GeV protons bombarded a thick heavy target placed on the axis of, and 1.9 m from the entrance of, a tunnel of square cross section (2.3-m side) lined with concrete (density 2.3 g/cm^3).

The transmission factor for fast neutrons was found to be well represented by

$$T(z) = \left(\frac{\ell}{\ell + z}\right)^2 \exp(-\ell + z/60), \qquad (6.74)$$

where ℓ is the distance from the target to the tunnel mouth,
z is the distance along the tunnel, measured from the tunnel mouth.

This formula fits the data obtained with $^{27}Al(n,\alpha)\ ^{24}Na$, $^{19}F(n,2n)\ ^{18}F$, and $^{12}C(n,2n)\ ^{11}C$ activation detectors with thresholds of 6, 11, and 20 MeV respectively (see Fig. 6.71). It is of interest to note that the value of attenuation length—60 m—confirms that reported in the measurements by Gilbert el al. for aluminum activation detectors. The data of Stevenson and Squier do not extend to sufficiently large distances to confirm the variation of attenuation length with energy threshold reported in the earlier work. Stevenson and Squier report that measurements made with moderated indium detectors and ^{7}LiF TLD detectors show transmissions similar to those of the higher-energy threshold detectors. However, the thermal neutron flux measurements indicate a considerable enhancement from wall scattering (see Fig. 6.71).

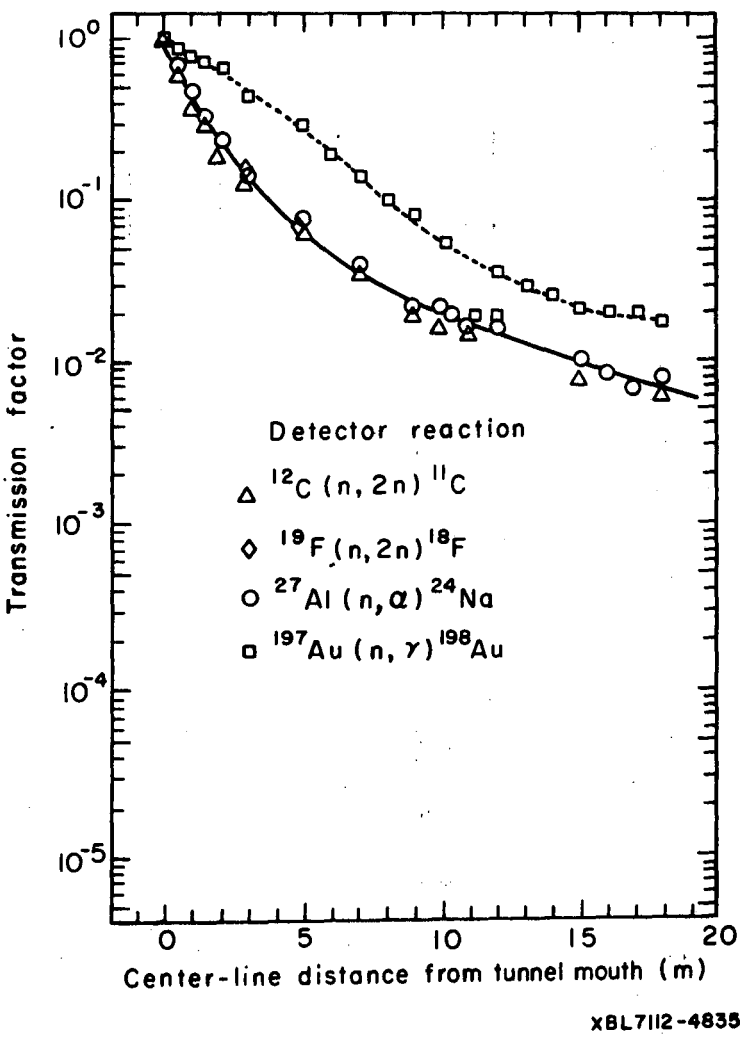

Fig. 6.71. Relative variation of particle flux density (as determined by several activation detectors) with distance along a straight tunnel. (After Stevenson and Squier).

CURVED TUNNELS

Shaw (SHA K 66) reported the first measurements of high energy neutron transmission along curved tunnels through the shielding of a high energy accelerator. Similar measurements were made, but in greater detail, in the shielding studies reported by Gilbert et al., who showed the higher energy component of the neutron flux (as measured by aluminum detectors and fast neutron films) is attenuated more rapidly than the thermal neutron flux. The decrease of the flux measured by the moderated indium foils is approximately exponential, with an e-folding length of 3.9 m, in excellent agreement with the value of 6.0 m derived from the data presented by Rindi and Tardy-Joubert for the same tunnel.

The measurements by Rindi and Tardy-Joubert facilitated the development of a Monte Carlo neutron transport program (ZEUS) for labyrinth design. This program randomly generates monoenergetic neutrons and follows their transmission through almost any desired labyrinth (GER F 68, d'HO M 68). Reflection of neutrons from the labyrinth walls is approximated by the albedo method. Gollon and Carrigan (GOL P 70) have described the use of this program, with albedo coefficients corresponding to neutrons in the energy region 3 to 4 MeV, to study radiation transmission along a variety of concrete tunnels. Their calculations for circular tunnels show the approximate exponential attenuation observed experimentally. Combining the theoretical and experimental data suggests that the effective attenuation length, λ, is a factor of tunnel radius of curvature, R, given by

$$\lambda = \approx 0.7 \sqrt{R,} \qquad (6.75)$$

with R in meters over the range $4 \text{ m} \leqslant R \leqslant 40$ m. No systematic study has been carried out, however.

LABYRINTHS

The earliest studies of neutron attenuation through labyrinths were theoretical. Alsmiller and Solomito (ALS R 69b) have calculated the thermal and epicadmium neutron fluxes as a function of position in labyrinth of concrete tunnesl of rectangular cross section. The radiation source at the labyrinth entrance was produced by 3-GeV protons interacting on a lead target to simulate the conditions of some measurements reported by Schimmerling and Awschalom in a four-legged labyrinth (SCH W 69). However, all incident charged particles and neutrons of energy greater than 10 MeV were neglected in the calculations, making comparisons with the experimental data somewhat ambiguous. Comparisons along the second and third legs indicate that the calculated flux densities were consistently lower than those measured, by a factor between two and three.

Gollon and his colleagues (GOL P 70, GOL P 71) have reported calculations with the program ZEUS to study neutron transmission through

labyrinths, and recently some careful measurements by Stevenson and Squier have facilitated a comparison of such calculations with experimental data. Figure 6.72 shows the experimental arrangement for these labyrinth measurements, which consisted of a-right angled bend, some 11 m from the tunnel entrance, that then extended a further 8 m. Figure 6.73 shows the experimental data obtained with the detectors previously discussed. After the bend all components suffer a more rapid attenuation than for the corresponding distance along a straight tunnel. This effect is more marked the higher the energy of the neutrons (note the clear separation between the aluminum and carbon-activation detector data).

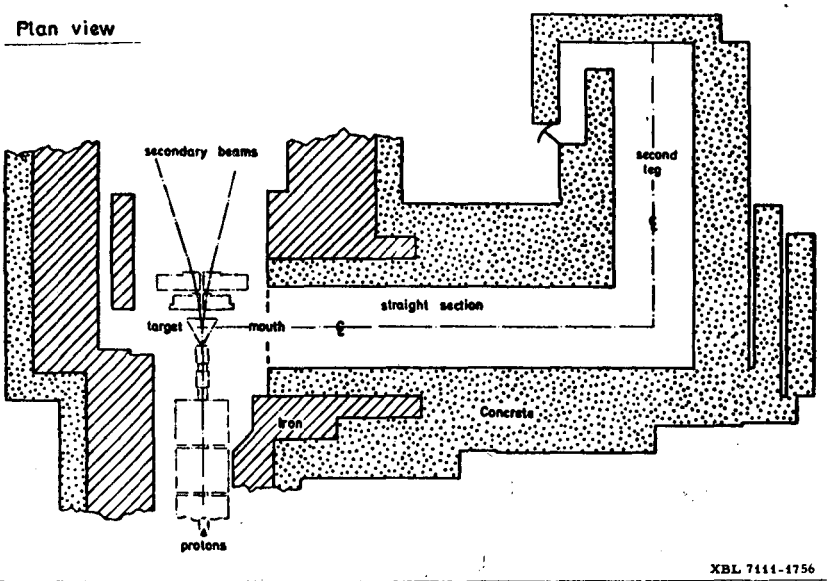

Fig. 6.72. Experimental layout used to study the transmission of neutrons around right-angled bends. (From Stevenson and Squier.)

From the flux density measurements Stevenson and Squier evaluated the resultant neutron dose-equivalent rates by the method first suggested by Shaw et al. (SHA K 69). Figure 6.74 shows a comparison between these dose-equivalent rate values and those calculated by using ZEUS with albedo coefficients corresponding to 3- to 4-MeV neutrons. The measured transmission is considerably higher than that calculated, and Stevenson and Squier attribute this to the choice of inappropriate albedo parameters in the calculations. Stevenson and Squier further suggest, from their experience with multileg accesses, that, following the first substantial bend in a labyrinth, the neutron spectrum does not significantly change further.

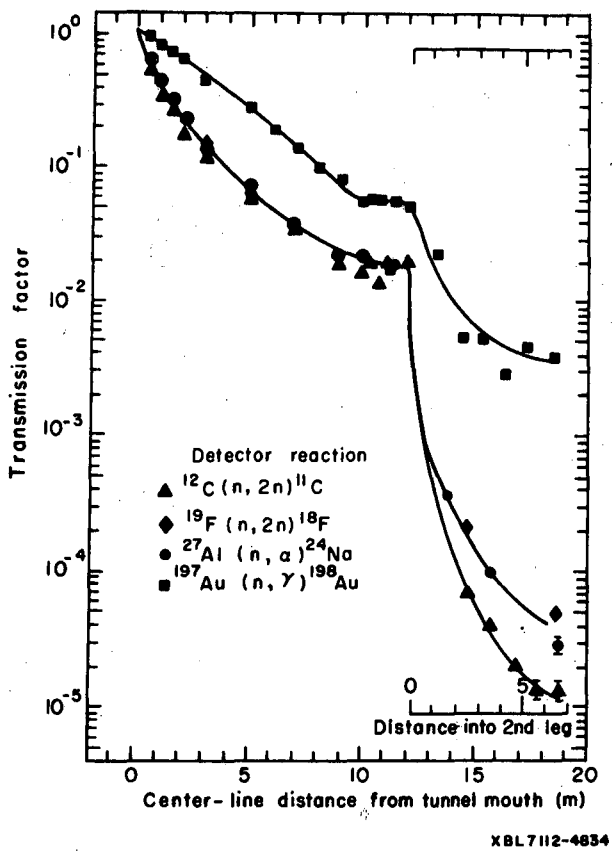

Fig. 6.73. Relative transmission of particle flux density along tunnel Layout shown in Fig. 6.72. (From Stevenson and Squier.)

The choice of the albedo coefficients in the ZEUS program was based on the measurement of radiation transmission along tunnels with a tissue-equivalent ionization chamber (RIN A 67). However, such an instrument doesn't discriminate between absorbed doses due to γ rays or to neutrons. It is possible therefore that the influence of a substantial γ-ray flux in the experiments by Rindi and Tardy-Joubert could have perturbed the selection of albedo coefficients. It would therefore seem appropriate to modify these coefficients to correspond to somewhat lower energies.

More experiments are needed to achieve reasonable precision in labyrinth design. However, this short review should indicate the steady increase in our understanding of tunnel transmission phenomena for neutrons of greater energy than a few MeV.

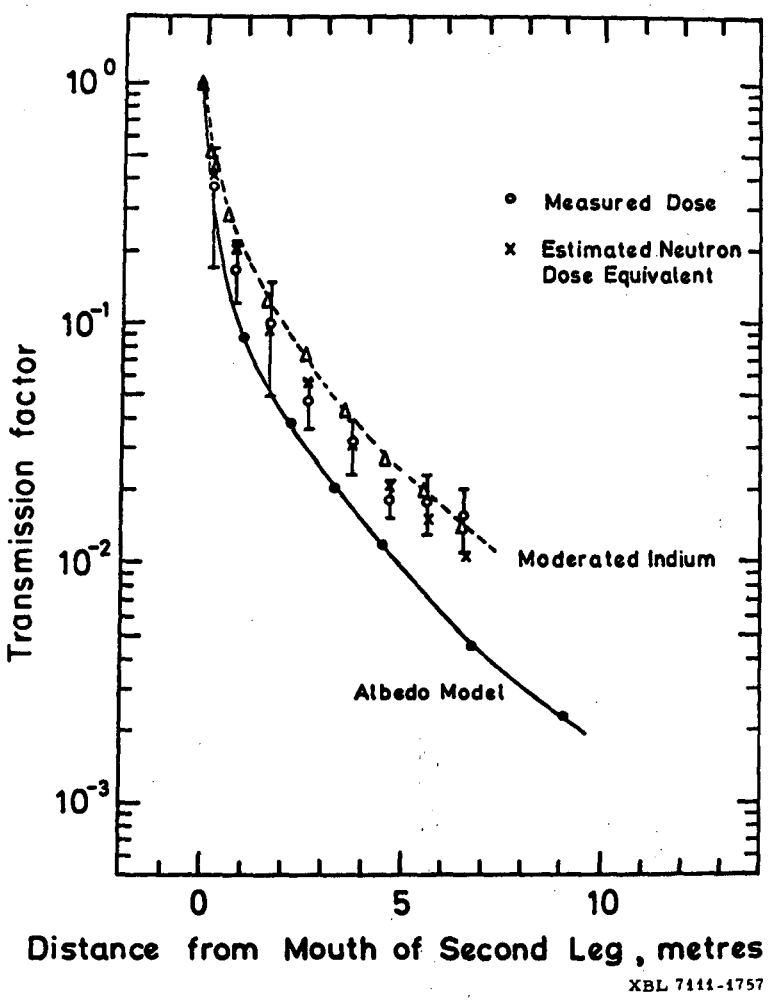

Fig. 6.74. A comparison between the transmission of absorbed dose, along the second leg of the tunnel (Fig. 6.72), as measured and as calculated by using the computer code ZEUS. (From Stevenson and Squier.)

SHIELD DESIGN—SOME EXAMPLES

Introduction

The variety of particle accelerators does not permit shield design to be reduced to rote. This chapter cannot therefore attempt to provide a shielding manual, but rather to indicate the general principles involved in shield design.

However, any efficient shield design progresses along a well-defined logical path, which is indicated here.

a. *Accelerator parameters* must first be roughly decided. Of greatest importance is knowledge of the particles to be accelerated, the energy, and the intensity. This knowledge will facilitate some general conclusions as to the quality of the radiation environment and its approximate magntiude (Chapters 3, 6, and 7).

b. *Accelerator location* will often determine the radiation levels that may be permitted outside the shielding. Quite different safety standards are required for, say, a research accelerator situated at the center of a remote site, access to which is controlled and limited to experienced radiation workers, and for an accelerator located in the center of a busy university campus open to young students and members of the general public (see Chapter 8).

c. *Primary radiation sources* will be determined by the accelerator, its mode of operation, and the primary interactions of the accelerated particles with accelerator components, shielding experimental setups, irradiated objects, or patients. We have discussed in Chapter 3 the characteristics of these primary interactions. The spatial distribution of these primary interactions around the accelerator, complex often referred to as the "beam loss distribution," must be determined.

d. *The extent of the transmission and modification* of the primary radiation by shielding material, discussed in this chapter, then determines the shield design. The fact that no shield is perfect, that it inevitably is penetrated by access tunnels, service ducts, and beam channels, must not be forgotten by the shield designer!

e. *The radiation environments* that may exist outside the shielding should be determined, as far as possible, in the design, so that reliable estimates of the dose-equivalent rates around the accelerator complex may be made.

PROTON LINEAR ACCELERATORS IN THE ENERGY RANGE 20 TO 100 MeV

Introduction

Despite the fact that proton linear accelerators have been in operation for some 20 years or more (ALV L 47), surprisingly little information describing *practical* experience of associated health physics problems has appeared in the scientific literature. This is no doubt in part because at many laboratories the problems have not hitherto been severe at accelerator energies up to 50 MeV. Thus, for example, radiation levels in the enivronment of the 20-MeV injector to the Bevatron and the 50-MeV injector to the AGS have been sufficiently low to permit personnel to work for limited periods, alongside these accelerators while they are in operation (EVE W 71). Because these accelerators were used to inject beam into proton synchrotrons, their major neutron production occurred in well-shielded regions of the accelerator complex. However, at those linear accelerators where the proton beam has been primarily used directly for experiments—for example, at the 50-MeV proton linear accelerator of the rutherford Laboratory (HAC R 66, HAC R 67a, HAC R 67b). Substantial shielding around targets, Faraday cups, beam collimators, etc. is found to be necessary at energies of 30 to 50 MeV and average proton beam currents of $\approx 1\mu$ A. Operational health physics experience at the Rutherford Laboratory thus provides one useful source of information. Unfortunately this accelerator is no longer in operation. However, before it was taken out of service considerable attention was given to its possible application for use as an injector to Nimrod, a 7-GeV proton synchrotron (PLA C 68a, PLA C 68b). This design study provided some estimates of losses along beam transport systems and the shielding required.

A second source of information is the design studies made at several laboratories for high-intensity high-energy linear accelerators. Thus design studies for a 750-MeV proton linac by a group at Yale included a comprehensive review of radiation problems up to 1964 (KNO H 65, YALE 64). A similar accelerator, designed to produce protons up to 800 MeV at a mean current of 1 mA, is presently under construction at Los Alamos. Cochran and Israel have discussed the radiation problems and shielding design of this accelerator (COC D 65, ISR H 69). Design studies for the 200- to 500-GeV proton synchrotron currently under construction at the National Accelerator Laboratory, carried out first at the Lawrence Berkeley Laboratory (LRL 65) and subsequently at Batavia (NAL 68, AWS M 70a), included shielding estimates for a 200-MeV proton linac. The work at Batavia depends on calculations based on neutron transport theory by O'Brien, who had previously reported similar calculations for the Los Alamos linear accelerator (OBR K 67, 68b).

As the new high-energy linacs come into operation we may expect a rapid increase in our understanding of radiation problems of these accelerators. Preliminary data obtained at the 70-MeV proton linac used as an injector for the 70-GeV synchrotron at Serpukhov have already been published (CHI M 69), and the operation of the 200-MeV injectors at Brookhaven and Batavia should yield interesting information. The construction of the 800-MeV LAMPF facility makes it particularly suited to shielding studies of the type already carried out at CERN (GIL W 68) should they be found necessary.

Table 6.XIX summarizes the sources of information on the radiation problems of proton linear accelerators.

Table 6.XIX

Accelerator	Energy (MeV)	Comments
Rutherford Laboratory PLA	50	(a) Operational experience (b) PLANIM design study
CERN PS injector	50	Operational experience
Bevatron Mark II linac injector	19.2	Operational experience
Yale meson factory	750	Design study
LAMPF	800	Mean current 1000 μA; design study
NAL synchrotron linac injector	200	Design study
Serpukhov synchrotron injector	100	Operational experience

Linear Accelerator Beam Losses

Quantitative estimates of beam losses along the accelerating structure of proton linear accelerators have not yet been satisfactorily predicted theoretically, and surprisingly few experimental studies have been made.

Proton losses in the accelerator are of no consequence as a source of radiation until they reach energies above the threshold for (p,n) reactions in the accelerator structure, typically 8 MeV in copper. Thus although substantial beam losses may occur from the preinjector output until after "bunching" (ALL R 69, ZAJ A 70), they do so at energies too small to produce neutrons. (EVE R 70).

Livdahl has suggested (LIV P 68) that operational experience of beam losses at the ANL, BNL, and CPS 50-MeV linacs indicates them to be less than 0.1% of the output current. However, because this conclusion requires inferences from measurements made with beam induction electrodes whose

sensitivity was ≈ 1% of the beam current, it would seem that the measurements indicate beam losses of 1% or less, rather than 0.1%. Indeed, this inference seems better supported by measurements at the Rutherford Laboratory and CERN.

Shaw has reported measurements of neutron flux density along the 50-MeV PLA of the Rutherford Laboratory (SHA K 65) and had interpreted his measurements to indicate beam losses of "a few percent." This accelerator is almost identical to the CERN PS injector, except that it utilizes grid focusing along the first 10-MeV section of the accelerating structure rather than quadrupole focusing. This difference might lead to somewhat higher beam losses, even at energies up to 50 MeV, than those experienced at CERN. However, Everette (EVE W 70) has used CERN PS injector operational data to estimate that from 1 to 2% of proton beam is lost along the accelerator structure at energies greater than a few MeV; this is in good agreement with the estimate made by Shaw for the Rutherford Laboratory accelerator (CAY L 63).

Zajec (ZAJ E 70) has reported measurements on the Bevatron Linac Mark II. At total output of 60 mA from the ion source some 40 mA are protons, and of this current 25 mA is accelerated to 19.2 MeV when the prebuncher is in operation. Beam-intensity measurements made with current transformers at 6.5 and 10.2 MeV indicate normal losses of 0.5 mA, or some 2% of the beam current.

Although there are significant difference between electron and proton linear accelerators, it is salutory to examine beam losses at the 20-GeV electron linac at Stanford. Beam losses are low at this accelerator and quite well understood. Under typical operating conditions beam losses may be as high as 1% to 2%, but when the accelerator is in perfect tune losses fall to about 0.5% (REA D 69).

In the design of the shielding for the 200-MeV proton linac injector at the National Accelerator Laboratory, it was judged prudent to assume an average beam loss of 1% (AWS M 70b). Beam losses under normal operational conditions have been found to be much smaller (HOW H 71).

Table 6.XX.

Accelerator	Beam loss (%)	Remarks
Rutherford laboratory PLA	"few %"	Measurement of neutron flux density
CPS injector	1-2	Operational data
Bevatron linac Mark II	2	Current transformer measurements at 6.5 and 19.2 MeV.
SLAC	0.5	"Perfect tune"
	1-2	Typical operation

Review of Shielding Design at Linear Accelerators

Prior to the design studies for the Los Alamos 800-MeV proton linac little information was available in the literature to aid in the design of proton linac shields. By 1965, however, shields had been designed for three linacs of somewhat different energy and intensity. The most important contribution was made by Cochran, Israel, and Mueller (COC D 65), who leaned heavily on experimental data supported by a Monte Carlo calculation in their shield design: "The shielding requirements for LAMPF are based on experimental data as much as possible. The mean free paths for the attenuation of high-energy neutrons in concrete that have been used are presented in the work of Wallace (WAL R 62) and in the review article of Lindenbaum. Most of the existing data on attenuation lengths and buildup factors apply to the forward or beam direction and it has been necessary to devise a means of applying the existing data to shielding in the transverse direction from the proton beam. Alsmiller et al. (ALS R 65) have calculated the effects as a function of depth of an 800-MeV proton beam incident on a shield and have found that neutrons contribute about 90% of the dose. For the purpose of calculation for LAMPF, no other particles need to be considered. In the shielding calculation, a revised version of the Monte Carlo cascade code of Metropolis et al. (MET N 58) is used to generate the energy and angular distribution of cascade neutrons from incident nucleons interacting in a given target material. By using the results of the cascade code once to generate the source and a second time for the first interaction of the cascade neutrons in the shield, an energy and angular distribution of high-energy neutrons near the beginning of the shield can be established. It is then possible to use the straight-ahead buildup factors and attenuation lengths to calculate the flux of neutrons external to the shield. The flux of neutrons is normalized to the cosmic-ray energy spectrum of Hess et al. (HES W 59) for the flux to dose conversion."

More recently O'Brien (O'BR K 67, O'BR K 68) has reported calculations extending the techniques of neutron transport theory (DAV B 67) to higher energies. Assuming cylindrical geometry, O'Brien has reported values of dose-equivalent rate outside shielding, assuming that protons interact uniformly in copper (simulating the drift-tube structure of the accelerator) along the axis of the accelerator.

A comparison of shield thicknesses estimated by the Yale, Los Alamos, and Berkeley groups with those obtained from O'Brien's calculations has been reported by Thomas (THO R 69b). A useful figure of merit in such comparisons is the parameter P/D, where P is the proton loss rate per unit distance (protons/cm/sec) and D is the dose-equivalent rate at the shield surface. Table 6.XXI tabulates these parameters, and Fig. 7.75 summarizes O'Brien's calculations.

Table 6.XXI. Comparison of shield thickness estimates for proton linear accelerators.

Design group	Proton energy (Mev)	Beam loss (protons/cm/sec)	Radiation level at shield surface (rem/h)	Proton less per unit dose rate (Protons/cm/sec/rem/h)	Shield thickness (g/cm^2)
Yale	100	3.75×10^{13}	1.44×10^{3}[a]	2.60×10^{10}	260
	200	3.75×10^{13}	1.44×10^{3}	2.60×10^{10}	382
	300	3.75×10^{13}	1.44×10^{3}	2.60×10^{10}	560
	400	3.75×10^{13}	1.44×10^{3}	2.60×10^{10}	688
Los Alamos	100	1.56×10^{13}	50×10^{-3}	3.12×10^{14}	873
	100	1.56×10^{13}	10×10^{-3}	1.50×10^{15}	993
	150	1.56×10^{13}	5×10^{-3}	3.12×10^{15}	1046
	150	1.56×10^{13}	2.5×10^{-3}	6.24×10^{15}	1100
	150	1.56×10^{13}	1×10^{-3}	1.56×10^{16}	1165
Berkeley	200	1.0×10^{8}	$<2.5 \times 10^{-3}$	$>4 \times 10^{10}$	549

[a] Entire beam assumed lost over 2 meters.

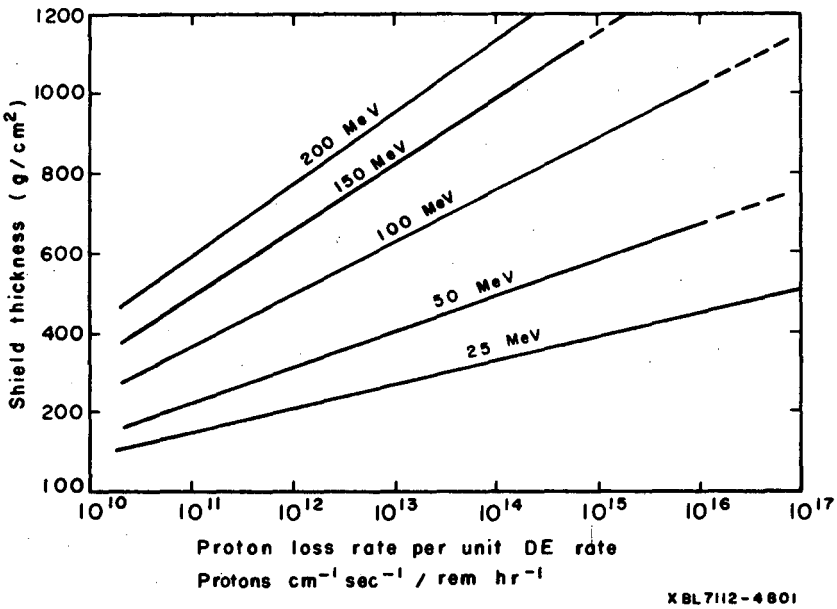

Fig. 6.75. Summary of calculations of proton linear accelerator shielding in the energy range 25 to 200 MeV. (From data by K. O'Brien.)

At values of P in the range 10^{10} to 10^{11} the agreement is rather (perhaps fortuitously) good. At higher values comparison between the Los Alamos and O'Brien calculations at 100 MeV show differences of about a factor of 3 in the radiation estimated at the surface of a shield 1000 g/cm^2 thick. (See Fig. 6.76.)

The shielding design of the 200-MeV linear accelerator at Batavia has utilized O'Brien's calculations. Figures 6.77 and 6.78 conveniently represent the dose equivalent rate outside anticipated outside shields of concrete and earth for the parameters shown. (AWS M 70b).

The simplest physically plausible parameterization of O'Brien's calculations, assuming cylindrical geometry, is

$$D = \frac{k(E) \cdot P}{(a + x/\rho)} \exp(-x/\lambda(E)), \qquad (6.76)$$

where D is the dose-equivalent rate at the shield surface (rem/h),
k(E) is a constant which varies with energy and shield composition,
P is the beam loss rate (protons/cm/sec),
x is the shield thickness (g/cm^2),

$\lambda(E)$ is the dose-equivalent attenuation length (g/cm^2) and is a function of energy,

ρ is the density of the shield (g/cm^3),

a is the distance from the beam to the inner face of the shield.

Table 6.XXII gives values of K(E) and $\lambda(E)$ derived from O'Brien's work.

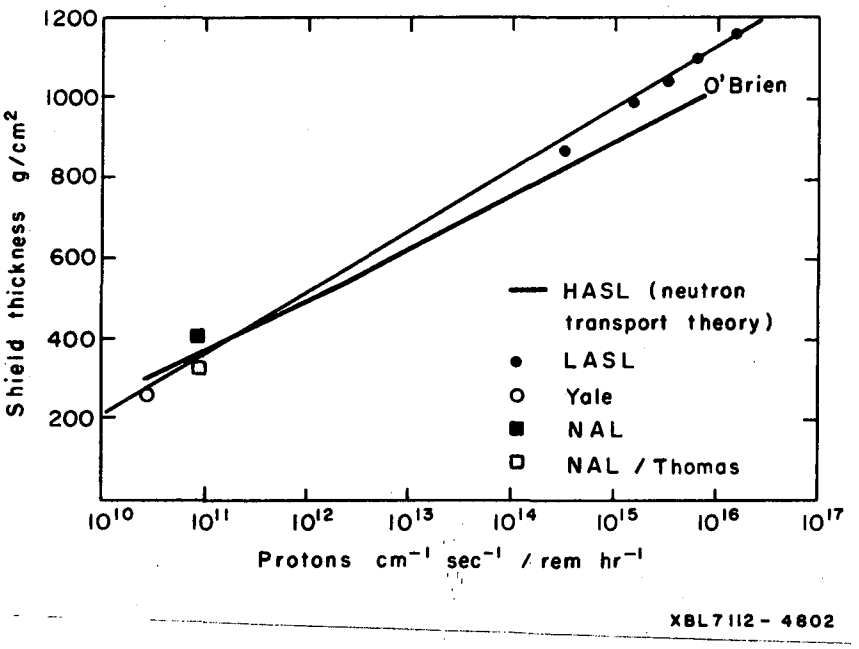

Fig. 6.76. Comparison of shielding estimates for a 100-MeV proton linear accelerator. (From Thomas.)

Table 6.XXII. Values of the parameters k(E) and λ(E) for calculation of concrete shielding.

Proton energy (MeV)	k(E)	λ(E) (g/cm^2)	Range of validity (g/cm^2)
25		24.4	120 to 480
50		44.6	180 to 600
100		74.2	300 to 1000
150			
200			

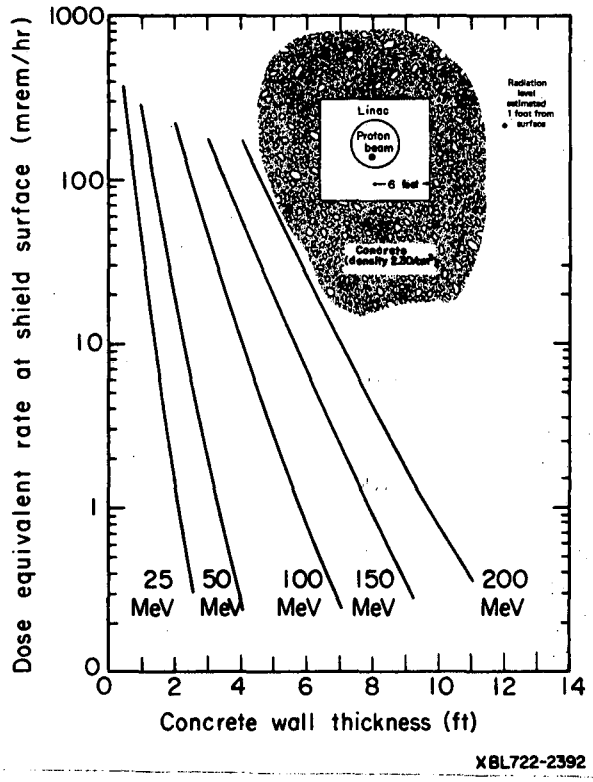

Fig. 6.77. Dose-equivalent rate at the surface of the concrete shield wall of a proton linear accelerator, as a function of proton energy and wall thickness. Calculations made for the geometry shown (inset). Density of concrete assumed to be 2.3 G/cm^3. Proton loss density taken as 6.8 X 10^8 protons/cm/sec. (From M Awschalom et al.)

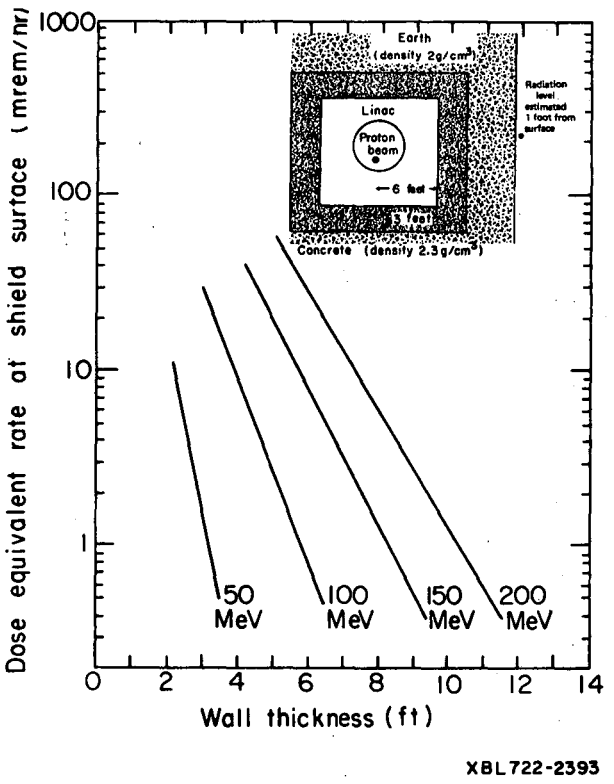

Fig. 6.78. Dose-equivalent rate at the surface of the earth shield of a proton linear accelerator as a function of proton energy and shield thickness. Calculations made for the geometry shown (inset)—with a 3-ft-thick concrete accelerator room wall. Density of concrete assumed to be 2.3 g/cm^3, density of earth assumed to be 1.7 g/cm^3. Proton loss density taken as 6.8 X 10^8 protons/cm/sec. (From M. Awschalom et al.)

If further accuracy is required, Awschalom (AWS M 70b) suggested a more detailed form of Eq. 6.76, which takes account of the variation of effective attenuation length with shield thickness due to small changes in the neutron spectrum. He writes D in the form

$$D = \frac{k(E) \cdot P}{(a + x/\rho)} \exp\left[-\left(\sum_{i=1}^{3} a_i(E)\, x^i\right)\right]. \qquad (6.77)$$

Values of the constants $k(E)$ $a_1(E)$, $a_2(E)$ and $a_3(E)$ are given by Awschalom for earth and concrete over the energy range 25 to 200 MeV. Unfortunately few experimental data are available to validate these calculations.

The use of transport theory to predict neutron dose rates at sea level due due to cosmic radiation suggests that estimates using this technique are good to about a factor of 3. It would perhaps be prudent, then, in using Eq. 6.76, to incorporate a safety factor of 3.

CYCLOTRON SHIELDING

The calculation of shielding of a cyclotron in the energy region of a few hundred MeV is, of course, similar to that for heavy-particle linear accelerators in the same energy range. In general, cyclotrons are capable of producing higher beam currents (Chapter 3) although, as we have seen, high-intensity and proton linear accelerators are now feasible. These higher beam intensities, however, merely affect the scale of the problems of shielding and induced activity, and it is not necessary to discuss the techniques used to achieve high beam currents.

Because cyclotrons were among the earliest of particle accelerators (see Chapter 3), they have provided us with substantial information on their radiation fields. This information is directly applicable to modern high-current (> 100-μ A) cyclotrons. In some early cyclotrons the shielding was treated as an accessory that could be added sometime after the initial construction costs had been absorbed. We have seen some of the disadvantages of such a policy in the historical resumé at the beginning of this chapter. A modern cyclotron in the few-hundred-MeV energy region is physically very large and the shielding expensive. It is not economic to use large safety factors in the estimation of shielding, and in consequence radiation problems form an integral and important part of the accelerator design studies. A modern high-current cyclotron cannot be used effectively at initial operation without adequate shielding. Induced radioactivity, too, presents problems in maintenance and subsequent modification of the accelerator, consideration of which must not be postponed until after construction.

The only radiation of concern for the design of a cyclotron shield in the several-hundred-MeV energy region arises from the production of secondary neutrons by the interaction of the accelerated beam with primary targets and

with the accelerator structure. Shielding that is adequate to attenuate these neutrons will be more than enough to contain charged particles or the electromagnetic cascade generated by high energy γ rays. Mu mesons, produced by the decay of π mesons, are of no consequence at these energies.

Shielding is normally calculated by using the Moyer Method, already described in this chapter. In the discussion of the nuclear cascade we have seen that only neutrons are of biological significance outside well-shielded proton accelerators, in this energy range.

In Chapter 3 we have discussed in some detail the production of neutrons resulting from the interactions of protons with different nuclei. Figure 6.79 shows the total production of neutrons in thick targets of carbon, aluminum, copper, and lead. As we have seen, these neutrons are produced in two ways, by evaporation and by cascade processes. Neutrons (and protons) produced by cascade processes are strongly forward directed relative to the incident proton direction, because of the requirements of momentum conservation. The yield of cascade-produced particles is such that they are unlikely to be important below an incident proton energy of 100 MeV. The evaporation particle yield is roughly isotropic.

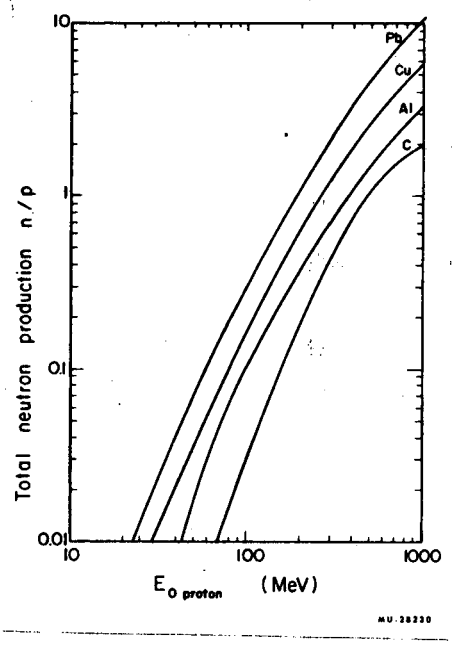

Fig. 6.79. Measured total neutron yield per proton stopping in thick targets of C, Al, Cu, and Pb. (After Moyer.)

Neutron Spectra

The resultant neutron spectrum (from a thick target), Fig. 6.80, may be quite naturally described as consisting of three energy regions:

a. Cascade neutrons of energy greater than 20 MeV.
b. Evaporation neutrons peaked in the few-MeV region.
c. Thermal neutrons arising from the slowing down of the evaporation and cascade neutrons.

It is not usually necessary to estimate this spectrum in great detail in order to design an adequate shield. The yield of neutrons of energy greater than 150 MeV must be determined with some accuracy, however, since it is these neutrons that control the penetration of the radiation through the shield. After neutron equilibrium has been established in the shield (within 2 to 3 mean free paths), no further gross changes occur in neutron spectrum with increasing depth. All particles in the entire spectrum are then transmitted with the same attenuation length as that of those of highest energies.

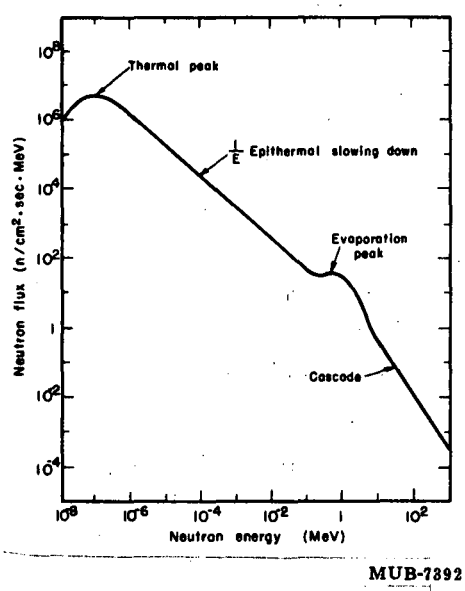

Fig. 6.80. Differential neutron spectrum emerging from accelerator shielding containing hydrogen. (From Wallace.)

The neutron spectrum in the thermal region may be written

$$\phi\,(E)\,dE = a\,E^{1/2}\,e^{-E/kT}\,dE; \tag{6.78}$$

the slowing-down spectrum, resulting from the degradation of evaporation and cascade neutrons, has the form (WAL R 70)

$$\phi\,(E)\,dE = bdE\int_{E}^{E_{max}} Q(\epsilon)\left(\frac{1}{E} - \frac{1}{\epsilon}\right)d\epsilon \tag{6.79}$$

where $Q(\epsilon)\,d\epsilon$ is the number of neutrons produced in unit time with energy between ϵ and $\epsilon+d\epsilon$,

and E_{max} is the maximum energy in the spectrum.

Data given in Chapter 3 give values of $Q(\epsilon)\,d\epsilon$. The normalization constant a of Eq. 6.79 may require

$$\int_{0}^{0.5\ eV} \phi(E)\,dE = 1.25\ Q/S, \tag{6.80}$$

where ϕ is the total source strength of fast neutrons
and S is the surface area over which they are thermalized (PAT H 58).

Radiation Emerging from the Shield

Now that the spectrum and angular distribution of the neutrons produced in the target and accelerator hardware by the primary protons have been estimated, a secondary calculation can be made of the penetration of the outer shield by these neutrons. This can be done by using similar data for cascade and evaporation particles produced by *neutrons* (instead of protons, as shown in Figs. 3.23, 3.29, 3.30, 3.32, and 3.35 through 3.39), secured from the same sources as given earlier for incident *protons.* Although evaporation data are the same as for incident protons, the cascade values are not. As would be expected, the neutrons are more numerous in neutron-induced cascades than in proton-induced cascades, and protons more numerous for proton-induced cascades. Cascade-produced mesons gradually increase in importance from 500 MeV incident energy on up.

The particles outside the shield consist of

a. directly transmitted primary neutrons of energy greater than 150 MeV,

b. evaporation fragments produced by the high energy reactions that suffer inelastic collision in the outer layers of the shield.

The number, N, of cascade neutrons making inelastic collisions in the outermost layer of thickness y is given by

$$N = N_0 (e^{-\gamma/\lambda} - 1) , \quad (6.81)$$

where N_0 is the number of cascade neutrons reaching the outside of the shield and λ is the inelastic mean free path for cascade neutrons.

An overestimate would be to assume that half the evaporation neutrons emerge. Few of the protons produced in early cascade events in the shield penetrate the shield; protons are stopped by ionization losses. Some protons emerge from the outer layers of the shield, however. Wallace (WAL R 70) estimates that each cascade neutron produced in the outer shield is accompanied by 0.6 fast neutron and 0.3 proton. There will in addition be a small flux of thermal neutrons and γ rays. Typically the thermal neutron flux density is comparable to the fast neutron flux density, and therefore contributes little to the dose-equivalent rate. Gamma rays arise from neutron capture in hydrogen in the shield material and from nuclear deexcitation processes.

HIGH ENERGY PROTON SYNCHROTRONS

The Bevatron

SHIELDING DESIGN OF THE BEVATRON

The 6.3-GeV weak-focusing proton synchrotron of the Lawrence Berkeley Laboratory, is of particular interest in that it led to the development of the Moyer Model, which, as we have seen, proved to be an extremely valuable means of estimating shielding

In 1954 the Bevatron first achieved full energy at an intensity of 10^{10} protons per pulse, and as experience developed the intensity has steadily increased. Shielding was added around the machine, but it was not possible to place shielding above the machine because of the high floor loading this would cause. Consequently it became clear that the upper operating intensity of the machine was limited to $\approx 10^{11}$ protons per pulse simply by the radiation levels produced in the control room experimental areas and even at the laboratory perimeter (where stricter regulations apply).

Concurrently with the establishment of this intensity limitation, for reasons discussed by Wenzel (WEN W 59), there developed a demand for even higher beam current and the development of an external beam area. Such an improvement program necessitated drastic revision of the shielding around the Bevatron. Comprehensive surveys of the radiation field around the Bevatron (SMI A 58) and measurements of the shielding properties of concrete by the LRL Health Physics Group (PAT H 62) made it possible for Moyer (MOY B 62) to estimate the shielding required by the increase in beam intensity up to 10^{13} protons per pulse. A new shield, which included roof shielding, was designed upon the basis of these calculations. In 1962 the necessary modifications

were made, including installation of a 20-MeV linac and inflector system, provision of adequate foundations for the new shielding, and installation of a beam-extraction system (WEN W 63). Lofgren and Hartsough (LOF E 63) described in detail the improvements made to the Bevatron during this shutdown, and Lambertson (LAM G 63) reported details of beam observations during the machine cycle. By 1964 the intensity had been increased to as much as 5×10^{12} protons per pulse.

Detailed descriptions of the Bevatron have been published in the literature (LOF E 59, BRO W 57). Figure 6.81 shows a plan view of the accelerator and its surrounding shielding.

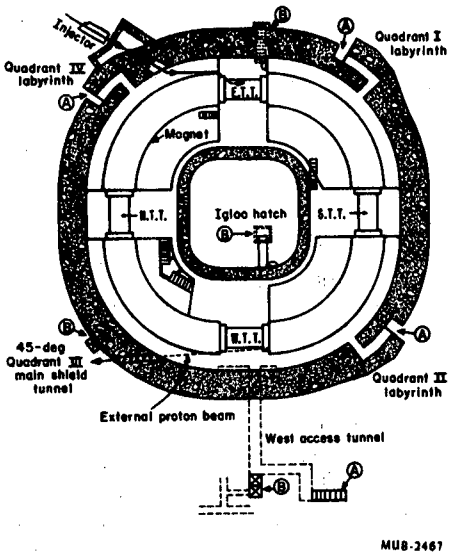

Fig. 6.81. Plan view of Bevatron shielding.

ESTIMATES OF SHIELDING FOR THE BEVATRON

Moyer's (MOY B 61) calculations of shielding for the Bevatron, based on an intensity of 10^{13} protons per pulse, are summarized below. As we have already seen, these calculations played an extremely important part in improving our understanding of shielding phenomena and are an outstanding example of the use of intuition in the absence of complete information.

Utilization of the circulating proton beam of a weak-focusing proton synchrotron for various experiments leads directly to production of radiation (THO R 68). When secondary beams of low intensity are produced by the use of internal targets almost all the circulating beam incident upon the target is lost to the vacuum chamber wall. The beam may be extracted with efficiencies of $\approx 50\,\%$ (from a weak-focusing synchrotron), in which case there is less radiation from the accelerator proper, but this is to some extent compensated by the radiation emitted by backstop necessary to absorb the extracted beam. The complexity of the detailed beam-loss distribution and its dependence upon many variables precluded any attempts at its precise determination. An alternative procedure adopted by Moyer was to identify those conditions which produce the highest radiation levels. Such conditions occur when a thick target is placed slightly upstream from one of the machine's straight sections. In this position there is no self-shielding from the magnet yoke itself. Calculations were made for a copper target ≈ 100 g/cm^2 thick in four different positions. By providing shielding to handle these situations one can be sure that less severe operating conditions will be adequately handled. It was estimated that primary proton interactions in a thick copper target produce about 20 neutrons per proton. Figure 6.82 shows their energy spectrum, which was derived by Moyer from cosmic-ray information, experiments at the Bevatron, and Monte Carlo calculations by Metropolis et al. (MET N 58).

We have previously summarized the results of neutron attenuation cross section measurements and seen that the shielding thickness is determined by the neutrons above about 150 MeV, the much higher yield of lower energy neutrons being more than compensated by the shorter attenuation lengths appropriate to these energies. From the data of Fig. 6.82 Moyer estimated that eight neutrons ($E > 150$ MeV) were produced by 6.3-GeV neutrons incident upon a thick copper target. From the Metropolis calculations Moyer inferred the angular distribution of neutrons of energy greater than 150 MeV shown in Fig. 6.83.

The basic assumptions used by Moyer in his shielding calculations may be summarized thus:

a. Beam intensity of 10^{13} protons per pulse; machine repetition rate of 11 pulses/min.

b. Attenuation length of high energy neutrons was taken as 160 g/cm^2, which corresponds to the half-value thicknesses:

Ordinary concrete ($\rho = 2.4$ g/cm^3), 18 in. ≈ 46 cm,

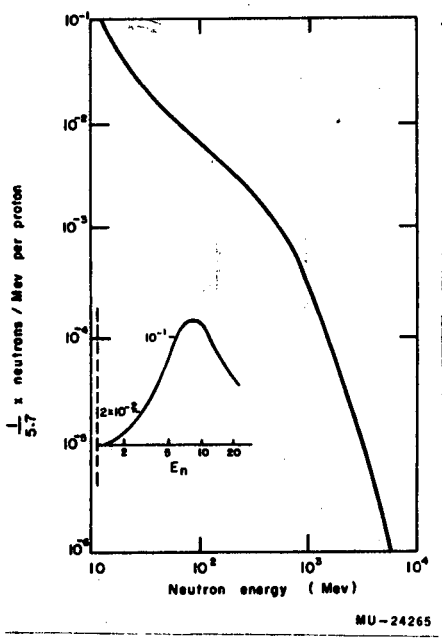

Fig. 6.82. Energy spectrum of neutrons from a thick copper target bombarded by 6.3-GeV protons (target thickness 1 nuclear mean free path; to obtain neutrons/MeV per incident proton multiply ordinate by 5.7), as estimated by Moyer.

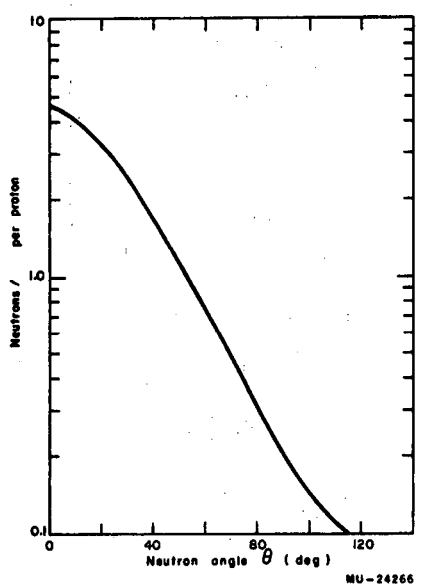

Fig. 6.83. Angular distribution of neutrons with energy greater than 150 MeV emitted by a thick copper target bombarded by 6.3-GeV protons, as estimated by Moyer.

Heavy concrete ($\rho = 3.5$ g/cm^3), 12.4 in. $\approx$ 31 cm,
Steel ($\rho = 7.8$ g/cm^3), 5.5 in. $\approx$ 14 cm.

c. Outside the shielding the biological dose equivalent due to low energy neutrons is not greater than that due to the surviving "primary" neutrons.*

d. The biological dose due to γ rays is not greater than 25% of the dose equivalent from neutrons.

e. The biological dose from μ mesons may be neglected.

f. One rem is taken to be equivalent to 10^7 high energy neutrons per cm^2.

CONSTRUCTION OF THE BEVATRON SHIELDING

A plan view of the accelerator and its shielding, has been shown in Fig. 6.81, Figs. 6.84 through 6.87 show the shielding being installed, in particular the arrangement of the roof blocks.

The shielding consists of a central monolithic concrete wall, 4 ft (122 cm) thick, within the Bevatron magnet. The thickness was determined by the loading of the roof blocks, which are keyed into this inner wall to prevent their slipping loose during an earthquake. A concrete wall 10 ft (305 cm) thick and 16 ft (488 cm) high is tacked on the outer side of the magnet. This wall is made up from blocks 4 ft high, the two middle courses (centered roughly on the median plane of the machine) being fabricated from heavy concrete ($\rho = 3.5$ g/cm^3), whereas the upper and lower courses are made from normal concrete blocks ($\rho = 2.4$ g/cm^3). Between the west and east tangent tanks, where the experimental area is situated, the median plane shielding is constructed from small blocks to allow beams to be set up. Figure 6.86 shows these blocks very clearly.

Long roof blocks span from the outer wall to a steel support rail, and shorter blocks cover the gap between the steel support and the "igloo' (Figs. 6.86 and 6.87). The outer roof shielding directly above the machine is in two staggered layers to prevent fast neutrons streaming along cracks in the wall, and provides a total thickness of 7 ft (214 cm) of ordinary concrete directly above the magnet. The shape of the long roof blocks was determined by the necessity to ensure that neutrons emitted at elevations up to 30 deg had to traverse a minimum of 10 ft of ordinary concrete.

As a consequence of high neutron output at the injection area, particularly where the beam strikes collimating slits, additional shielding is added in this region. A 2-ft-thick (61 cm) concrete "blister" surrounds the beam

*More recent studies would allow some improvement on the choice of the input parameters if these calculations were to be repeated today, but this should not have a large impact on the final shield thickness calculated because it is quite insensitive to the choice of impact.

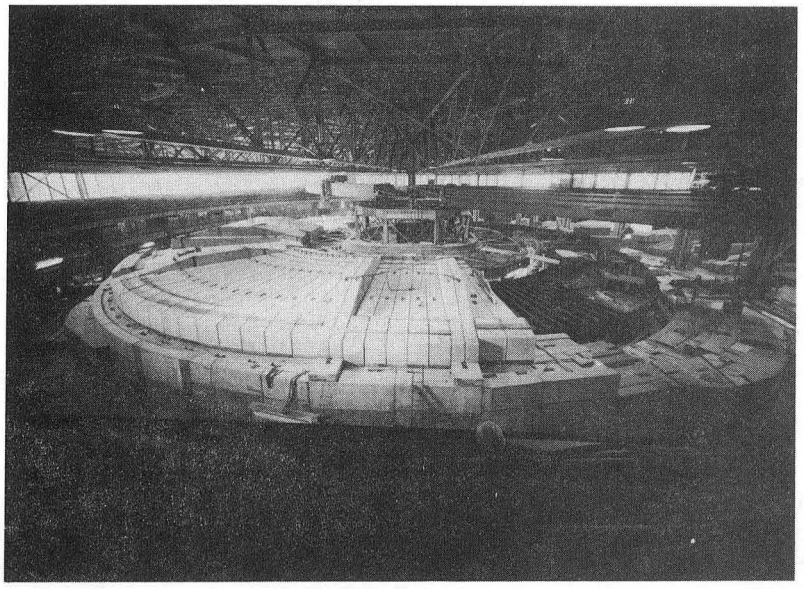

Fig. 6.84. View of Bevatron shielding under construction.

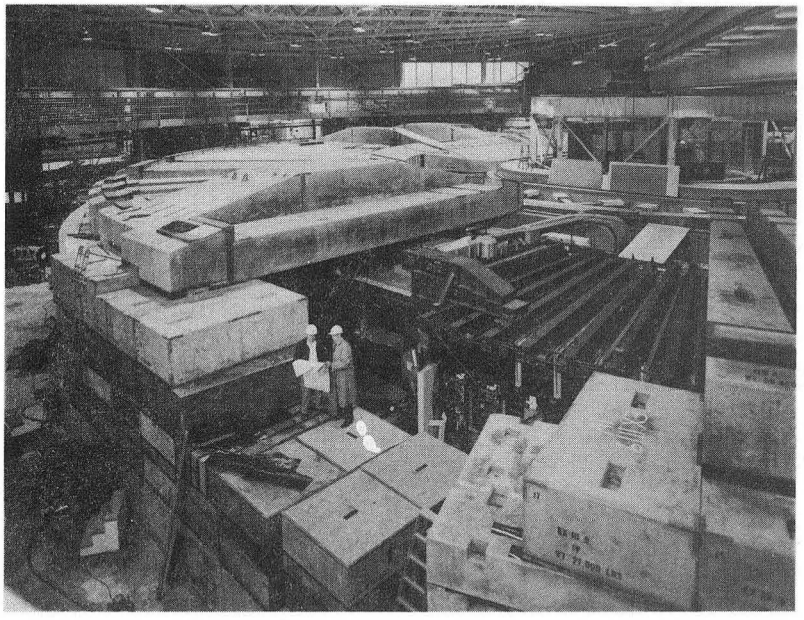

Fig. 6.85. View of Bevatron shielding under construction.

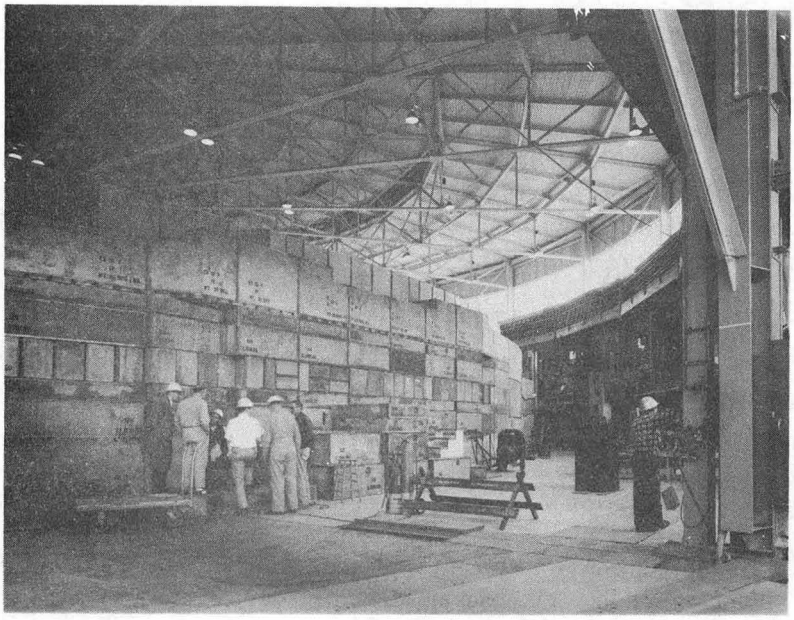

Fig. 6.86. View of wall construction, showing slot blocks.

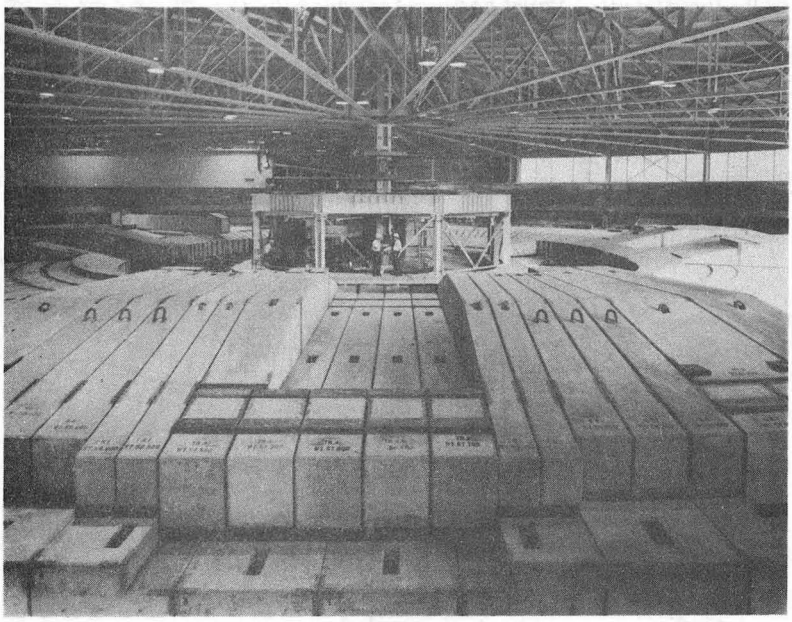

Fig. 6.87. View of completed roof shielding.

chopped at the end of the linear accelerator. The thickness of this shielding was based on estimates of the neutrons produced when the linac beam struck graphite beam cups, from experimental data supplied by Patterson (JOH R 62).

Access to the machine is obtained by four labyrinths, shown in Fig. 6.81. The positions of these access points were chosen so as to avoid looking directly at targets or other sources of high-level radiation, and they were designed to provide adequate attenuation of the neutron flux that streams down such tunnels.

METHOD OF CALCULATION

As we have shown, the flux of high energy neutrons ($E > 150$ MeV) outside a shield of thickness d at a point distant r from the source of radiation may be written

$$\phi\,(E > 150\ \text{MeV}) = \frac{N\,g(\theta)}{r^2}\ \exp\left(-\frac{d\ \text{cosec}\ \theta}{\lambda}\right). \qquad (6.43b)$$

Moyer made estimates of the shielding required in four different target situations, and these examples are quoted directly.

"Example No. 1

The target located in position 1 shown" in Fig. 6.88 "will deliver its forward-hemisphere neutrons through the magnet iron and the 10-ft concrete wall. It represents a target position for which the radiation escape is not dominated by a tangent tank area, and we inquire whether or not the concrete wall can be made solely of ordinary concrete (2.4 g/cm^3) in this case.

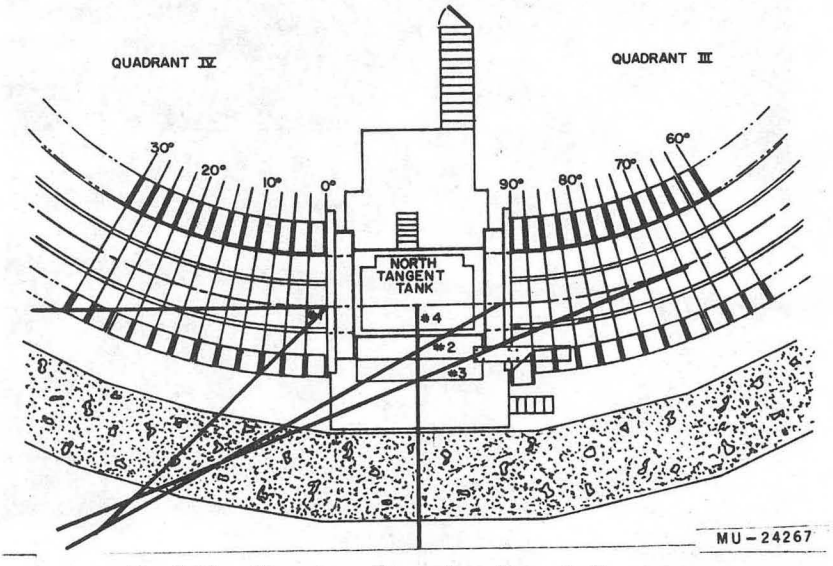

Fig. 6.88. Plan view of target positions in Bevatron vacuum chamber. (From Moyer.)

"The answer is as follows: In the 0-deg direction from this target the obliquity and distance factors provide sufficient attenuation to allow ordinary concrete to be used. But for direction angles greater than 30 deg, the 10 ft of ordinary concrete is clearly insufficient; and beyond 45 deg the full 10 ft of the median course of blocks must be of heavy (3.5 g/cm^3) concrete. Even then, at 90 deg, the surviving primary neutron flux density is calculated to be 15 n/cm^2/sec at the outer surface of the shield; and to this must be added an approximately equal additional exposure from the secondary neutrons and gamma rays emerging from the shielding. At 45 deg the corresponding flux density of surviving primary neutrons is 13 n/cm^2/sec.

"Thus it is clear that the median course must be of heavy concrete in any quadrant where a target is to be placed if complete freedom of target location within the quadrant is desired.

"Example No. 2

"In this example we choose a situation very clost to frequent practice. A target is located near the end of a quadrant, where its primary neutrons can escape through the tangent tank wall and strike the shield wall without any intervening magnet iron. The distance from the target to the point of concern is 45 ft. The oblique path length through the concrete is 15 ft. The surviving neutron flux density if the 10-ft wall is of heavy concrete is found to be 92 n/cm^2/sec. It is clear that we need a greater attenuation than the 10-ft wall will provide. Additional shield thickness of 27 in. of heavy concrete, or its equivalent, will be required in the region 'illuminated' by the neutrons emerging through the tangent tank from this target.

"Example No. 3

"We place the target in a quadrant at such a point that the 0-deg neutron yield can escape through the aperture at the end of the quadrant iron and thus impinge upon the concrete shield as indicated on beam 3 of" Fig. 6.88. "The distances from the target to the point just outside the shield is 68 ft, and the oblique path through the 10-ft concrete wall is 17.5 ft. The surviving flux density is 16 n/cm^2/sec for a 10-ft wall, indicating that a slightly greater thickness is required; but this need is more than fulfilled by the requirements of Example 2.

"Example No. 4

"In this rather unlikely case,* we place the copper target in the tangent tank and consider the result of the neutron flux at 90 deg directly striking the

---

* At the time of these calculations this was in fact an unlikely situation. The two plunging magnets of the beam extraction system described by Wenzel (WEN W 59) "intercept the circulating beam and effectively act as thick targets. Measurements of the radiation levels above the S and W tangent tanks indicated the need for additional shielding as predicted by Moyer." (This has been installed.)

concrete wall. The distance from the target to the nearest point of exposure is 25 ft if we consider a 10-ft wall. In this case, the surviving primary flux density is 650 n/cm^2/sec. The wall thickness in the 90-deg direction from this target would need to be 15 ft of heavy concrete to adequately attenuate the primary neutron flux. But since this is an unlikely target situation, and since the platforms of sufficient strength to support additional shadow shielding are provided, we consider that it is unnecessary to call for greater attenuation in the shield wall than would be provided by the 12.5 ft of heavy concrete already required by Examples 2 and 3.

Finally Moyer made estimates of the neutron flux densities that would be observed at the boundaries of the laboratory, approximately 1500 ft ($\approx$ 460 m) from the Bevatron. With a target situated at the entrance end of the tangent tank, neutrons emitted between 45 and 90 deg to the beam direction could penetrate the minimum thickness of shielding near the junction of the roof blocks and the side wall. With only 7 ft of overhead shielding Moyer estimated the surviving primary neutron flux density at the project boundary is 6 n/cm^2/sec, a factor $\approx$ 36 too high if the Bevatron were to operate entirely at 10^{13} protons per pulse. As a consequence, Moyer recommended that roof shielding at tangent tanks should be increased so as to provide at least 10 ft (305 cm) of concrete in neutron ray directions at 90 deg with respect to the beam for elevation angles up to 30 deg. Measurements of the neutron flux observed at the laboratory boundary would indicate whether further shielding should be installed above tangent tanks.

A calculation of the neutron flux density observed 1500 ft away from the Bevatron due to uniform beam loss indicated levels $\approx$ 0.2 n/cm^2/sec, showing that thick targets placed in the tangent tank are the major source of large radiation fields at large distances.

REFERENCES

AAL E 68 E. Aalto, Liquid-Filled Cylindrical Ducts, in *Engineering Compendium*, Vol. 1 (Springer-Verlag, Berlin, 1968), Sect. 8.2.3.

AKA M 62 M. Akashi, K. Shimizu, Z. Watanabe, T. Ogawa, N. Ogita, A. Misaki, I. Mito, S. Oyama, S. Tokunaga, M. Fujimoto, S. Hasegawa, J. Nishimura, K. Niu, and K. Yoki, J. Phys. Soc. Japan *17*, Suppl. A-III, Part III, 427 (1962).

ALL F 63 F. J. Allen and A. T. Futterer, Neutron Transmission Data, Nucleonics *21* [8], 120 (1963).

ALL L 55 L. Allen, Photodisintegration of the Deuteron by 95-MeV Bremsstrahlung, Phys. Rev. *98*, 705 (1955).

ALL R 69 R. W. Allison, Jr. (Lawrence Radiation Laboratory), private communication, Oct. 1969.

ALS F 65 F. S. Alsmiller, A General Category of Soluble Nucleon-Meson Cascade Equations, ORNL-3746, 1965.

ALS R 62 R. G. Alsmiller, F. S. Alsmiller, and J. E. Murphy, Neutron Meson Cascade Calculations: Transverse Shielding for a 45-GeV Electron Accelerator (Part I), Oak Ridge National Laboratory Report ORNL-3289, 1962.

ALS R 63a R. G. Alsmiller and J. E. Murphy, Nucleon Meson Cascade Calculations: The Star Density Produced by a 24-GeV Proton Beam in Heavy Concrete, Oak Ridge National Laboratory Report ORNL-3367, 1963.

ALS R 63b R. G. Alsmiller, F. S. Alsmiller, and F. E. Murphy, Neutron-Meson Cascade Calculations: Transverse Shielding for a 45-GeV Electron Accelerator (Part II), Oak Ridge National Laboratory Report ORNL-3365, 1963.

ALS R 65 R. G. Alsmiller, Shielding Calculations for High Energy Accelerators, CONF-651109, p. 327.

ALS R 69a R. G. Alsmiller, Electromagnetic and Nuclear-Cascade Calculations and Their Application in Shielding and Dosimetry, CONF-691101, p. 166.

ALS R 69b R. G. Alsmiller and E. Solomito, The Transport of Neutrons Produced by 3-GeV Proton-Lead Nucleus Collisions Through a Labyrinth and Comparison With Experiment, in *Proc. Second International Conference on Accelerator Dosimetry and Experience, Stanford, California Nov. 1963*, CONF-691101, p. 447.

ALS R 70 R. G. Alsmiller, F. C. Mynatt, M. L. Gritzner, J. V. Pace, and J. Barish, The Lateral Spread of High Energy ($\leq$400-MeV) Neutron Beams and Earthshine, Aug. 1970. J. Nucl. Instr. Methods *89*, 53 (1970).

ALV L 47 L. W. Alvarez et al., Initial Performance of a 32-MeV Proton Linear Accelerator, Science *106*, 506(1947).

ASH A 60 A. Ashmore, G. Cocconi, A. N. Diddens, and A. M. Wetherell, Total Cross Sections of Protons with Momentum Between 10 and 28 GeV/c, Phys. Rev. Letters *5*, 576 (1960).

ATK J 61 John H. Atkinson, Wilmot N. Hess, Victor Perez-Mendez, and Roger Wallace, 5-BeV Neutron Cross Sections in Hydrogen and Other Elements, Phys. Rev. *123*, 1850 (1961).

AWS M 68 M. Awschalom, J. N. DeWire, M. S. Livingston, A. Mashke, A. L. Read, and R. H. Thomas, Design Report, National Accelerator Laboratory Report, July 1968, Chapter 12, Radiation and Shielding, p. 7-8.

AWS M 70a M. Awschalom, Lateral Shielding for the 8-GeV and 200-GeV Synchrotrons, National Accelerator Laboratory Internal Report TM-241, May 25, 1970.

AWS M 70b M. Awschalom, Linac Shielding, National Accelerator Laboratory Internal Report TM-236, May 5, 1970.

AWS M 70c M. Awschalom, T. Borak, P. J. Gollon, and D. Theriot, Radiation Physics Aspects of NAL Construction, National Accelerator Laboratory Internal Report FN-211 1100, May 26, 1970.

BAA J 64 J. Baarli, The Radiation Protection of the CERN Laboratory and its Surroundings When Operating the CERN Accelerators, CERN Internal Report DI/HP/59, Nov. 4, 1964.

BAA J 65 J. Baarli, K. Goebel, and A. H. Sullivan, Shielding Studies in Steel With 10-20-GeV Proton Beam in Steel Using Ionization Chambers and Plastic Phosphors, Nucl. Instr. Methods *32*, 57 (1965).

BAC G 63 G. Backenstoss, B. D. Hyams, G. Knop, and U. Stierlin, A Total Absorption Scintillation Detector for Electrons, Photons, and Other Particles in the GeV Region, Nucl. Instr. Methods *21*, 155 (1963).

BAL W 52 W. P. Ball, Nuclear Scattering of 300 MeV Neutrons, Thesis, UCRL - 1938, 1952.

BAR A 61a A. Barbaro-Galtieri, A. Manfredini, B. Quassiati, C. Castagnoli, A Gainotti, and I. Ortalli, Experimental Results on the Proton-Nucleus Collisions at 27 GeV in Emulsion, Nuovo Cimento *21*, 469 (1961).

BAR A 61b A. G. Barkow, B. Chamany, D. M. Haskin, P. L. Jain, E. Lohrmann, M. W. Teucher, and M. Schein. Nuclear Interactions of Protons, Neutrons, and Shower Particles of Very High Energy in Nuclear Emulsion, Phys. Rev. *122*, 617 (1961).

BAT G 65 G. Bathow, E. Freytag, and K. Tesch, Shielding Measurements on 4.8-GeV Bremsstrahlung, Nucl. Instr. Methods *33*, 261 (1965).

BAT G 67a G. Bathow, E. Freytag, and K. Tesch, Measurements on 6.3-GeV Electromagnetic Cascade and Cascade-Produced Neutrons, Nucl. Phys. *B2*, 669 (1967).

BAT G 67b G. Bathow, E. Freytag, and K. Tesch, Shielding of High-Energy Electrons: The Neutron and Muon Components, Nucl. Instr. Methods *51*, 56 (1967).

BAT G 67c G. Bathow, V. Clausen, E. Freytag, and K. Tesch. Skyshine-Messungen und ihr Vergleich mit Abschätzungen, aus der Diffusiontheorie, Nukleonik *9*, 14 (1967).

BAT G 69 G. Bathow, E. Freytag, K. Tesch, R. Kajikawa, and M. Köbberling, Measurements of the Longitudinal and Lateral Development of the Electromagnetic Cascade in Lead, Copper, and Aluminum at 6 GeV, CONF-691101, p. 222.

BAT H 10 H. Bateman, Proc. Cambridge Phil. Soc. *15*, 423 (1910).

BEC E 64 E. E. Becklin and J. A. Earl, Experiments on the Average Characteristics of Cascade Showers Produced in Lead by 500- and 1000-MeV Electrons, Phys. Rev. *136*, B237 (1964).

BEL S 59 S. Z. Belenkii and I. P. Ivanenko, Usp. Fiz. Nauk *69*, 591 (1959) [English Transl.: Soviet Phys.—Usp. *2*, 912 (1960)].

BEN G 71a G. W. Bennet et al., Study of a Uniform Beam Stop at 28 GeV, IEEE Trans. Nucl. Sci. NS *18* [3], 776 (1971).

BEN G 71b G. W. Bennet, H. Foelsche, D. Lazarus, G. Levine, W. Moore, and T. Toohig, Flux Attenuation in a Steel Side Shield at the AGS, IEEE Trans. Nucl. Sci. NS *18* [3], 778 (1971).

BER B 68a B. R. Bergelson and V. P. Maskovitch, Empty Cylindrical Ducts, in *Engineering Compendium*, Vol. 1 (Springer-Verlag, Berlin, 1968), Sect. 8.2.1.

BER B 68b B. R. Bergelson and V. P. Maskovitch, Straight Cylindrical Ducts Filled with Material Differing from Shield Material, in *Engineering Compendium*, Vol. 1 (Springer-Verlag, Berlin, 1968), Sect. 8.2.2.

BER H 69 H. Bertini, Calculations of Nuclear Reactions for Incident Nucleons and π Mesons in the Energy Range 30 to 2700 MeV, CONF-691101, p. 42.

BLO W 50 W. Blocker, R. W. Kenney, and W. K. H. Panofsky, Transition Curves of 330-MeV Bremsstrahlung, Phys. Rev. *79*, 119 (1950).

BNL 325 Neutron Cross Sections, Ed. D. J. Hughes and C. B. Schwartz, Brookhaven National Laboratory Report BNL 325—2nd Edition, July 1958.

BNL 64 A Proposal for increasing the Intensity of the Alternating-Gradient Synchrotron at the Brookhaven National Laboratory. Brookhaven National Accelerator Report BNL-7956, May 1964.

BNL 65 *Proceedings of the USAEC First Symposium on Accelerator Radiation Dosimetry and Experience, held at Brookhaven National Laboratory, New York, November 3-5, 1965,* CONF-651109.

BOG N 58 N. P. Bogachev, S. A. Bunyatov, Yu P. Merekov, and V. M. Sidorov, Interaction of 9-BeV Protons with Free and Bound Nucleons in Emulsion, Dokl. Akademiia Nauk USSR *121,* 617 (1958).

BRO D 59 D. L. Broder, A. A. Kutuzov, V. V. Levin, V. V. Orlov, and A. Z. Turusova, The Passage of Fast Neutrons Through Lead and Iron, Atomnaya Energiya *6,* 578 and *7,* 313 (1959).

BRO W 57 W. M. Brobeck, Design and Construction of the Bevatron, Lawrence Radiation Laboratory Report UCRL-3912, Sept. 1957.

CAR T 69 T. G. Carter and R. H. Thomas, Radiation Surveys HEPL Mark III Electron Linac: I - Film Badge Measurements, Stanford University Internal Report RHT/TN/69-10, Sept. 1969.

CAS K 53 K. M. Case, F. de Hoffmann, and G. Placzek, *Introduction to the Theory of Neutron Diffusion,* Vol. 1, Los Alamos, 1953.

CAS N 67 N. R. Casey, C. H. Distenfeld, G. S. Levine, W. H. Moore, and L. W. Smith, Sand as a Side Shield for 30-GeV Protons Stopping in the Brookhaven AGS, Nucl. Instr. Methods *55,* 253 (1967).

CER N 64 *Report on the Design Study of a 300-GeV Proton Synchrotron by the CERN Study Group on New Accelerators* (2 vol.), CERN/563, Nov. 1964.

CHA G 55 G. T. Chapman and C. L. Storrs, Effective Neutron Removal Cross Sections for Shielding, USAEC Report AECD-3978, 1955.

CHA S 67 S. J. Charalambus, K. Goebel, and D. Nachtigall, Angular Distribution of Secondary Particles and Dose Rates Produced by 19.2-GeV/c Protons Bombarding Thin Be, Al, Cu, and U Targets, CERN DI/HP, March 14, 1967.

CHA V 69 V. M. Chakalian and R. H. Thomas, Radiation Surveys—HEPL Mark III, Electron Linac: II – Activation Detector Measurements, Stanford University Internal Report RHT/TN/69-11, Sept. 1969.

CHE F 55 F. F. Chen, C. P. Leavitt, and A. Shapiro, Attenuation Cross Sections for 860-MeV Protons, Phys. Rev. *99*, 857 (1955).

CHI M 69 M. N. Chimankov, A. M. Biskupchuck, V. Ye. Borodin, V. N. Lebedev, and Ye. G. Maltzev, Radiation Situation Around the Linac Injector of the 70-GeV Proton Synchrotron, Preprint, Institute of High Energy Physics, Serpukhov, IHEP 69-67.

CHI R 65 R. L. Childers, C. D. Zerby, C. M. Fisher, and R. H. Thomas, Shielding Studies in Steel With 10- and 20-GeV/c Protons, Part III. Measurement of the Nuclear Cascade at 10 GeV/c with Emulsions, Nucl. Instr. Methods *32*, 53 (1965).

CIT A 61 A. Citron, L. Hoffmann, and C. Passow, Investigation of the Nuclear Cascade in Shielding Materials, Nucl. Instr. Methods *14*, 97 (1961).

CIT A 65 A. Citron, L. Hoffmann, C. Passow, W. R. Nelson, and M. Whitehead, Shielding Studies in Steel With 10- to 20-GeV Protons. Part II. A Study of the Nuclear Cascade in Steel Initiated by 19.2-GeV/c Protons, Nucl. Instr. Methods *32*, 48 (1965).

CLA F 71 F. H. Clark, Shielding Data, Appendix E in *Protection Against Neutron Radiation*, NCRP Report No. 38, National Council on Radiation Protection and Measurements, Washington, D.C., 1971.

CLE G 65 G. Clement and P. Kessler, Electroproduction of Muons of Very High Energy, Nuovo Cimento *37* [10], 876 (1965).

CLO E 67 E. Close, FLUXFT—A CDC 6600 Code for Fitting Radiation Data Associated with the CERN PS, Lawrence Radiation Laboratory Report UCID-3061, July 1967.

COC D 65 D. R. F. Cochran, H. I. Israel, and D. W. Mueller, Radiation Problems Associated with the Lampf Facility, in *Proceedings of the First Symposium on Accelerator Radiation Dosimetry and Experience, held at Brookhaven National Laboratory, New York, November 3-5, 1965*, CONF 651109.

COL F 71 F. J. Coleman, D. C. Thomas, and G. Saxon, An Experiment to Determine Shielding Requirements for a Multi-GeV Electron Synchrotron Ring, Daresbury Nuclear Physics Laboratory Report DNPL, p. 72, May 1971.

COO T 55 T. Coor, D. A. Hill, W. F. Hornyak, L. W. Smith, and G. Snow, Nuclear Cross Sections for 1.4-BeV Neutrons, Phys. Rev. *98*, 1369 (1955).

COW F 53 F. P. Cowan and J. S. Handloser, Health Physics Program for the Brookhaven Cosmotron, Brookhaven National Laboratory Report BNL-264 (T-43), 1953.

CRA D 65a D. F. Crawford and H. Messel, The Electron-Proton Cascade in Lead, Emulsion, and Copper Absorbers, Nucl. Physics *61*, 145 (1965).

CRA D 65b D. F. Crawford and H. Messel, Energy Distribution in Low-Energy Electron-Photon Showers in Lead Absorbers, Phys. Rev. *128*, 2352 (1965).

CRE A 59 A. Crewe, Notes on External Particle Beams from the Argonne 12.5 - BeV Synchrontron, in *Proceedings of an International Conference on High Energy Accelerators and Instrumentation, CERN, Sept. 1959*, p. 400 (see also p. 359).

CRO E 57 E. Crosbie, Argonne National Laboratory 12.5 - BeV Proton Synchrotron, in *Proceedings of an International Conference on Shielding of High Energy Accelerators, New York, April 11-13, 1957*, TID-7545, p. 167.

CRO J 57 J. W. Cronin, R. L. Cool, and A. Abashian, Cross Sections of Nuclei for High-Energy Pions, Phys. Rev. *107*, 1121 (1957).

CRO J 62 J. W. Cronin, P. Engles, M. Pyka, and R. Roth, Electron Showers in a Lead Plate Spark Chamber, Rev. Sci. Instr. *33*, 946 (1962).

CVI G 61 G. Cvijanovich et al., Nuclear Excitation and Multiple Production in Proton-Nucleus Collisions at CERN-PS Energies, Nuovo Cimento *20*, 1012 (1961).

DAK H 61 H. S. Dakin (Lawrence Radiation Laboratory), private communication, 1961.

DAK H 62 H. S. Dakin (Lawrence Radiation Laboratory), private communication, 1962.

DAV B 58 B. Davidson, *Neutron Transport Theory* (Oxford, 1958).

DEK D 65 D. Dekkers et al., Experimental Study of Particle Production at Small Angles in Nucleon-Nucleon Collisions at 19 and 23 GeV/c, Phys. Rev. *137*, B962 (1965).

DES H 62 H. DeStaebler, Transverse Radiation Shielding for the Stanford Two-Mile Accelerator, USAEC Report SLAC-9, Nov. 1962.

DES H 63 H. DeStaebler, Radiation Measurements in the CEA Labyrinth, Stanford Linear Accelerator Report SLAC TN-63-62, 1963.

DES H 65 H. DeStaebler, Similarity of Shielding Problems at Electron and Proton Accelerators, in *Proceedings of the Symposium on Accelerator Dosimetry and Experience, Brookhaven, Nov. 3-5, 1965*, CONF-651109, p. 429.

d'HO M 68 M. M. d'Hombres, C. Devillers, F. Gervaise, B. de Séréville, and Ph. Tardy-Joubert, Propagation des neutrons dans les tunnels d'accès à un accélérateur de haute energie à protons, CEA-R-3941.

DIS C 65 C. Distenfeld and R. D. Colvett, AGS Conversion – A Summary, CONF 651109, p. 490.

DIS C 66 C. Distenfeld and R. D. Colvett, Skyshine Considerations for Accelerator Shielding Design, Nucl. Sci. Eng. *26*, 117 (1966).

DOT D 64 D. R. Doty, Dose Measurements for Neutron Streaming in Ducts, U.S. Navy, Port Hueneme, California, report R 282, March 1964.

DOV O 63 O. I. Dovzhenko and A. A. Pomanskii, Radiation Units and Critical Energies for Various Substances, Zh. Eksperim. i Teor. Fiz. *45*, 268 (1963) [English transl.: Soviet Phys.–JETP *18*, 187 (1964)].

EVA R 55 R. D. Evans, *The Atomic Nucleus* (McGraw-Hill, New York, 1955), Chap. 15.

EVE W 70 W. Everette, Radiation Shielding for Bevatron 50-MeV Linac, Bevatron Internal Note, Lawrence Radiation Laboratory, Dec. 1970.

EVE W 71 W. Everette (Lawrence Berkeley Laboratory), private communication, 1971.

FAL C 57 C. E. Falk, in Introductory Remarks, in *Proceedings of the Conference on Shielding of High-Energy Accelerators, New York, April 11-13, 1957*, TID-7545, p. ix.

FAR E 63 E. Farrow et al., Nuclear Interaction of the Secondary Particles of High-Energy Cosmic-Ray Jets, Nuovo Cimento *28*, 1238 (1963).

FIS C 63 C. M. Fisher, Notes on the Nuclear Cascade in Shielding Materials in *Report of the Shielding Conference held at the Rutherford Laboratory on September 26 and 27, 1962*, R. H. Thomas, Ed., Rutherford Laboratory Internal Report NIRL/R/40, June 1963.

FOR R 67 R. D. Fortune, W. S. Gilbert, and R. H. Thomas, Shielding Experiment at the CERN PS, Lawrence Radiation Laboratory Internal Report UCID-10199, April 1967.

FRE E 71 E. Freytag and J. Ranft, Hadronic and Electromagnetic Cascades in Radiation Problems Encountered in the Design of Multi-BeV Research Facilities, K. Goebel, Ed., CERN-71-21, 29, Sept. 1971.

FRI W 65 W. R. Frisken (Brookhaven National Laboratory), private communication to W. H. Moore (Brookhaven National Laboratory), 1965.

GEI J 65a J. A. Geibel and J. Ranft, Shielding Studies in Steel With 10- and 20-GeV/c Protons, Part VI. Monte Carlo Calculations of Nucleon-Meson Cascade in Shielding Materials, Nucl. Instr. Methods *32*, 65 (1965).

GEI J 65b J. Geibel, K. H. Reich and J. Seetzen, Shielding Studies in Steel With 10–20-GeV/c Protons, Part I. General Description of the Experiment, Nucl. Instr. Methods *32*, 45 (1965).

GER F 68 F. Gervaise and M. M. d'Hombres, Variante du programme Zeus appliqué à des problèmes de tunnels, CEA-N-933.

GIL W 67a W. S. Gilbert, Radiation Problems With High-Energy Proton Accelerators, *Proceedings of the 1967 U.S. National Particle Accelerator Conference, Washington, D.C., March 1-3, 1967*, IEEE Trans. Nucl. Sci. NS-*14* [3] (1967).

GIL W 67b W. S. Gilbert, Beam Loss and Shielding Experiment, in *Proceedings of the Sixth International Conference on High Energy Accelerators, Cambridge, Mass., September 11-15, 1967*, p. 221.

GIL W 68 W. S. Gilbert et al., 1966 CERN-LRL-RHEL Shielding Experiment at the Cern Proton Synchrotron, Lawrence Radiation Laboratory Report UCRL-17941, Sept. 1968.

GIL W 69 W. S. Gilbert, Shielding Measurements of the CERN 25-GeV Proton Synchrotron, in *Proceedings of the Second International Conference on Accelerator Dosimetry and Experience held at the Stanford Linear Accelerator Center, Stanford, California, November 5-7*, 1969, CONF-691101.

GOE K 69 K. Goebel and J. Ranft, Radiation Measurements Around a Beam Stopper Irradiated by 19.2-GeV/C Protons and Neutron Energy Spectra by Monte-Carlo Nucleon-Meson Cascade Calculations, CONF-691101, p. 394.

GOE K 71 K. Goebel, Ed., Radiation Problems Encountered in the Design of Multi-GeV Research Facilities, CERN 71-21, Sept. 1971.

GOL P 70 P. J. Gollon and R. A. Corrigan, Design of Personnel and Vehicle Access Labyrinths, National Accelerator Laboratory internal report TM-239, May 1970.

GOL P 71 P. J. Gollon and M. Awschalom, The Design of Penetrations in Hadron Shields, in *Proceedings of the Internal Congress on Protection Against Acceleration and Space Radiation, CERN, April 1971.*

GOL V 69 V. T. Golovachik et al., Induced Radioactivity at the IHEP Proton Synchrotron, IHEP 69-76.

GOL V 70 V. T. Golovachik et al., Recent Radiation Measurements at the Serpukhov Proton Synchrotron, Preprint 1970.

GRE K 56 K. Greisen, Extensive Air Showers, Progr. Cosmic Rays *3*, 1 (1956).

GRE K 57 K. Green, Reported in Discussion Session, in *Proceedings of the Conference on Shielding of High Energy Accelerators, New York, April 11-13, 1957*, TID 7545, p. 63.

GRE K 60 K. Greisen, Cosmic Ray Showers, Ann. Rev. Nucl. Sci. *10*, 63 (1960).

HAC J 67 J. Hacke, Dosimetry and Shielding with a 14-MeV Neutron Generator, Intern. J. Appl. Radiat. Isotopes *18*, 33 (1967).

HAC R 66 R. C. Hack, Health Physics, Section 9 in *PLA Progress Report*, C. J. Batty and J. M. Dickson Eds., Rutherford Laboratory Report RHEL/R156, 1966.

HAC R 67 R. C. Hack, Health Physics, Section 9 in *PLA Progress Report*, C. J. Batty and J. M. Dickson Eds., Rutherford Laboratory Report RHEL/R156, 1967.

HAR D 68 D. M. Hargreaves, Studies of the Stray Radiation Field Around Proton Synchrotrons (M. Sc. Thesis) University of London, 1968.

HAR W 69 *Proceedings of the Conference on Radiation Protection in Accelerator Environments held at the Rutherford Laboratory, England, March 1969.*

HES W 59 W. N. Hess, H. W. Patterson, R. Wallace, and E. L. Chupp, Cosmic Ray Neutron Energy Spectrum, Phys. Rev. *116*, 445 (1959).

HEU C 64 C. A. Heusch and C. Y. Prescott, Longitudinal Behavior of Electromagnetic Showers, Phys. Rev. *135*, B772 (1964).

HOF L 63 L. Hoffmann, A Summary of the Shielding Experiments Using 20-GeV Protons of the CERN PS, NIRL/R40, p. 3.

HOF L 65 L. Hoffmann and A. H. Sullivan, Shielding Studies in Steel With 10- and 20-GeV Protons, Part V: Studies of the Shielding Required for the Secondary Radiation Produced by a Target in a High-Energy Proton Beam, Nucl. Instr. Methods *32*, 61 (1965).

HOW H 71 H. Howe (National Accelerator Laboratory, Batavia), private communication, 1971.

HUG E 69 E. B. Hughes, W. L. Lakin, I. Sick, and R. Hofstadter, On the Design of NaI (Tl) Total Absorption Detectors for Strongly Interacting Particles at GeV Energies, Nucl. Instr. Methods *75*, 130 (1963).

ISR H 69 H. Israel, DTF Shielding Calculations at 800 MeV – LAMPF, in *Proceedings of the Second International Conference on Accelerator Dosimetry and Experience, Stanford, November 1969*, CONF-691101, p. 341.

JAE R 68 R. G. Jaeger, Ed., *Engineering Compendium on Radiation Shielding* Vol. 1 (Springer-Verlag, Berlin, 1968).

JAE R 70 R. G. Jaeger, Ed., *Engineering Compendium on Radiation Shielding* Vol. 3 (Springer-Verlag, Berlin, 1970).

JAE T 60 T. Jaeger, *Grundzeuge der Strahlenschutztechnik* (Springer-Verlag, Berlin, 1960).

JAI P 61 P. L. Jain, H. G. Glahe, G. N. Srivastava, and P. D. Bharadwaj, Interaction of Protons from Brookhaven Alternating-Gradient Synchrotron with Nuclear Emulsion, Nuovo Cimento *21*, 859 (1961).

JOH R 62 R. M. Johnson, Neutron Shielding Required for Linac: II. Proton Beam Striking a Carbon Target, UCRL internal document BeV–730, March 1962.

JOR B 65 B. Jordan, Experimental Study of The Production of Particles at Small Angles in Proton-Proton and Proton-Nucleus Collisions at 20 GeV, CERN 65-14, April 1965.

KAJ R 63 R. Kajikawa, Direct Measurement of Shower Electrons with "Glass-Metal" Spark Chambers, J. Phys. Soc. Japan *18*, 1365 (1963).

KAM K 58 K. Kamata and J. Nishimura, The Lateral and Angular Structure Functions of Electron Showers, Progr. Theor. Phys. Suppl. *6*, 93 (1958).

KAN A 63 A. Kantz and R. Hofstadter, Electron-Induced Showers in Copper, Phys. Rev. *89*, 607 (1953); Large Scintillators, Cerenkov Counters for High Energies, Nucleonics *12*, 36 (1951).

KAO S 63 S. Kao and G. Voss, Effectiveness of Ilmenite-loaded Concrete in Attenuating Neutron Radiation Produced by a 5-BeV Photon Beam, USAEC Report CEAL-1007 (Cambridge, Mass.), December 1963.

KAS K 72 K. Kase and W. R. Nelson, Concepts of Radiation Dosimetry, SLAC report 153, June 1972.

KEC K 56 J. C. Keck and A. V. Tollestrup, Photodissociation of the Deuteron From 150 to 450 MeV, Phys. Rev. *101*, 360 (1956).

KEE D 64 D. Keefe, μ-Meson Shielding Problems at 200 GeV: Approximate Calculations, Lawrence Radiation Laboratory Internal Report UCID-10018, May 20, 1964.

KEE D 66 D. Keefe and M. Scolnick, Table of Mean Free Path and Radiation Length for Various Materials, Lawrence Radiation Laboratory Accelerator Study Internal Report, AS/EXP 01, Dec. 1966.

KNO H 65 H. B. Knowles, Radiation Hazards Peculiar to a Linear Accelerator Meson Factory, in *Proceedings of the First Symposium on Nuclear Dosimetry and Experience, Brookhaven, Nov. 1965*, CONF-651109, p. 472.

KOM M 70 M. M. Komochkov, The Dubna Synchrophasotron, in *Engineering Compendium on Radiation Shielding*, Vol. III, Ed. R. G. Jaeger (Springer-Verlag, Berlin, 1970), Section 10.7.32.

LAD M 65 M. Ladu, M. Pellicioni, and E. Rotondi, Misure di Neutroni di Skyshine Interno al Sincrotrone di Frascati, Energia Nucleare *12*, 1 (1965).

LAD M 69 M. Ladu, Problems of Safety and Radiation Protection Around High Energy Accelerators, in *Health Physics*, Vol. 2, A. M. F. Duhamel, Ed. (Pergamon Press, Oxford, 1969), Part 1, p. 365.

LAL S 62 S. Lal and A. Subramanian, On the Growth and Decay of Electron-Photon Showers in Materials of High Atomic Number, Nuovo Cimento *26*, 1245 (1962).

LAM G 63 G. R. Lambertson, High Intensity Phenomena at the Bevatron, in *Proceedings of the International Conference on High-Energy Accelerators, Dubna, August 21-27, 1963*, p. 153.

LAS L 64 A Proposal for a High-Flux Meson Facility, Los Alamos Scientific Laboratory report, Sept. 1964.

LEB V 65 V. N. Lebedev, L. S. Zolin, and M. I. Salatskaya, A Distribution of the Penetrating Radiation Field Over the Protective Zone of the 10-GeV Synchrophasotron, Joint Institute for Nuclear Research, Dubna, USSR, Internal Report P-2177, 1965.

LEN H 63 H. Lengeler, W. Tejessy, and M. Deutschmann, Measurement of Electron Showers in Lead and Copper With the Help of a Bubble Chamber, Z. Physik *175*, 283 (1963).

LEV J 51 J. S. Levinger, The High Energy Nuclear Photoeffect, Phys. Rev. *84*, 43 (1951).

LEV J 60 J. S. Levinger, *Nuclear Photodisintegration* (Oxford University Press, 1960).

LEV G 69a G. S. Levine and W. H. Moore, Beam Stop Studies at the Brookhaven AGS, CONF-691101, p. 440.

LEV G 69b G. S. Levine and W. H. Moore, Beam Stop for 28-GeV/c Protons, CONF-691101, p. 836.

LIN S 57a S. J. Lindenbaum, Brookhaven National Laboratory Proton Synchrotron, in *Proceedings of the Conference on Shielding of High Energy Accelerators, New York, April 11-13, 1957*, TID-7545, p. 28.

LIN S 57b S. J. Lindenbaum, Skyshine, in *Proceedings of the Conference on Shielding of High Energy Accelerators, New York, April 11-13, 1957*, TID-7545, p. 101.

LIN S 61 S. J. Lindenbaum, Shielding of High Energy Accelerators, Ann. Rev. Nucl. Sci. *11*, 213 (1961).

LIN S 65 S. J. Lindenbaum, quoted by J. Baarli et al., BAA J 65.

LIV M 52a M. S. Livingston, High-Energy Accelerators—Synchro-cyclotron, Ann. Rev. Nucl. Sci. *1*, 167 (1952).

LIV M 52b M. S. Livingston, High Energy Accelerators—Standard Cyclotron, Ann. Rev. Nucl. Sci. *1*, 160 (1952).

LIV M 62 M. S. Livingston and J. P. Blewett, *Particle Accelerators* (McGraw-Hill, New York, 1962).

LIV P 68 P. Livdahl, private communications, quoted in Design Report, National Accelerator Laboratory, July 1968.

LOF E 57 E. J. Lofgren, reported in Discussion session, in *Proceedings of the Conference on Shielding of High-Energy Accelerators, New York, April 11-13, 1957*, TID-7545, p. 64.

LOF E 59 E. J. Lofgren, The Bevatron, Proc. Natl. Acad. Sci. *45*, 451 (1959).

LOF E 63 E. J. Lofgren and W. D. Hartsough, Bevatron Improvements, in *Proceedings of the International Conference on High-Energy Accelerators, Dubna, August 21-27, 1963*, p. 146.

LOH E 61 E. Lohrman, M. W. Teucher, and M. Schein, Nuclear Interactions and Mean Free Paths of Protons, Neutrons, and Alpha Particles at Energies Around 250 BeV/Nucleon, Phys. Rev. *122*, 672 (1961).

LRL 65 Lawrence Radiation Laboratory, 200 BeV Accelerator Design Study Report (2 vol.), Lawrence Radiation Laboratory Report UCRL-16000, June 1965, Ch. 12.

MAC M 58 M. H. MacGregor, W. P. Ball, and R. Booth. Neutron Nonelastic Cross Sections at 21.0, 25.5, and 29.2 MeV, Phys. Rev. *111*, 1155 (1958).

MAE R 68 R. E. Maerker, H. C. Claiborne, and C. E. Clifford, Neutron Attenuation in Rectangular Ducts, in *Engineering Compendium*, Vol 1 (Springer-Verlag, Berlin, 1968). Sect. 8.25.

MAR T 70 T. O. Marshall, The Attenuation of 14-MeV Neutrons in Water, Health Phys. *19*, 571 (1970).

MES H 62 H. Messel, A. D. Smirnov, A. A. Varfolomeev, D. F. Crawford, and J. C. Butcher, Radial and Angular Distributions of Electrons in Electron-Photon Showers in Lead and in Emulsion Absorbers, Nucl. Phys. *39*, 1 (1962).

MET N 58 N. Metropolis, R. Bivins, M. Storm, A. Turkevitch, J. M. Miller, and G. Friedlander, Monte Carlo Calculations in Intranuclear Cascades, I and II, Phys. Rev. *110*, 185 (1958).

MEY H 61 H. Meyers, R. Gomez, D. Guinier, and A. V. Tollestrup, Phys. Rev. *121*, 630 (1960).

MOO W 66 W. H. Moore, Source of High-Energy Particles from an Internal Target in the AGS, Brookhaven National Laboratory Report AGSCD-62, Jan. 1966.

MOY B 57 B. J. Moyer, Buildup Factors, in *Proceedings of the Conference on Shielding of High Energy Accelerators, New York, April 11-13, 1957*, TID 7546, p. 96.

MOY B 61 B. J. Moyer, Evaluation of Shielding Required for the Improved Bevatron, Lawrence Radiation Laboratory Report UCRL-9769, June 1961.

MOY B 62 B. J. Moyer, Method of Calculating the Shielding Enclosure of the Bevatron, in *Premier Colloque International sur la Protection Auprès des Grands Accélérateurs* (Presses Universitaires de France, Paris, 1962), p. 65.

MUR Y 65 Y. Murata, Investigation of Cascade Showers in Lead with X-Ray Films, J. Phys. Soc. Japan *20*, 209 (1965).

NAG H 65 H. H. Nagel, Electron-Photon Cascades in Lead and Monte Carlo Calculation for Primary Electron Energies Between 100 and 1000 MeV, Z. Physik *186*, 319 (1965).

NAL 68 National Accelerator Laboratory Design Report, Jan. 1968.

NEA R 56 R. B. Neale and W. K. H. Panofsky, The Stanford Mark III Linear Accelerator and Speculations Concerning Multi-BeV Applications of Electron Linear Accelerators, in *Proceedings of the CERN Symposium on High Energy Accelerators and High Energy Physics, CERN, 1956*, Vol. 1, p. 530.

NEL W 66 W. R. Nelson, T. M. Jenkins, R. C. McCall, and J. K. Cobb, Electron-Induced Cascade Showers in Copper and Lead at 1 GeV, Phys. Rev. *149*, 201 (1966).

NIL J 68 J. Nilssen and R. Sandlin, Annular (Cylindrical) Ducts—Straight Ducts, in *Engineering Compendium*, Vol. 1 (Springer-Verlag, Berlin, 1968), Sect. 8.2.4.1.

NIS J 67 J. Nishimura, Theory of Cascade Showers. Handbuch der Physik Vol. XLVI/2, Kosmiche Strahlung II, Ed. S. Flügge (Springer-Verlag, Heidelberg, 1967).

O'BR K 67 K. O'Brien, The Neutron Shielding of the Los Alamos Meson Physics Facility, USAEC Health and Safety Laboratory Report HASL-188, Nov. 1967.

O'BR K 68a K. O'Brien and J. McLaughlin, Propagation of the Neutron Component of the Nucleon Cascade at Energies Less Than 500 MeV: Theory and a Solution to the Accelerator Transverse Shielding Problem, Nucl. Instr. Methods *60*, 129 (1968).

O'BR K 68b K. O'Brien, Transverse Shielding for the Components of a ½-TeV Proton Synchrotron, USAEC Health and Safety Laboratory Internal Report HASL-199, Aug. 1968.

O'BR K 70 K. O'Brien and J. E. McLaughlin, Calculation of Dose and Dose-Equivalent Rates to Man in the Atmosphere from Galactic Cosmic Rays, Health and Safety Laboratory Report HASL-228, May 1970.

O'BR K 71 K. O'Brien, Cosmic Ray Propagation in the Atmosphere, Nuovo Cimento, *3A*, [3], 521 (1971).

OTT K 53 K. Ott, in *Kosmische Strahlung*, Ed. W. Heisenberg (Springer-Verlag, Berlin, 1953).

PAN W 57 W. K. H. Panofsky, Shielding Work at Stanford, in *Proceedings of the Conference on Shielding of High Energy Accelerators, New York, April 11-13, 1957*, TID 7545, p. 199.

PARIS 62 Proceedings of Premier Colloque International sur la Protection Auprès des Grands Accélérateurs (Presses Universitaires de France, Paris, 1962).

PAS C 62 C. Passow, "Phenomenologische Theorie Zur Berechnung einer Kaskade aus schweren Teilchen (Nukleonen-Kaskade) in der Materie," Deutsches Electron Synchrotronen Laboratorie, Hamburg Internal Publication DESY Notiz A285, Feb. 1962.

PAT H 57 H. W. Patterson, University of California Laboratory Synchrocyclotron, in *Conference on Shielding of High Energy Accelerators, New York, April 11-13, 1957*, TID-7545, pp. 3-7.

PAT H 58 H. W. Patterson and R. Wallace, A Method of Calibrating Slow-Neutron Detectors, Lawrence Radiation Laboratory Report UCRL-8359, July 1958.

PAT H 59 H. W. Patterson, W. N. Hess, B. J. Moyer, and R. W. Wallace, The Flux and Spectrum of Cosmic-Ray-Produced Neutrons as a Function of Altitude, Health Phys. *2*, 69 (1959).

PAT H 62 H. W. Patterson, The Effect of Shielding on Radiation Produced by the 730-MeV Synchrocyclotron and the 6.3-GeV Proton Synchrotron at the Lawrence Radiation Laboratory, in *Proceedings Premier Colloque International sur la Protection Auprès des Grands Accélérateurs* (Presses Universitaires de France, Paris, 1962).

PAT H 71 H. W. Patterson and R. H. Thomas, Studies at High Energy Proton Accelerators—A Review, Particle Accelerators *2*, 77, (1971).

PER D 60 D. H. Perkins, Observations on Cosmic Ray Jet Interactions in Nuclear Emulsions, Progr. Cosmic Ray Phys. *5*, 257 (1960).

PER D 63 D. H. Perkins, Results from Cosmic Ray Experiments, in "High Energy Physics Study," Lawrence Radiation Laboratory report UCRL-10022, 1963, p. 587.

PER D 65 D. R. Perry and K. B. Shaw, Radiation Levels In and Around Nimrod, CONF-651109, p. 20.

PIC T 59 T. G. Pickavance, 7-GeV Proton Synchrotron ("Nimrod"), in *Proceedings of the International Conference on High Energy Accelerators and Instrumentation, CERN, September 1959*, p. 343.

PIL J 70 J. E. Pilcher and C. Rubbia, Sampling Total Absorption Detector (SANC) for Hadrons at High Energies, Harvard University preprint, 1970.

PLA C 68a C. W. Planner and T. R. Walsh, The Possibility of a Linac Booster for Nimrod, Rutherford Laboratory Internal Report RHEL/M/156, Nov. 1968.

PLA C 68b C. W. Planner, A Study of the Feasibility of Transporting Beam from the 50-MeV PLA for Injection into Nimrod, Rutherford Laboratory Internal Report RHEL/R141, 1968.

PRI B 57 B. T. Price, C. C. Horton, and K. T. Spinney, *Radiation Shielding* (Pergamon Press, Oxford, 1957), Chap. 4.

RAJ V 60 V. J. Rajopadhye, Nuclear Interactions of 5.7-BeV Protons in Photographic Emulsion, Phil. Mag. *5*, 537 (1960).

RAN J 67a J. Ranft, Improved Monte Carlo Calculation of the Nucleon-Meson Cascade in Shielding Material, I and II, Nucl. Instr. Methods *48*, 133 (1967) and *48*, 261 (1967).

RAN J 67b J. Ranft, Monte Carlo Calculations of Particle-Loss Distributions Along the Vacuum Chamber of the CPS Near Internal Targets and of the Transverse Attenuation of Strongly Interacting Particle Fluxes in the CPS Magnet Units and Earth Shield, CERN-MPS/INT.MU/EP 67-5.

RAN J 72 J. Ranft, Particle Accelerators, *3*, 129 (1972).

RAR W 64 W. Rarita, Regge-Pole Expansion of High-Energy Peripheral Collision Amplitudes, Lawrence Radiation Laboratory Internal Report, UCID-10111, April 1964.

REA D 69 D. Reagan (Stanford Linear Accelerator Center), private communication, April 1969.

RID R 65 R. J. Riddell, High Energy Nuclear Cascades in Matter, Lawrence Radiation Laboratory Report UCRL-11989, 1965.

RIN A 63 A. Rindi and J. Baarli, Scattered Radiation at Large Distances from the CERN 600-MeV Synchrocyclotron, CERN Internal Report DI/HP/19, July 18, 1963.

RIN A 67 A. Rindi and P. Tardy-Joubert, Contribution to the Experimental Study of the Transmission of Radiation Through Service Tunnels in the Shielding of High Energy Accelerators, Industries Atomiques 3/4, 53 (1967) (in French); also available in translation, UCRL Transl. 350.

ROC T 56 T. Rockwell, *Reactor Shielding Design Manual* (Office of Technical Services, Department of Commerce, Washington, 1956).

ROS B 41 B. Rossi and K. Greisen, Cosmic-Ray Theory, Rev. Mod. Phys. *13*, 260 (1941).

ROS B 52 B. Rossi, *High Energy Particles* (Prentice-Hall, New York, 1952).

ROT J 50 J. Rotblat, in *The Acceleration of Particles to High Energies* (Institute of Physics, London, 1950), p. 54.

ROU J 69a J. T. Routti, High Energy Neutron Spectroscopy with Activation Detectors, Lawrence Radiation Laboratory Report UCRL-18514, April 1969.

ROU J 69b J. T. Routti and R. H. Thomas, Moyer Integrals for Estimating Shielding of High Energy Accelerators, Nucl. Instr. Methods *76*, 157 (1969).

SCH W 69 W. Schimmerling and M. Awschalom, Neutron Flux in a Labyrinth Due to a 3-GeV Proton Beam Incident on Lead, in *Proceedings of the 1969 Particle Accelerator Conference, Washington, D.C., Mar. 5-7, 1969*, p. 604.

SHA K 64 K. B. Shaw (Rutherford Laboratory), private communication to R. H. Thomas, 1964.

SHA K 65 K. B. Shaw, private communication quoted in 200 BeV Accelerator Design Study, UCRL - 16000, Dec. 1964.

SHA K 66 K. B. Shaw, Neutron Studies in Shields and Tunnels of the 7-GeV Proton Synchrotron Nimrod; in *Proceedings of the Conference on Radiation Measurements in Nuclear Power, Berkeley, Gloucestershire, England, 1966* (Institute of Physics and the Physical Society, London, England, 1966).

SHA K 68 K. B. Shaw, Radiation Protection Problems Associated with High Energy Proton Accelerators (M. Sc. Thesis), University of London, 1968.

SHA K 69 K. B. Shaw, G. R. Stevenson, and R. H. Thomas, Evaluation of Dose Equivalent from Neutron Energy Spectra, Health Phys. *17*, 459 (1969).

SIM P 62 P. W. Simpson and D. Laws (Rutherford Laboratory), private communication, 1962.

SMI A 58 A. R. Smith, The Stray Radiation Field at the Bevatron, UCRL-8377, July 1958.

SMI A 64 A. R. Smith, J. B. McCaslin, and M. Pick, Radiation Field Inside a Thick Concrete Shield for 6.2-BeV Incident Protons, Lawrence Radiation Laboratory Report UCRL-11331, September 18, 1964.

SMI A 65 A. R. Smith, Some Experimental Shielding Studies at the 6.2-BeV Berkeley Bevatron, in *Proceedings of the First Symposium on Accelerator Radiation and Experience, held at Brookhaven National Laboratory November 3-5, 1965.*

SMI L 56 L. W. Smith, Operation of the Cosmotron, in *Proceedings of the CERN Symposium on High Energy Accelerators and High Energy Physics, CERN 1956,* Vol. 1, p. 493.

STAN 69 *Proceedings of the Second International Conference on Accelerator Radiation and Experience, held at Stanford, California, November 5-7, 1969,* CONF-691101.

STE G 71 G. R. Stevenson and D. M. Squier, An Experimental Study of the Attenuation of Radiation in Tunnels Penetrating the Shield of an Extracted Beam of the 7-BeV Proton Synchrotron Nimrod, Rutherford Laboratory Preprint, Sept. 1971.

STE L 63 L. D. Stephens and H. Aceto, Variation of a Fission-Neutron Flux and Spectrum from a Fast Reactor Measured Over Large Distances, in *Neutron Dosimetry,* Vol. 1 (IAEA, Vienna, 1963), p. 535.

TAR P 63 P. Tardy-Joubert and H. de Kerviler, Neutrons Scattered Around Saturne, Centre d'Etudes Nucléaire de Saclay, Internal Report CEA-2303, 1963.

TAR P 65 P. Tardy-Joubert, Methods and Experience in Dosimetry at the Saturne Synchrotron, in *Proceedings of the USAEC First Symposium on Accelerator Radiation Dosimetry and Experience, held at Brookhaven National Laboratory, New York, November 3-5, 1965,* CONF-651109.

TAY C 63 C. S. Taylor, High Current Performance of the CERN/PS Linac, in *Proceedings of the International Conference on High Energy Accelerators, Dubna,* Vol. 1, p. 616, 1963.

THO H 64 H. Thom, Showers in Lead Produced by Electrons With Energies from 300 MeV to 1 BeV, Phys. Rev. *136,* B447 (1964).

THO R 60 R. H. Thomas, Neutron Background at Large Distances from the PLA, Rutherford Laboratory Internal Report NIRNS/M/12, Oct. 1960.

THO R 61 R. H. Thomas, Neutron Shielding Properties of Various Materials in the Energy Region 1-100 MeV, Rutherford Laboratory Internal Report NIRL/M/13, March 1961.

THO R 62a R. H. Thomas, Skyshine Measurements Around the Rutherford Laboratory Proton Linear Accelerator, in *Proceedings of the First International Conference on Shielding Around High Energy Accelerators, Paris, January 1962* (Presses Universitaires de France, Paris 1962), p. 108.

THOR R 62b R. H. Thomas, K. B. Shaw. P. W. Simpson, and J. F. MacEwan, Neutron Surveys Around the Rutherford Laboratory 50-MeV Proton Linear Accelerator, Rutherford Laboratory Internal Report NIRL/M/30, March 1962.

THO R 63 R. H. Thomas, Ed., *Report of the Shielding Conference held at the Rutherford Laboratory September 26-27, 1962*, NIRL/R40.

THO R 64 R. H. Thomas, Shielding Experiment at 6 GeV (I), Lawrence Radiation Laboratory Internal Report UCID-10023, Feb. 1964.

THO R 65 R. H. Thomas, Discussion (comment), in *Proceedings of the First International Symposium on Accelerator Radiation and Experience, Held at Brookhaven National Laboratory, November 3-5, 1965*, p. 273.

THO R 67 R. H. Thomas, The Radiation Field Observed Around High-Energy Nuclear Accelerators, in *Progress in Radiology* (Excerpta Medica Foundation, Amsterdam 1967), Vol. 2, p. 1849.

THO R 68 R. H. Thomas, The Proton Synchrotron as a Source of Radiation, in *Engineering Compendium on Shielding* Vol. 1 (Springer-Verlag, Berlin, 1968).

THO R 69a R. H. Thomas, Radiation Surveys—HEPL Mark III Electron Linac III—Bonner Sphere Measurements, Stanford University Internal Report RHT/TN/69-18 Sept. 30, 1969.

THO R 69b R. H. Thomas, Preliminary Estimates for Transverse Shielding of a Superconducting Linac, Stanford University Internal Report RHT/TN/69-12, May 8, 1969.

THO R 70 R. H. Thomas, Shield Design Examples—The Bevatron, in *Engineering Compendium on Radiation Shielding*, Vol. 3 (Springer-Verlag, Berlin, 1970).

TIN H 64 H. Tinlot (BNL), private communication to S. J. Lindenbaum, 1964.

TSA C 58 C. J. Tsao, R. B. Curtis, B. K. Harrison, and G. K. O'Neill, Monte Carlo Calculations of the Shielding of the Princeton-Pennsylvania 3-BeV Proton Synchrotron, Preprint 1958.

UCRL-5351 Semiempirical Neutron Cross Sections, 0.5—15 MeV, Part II. Ed., R. J. Howerton, Lawrence Radiation Laboratory Report UCRL-5351, Nov. 1958.

VAN A 71 A. Van Ginniken, M. Awschalom, and T. Borak, Comparison of Measurements and Calculations for a 29.4-GeV/c Steel Backstop, in *Proceedings of the International Congress on Protection Against Accelerator and Space Radiation, Geneva, April 1971*, CERN 71-16, Vol. 2, p. 816.

VES W 68 W. E. Veseley, Annular (Cylindrical) Ducts—Stepped Ducts, in *Engineering Compendium*, Vol. 1 (Springer-Verlag, Berlin, 1968), Sec. 8.2.4.2.

VÖL U 65 U. Völkel, Electronen-Photon-Kaskaden in Blei Für Primär Teilchen der Energie 6 GeV, Deutsches Electronen-Synchrotron, DESY, Hamburg, Internal Note DESY 65/6.

VOS R 56 R. G. P. Voss and R. Wilson, Analysis of High-Energy Neutron Cross Sections, Proc. Roy. Soc. (London) *A 236*, 41 (1956).

WAL R 62 R. W. Wallace, Shielding and Activation Considerations for a Meson Factory, Nucl. Instr. Methods *18, 19,* 405 (1962).

WAL R 70 R. Wallace, Cyclotron: Neutron Emission and Attenuation, in *Engineering Compendium On Radiation Shielding,* Vol. 3 (Springer-Verlag, Berlin, 1970), p. 157.

WEN W 59 W. A. Wenzel, Bevatron Improvements, Proposal for evatron Improvements, UCRL internal document, BeV-407, March 1959.

WEN W 63 W. A. Wenzel, Bevatron External Proton Beam, in *Proceedings of the International Conference on High-Energy Accelerators, Dubna, August 21-27, 1963,* p. 698.

WHI M 56 M. G. White, F. C. Shoemaker, and G. K. O'Neill, A 3-BeV High Intensity Synchrotron, in *Proceedings of CERN Symposium on High Energy Accelerators and High Energy Physics, CERN,* 1956, Vol. 1, p. 525.

WIL M 62 M. D. Wilson and I. B. McDiarmid, Electron Shower Curves in Lead for Energies of 3 to 40 BeV, Can. J. Phys. *40,* 573 (1962).

WIL R 52 R. R. Wilson, Phys. Rev. *86,* 261 (1952); Wilson's original results have been corrected by H. Thom, Phys. Rev. *136,* B447 (1964).

WIL R 64 R. W. Williams, Empirical Formula for Absorption Cross Sections in Nuclei, University of Washington preprint, 1964.

WIN H 60 H. Winzeler, B. Klaiber, W. Koch, M. ikolič, and M. Schneeberger, Interactions of 6.2-GeV Protons in Emulsion. I—General Results, Nuovo Cimento *17,* 8 (1960).

YALE 64 Yale University Design Study Staff, A Final Report on the Design of a Very-High-Intensity Proton Linear Accelerator as a Meson Factory of 750 MeV, Yale Report Y-12, Oct. 1964.

ZAI O 67 O. A. Zaimidoroga, Y. D. Prokoshkin, and V. M. Tsupko-Sitnikov, ZhETF (USSR) *51,* 749 (1966), *52,* 89 (1967).

ZAJ E 70 E. Zajec (Lawrence Berkeley Laboratory), private communication, Nov. 1970.

ZER C 62a C. D. Zerby, Theoretical Studies on the Transport of High Energy Radiation Through Shielding Materials in *Premier Colloque International sur la Protection Auprès des Grands Accélérateurs,* p. 57.

ZER C 62b C. D. Zerby and H. S. Moran, High Energy Electron Photon Cascade Showers in Cu, Oak Ridge National Laboratory Report ORNO-3329, 1961.

ZER C 62c C. D. Zerby and H. S. Moran, Calculation of Electron-Photon Cascade Showers, Oak Ridge National Laboratory Report ORNL-TM-442, 1962.

ZER C 63 C. D. Zerby and H. S. Moran, Studies of the Longitudinal Development of Electron-Photon Cascade Showers, J. Appl. Phys. *34*, 2445 (1963).

CHAPTER 7

INDUCED ACTIVITY AT ACCELERATORS

TABLE OF CONTENTS

INDUCED RADIOACTIVITY AT ACCELERATORS

GENERAL INTRODUCTION

The problems posed by induced radioactivity in the structure of accelerators and their local environments are not likely to be foremost in the mind of an accelerator health physicist. Indeed, at many accelerators they may be nonexistent. The practical energy threshold for production of radioactivity by accelerators is 5 to 10 MeV (with a few notable exceptions--for example, photoneutron production in Be and D, with thresholds of 1.7 and 2.2 MeV respectively). All neutron generators, of whatever energy, are potential sources of radioactivity, even at the lowest energies, because of capture of neutrons thermalized close to the accelerator.

Table 7.I provides a convenient means of deciding whether induced activity will be produced by an accelerator and how important it may be (NBS 70).

Table 7.1. Production of induced radioactivity in particle accelerators.

Particle	Energy range (MeV)	Induced radioactivity in Target	Vicinity
Electrons	< 1.67	none	none
Electrons	1.67-10	limited	very slight
Electrons	> 10	probable	suspect
Protons, helium ions	< 1	limited	none
Protons, helium ions	1-10	limited	suspect
Deuterons, tritons	any energy	probable	suspect
All ions of light atomic weight	> 10	certain	suspect

The majority of accelerators used in medicine and industry are still below the energy at which induced activity can be a problem. Nevertheless, Burrill (BUR A 69) reports that as of 1969 more than 100 electron accelerators of energy greater than 10 MeV were used for therapy, radiography, and radiation processing in the USA. Also, there is increasing interest in the use of neutron generators for neutron-activation studies and radiotherapy, of heavy-ion accelerators in radiotherapy, of various accelerators in radiopharmaceutical production, and of electron accelerators in radiography. Thus although the problems of induced activity are of less moment than those of shielding design or measurements of the radiation environments at accelerators, they may be of some importance. At larger research installations, at which frequent maintenance of, or changes in, the accelerator structure are required, induced radioactivity is often the major cause of

radiation exposure to personnel. This is particularly so if the workers are well shielded from the prompt radiation field (discussed in Chapter 3). At high-intensity accelerators this source of radiation exposure to the operating crew and maintenance workers may be so great as to actually limit accelerator operation. Figure 7.1 shows how the exposure to maintenance workers at the Brookhaven AGS has increased with the intensity of the accelerator. Indeed, this problem is of such severity in some cases as to demand the use of remote manipulators similar to those used in nuclear reactor operations (GOR A 65, FLA C 65). It should be remembered, however, that in general the specific activity induced in accelerator structure is much lower than that found in reactor-irradiated material. With the notable exception of targets, collimators, etc., placed directly in the beam, or beam dumps, the specific activity is not high. The extent of the activity is widespread, however; it is not "concentrated and confined," but rather diluted and dispersed. In consequence the total quantities of induced activity in accelerators may be large. Control of this low-specific-activity material at an accelerator laboratory may represent a major administrative problem.

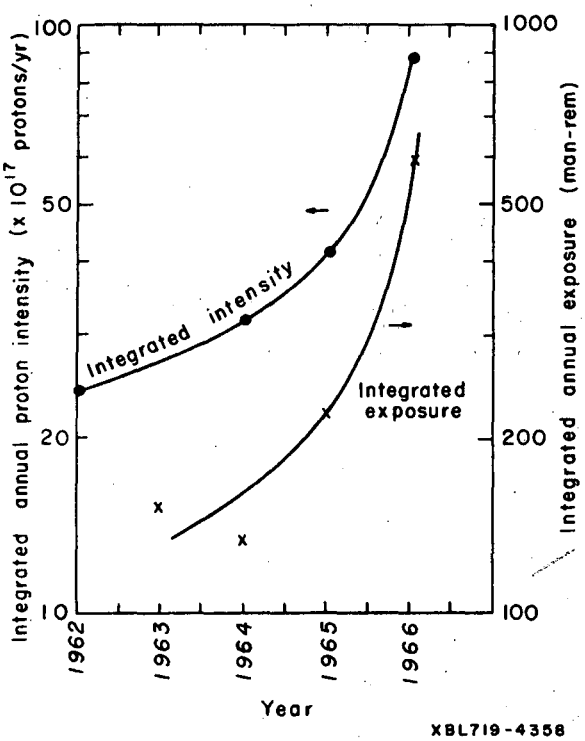

Fig. 7.1. Correlation between personnel exposures at the Brookhaven National Laboratory 30-GeV proton synchrotron and beam intensity.

One other important difference between isotopes produced in reactors and isotopes produced by accelerators is in the decay modes of the radionuclides. Accelerator-induced reactions produce radionuclides with a high proton-to-neutron ratio which tend to decay by positron emission, as contrasted with the β^--decay modes of the neutron-rich radionuclides produced by neutron capture and fission.

RADIOACTIVITY OF ACCELERATOR STRUCTURES

RADIONUCLIDES INDUCED IN ACCELERATOR STRUCTURES

Fortunately, not many materials are used in the construction of accelerators; the most important are iron, several stainless steels, copper, aluminum and aluminum alloys, and various hydrocarbons. Even so the number of possible radionuclides that may be produced is theoretically very large. Figure 7.2 shows how the production cross sections for various nuclides from proton bombardment of a target vary with proton energy. At energies of about 50 MeV the radionuclides produced with greatest probability are those with a mass number close to that of the target bombarded. As the energy increases, however, the probability of producing radionuclides of mass numbers remote from that of the target increases. (Indeed, in rough calculations it is often convenient to assume a production cross section of about 10 mb for all radionuclides.)

Precise calculations have in the past been very difficult, because it is necessary to include the effects due to secondary particles produced in the nuclear or electromagnetic cascades generated in the accelerator structure. One cannot assume that these cascades have achieved equilibrium (as may often be done, for example, in shielding calculations), because the greater part of the induced activity is produced in the transition region. Experimental studies have to date provided essentially all our available data on accelerator-produced radionuclides. Recently, however, advances in cascade calculations have made it possible to make some estimates of the activity induced in accelerator structures (ARM T 69a,b)

Experimental studies at a variety of accelerators by Boom, Toth, and Zucker (BOO R 61), Baarli (BAA J 62), Perry and Shaw (PER D 65), and Wyckoff (WYC J 67) have shown that in practice only a few radionuclides control the radiation field that is observed after accelerator shutdown.

Table 7.II summarizes the radionuclides commonly identified in materials irradiated around accelerators. Only nuclides with half-lives between 10 minutes and 5 years are listed, and--except for ^{11}C pure β^- or β^+ emitters are excluded. Most of these nuclides are produced by simple nuclear reactions such as (γ,xn), (p,xn), (n,xp), (p,pn), etc., but some are the result of spallation or fragmentation reactions, e.g. the production of ^{22}Na in steel.

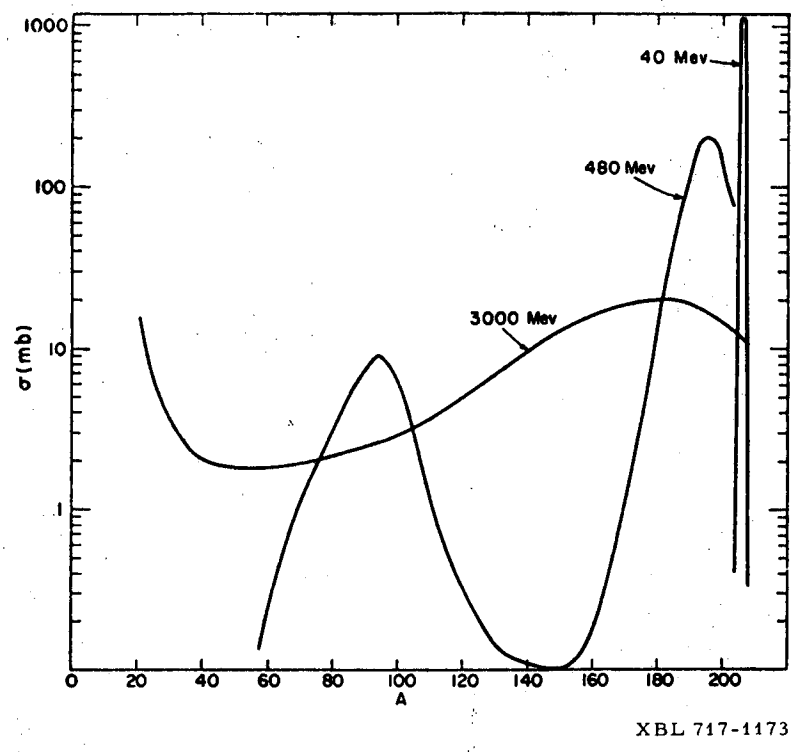

Fig. 7.2. Mass-yield curves for the proton bombardment of bismuth. The 40-MeV curve was taken from Bell and Skarsgard (BEL R 56); the 480-MeV curve was constructed from data of Hunter and Miller for 380-MeV protons on bismuth (HUN E 59), Murin et al. for 660-MeV protons on Bi(MUR A 58), and Vinogradov et al. for 480-MeV protons on bismuth (VIN A 55); the 3000-MeV curve was constructed from data of Wolfgang et al. for 3000-MeV protons on Pb (WOL R 56).

Table 7. II Summary of radionuclides commonly identified in materials irradiated around accelerators.

Target material	Radionuclides	Half-life	
Plastics and oils	^{7}Be	53.6	days
	^{11}C	20.4	minutes
Duralumin	As above, plus[a]		
	^{18}F	110	minutes
	^{22}Na	2.60	years
	^{24}Na	15.0	hours
	^{42}K	12.47	hours
	^{43}K	22.4	hours
Steel	As above, plus[a]		
	^{44}Sc	3.92	hours
	^{44m}Sc	2.44	days
	^{46}Sc	84	days
	^{47}Sc	3.43	days
	^{48}Sc	1.83	days
	^{48}V	16.0	days
	^{51}Cr	27.8	days
	^{52}Mn	5.55	days
	^{52m}Mn	21.3	minutes
	^{54}Mn	300	days
	^{56}Co	77	days
	^{57}Co	270	days
	^{58}Co	72	days
	^{55}Fe	2.94	years
	^{59}Fe	45.1	days
Stainless steel	As above, plus		
	^{60}Co	5.27	years
	^{57}Ni	37	hours
	^{60}Cu	24	minutes
Copper	As above, plus		
	^{65}Ni	2.56	hours
	^{61}Cu	3.33	hours
	^{62}Cu	9.80	minutes
	^{64}Cu	12.82	hours
	^{63}Zn	38.3	minutes
	^{65}Zn	245	days

[a]Produced with small cross section

VARIATION OF DOSE RATE FROM THE INDUCED ACTIVITY OF ACCELERATOR STRUCTURES

Because the number of radionuclides produced in accelerator components is large and accelerator operation is often quite variable, the buildup and decay of gross γ activity is a complex function of time.

The decay of dose rate near the 600-MeV CERN synchrocyclotron has been reported by Baarli (BAA J 62) and by Rindi (RIN A 64). Reliable experimental data of this type are few because of the difficulty of obtaining them at most accelerators. In periods of accelerator shutdown gross changes in the remanent radiation field may result from structural changes in the accelerator and its shielding. What data are available, however (Fig. 7.3), show that the dose rate decays by about a factor of two within 50 hours, in agreement with measurements at all the accelerators at the Lawrence Radiation Laboratory, Berkeley (BOO R 61) and elsewhere (AWS M 65) (see Fig. 7.3). Indeed it seems confirmed by general experience that the gross features of the decay of induced activity near accelerators that have been in operation for several years are nearly independent of the type of particles accelerated and their maximum energy.

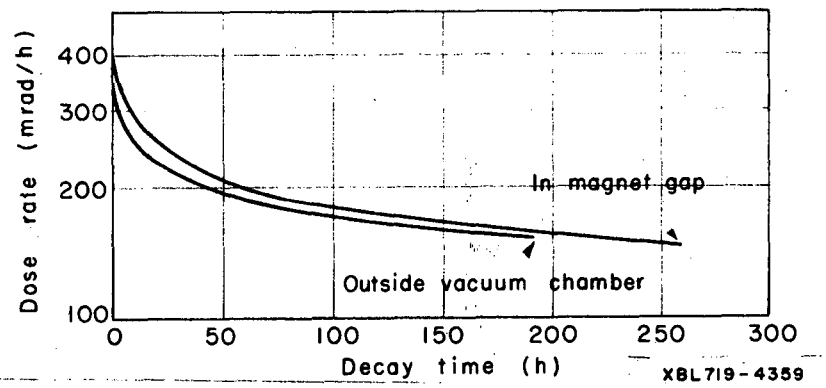

Fig. 7.3. Decay of dose rate from induced radioactivity of the CERN 600-MeV synchrocyclotron. Measurements shown were made in the air space between the accelerator vacuum chamber and the shield wall (upper curve) and between the vacuum chamber and the magnet yoke (lower curve). (After Baarli.)

Armstrong and Barish (ARM T 69a) have reported calculations of the relative photon dose rate outside a steel cylinder surrounding beams of 200-MeV and 3-GeV protons traveling along the axis (corresponding roughly to a typical accelerator structure). Figure 7.4 shows the relative dose rate at the cylinder surface after an infinitely long irradiation. The principal contributors to the γ dose rate are ^{54}Mn, ^{48}V, ^{51}Cr, ^{52m}Mn, ^{52}Mn, and ^{56}Mn.

Figure 7.5 shows how the variation of dose rate depends upon irradiation time. These calculations confirm the qualitative features observed experimentally.

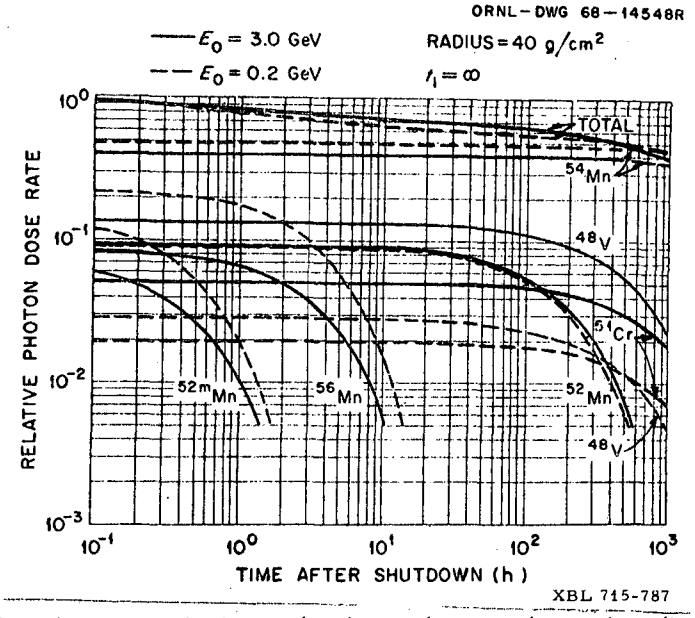

Fig. 7.4. Relative contribution to the photon dose rate due to six radionuclides at the surface of an iron cylinder (diameter 80 g/cm²) irradiated axially by 200-MeV and 3-GeV protons for an infinite time. (From Armstrong and Barish.)

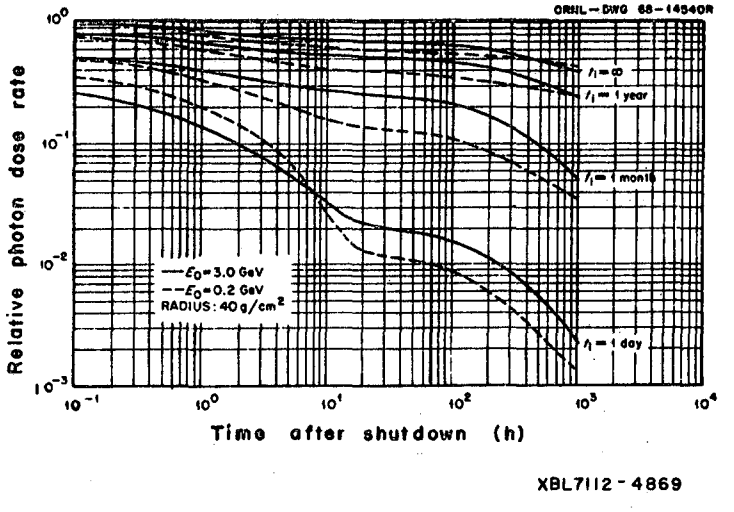

Fig. 7.5. Relative total photon dose rate at the surface of an iron cylinder axially irradiated by 200-MeV and 3-GeV protons as a function of irradiation and decay time. (From Armstrong and Barish).

Sullivan and Overton (SUL A 65) have derived approximate analytical expressions for the buildup and decay of dose rates in accelerator-irradiated material. The variation D(t), with time, of dose rate due to a single nuclide may be written as

$$D(t) = G\,I\,(1 - e^{-\lambda T})\,e^{-\lambda t}, \qquad (1)$$

where T is the irradiation time,
I is the accelerator intensity (assumed constant),
t in the decay time,
and G is a parameter that is a function of
(a) the macroscopic production cross section for the nuclide considered,
(b) accelerator parameters,
(c) particle spectrum in which the sample is irradiated,
(d) self-shielding of the decay products,
(e) geometrical factors.

Assume that dn radionuclides are produced with decay constants between λ and $d\lambda$; then the dose rate d D(t) produced by these dn radionuclides is given by

$$d\,D(t) = G\,I\,(1 - e^{-\lambda T})\,e^{-\lambda t}\,dn, \qquad (2)$$

provided G is assumed to be independent of λ. The variation in dose rate is then given by

$$D(t) = G\,I \int_{\lambda_o}^{\infty} (1 - e^{-\lambda T})\,e^{-\lambda t}\,\frac{dn}{d\lambda}\,d\lambda \qquad (3)$$

where λ_o is the smallest decay constant considered.

Sullivan and Overton suggest that for heavy target nuclei the distribution of radionuclides with decay constant greater than λ may be represented by $n = a \ln \lambda$ within about 10%.

Thus, substituting for $dn/d\lambda$ into Eq. (3) and solving, we obtain

$$D(t) = a\,G\,I\left[\ln\left(\frac{T+t}{t}\right) - \lambda_o T + O[\lambda_o^2]\right]; \qquad (4)$$

since $\lambda_o \to 0$, we have

$$D(t) = a\,G\,I \ln\left(\frac{T+t}{t}\right). \qquad (5)$$

Figures 7.6 and 7.7 show the buildup and decay of dose rate around an accelerator predicted by use of Eq. (5). These diagrams give an extremely graphic indication of the importance of accelerator operation time on the residual dose rate. Figure 7.6 shows that an accelerator that has been inoperative for a long time has the quickest buildup of radioactivity; conversely

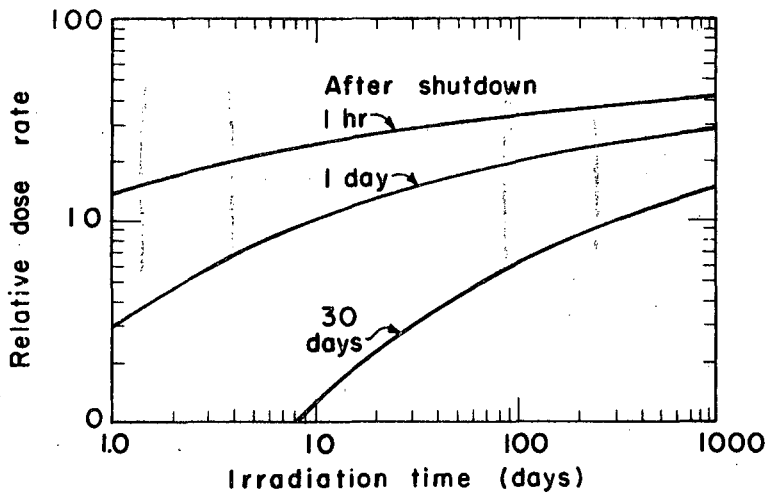

Fig. 7.6. Predicted buildup of induced radioactivity in an accelerator assuming constant intensity of irradiation. (After Overton and Sullivan.)

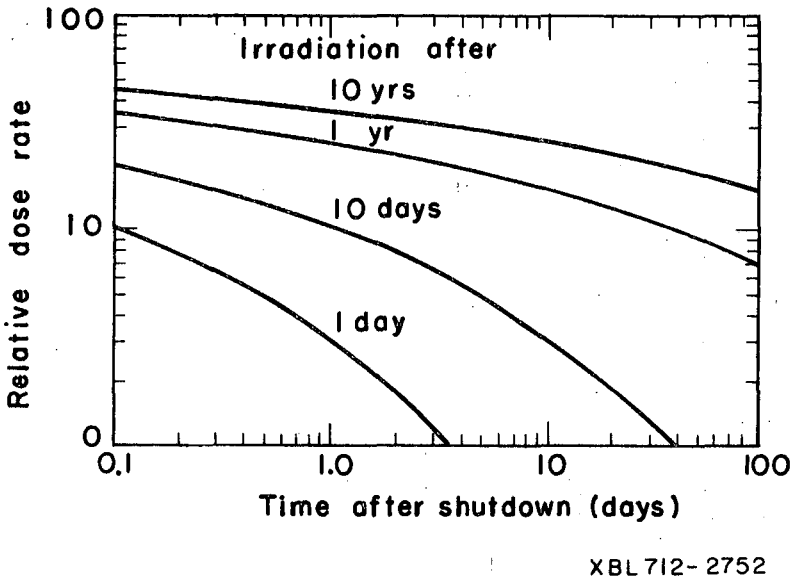

Fig. 7.7. Predicted decay of induced radioactivity following constant irradiation. (After Overton and Sullivan.)

the dose rate after accelerator shutdown decreases more slowly after long irradiations (Fig. 7.7).

Sullivan and Overton have confirmed the validity of Eq. (5) for a limited range of exposures and materials. The basic limitations of the derivation should be borne in mind, however, when their formula is used.

Fulmer et al. (FUL C 64) have described the methods for calculating γ dose rates outside thick slabs of materials irradiated with fast particles, provided the relevant production cross sections are known. Ball and Fulmer (BAL J 64) have described a computer program for such calculations that includes corrections for attenuation in the incoming beams and absorption of γ rays in the target material. Calculated decay curves for carbon, aluminum, iron, and copper (common accelerator structural materials) were compared with experimental curves obtained from exposures to neutrons of about 500 and 600 MeV, and to protons at 19 to 26, GeV, and found to agree within a factor of three (FUL C 64, FUL C 65).

Figure 7.8 shows a comparison between calculated decay curves and measured data from Al, Fe, and Cu samples irradiated for 15 minutes by 500-MeV protons. Measurements were made of the integral counts for γ rays with an energy greater than 500 keV. ^{22}Na is responsible for the dominant activity in aluminum after about 300 hours, and the experimental data presented are normalized at this point. Calculated absolute dose rates agreed with measured rates to within a factor of two. Thus it seems clear that, provided complete production cross-section data are available, residual radiation levels may be predicted. Unfortunately, for many materials of interest such cross sections are not well known.

Toth et al. (TOT K 66) have utilized the experimental and theoretical decay curves for aluminum to obtain a normalization factor that enabled them to convert their experimental relative decay curve data to dose rates for many materials. Figure 7.9 shows dose rates at 1 meter from 20-cm-thick samples irradiated for 2 years by 600-MeV protons. Figure 7.10 shows dose rates from aluminum samples of different thicknesses as functions of time. Dose rate increases with sample thickness, although the effect is not large for samples greater than about 10 cm. Thus the dose rates given in Fig. 7.9 for 20-cm-thick samples are only about 25% smaller than would be obtained from an infinitely thick target. It may be seen from these data that extremely high surface dose rates are obtained from accelerator targets, beam collimaters, etc., struck by the direct beam. A 2-cm-thick aluminum target, for example, produces a dose rate of 200 to 400 mR/h at 1 meter soon after accelerator turnoff. Dose rates at the target surface are in excess of 2000 R/h. Accelerator targets should never be handled!

Barbier (BAR M 69) has confirmed and extended these data. He shows that the production and decay of radionuclides in most materials are nearly independent of incident proton energy over the range 50 to 2900 MeV. Deuterons or α particles increase the yield by a factor of 2 to 4 over protons

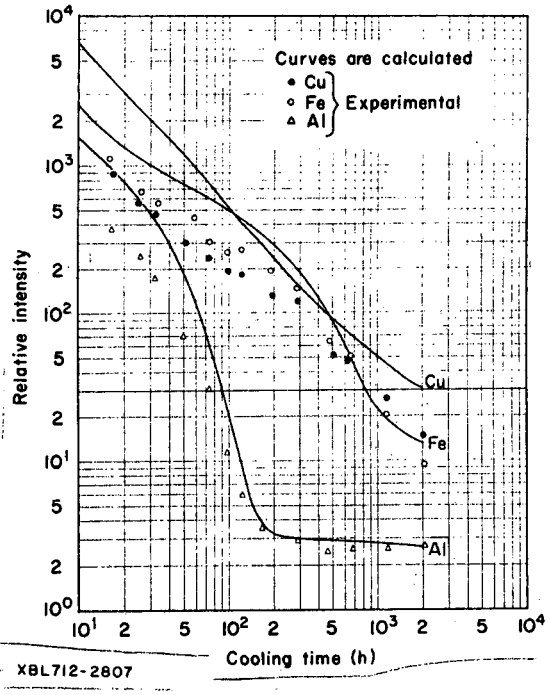

Fig. 7.8. Calculated and experimental residual radiation decay curves for samples irradiated with 500-MeV protons (15-min exposure at beam intensity of $3.2X10^{13}$ protons). (After Toth et al.)

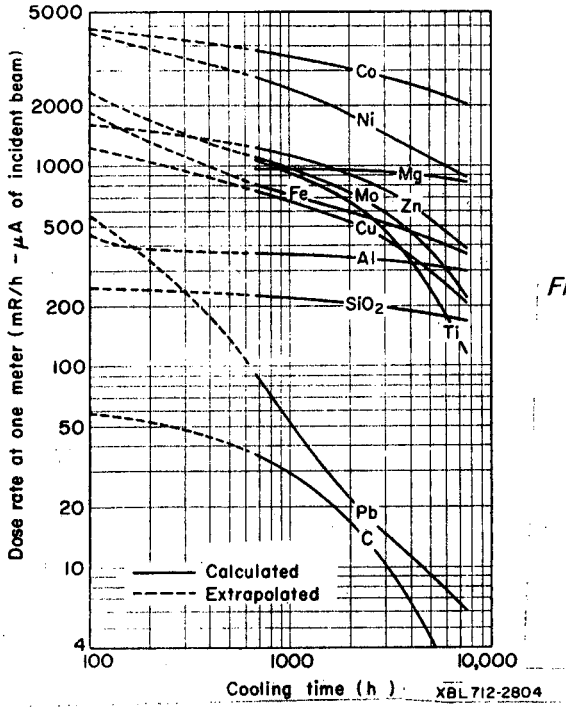

Fig. 7.9. Residual radiation levels for 20-cm-thick samples irradiated for 2 years with 600-MeV protons. The ordinate scale is also applicable for dose rates outside large 20-cm-thick slabs irradiated with a uniform flux of 10^8 protons/cm^2 sec for 2 y. (After Toth et al.)

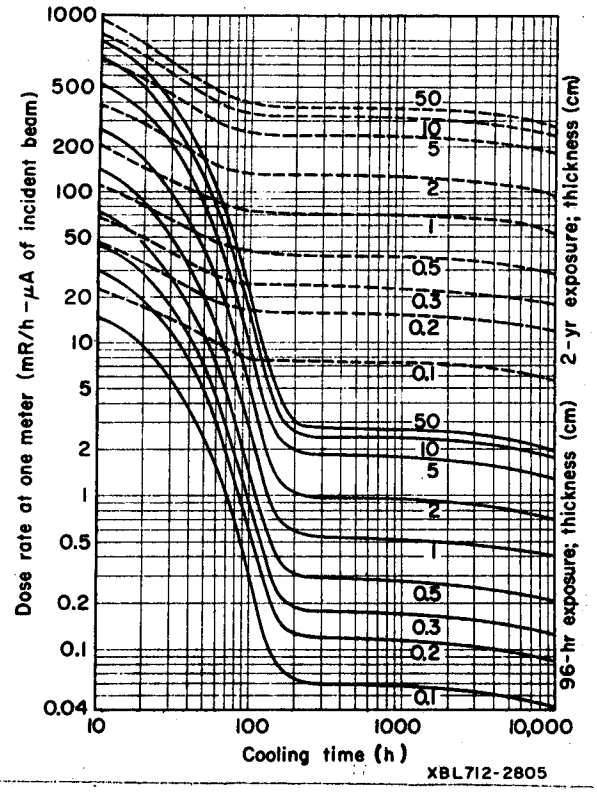

Fig. 7.10. Dose rate vs cooling time for aluminum samples of various thicknesses irradiated with 600-MeV protons for periods of 96 h and 2 y. (After Toth et al.)

of the same energy. Some anomalies appear occasionally, but it seems clear that the suggestion by Toth, Fulmer, and Barbier holds good that dose rates may be predicted within a factor of three over a wide range of materials, sample thicknesses, irradiation times, and decay times for bombardment by protons, deuterons, or α particles (TOT K 66).

RADIOACTIVITY OF THE ACCELERATOR ROOM

High intensity accelerators are usually placed in a concrete-shielded room or, alternatively, surrounded by concrete shielding blocks. The hydrogen content of concrete has an important influence in that neutron-slowing-down theory may be used to obtain the neutron spectrum inside the room. The production of high energy neutrons inside such a vault results in a thermal neutron flux density, ϕ_{th}, the magnitude of which may be obtained from the relation (PAT H 58)

$$\phi_{th} \approx \frac{1.25\,Q}{S} \quad , \tag{6}$$

where Q is the number of fast neutrons produced in the accelerator room per sec (n/sec),

and S is the inside surface area of the accelerator room (cm^2).

The spectrum of neutrons inside the accelerator vault may be obtained from two assumptions:

(a) The total thermal neutron flux density is distributed in a thermal spectrum,

$$\phi_{th}\,dE = a\,E^{1/2}\,e^{-E/kT}dE; \tag{7}$$

the normalization constant a is obtained from the known total thermal flux density:

$$a\int_0^{0.5\ eV} E^{1/2}\,e^{-E/kT} = 1.25\,Q/S. \tag{8}$$

(b) This thermal flux distribution is joined smoothly to that due to the slowing down of fast neutrons, $\phi(E)\,dE$, where

$$\phi(E)\,dE = \beta dE \int_{E_{min}}^{E_{max}} Q(E)\left(\frac{1}{E_{min}} - \frac{1}{E}\right) dE, \tag{9}$$

where β is a constant,

and $Q(E)dE$ is the number of fast neutrons of energy E produced in the vault per sec.

Substantial thermal- and fast-neutron flux densities may thus be generated in the vaults of high intensity accelerators and induce radioactivity resulting in remanent radiation levels after accelerator turnoff.

These radiation levels inside an accelerator room are from two sources--the activity induced in the walls of the room and that of the accelerator components themselves.

It is fairly easy to show that the dose rate due to remanent radioactivity inside a cylindrical void whose walls have been uniformly irradiated is constant and equal to the dose rate at the tunnel wall (ARM T 69b). The dose rate from the accelerator structure, however, is a function of distance from the accelerator. The resultant radiation level is therefore a function of position inside an accelerator room.

Armstrong and Barish (ARM T 69b) have calculated the residual photon dose rate inside an accelerator tunnel due both to the iron of the accelerator and to the concrete of the accelerator room for one particular case (though results may be extended to other situations as required) in which protons of 3 GeV travel along the axis of an infinitely long iron cylinder of 40 g/cm^2 in radius. The iron is situated along the axis of cylindrical void i.d. 14.68 ft) in an infinite slab of concrete. The reader is referred to the original paper for details of these calculations, but their general conclusion is summarized here. Figure 7.11 shows how the dose rate due to accelerator structure and tunnel wall varies as a function of position; Fig. 7.12 shows the ratio of the total dose rate to that contributed by the magnet.

Measurements of the residual radiation levels inside the Brookhaven AGS tunnel (which approximates the model used by Armstrong et al.--(ARM T 69b) indicate such a general background due to radioactivity of the concrete walls. Figure 7.13 shows an isodose contour diagram taken at the midsection of an accelerator gradient magnet. Not surprisingly, the highest radiation levels are due to the high levels of radioactivity in the magnet pole faces and are found opposite the open side of the C magnet. Figure 7.14 indicates the contribution due to the magnet alone, a residual background level of about 1 mrem/h having been substracted. Comparison of Figs. 7.13 and 7.14 reveals that it is quite feasible to place limited shielding around the accelerator magnet so that the radiation field in the accelerator room is largely determined by the activity of the concrete walls.

Several studies have been made of the latter contribution. Calculations by Armstrong and Barish (ARM 69b) show that ^{24}Na dominates for about 30 h after accelerator shutdown, and this has been confirmed experimentally (see Fig. 7.15) (DES H 62, GIL W 64a b c, MID W 65, GIL W 65, NAC D 66). This isotope emits exceptionally penetrating γ radiation, and consequently poses the most serious problem of induced activity from such a shield. For multi-GeV proton accelerators, it has been suggested that the capture of thermal neutrons by elemental sodium (^{23}Na) in concrete be reduced by adding a neutron "poison" (boron, for example) to the concrete aggregate (GIL W 65).

An experimental study to determine the influence of boron in concrete was undertaken by Nachtigall and Charalambus (NAC D 66), who measured dose rates and induced activity in ordinary and borated concrete at the 28-GeV proton synchrotron in CERN, Geneva, Switzerland. These measurements show that dose rate and induced activity can be considerably reduced

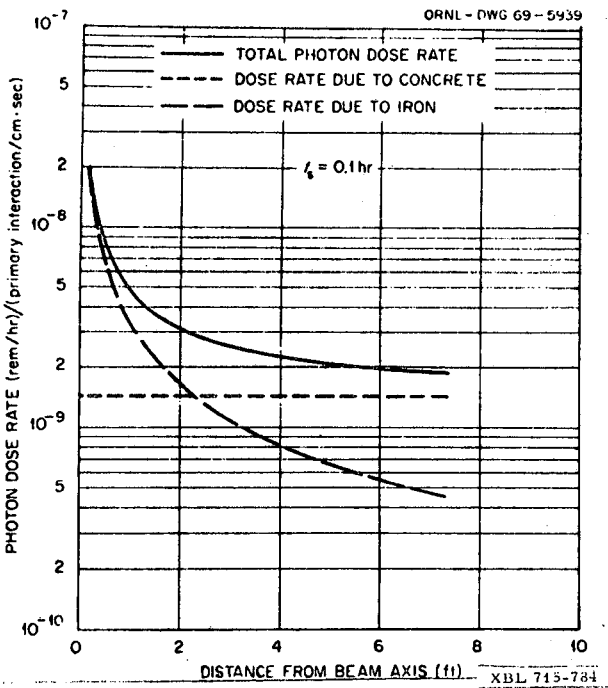

Fig. 7.11. Dose rate inside accelerator tunnel as a function of distance from the beam axis after a shutdown time of 0.1 h. (Infinitely long steel cylinder--80 g/cm^2 diam--axially irradiated by 3-GeV protons). (From Armstrong and Barish.)

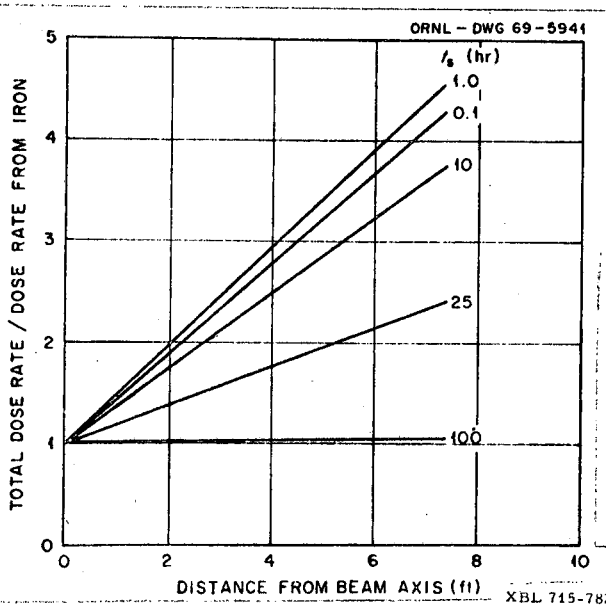

Fig. 7.12. Relative contribution to the dose rate in the iron magnet as a function of shutdown time and position. (After Armstrong and Barish.)

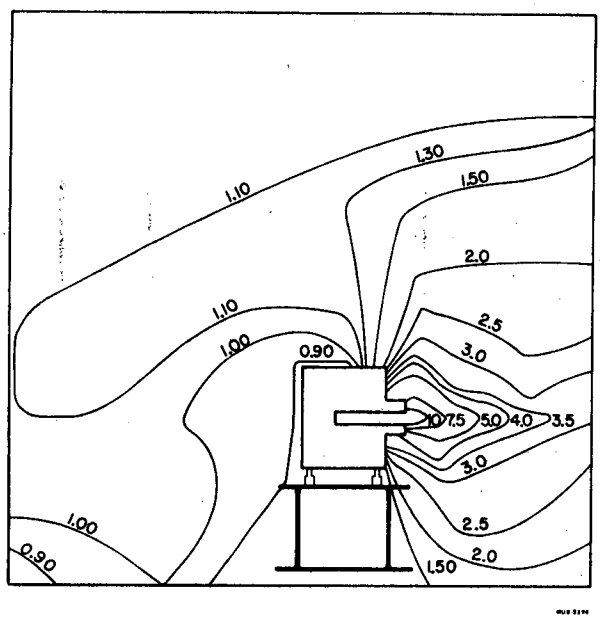

Fig. 7.13. Isodose contours (in mr/h) inside the accelerator tunnel of the BNL 30-GeV AGS. Measurements taken at mid-magnet about 6 h after accelerator shutdown. (After Gilbert and Thomas.)

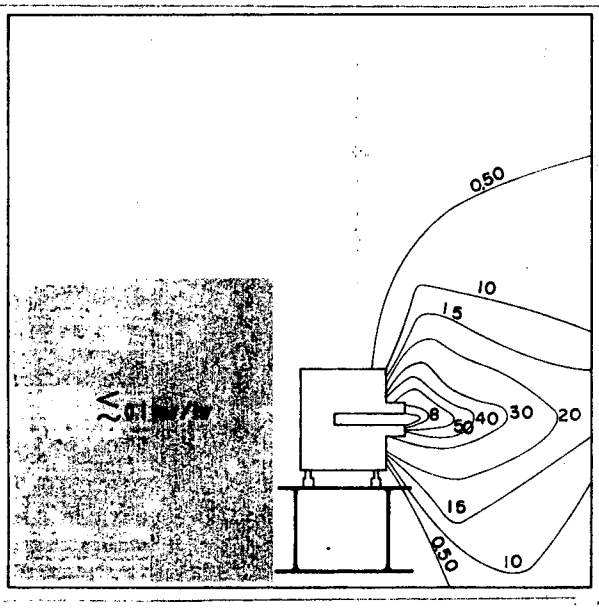

Fig. 7.14. Isodose contours with tunnel contribution removed (after Gilbert and Thomas).

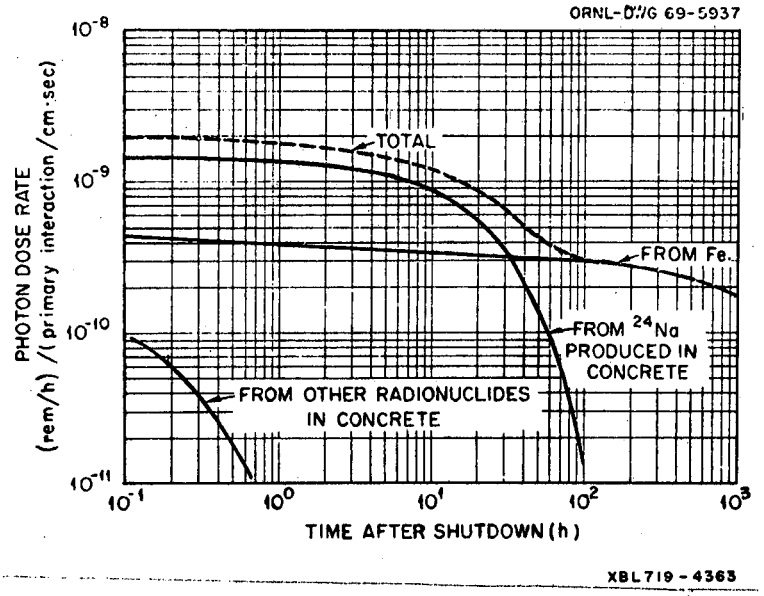

Fig. 7-15. Photon dose rate at surface of tunnel wall after finite irradiation time for concrete containing one percent sodium by weight (from Armstrong and Barish.)

by adding as little as 0.3% boron to this concrete. They did not, however, measure production of ^{24}Na in the different constituents of the concrete. In a previous preliminary experiment Middlekoop and de Raad measured the ^{24}Na contribution in the main constituents of this concrete at two positions on the concrete surface inside the proton synchrotron ring tunnel (MID W 65). They could show, as expected, that ^{24}Na production was highest in Na, but that some ^{24}Na was also produced in Mg, Al, and Si by particles of higher energy.

Gilbert et al. have reported the results of a very thorough analysis (GIL W 69). ^{24}Na activity produced in concrete aggregate and its major elemental constituents (Na, Mg, Al, Si, and Ca) was measured as a function of depth in ordinary and boron-loaded concrete at the Berkeley 6.2-GeV Bevatron. These measurements were made at two locations in the Bevatron main shielding wall adjacent to strong local radiation sources. At one site, additional exposures were made with a boric acid wall in front of the concrete shield wall, in order to study the influence of boron spatial distribution on thermal-neutron production of ^{24}Na from sodium. The influence of several ^{24}Na-producing reactions on the dose rate in the main vault was evaluated for the different experimental conditions. Suppression of thermal flux was assessed by introducing a neutron poison, either into the structural concrete of the shield or as a thin layer on the inner surface of the shield.

It was shown the ^{24}Na production in the constitutents selected for the measurements accounts for practically all ^{24}Na found in aggregate following irradiation. In this way the ^{24}Na measured in the aggregate was completely accounted for. The depth dependence of ^{24}Na production in the different constituents followed the simple attenuation pattern for the reaction with the highest-energy threshold, upon which was superimposed the production by lower-energy radiation (penetrating the concrete to a depth of 2 ft at most).

The large effects on ^{24}Na production of the boron content of concrete and of the presence of a boron layer in front of the concrete were quantitatively determined. It was further shown that, if the boron and sodium contents of different concrete mixtures are taken into account, the results of other experiments are in accordance with findings by Gilbert et al. (GIL W 69). This allows evaluation of the contribution to the dose rate in an accelerator vault from different constituents at different depths in a shield, not only for the Bevatron but also for the general case.

AIRBORNE RADIOACTIVITY PRODUCED AT ACCELERATORS

INTRODUCTION

During accelerator operation radioactive gases are produced by the interaction of primary or secondary particles with air. Such airborne radioactivity is in general short-lived, and even if it is produced in unacceptably high levels, radioactive decay and (or) dilution with inactive air very quickly

reduce concentrations to acceptable levels. Indeed, only in very unusual circumstances would exposure from radioactive gases be the limiting factor for personnel access to accelerator buildings. Nevertheless, it is important that the accelerator health physicist be able to compute the exposure both to accelerator personnel and to members of the general public who may be exposed at the accelerator-site perimeter.

A second source of airborne radioactivity is dust, formed by natural erosion and wear or by maintenance work on radioactive accelerator components. A third source of radioactivity in the air close to an accelerator has recently been reported: Warren et al. (WAR G 69) have studied the production of CO_2, which acts as a carrier for ^{11}C and ^{15}O produced in water beam dumps at the Stanford Linear Accelerator.

GASEOUS RADIONUCLIDES PRODUCED IN AIR

Table 7.III lists the isotopes found most abundantly in the atmosphere.

Table 7.III. Most abundant isotopes found in the atmosphere.

Isotope	Percentage by volume in the atmosphere
^{14}N	78.1
^{16}O	21.2
^{40}A	0.46
^{15}N	0.28
^{18}O	0.04
^{12}C	0.015
^{17}O	0.008
^{36}A	0.0016

Rindi and Charalambus (RIN A 67) have summarized all the radionuclides with a half-life greater than 1 second that may be produced from the target nuclei given in Table 7.III by thermal-neutron capture and by (γ,n) and spallation reactions. Table 7.IV lists these radionuclides in order of decreasing half-life and summarizes their modes of production and decay.

The total specific activity S, of the radioactive air, produced close to an accelerator may be written generally as

$$S = C \sum_{ijk} N_j \int_{E_{ijk}}^{E_{k\,max}} \sigma_{ijk}(E)\, \phi_k(E)\, dE\, (1-e^{-\lambda_i T})\, e^{-\lambda_i t} \qquad (10)$$

where S is the total specific activity of radioactive air (per liter),
C is a constant,
i represents the radionuclide of type i,
j represents the target nuclide, j,
k represents the interacting particle, γ, p,n, etc.,
N_j is the number of target nuclei of type j in a liter of atmospheric air,
$\sigma_{ijk}(E)$ is the cross section for the production of the radionuclide of type i from the target j by a particle k at energy E,
$\phi_k(E)$ is the flux density of particles of type k between E and E+dE,
E_{ijk} is the threshold for the reaction $i \rightarrow j$ by a particle of type k,
$E_{k\,max}$ is the maximum energy of particles of type k,
λ_i is the decay constant of the radionuclide i,
T is the irradiation time,
and t is the decay time.

Equation (10) may be simplified considerably by two simple approximations.

a. Production by only three modes is considered:
   (i) thermal neutron capture,
   (ii) high-energy particle spallation,
   (iii) γ,n reactions [k = γ, th, HE]
b. The integrals of Eq. (10) are replaced by average fluxes and cross sections:

$$\left[\int_{E_{ijk}}^{E_{j\,max}} \sigma_{ijk}(E)\, \phi_k(E)\, dE = < \sigma_{ijk} > \Phi_k \right]. \qquad (11)$$

Thus Eq. (10) simplifies to (RIN A 67)

$$S = C \sum_i \left[\sum_j \Phi_\gamma N_j \bar{\sigma}_{ij\gamma} + \sum_j \Phi_{th} N_j \bar{\sigma}_{ijth} + \sum_j \Phi_{HE} N_j \bar{\sigma}_{ijHE} \right] X\,(1-e^{-\lambda_i T})\, e^{-\lambda_i t}, \qquad (12)$$

where Φ_γ, Φ_{th}, and Φ_{HE} are the average photon, thermal neutron, and high-energy particle flux densities,

and $\bar{\sigma}_{ij\gamma}$, $\bar{\sigma}_{ijth}$ and $\bar{\sigma}_{ijHE}$ are the corresponding average cross sections.

To use the simple expressions one must determine which nuclides are of greatest concern. Radionuclides with half-lives less than 1 minute are of no concern, decaying to negligible activities before personnel may enter the accelerator room. They may also be similarly discounted with

Table 7.IV. Radionuclides produced from gases of atmospheric air. (After Rindi and Charalambus).

Radionuclide	Half-life	Type of decay energy (MeV) and percent	Parent element	Fraction by weight of parent element in air	Production reaction	Cross section (mb)
$^{3}_{1}H$	12.2y	β^-(0.018)–100%	C	1.6×10^{-4}	spallation	[a]
			N	0.755	spallation	30
			O	0.23	spallation	30
$^{7}_{4}Be$	53d	γ(0.48) 12% E.C.	C		spallation	[a]
			N	see above	spallation	10
			O		spallation	10
$^{41}_{18}A$	1.8h	β^-(1.2) 99% γ(1.3) 99%	^{40}A	0.013	thermal capture	610
$^{11}_{6}C$	20.5 min	β^+(0.9) 100%)	C			[a]
			N	see above	spallation	20
			O		spallation	20
$^{13}_{7}N$	10 min	β^+(1.25)–100%	N		spallation and (γ,n)	30[a]
			O	see above	spallation	10
$^{15}_{8}O$	2.1 min	β^+(1.7) 100%	O		(n, 2n) and (γ,n)	60[b]
$^{14}_{8}O$	74 sec	β^+(1.8) 99% γ(2.3) 99%	O	see above	spallation	5
$^{19}_{8}O$	29 sec	β^-(4.5) 30% β^-(2.9) 70% γ: various	^{18}O	4.2×10^{-4}	thermal capture	*
$^{19}_{6}C$	19 sec	β^+(2.1)–99% γ(0.7) 99%	C	see above	spallation	*
$^{16}_{7}N$	7.3 sec	β^-: various	^{15}N	0.0028	thermal capture	
		γ: various	O	see above	(n,p) spallation	60
$^{17}_{7}N$	4.1 sec	β^-,n			**	
$^{15}_{6}C$	2.3 sec	β^-(4.5–80%) and (9.5–20%) γ(5.3–20%)			**	

*This reaction has not been taken into consideration owing to the small fraction of parent element.
**The production of these isotopes is very improbable.
[a]This is the total cross section. The spallation cross section is about 10 mb and the (γ,n) reaction cross section is assumed to be 10 mb. We suppose that the high-energy γ-ray flux is double that produced by high-energy particles; consequently, a total cross section of 30 mb can be used.
[b]Total cross section. The (n,2n) reaction cross section is 40 mb. On the same assumption as above a total cross section of 60 mb can be used.

Table 7.V. Radionuclides identified in the air around several accelerators.

Laboratory	Accelerator	Radionuclides identified	Comments
RPI	50-MeV electron linac	^{15}O, ^{13}N	
Saclay	330- to 560-MeV 100-kW beam power	^{13}N, ^{15}O, ^{11}C, ^{41}A, ^{38}Cl, ^{7}Be	
CERN	600-MeV proton synchrotron	^{11}C, ^{13}N, ^{41}A	
PPA	3-GeV proton synchrotron, 10^{11} p/sec	^{14}O, ^{15}O, ^{13}N, ^{11}C	^{13}N, ^{11}C, levels negligible ^{14}O, ^{15}O same order of magnitude as $(MPC)_a$
RHEL	7-GeV proton synchrotron	^{16}N, ^{15}O, ^{13}N, ^{11}C	Maximum concentrations $\approx 2 \times 10^{-6}$ per/cm^3 close to target
CERN	25-GeV proton synchrotron	^{13}N, ^{11}C, ^{41}A	
BNL	30-GeV proton synchrotron	^{13}N, ^{11}C, ^{41}A	

respect to exposure from gases leaking from the accelerator room during operation. Long-lived activities, on the other hand, may be discounted because of their low production rate. In usual facilities, where complete air changes occur 2 to 3 times per hour, even normal leakages may amount to 10% of the volume of enclosed air per hour. Unless special steps are taken to prevent air from leaving the accelerator room its residence time is considerably less than 1 day. It is not possible, therefore, to produce ^{7}Be or ^{3}H at levels higher than a small fraction of saturated specific activity.

Because of the extremely small thermal neutron absorption cross section of ^{18}O and its low isotopic abundance, no significant quantity of ^{19}O would be expected.

Such arguments suggest that only four radionuclides need be considered--^{15}O, ^{13}N, ^{11}C, and ^{41}A.

Several experimental studies at various accelerators have confirmed these conclusions. At electron accelerators George et al. (GEO A 65) have reported measurements at a 50-MeV electron linac, and Vialettes (VIA H 69) has reported studies at energies up to 560 MeV. At proton accelerators studies have been reported at the (PPA) Princeton-Pennsylvania Accelerator 3-GeV synchrotron (AWS M 69), the Rutherford Laboratory 7-GeV synchrotron (SHA K 67), the Brookhaven AGS (BNL 64), and CERN accelerators (RIN A 67). Table 7.V summarizes the general findings of these studies.

The most extensive study at an electron accelerator reported to date is that due to Vialettes (VIA H 69). This study is noteworthy because of the large number of radionuclides identified in air; of particular interest is the identification of ^{38}Cl and ^{39}Cl produced by (γ,pn) and (γ,p) respectively with ^{40}A. Vialettes finds that with the accelerator operating at 550 MeV and a beam power of 100 kW the concentration of radioactive gases in the effluent stack is greater than the maximum permissible concentration (MPC). It is possible to operate this accelerator using a closed air circuit and thus substantially reducing the quantity of activity released to the environment. Figure 7.16 shows a γ spectrum of the radionuclide emerging from the target-room effluent stack. Vialettes concludes that the contribution to exposure from radioactive gases to anyone entering the accelerator room is negligible compared with that from the induced activity of the accelerator structures.

The most extensive series of measurements of gaseous radioactivity at proton accelerators has been made at the CERN 600-MeV synchrocyclotron (SC) and the 28-GeV proton synchrotron (PS) (RIN A 67). Typical measurements are summarized in Table 7.VI.

Figure 7.17 shows the decay of the induced activity measured at both accelerators compared with the decay curve calculated by assuming a 30-minute irradiation and 5-minute decay period, and that the radionuclides ^{41}A: ^{11}C: ^{13}N: ^{15}O are produced in the relative proportions 0.14: 0.31: 0.47: 0.08.

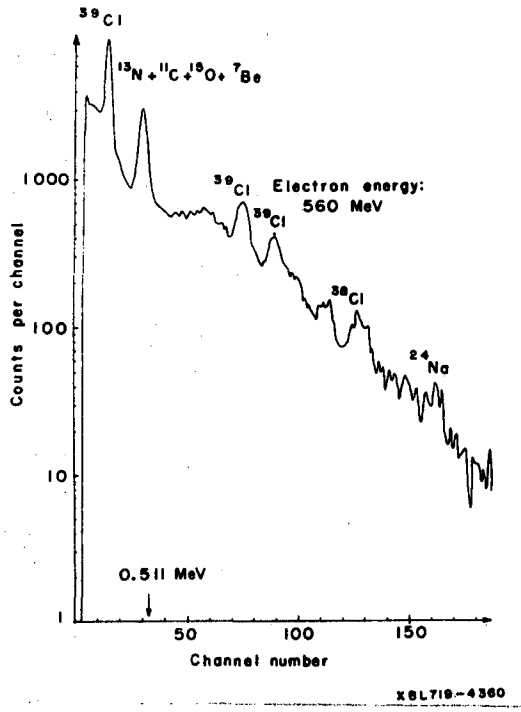

Fig. 7.16. Gamma spectrum of the radionuclides in the air emerging from the stack of the target room of a 550-MeV electron linac. (After Vialettes.)

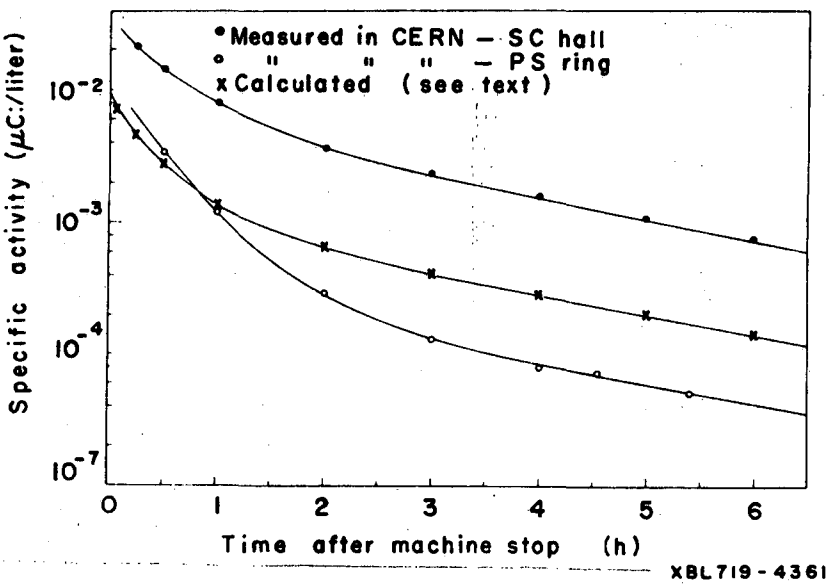

Fig. 7.17. Decay of the radioactivity in air produced at the CERN accelerators. (After Rindi and Charalambus.)

Table 7.VI. Maximum values of specific radioactivity of the air measured at the CERN accelerators (5 min after machine stop). [After Rindi and Charalambus].

Location	Total (μCi/liter)	Contribution from different radioisotopes
In the ring of the CERN proton synchrotron (near target region)	$\approx 10^{-2}$	$^{13}N \approx 50\%$; $^{11}C \approx 30\%$; $^{41}A < 10\%$; other isotopes $> 10\%$.
In the hall of the CERN synchrocyclotron (near target region)	$\approx 3.5 \times 10^{-2}$	$^{11}C \approx 55\%$; $^{41}A \approx 22\%$; $^{13}N \approx 12\%$; other isotopes $\approx 10\%$.
In the extracted 600-MeV proton beam of the CERN synchrocyclotron	8	$^{11}C \approx 67\%$; isotopes with half-life < 20 min $\approx 32\%$ (^{85m}Kr present; no ^{41}A)
Near a target placed in the path of the extracted 600-MeV proton beam of the CERN Synchrocyclotron.	2×10^{-1}	$^{11}C \approx 23\%$; isotopes with half-life < 20 min $\approx 76\%$ (^{85m}Kr present; no ^{41}A.

Table 7.VII gives values of the maximum permissible concentrations of radionuclides in air, $(MPC)_a$, calculated by using the formula recommended by the ICRP (ICRP 60).

Table 7.VII. Maximum permissible concentrations in air.

Radionuclide	$(MPC)_a$ (μ Ci/liter)
$^{3}_{1}H$	2
$^{7}_{4}Be$	6×10^{-3}
$^{41}_{18}A$	2×10^{-3}
$^{11}_{6}C$	8×10^{-3}
$^{13}_{7}N$	5×10^{-3}
$^{15}_{8}O$	3×10^{-3}
$^{16}_{7}N$	5×10^{-4}

Rindi and Charalambus conclude that under normal accelerator operating conditions specific activities from 10 to 30 $(MPC)_a$ are found 5 minutes after cessation of operation at the CERN accelerators. Air confined around targets or in particle beams may reach levels as high as 1000 $(MPC)_a$.

The observation of specific activities exceeding the maximum permissible concentration in air, $(MPC)_a$, need not necessarily be (and in general is not) a serious matter, however, for several reasons:

a. The gaseous radionuclides of greatest concern emit positrons or γ rays (or both), and use of ordinary portable survey instruments indicates abnormally high radiation levels due to their presence. Normal survey procedures therefore prevent high external exposures.

b. The high levels measured are of extremely short duration after accelerator turnoff, because of the short half-lives of the important nuclides and dilution with inactive air. Workers are not, in general, continuously exposed to levels exceeding $(MPC)_a$ for periods comparable to 40 hours per week, for which they are estimated.

c. The criteria used in the calculation of MPC's are often unduly conservative. For gaseous radionuclides that are not fixed metabolically and are β and (or) γ emitters, MPC's are calculated by assuming immersion in an infinite cloud (ICRP 60). Attention was drawn to the inadequacy of the infinite-cloud computation in the design study report for a 200-GeV accelerator (LRL 65): "A comment may be made on the low value of the $(MPC)_a$ for

Table 7.VIII Results of survey of accelerator workers. (Numbers in parentheses indicate number of workers in whom isotopes were found.) [From Patterson et al.]

Location and type of determination	Individuals	Determinations	Individuals positive	Isotope or energy		Values (or range) (μCi)	
184-inch *cyclotron*							
A. Radiochemical							
1. alpha	11	16[a]	3[b]	^{237}Np[c]	(2)	0.15 to 1.0 X 10^{-6}[d]	
2. beta	11	14	12			4.2 to 42 X 10^{-6}[d]	
3. gamma	11	11	0				
B. Whole-body count	14	14	2	0.825 MeV	(1)	trace	
				^{65}Zn	(2)	3×10^{-3}	(1)
						7×10^{-3}	(1)
Bevatron							
A. Radiochemical							
1. Alpha	42	42	1			0.3 X 10^{-6}[d]	
2. beta	42	42	38			1.7 to 120 X 10^{-6}[d]	
3. gamma	42	42	0				
B. Whole-body count	44	44	1	^{65}Zn		1×10^{-3}	
Heavy-ion linear accelerator							
A. Radiochemical							
1. alpha	10	11	1	^{237}Np	(1)	1 X 10^{-6}[d]	
2. beta	10	10	9			2.7 to 6.7 X 10^{-6}[d]	
3. gamma	10	10	0				
B. Whole-body count	13	13	0				
88-inch *cyclotron*							
A. Radiochemical							
1. alpha	21	21	1			0.7 X 10^{-6}[d]	
2. beta	21	21	20			1-10 X 10^{-6}	
3. gamma	21		0				
B. Whole-body count	22	22	3	^{181}W ?	(2)	7×10^{-3}	(2)
				$^{58,57}Co$	(1)	3×10^{-3}	(1)

[a]Multiple determinations on cases thought to be positive.

[b]One individual not confirmed.

[c]What appeared to be clearly a ^{237}Np peak, energy 4.77 MeV, was present in each of the samples examined by alpha pulse-height analysis. In addition, a number of smaller peaks were seen in all the samples.

[d]Per 24-hr urine sample.

Table 7.IX. Radionuclides identified in dust samples at CERN proton synchrotron (after Charalambus and Rindi).

Radionuclide	Decay Mode	Relative quantity (%)
^{54}Mn	EC,γ	≈ 50
^{7}Be	EC,γ	≈ 25
^{51}Cr	EC,γ	≈ 7
^{59}Fe	β^-, γ	≈ 9
^{68}V	β^+,γ	≈ 9

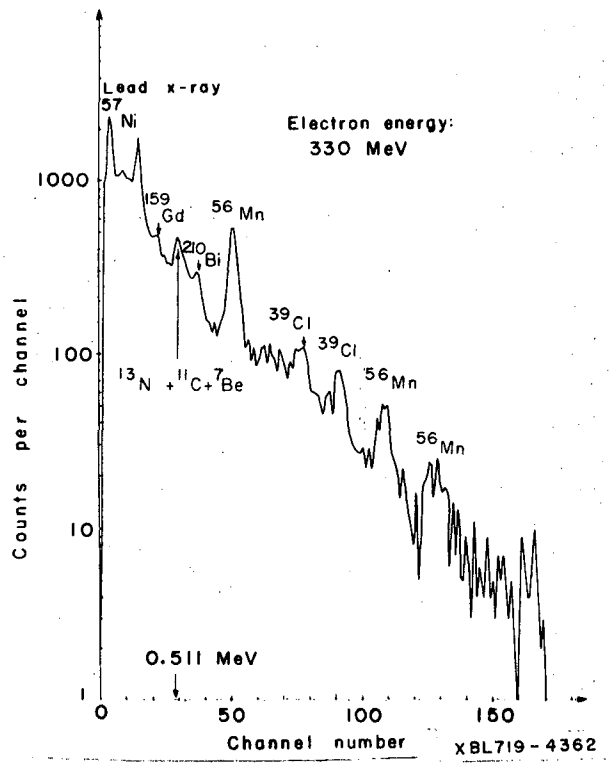

Fig. 7.18. Gamma spectrum of radionuclides found in the filter of an air sampler operating in the target room of 500-MeV electron linac. (After Vialettes.)

components by (n,γ) and (γ,p) reactions. ^{57}Ni is produced by the (γ,n) reactions in ^{58}Ni. The 0.072-MeV and 0.6-MeV γ's are attributed to ^{212}Pb and ^{214}Bi respectively, which are decay products of atmospheric radon and thoron.

Busick and Warren (BUS D 69) have studied the problem of machining radioactive accelerator components and the possible internal contamination of personnel that might result. Air sampling close to machining operations on stainless steel and copper showed no airborne radioactivity. Busick and Warren conclude that the chemical toxicity and external dose rate are the factors that limit the machining of radioactive accelerator components rather than inhalation of radioactive dust.

RADIOACTIVITY INDUCED IN WATER

COOLING WATER AND BEAM DUMPS

The radioactivity induced in cooling-water circuits of accelerators of high intensity may be of concern either because of the high dose rates close to loops carrying highly radioactive water or because of the difficulties in its disposal.

Rose et al. (ROS B 58) reported that external radiation levels as high as 100 millirem per hour were found at various regions close to the cooling system of the Harwell 150-MeV cyclotron when it was operated with an internal beam of about 1 μA. Warren et al. (WAR G 69) have reported dose rates of between 0.5 and 4 mr/h from cooling-water circuits along the accelerator structure of the Stanford 20-GeV electron linear accelerator. Considerably higher levels, however, are found from heat exchangers for high-power beam dumps, rates up to 120 R/h being observed.

Distenfeld (DIS C 64) has concluded from measurements at the Brookhaven AGS that with a proton beam intensity of 10^{13} protons/sec the external radiation hazard from induced activity in cooling water would be trivial. However, the dose rate from large volumes of water, such as heat exchangers or storage tanks, would be measurable during accelerator operation.

Table 7.X lists the radionuclides produced by spallation of oxygen. Bruninx (BRU E, 61, BRU E 62, BRU E 64) has tabulated high-energy nuclear-reaction cross sections for charged-particle energies greater than 50 MeV which are of value in estimating spallation yields. When cross-section data are unavailable they may often be obtained with sufficient accuracy by theoretical techniques (RUD G 66, BER H 69). Some rough experimental studies of the production of radionuclides in typical high-energy neutron spectra have been reported (STA G 67a,b), the general results being that

(a) ^{11}C was found to be the dominant short-lived radionuclide 1 to 5 hours after irradiation.

(b) The only long-lived γ emitter found with half-life greater than approximately 10 hours was ^{7}Be. The production cross section for ^{7}Be production

Table 7.X. Spallation products from ^{16}O.

Nuclide	Half-life
^{10}C	19 sec
^{14}O	71 sec
^{15}O	124 sec
^{13}N	10 min
^{11}C	20.5 min
^{7}Be	53 days
^{3}H	12.2 years

by 7-GeV proton spallation of ^{16}O was measured as 9.1±1.8 mb.

(c) An upper limit for the tritium production cross section from 7-GeV proton spallation of ^{16}O was determined as $\sigma(^{3}H) \leqslant 50$ mb--not significantly different from the more precise published values of 30 to 35 mb.

(d) The ratio of the saturated specific activities of tritium and ^{7}Be in samples of water irradiated under several different conditions varied between 1.3 and 5.8. Since the accuracy of these experiments was rather low (about a factor of 2), it was concluded that the production cross section for tritium production is approximately three times that for ^{7}Be under a variety of experimental conditions, and the data obtained are consistent with a ^{7}Be production cross section of approximately 10 mb.

Disposal of irradiated water to streams would generally be controlled bythe tritium content, since ^{7}Be is strongly absorbed on rock surfaces (STA G 70).

Careful studies of the radioactivity produced in water irradiated by high-energy electrons (WAR G 69) have identified ^{15}O, ^{11}C, and ^{7}Be as the most important radionuclides. ^{7}Be is readily absorbed in mixed-bed resins (BUS D 68).

POSSIBLE CONTAMINATION OF GROUND WATER BY ACCELERATORS

Particle accelerators are not often thought of as potential polluters of the environment. Indeed, by comparison with nuclear reactors, they are rather puny in their ability to produce radioactivity. Thus, for example, Thomas (THO R 70) has shown that the total inventory of tritium in the ground water in the earth shield of a 500-GeV proton accelerator is only about 50 curries at saturation. However, because it is necessary for economic reasons to bury such accelerators underground (NAL 68, ADA J 70), the surrounding earth is in fairly close proximity to the accelerator, and, if sub-

stantial particle fluxes are generated in the earth and ground water, it is possible that radioactivity may ultimately appear in local ground-water systems. Thus, although the total inventory of tritium in the ground water of the shield is only several tens of curies it is produced directly in the environment--a release comparable to or in excess of that reported for many power reactors (MAR J 70). Although the particle fluxes appearing in the earth may be quite small compared with those produced by nuclear reactors, they may nevertheless be sufficient to induce specific activities in excess of those recommended by the International Commission on Radiological Protection (ICRP 60) as fit for human ingestion. Thus, for example, a high energy flux only $\approx 10^5$ neutrons/cm^2 sec produces a maximum permissible concentration (MPC) of tritium by spallation in water.

The first reported study of possible contamination of ground water by accelerator-produced radionuclides is due to Nelson (NEL W 65) at the Stanford Linear Accelerator Center, who estimated the radioactivity induced in ground water close to beam dumps at the SLAC 20-GeV electron linear accelerator. The expectation that no significant water contamination would arise has been subsequently confirmed by environmental radioassays at SLAC (BUS D 71).

Indeed it is emphasized that to date no serious concentration of radionuclides in the ground water systems near existing accelerators has been reported. However, it is clear that the question of possible ground-water contamination by accelerators merits some study, since it could be an important factor in accelerator design or siting and, in any case, such preoperational studies are good health physics practice. Furthermore, in a climate of increasing public concern about water pollution it is valuable to have a closely documented study available for public information.

The design studies for the large strong-focusing accelerators now under construction at Batavia and CERN have included detailed consideration of this problem. Hoyer (HOY F 68) has reported measurable quantities ^{22}Na and ^{45}Ca in the drainage water of the CERN 25-GeV proton synchrotron. He finds fair agreement (within about a factor of 3) with his measurement and with concentrations calculated from the known flux distribution in the accelerator shield (GIL W 68). Stapleton and Thomas (STA G 70, STA G 71b) have reported studies of possible ground-water contamination around a 300-GeV accelerator situated on a chalk site. Fairman et al. FAI W 70, BOR T 70) have reported measurements of the nuclides produced in glacial till (the soil at the Batavia accelerator site) and their solubility in water. Gabriel et al. (GAB T 70a,b) have reported approximate calculations of the induced activity in soil surrounding high-energy accelerator target areas.

GENERAL FORMULATION OF THE PROBLEM

Assessment of potential contamination of drinking water supplies falls into three stages:

a. Consideration, from a knowledge of the chemical composition of rock and water impurities, of the radionuclides that could possible be produced.

b. Estimation of the yield of these radionuclides from the known production cross section, radioactive half-life, particle flux densities, and energy spectra.

c. Estimation of the final specific concentration of radionuclides in local water supplies, taking into account site hydrology, dilution, radioactive decay, and chemical sorption.

In general, when the specific activity of a radionuclide appearing in the ground-water system contiguous to a high-energy accelerator merits concern, estimates of the residence time in the activation zone, transport time into the public water supply, and time for mixing, dilution, and sorption in the aquifer will be needed.

Thus, if the total inventory of a particular nuclide at saturation in the activation zone is Q_0 curies, the quantity of activity reaching the public water supply, Q, can be written .

$$Q = \epsilon Q_0 (1-e^{-T/\tau})\, e^{-t/\tau}, \tag{14}$$

where τ is the mean life of the nuclide,

T is the residence time in the activation zone,

t is the time taken to reach the public water supply after leaving the activation zone,

and ϵ is the fraction of activity produced that flows freely in the ground water.

Dilution is difficult to estimate, but limits may be set by considering dilution resulting from pumping water from the general area. Thus the specific activity, S, of water reaching public water supplies may be written $S = DQ$, where D is a dilution factor discussed later.

The total specific activity reaching the public water supply in units of MPC is given by

$$S_{MPC} = D \sum_i \frac{\epsilon_i Q_i (1-e^{-T/\tau_i})\, e^{-t/\tau}}{M_i} \tag{15}$$

where M_i is the MPC of the ith nuclide.

The logical sequence of any pollution study is, then, an evaluation of the parameters of Eq. (15). It will be seen later that the chemical sorption parameter ϵ plays an extremely important role.

MAGNITUDE OF THE PROBLEM

Equation (15) permits a fairly crude assessment of the magnitude of the water pollution problem at an accelerator site.

The maximum rate of release of activity occurs at small residence times when

$$\left[S_{MPC}\right]_{max} = D \sum_i \frac{\epsilon_i Q_i e^{-t/\tau}}{M_i \tau_i} \qquad (16)$$

At an accelerator site where the water table is not disturbed by pumping of water the out flow of water would equal the inflow due to rainfall (corrected for evaporation tables), and the activity released can be considered to be associated with this outflow. As an example, the average rate of outflow of water from a site some 20 km^2 in area with net average inflow due to rainfall (corrected for evaporation and runoff) of 0.20 m/yr would be approximately 10^{10} cm^3/day.

Fairly elementary considerations lead one to conclude that the total radionuclide production of a 500-GeV accelerator losing some 10% of its beam intensity of 10^{13} protons/sec^{-1} (this would be considered an unusually high beam loss) would be about 500 curies in the earth shield. Because short-lived nuclides are of no concern, we might expect that some 10% of the total activity produced in the shield--≈ 50 curies--could in principle contribute to groundwater contamination.

Gabriel et al. (GAB T 70a,b) have estimated the mean life of a mixture of radionuclides produced in the earth shield of a high energy accelerator as ≈ 1 to 2 years. Thus, substituting the values

$$\sum Q_i = 50 \text{ Ci},$$

$$D = 10^{-10}/\text{ml},$$

$$\tau = 365 \text{ days},$$

and $M = 3 \times 10^{-6}$ μCi/ml for unidentified accelerator-produced radionuclides

into Eq. (16), we obtain

$$\left[S_{MPC}\right]_{max} \leqslant 5 \text{ MPC}. \qquad (17)$$

Although this simple argument does not eliminate the possibility of ground-water contamination, it does indicate that such an eventuality is unlikely. In general not all the long-lived radionuclides are released to the

ground water, and they are not produced at maximal quantities, moreover, the MPC's are larger than the restrictive value of 3×10^{-6} μCi/ml.

Table (7.XI) gives the quantity of some typical accelerator-produced radionuclides that would give a concentration of 1 MPC if released at maximum production rate into 10^{10} ml water per day.

Although the number of radionuclides produced in the earth and ground water in an accelerator shield is potentially very large, only a few can actually be produced in maximal quantities in ground-water systems.

Equation (15) shows that radionuclides of greatest concern

(a) are produced in large quantities, and (or)
(b) have a low MPC,
(c) pass efficiently into the ground-water system,
(d) do not decay significantly in being transported to a public water supply.

Nuclides with short half-lives will decay so rapidly as to be of no potential hazard by the time they reach a public water supply. Conversely, if the half-life is long the production rate will be too small and the nuclides will not appear in significant quantities. Knowledge of the hydrogeology of the accelerator site being studied will indicate the range of radioactive half-lives that are of interest. It is usually reasonable to study radionuclides with half-lives in the range 10 hours $< T <$ 100 years, but detailed investigation of site conditions will identify the appropriate range to be investigated. Those nuclides in this range of half-life that also satisfy conditions (a), (b), and (c) are fortunately few in number.

This topic is not of sufficient general interest to be dealt with in great detail here, and the interested reader is referred to literature for a complete discussion.

Figure 7.19 shows a model suggested to estimate the upper limit to the specific activity present in ground water at an accelerator site (THO R 70).

It is assumed that rainfall absorbed into the earth moves vertically downward past the accelerator to the water table. An estimate of the residence time of water flowing through regions of high flux density may be obtained from the size of the activation zone and the rate of inflow of water from rainfall. Estimates so obtained indicate water residence times of $\approx$ 2000 days, but hydrological studies at accelerator sites will be needed to establish reliable values.

After leaving the activation zone water will continue to move downward to the water table and then be transported horizontally beyong the accelerator site. Radioactive decay subsequent to production is an important mitigating factor only for shorter-lived nuclides. Thus, for example, in a journey of 7 days ^{7}Be will not have decayed appreciably. On the other hand, for short-lived nuclides--e.g., ^{11}C, ^{15}O, and ^{13}N--the decay factor is very large ($\approx 10^{15}$), making them of no account.

Table 7.XI. Quantity of typical accelerator-produced radionuclides, Q, that would result in a concentration of 1 MPC if released at maximum rates.

Nuclide	MPC M,(μCi/cm^3)	Mean life, τ (days)	Q (Ci)
^{32}P	2×10^{-5}	20.63	4.1
^{59}Fe	6×10^{-5}	65	39
^{7}Be	2×10^{-3}	77.04	1 540
^{46}Sc	4×10^{-5}	121	48
^{35}S	6×10^{-5}	126	76
^{45}Ca	9×10^{-6}	220	20
^{54}Mn	1×10^{-4}	410	410
^{22}Na	4×10^{-5}	1370	550
^{3}H	3×10^{-3}	6428	190000

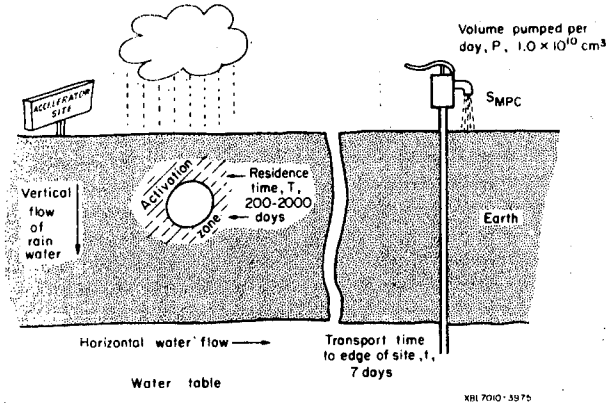

Fig. 7.19. Model illustrating mechanisms by which accelerator-produced radioactivity may appear in ground water.

On the assumption that the activity produced in the activation zone is released steadily during the residence time of water in the activation zone, the rate of release of activity at the perimeter of the accelerator site, R, is given by

$$R = \frac{\epsilon Q_0 (1-e^{-T/t}) e^{-t/\tau}}{T} \text{ Ci/day.} \qquad (18)$$

Thus if the quantity of water pumped from the site is P cm^3/day, the specific activity of water reaching the water supply (in MPC) is given by

$$S_{MPC} = \frac{10^6}{P} \sum_i \frac{\epsilon_i Q_i (1-e^{-T/\tau_i}) e^{-t/\tau_i}}{M_i T}, \qquad (19)$$

with Q_i in curies,

M_i in μCi/cm^3,

T, t, and τ_i in days,

and P in cm^3/day.

Figure 7.20 shows the concentration calculated as a function of residence time, on the assumption that all the activity produced in earth and water can be released directly to the ground water for nuclides produced in the shield of a 500-GeV accelerator losing 10^{12} protons/sec (THO R 70). A value of 10^{10} ml/day was used for the total volume of water abstracted from the accelerator site area, and a transport time in the water table of 7 days was assumed.

Inspection of Fig. 7.20 shows that the specific activity of the water never exceeds 0.03 MPC and decreases only very slowly with residence time up to $\approx$ 1000 days.

Chemical sorption prevents several of the nuclides from appearing in the ground water and considerably reduces the MPC actually observed.

Mawson (MAW C 69) has recently reviewed information on the movement of radioactive wastes buried in the ground. He says, "With few exceptions, adsorption and exchange processes occur between the radionuclides and constituents of the soil." He concludes his revies by saying, "The burial of radioactive waste is usually a very safe operation. If the site is selected with care any radionuclides that enter the soil will progress quite slowly down to the water table. Once in the ground water they will move faster, but still at a rate of one to several orders of magnitude less than the rate of movement of the gound water. These statements apply to most cations--many anions move at about the same speed as the gorund water."

^{7}Be is produced in a form very strongly absorbed onto surfaces in carrier-free solutions (MEL C 64). Similarly, studies by Blythe (BLY H nd) show that ^{32}P is fixed in chalk soils predominantly in the form of calcium

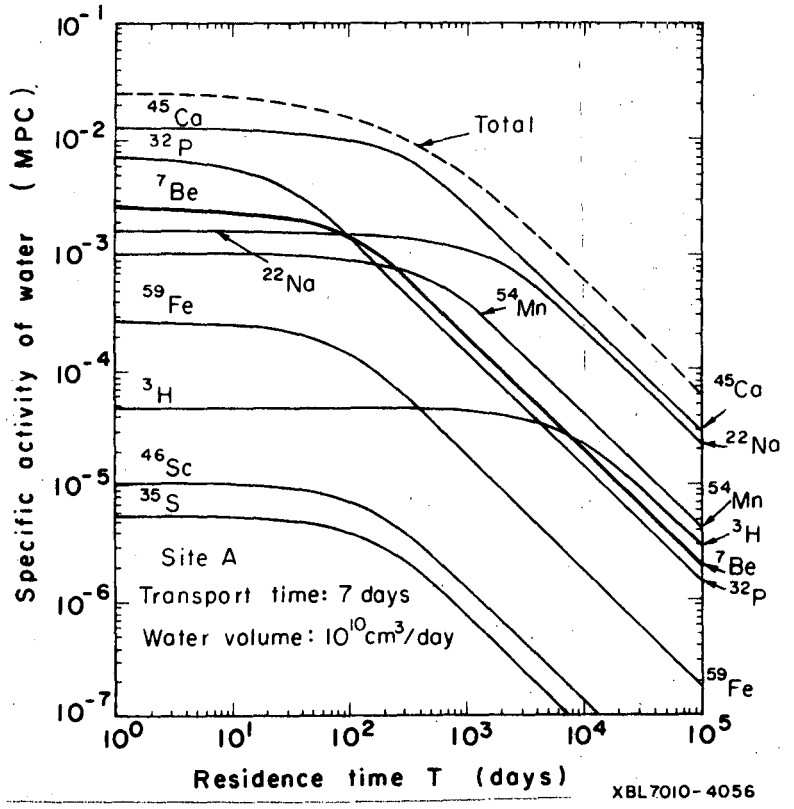

Fig. 7.20. Specific activity of ground water at accelerator site perimeter.

phosphate. Borak et al. (BOR T 70) report that, of the long-lived radionuclides produced in glacial till, only ^{3}H, ^{22}Na, ^{45}Ca, and ^{54}Mn were found in leach water; Thomas (THO R 71) has reported the solubility of gross γ activity produced in earth as $< 1\%$. Detailed sorption studies may be necessary for particular accelerator sites, but available information suggests many accelerator nuclides will be strongly retained. Tritium may pass freely into the ground water.

General consideration of the total quantity of radionuclides produced in the earth shield of high-energy high-intensity accelerators suggests no serious contamination problems in volumes of water comparable to rainfall on the site. More precise estimates indicate maximum specific activities in ground water of $\approx 3 \times 10^{-2}$ MPC if all long-lived nuclides are released. However, chemical sorption plays an extremely important role in limiting the release of radionuclides to the general environment, and if only tritium is mobile levels of $\approx 10^{-5}$ MPC are estimated.

REFERENCES

ADA J 70 J. B. Adams and E. J. N. Wilson, Design Studies for a Large Proton Synchrotron and Its Laboratory, CERN 70-6, Feb. 1970.

AND A 66 A. L. Anderson and C. T. Schmidt, ^{65}Zn Content in 90-Inch Cyclotron Workers at Livermore, Livermore Lawrence Radiation Laboratory Hazards Control Progress Report No. 25, April-August 1966, UCRL-50007 66-1.

ARM T 69a T. W. Armstrong and J. Barish, Calculation of the Residual Photon Dose Rate Induced in Iron by 200 MeV Proton, *In Proceedings of the Second International Conference on Accelerator Radiation Dosimetry and Experience, held at Stanford, Nov. 5-7, 1969.*

ARM T 69b R. W. Armstrong and J. Barish, Calculation of the Residual Photon Dose Rate Due to the Activation of Concrete by Neutrons from a 3-GeV Proton Beam in Iron, in *Proceedings of the Second International Conference on Accelerator Radiation Dosimetry and Experience, held at Stanford, Nov. 5-7, 1969.*

AWS M 65 M. Awschalom, F. L. Larsen, and R. E. Sass, The Radiation Measurements Group at the Princeton Pennsylvania 3-GeV Proton Synchrotron, *in Proceedings of the USAEC First Symposium on Accelerator Radiation Dosimetry and Experience, held at Brookhaven National Laboratory, Nov. 3-5, 1965,* p. 57.

AWS M 69 M. Awschalom, F. L. Larsen, and W. Schimmerling, Activation of Air Near a Target Bombarded by 3-GeV Protons, Princeton Report PPAD-661 E, May 1969 (unpublished).

BAA J 62 J. Baarli, Induced Radioactivity in the CERN Accelerators, *First International Conference on Shielding Around High Energy Accelerators, January 1962* (Presses Universitaires de France 108 Boulevard St. Germain, Paris), p. 123-128.

BAR M 69 M. Barbier, *Induced Radioactivity* (John Wiley and Sons, Inc. New York, 1969).

BAL J 64 J. B. Ball and C. B. Fulmer, Fortran Program for Estimating Residual Radiation Levels in Accelerators, Oak Ridge National Laboratory Report ORNL-3554, 1964.

BEL R 56 R. E. Bell and H. M. Skarsgard, Cross Sections of (p,xn) Reactions in the Isotopes of Lead and Bismuth, Can. J. Phys. *34,* 745 (1956).

BER H 69 H. Bertini, Calculations of Nuclear Reactions for Incident Nucleons and π Mesons in the Energy Range 30-2700 MeV, in *Proceedings of the Second International Conference on Accelerator Dosimetry and Experience, held at Stanford, California, November 5-7, 1969,* CONF-691101, p. 42.

BLY H nd H. J. Blythe, Some Field Trials on Ground Disposal by the Industrial Chemical Group, AERE GDE/P2, undated.

BNL 64 Brookhaven National Laboratory, A Proposal for Increasing the Intensity of the AGS at BNL, Brookhaven National Laboratory Internal Report BNL-7956, May 1964, p. 225.

BOO R 61 R. W. Boom, K. S. Toth, and A. Zucker, Residual Readiation of the LRL 184-Inch Cyclotron, Oak Ridge National Laboratory Report ORNL-3158, June 1961 (unpublished).

BOR T 70 T. B. Borak, M. Awschalom, W. D. Fairman, W. M. Hranka, and J. Sedlet, The Production in Soil and Transport by Water of Radionuclides Near a High-Energy Particle Accelerator (paper read at the Health Physics Society Annual Meeting, Chicago, Ill., June 1970), Abstract: Health Phys. *19*, 351 (1970).

BRU E 61 E. Gruninx, High-Energy Nuclear Reaction Cross Sections, Vol. 1, CERN Internal Report 61-1, 1061.

BRU E 62 E. Bruninx, High-Energy Nuclear Reaction Cross Sections, Vol. 2, CERN Internal Report 62-9, 1962.

BRU E 64 E. Bruninx, High-Energy Nuclear Reaction Cross Sections, Vol. 3, CERN Internal Report 64-17, 1964.

BUR A 69 E. A. Burrill, The Expanding Use of Particle Accelerators in Research, Medicine, and Industry, in *Proceedings of the Second Conference on Accelerator Radiation Dosimetry and Experience held at Stanford, November 5-7, 1969*, p. 1.

BUS D 68 D. D. Busick, ^{7}Be Buildup in a Large Water Beam Dump System at SLAC, Stanford Linac Accelerator Center Internal Report, SLAC-Pub-521, 1968.

BUS D 69 D. D. Busick and G. J. Warren, Operational Health Physics Associated With Induced Radioactivity at the Stanford Linear Accelerator Center, in *Proceedings of the Second International Conference on Accelerator Dosimetry and Experience, held at Stanford, California, November 5-7, 1969*, CONF-691101, p. 139.

BUS D 71 D. D. Busick, A Three-Year Summary of Environmental Radiation Measurement at SLAC, private communication, 1971.

CHA S 67 S. Charalambus and A. Rindi, Aerosol and Dust Radioactivity in the Halls of High Energy Accelerators, Nucl. Instr. Methods *56*, 125 (1967).

DES H 62 H. De Staebler, Average Radiation Levels Inside the Accelerator Housing When the Machine is Off, SLAC TN-6270, Oct. 1962.

DIS C 64 C. Distenfeld, in a Proposal for Increasing the Intensity of the AGS at the Brookhaven National Laboratory, Brookhaven National Laboratory Internal Report BNL-7956, May 1964.

FAI W 70 W. Fairman, W. Hranka, J. Sedlet, M. Awschalom, and T. B. Borak, The Extraction and Transport of Radionuclides Produced in Soil by High-Energy Hadrons, National Accelerator Laboratory Internal Report TM 247, June 24, 1970.

FLA C 65 C. R. Flateau, Proposed Remote Handling Method for a Modified AGS, Proceedings IEEE Trans. Nucl. Sci. *12*, 656 (1965).

FUL C 65 C. B. Fulmer, K. S. Toth, and M. Barbier, Residual Radiation Studies, IEEE Trans. Nucl. Sci. *12*, 673 (1965).

FUL C 64 C. B. Fulmer, K. S. Toth, and M. Barbier, Residual Radiation Studies for Meson Factories, Nucl. Instr. Methods *31*, 45 (1964).

GAB T 70a T. A. Gabriel, Calculation of Long-Lived Activity in the Soil Around High-Energy Accelerator Target Areas, Oak Ridge National Laboratory Report ORNL-TM-3033, 1970.

GAB T 70b T. A. Gabriel et al., Calculation of the Long-Lived Induced Activity in the Soil Around High-Energy Accelerator Target Areas. II, Oak Ridge National Laboratory Report ORNL-4599, 1970.

GEO A 65 A. C. George, A. J. Breslin, J. W. Hoskins, Jr., and R. M. Ryan, in *Proceedings of the First Symposium on Accelerator Radiation Dosimetry and Experience, Brookhaven National Laboratory*, CONF-65119, p. 513-555.

GIL W 64a W. S. Gilbert, Induced Activity and Radiation Damage, Lawrence Radiation Laboratory internal report UCID-10014, April 17, 1964.

GIL W 64b William S. Gilbert, Self-Shielding of γ's from Induced Activity in Accelerator Shielding Walls, Lawrence Radiation Laboratory internal report UCID-10013, July 15, 1964.

GIL W 64c W. S. Gilbert, Decay of Shut-Down Field in BNL AGS Tunnel, Lawrence Radiation Laboratory internal report UCID-10119, Aug. 11, 1964.

GIL W 64d W. S. Gilbert, Shutdown Radiation Fields in an AGS Tunnel Causes and Cures, Lawrence Radiation Laboratory internal report UCID-10137, Dec. 1964.

GIL W 65 W. S. Gilbert and R. H. Thomas, Problems of Induced Radioactivity Around the 200-BeV Alternating Gradient Synchrotron, in *Proceedings of the First International Particle Accelerator Conference. Washington, DC, March 10-12, 1965*, Proc. IEE Trans. Nucl. Sci. 12, 665 (1965).

GIL W 68 W. S. Gilbert et al., CERN-LRL-RHEL Shileding Experiment at CERN, Lawrence Radiation Laboratory Report UCRL-17941, Sept. 1968.

GIL W 69 W. S. Gilbert, K. Goebel, H. W. Patterson, and A. R. Smith, Concrete Activation Experiment at the Bevatron, Lawrence Radiation Laboratory Report UCRL-19368, December 1969 (unpublished).

GOR A 65 A. J. Gorka, Induced Radioactivity and Remote Handling Methods for Accelerators, Proceedings IEEE Trans. Nucl. Sci. NS-12, 656 (1965).

GRE K 66 K. Green (BNL) private communication to W. S. Gilbert, 1966.

HOY F 68 F. E. Hoyer, Induced Radioactivity in the Earth Shielding on Top of High-Energy Particle Accelerators, CERN 68-42, Dec. 1968.

HUN E 59 E. T. Hunter and J. M. Miller, Spallation of Bismuth by 380-MeV Protons, Phys. Rev. *115*, 1053-7 (1959).

ICRP 60 ICRP Publication 2, Report on Committee II on Permissible Dose for Internal Radiation, 1959 (Pergamon Press, Oxford, 1960).

KAS K 68 K. Kase, $(MPC)_a$ for ^{13}N, Health Phys. *15*, 283 (1968).

LRL 65 200 BeV Accelerator Design Study, Chapter 12—Radiation Problems, P XII-53, UCRL-16000, June 1965.

MAR J 70 J. E. Martin et al., Radioactivity from Fossil Fuel and Nuclear Power Plants, Proceedings of a Symposium on Environmental Aspects of Nuclear Power Stations, New York, August 1970, Paper SM-146/19.

MAW C 69 C. A. Mawson, Consequences of Radioactive Disposals Into the Ground, *Health Phys.* Vol. *2* Part I edited by A. M. F. Duhamel (Pergamon Press, Oxford, 1969.

MEL C 64 C. E. Mellish, J. A. Payne, and G. Worrall, The Adsorption and Sedimentation of Clean, Carrier-Free Yttrium Solutions, Radiochim. Acta *2*,204 (1964).

MID W 65 W. C. Middelkoop and B. de Raad, Induced ^{24}Na Activity in the Concrete of the CPS Tunnel, AR/Int. SG/65-13, June 11, 1965.

MIT 59 Massachusetts Institute of Technology, Annual Progress Report, May 1959.

MUR A 58 A. N. Murin, B. K. Preobrazhenskii, and N. E. Titov, Radiochemical Investigation of Spallation and Fission Reaction Products Resulting from the Bombardment of Bismuth by 660-MeV Protons, in *Soviet Research on the Lanthanide and Actinide Elements, 1949-1957. Part III. Nuclear Chemistry and Nuclear Properties* (Engl. Transl.) (Consultants Bureau Inc., New York, 1959).

NAC D 66 D. Nachtigall and S. Charalambus, Induced ^{24}Na Activity in the Concrete Shielding of High Energy Accelerators, CERN Report 66-28, Sept. 16, 1966.

NAL 68 National Accelerator Laboratory, Design Report, January 1968 (Revised July 1968), Batavia, Ill.

NBS 70 Radiological Safety in Design and Operation of Particle Accelerators, National Bureau of Standards Handbook 107, American National Standard N43.1-1969, June 1970.

NEL W 65 W. R. Nelson, Radioactive Ground Water Produced in the Vicinity of Beam Dumps, SLAC-TN 65-16, July 1965.

PAT H 58 H. W. Patterson and R. Wallace, A Method of Calibrating Slow Neutron Detectors, Lawrence Radiation Laboratory report UCRL-8359, July 1958.

PAT H 69 H. W. Patterson, A. D. Low-Beer, and T. W. Sargent, Whole-Body Counting and Bioassay Determination of Accelerator Workers, Health Phys. *17*, 621 (1965).

PER D 65 D. R. Perry and K. B. Shaw, Radiation Levels In and Around Nimrod, in *Proceedings of the First Symposium on Accelerator Radiation Dosimetry and Experience* held at Brookhaven National Laboratory, November 3-5, 1965, CONF-651109, p.20.

RIN A 64 A. Rindi, Le Danger Presenté par L'activation du Synchro-cyclotron de 600 MeV du CERN, Colloque International sur la Dosimetrie des Irradiations dues à des Sources Externes, Paris, November 1964 - Vol. II. (SCPRI, Le Vesinet, 1967) p. 153.

RIN A 67 A. Rindi and S. Charalambus, Airborne Radioactivity Produced at High Energy Accelerators, Nucl. Instr. Methods *47*, 227 (1967).

ROS B 58 B. Rose et al. Radioactivity of Synchrocyclotron Cooling Water, AERE Harwell Internal Report AERE NP/R 2768, 1958.

RUD G 66 G. Rudstam, Systematics of Spallation Yields, Z. Naturforschung *21a* 1027 (1966).

SAR T 62 T. W. Sargent, (Lawrence Radiation Laboratory), private communication, 1962, quoted in PAT H 69.

SHA K 67 K. B. Shaw and R. H. Thomas, Problems Associated with a High Energy Proton Beam, Health Phys. *13*, 1127 (1967).

STA G 67a G. B. Stapleton and R. H. Thomas, Radioassay of Irradiated Water Samples at Nimrood, Rutherford Laboratory internal report RP/PN/45, July 1967.

STA G 70 G. B. Stapleton and R. H. Thomas, Experimental Studies of the Sorption of ^{7}Be on Chalk, Rutherford Laboratory Memorandum RHEL/M/E/1, June 1970.

STA G 71 G. B. Stapleton and R. H. Thomas, The Production of ^{7}Be by 7-GeV Proton Interactions with Oxygen, Nucl. Phys. Vol. A 175, p. 124 (1971).

STA G 71 G. B. Stapleton and R. H. Thomas, Estimation of the Induced Radioactivity of the Ground Water System in the Neighbourhood of a Proposed 300-GeV High Energy Accelerator Situated on a Chalk Site, Rutherford Laboratory internal report R-216, 1971. (in press).

SUL A 65 A. H. Sullivan and T. R. Overton, Time Variation of the Dose Rate from Radioactivity Induced in High-Energy Particle Accelerators, Health Phys. *11*, 1101 (1965).

THO R 70 R. H. Thomas, Possible Contamination of Ground Water System by High Energy Proton Accelerators, in *Proceedings of the Symposium on Health Physics, Aspects of Nuclear Facility Siting, Idaho Falls, November 3-6, 1970.*

THO R 71 R. H. Thomas, Radioactivity in Earth Induced by High Energy Electrons, Nucl. Inst. Methods (in press).

TOT K 66 K. S. Toth, C. B. Fulmer, and M. Barbier, Estimates of Residual Radiation Levels Induced by High Energy Nucleons, Nucl. Instr. Methods *42*, 128 (1966).

VAN M 60 M. A. Van Dilla and M. J. Engelke, Zinc-65 in Cyclotron Workers. Science *131*, 830 (1960).

VIA H 69 H. Vialettes, Gas and Dust Activation in the Target Room of the Saclay Electron Linac, in *Proceedings of the Second International Conference on Accelerator Dosimetry and Experience, held at Stanford, California, November 5-7, 1969,* CONF-691101, p. 121.

VIN A 55 A. P. Vinogradov, I. P. Alimarin, V. I. Baranov, A. K. Lavrukhina, T. V. Baranova F. I. Pavlotskaya, A. A. Bragina, and Yu. V. Vaklovev, Radiochemical Study of the Fission Products of Be, Th, and U upon Bombardment with 480-MeV protons, Session of Acad. Sci. USSR on the Peaceful Uses of Atomic Energy, July 1-5, 1955 Moscow in, *Meetings of the Division of Chemical Sciences*, p. 97-119 (Moscow 1955).

WAR G 69 G. J. Warren, D. D. Busick, and R. C. McCall, Radioactivity Produced and Released from Water at High Energies, in *Proceedings of the Second International Symposium on Accelerator Dosimetry and Experience, held at Stanford, California, November 5-7, 1969,* p. 99.

WOL R 56 R. L. Wolfgang, E. W. Baker, A. A. Caretto, J. B. Cumming, G. Friedlander, and J. Hudis, Radiochemical Studies of the Interaction of Lead With Protons In the Energy Range

WOL R 56 R. L. Wolfgang, E. W. Baker, A. A. Caretto, J. B. Cumming, G. Friedlander, and J. Hudis, Radiochemical Studies of the Interaction of Lead With Protons In the Energy Range 0.6 to 3.0 BeV, Phys. Rev. *103*, 394 (1956).

WYC J 67 J. Wyckoff, Radioactivity Produced by a Linac, IEEE Trans. Nucl. Sci. *14*, 990 (1967).

CHAPTER 8

ADMINISTRATION OF AN ACCELERATOR HEALTH PHYSICS PROGRAM

TABLE OF CONTENTS

ADMINISTRATION OF AN ACCELERATOR HEALTH PHYSICS PROGRAM

Accelerator Health Physics is a subdivision of Health Physics, which is the profession devoted to the protection of man and his environment from unwarranted radiation exposure. Health Physics is multidisciplinary, and through this volume we have indicated the most important areas with which the Accelerator Health Physicist should be familiar in order to efficiently meet his responsibilities and to provide the services required of him. These responsibilities specifically include:

1. Familiarity with the immediate program of accelerator operation.
2. Periodic surveys of all radiation produced.
3. Studies of induced radioactivity.
4. Evaluation of shielding
5. Proper use, calibration, and interpretation of radiation monitors, including personnel monitors.
6. Radiation safety training.
7. Knowledge of rules and regulations regarding personnel exposure.
8. Public relations.

Knowledge of the characteristics of particle accelerators and their intended modes of operation will aid assessment of their radiation output (Chapter 3). Adequate shielding can be designed and constructed to maintain radiation levels below any desired limits (Chapter 6). Requirements for beam dosimetry and personal and area monitoring may then be determined (Chapters 2 and 5). The magnitude of the problem posed by induced radioactivity (if any) can be estimated from the data presented in Chapter 7.

RADIATION SAFETY PROGRAMS AT ACCELERATOR INSTALLATIONS

Great diversity exists in the organization and administration of radiation safety programs at different accelerator installations. Every program is unique and is shaped by the size of the supporting institution, the administrative structure of coexisting safety and medical services with which the radiation safety program must interrelate, the presence of individuals with particular qualifications and personal interests, and many other factors. Therefore, we do not attempt to give a prescription for organizing a radiation safety program except in general terms.

A basic requirement for any program is the preparation of a clear and concise safety manual. Guidance for preparing such a manual will be found in *Radiological Safety in the Design and Operation of Particle Accelerators* (NBS 70), and in *Particle Accelerator Safety Manual* (HEW 68). As a minimum the contents of an adequate safety manual should include:

1. Authorities and responsibilities of accelerator operator, management, and radiation safety personnel.
2. Standard operating procedures (monitoring, interlocks).
3. Emergency operating procedures.
4. Search and access regulation.
5. Radioactivity handling and waste disposal.
6. Descriptions of the accelerator, the facility, and any special problems.

The manual should be available and familiar to those involved and should be reviewed and updated periodically.

As we have already discussed, it is possible to set down only the general requirements for any accelerator radiation safety program. Specific details must depend upon the actual installation. It is instructive, however, to study programs that have proved effective at existing installations. Rich and Kase have described the excellent program designed for the nine accelerators of the Lawrence Livermore Laboratory (RIC B 69). We derive some details from their report for illustrative purposes.

THE LAWRENCE LIVERMORE LABORATORY ACCELERATOR SAFETY PROGRAM

INTRODUCTION

The Lawrence Livermore Laboratory (LLL) has as part of its research facilities nine major accelerators and three Van de Graaff accelerators in use or under construction. The newer accelerators include two 10-to 13-MeV electron linear accelerators (Linacs) used for radiography; one 4-MeV Linac used for thermonuclear research; one 40-MeV Linac used for both research and radiography; one 35-MeV Linac in use and one 100-MeV Linac under construction for physics research; one Insulating Core Transformer (ICT) neutron generator; one 90-inch cyclotron; and a combination 12-MeV tandem Van de Graaff accelerator-30-inch cyclotron under construction, also for physics research. This paper deals with (a) a brief description of the LLL accelerator facilities, (b) examples of procedural variance, and (c) description of a uniform LLL safety guide for all accelerator facilities.

ACCELERATOR FACILITIES DESCRIPTION

Of the nine accelerators in use or under construction at LLL, six are electron Linacs. As these Linacs are used for a variety of purposes, the facilities housing them vary.

Two Linace are in use for routine radiography. One of these is a portable unit operating at 13 MeV and generally housed in a remote facility shielded only by earth berms. The accelerator controls are housed in a trailer, and access to the Linac is controlled through a chain-link fence.

The other radiography Linac is a variable-energy unit ranging up to 15 MeV but normally operated at 10 MeV. It is housed in a concrete- and earth-shielded underground facility. The versatility of both these Linacs has made them valuable for health-physics-related radiation measurement and scattering studies in addition to the normal radiography work.

The 40-MeV Linac is installed at a firing bunker at the LLL High Explosive Test Site. It is used for radiography of explosive devices during detonation. It has also occasionally been used for research. The bremsstrahlung beam is directed onto an open firing table, and access is controlled through the firing bunker and a chain-link fence.

The remaining three Linacs are basically research machines. A 4-MeV 1000-A Linac is currently in use in the Controlled Thermonuclear Research program associated with the Astron machine. This accelerator is housed in a large concrete-shielded structure, but can be beamed into a large room with no roof shield.

The 35-MeV Linac used for physics research is currently being phased out of operation and will soon be replaced with a new 100-MeV Linac now

undergoing preliminary testing. Both accelerators are housed in concrete-shielded facilities. Further, the 100-MeV Linac facility is underground with about 11 feet of earth overburden.

The remaining accelerators are used for physics research and are housed in concrete- and wood-shielded facilities. An insulating core transformer is used to accelerate deuterons bombarding a tritium target to produce 14-MeV neutrons. A 90-inch cyclotron is used to accelerate protons, deuterons, and particles to variable energies ranging from 2.6 to 30 MeV. A new combination 12-MeV tandem Van de Graaff accelerator-30-inch cyclotron is currently under construction and will replace the 90-inch cyclotron when completed.

ACCELERATOR SAFETY PROGRAM INVESTIGATION

Approximately two years ago a fairly formal internal radiation safety review committee was established. Three supervisory Hazards Control personnel periodically (approximately once per year) visit each major facility at the Laboratory and evaluate the radiation safety program in that facility. The responsible health physicist is interviewed, along with other members of the safety team supporting his program (monitors and their supervisor) to determine the adequacy and consistency of the radiation safety program with "state of the art" standards in mind.

Although complete uniformity is not necessarily a desirable objective, the committee felt that certain minimum safety standards can and should be established and made applicable to all facilities.

Specific areas of concern to the committee are listed below.

1. Are interlock systems routinely checked?
2. Are warning signs standardized?
3. Are door interlocks to cells always present in pairs?
4. Is "sweeping" or clearing of the area prior to a run rigorously performed in all facilities?
5. Are audio alarms standardized?
6. Is wearing of personnel alarming dosimeters consistent and adequate?
7. Is area monitoring consistently and adequately accomplished in all areas?
8. Is the general education program for personnel concerning radiation hazards, alarm systems, and safety procedures, adequate?
9. Are effluent monitoring systems being reconsidered in facilities not presently equipped?
10. Are key permissive systems always used?
11. Are remote area monitoring systems (RAMS)consistently used in each facility?
12. Are portable survey instruments used at every facility before entry?
13. Are beam areas consistently controlled at all facilities?

Following the review and as a result of the findings, the committee drew up a uniform safety guide to be applied to all LLL accelerator facilities. The proposed guide was discussed with the operations personnel and experimenters at each accelerator, and a final form of the guide incorporating thier comments was drawn up.

UNIFORM ACCELERATOR SAFETY GUIDE

Basically, the guide is applied to all accelerators. The purpose of the guide is to assure that every conceivable problem has been carefully considered and adequately solved. If compliance with a certain portion of the guide involves undue operational inconvenience or undue expense, a variance can be permitted, provided appropriate substitute procedures or administrative controls are instituted to provide the intended protection.

The policy at LLL is to write building or facility operating procedures which, among other things, formally establish responsibilities, define potential hazards, and establish the safety program and procedures. These procedures are reviewed and updated at least once annually. The uniform accelerator safety guide is used in establishing the facility operating procedures as a guideline to be followed unless variances are established. The safety programs at the older facilities were reviewed "point by point" with the guide. Where variances were necessary, the necessity was documented with a description of circumstances requiring the variance and with the controls or safety program which provided the protection intended by the guide. New accelerators constructed since the guide was established comply with nearly every point and, as a consequence, are considered to have model protection programs. The guide will be useful in the establishment of new facilities as well as in the periodic safety review of existing facilities.

The guide is divided into five areas: interlocks, remote area monitors, portable survey instruments, personnel dosimetry, and administrative procedures; these are detailed below.

A. Interlocks

1. In general, a key permissive system should be used at all accelerators. This system would require that the master key to the accelerator control console be used for access to the cell gates and other hazardous areas. Removing the key deactivates the accelerator power source.

2. Interlocks on access gates into the accelerator areas or to beam areas where hazardous fields may exist should be installed in pairs to provide increased reliability. These gate interlocks should be designed to be "fail safe."

3. Where applicable, a sequential area-sweep permissive system is desirable. This would require the operator making the area sweep to actuate the system by pressing buttons or turning a key in all the hazardous areas in sequence to assure that a complete area sweep has been completed (or at least that an operator has been through all accessible areas prior to "beam on"). In any case, a permissive system requiring an area sweep should be installed.

4. Manual reset at both the accelerator console and interlock field location should be required before the accelerator can resume operation.

B. Remote Area Monitors

1. A RAM system should be installed and used with the primary goal to alert personnel to hazardous or increasing levels of radiation. Alarm set points should be established such that a significant increase in radiation level will sound a local alarm, alerting personnel to the change.

2. A reliable RAM system can be used effectively to determine, in advance, the conditions to be expected before a cell is entered and to provide a record of radiation conditions. These systems should not replace the use of portable survey meters during entry.

3. In certain areas, the RAM should be interlocked with the machine in such a manner that malfunctions whereby beams would penetrate occupied areas would result in immediate shutdown of the accelerator.

4. The RAM systems should be installed in accelerator cells in such a manner that the gate interlocks deactivate the alarm. If the gate is opened while the radiation level still exceeds the predetermined set point, the local alarm will sound, alerting personnel to hazardous levels.

5. The accelerator supervisor and the health physicist should establish criteria for an effective RAM system for each facility.

C. Portable survey instruments

1. As a general policy, portable survey instruments should be used on each initial reentry in a high radiation area following accelerator operation and at other times when the levels of radiation are not known.

2. A rigorous maintenance program should be established to maintain these instruments in excellent repair and calibration.

D. Personnel dosimetry

1. Personnel accident dosimeters (PAD) should be considered for use at accelerator installations to assist in preventing inadvertent exposures. These dosimeters come in three general types:

a. Dosimeters that sound an alarm at a preset accumulated dose.

b. Dosimeters that sound an audible "chirp" or "beep" at decreasing intervals as increased radiation fields are entered.

c. A nonaudible dosimeter from which the accumulated dose can be read directly. This type of detector requires the user to read the dosimeter periodically.

Care must be exercised to use the right type of detector in both the No. 1 and 2 detectors. GM-type detectors may be so dose-rate-dependent that their use may be a hazard. There are instruments using ionization chamber detectors which would be more reliable and less dose-rate-dependent.

2. Standard personnel dosimetry using at least a monthly badge exchange cycle should be provided for all persons working in the vicinity of an accelerator.

E. Administrative procedures

1. As a general policy, a voice announcement that the accelerator is about to be operated should be made prior to closing the cell, and again immediately before the accelerator is operated. If feasible, this announcement should be on an automatic tape recorder, which is programmed to play at a preset time and must play to complete the startup sequence. This would preclude inadvertent omission by the operator.

2. In addition to the voice announcement on #1 above, the lights in the accelerator and target areas should be dimmed prior to "beam on."

3. The alarm sounds should be made consistent at all accelerators, so that all Laboratory personnel can be oriented to their meaning. The following sounds should be used:

a. Radiation – "chimes"
b. Beam on elert – "ooga" or "dive"
c. Evacuation – steady klaxon

4. Radiation alarms (chimes) should be actuated whenever conditions are such (i.e., beam on) that hazardous radiation levels could exist. (There should also be an alarm to indicate a significant increase of radiation above "background.")

5. A rigorous area sweep should be performed prior to each startup. Note the recommendation on a sequential permissive sweep system in A. 3., above.

6. A routine and consistent education program should be developed, not only to educate personnel to the radiation safety procedures and requirements, but also to avoid the hazards of becoming too familiar with the operation.

7. Reentry delays to allow cathode cooling and (where applicable) ventilation of toxic products should be considered

8. Interlocks should be bypassed only upon specific written approval by the responsible person in charge. A system should be devised for assuring that these bypasses are temporary only. A log of bypasses should be maintained in a prominent location at each accelerator.

9. A written approved safety procedure should be observed at each accelerator.

10. All the interlocks and safety systems should be routinely checked according to a written procedure.

11. All warning signs and lights should be consistent in color, message, etc.

12. Emergency shutoff switches should be installed in convenient locations and personnel instructed in their use.

13. Hand-held survey instrument surveys should be made prior to initial cell entries following accelerator operation.

14. The health physicist for each accelerator should establish a formal training program for accelerator operators in radiation safety practices and use of survey instruments.

ACCELERATOR RADIATION SAFETY CHECK LIST

Following is a check list of a number of areas found to be important in many accelerator radiation-safety programs. The list, though not applicable to all accelerators, should prove useful in many circumstances. The reader may wish to add items or put greater emphasis on some, but probably nothing should be omitted.

I. Shielding

a. Design and Calculations. Are the calculations available on which shielding design is based? What is the source of the input data for the calculations?

b. Measurements. Have measurements been made to check the accuracy of the calculations and the efficacy of the shield?

II. Radiation Damage Estimates for Sensitive Components.

Are sensitive components of the radiation-monitoring system or the interlock system so located that their function cannot be impaired by exposure to very high radiation doses?

III. Accelerator Controls

a. Lockability. Can accelerator controls be locked to prevent unauthorized use?

b. Position. Are the position and location of accelerator controls convenient for the operators?

c. Identification. Is the function of each important accelerator control clearly identified?

IV. Interlocks

a. Manual reset. Can tripped interlocks be reset only manually at the location of the interlock, rather than remotely from the control console?

b. Run-safe switches. Are there switches in the radiation and high-radiation areas that make it impossible for the accelerator to operate or beam to be admitted to the area when the switch is in the "safe" position?

c. Regular tests. Is the function of the entire interlock system tested at regular intervals and are the results recorded?

d. Up-to-date circuit diagrams. Are up-to-date circuit diagrams maintained?

V. High Radiation Areas

a. Markings. Are all high-radiation areas properly marked and interlocked?

b. Magenta lights. Are magenta lights used to warn of the presence of radiation?

c. Audible warning. Is an audible warning given to alert personnel that the accelerator is about to be turned on or that beam is about to be admitted to a specific area?

d. Radiation monitors. Are suitable radiation monitors available to indicate the presence of radiation in high radiation areas?

1. Calibration. Are monitors calibrated at regular intervals?
2. Testing. Is the functioning of monitors tested regularly?
3. Readout. Is monitor readout conveniently available to the operators?
4. Records. Are suitable records maintained with respect to the above three items?
5. Portable instrument. Is a portable instrument used to monitor for unsuspected radiation upon entry to a shut-down accelerator or high radiation area?

VI. Procedures

a. Widespread understanding. Are procedures posted, read, and familiar to operators and support personnel and to visitors?

b. Validity. Are procedures reviewed and updated at suitable intervals?

c. Inclusiveness. Do Procedures include

1. A clear statement of responsibilities of management, accelerator operators, and radiation safety officers?
2. Standard operating procedures and procedures for emergency situations?
3. Access rules and regulations and search procedures to be used before turning on the accelerator?
4. Instructions for the proper handling of radioactivity and disposal of radioactive waste?
5. Descriptions of the facility and the accelerator giving enough information so that people unfamiliar with it can make some estimate of the relative hazard that prevails? Are any special problems described?

VII. Personnel Monitoring

a. Requirement. Is suitable personnel monitoring required?

b. Calibration. Is the calibration correct for the circumstances under which the monitors are used?

c. Interpretation. Is there adequate justification for the interpretation of results and assumptions made in deriving dose equivalent?

d. Records. Are adequate monitoring records maintained and are they available to the supervisor and employees?

VIII. Area Monitoring and Surveys

a. Instruments

1. Calibration. Is their calibration correct for the circumstances under which monitoring or survey instruments are used?
2. Interpretation. Is there adequate justification for the interpretation of results and assumptions made in deriving dose equivalent?

b. Repetition. Are area radiation surveys performed at regular intervals?

c. Records. Do the records of radiation surveys include

1. Date and time and person doing?
2. Particle, energy, and current?
3. Target?
4. Collimator and magnets?
5. Purpose and detector used?
6. Location?
7. Results and recommendations?

d. Induced Activity

1. Atmosphere. Have suitable measurements or estimates been made of radioactivity induced in air? If this is a problem, is ventilation adequate, and where does the exhausted air go?
2. Accelerator. Have suitable measurements been made of the radioactivity induced in the accelerator itself, in targets, and in shielding? Are suitable methods used to reduce personnel exposures from this source?
3. Workers. Are bioassay and whole-body counting procedures used occasionally to check for ingested or inhaled radioactivity?

IX. Education and Training of Operators, Support Personnel, and Others

Is there a regular program of educational training available? Does it include at least the following topics?

a. Radiation Safety

1. Interaction of radiation with matter
2. Units of dose and radioactivity
3. Biological hazards
4. Methods of control of exposure
5. Procedures

b. Radiation Detection

1. Use of instruments and personnel monitors
2. Survey and measurement techniques

c. Equipment

1. Accelerator
2. Remote handling devices
3. Interlocks

X. Relations Between Health Physics, Accelerator Operators, and Experimenters.

Are the technical and personal relations between Health Physics, accelerator operators, experimenters, and management good? Are there frequent interchanges of views and positions? Is there a radiation safety committee? If not, what takes its place?

PLANNING IN EMERGENCIES—RADIATION ACCIDENTS.

We have seen in Chapter 4, that it is unlikely that lethal *whole-body* radiation exposures will be delivered by particle accelerators. Severe partial-body exposures are much more probable, even though many might be avoided by elementary precautions--for example, by locating particle beams well above head height (see Chapter 4).

It is an unfortunate fact that in recent years almost half the serious radiation accidents reported by the USAEC have occurred at particle accelerator institutions.

We have prepared from various sources a summary of some sixteen accidents which occurred during the period 1944-1970 and involved particle accelerators not used for medical purposes. We quote them in full.

DETAILS OF SOME ACCELERATOR ACCIDENTS

Incident # 1

Equipment involved: 1200-kV electrostatic generator.

Date and location of incident: 1944, Massachusetts.

Exposure: Approximately 1000 to 2000 "tissue rem."

Injury: Severe radiodermatitis developed over much of the body areas of the exposed individuals.

Circumstances: The target of an electrostatic generator, used for medical purposes in a large hospital, was removed in order to determine the size and location of a focal spot using a piece of film. It was known that there was a definite danger in exposure to the direct beam, but it was thought that it would be safe to stand at a distance of several feet. Consequently, six staff members entered the room while the machine was in operation to observe the fluorescence due to the electron beam, thus resulting in their exposure.

Incident # 2

Equipment involved: Electron linear accelerator.

Date and place of incident: 1959, California.

Exposure: Seven individuals were exposed. It was determined that film badges had been exposed to 200-keV γ radiation. An exposure dose of 41 r was estimated for one physicist. This dose was received in a period of about 1 minute, which was the established time that the physicist worked alone in certain places in the cell. The next highest reading, 400 mr, was received by another physicist. All other individuals received less than 50 mr.

Injury: No clinical manifestation of radiation injury was reported.

Circumstances: A new electron linear accelerator was being operated to accumulate data to enable the engineering section to design a permanent piece of equipment for this machine. A number of remote operating circuits were not in operation. The barrier was temporarily replaced by a 4 X 4-ft piece of plywood and a warning sign. A series of adjustments was being made on beam-defining plates. Radiation surveys were made with negative results when personnel entered the cell after the first three adjustment runs. No survey was made after the fourth and fifth runs. A survey made after the sixth run showed an approximate radiation level of 1000 r per hour. During all entries to the cell, the key which was designed to lock all controls in the "off" position was removed from the control panel. Reliance was placed for safe operation on an incomplete safety interlock circuit.

Incident # 3

Equipment involved: Linear accelerator.

Date and place of incident: Date not specified, unknown University.

Exposure: Not stated.

Injury: No clinical manifestation of injury was found.

Circumstances: Two research assistants entered a target area of a linear accelerator without notifying the operator. They failed to remove an interlock key and ignored warning lights, signs, and the sound of accelerator klystron pulsers. One worker adjusted the target by hand and made a visual alignment. He realized that a blueish irridescence occurred in his eyeglasses and left the target area immediately.

Incident # 4

Equipment involved: Linear accelerator.

Date and place of incident: Date not specified, unknown university.

Exposure: Not stated.

Injury: No sign of biological damage was found.

Circumstances: A part-time worker, whose job it was to fill vacuum pump traps, ignored warning devices and signs, and climbed across the top of the accelerator shielding into an exposure area. He thus avoided the interlocked gates. The operator, assuming the worker was through with his work, proceeded to warm up the machine and operate it. The worker was not exposed to the primary beam, however.

Incident # 5

Equipment involved: Van de Graaff accelerator

Date and place of incident: 1960, New Mexico.

Exposure: By indirect measurements using film badges, a dose of approximately 760 rads to the face of one employee was estimated and approximately 53 rads total body dose to another employee was estimated.

Injury: The individual receiving the larger dose showed multiple radiation burns in the middle section of the face, abdomen, and both hands. No clinically manifested radiation injury was shown for the other individual.

Circumstances: While setting up an experiment in front of the beam tube, an employee was accidentally exposed to the electron beam emanating from the Van de Graaff accelerator. The machine operator put the machine on self charge, with the employee's consent and knowledge. The employee

entered the beam room. This was done to check the self-charge rate and limit of the machine. The beam current and belt charge were not turned on, these being the normal source of electrons. The employee proceeded to the end of the beam tube and began setting up his experiment. After approximately 2 minutes, he came out of the beam room, since his face felt warm. He then went to the washroom and washed his face. The employee asked the operator if there was any residual beam current. The operator stated that the beam current was not on but that he would check. The operator then entered the beam room with a low-range survey meter and made a measurement in front of the beam tube. The meter pegged at 20 mrem.

Incident # 6

Equipment involved: synchrotron

Date and Place of incident: 1963, Illinois.

Exposure: Two individuals received whole-body exposure of 3.8 and 2.8 rem respectively.

Injury: No injury specified.

Circumstances: Employees were exposed while making adjustments on a gradient synchrotron. Before the work of adjusting the synchrotron began, the beam stopper was inserted into the synchrotron to prevent exposure to the employees. However, the correct beam stopper was not inserted, and the employees carried on their assignment unaware of this

Incident # 7

Equipment involved: Cyclotron.

Date and place of incident: 1964, California.

Exposure: One individual received a whole-body dose of approximately 3.4 rem.

Injury: Not specified.

Circumstances: An employee was exposed to radiation while removing targets, which had been bombarded by the cyclotron. These targets were removed from a vacuum chamber in a high-level cave.

Incident # 8

Equipment involved: Cyclotron.

Date and place of incident: 1965, California.

Exposure: One individual was estimated to have received an external whole body radiation exposure of approximately 3-1/3 rem. This was concluded from a film badge reading.

Injury: No clinical manifestation of radiation injury was specified.

Circumstances: An employee was preparing for an experiment in a cave area. The radiation exposure was presumed to have occurred during a beam tuning period, while the employee was working in a cave adjacent to a cyclotron vault. The exposure was assumed to have occurred because of a narrow crack in the shielding wall between the cave and the vault. Although there was reasonable doubt that the film badge reading was sustained as a whole-body exposure, nevertheless, it was charged to the employee's record.

Incident # 9

Equipment involved: Van de Graaff accelerator.

Date and place of incident: 1965, Tennessee.

Exposure: One individual received an exposure of approximately 51 rem to the left forefinger.

Injury: Not specified.

Circumstances: An experiment was being conducted by a physicist involving the use of the Van de Graaff machine. While he was in the target room, the beam shutter failed, permitting the proton beam to impinge on a tritium gas target in the shielded target room. This resulted in a yield of about 6×10^9 neutrons per second. He worked in the vicinity of the neutron source for approximately 15 minutes and held his finger adjacent to the tritium target for approximately 10 seconds.

Incident # 10

Equipment involved: Ion linear accelerator.

Date and place of incident: 1965, California.

Exposure: One individual received approximate whole-body quarterly exposure of 3 rem.

Injury: No clinical manifestation of radiation injury was specified.

Circumstances: Modification of the water cooling system for the post-stripper tank, and adjustments of focusing magnets in an ion linear accelerator in preparation for startup, were being performed. The employee has been forewarned that his exposure was approaching the quarterly limit, but he continued to start up preparations although he knew that he might exceed the quarterly limit.

Incident # 11

Equipment involved: Linear accelerator.

Date and place of incident: 1965, Illinois.

Exposure: One individual received the following doses: to the interior of the body, 0.2 to 5 rads; to the right hand, 42000 to 240000 rads; to the right foot, 200 to 29000 rads.

Injury: Double amputation, right hand and right foot.

Circumstances: An industrial worker was accidentally exposed to an electron beam when he walked into a room to place an octagonal mold on a conveyor belt near the output port of an operational accelerator. The accelerator was mounted so that 10.8-MeV electrons were directed downward after emerging into the air from a vacuum chamber at a height of 75 cm from the floor. The electron beam spread rapidly in its downward course due to its intrinsic angular distribution coupled with multiple scattering in the window and air. At 46 cm above the floor, it struck a conveyor belt, whose function it was to carry industrial products to the beam. The conveyor system occupied part of the entryway to the accelerator room. In order to accommodate this conveyor system, the bottom of the door guarding the entryway had been sawed off. The worker gained entrance to the accelerator room through the resulting gap without tripping the electrical interlocks.

Incident # 12

Equipment involved: Linear accelerator.

Date and place of incident: 1966, California

Exposure: One individual was exposed to a dose of approximately 300 rem to one foot.

Injury: No evidence of erythrema.

Circumstances: While tuning an RF circulator, an employee received an estimated quarterly radiation exposure, to the left foot, of 300 rem of soft x-rays of less than 35 kV.

Incident # 13

Equipment involved: Proton synchrotron

Date and place of incident: 1966, California.

Exposure: Two individuals received respectively 4.6 and 3 rems.

Injury: None.

Circumstances: Two members of a bubble chamber crew received neutron exposures during normal operations. Their estimated external quarterly whole-body neutron exposures were 4.6 and 3 rem.

Incident # 14

Equipment involved: Proton synchrotron.

Date and place of incident: 1966, Illinois.

Exposure: One individual received 3.2 rem.

Injury: None.

Circumstances: While engaged in the removal, repair, maintenance, and installation of target manipulators, an employee received an estimated external whole-body cumulative radiation exposure of 3.2 rem.

Incident # 15

Equipment involved: 3-MeV van de Graaff accelerator.

Date and place of incident: 1967, Pennsylvania.

Exposure: Three individuals were involved in the exposure. Two men received approximately 500 to 600 rem whole-body dose. The third individual received approximately 100 to 200 rem whole-body dose. Exposure to the extremities may have been higher.

Injury: One technician had both hands amputated, and a spot of tissue deterioration recently appeared on the foot of this individual. Further information regarding injury to the technician and the two other research chemists has not been reported.

Circumstances: A Van de Graaff accelerator was being used for activation analysis. The exposure took place apparently because the accelerator did not shut off after the irradiation of a sample of oil. The three men entered the target room, removed the sample, and then attempted to locate the source of the trouble with the target cooling system. Possible reasons for the exposure appeared to be the failure of the safety interlock system to shut off the accelerator and the lack of, or failure to adhere to, proper operating and radiation safety procedures.

Incident # 16

Equipment involved: Linear accelerator.

Date and place of incident: 1967, California.

Exposure: Six graduate students at a university were exposed to x radiation, ranging from 920 to 2690 mrem, from a linear accelerator.

Injury: No clinically manifested radiation injury was reported

Circumstances: Six graduate students, who were involved in the initial tune-up of the linear accelerator, entered a high radiation area by overriding the interlocks on the doors that should have prevented access to this area. During the tune-up of the RF phase of the linac operation, the students were exposed to x radiation.

Incident # 17

Equipment involved: Linear accelerator.

Date and place of incident: 1967, California.

Exposure: Employee received an occupational exposure of 2100 mrem in the second month of a quarter and a subsequent exposure of 900 mrem in the final month of the quarter, thereby exceeding permissible quarterly exposures.

Injury: No injury was specified.

Circumstances: An investigation indicated that the over-exposure was received while tuning a klystron amplifier without adequately estimating and controlling anticipated exposures.

Incident # 18

Equipment involved: Linear accelerator.

Date and place of incident: 1967, Utah.

Exposure: One individual was exposed to approximately 1 rem.

Injury: Not specified.

Circumstances: A radiographic technician turned off a 24-MeV linear accelerator and proceeded through two interlocked doors to the accelerator room. He noted an unusual humming sound coming from the accelerator and upon returning to the control console noted the machine indicated x radiation without the "exposure on" button being pushed. Subsequent investigation revealed carbonized material had formed on a relay in the safety interlock system. An independently operated lead shutter in front of the x -ray port operated normally and saved the technician from a higher radiation exposure

EXPECTING THE UNEXPECTED

A well-thought-out safety system should eliminate the possibility of forseeable accidents but cannot avoid the unexpected. We know with Burns that "The best laid schemes o' mice and men gang aft a-gley."

As an example of how the unexpected can lead to radiation incidents, Karzmark (KAR C 67) has described the effect of radiation damage to the

insulation of ionization chambers and the hardening of grease in high-radiation environments, leading to interlock problems. It is imperative that the accelerator health physicist keep himself well informed on the results of the investigations that follow all radiation accidents or "incidents," constantly applying what he learns to his own safety procedures.

It also is essential to anticipate the possibility of an overexposure and develop a clear procedure to be followed should any overexposure be suspected. In most cases the possibility of overexposure will be surmised by the victim, his colleagues, or the accelerator operator within a short time of the "suspected overexposure." The accelerator operator should contact the responsible health physicist, who should initiate the sequence of events given in the following check list.

OUTLINE TO FOLLOW IN POSSIBLE ACCIDENTAL ACCELERATOR OVEREXPOSURE

1. Check for induced activity in and on individual

2. Get additional information

When did the incident occur? What was its duration? Where did it occur? Did equipment fail? Were procedures overlooked? Who was involved? What was the sequence of events both before and after the incident?

3. Notify others

   Operations:

   So that they can verify any equipment failure and the occurrence of the incident, and prevent other accidents.

   So that they can establish and verify the record of machine operation.

   Medical: For physical and medical examinations and treatment.

   Health Physics: For technical support.

   Management: For information, and for handling public relations if required.

4. Collect and process personnel dosimeters. Check previous exposure records.

5. Initiate confirmatory dosimetry, if required.

These activities should be initiated promptly, but there is no merit in undue hurry. Several hours must elapse before the manifestation of any clinical symptoms of overexposure.

INTERNATIONAL ORGANIZATIONS ASSOCIATED WITH RADIATION PROTECTION

International Congress of Radiology (ICR)

The concern expressed by these various national organizations was taken up by the International Congress of Radiology. At its first meeting, held at London in 1925, the congress created the International Commission on Radiological Units (name later changed to International Commission on Radiation Units and Measurements-ICRU).

International Commission on Radiation Units and Measurements (ICRU)

This organization was charged with the task of dealing with the technical aspects and standardization of radiation measurements in radiology. Since its inception the ICRU has had as its principal objective the development of internationally acceptable recommendations regarding

(a) quantities and units of radiation and radioactivity,
(b) procedures suitable for the measurement and application of these quantities in clinical radiology and radiobiology,
(c) physical data needed in the application of these procedures, the use of which tends to assure uniformity in reporting.

The Commission also considers and makes recommendations in this field of radiation protection. In this connection, its work is carried out in close cooperation with the International Commission on Radiological Protection (ICRP).

International Commission on Radiological Protection (ICRP)

The ICRP was the creation of the Second International Congress on Radiology, held at Stockholm in 1928. Since then the Commission has had a close relationship with succeeding Congresses, and it has also been looked to as the appropriate body to give general guidance on the more widespread use of radiation sources caused by the rapid developments in the field of nuclear energy. The Commission wishes to maintain fully its traditional contact with medical radiology, and to fulfill its responsibilities to the medical profession. In addition, the Commission recognizes its responsibility to other professional groups and its obligation to provide guidance within the field of radiation protection as a whole.

The policy adopted by the Commission in preparing its recommendations is to deal with the basic principles of radiation protection, and to leave to the various national protection committees the responsibility of introducing the detailed technical regulations, recommendations, or codes of practice best suited to the needs of their individual countries.

The Commission has kept its recommendations continually under review in order to cover the increasing number and scope of potential radiation hazards, and to amend safety factors in the light of new knowledge on the effects of ionizing radiations.

These two international bodies, the ICRU and the ICRP, are generally regarded as authoritative in their respective fields of competence and maintain close contact with both each other and with those other international organizations having an interest in radiation protection. Thus since 1955, the ICRU has had an official relationship with the World Health Organization (WHO) whereby the ICRU is looked to for primary guidance in matters of radiation units and measurements, and in turn, WHO assists in the worldwide dissemination of the Commission's recommendations. In 1960 the ICRU entered into consultative status with the International Atomic Energy Agency. The Commission has a formal relationship with the United Nations Scientific Committee on the Effects of Atomic Radiation (UNSCEAR), whereby ICRU observers are invited to attend UNSCEAR meetings. The Commission and the International Organization for Standardization (ISO) informally exchange notifications of meetings and the ICRU is formally designated for liaison with two of the ISO Technical Committees. The ICRU also corresponds and exchanges final reports with the following organizations:

Bureau International des Poids et Mésures

Council for International Organizations of Medical Sciences

Food and Agriculture Organization

International Council of Scientific Unions

International Electrotechnical Commission

International Labor Organization

International Union of Pure and Applied Physics

United Nations Educational, Scientific, and Cultural Organization

The ICRP has maintained close contact with the World Health Organization (WHO) and with the International Atomic Energy Agency (IAEA), with both of which the Commission has an official relationship. The Commission has been represented by observers at a number of meetings organized by WHO and IAEA. Cooperation has also been maintained with the International Labor Office (ILO), the Food and Agriculture Organization, and UNSCEAR, all of which have been invited to send observers to technical meetings of the Commission and its committees.

The International Atomic Energy Agency

The International Atomic Energy Agency (IAEA) is an autonomous intergovernmental organization with headquarters in Vienna, Austria; it is related to the United Nations by the terms of an Agreement which recognizes it as "the agency under the aegis of the United Nations responsible for international activities concerned with the peaceful uses of atomic energy."

The IAEA fosters and encourages the beneficial use of nuclear energy in science and industry throughout the world. It also functions as a guide and adviser, as far as it is able, to prevent harmful consequences resulting from the use of nuclear energy.

In accomplishing these objectives, the activities of the IAEA encompass many fields, extend to many countries, and employ many techniques. It operates three laboratories, publishes books, organizes international meetings, and establishes safety standards for all types of nuclear operations. It sends more than 150 experts to developing countries annually. It advises governments on nuclear energy programs, awards fellowships, arranges the loan of equipment, finances research, and acts as an intermediary in supplying nuclear materials. This work is done in cooperation with dozens of other organizations, both national and international

In the area of health and safety and in cooperation with other international organizations, the Agency has established basic standards and recommendations relating to all aspects of radiation safety under both normal and emergency conditions. Thirty publications concerning these standards and recommendations have been issued.

The agency has also convened many Symposia. Of particular interest to accelerator health physicists were those on Neutron Dosimetry at Harwell, England, in 1962; on Biological Effects of Neutron and Proton Irradiation at Brookhaven National Laboratory, USA, in 1963; and on Neutron Monitoring at Vienna, Austria, in 1966.

International Radiation Protection Association (IRPA)

IRPA was organized in 1966 with the ultimate goal of bringing together in one world-wide organization all persons professionally engaged or actively interested in the problems of radiation protection. Following the favorable response by several national and regional professional organizations to initiatives by the Health Physics Society the first IRPA Congress was held in Rome in 1966. At that meeting 15 professional organizations representing 5000 members affiliated to form IRPA.

A second congress was held at Brighton, England, in 1970, by which time 21 organizations, representing more than 6000 persons, were affiliated.

At present the efforts of IRPA are largely directed towards the organization of congresses, at intervals of 4 years, at which truly international exchanges

of scientific information are possible. As the strength of IRPA grows, however, it seems likely that it will extend its activities. It has been suggested, for example, that IRPA might join with the International Congress of Radiology in supporting the ICRP. Already some small financial assistance has been possible.

HISTORY OF RADIATION PROTECTION STANDARDS

One of the most important functions of these international organizations has been to draw together the collective wisdom of many nations and offer advice on the control of man's exposure to radiation.

Excellent summaries of the history of radiation protection standards have been given by Taylor and Harris (TAY L 59), Browing (BRO E 59), and Morgan (MOR K 67a).

Soon after the discovery of ionizing radiations it was recognized that they presented a hazard to man. Indeed, in the same year as Roentgen announced the discovery of x rays, the first reports of radiation damage to human beings also appeared. Morgan (MOR K 67b) has summarized man's early experience of the harmful effects of ionizing radiations. Although no accurate estimates are possible of the total number of persons seriously harmed by the uncontrolled use of x rays and radium, it was sufficiently large to cause serious concern among members of the medical profession. As an example, Ledoux-Lebard (MOR K 67b) suggested that by 1922 more than 100 radiologists had died of occupationally induced cancer.

Since the early 1920's, therefore, there has been a serious effort to study and control the harmful effects due to ionizing radiations. Early work was naturally concerned with the problems posed by the use of x rays and radium by the medical profession.

The first standards were expressed in terms of dose rate; for example, in 1925 Mutscheller (MUT A 25) suggested a protection standard of 1/100 of skin erythema dose in 30 days; this was slightly modified the same year in a joint suggestion by Mutscheller and Deivert (STO R 52) to 1/10 an erythema dose per year (roughly corresponding to 25 R per year for 100-KV x rays or 50 R per year for 200-kV x rays.)

In the period prior to 1930 very different standards prevailed in different countries. In France a suggested limit could have resulted in exposures as high as 4000 R/yr (SOL I 24), whereas in Britain 0.7 R per day was recommended.

The establishment of the ICRP in 1928 led the way to international uniformity in protection standards, and in 1934 a limit of 0.2 R/day was chosen (TAY L 59), a value similar to that then used in Great Britain of 1 R per week (RAD 34). The ICRP limit remained in worldwide use until 1950.

Protection standards in the United States were based upon the reccommendations of the NCRP, founded in 1929. In 1963 a value of 0.1 R per day was suggested, providing an additional safety factor over the ICRP

recommendation, and this was the basic standard for radiation protection during the Manhatten Project (NBS 34). Recommendations in the United States and the United Kingdom were brought into line in 1947, after the Medical Research Council (United Kingdom) recommended a reduction of the acceptable level to 0.5 R per week on the basis of studies of blood disease, development of cancer, and genetic effects induced by radiation (BRO E 59). Two years later, however, the NCRP advised a reduction to 0.3 rem/week (NBS 49), and this value was adopted internationally in 1950 (NBS 51).

The last substantial change in radiation standards occurred in 1956, when maximum permissible doses were reduced by a factor of 3, primarily based on based on consideration of possible genetic effects (ICRP 59). See Table 8.I, Fig. 8.1.

Table 8.I. Recommended permissible radiation levels for radiation workers

Year	Country	Recommendation	Approximate integral dose/year (rem) possible under recommendation
1924	France	---	4,000
	U.K.	0.7 R per day	326
1925	USA, Sweden	1/10 erythema dose/year	50
1934	ICRP	0.2 R per day	73
	U.K.	1 R per week	52
1936	USA (NCRP)	0.1 R per day	36
1947	U.K.	0.5 R per week	26
1949	USA (NCRP)	0.3 R per week	15
1950	ICRP	0.3 R per week	15
1956	ICRP	5 rem per year	5

One cannot avoid inquiring why the evident reductions in radiation standards have occurred.

Perhaps the first thought that might be considered—that of evidence of harmful effects at the suggested permissible levels—can be summarily dismissed. Since 1925, when the MPD suggested by Mutscheller and Sievert amounted to approximately 25-50 rem per year, no MPD has been changed because of positive evidence of radiation damage, or harmful effects under their regime. The NCRP (NBS 58) has suggested how the changes came about:

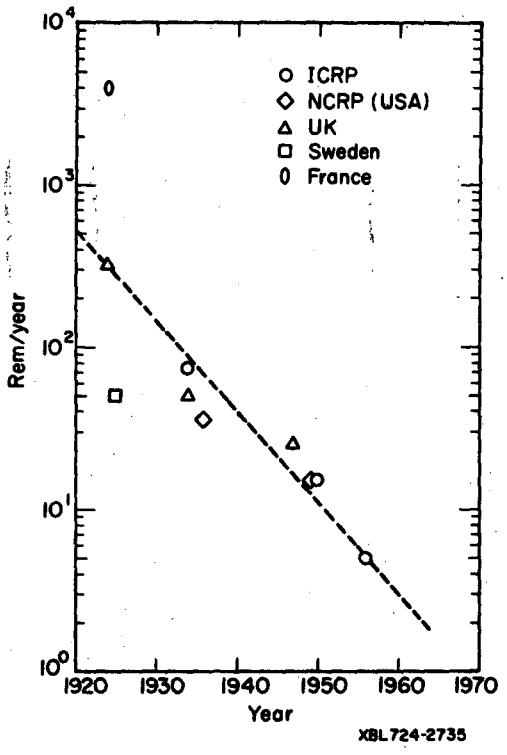

Fig. 8.1. Reduction with time of whole body radiation limits for radiation workers.

"The changes in the accumulated MPD (Maximum Permissible Dose) are not the result of positive evidence of damage due to use of the earlier permissible dose levels, but rather are based on the desire to bring the MPD into accord with the trends of scientific opinion; it is recognized that there are still many uncertainties in the available data and information. Consideration has been given also to the probability of a large future increase in radiation uses."

Taylor (TAY L 65) has suggested that the changes in radiation safety standards were primarily brought about by changes in philosophy and approach to radiation safety with the recognition of problems and development of new knowledge.

Until the mid-30's ionizing radiations was used primarily by the medical profession, and radiation standards were designed to protect the physician, his

staff, and patients. As the voltage of available x-ray tubes increased, industrial radiography became possible in the late 30's, and the widespread use of this technique in industry by relatively unskilled workers became an important consideration.

Until the mid-40's the driving purpose of radiation protection recommendations was to prevent acute radiation effects, and in this they were demonstrably successful. One example of this success has been given in the several studies of longevity and the incidence of cancer in radiologists compared with other members of the medical profession. The early radiologists died earlier than their colleagues and were subject to a higher risk of cancer. Subsequent studies have given good support to the thesis that as protection standards improved so did the general well-being of U.S. radiologists.

It is of interest to note that in the attempts to eliminate the accute effects of radiation (skin erythema, epilation, all phases of the acute radiation syndrome, etc.) the early concept of a threshold—that dose below which a biological response to a radiation insult does not appear—was shown to have scientific validity. In addition to more direct evidence, the fact that no patient has ever developed erythema or displayed any manifestation of the acute radiation syndrome as the result of *diagnostic* radiology lends support to the view that acute radiation effects do not appear, even statistically, below a given threshold.

Taylor points out that the guidelines established in 1936—designed, as they were, primarily for medical use and secondarily for industrial guidance—were applied throughout the extensive operations of the Manhattan District and "resulted in an almost unbelievable absence of radiation injury." In retrospect, considering the state of knowledge in the mid-30's, Taylor considers it "as almost fortuitous that the permissible levels then established would apply so well to the rigorous requirements of the Atomic Energy Project."

Genetic considerations became of increasing relevance as the results of exposure of large populations to small doses of radiation were studied. Taylor (TAY L 65) reports how, as early as 1933, Failla foresaw the importance of the work of Mueller in this general area. By the late 40's several geneticists were working with the NCRP, and Charles, Mueller, and Stern played an important role in the formulation of NCRP policy. An important realization was that for *genetic effects* "there might be an element of risk in the use of radiation and that, however small, the element of risk could never completely disappear."

The year 1949 is important in another sense in that, as Taylor points out, the NCRP regulations published then contain certain changes in radiation standards made "in spite of absence of a demonstrated need" but rather because "we had developed the first recognized and conscious use of judgment in addition to purely technical considerations in the setting of standards." Thus the 1949 NCRP report defined many of the areas of interest in radiation

control that are live topics today. The items discussed include risk philosophy, genetic effects, short- and long-range somatic effects, high-dose versus low-dose effects, recovery and repair, life-span shortening, and population exposure.

The current ICRP and NCRP recommendations are based primarily on genetic considerations.

UNITED STATES ORGANIZATIONS ASSOCIATED WITH RADIATION PROTECTION

Both the ICRU and the ICRP believe it to be their role to lay down the basic principles of radiation measurement and radiation protection respectively, leaving the responsibility of providing detailed technical procedures to national organizations. In this way each nation may decide upon the particular applications of ionizing radiations pertinent to its own particular problems, but within limits of safety that are internationally acceptable.

In consequence all industrial nations have developed their own national organizations to deal with radiation protection and its associated problems. As might be expected the structure and interrelationships between these national organizations varies widely from country to country depending upon, among other things, the state of industrial development of, the governmental and legal systems, and the availability of trained specialists in radiation protection in the country concerned.

National Council on Radiation Protection and Measurements (NCRP)

In the United States of America the national system is complex. The authoritative advisory national body on radiation protection matters is the National Council on Radiation Protection and Measurements (NCRP), a non-profit corporation chartered by Congress in 1964 to

"1. Collect, analyze, develop, and disseminate in the public interest information and recommendations about (a) protection against radiation and (b) radiation measurements, quantities, and units, particularly those concerned with radiation protection;

"2. Provide a means by which organizations concerned with the scientific and related aspects of radiation protection and of radiation quantities, units, and measurements may cooperate for effective utilization of their combined resources, and to stimulate the work of such organizations;

"3. Develop basic concepts about radiation quantities, units, and measurements, about the application of these concepts, and about radiation protection;

"4. Cooperate with the International Commission on Radiological Protection, the International Commission on Radiation Units and Measurements, and other national and international organizations, governmental and private, concerned with radiation quantities, units, and measurements and with radiation protection.

"The Council is the successor to the unincorporated association of scientists known as the National Committee on Radiation Protection and Measurements and was formed to carry on the work begun by the Committee.

"The Council is made up of the members and the participants who serve on the thirty-four Scientific Committees of the Council. The Scientific Committees, composed of experts having detailed knowledge and competence in the particular area of the Committee's interest, draft proposed recommendations. These are then submitted to the full membership of the Council for careful review and approval before being published."

The NCRP seeks to promulgate information and recommendations based on leading scientific judgment on matters of radiation, protection, and measurement, and to foster cooperation among organizations concerned with these matters. These efforts are intended to serve the public interest, and the Council welcomes comments and suggestions on its reports or activities from those interested in its work.

An extremely important function of the NCRP has been to "facilitate and stimulate cooperation among organizations concerned with the scientific and related aspects of radiation protection and measurement... At present 28 collaborating organizations maintain liaison with the NCRP."

Other National (U.S.) Regulatory Organizations

Other organizations in the United States that have stubstantial interests in radiation protection are the Atomic Energy Commission, the Public Health Service, the Environmental Protection Agency, the Department of Labor, and the Public Health Departments of the various states. One or more of these may be concerned with the radiation safety aspects of a particular accelerator or facility. However, the division of responsibility between them is complicated and subject to change, and it is not possible to give a detailed description of it. It is perhaps sufficient to understand that the radiation-protection standards that each uses is derived from the standards suggested by NCRP. For a full discussion of these standards the reader is referred to NCRP Report No. 39, Basic Radiation Protection Criteria, National Council on Radiation Protection and Measurements.

To simplify the use of the recommendations given in the full report the NCRP has summarized them in a table which is given below in a slightly modified form.

Table 1. NCRP recommendations.

Maximum Permissible Dose Equivalent for Occupational Exposure	
Combined whole-body occupational exposure	
Prospective annual limit	5 rem in any one year
Retrospective annual limit	10 to 15 rem in any one year
Long-term accumulation to age *N* years	(N – 18) X 5 rem
Skin	15 rem in any one year
Hands	75 rem in any one year (25/qtr)
Forearms	30 rem in any one year (10/qtr)
Other organs, tissues and organ systems	15 rem in any one year (5/qtr)
Fertile women (with respect to fetus)	0.5 rem in gestation period
Dose Limits for the Public, or Occasionally Exposed Individuals	
Individual or occasional	0.5 rem in any one year
Students	0.1 rem in any one year
Population Dose Limits	
Genetic	0.17 rem average per year
Somatic	0.17 rem average per year
Emergency Dose Limits—Life Saving	
Individual (older than 45 years if possible)	100 rem
Hands and forearms	200 rem, additional (300 rem total)
Emergency Dose Limits—Less Urgent	
Individual	25 rem
Hands and forearms	100 rem, total

Professional Organizations

In common with the other learned professions, Health Physicists have developed their own professional organizations des gned to provide opportunities for the interchange of information, mutual education of their members, and elevation of professional goals and standards of Health Physicists.

HEALTH PHYSICS SOCIETY

Within the United States the principal professional organization is the Health Physics Society, whose objective is stated to be "...the development of scientific knowledge and practical means for the protection of man and his environment from the harmful effects of radiation, while encouraging its optimum utilization for the benefit of mankind."

The activities of the Health Physics Society are those appropriate to the accomplishment of the primary objective, and its purpose will be to (1) encourage the establishment of local chapters as a means of achieving cooperation among persons engaged in radiation protection activities within particular geographical areas, (2) provide for and give support to meetings at which the members may discuss their scientific endeavors, (3) encourage scientific publications dedicated to the science of radiation protection, (4) encourage scientific research and educational opportunities among those scientific disciplines which support the science of radiation protection, (5) encourage the establishment of universally acceptable radiation protection standards or recommendations through domestic and international bodies concerned with continuous review of these matters, and (6) undertake any other appropriate matters essential to the accomplishment of the primary objective. Organized in 1955, the Society was incorporated in 1961.

As of June 1, 1971, the Health Physics Society has more than 3100 paid-up members in 40 countries, with 30 local chapters.

The Society edits the journal HEALTH PHYSICS, the official publication of the Society and the only journal devoted exclusively to the field of health physics.

Annual meetings are organized at which papers are presented covering the entire multidisciplinary field of radiation protection. In addition topical symposia are organized each year (normally during the winter months) which deal with specialized topics in some depth.

OTHER AMERICAN PROFESSIONAL SOCIETIES

Other professional organizations in the United States with an interest in Health Physics include the American Association of Physicists in Medicine (AAPM), the American Board of Radiology, and the American Public Health Association. The AAPM, in collaboration with Hospital Physicists' Association of the United Kingdom, publishes the journal "Physics in Medicine and Biology," which contains many scientific papers of interest to Health Physicists.

AMERICAN BOARD OF HEALTH PHYSICS (ABHP)

Shortly after its organization, the Health Physics Society established a Committee to study the need for certification of health physicists and to develop plans for certification if this appeared to be desirable. After an intensive study, the Committee recommended that an American Board of Health Physics be established to develop standards and procedures, to examine candidates, and to issue written proof of certification to individuals who have satisfied the requirements established by the Board.

The ABHP was incorporated in the State of New York on December 1, 1960. Provision was made for organizations other than the Health Physics Society to be represented on the Board.

The Board has seven members. Five are sponsored by the Health Physics Society, one by the American Association of Physicists in Medicine, and one by the American Public Health Association. Each member serves a 5-year term.

An Examination Panel consisting of 16 Certified Health Physicists appointed by the Board prepares, administers, and grades the written certification examination under the guidance and approval of the Board.

The certificate indicates that its holder has completed certain requirements of study and professional experience, which the Board considers to constitute an adequate foundation in health physics, and has passed an examination designed to test his competence in this field.

Requirements for Candidates for certification are as follows:

1. ACADEMIC: The applicant must have a Bachelor's Degree in a physicsl science, or in a biological science with a minor in a physical science

2. AGE: An applicant must have passed his twenty eighth birthday before the date of the examination.

3. EXPERIENCE: An applicant must have at least 6 years of responsible professional experience in health physics. At least 3 years of the experience must have been in applied radiation-protection work. Additional education may be substituted for up to a maximum of 2.5 years of experience.

4. PROFESSIONAL: Each applicant must be engaged in the professional practice of health physics a substantial portion of his time. Reference statements are required from the applicant's supervisor (if appropriate) and from at least two other individuals who are professionally qualified to evaluate the applicant's ability in health physics. It is recommended (but not required) that at least one reference by from a health physicist already certified by the ABHP.

5. WRITTEN REPORT: The Board, after examination of the application for certification, may request reports on radiation-protection evaluations made personally by or under the supervision of the applicant.

6. EXAMINATION: Written examinations will be mandatory; additional oral examinations will be at the discretion of the Board. The written examination has two parts. Part I determines competence of the applicant in fundamental aspects of health physics, and Part II determines his competence in practical health physics topics.

Examinations are usually given once a year—at the time of the Annual Meeting of the Health Physics Society. They are held at the location of the Society's meeting and at other selected locations where the demand warrants.

Applicants are not permitted to take Part I of the written examination until they have fulfilled the academic requirements and have had 2 years of professional experience at the time of the examination. Admission to Part II requires an additional 4 years of professional experience, additional professional references, and attainment of age 28 at the time of the examination.

REFERENCES

BRO E 59 E. Browing, *Harmful Effects of Ionizing Radiations* (Elsevier Publishing, Amsterdam, 1959).

GIB R 68 R. W. Gibson et al., New England J. Med *279*, 906 (1968).

GOF J 69 J. W. Gofman and A. R. Tamplin, Hearings before Joint Committee on Atomic Energy-Congress of U. S., Oct. 28-Nov. 7, 1969. Part I U. S. Government Printing Office, Washington, D. C. (1969).

HEW 68 *Particle Accelerator Safety Manual*, U. S. Department of Health Education, and Welfare, MORP 68-12, Oct. 1968.

ICRP 59 Recommendations of the ICRP, ICRP Publication 1, Pergamon Press, London (1959).

ICRP 66 ICRP Publication 8, *The Evaluation of Risks from Radiation* (pergamon Press, London, 1966).

KAR C 67 C. J. Karzmark, Some Aspects of Radiation Safety for Electron Accelerators Used for Both X-Ray and Electron Therapy, Brit. J. Radiol. *40*, 697 (1967),

MOR K 67a K. Z. Morgan and J. E. Turner, Maximum Exposure Levels External and Internal, in *Principles of Radiation Protection* (John Wiley and Sons, New York, 1967), Chap. 14.

MOR K 67b K. Z. Morgan, History of Damage and Protection from Ionizing Radiation op. cit. Chap. 1.

MOR K 67c K. Z. Morgan op. cit. Ref. p. 518 *Principles of Radiation* John Wiley and Sons, Inc. New York (1967).

MOR P 68 Particle Accelerator Safety Manual, U. S. Department of Health, Education, and Welfare, Publication MORP 68-12

MRC 60 Hazards to Man, Medical Research Council Report H.M.S.O. London, 1956 Second Report 1960.

MUT A 25 A. Mutscheller, Physical Standards of Protection Against Roentgen-Ray Dangers, Am. J. Roentgenol. Radium Therapy *13*, 65 (1925).

NBS 34 *Radium Protection for Amounts Up to 300 Milligrams*, NBS Handbook 18, 1934.

NBS 49 Safe Handling of Radioactive Isotopes, NBS Handbook 42 (1949).

NBS 51 Recommendations of the ICRP and ICRU 1950, NBS Handbook 47 (1951).

NBS 58 Maximum Permissible Radiation Exposures to Man, Supp. NBS Handbook 59 (1958).

NBS 70 Radiological Safety in the Design and Operation of Particle Accelerators, American National Standards N 43-4, NBS Handbook 107, 1970.

RAD 34 Recommendations for X-Ray and Radium Protection, Radiology *23*, 682 (1934).

RIC B 69 B. L. Rich and K. R. Kase, The Lawrence Radiation Laboratory Accelerator Safety Program, Second International Conference on Accelerator Dosimetry and Experience, SLAC, Nov. 1969, CONF-691101, p. 435.

SOL I 24 I. J. Solomon, Radiol. Electrol. *8*, 351 (1924).

STO R 52 R. S. Stone, The Concept of a Maximum Permissible Exposure, Carman Lecture, Radiology 58, 639 (1952).

TAY L 58 L. S. Taylor, Health Physics *1*, 97 (1958).

TAY L 59 L. S. Taylor and S. J. Harris, Exposure Standards and Radiation Protection Regulations, in *Radiation Hygiene Handbook* Ed. H. Blatz (McGraw-Hill, New York 1959, Sec. 3.3.

TAY L 65 Philosophical Influences in Radiation Protection Standards, Health Physics *11*, 859 (1965).

THO R 60 R. H. Thomas, History of Radiation Protection Standards UCID-10104, February 18, 1969.

BIBLIOGRAPHY ON RADIATION ACCIDENTS AND SAFETY PROCEDURES

1. Operational Accidents and Radiation Exposure Experience Within the United States Atomic Energy Commission, 1943-1970, Division of Operational Safety, Washington, D. C., Wash 1192 UC 41.
2. L. H. Lanzl, M. Rozenfeld, and A. R. Tarlov, Injury Due to Accidental High-Dose Exposure to 10-MeV Electrons, Health Physics *13*, 241 (1967).
3. Safety Guidelines for High Energy Accelerator Facilities, The National Accelerator Safety Committee, 1967.
4. Eugene L. Saenger, Radiation Accidents, Am. J. Roent. Rad. Therapy *84*, [4], 715 (1960).
5. Handling of Radiation Accidents, Proceedings of a Symposium, Vienna, 19-23 May 1969 (International Atomic Energy Agency, Vienna, 1969).

6. Handling of Radiation Accidents, Ed. B. Kaufmann and C. N. Welsch, (International Atomic Energy Agency, Vienna, 1969).

7. *Atomic Medicine*, Ed. C. F. Behrens, E. R. King, and J. W. J. Capender (Williams and Wilkins Company, Baltimore, 1960).

8. C. N. Welsh, Personnel Dosimetry for Radiation Accidents (International Atomic Energy Agency, Vienna, 1965).

9. *Radiation Accidents and Emergencies in Medicine, Research and Industry*, Ed. L. H. Lanzl, J. H. Pingel, and J. Rust (Charles C. Thomas, Springfield, Illinois, 1965).

10. Eugene L. Saenger, *Medical Aspects of Radiation Accidents*, Ed. USAEC (Government Printing Office, Washington, D.C. 1963).

APPENDIX—LABORATORY MANUAL

CONTENTS

LABORATORY MANUAL

INTRODUCTION

The practical features of the Berkeley Accelerator Health Physics Training Course are equal in importance to the lecture material presented. The student spends roughly equal time listening to lectures and carrying out laboratory experiments or radiation surveys at accelerators. It is our—the authors'—view that, since the problems presented by accelerator radiation measurement are fundamental, such practical experience is vital for a comprehensive understanding of Accelerator Health Physics. Our belief in this respect is reinforced by the concurrence of the vast majority of our students.

It has been our practice to send questionnaires to students, after they have taken the course, asking for constructive criticism. To date *all* those returning the questionnaire have recognized the great importance of these practical studies.

The course at Berkeley is still evolving, and precise details of the experiments performed by students may change as new and more appropriate techniques develop and become widely used. Although some details given here relate to the course given at Berkeley, we believe the material presented is sufficiently general that it may be adopted for use at other laboratories. It is therefore hoped that this appendix material may be used either independently as a laboratory manual or in conjunction with the main text.

In preparing this appendix the authors are deeply indebted to their colleagues in the Health Physics Group of the Lawrence Berkeley Laboratory, who were instrumental in development of the experimental program of the Accelerator Health Physics Training Course. Joseph B. McCaslin, A. Jerry Miller, Alessandro Rindi, Jorma T. Routti, Alan R. Smith, Lloyd D. Stephens, and Harold A. Wollenberg have all assisted in the planning of the experiments performed during the course, in the guidance of students, and in the preparation of the notes presented here.

USE OF β,γ PERSONAL FILM DOSIMETERS

ALESSANDRO RINDI

Experiment 1

Purpose

The student is to gain knowledge in the theory and use of photographic film as a personal dosimeter for β and γ radiation around high energy accelerators. A density-exposure calibration for Eastman Kodak Type 3 film in the bare packet is to be obtained for γ rays from a radium source. The student should realize that bare film packets are seldom used for γ-ray dosimetry when γ rays of energy lower than a few hundred keV have to be monitored. In such cases film packets are used in combination with suitable metallic filters (see references). However, around high energy accelerators the contribution of the low energy component to the total γ-ray dose is generally very small, so that complicated filtration methods can be avoided. The standard badge container used at LBL has only one metallic filter.

Theory

Photographic emulsions consist of a microscopic suspension of silver halide crystals in gelatin. Exposure to visible light or ionizing radiation results in energy absorption in individual halide grains that manifests itself in chemical changes—the formation of a so-called "latent image." These exposed grains may be reduced to metallic silver under the chemical action of development and made permanent by the chemical action of the fixer. The greater the amount of incident radiation the greater the production of silver. As metallic silver deposited in the emulsion impairs the transmission of visible light, the optical density of the emulsion may be related to radiation exposure.

The emulsion is usually placed, for rigidity, on a backing of cellulose acetate or polyester film. Typically, for radiation-monitoring purposes, films similar in size to those used in dental radiography (3 X 4 cm) are used. In the Kodak Type 3 film packages used in this experiment two films of different sensitivity are provided in each package. One film permits measurements from about 20 mR to about 1 R, the other from about 1 to 100 R. If the more sensitive one is fully blackened, the measurement is made with the other.

Optical density, D, is defined as the logarithm of the ratio of the incident light intensity, I_0, to the transmitted intensity, I_T:

$$D = \log_{10} (I_0/I_T).$$

Over a large portion of the sensitive range of the film the optical density is experimentally found to be proportional to the logarithm of the exposure E:

$$D \propto \log_{10} E.$$

Equipment

a. Nine Kodak Type 3 film badges.

b. Calibrated ^{226}Ra source. In this experiment the source used will be 901.5 mg radium.

c. Film-exposure facilities—an irradiation jig will be provided.

d. Film-processing facilities—a dark room and developing, fixing, and wash baths will be available by arrangement.

e. Optical densitometer.

f. Semilog graph paper (three cycles).

Laboratory Procedures

Identify the film badges by writing on the film wrapping with a soft pencil. These identification numbers will be permanently punched onto the films in the dark room.

Use one film as a processing control and background monitor and expose the other eight to the radium source. It is suggested that increasing exposures in the range from 25 mR to about 1.5 R be given;

Table 1.1. Suggested exposure scheme for Kodak Type 3 films placed at 1 meter from the 901.5-mg radium source.

Film No.	Exposure time	Exposure
1	0	background
2	2 min	25 mR
3	5 min	63 mR
4	15 min	189 mR
5	30 min	378 mR
6	45 min	568 mR
7	1 h	757 mR
8	1.5 h	1.13 R
9	2 h	1.51 R

the films can be exposed for the same time period at different distances from the source, or at the same distance from the source for different time periods, or a combination of methods can be used. We choose the second alternative.

The distance at which the exposure is made should be selected so as to optimize the conflicting requirements of uniform exposure, minimum influence from scattered radiation, and convenient irradiation times.

The 901.5-mg radium source provided will produce an exposure rate of 757 mR/h at a distance of 1 meter, and suggested exposure scheme is given in Table 1.1.

After the exposure, the films must be processed in the dark-room. The procedure to follow in the darkroom is the following:

1. Switch the main light off and the safe lights on (Kodak Wratten series OA filter.)
2. Punch the number on the badge, using the special punching machine (perforator).
3. Open the film packets.
4. Separate the two films contained in each packet and place them in special film holders.
5. Develop films for 3.25 minutes in the Kodak X-Ray Developer solution at a temperature of 68° F.
6. Wash in water at a temperature of 68° F for 2 minutes.
7. Place films in the Kodak X-Ray Fixer bath at 68° F for 10 minutes.
8. Turn on the main light.
9. Wash films in water for at least 20 minutes.
10. Dry films in air at room temperature.

Because the time required for drying the films is more than 6 hours, it is best to plan to determine the density of the processed films at least a day later than the exposure and processing.

The optical density of the processed films is measured by using a photo-electric densitometer. The density of the background (Film 1), representing the fogging of the emulsion prior to exposure, must be subtracted from the measured density of the exposed films. Plot the corrected density versus the log of the exposure for the more sensitive film. (Because of the low intensities to which the films were exposed, insufficient data will be obtained for the less sensitive film.) In Fig. 1- 1 standard curves of density versus dose for the Kodak Type 3 films are shown.

Possible Errors in the Experimental Procedure

Several errors can affect the final results obtained; the most important are discussed below.

a. DURING EXPOSURE OF THE FILM

(i) Errors in evaluation of the source-to-film distance (negligible for large enough distances).

(ii) Variation of the calculated dose rate due to backscattering, diffusion, etc. in the exposure room (negligible if the calibration room is large and the exposure is carried out high above the floor).

(iii) Errors in evaluation of the exposure time (negligible for long exposures).

b. DURING PROCESSING OF THE FILM

Variation of the temperature of the developing baths, the developing time, or the chemical condition of the developing fixing solutions, all of

which influence strongly the darkening of the developed film. (Errors can be minimized by accurate processing and by use of fresh solutions.)

c. DURING READING OF THE FILM

Errors in evaluation of the optical density due to nonuniform blackening of the film. (Errors can be minimized by the appropriate choice of film and by accurate processing.)

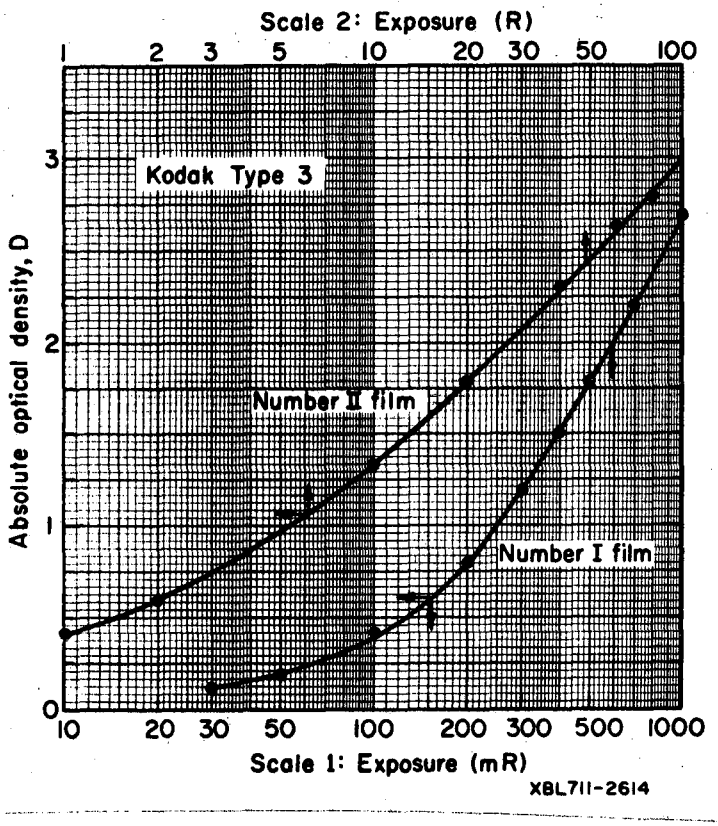

Fig. 1.1. Typical density exposure curves for the two films contained in the Kodak Type 3 β - γ package, obtained by Lawrence Berkeley Laboratory film badge service (after Camp and Hadley).

Background Reading

This text, Chapter 5.

K. Becker, *Photographic Film Dosimetry* (Focal Press, London, 1966).

W. H. Barkas, *Nuclear Research Emulsions* (Academic Press, New York, 1963), Vol. *15* Part I.

R. A. Dudley, Dosimetry With Photographic Emulsions, in *Radiation Dosimetry*, Vol. II F. H. Attix and W. C. Roesch, eds. (Academic Press, New York, 1966), Chapter 15.

R. A. Dudley, Photographic Film Dosimetry, in *Radiation Dosimetry* G. Hine and G. Brownell, eds. (Academic Press, New York, 1956), Chapter 7.

PERSONNEL NEUTRON DOSIMETRY WITH NUCLEAR EMULSIONS

ALESSANDRO RINDI

Experiment 2

Purpose

The student is to become familiar with the theory and use of nuclear emulsion for the detection of fast neutrons (0.5 to 15 MeV). Kodak NTA films are calibrated by using neutrons from a PuBe source (average neutron energy $\approx$ 4 MeV).

Theory

The grain size in ordinary emulsions (as, for example, those used for γ-ray dosimetry) is too large and the grains are too widely spread to permit identification of tracks of charged particles. Nuclear track emulsions, however, are specially produced with grain sizes small enough and grain density large enough to permit observation of individual particle tracks under the microscope. Thus emulsions may be used to detect, for example, proton recoil tracks produced by the elastic scattering of neutrons in a hydrogenous medium placed adjacent to the emulsion (or the acetate backing of the emulsion).

A widely used system of personnel neutron dosimetry is based on proton track counting in Kodak Personnel Neutron Monitoring Film, Type A (NTA). Measurements of sensitivity have been reported by Lehman (LEH R 60).

Neutrons hitting the badge scatter the hydrogen nuclei of the paper in which the film is wrapped, of the plastic support of the film, and of the gelatin that supports the emulsion. These elastically scattered protons interact with the grains of the emulsion, and the path of each is shown as a set of dark aligned grains (a track) in the processed film. Usually three or more aligned grains define a track. The number of tracks generated in the film is proportional to the number of incident neutrons in a given neutron spectrum. (The overall efficiency of the film as a neutron detector is a function of neutron energy.) Thus by counting the number of tracks generated in the emulsion, the number of incident neutrons may be determined. Knowing the energy (or the spectrum) of the neutrons, one can relate the number of tracks to the dose equivalent. The film is generally scanned by a microscope with total magnification between 400 X and 800 X.

Equipment

a. Four Kodak Personnel Neutron Monitoring films (Type A).

b. A ^{238}Pu-Be neutron source (the LBL source No. 581 provided has an absolute yield of 1.56 X 10^6 n/sec).

c. Exposure facilities.

d. Darkroom facilities.

e. Microscopes.

Laboratory Procedure

Number the four badges with soft pencil (the films will be permanently identified in the dark room) and expose three of them to different fluences from the PuBe source. (The unexposed film will have on it the background number of tracks, which is to be subtracted from the other readings.) As in Experiment 1 it is suggested that films be exposed at the same distance from the source for different times. To facilitate easy scanning the films should be exposed to dose equivalents in the range 50 to 400 mrem.

After exposure the four films must be processed in the darkroom. The developing and fixing baths and times have been standardized for the γ-ray and neutron films, so that the procedure for processing the neutron films is identical to that for the γ-ray films (see Experiment 1).

After complete drying, each film is to be scanned under the microscope provided. Use the 43 X objective and the 10 X eye piece for a total magnification of 430 X. At Berkeley "random scanning" is used: Select a microscope field at random by moving either the horizontal or vertical stage adjustments (or both) of the microscope. Count the tracks in this field, then select another field at random and count the tracks in it. Continue this procedure until enough tracks have been counted to give a standard deviation less than 10%. (When a field count is started it must be completed.) The final result of the scanning is expressed in tracks per field (the total number of counted tracks divided by the number of fields explored) or in number of tracks per cm^2 (the field area of the microscope provided is 6.0×10^{-4} cm^2). Subtract from the number of tracks per field counted on the exposed film the number counted per field on the background film. Plot on a linear scale the number of tracks per field versus dose equivalent for the exposed films (indicate the statistical error bars); the three points should lie on a straight line. It may be necessary to count more fields so as to improve the statistical accuracy of each measurement to obtain this linear relationship.

Evaluate the calibration factor in tracks/field per mrem from the known output of the PuBe source. Figure 2.1 shows typical results obtained by using a PuBe neutron source. The film was rotated during exposure and scanned for tracks more than 5 μ long. For a field size of 245 X 245 μ a calibration factor of 7.4 tracks/field per rem was obtained. A value of 7.2 n/cm^2 sec per mrem/hr was used to convert flux density to DE rate. (For purposes of comparison, the calibration factor used at the Lawrence Berkeley Laboratory for typical accelerator environments is 8 tracks per field per rem.)

Experimental Errors

Experimental errors during exposure and film processing are identical to those described in Experiment 1. Substantial errors may be introduced during track counting by uncertainty in track identification. Having an experienced scanner look at your microscope fields and comparing notes with him will prove helpful in resolving many difficulties.

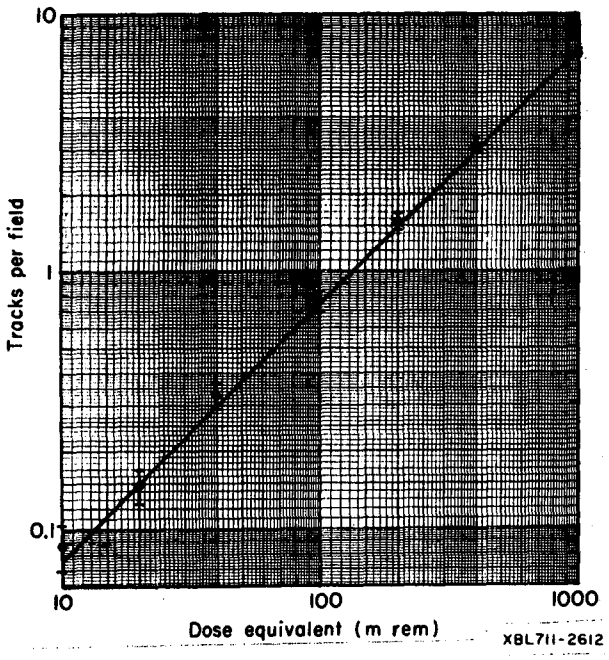

Fig. 2.1. Calibration curve for NTA film obtained with a PuBe neutron source with the film isotropically irradiated (film rotated). Calibration obtained: 7.36 ± 0.36 tracks/field per rem for tracks greater than 5 μ in length and a field size of 245 X 245 μ (after Masao Oshino).

REFERENCE

LEH R 60 R. L. Lehman, Energy Response and Ph ysical Properties of NTA Personnel Dosimeter Nuclear Track Film, UCRL-9513, 1960.

Background Reading

This Manual, Vol. 1, Chapter 5.

R. A. Dudley, Dosimetry With Photographic Emulsions, in *Radiation Dosimetry*, Vol. II, F. H. Attix and W. C. Roesch, eds. (Academic Press, New York, 1966), Chapter 15.

M. Oshino, Response of NTA Personnel Neutron Monitoring Film Worn on a Human Phantom, LBL-342, Sept. 1971.

E. Piesch, Some Remarks on Fast Neutron Dosimetry With Nuclear Track Film, in *Personnel Dosimetry Techniques for External Radiation* (ENEA, Paris, 1963), p. 267.

USE OF A MODERATED BF_3 PROPORTIONAL COUNTER TO DETECT FAST NEUTRONS

LLOYD D. STEPHENS

Experiment 3

Purpose

In addition to using personal radiation monitors of the type studied in Experiments 1 and 2, we must also make environmental surveys of working areas around accelerators. Instruments capable of giving instantaneous readings must be available. The BF_3 proportional counter is one of the most useful, reliable, stable, and rugged instruments available for thermal-neutron measurement. When used in conjunction with a hydrogenous moderator it may be calibrated to measure fast neutrons.

Theory

Neutrons, being neutral particles, are not directly detectable in their passage through matter. It is only after they have interacted with matter that their effects are detectable.

The reaction utilized in the BF_3 counter is the interaction of thermal or slow neutrons (a few eV) with a ^{10}B nucleus. This is an exothermic reaction which gives rise to an α particle by the reaction $^{10}B(n,\alpha)\,^{7}Li$, with an energy release of 2.78 MeV. The ground state of ^{7}Li may be formed directly, with the entire energy being shared by the ^{7}Li and the ^{4}He nuclei, or an excited state of ^{7}Li may be formed, with the emission of a 0.48-MeV γ ray:

$$^{1}_{0}n + {}^{10}_{5}B \rightarrow {}^{7}_{3}Li + {}^{4}_{2}He + 2.78\ \text{MeV}$$

$$\rightarrow {}^{7}_{3}Li^{*} + {}^{4}_{2}He + 2.30\ \text{MeV};$$

$${}^{7}_{3}Li^{*} \rightarrow {}^{7}_{3}Li + E_{\gamma}\ (0.48\ \text{MeV}).$$

Simple kinematic considerations show that the minimum energy available to each charged particle is

$$E_{Li} = [M_{\alpha}/(M_{\alpha} + M_{Li})] \times 2.30\ \text{MeV},$$

$$E_{\alpha} = [M_{Li}/(M_{\alpha} + M_{Li})] \times 2.30\ \text{MeV},$$

where M_{α}, M_{Li} are the helium and lithium ion masses

and E_{α}, E_{Li} are their respective energies.

Substituting for M_α and M_{Li}, we obtain

$$E_{Li} = 0.84 \text{ MeV},$$

$$E_\alpha = 1.46 \text{ MeV}$$

for the minimum energies of the charged reaction products.

The capture cross section, σ, of ^{10}B for slow neutrons is inversely proportional to neutron velocity, v, up to an energy of about 100 eV, and can be represented by

$$\sigma = \sigma_0 v_0,$$

where σ_0 is the absorption cross section at 0.025 eV,

v_0 is the neutron velocity at 0.025 eV (2.2×10^5 cm/sec).

Substituting the values

$$\sigma_0 = 3837 \times 10^{-24} \text{ cm}^2$$

and

$$v_0 = 2.2 \times 10^5 \text{ cm/sec},$$

we obtain $\sigma = 8.44 \times 10^{-19}/v)$ cm^2 (with v in cm/sec). (1)

The sensitivity of a BF_3 counter to neutrons distributed in a Maxwell-Boltzman distribution may be estimated by using Eq. 1. In this case the mean neutron velocity is 2.48×10^5 cm/sec, whence

$$\sigma = 3404 \times 10^{-24} \text{ cm}^2.$$

The sensitivity S in counts/sec per unit neutron density then has an upper limit given by

$$S \leqslant 3404 \times 10^{-24} \text{ NV counts/sec per neutron/cm}^2 \text{ sec}, \quad (2)$$

where N is the number of ^{10}B atoms/cm^3,

V is the sensitive volume of the counter.

This estimate, although only approximate, is sufficiently accurate for out purposes, and the sensitivity is assumed equal to the upper limit given be Eq. 2.

For a typical counter used at Berkeley the parameters are

gas pressure = 20 cm Hg,

^{10}B enrichment = 96%,

sensitive volume, V = 430 cm^3.

Because 1 gram molecule BF_3 (67 g) occupies 22.4 liters at STP, the density of BF_3 at STP = $(67/22.4) \times 10^{-3}$ g/cm^3; density of BF_3 at 20 cm Hg pressure and 20°C

$$= \frac{67}{22.4} \times \frac{273}{293} \times \frac{20}{76} \times 10^{-3} \text{ g/cm}^3.$$

Finally, the number of molecules BF_3 per cm^3 in the counter is

$$N = \frac{1}{67} \times \frac{67}{224} \times \frac{273}{293} \times \frac{20}{76} \times 10^{-3} \times 0.602 \times 10^{23} \text{ molecules.}$$

Thus from Eq. 2 the sensitivity S is given by

$$S \leqslant 3560 \times 10^{-24} \times \frac{430}{67} \times \frac{67}{22.4} \times \frac{273}{293} \times \frac{20}{76} \times 10^{-3} \times 0.602 \times 10^{24}$$

$$\leqslant \underline{10 \text{ counts/sec per unit flux density.}}$$

The BF_3 counter is surrounded by 2.5-in.-thick paraffin moderator, and under these conditions its sensitivity remains nearly constant between neutron energies of 30 keV and 15 MeV (Fig. 3.1). Response to incident thermal neutrons is eliminated by surrounding the moderator with cadmium; only neutrons with energy greater than the "cadmium cutoff" (0.5 eV) can enter the moderator, become thermalized, and be detected.

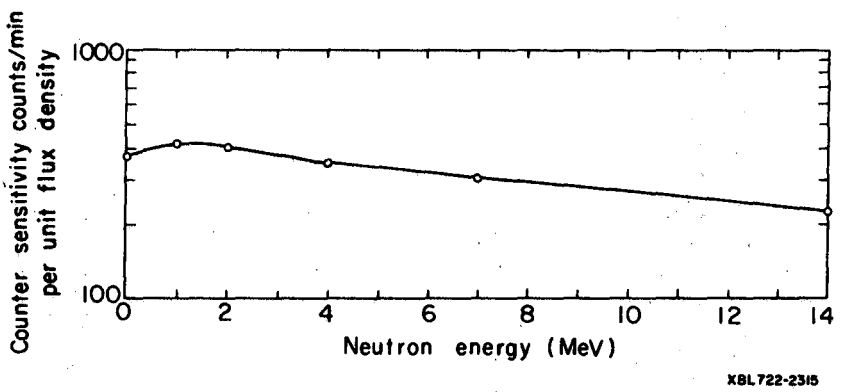

Fig. 3.1. Variation of resistivity of moderated BF_3 counter with neutron energy. (Moderator thickness, 2.5 in. paraffin.)

Equipment

a. BF_3 proportional counter.
b. Moderator.
c. Electronic equipment consisting of
   amplifier,
   discriminator-scaler,
   high voltage supply,
   oscilloscope,
   pulse generator.
d. Neutron sources (PuBe, PuLi, PuF, PuB).

Laboratory Procedure

Connect all the electronics as shown in Fig. 3.2.

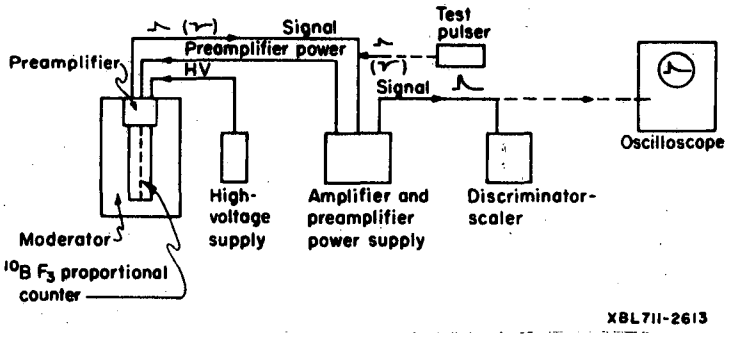

Fig. 3.2. Schematic diagram of moderated BF_3 proportional counter and ancillary electronic equipment.

After all connections have been made, turn on the amplifier, scaler, and oscilloscope. The preamplifier output impedance should match the input of the amplifier. Discriminator-scalers used in this experiment require positive-going signals, as provided by the amplifiers used.

The proportional counters require a positive high voltage on the center wire, since we are collecting electrons. A test pulser may be used to be certain that the amplifier and scaler are operating correctly.

Using a neutron source of known strength and a fixed discriminator level, prepare a voltage plateau curve (such as shown in Fig. 3.3). For most purposes 50-volt steps in the high voltage are sufficient. The operating high voltage should be selected on the flat portion of the curve to minimize changes in counting rate resulting from fluctuations in the high voltage (HV) supply.

It is also a wise precaution to set the amplifier gain at a point that will permit minor changes to be made, so that small fluctuations in gain can be compensated for.

Selection of a HV operating point near the upper end of the plateau will require less amplifier gain but at the same time increase the posibility of spurious voltage breakdowns. One the other hand, a HV operating point that is low will reduce breakdown to a minimum (or completely eliminate it), but will require maximum amplifier gain—a condition which then amplifys the electronic noise common to all high-gain systems and increases background noise. An optimum operating voltage must be chosen (see Fig. 3.3).

Once this setting has been selected, the effect of discriminator adjustment should be studied. This is done by using a neutron source and studying the variation of the counting rate with discriminator settings. The curve (Fig. 3.4) drawn from the data will rise steeply near zero bias but will soon flatten out. The steep portion is due to electronic noise and small γ-ray pulses.

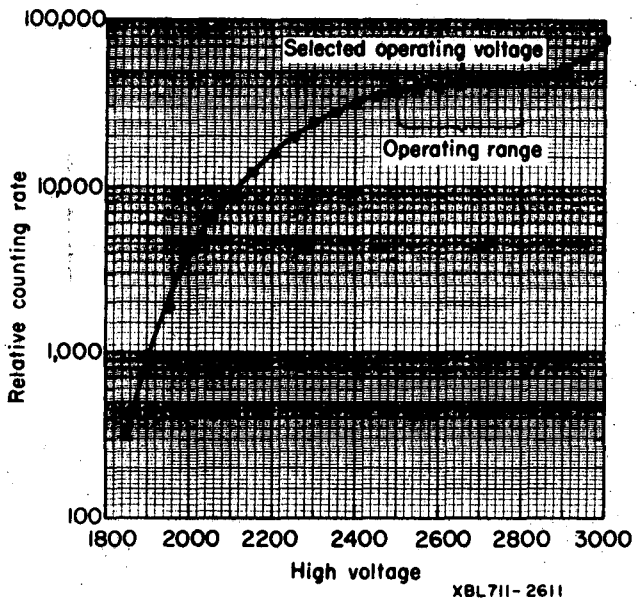

Fig. 3.3. Typical high voltage characteristic curve for moderated BF_3 counter obtained with a PuBe neutron source. The discriminator voltage was set at 0.5 V.

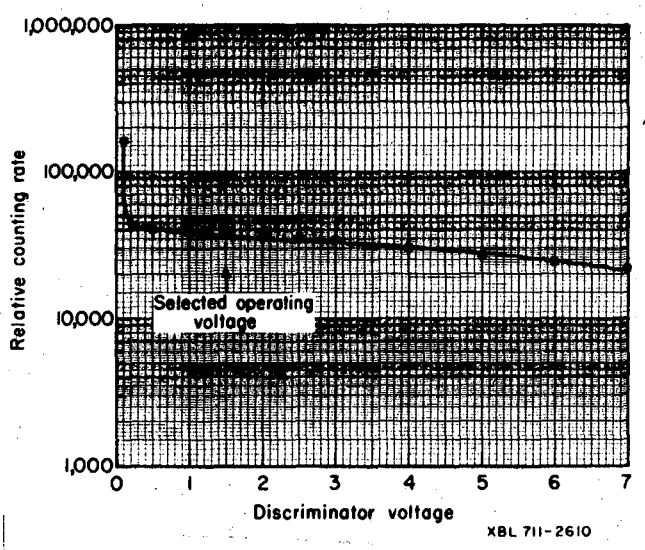

Fig. 3.4. Typical discriminator voltage curve for moderated BF_3 counter. High voltage set at 2650 V.

The discriminator should be set at a point that will discriminate against these pulses. This is sometimes termed biasing out the noise signals. The flatness of the remainder of the curve is due to the large amount of energy released in the counter for each neutron detected. Most of these events drive the amplifier to its full output, resulting in nearly constant counting rates for all discriminator or bias settings.

One of the useful features of the BF_3 counter is its relative insensitivity to γ rays. The effect of γ rays should be observed by noting the change in counting rate when a Ra source is placed near the BF_3 counter. The effect, if noticeable at all, should be quite small.

Data

Record all electronic equipment settings for future reference; record source number, type, and output.

Obtain

a. HV plateau curve,
b. discriminator curve,
c. selected operating points.

Precautions

a. Observe high voltage polarity.
b. Increase high voltage slowly.
c. Make sure that cable connections are reasonably tight, to eliminate spurious counts.

Background Reading

William J. Price, *Nuclear Radiation Detection* (McGraw-Hill Book Company, New York, 1958).

Richard Stephens, *Introduction to Nuclear Engineering*, second edition (McGraw-Hill Book Company, New York, 1958).

THE POLYETHYLENE-LINED PROPORTIONAL COUNTER

LLOYD D. STEPHENS

Experiment 4

Purpose

Experiment 3 has shown how neutron flux density may be measured by using a moderated BF_3 counter. In this experiment one learns how to use a polyethylene-lined counter to measure neutron energy density and thus facilitate an estimation of average neutron energy.

Theory

As we have seen in Experiment 1, neutrons may be detected from recoil protons produced in (n ,p) scattering processes. If these recoil protons are generated in either the wall or the gaseous filling of a proportional counter they may be detected. On this basis Hurst et al. (HUR G 54, HUR G 61) designed an ethylene-filled polyethylene-lined proportional counter to measure absorbed dose due to neutrons. Dennis and Loosemore (DEN J 60) designed a counter whose response is approximately proportional to dose equivalent in the energy range 0.1 to 14 MeV.

Evaluation of neutron flux density for monoenergetic neutrons is relatively straightforward (ROS B 49), but radiation-protoection measurements must be made in neutron spectra covering a wide range of energies. Experiments 3, 5, and 8 show how flux densities in such spectra may be measured. It is of great value, when the neutron spectrum covers wider ranges, to measure the energy flux density that is carried by fast neutrons. Then if the neutron spectrum is known well enough to permit an estimate of effective mean energy, the numerical flux density may be independently approximated. Alternatively if the neutron spectrum is not known, a measurement of both particle number and energy density will give a value of effective energy. This concept was developed by Mather et al. (MAT R 52) and described in detail by Moyer (MOY B 52).

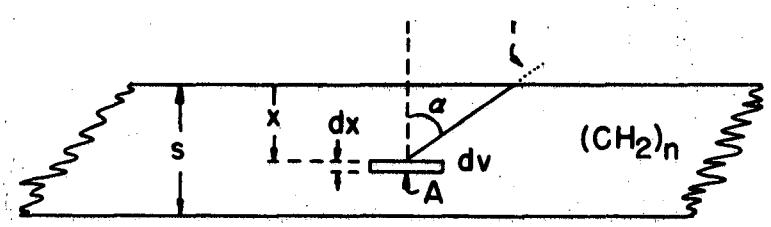

$$\text{MAXIMUM ANGLE} = \alpha = \cos^{-1}\frac{X}{R-r}$$

MU3174

The analysis of the energy-flux counter designed by Mather et al. proceeds in five steps, as follows.

1. Consider a plane sheet of hydrogenous material of thickness S immersed in an isotropic flux of neutrons of energy E (Fig. 4.1). Recoil protons originate from any volume element with equal probability in any direction, and with equal probability of having any energy up to the maximum possible value of E. The number dF(X,E) of protons produced in dV at depth X that will emerge with sufficient residual range to be detected may be shown (MAT R 52) to be

$$dF(X,E) = \frac{1}{2}\,\phi(E)\,\sigma_{np}(E)\,N_H dV \int_{\epsilon_x}^{1} [1 - x/R(\epsilon) - r)]\,d\epsilon, \qquad (1)$$

where $\phi(E)$ = flux density of neturons with energy between E and E+dE,
$\sigma_{np}(E)$ = total n-p cross section for a neutron of energy E,
N_H = number of hydrogen atoms per cm^3 of polyethylene,
$\epsilon = E_p/E$ = fractional energy delivered to a recoil proton,
ϵ_x = minimum fractional energy for emergence of a proton from depth x,
$R(\epsilon)$ = range in the hydrogenous material of a proton with fractional energy ϵ,
and r = residual range required upon emergence to allow detection.

2. If now $R(\epsilon)$ is approximated by $R(E) = \epsilon^{3/2}$, where R(E) is the proton range for $\epsilon = 1$, and if, to begin with, the required residual range r is set equal to zero, Eq. 1 may be integrated to yield

$$dF(X,E) = \frac{1}{2}\,\phi(E)\,\sigma_{np}(E)\,\{1+[2x/R(E)] - [3x/R(E)]^{2/3}\}\,N_H dV. \qquad (2)$$

This last approximation of $r = 0$ is *not* employed in more precise calculations (MAT R 52), which space does not allow here.

3. The contributions from all depths x are now to be summed. Denote volume element dV by Adx, where A is a plane area parallel to the surface. Then by integration over x the results may be obtained for the two cases (a) $S \geq R(E)$, and (b) $S < R(E)$.

(a) For $S \geq R(E)$:

$$F(E) = \frac{1}{2}\,\phi(E)\,\sigma_{np}(E) N_H A \int_0^{R(E)} \left\{1 + \frac{2x}{R(E)} - 3\,\frac{(x)^{2/3}}{R(E)}\right\} dx$$

$$= \frac{1}{10}\,N_H A\,\phi(E)\,\sigma_{np}(E)\,R(E). \qquad (3)$$

(b) For $S < R(E)$:

$$F(E,S) = \frac{1}{2}\,\phi\,\sigma N_H A \int_0^S \left\{1 + \frac{2X}{R} - 3\,\frac{(X)^{2/3}}{R}\right\} dX$$

$$= \frac{1}{2}\,N_H A\,\phi(E)\,\sigma_{np}(E)\,R(E)\left\{\frac{S}{R} + \frac{S^2}{R^2} - \frac{9}{5}\left(\frac{S}{R}\right)\right\}^{5/3} . \quad (4)$$

Expression 3 or 4 gives the number of protons, produced within the parallelepiped volume A_S by neutrons of energy E, that emerge each second from one face of the sheet.

4. The total number of protons emerging per second is to be obtained by integrating over the energy spectrum. This integration is divided into two parts: (a) energy interval from E = 0 to $E = E_S$, where E_S is the energy required to give range S in the sheet material, and (b) energy interval from E_S to infinity, or to E_{max} for the spectrum of the neutrons. Thus if every proton that emerges can be counted, the counting rate arising from area A is

$$C = \int_0^{E_S} F(E)dE + \int_{E_S}^{E_{max}} F(E,S)dE, \quad (5)$$

where F(E) and F(E,S) are expressions 3 and 4, respectively.

In many instances $S > R(E_{max})$, so that only the first term of Eq. 5 is involved. [For example, the range of a 15-MeV proton in polyethylene is only 0.24 cm (or 3/32 in.), which would be a quite reasonable wall thickness.] Advantage is now taken of the fact (evident from Fig. 4.2) that over a wide range of energies in this region the product $\sigma_{np}(E)\,R(E)$ is very nearly proportional to E. From less than 0.1 MeV up to 20 MeV the approximation

$$\sigma R = (1.0 \times 10^{-26})E,$$

with E expressed in MeV and the product σR in cm^3, is nowhere in error by more than 15%.

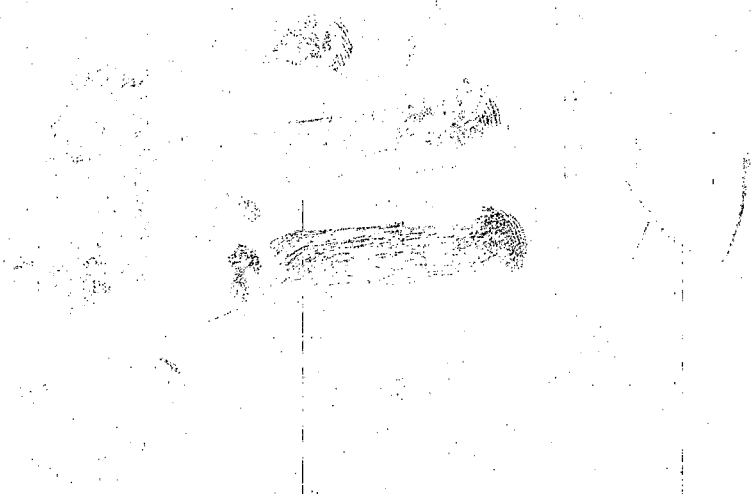

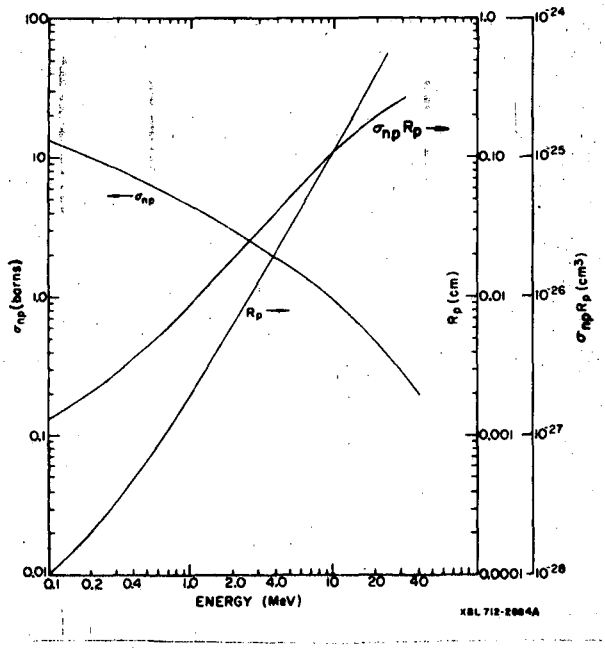

Fig. 4.2. σ_{np}, proton range, R_p, (in polyethylene of density 0.95 g/cm^2), and the product $\sigma_{np}R_p$ as a function of energy.

Thus for a sheet whose thickness is greater than $R(E_{max})$, so that only the first integral of Eq. 5 is required, C becomes, in view of Eqs. 3 and 6,

$$C = (1.0 \times 10^{-27}) N_H A \int_0^{E_{max}} \phi(E) E dE \text{ counts/sec.} \quad (6)$$

The integral appearing here gives the total density energy flux carried by fast neutrons. Corrections to this somewhat oversimplified discussion are mentioned in the next step.

5. The sheet of $(CH_2)_n$ is now bent into a cylinder whose radius is large compared with S, and is very lightly graphited with Aquadag to provide conduction. It is then made to serve as the cathode of a proportional counter filled with argon plus a small percentage of CO_2.

The refinements to the foregoing calculation involve the following items:

a. treatment of the problem with r not zero, i.e., with a specifiec residual range required for detection;
b. allowance for effects of argon and carbon recoils;
c. allowance for geometrical effect of bending the flat sheet into a cylinder;
d. inclusion of neutron energies for which $R(E) > S$, i.e., the use of both terms of Eq. 5.

The results of a calculation including corrections (refinements) a and d are displayed for various $(CH_2)_n$ sheet thicknesses in Fig. 4.3, in which the ordinate is efficiency in counts/unit area per unit flux density of neutrons in unit energy interval at E. It is evident that below 1 MeV the requirement of a residual range that will provide as much as a 0.2-MeV energy loss in the counter gas reduces the efficiency so that it is no longer proportional to neutron energy: 0.2 MeV is possibly a more stringent requirement than is necessary if counter design is such that electron path lengths are short. Correction c can be estimated to be small for a typical counter diameter of 5 cm, though its effects at the higher-energy end begin to be appreciable.

From Fig. 4.3 it is seen that if the spectral region of interest lies between 0.8 MeV and nearly 20 MeV, a 1/8-in.-wall counter has a sensitivity essentially proportional to energy, and the simple relationship of Eq. 6 may be used. If values of residual proton range r smaller than 0.2 MeV equivalent are possible, the lower-energy limit of this proportional region is moved downward, as is indicated by the ideal curve for r = 0.

Moyer (MOY B 52) has reported the development of such survey instruments at Berkeley. To avoid errros due to the anisotropy of the incident neutrons, a spherical detector was constructed, but comparisons with a cylindrical counter showed agreement to within 15%. The instrument currently consists of a polyethylene-walled cylindrical proportional counter.

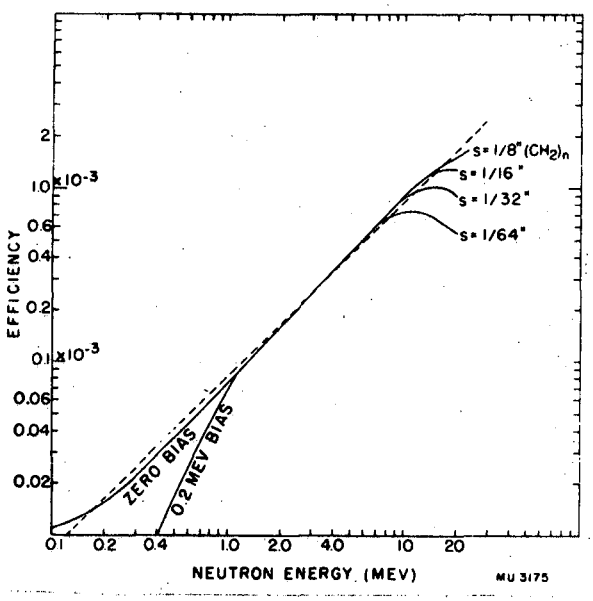

Fig. 4.3. Calculated counter efficiency versus neutron energy, in recoil counts per second per unit area per unit flux density and per unit energy interval, for various wall thicknesses. The $\frac{1}{N_N A\phi(E)} \frac{dC}{dE}$, *from Eq. 2 in text.*

The counter used is filled with a mixture of 96% Ar-4% CO_2 to a pressure of 1 atm and lined with 0.32 cm of polyethylene. A discriminator bias curve is obtained by counting recoil-proton events under conditions of constant amplifier gain and high voltage. The counter is calibrated by extrapolating the discriminator bias curve obtained with a calibrated neutron source back to the counting rate at zero bias. Calculations indicate the sensitivity in the energy range 0.1 to 20 MeV to be 15 MeV/cm^2 per count.

Laboratory Procedure

1. Connect the detector to the associated electronic equipment.
2. Turn on the amplifier and scaler.
3. Test scaler and amplifier, using negative pulses from the pulse generator.
4. Select amplifier and high voltage settings as in Experiment 3.
5. Set the high voltage supply to its lowest setting before turning it on. Slowly increase the high voltage to approximately 1800 V.
6. Bring a neutron source up to the counter and observe pulses on the oscilloscope. The pulses should be clean and there should be no noise.
7. Place calibrated neutron source at a measured distance from the counter and obtain a series of bias curves (discriminator voltage versus

counting rate) at several high voltage settings. The range of high voltage suggested is 1800 to 2000 V in steps of 50 V. Discriminator settings should be varied in 1-V steps in the range 0.5 to 7 V.

8. Select the operating region from the bias curves. It is recommended that the operating counting rate be approximately 80% of the extrapolated zero-bias counting rate.

9. The calibration factor for the counter is then obtained by extrapolating the zero-bias counting rate at the known energy-flux density incident upon the detector.

A value of approximately 15 MeV/cm^2 sec per count/sec should be obtained. Figure 4.4 shows examples of bias curves obtained.

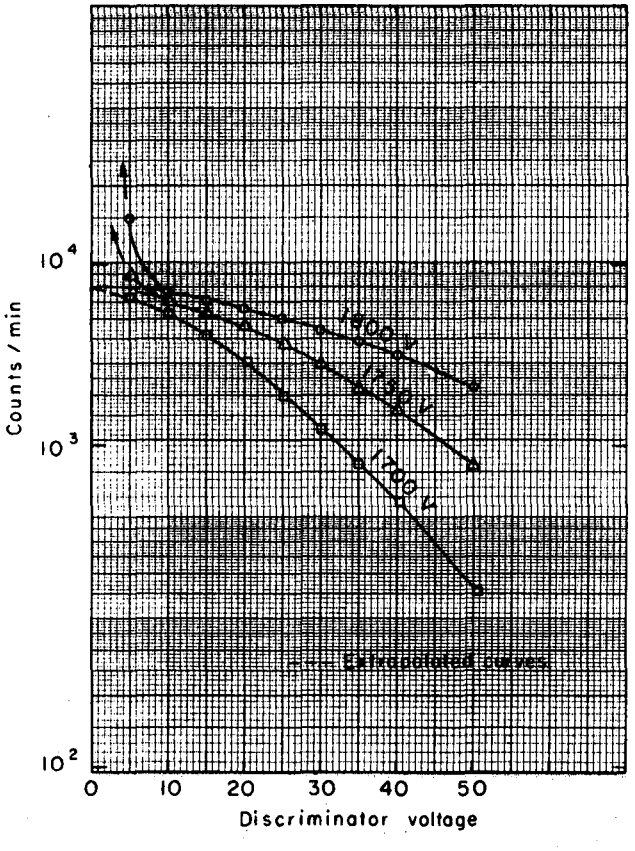

Fig. 4.4. Family of discriminator voltage curves for the LBL polyethylene-lined counter obtained with a PuBe source. At low voltage the counting rate increases due to sensitivity to γ rays. All curves extrapolate back to the same zero-bias counting rate.

REFERENCES

DEN J 60 J. A. Dennis and W. R. Loosemore, A Fast Neutron Counter for Dosimetry, Harwell Report AERE-R-3302, 1960.

HUR G 54 G. S. Hurst, An Absolute Tissue Dosimeter for Fast Neutrons, Brit. J. Radiol. *27*, 353 (1954).

HUG G 61 G. S. Hurst and E. B. Wagner, Special Counting Techniques in Mixed Radiation Dosimetry, in *Selected Topics in Radiation Dosimetry* (IAEA, Vienna, 1961).

MAT R 52 R. L. Mather, B. J. Moyer, and B. W. Thompson, quoted by MOY B 52.

MOY B 52 B. J. Moyer, Survey Methods for Neutron Fields, Nucleonics *10* [5], 14 (1952).

ROS B 49 B. B. Rossi and H. Staub, *Ionization Chambers and Counters*, National Nuclear Energy Series (McGraw-Hill Book Co., New York, 1949), Chapters 4 and 7.

Background Reading

William J. Price, *Nuclear Radiation Detection* (McGraw-Hill Book Co., New York, 1958).

E. W. Emergy, Geiger-Muller and Proportional Counters, in *Radiation Dosimetry* Vol. 2, F. H. Attix and W. C. Roesch, eds. (Academic Press, New York, 1966).

MODERATED INDIUM FOILS

A. JERRY MILLER and LLOYD D. STEPHENS

Experiment 5

Purpose

Nuclear track emulsions are limited to detection of neutrons in the energy range between 0.5 and 15 MeV (Experiment 2), and counters may be limited by time resolution (Experiments 3 and 4). It is often necessary therefore to use alternative techniques in neutron surveys. This experiment shows how neutrons of energy up to about 15 MeV (including intermediate-energy neutrons) may be measured by use of a moderated-thermal-neutron detector.

Theory

Nuclear transmutations frequently produce radioactive species. The activity of the radioisotope produced may be used to determine the incident neutrons, but the technique may be employed for any other strongly interacting particles (e.g., p,π). A detector employing this technique is referred to as an *activation detector.*

In neutron measurements by induced activity, a stable element is exposed to the neutron flux for a measured period of time. Following the irradiation, the element is removed from the neutron field, and the activity induced in it is determined.

Neutron activation detectors have a number of advantages:

a. Many simultaneous measurements are possible.

b. The locations where foils may be placed are quite unrestricted.

c. The results are unambiguous, as the induced activity is caused solely by neutrons.

d. Foils are not disabled by high neutron flux rates, as conventional electronic counters may be.

e. They respond correctly in pulsed radiation fields.

Thermal neutron flux densities are frequently measured by activation techniques, for which it is common practice to use a small piece of gold or indium as the irradiated target.

When indium is used, foils of mass 300 to 400 mg are convenient. The nuclear reactions for foil activation and decay are

$$^{115}_{49}\mathrm{In} + ^{1}_{0}\mathrm{n} \rightarrow ^{116}_{49}\mathrm{In} \qquad (1)$$

and

$$^{116}_{49}\mathrm{In} \rightarrow \beta^{-} + ^{116}_{50}\mathrm{Sn}\,. \qquad (2)$$

The β^- decay of the ^{116}In follows a 54.0-min half-life, which may be detected in a gas-flow proportional counter with standard radiation laboratory

counting equipment. The gas used in the proportional counter is ordinary gas supplied by the local utility company.

After the activated foils have been counted, corrections must be made both for decay following irradiation and for the fraction of saturation achieved. The corrected counts then correspond to the activity the foil would have at the moment the activation ended if the activation time had been infinitely long.

The following equations are used to make these corrections.

$$\text{Decay correction factor} = e^{-\lambda t}\ \text{decay} \qquad (3)$$

and $$\text{Activation correction factor} = [1-\exp(-\lambda\, t_{act})],$$

where λ is the decay constant, t_{decay} is the decay time in the same time units as λ, and t_{act} is the activation time in the same time units as λ.

Although indium foils essentially detect only thermal neutrons, they may be used to measure fast neutrons by placing them in a cadmium-covered paraffin moderator of 6 in. diam (STE L 58). The effect of the cadmium is to absorb the thermal neutrons present in the incident neutron flux. The paraffin thermalizes the high-energy neutrons, which then activate the indium foils. Stephens and Smith (STE L 58) have shown that such a detector has a fairly uniform energy sensitivity from a few keV to about 20 MeV.

To calibrate the indium foils for fast-neutron detection the loaded moderators are placed in a known neutron flux density, ϕ, and the corrected activity is calculated:

$$A_{corr} = \frac{A_{meas}\exp(\lambda t_{decay})}{[1-\exp(-\lambda t_{act})]} \qquad (4)$$

The corrected activity per unit mass m is then

$$A_{corr}/m \ \text{counts/min/g},$$

and the calibration factor, k, is given by

$$k = (A_{corr}/m\phi)\ \text{counts/min/g per unit flux density},$$

where ϕ is flux density.

Note on Gas-Flow Proportional Counters

The interested student is referred to Price (PRI W 58) for a discussion of the theory of gas-flow proportional counters. Two other corrections are of importance. These are the bias correction and counting-shelf corrections.

The counter used in this experiment is operated on its β plateau and has a bias correction of almost unity. The counter is provided with several counting-shelf positions, and in general the flux density, ϕ, is given by

$$A_{corr}\ X\ \frac{\text{bias correction factor X shelf correction factor}}{k \cdot m}.$$

where the shelf corrections vary from 1 to 23 depending upon the shelf chosen.

Equipment

a. Calibrated neutron source.
b. Indium foils,
c. Cadmium-paraffin moderators.
d. Stopwatch.
e. Gas-flow proportional counter and associated electronic equipment.
f. ^{137}Cs check source.

Laboratory Procedure

1. From the known source neutron output calculate a reasonable source-detector distance for foil irradiation. Distances should be calculated from the center of the source to the center of the detector. In deciding the irradiation distance take into account the influence on the results of measurement accuracy and scattered radiation.

2. Irradiate foil for a known length of time.

3. Check the operating gain of the gas-flow system with a standard ^{137}Cs source to make sure that it has not drifted.

4. Count the irradiated foils for 1-min intervals, using the gas-flow proportional counter. Count foils enough times so that an accurately representative plot of activity vs time after irradiation can be obtained.

5. With measured foil activity data, make the necessary decay and activation corrections and determine the calibration factor of the system. (Information on how bias correction and shelf-correction factors are made will be discussed and the actual values will be supplied.)

Suggested Data Format

Foil No.	10	12	15	15	etc.
Shelf	1	1	1	1	etc.
Time (after end of irradiation) min	10	12	14	16	etc.
Count time	1	1	1	1	etc.
Counts	3106	3716	283	4321	etc.

Errors that should be taken into account include:

a. Absolute errors on source calibration.
b. Error in measurement of distance between detector and source. (This should also include an assessment of the error in assuming the effective detector position to be at its physical center.)
c. Contribution from scattered radiation due to floor, walls, air, etc.
d. Statistical counting errors.

From your experimental data how may the half-life of ^{116}In be calculated? This calculation is of importance because it assures the health physicist that he has used the proper foil, that it is not contaminated, and that the background in the counter is not elevated or varying due to a strong source in the vicinity of the counting system.

REFERENCES

PRI W 58 W. J. Price, *Nuclear Radiation Detection* (McGraw-Hill Book Company, Inc., New York, 1958), Chapters 6 and 9.

STE L 58 L. D. Stephens and A. R. Smith, Fast Neutron Surveys Using Indium-Foil Activation, UCRL-8418, 1958.

Background Reading

This Manual, Vol. 1, Chapter 5.

G. Friedlander and J. W. Kennedy, *Nuclear and Radio-Chemistry* (John Wiley and Sons, Inc., New York, 1958), Chapter 5.

SHIELDING MEASUREMENT AT THE LBL 184-INCH CYCLOTRON

LLOYD D. STEPHENS

Experiment 6

Purpose

The attenuation of neutrons through a thick concrete shield is to be studied.

Theory

The penetration of neutrons through a shield depends on the behavior of the highest-energy component. High energy neutrons lose energy by either elastic or inelastic scattering, of which the latter is predominant. Inelastic scattering produces low energy secondary particles; when high energy neutrons produced in a cyclotron target enter the shield they generate low energy neutrons. An increase in low energy neutron intensity (or "buildup") should therefore be detected in the shield.

The intensity, I_x, of high energy neutrons surviving at depth x in the shield is given by

$$I_x = I_0 e^{-N\sigma x}, \qquad (1)$$

where I_0 is the incident intensity,

N is the number of atoms/cm^2,

σ is the inelastic cross section.

We can define buildup as the ratio of the neutron flux actually detected to that calculated by using Eq. 1.

Within a short distance into the shield particle equilibrium is achieved and exponential reduction of intensity is observed. Near the outside of the shield backscattering into the shield is indicated by a flattening of the transmission curve (see Fig. 6.1).

At neutron energies below about 50 MeV, elastic scattering processes can become increasingly important, but the general character of neutron transmission is governed by the high energy neutrons. Elastic scattering is extremely important, however, in energy reduction and thermalization (leading to capture) of neutrons.

Equipment

a. Gold foils (0.005 in. thick, 1 in. diam) suitably mounted for use in a gas-flow proportional counter.

b. Aluminum strip 1.5 in. wide, 13 ft long.

c. Gas-flow proportional counter and ancillary electronics.

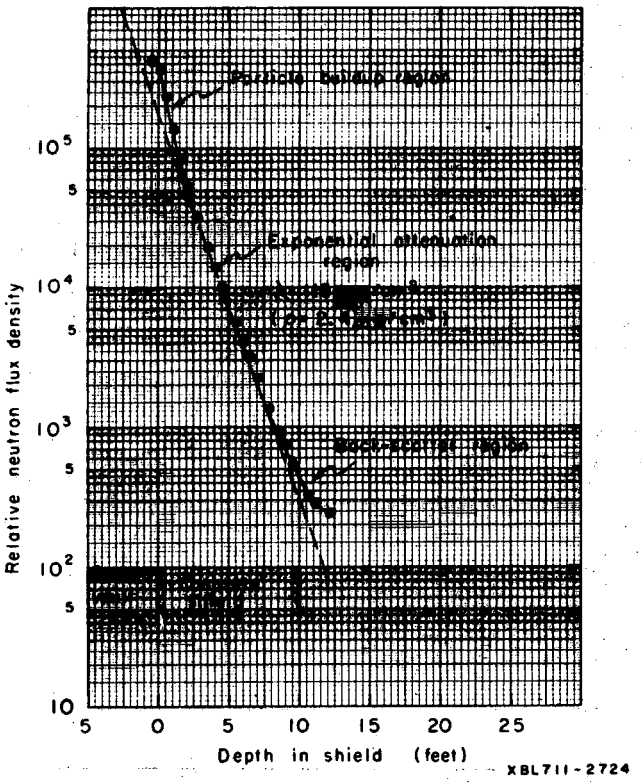

Fig. 6.1. Typical neutron transmission curve measured at the 184-inch synchrocyclotron with gold foils. The slope of the exponential attenuation region is 115 g/cm^2.

Laboratory Procedure

Gold foils are mounted at 6-in. intervals on the aluminum strip. The location of each identified foil on the aluminum strip is noted and the strip is then inserted in a very narrow crack in the east shield wall of the 184-inch synchrocyclotron. Irradiation of the foils should continue for about a week.

The relative transmission of thermal neutrons through the shield wall may be obtained from the relative activities of the gold foils. Thermal neutrons are captured in stable ^{197}Au to give radioactive ^{198}Au:

$$^{0}_{1}n + {}^{197}Au \rightarrow {}^{198}Au \xrightarrow[2.7\ \text{days}]{\beta^-} {}^{198}Hg.$$

Because the half-life of ^{198}Au is long (2.7 days), decay correction to the measured activities is inconsequential if counting is completed quickly (say within 1 to 2 hr). It will, however, be necessary to make corrections for individual variations in the masses of the gold foils. Counting should continue until individual statistical accuracies are within less than 1%. Plot

the relative corrected counting rates as a function of location in the cyclotron shield. If the logarithm of the relative counting rate is plotted against shield depth (it is convenient to use semilog graph paper) a straight line results at large depths in the shield. As shown in the theory section, a buildup of thermal neutrons is seen close to the accelerator, whereas near the outside of the shield backscattering into the shield is observed. Figure 6.1 shows a typical profile. Over a substantial range, however, the relative counting rate C_x at depth of x is represented by

$$C_x = C_0 e^{-x/\lambda}, \tag{2}$$

where x is the depth in the shield,

C_x is the relative counting rate at depth x,

C_0 is the relative counting rate at depth zero,

and λ is defined to be the *relaxation length*, or *attenuation length*, of neutrons in the shield.

An increase in shield thickness by one attenuation length, λ, reduces the neutron intensity by a factor of e. The attenuation length may be expressed in cm or, more usually, in g/cm^2. (The density of concrete in the cyclotron shield is 2.45 g/cm^3.)

It is often convenient in practice to evaluate the shield thickness that will reduce neutron intensity by a factor of 2 (half-value thickness, $x_{1/2}$) or 10 (tenth-value thickness, $x_{1/10}$). These are related to the attenuation length by the relations.

$$x_{1/2} = 0.693\,\lambda, \tag{3}$$

$$x_{1/10} = 2.30\,\lambda. \tag{4}$$

A good value of attenuation length is 120 g/cm^2.

Additionally, the reaction ^{27}Al (n,α)^{24}Na can be used to measure the neutron (or proton) flux of energy greater than about 6 MeV. The radionuclide ^{24}Na is a β^- emitter of 15-hr half life; its β decay is accompanied by emission of a cascade of γ rays at energies 2.754 and 1.368 MeV, each at 100% abundance. The high abundance of these γ rays, the relative transparency of our matrix material (aluminum), and the convenient magnitude of half-life favor the possibility of measuring very small quantities of ^{24}Na in large samples; that is, achieving quite high sensitivity from such a detector (SMI A 65, GIL W 68).

The induced ^{24}Na activity in the aluminum foil-holder strip can be measured with our high-sensitivity S7 γ-ray spectrometer system (see Experiment 10). The strip width and thickness have been chosen so that ^{24}Na activity can be accurately determined through the entire shield thickness, given a suitable irradiation period of normal high-intensity cyclotron operation. The strip should be marked off into 3-in. lengths, with each piece positively identified, and then cut into sections as marked.

The process of γ-ray counting may last 20 to 24 hours. Students are not expected to participate throughout this lengthy counting period; however, they are expected to keep track of progress, to weigh each sample so that counting data can be properly corrected, and to apply all other corrections to counting data so that experimental results can be obtained. Corrected counting data should be plotted and treated in the same fashion as the gold-foil data.

Plotted results from the two detectors should be carefully compared, to note—and explain—similarities or differences or both. Particular attention should be given three broad categories of sample location: near the inside shield surface, in the relatively thick shield interior, and near the shield exterior surface. Note that some of your conclusions could not be derived from the profile of either detector alone, although *much* information can be obtained from only one profile. In particular, the attenuation length can be derived from either profile.

REFERENCES

GIL W 68 W. S. Gilbert, D. Keefe, J. B. McCaslin, H. W. Patterson, A. R. Smith, L. D. Stephens, K. B. Shaw, G. R. Stevenson, R. H. Thomas, R. D. Fortune, and K. Goebel, 1966 CERN-LRL-RHEL Shielding Experiment at the CERN Proton Synchrotron, UCRL-17941, Sept. 1968.

SMI A 65 A. R. Smith Threshold Detector Applications to Neutron Spectroscopy at the Berkeley Accelerators, and Some Experimental Shielding Studies at the 6.2-BeV Berkeley Bevatron, in *Proceedings of the USAEC First Symposium on Accelerator Radiation Dosimetry and Experience, Brookhaven National Laboratory, November 3-5, 1965, 1965,* CONF-651109, pages 224, 365.

Background Reading

Samuel Glasstone and Milton C. Edlunds, *The Elements of Nuclear Reactor Theory,* second edition (D. Van Nostrand Co., Inc., 1954).

H. W. Patterson and R. H. Thomas, Experimental Shielding Studies at Accelerators--A Review, Particle Accelerators *2,* 77 (1971).

Richard Stephenson, *Introduction to Nuclear Engineering,* second edition (McGraw-Hill Book Company, New York, 1958).

RADIATION SURVEY AT THE BEVATRON, A 6-GeV PROTON SYNCHROTRON

A. JERRY MILLER

Experiment 7

Purpose

One of the activities of a Health Physicist at an accelerator installation is to measure and understand the radiation fields existing around the accelerator. Laboratory surveys with activation detectors take several hours or days to complete (Experiments 5 and 6). An alternative method using a moderated BF_3 counter has been studied in Experiment 3. An inexpensive and rugged detector combining activation and counter techniques has been used with success for many years at the Bavatron.

Theory

1. Detector System

The use of moderated thermal neutron detectors to monitor fast neutrons has previously been studied in Experiments 3 and 5. Silver may be used to detect thermal neutrons, through two capture reactions in ^{107}Ag and ^{109}Ag that occur in roughly equal quantities in naturally occurring silver:

$$\text{(a)}\quad {}^{109}\text{Ag}(n,\gamma)\,{}^{110}\text{Ag}. \qquad (1)$$

$${}^{110}\text{Ag} \rightarrow {}^{110}\text{Cd};$$

$$\beta^-,\ 24\ \text{sec}$$

$$\text{(b)}\quad {}^{107}\text{Ag}(n,\gamma)\,{}^{108}\text{Ag}, \qquad (2)$$

$${}^{108}\text{Ag} \rightarrow {}^{108}\text{Cd}.$$

$$\beta^-,\ 23\ \text{min}$$

Because the cross section for the first reaction is 110 b, almost four times as great as for the second reaction, the production of ^{110}Ag with a half-life of 24 sec dominates.

Exposure of a silver foil to thermal neutrons results in reaching an equilibrium activity very quickly (70% saturation in 1 min). The activity induced in silver therefore provides a convenient monitor of accelerator neutrons produced at a repetition rate of 1 per sec of slower. Detectors based on this principle have been used with great success at the Bevatron (SMI A 58), which has a pulse repetition rate of 10 pulses/min. Thin silver sheet ($\approx$ 0.010 in. thick) is wrapped around a halogen-quenched thin-walled Geiger-Müller counter. Fast neutrons are thermalized in a cadmium-covered polyethylene jacket and the radioactivity induced in the silver foil is

sampled by the counter. Output pulses from the GM tube are fed to an indicator unit consisting of a pulse amplifier, gating circuits, and scaling and readout stages. The gating circuits ensure that sampling occurs at a time when there is no production of prompt radiation. Changes in the level of radiation field are then indicated by changes in the detector readings presented after every accelerator pulse or group of pulses.

2. Use of Detector for Radiation Surveys

The stray radiation field of a large accelerator depends upon many variables. For example, at the Bevatron (the 6-GeV weak-focusing synchrotron at LBL) the positions and operation of internal targets, magnets, and related operational and experimental equipment often have a great influence on the neutron radiation levels. The study of the stray neutron fields outside its thick concrete shield yields information that can be directly related to the accelerator's mode of operation. This information in turn is valuable in predicting personnel exposure rates in certain work areas as a function of the accelerator's mode of operation and beam intensity.

Equipment

a. Four Ag GM fast-neutron detectors.
b. Four each amplifier, scaling, and readout units.
c. Scaler gating circuitry.
d. Oscilloscope.

Laboratory Procedure

a. Examine Figs. 7.1 and 7.2, which represent the Bevatron roof shielding itself.
b. Use one Ag GM detector as a monitor located on the "igloo roof."
c. Place the remaining three detectors on the roof shield directly above the beam orbit.
d. Observe the output pulses from the detectors to check that the counters are not saturated.
e. Integrate the detector readout over a convenient number of Bevatron pulses (the sampling counting period after each accelerator pulse is 3 sec). The readout is calibrated directly in neutron flux density. Reset scaler readouts and repeat until good statistical accuracy has been obtained.
f. Relocate three detectors, wait for 2 min to allow the silver activity to equilibrate in the new position, and continue as in Step 5.
g. Plot a graph showing the normalized flux densities as a function of position.

Errors

Possible sources of errors in the measurement are:

a. Incorrectly evaluated sensitivity of the detector because of inaccuracies in the original calibration.
b. Incorrect sample-counting time.

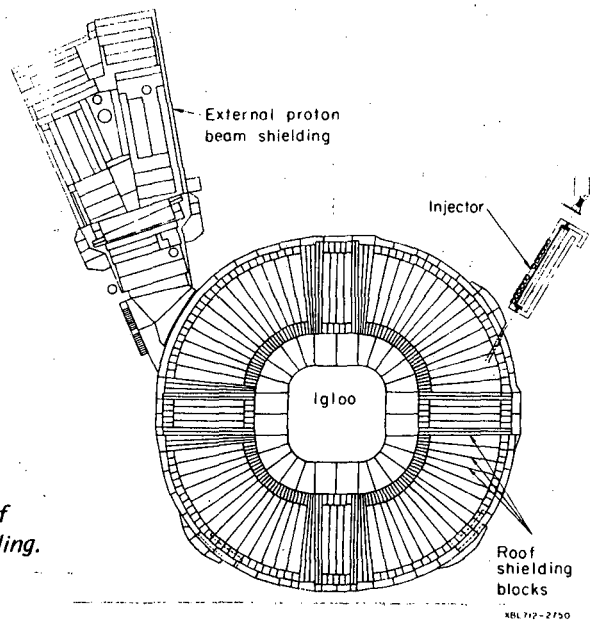

Fig. 7.1. Plan view of Bevatron shielding.

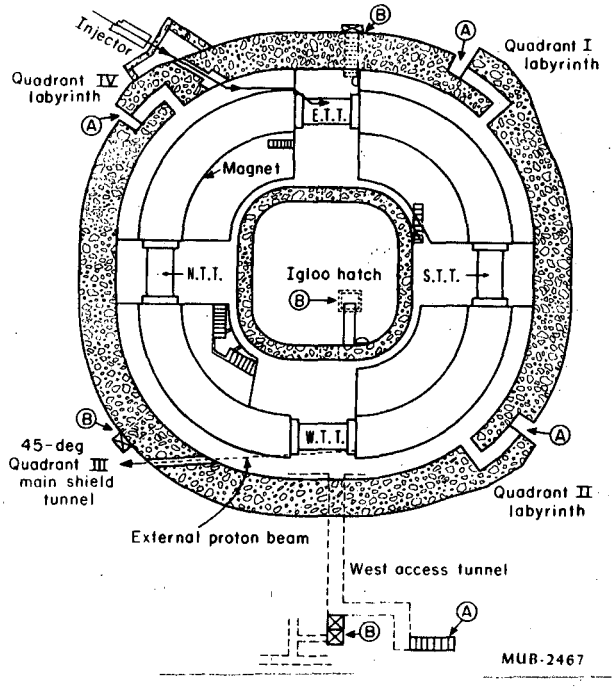

Fig. 7.2. Plan view of the Bevatron, showing relationships of accelerator to its shielding.

c. Failure to allow silver activity to reach equilibrium before recording data.

d. Dead-time counting losses (about 10% at counting rates of 2000 counts/sec).

REFERENCE

SMI A 58 Alan R. Smith, Measurement of Radiation Field Around High Energy Accelerators, in *Premier Colloque International sur la Protection auprés des Grands Accélérateurs, Orsay et Saclay, 18-20 January, 1962* Presses Universitaires de France, Paris, 1962), p. 137.

Background Reading

B. J. Moyer, Evaluation of Shielding Requried for the Improved Bevatron, UCRL-9769, 1961.

B. J. Moyer, Method of Calculation of the Shielding Enclosure for the Berkeley Bevatron, in *Premier Colloque International sur la Protection auprés des Grands Accélérateurs, Orsay et Saclay, 18-20 January, 1962* (Presses Universitaires de France, Paris, 1962), p. 137.

A. R. Smith, The Stray Radiation Field of the Bevatron, UCRL-8377, 1958.

Some Experimental Shielding Studies at the 6.2-BeV Berkeley Bevatron, in *Proceedings of the First Symposium on Accelerator Radiation and Experience, Brookhaven, November 3-5 1965;* CONF-651109, p. 365.

R. H. Thomas, The Radiation Field Observed Around High Energy Nuclear Accelerators (UCRL-16267m 1965, in *Progress in Radiology* Vol. 2 (Excerpta Medica Foundation, Amsterdam, 1967), p. 1849.

Shield Design Examples—The Bevatron (UCRL-16459, 1965), in *Engineering Compendium on Radiation Shielding,* Vol. 3 (Springer-Verlag, Berlin, 1970).

DETECTION OF NEUTRONS OF ENERGY GREATER THAN 20 MeV FROM THE PRODUCTION OF ^{11}C

JOSEPH B. McCASLIN

Experiment 8

Purpose

The methods of neutron measurement investigated in Experiments 2 through 6 have been limited to neutron energies below 20 MeV. At some high energy accelerators, however, the contribution to dose equivalent by neutrons of energy greater than 20 MeV is substantial and high energy neutron surveys must be made. This experiment studies one of the best techniques presently available, the ^{11}C counting system.

Theory

Use of the reactions $^{12}C(n,2n)\ ^{11}C$ and $^{12}C(p,pn)\ ^{11}C$ for health physics purposes has had a long history.

First use was reported by Sharpe and Stafford (SHA J 51), who counted the scintillations produced by ^{11}C positron decay in an organic crystal (anthracene) in order to measure the extraneous high energy neutron levels aroung the AERE 110-inch cyclotron at Harwell. Following this, Baranov and Goldanskii (BAR P 55) reported the use of stilbene or toluene, and later—with Roganov (BAR P 57)—used liquid organic scintillator material for this purpose. The first use of plastic scintillator material to monitor high energy neutron and proton fluxes was at the Bevatron and the 184-inch cyclotron (at Berkeley), as reported by McCaslin (McC J 60).

Neutrons and protons of energy greater than 20.4 MeV interact with ^{12}C nuclei to produce ^{11}C by (n,2n) and p,pn) reactions. ^{11}C decays with a half-life of 20.34 min through emission of positrons of maximum energy 0.98 MeV.

Plastic scintillator LBL or Pilot B) is used both for the target material and for the detecting medium; 1700-gram plastic scintillators (5 in. diam X 5 in.) are often used. They are exposed to an unknown neutron flux for a time usually not longer than 1 hour, and are then placed on top of 5-in.-diam photomultipliers for counting.

The positron energy is wholly contained in the scintillator (except for a negligible region near the surface), and a portion of the annihilation γ-ray energy is also contained. Each ^{11}C decay therefore produces a scintillation in the plastic and is detected and amplified by the multiplier phototube. This type of detector is called a 4π counting system; that is, essentially all the events occurring within the scintillator are detected regardless of their position within the scintillator or the direction of the emitted positron.

Neutron flux estimates are based on the amount of carbon in the scintillator and a reaction cross section of 22 mb. For 1700-g detectors

irradiated to saturation, 104 counts/min per unit flux density are obtained at zero bias (100% efficiency point) and zero time following irradiation.

It can be seen from Fig. 8.1 that for discriminator settings higher than about 5 V the ^{11}C count rate diminishes rapidly relative to the background count rate. For this reason a second discriminator is set at some high bias (or discriminator) level so that no events (^{11}C or background) that exceed this level are counted. A small percentage ($\approx$ 1%) of ^{11}C events is lost because their pulse heights exceed this level, but a large percentage ($\approx$40%) of background events is also lost, so that there is a net gain in sensitivity. (It will be recognized that a high background count rate can limit the sensitivity of a system by obscuring the events of real interest.)

Equipment

a. Plastic scintillator, 1700 g.
b. Lighttight photomultiplier assembly in low-level cave.
c. Preamplifier in low-level cave.
d. High voltage supply in counting area.
e. Amplifier and pulse shaper in counting area.
f. Single-channel analyzer in counting area.
g. Three decade scalers in counting area.
h. Timer in counting area.

Laboratory Procedure

1. Irradiate the plastic scintillator for up to 60 min in the neutron field to be investigated. (Longer irradiations will not significantly increase the measurable quantity of ^{11}C, but can lead to some longer-lived radionuclide production from reactions in the clay-based reflective paint on the scintillator surface, and are therefore to be avoided.) During irradiation the scintillators should be kept in plastic bags to prevent accidental contamination of, or electrostatic adherence of atmospheric radon to, the scintillator.

Plastic scintillators that are not protectively wrapped prior to being counted may exhibit a significant increase in background counting rate. This will be the case if there is a substantial concentration of radon daughter products in the air. The decay of these products and their rate of detachment from the scintillator combine to exhibit an effective half-life similar to that of ^{11}C, so that the radon could easily be mistaken for the carbon, especially when low-level measurements are being made.

2. Pulses from cosmic ray events are typically one or two orders of magnitude larger than those for ^{11}C. Many of these large pulses overdrive the amplifier and perhaps also overdrive the preamplifier. If this happens, an afterpulse may follow the initial pulse, and if this afterpulse is of sufficient amplitude it also is counted. Many amplifiers are designed to handle overload pulses in such a way that afterpulsing is not a problem. Preamplifiers are not usually so well suited to cope with overly large pulses. For that reason the photomultiplier and preamplifier gain must be limited to prevent overdriving the preamplifier (Fig. 8.2).

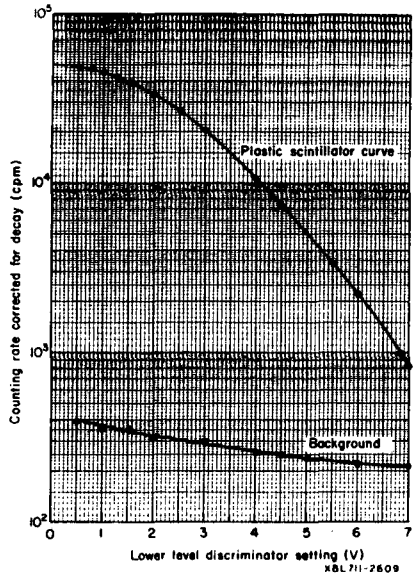

Fig. 8.1. Typical integral bias curves for ^{11}C counting systems. Efficiency between 0.5 and 7 V is 95%.

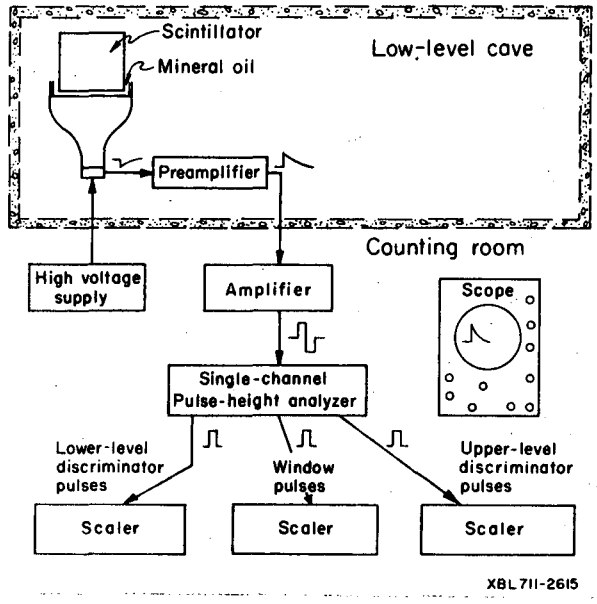

Fig. 8.2. Schematic diagram of ^{11}C counting electronics.

The oscilloscope can be used to determine if after pulsing is a problem by setting it to trigger only on the largest signals. The vertical sensitivity is then adjusted to about 0.5 V/cm, so that any disturbance of the base line following these large pulses can easily be seen. If base-line distrubances or afterpulsing exists, and if the magnitude of such disturbances exceeds the lower-level discriminator setting of the counting system, then corrective measures must be taken. This may mean only that the gain of the main amplifier must be increased while the photomultiplier-preamplifier gain is decreased, or it may be necessary to select a higher-quality nonoverloading main amplifier.

The high voltage setting is given at +900 V. Remember the discussion concerning the partitioning of gain between photomultiplier and main amplifier because of very large cosmic ray pulses in the scintillator. *High voltage must be turned off* before a scintillator is replaced or removed.

3. When the scintillator is brought into the room following irradiation, set the timer to the decay time, t_d (the time from the end of the irradiation to the start of the count).

4. With high voltage off (turned down slowly in 100-V steps and then off), place the scintillator, unpainted end down, on top of the photomultiplier, making certain first that there is sufficient mineral oil on the photomultiplier for optical coupling. Replace the lid and roll the shielding back over the top.

5. Turn high voltage on and increase the voltage slowly, in steps of 100 V, to 900 V.

6. On the oscilloscope note the size of the largest background pulses and the size of the largest ^{11}C pulses.

To determine whether the large background pulses are causing base-line distrubances, set the oscilloscope to 0.5 V/cm, and trigger the oscilloscope on the largest pulses. Note how much (in volts) the base shifts following large pulses. These distrubances must not be larger than the level selected for the lower-level discriminator.

7. With the oscilloscope on 5 V/cm and 10 μsec/cm and with single-sweep operation, look at several sweeps and see if the counting rate is too high. That is, with a pulse-pair resolution time of 8 μsec assumed, is a large fraction of the single sweeps such that pairs are close to 8 μsec apart? If so, the scintillator must be allowed to decay until counting losses become negligible. If not, proceed to the next step.

8. Run a discriminator curve at 0.5-V intervals from 0.5 to 3 V and at 1-V intervals from 3 to 10 V.

Correct the observed counts, N_d, for decay and saturation and calculate the saturated counting rate, A, at the end of the irradiation from

$$A\ (\text{counts/min}) = \frac{N_d - (B \times t_c)}{T\left|e^{-\frac{t_d}{T}} - e^{-\frac{(t_d + t_c)}{T}}\right|\left|1 - e^{-\frac{t_i}{T}}\right|}, \quad (1)$$

where N_d = observed counts (includes background),

B = background counting rate,

T = mean life = half-life/0.693,

t_c = counting time,

t_i = irradiation time,

t_d = decay time.

Equation 1 takes into account the decay during the counting interval, t_c.

10. Plot these results (draw an integral bias curve), and extrapolate to zero bias to get disintegrations/min. Compute the fraction of the total activity that falls within a given window, say 0.5 to 7 V, 1 to 7 V, 0.5 to 8 V, 1 to 8 V, 0.5 to 9 V, 1 to 9 V, etc. This fraction, for a particular window width, expressed as a percentage, is the efficiency.

Compare the number of counts in various window widths with the background in the same window. The % standard deviation in the observed count, when the background is well known and does not vary, can be computed from

$$\%\ \text{S.D.} = 100\sqrt{N_d/(N_d - Bt_c)}\ . \quad (2)$$

Use the window that minimizes the error.

Which window width would you use?

11. Find the neutron flux density, ϕ, that produced this activity in the scintillator:

$$\phi = \frac{A_w}{104\ E_w}\ \text{n/cm}^2\ \text{sec}, \quad (3)$$

where 104 counts/min per unit flux density is the calibration for 1700-g scintillators, and E_w is the counting efficiency in the window. A_w is the decay-corrected saturated counts/min in the window.

12. Now that the efficiency for a given window has been determined, all subsequent scintillators that one may wish to count can be counted on the scaler connected to the window of the single-channel pulse-height analyzer. This count is corrected to zero time and saturation by use of Eq. 1. The neutron flux density is then determined from Eq. 3.

How would the use of a multichannel/pulse-height analyzer assist in setting up a ^{11}C counting system?

REFERENCES

BAR P 55 P. S. Baranov and V. I. Goldanskii, Zh. Eksperim. i Teor. Fiz. *28* [5], 621 (1955).

BAR P 57 P. S. Baranov, V. I. Goldanskii, and V. S. Roganov, Rev. Sci. Instr. *28* [12], 1029 (1957).

McC J 60 Joseph B. McCaslin, A High-Energy Neutron Detector, Health Phys. *2*, 399 (1960).

SHA J 51 J. Sharpe and G. H. Stafford, Proc. Phys. Soc. (London) *A64*, 211 (1951).

184-INCH SYNCHROCYCLOTRON RADIATION SURVEY

ALESSANDRO RINDI

Experiment 9

Purpose

Experiments 3 through 5 have indicated some specialized techniques available to the accelerator health physicist in making surveys around an accelerator. A radiation survey around the 184-inch synchrocyclotron at the Lawrence Berkeley Laboratory (Fig. 9.1), using moderated BF_3 counters, puts these techniques into practice, showing how the data obtained are interpolated in terms of dose-equivalent (DE) rate. From these measurements the radiation safety procedures may be established.

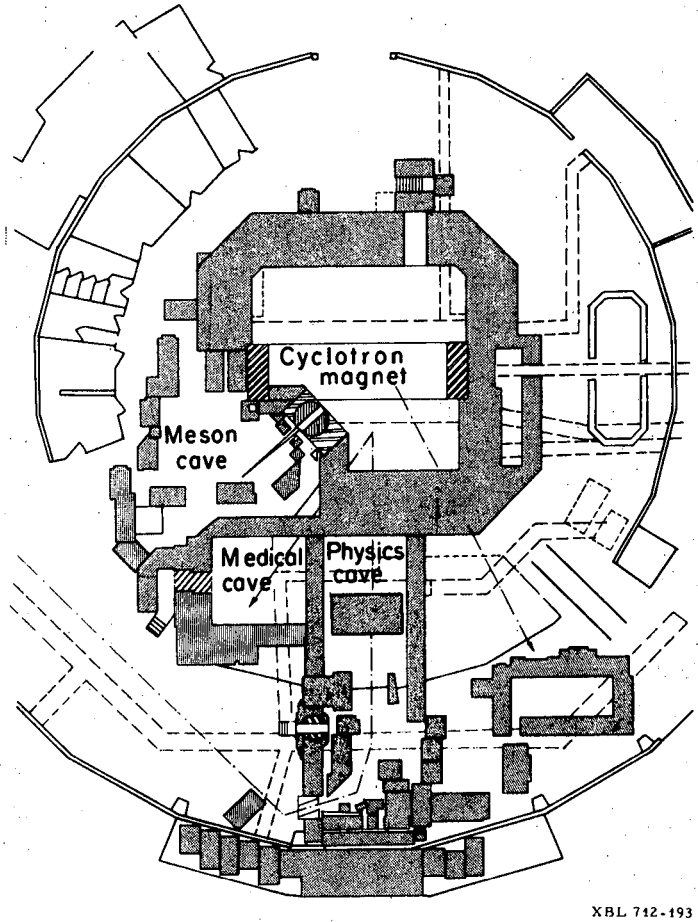

Fig. 9.1. Plan view of the 184-inch cyclotron.

Theory

In routine surveys it is often convenient to use only one detector rather than a complete set of threshold detectors (Experiment 11). Furthermore, in some circumstances radiation levels are too low to permit the use of activation detectors, in which case a convenient detector is a moderated BF_3 counter, provided the γ-ray and charged-particle contributions to dose are known to be small. Since this detector responds only to neutrons between about a few tens of keV and 15 MeV, it is necessary to correct its readings for the dose contribution from high energy neutrons. In practice it is found that these high energy neutrons contribute between 10% and 50% of the total dose equivalent. The fraction A of dose equivalent that falls within the range of the detector is given by

$$A = \int_{E_1}^{E_2} \phi(E)\, p(E)\, dE \Big/ \int_{E_{min}}^{E_{max}} \phi(E)\, p(E)\, dE, \qquad (1)$$

where $\phi(E)$ is the neutron spectrum,
$p(E)$ is a factor that converts flux density to dose equivalent,
E_1 and E_2 are the energy limits of sensitivity of the detector,
E_{min} and E_{max} are the energy limits of the spectrum.

If A is known for different neutron spectra, then a correction may be made to the readings of the instrument. Rindi (RIN A 68) and Gilbert et al. (GIL W 68) have reported such values for typical accelerator spectra. When used with spectra obtained at the 184-inch synchrocyclotron, a value of 6 n/cm^2 sec per mrem/h is appropriate if the moderated BF_3 counter is calibrated with a PuBe radium source. This conversion factor provides a small but not excessive overestimate of DE rate.

Equipment

a. Two portable moderated BF_3 counters.
b. Calibrated PuBe neutron source.
c. Plan of survey area.

Laboratory Procedure

Use one BF_3 counter as a monitor in a fixed position. The location chosen should be one where the radiation level is indicative of beam intensity and not strongly influenced by local perturbations.

Measure with the second counter at a sufficient number of locations to permit isodose contours to be drawn (to facilitate planning of radiation safety procedures). Individual measurements should be made with a statistical accuracy to within 10% or better, and the flux values should be normalized to constant monitor reading (proportional to internal beam intensity). Convert the normalized readings to DE rate.

Finally, on the basis of the findings, address a memorandum to the accelerator personnel responsible for operations and the experimental teams working in the area surveyed, setting out the results of the measurements and the safety measures to be adopted in consequence.

REFERENCES

RIN A 68 A. Rindi, Evaluation of Fluxes and Dose-Equivalent Rates in Neutron Fields Around High Energy Accelerators, UCRL-18424, Aug. 1968.

GIL W 68 W. Gilbert, D. Keefe, J. B. McCaslin, H. W. Patterson, A. R. Smith, L. D. Stephens, K. B. Shaw, R. Stevenson, R. A. Thomas, R. D. Fortune, and K. Goebel, CERN-LRL-RHEL Shielding Experiment at the CERN Proton Synchrotron, UCRL-17941, Sept. 1968.

GAMMA-RAY SPECTROSCOPY

ALAN R. SMITH

Experiment 10

Purpose

Both type and quantity of radionuclides can often be identified through detection of γ rays that accompany many radioactive decay processes. Among the numerous purposes for γ-ray detection, we will deal with the following three: γ-ray detection for determining the amount of a particular isotope present, as in measuring ^{65}Zn in dust from a cyclotron vault; γ-ray measurement to indicate the nature of an incident particle flux, as in activation-detector neutron spectroscopy (RIN J 63, ROU J 69a, SMI A 65); γ-ray measurement to indicate the quantities of stable trace elements present in certain matrix materials, as in neutron-activation analysis. The methods of γ-ray spectroscopy that employ a multichannel pulse-height analyser (PHA) are applicable in each of these cases, and serve as the basis for this laboratory study.

We proceed with these five objectives in mind:

a. To familiarize the student with the interaction of γ rays in matter and to indicate how the different interaction modes influence spectrometer response.

b. To familiarize the student with the operational principles of a large γ-ray spectrometer system, stressing the use of a pulse-height analyzer (particularly the analog-to-digital conversion unit), readout modes, and system gain stabilization.

c. To indicate the uses of γ-ray spectrometry to the accelerator health physicist in his routine operations. As a practical example the technique is applied to shielding measurements at the LBL 184-inch synchrocyclotron (Experiment 6).

d. To show the student how data obtained from γ-ray spectrometers are analyzed by computer techniques. We discuss and illustrate the processing of typical data. The scheme of peak area integration is thoroughly examined, and its application to simple-structured gain-stabilized spectra is the basis of an important part of the laboratory work.

e. To compare the relative merits of spectrometer systems, the characteristics and uses of the high-resolution Ge(Li) semiconductor crystal γ-ray spectrometer are discussed and illustrated. A Ge(Li) spectrometer system is used in the laboratory period, and this is contrasted with a NaI(Tl) spectrometer).

Theory

Ringle (RIN J 63) has summarized the basic theory of γ-ray spectroscopy in his Ph.D. thesis. His discussion of γ-ray spectrum formation is appended to this experiment, so the following discription is quite brief. (The student should familiarize himself with Ringle's summary, or equivalent, before undertaking the laboratory work.)

Gamma rays interact in the detector [NaI(Tl) or Ge(Li) in this case] by essentially three mechanisms: (i) photoelectric effect, (ii) Compton effect, and (iii) pair production. All three of these interaction modes produce secondary electrons, which deposit their energy in the detector, resulting in a scintillation in the NaI detector or an electronic pulse in the Ge(Li) detector. Figure 10.1 shows the absorption coefficients for the three basic processes for NaI. In the energy range of interest here (about 0.1 to 3 MeV) photoelectric and Compton processes are of most importance, although pair production becomes increasingly important above ≈ 1.3 MeV—particularly for Ge(Li) crystals.

The electronic pulses produced either by a solid-state detector of by a photomultiplier from a scintillation detector are proportional to the energy deposited and are amplified, amplitude-sorted, and stored in a pulse-height analyzer.

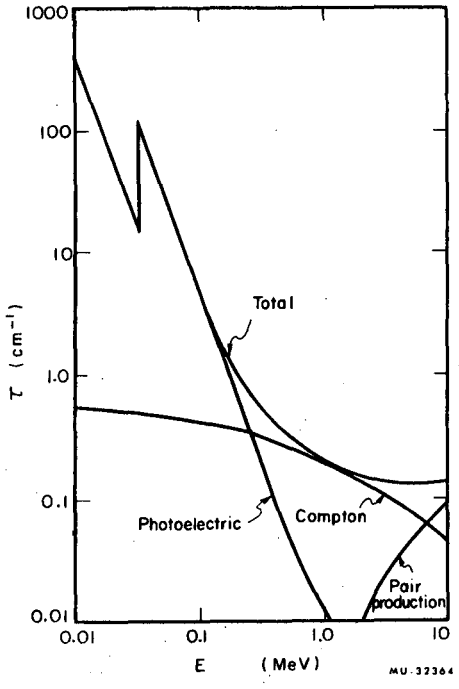

Fig. 10.1. Total linear γ-ray absorption coefficients as a function of energy for NaI (after Ringle).

Figure 10.2 shows a typical spectrum for ^{24}Na, which emits two γ rays of energy 1.368 and 2.754 MeV and β^- particles of maximum energy 1.39 MeV. In consequence the pulse-height spectrum is somewhat complex. A small peak corresponding to an energy of 4.12 MeV is seen, the so-called "sum peak" when two γ rays simultaneously deposit their entire energy in the detector; a peak occurs in the spectrum at an energy equal to the sum of the two individual γ-ray energies. The intensity of this peak is much less than that of either individual photopeak because of the small probability of the occurrence. Above energies of about 1.5 MeV, pair production is an important mechanism, and it is possible for some annihilation photons to be lost from the detectors. Figure 10.2 demonstrates that peaks occurring at energies of 0.51 and 1.02 MeV below the photopeak may be observed—corresponding to loss of one or both photons.

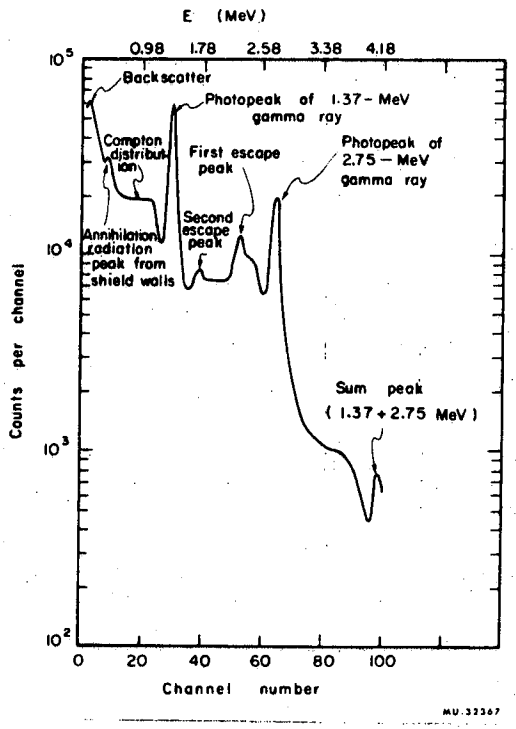

Fig. 10.2. Pulse-height distribution (γ-ray spectrum) obtained for ^{24}Na (after Ringle).

Because of the complexity of pulse-height spectra for even one radionuclide, the decomposition of a spectrum due to several emitters into its separate components may in practice be quite difficult. Ringle (RIN J 63) has summarized γ-ray spectrum-unfolding methods available up to 1963. More recently Routti (ROU J 69a, 69b) and Routti and Prussin (ROU J 69c) have studied this problem in Ge(Li) detectors and have written a general-purpose computer program for analysis of γ-ray spectra called SAMPO. For a discussion of these programs the interested reader is referred to the literature.

Equipment

Two spectrometer systems are available in the Health Physics group, the first utilizing a NaI(Tl) detector and the second using a Ge(Li) crystal. Detectors for both systems are located in the low-background counting facility.

The NaI(Tl) γ-ray spectrometer (the S7 system) consists of a crystal 20.3 cm in diam by 10.2 cm thick used in conjunction with a 400-channel pulse-height analyzer. In work in which detection of low activities is involved, high sensitivity, low background, and high stability are important. Because high sensitivity is an intrinsic property of a large NaI crystal, the response to background may also be correspondingly high. By careful selection of detector components and shield materials for low radioactivity, full advantage may be taken of the intrinsic high sensitivity of the detector.

The crystal is contained in a stainless steel case with a 17.8-cm-diam optical end window of fused quartz. A single 12.7-cm-diam EMI type 9530-Q photomulitplier—selected for its low activity, as its face plate and envelope are constructed of quartz—is optically coupled to the window with Dow-Corning silicone grease. The Teflon tube socket, voltage divider, phototube, and crystal assembly were incorporated into a single unit in our Laboratory.

The detector assembly is mounted in a vertical position inside a 10.2-cm-thick Pb brick shield. The crystal faces upward, and the entire assembly is supported on a low-mass styrofoam structure. Samples are usually placed on a thin steel plate that rests directly on the crystal case and serves to protect the crystal as well as to provide centering marks for sample placement. Styrofoam spacers are used to provide counting distances other than against the crystal. The preamplifier is located outside the Pb shield; thus, only the detector assembly and the two connecting cables are inside the shield. The shield interior volume has a 25-cm-square horizontal cross section with about 25 cm of vertical clearance above the crystal for sample placement. The shield opens at the top by means of a rolling door, also 10.2-cm-thick Pb.

Bricks for the inner 5 cm thickness were obtained from the St. Joseph Mine in Missouri, selected because of the known low activity of Pb from this source. The outer 5 cm thickness is also of low-activity Pb.

Background characteristics of this detector-shield combination as measured at LBL are shown on Table 10.1. Here we list the isotopes measured, the selected channel intervals, the spectral features included in these intervals,

the corresponding background rates, and the appropriate digital gain stabilizer (DGS) settings. We observe the γ-ray energy interval 0.1 to 4 MeV, at energy calibration of $\approx$ 10 keV/channel for 400-channel spectra. On Figs. 10.3 and 10.4 we show typical spectra of the measured isotopes as observed in our activation elements, together with a background spectrum; vertical bars on sample spectra indicate the selected analysis intervals.

Table 10.I. Characteristics of scintillation spectrometer (400-channel spectra).

Isotope	Channel interval	Spectral features included	Background at LBL (cpm)	DGS channel
^{7}Be	43-54	0.477-MeV peak	43.6	48
^{22}Na	45-59	0.511-MeV peak	47.9	51
	160-190	Sum peak (0.511 plus 1.27 MeV)	13.2	51
^{24}Na	120-289	1.37-MeV peak through 2.75-MeV peak	72.4	134
^{116m}In	100-144	1.10-MeV peak through 1.29-MeV peak	46.8	126
^{198}Au	37-47	0.412-MeV peak	37.0	41

NaI(Tl) data are acquired as 400-channel spectra, providing sufficient spectral detail for computer analysis of the structure revealed by this detector without employing an unnecessarily large number of data channels. Digital channel count information from each spectrum is permanently recorded on punched paper tape, and may also be plotted in analog format on an X-Y point plotter. Each spectrum is assigned a *run number*, and pertinent indicative data concerning the sample spectrum are also recorded; the digital spectrum and all indicative data are then transferred to a computer-compatible format on standard magnetic tape, for preservation in a data library and for any subsequent computer processing. The spectrometer system includes a *digital gain stabilizer* (DGS) to enable the operator to fix exactly and maintain indefinitely the gain (energy calibration) parameter for acquisition of any spectrum that contains a peak—or a valley— in its structure. Thus unit derives its corrective signal from digital channel-address information generated in the PHA, and uses this information in such a way that the action taken is not count-rate-dependent. Its use is demonstrated in the laboratory, in particular to illustrate the well-known gain-vs-count-rate problem associated with scintillation crystal spectrometers. The relationship of this problem to computer processing of spectrometer data will also be discussed.

Correct energy calibration of the spectrometer system is nominally maintained by occasional checks with a ^{137}Cs source; of course, use of the DGS unit insures the correct energy calibration for all cases that contain peaks of known energy. Detector efficiency is monitored with the same ^{137}Cs source, an IAEA standard with a listed absolute emission rate known to within $\pm$2%.

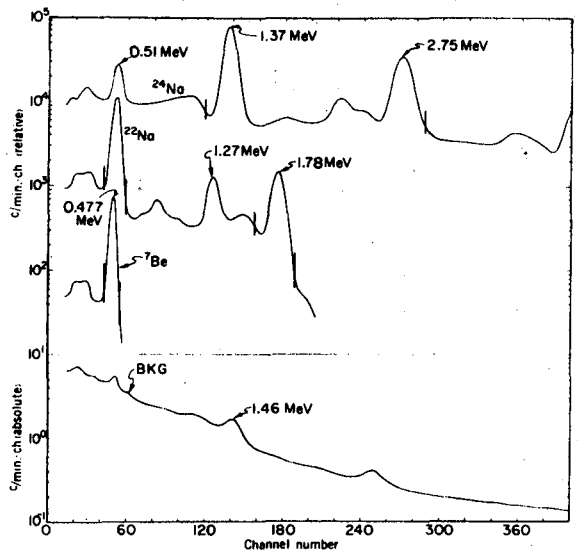

Fig. 10.3. Typical γ-ray spectra obtained from ^{7}Be, ^{22}Ne, and ^{24}Na with the LBL NaI detector.

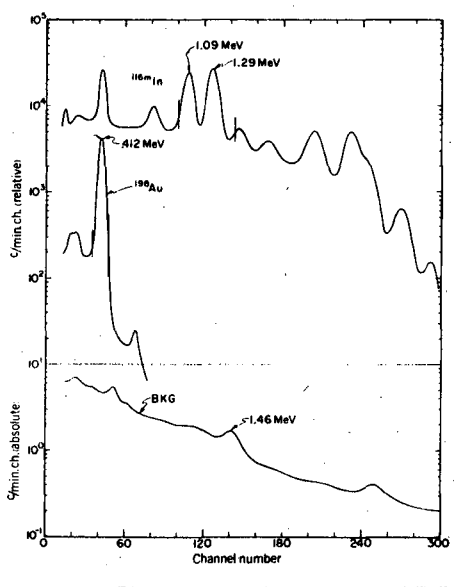

Fig. 10.4. Typical γ-ray spectra obtained from ^{116m}In and ^{198}Au with the LBL NaI detector.

Data from the high-resolution Ge(Li) detector (the G3 spectrometer system) are obtained as 1600-channel spectra at gain conversions of approximately 0.25 or 1.0 keV/channel. The G3 crystal is a 10-cm^3 volume planar detector of circular shape and approximately 1.0 cm active thickness. It is housed in a cryogenic vacuum system and employs a cooled-FET input-stage preamplifier with electronic feedback. A high-rate RC-shaping amplifier sends these pulses to the PHA for amplitude sorting and data storage.

Ge(Li) spectra are characterized by very narrow peaks (typically less than 1/10 the width of NaI peaks) that lie on relatively simple continuous distributions. Compton edges and their respective total absorption peaks are widely separated and completey noninterfereing. Single and double escape peaks, from γ rays of energies above $\approx$ 1.3 MeV, are prominent features of these spectra; although increased spectral complexity arises from this effect, such peaks can be extremely useful for analysis purposes. In Figure 10.5 we contrast NaI and Ge(Li) spectral shapes for the single 661.6 keV γ ray from ^{137}Cs decay. The Ge(Li) points represent actual counts per channel as indicated by the ordinate scale; NaI data have been adjusted to fit conveniently on the graph. If the two data sets were normalized in terms of absolute detection efficiency, the NaI peak would lie about two orders of magnitude above the Ge(Li) peak. Herein resides the greatest single disadvantage of the Ge(Li) crystal: its low absolute detection efficiency for γ-ray energies above about 200 keV.

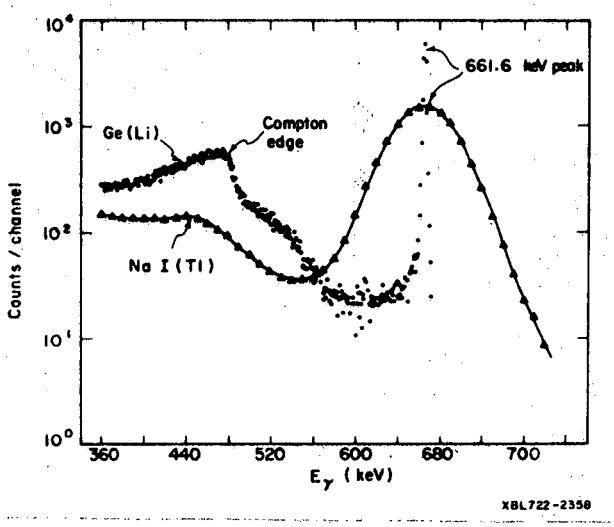

Fig. 10.5. Comparison of NaI (Te) and Ge (Le) spectra for ^{137}Cs 661.6 keV-γ rays.

In order to take full advantage of the intrinsic high resolution of the Ge(Li) crystal, a large number of data channels is required, and a sophisticated general-purpose computer program must be available to process so large a volume of information. Typical spectra, from either threshold-detector neutron spectroscopy or neutron-activation analysis, may contain 20 to 200 peaks in the energy interval 50 to 1600 keV. Peaks of interest often overlap (are not clearly separate from adjacent peaks) in a multiplet structure, and cannot be successfully analyzed by hand computation on a routine basis. Computer program SAMPO is used for all analysis of these spectra. (The SAMPO program will be explained or demonstrated—or both—to interested students.) Through use of SAMPO, certain *spectral quality* requirements become evident. For example, we are limited to 1600 data channels, and often accumulate spectra for the energy range 50 to 1600 keV at 1 keV per channel. Although singlet and doublet peaks are properly treated, the program has difficulty resolving triplets when member peaks are spaced closer than the detector resolution parameter. (The resolution, full width at half-maximum, is 1.5 keV at 120 keV.) There are simply not enough data points for the fitting routines. However, if the energy scale is expanded to 0.25 keV/channel, SAMPO fitting of the above triplet case proceeds with complete success. The implication is clear, and somewhat sobering: to use the full capability of an analysis program of the SAMPO type, 8000 to 10000 data channels should be employed when the energy interval of 50 to 2000 or to 3000 keV is to be analyzed from spectra that cover the complete energy range. Note that it is always inconvenient, often impractical, and sometimes impossible to study this energy interval by means of several spectra, each covering a fraction of the total interval.

Procedure

The characteristics of spectra obtained from several γ-ray emitters are studied. Spectra are displayed both for isotopically pure radionuclides and for materials irradiated under laboratory conditions. The relative importance of photoelectric scattering, Compton scattering, pair-production processes, and energy losses from the detectors to the observed pulse-height spectra are demonstrated. The relative merits of the NaI(Tl) and Ge(Li) detectors are indicated. Use of the Ge(Li) detector for quick identification of unknown γ-ray emitters will be demonstrated, as well as its application to nondestructive analysis of samples that contain very complex mixtures of γ-ray emitters. Both these applications will make evident the need for a library containing high-precision data for energies and intensities of γ rays from the various radionuclides.

As a practical example of the use of the NaI γ-ray spectrometer in routine accelerator health physics, we refer to Experiment 6. In this shielding study, use was made of a thermal-neutron capture reaction to establish the attenuation profile through the concrete structure. The aluminum strip,

nominally the gold foil holder, was also analyzed for ^{24}Na activity, the product of a reaction whose threshold is about 6 MeV neutron energy. The similarities and differences between these two profiles draw attention to important concepts of shield design and performance. Significant conclusions can be obtained from this comparison that would not be evident from either profile alone.

APPENDIX A

Formation of γ-Ray Spectra (from RIN J 63)

Interactions of γ rays with matter are discussed in the background reading and references. The interactions discussed only briefly here, as they are generally common knowledge, and the above references supply much more detail on any particular aspect. In this problem the interactions in a sodium iodide thallium-activated [NaI(Tl)] scintillation crystal are the main consideration, since our detector is of this type.

Gamma rays interact in a NaI(Tl) crystal (as in all other matter) in essentially three ways: the photoelectric effect, the Compton effect, and pair production. All three of these processes produce secondary electrons which deposit their energy in the crystal and produce the scintillations. Also in all three processes it is predominantly the iodine that interacts with the γ rays because of its high charge (Z).

In the photoelectric effect a γ ray interacts with a bound electron, and all the γ-ray energy is transferred to the electron. The electron is ejected from the atom with a kinetic energy equal to the γ-ray energy less its binding energy in the atom. This electron vacancy usually occurs in the K shell, and when this vacancy is filled by another electron a K x ray is emitted. For iodine this x ray has an energy of 0.028 MeV. The absorption coefficient (or cross section) for this process varies as Z^5 and decreases rapidly for increasing γ-ray energy.

The Compton effect can be considered as an elastic collision between the γ ray and a free electron; the γ ray gives some of its energy to the electron, and it may then interact again by the Compton effect or the photoelectric effect. The kinetic energy given to the scattered electron is a variable fraction of the initial γ-ray energy, depending upon the scattering angle. The absorption coefficient for this process varies as Z and decreases slowly with increasing γ-ray energy.

Pair production must occur in the Coulomb field of an atomic nucleus, and in this process the γ ray disappears and an electron and a positron are created. The kinetic energy of the pair is essentially equal to the initial γ-ray energy less 1.02 MeV (the rest mass of the pair); thus the initial γ-ray energy must be at least 1.02 MeV for this interaction to occur. The absorption coefficient for this process varies as Z^2 and increases with increasing γ-ray energy.

Other minor γ-ray interactions can occur, such as (i) the nuclear photoelectric effect, in which high-energy photons eject neutrons from high-Z materials, and (ii) Compton scattering by nuclei rather than electrons. For practical purposes all these other minor effects can be neglected.

The absorption coefficients for the three basic processes, along with the total absorption coefficient, are shown in Fig. 10.6 for NaI. Below about 0.1 MeV the photoelectric process is dominant. From about 0.1 to 0.4 MeV the photoelectric and Compton processes are both important; from about 0.4 to 2 MeV the Compton process alone is dominant. From about 2. to 7 MeV both the Compton and pair-production processes are significant, and above about 7 MeV the pair-production process alone becomes predominant.

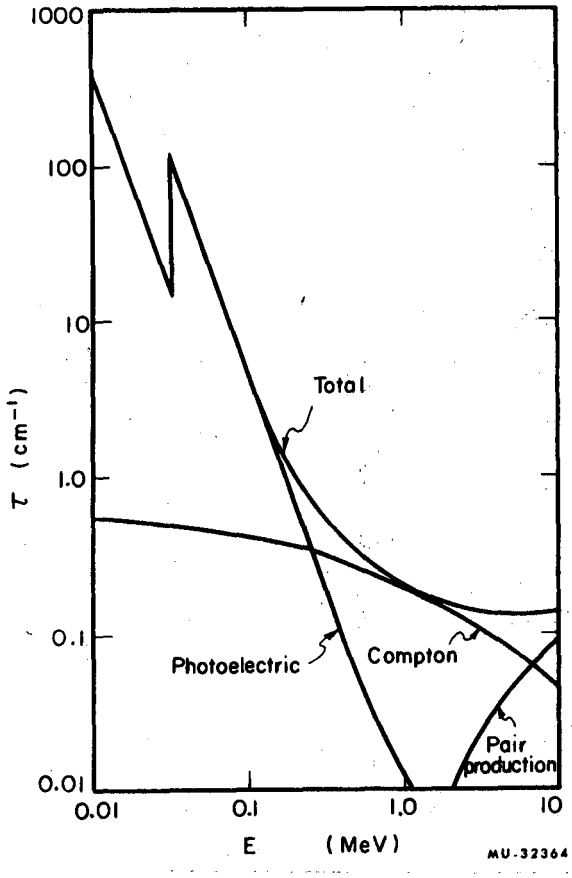

Fig. 10.6. Total linear γ-ray absorption coefficient vs. energy for NaI.

The γ rays we will be observing primarily have energies in the range 0.1 to 2 MeV; thus, photoelectric and Compton processes are our main consideration, although some pair production is observed around 2 MeV.

After the γ rays interact and deposit energy in the NaI(Tl) crystal this energy is released as a light pulse, or scintillation. This process is explained in detail in the background reading and is discussed here only so far as it affects the observed pulse-height spectrum. The light pulses emitted by the scintillation crystal are proportional to the energy deposited in the crystal by the γ ray. These pulses are collected and stored in a PHA and are displayed as the number of pulses of a given height vs pulse height (or channel number in the PHS). This is called a pulse-height spectrum, or a γ-ray spectrum, since the pulse height is proportional to the γ-ray energy.

To show that this is true, let us consider the γ-ray energy deposited by each process. In the photoelectric process, the secondary electron is quickly stopped and gives its energy to the NaI (Tl) crystal. Photoelectric processes occur most readily when the γ-ray energy is low, thus the γ ray does not penetrate very far into the crystal and the interaction usually occurs near the surface of the crystal. The K x ray then has a good chance of escaping from the crystal without depositing its energy. In this case the total energy deposited in the crystal equals the initial γ-ray energy less the K x-ray energy. In the pulse-height spectrum a peak would appear at a pulse height corresponding to the initial γ-ray energy less the K x-ray energy. The γ ray γ_1 in Fig. 10.7 illustrates this process.

When the incident γ-ray energy increases, the γ ray penetrates further into the crystal before interacting, and there is a higher probability that its K x ray will be captured in the crystal. When this happens the total energy deposited in the crystal is equal to the total energy of the incident γ ray, and a peak appears in the pulse-height spectrum at a pulse height corresponding to the total energy of the incident γ ray. This is illustrated by γ_2 in Fig. 10.7.

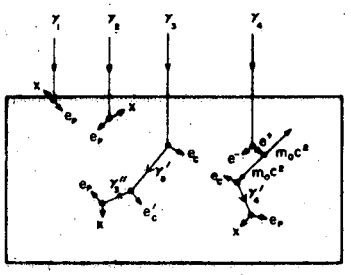

Fig. 10.7. Various γ-ray interactions in NaI(Tl) crystal.

Thus, at low γ-ray energies two peaks can occur in the pulse-height spectrum: one at a pulse height corresponding to the incident γ-ray energy, and one 0.028 MeV below this. Because the difference between these two peaks is small in absolute magnitude, and because at higher γ-ray energies the K x-ray energies the K x ray is almost always captured in the crystal, these two peaks are not observed separately at γ-ray energies above 0.170 MeV. Only one peak occurs at a pulse height corresponding to the incident γ-ray energy: this is called the photoelectric absorption peak or photopeak. The photopeak of ^{65}Zn is shown in Fig. 10.8.

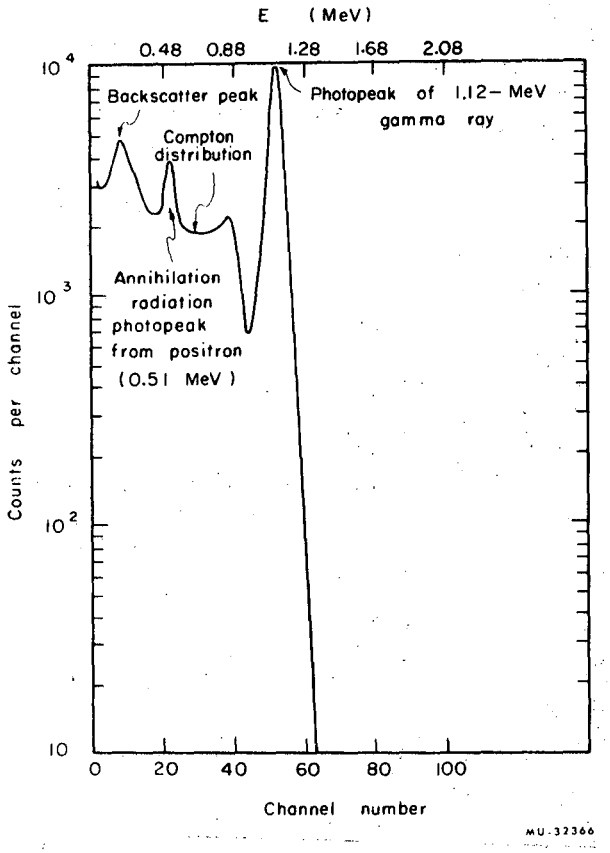

Fig. 10.8. Gamma-ray spectrum of ^{65}Zn.

The energy deposited in the Compton process is more variable. The energy of the Compton electron, e_c, is quickly deposited in the crystal, but the scattered γ ray γ_3' may escape from the crystal or interact further. If it escapes, a peak appears in the pulse-height spectrum corresponding to the energy of e_c. If γ_3' scatters and produced e_c' and γ_3'' (which then escapes), a peak appears at the energy of $e_c + e_c'$. If γ_3 is completely contained, as shown in Fig. 10.8, then a photopeak appears at an energy $e_c + e_c' + e_p + X$, i.e., the total energy of γ_3. The time of these interactions is so fast with respect to the decay time of a light pulse from NaI(Tl) that these events appear to be simultaneous, and only one light pulse corresponding to the photopeak is emitted by the crystal. This is called a multiple process—photoelectric plus Compton.

Usually in the Compton process, however, one of the scattered γ rays (γ_3' or γ_3'') escapes from the crystal, and a pulse appears in the spectrum at an energy below the photopeak (or incident γ-ray) energy. These pulses can appear at any fraction of the incident γ-ray energy, depending upon the scattering angle. When many γ rays interact having about the same number of pulses at each pulse height, from the incident γ-ray energy down to essentially zero energy. This continuous Compton distribution is shown for ^{65}Zn in Fig. 10.8.

One anomaly in this continuous distribution is the dip or "valley" at an energy just below the photopeak energy. A pulse in this region corresponds to the escape of a low-energy scattered γ ray (the rest of the incident γ-ray energy has been deposited in the crystal by the Compton electrons), and the escape probability of such a scattered γ ray is low unless the final interaction occurs near the crystal surface. Fewer of these events occur, hence the dip from the continuous distribution.

The pair-production process, illustrated by γ_4 in Fig. 10.7, presents the most complications. The initial process forms an electron, e^-, and a positron, e^+. The electron quickly deposits its energy in the crystal and the positron readily annihilates with another electron and emits two annihilation γ rays of m_0c^2 (0.511 MeV) each. These two γ rays may then interact by the Compton or photoelectric process, or one or both may escape. If one escapes and the other, by various processes, deposits all its energy in the crystal, a peak occurs at an energy of 0.511 MeV less than the incident γ-ray energy. This is called the single-escape peak. If both escape, a double-escape peak occurs at an energy of 1.02 MeV less than the incident γ-ray energy. If neither escapes and all the energy is deposited in the crystal, a pulse occurs at the incident γ-ray energy. Continuous Compton distributions are also possible between these three peaks and below the double-escape peak. These correspond to the escape of scattered γ rays of various energies.

The pair-production effect is not observed for incident γ-ray energies below about 1.5 MeV, and for a crystal of our size the double-escape peak is understandably small. Figure 10.9 illustrates this effect for ^{24}Na.

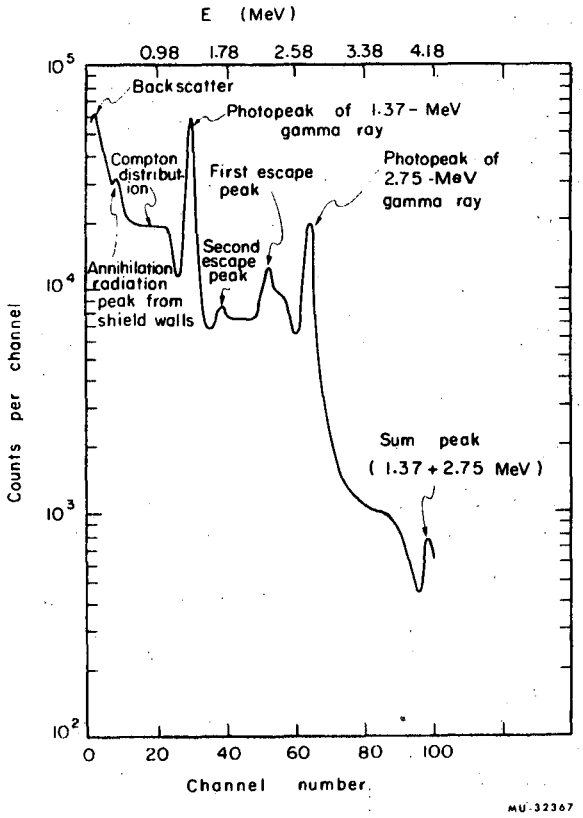

Fig. 10.9. Gamma-ray spectrum of ^{24}Na.

Another phenomenon occurs which complicates the pulse-height spectrum: the backscatter peak (see Figs. 10.8 and 10.9). This results when the incident γ ray undergoes a large-angle Compton scattering from the shield walls, then enters the crystal and deposits its remaining energy. The remaining energy of this scattered γ ray is nearly independent of the incident γ-ray energies from 0.2 to 2.0 MeV. Due to the small interior dimensions of our cave a large backscatter peak at about 0.200 MeV is always present in our spectra.

The incident γ rays can also interact by the photoelectric effect in the lead shield walls, and the lead K x ray of 0.072 MeV can escape from the walls and be detected by the crystal. Our detector system has a low-energy threshold of 0.080 MeV, however, so this effect is not observed.

When the incident γ-ray energy is above about 1.5 MeV, a peak at 0.511 MeV usually is observed in the pulse-height spectrum. The incident γ rays interact by pair production in the lead shield walls, and some of the

annihilation γ rays escape from the walls and deposit their energy in the crystal.

When the source emits positrons these are annihilated quickly in the source material, the shield walls, or the NaI(Tl) crystal. The annihilation radiation that is deposited in the crystal appears as a photopeak at 0.511 MeV, and this is a prominent feature in the spectrum of any source emitting a positron. Figure 10.8 illustrates this.

If the source emits β particles, these lose energy by radiation when they pass through the Coulomb field of a nucleus. This radiation is called bremsstrahlung; it results in a continuous energy distribution of photons from zero energy to the β-particle end-point energy. When these photons deposit their energy in their crystal, a pulse-height spectrum continuous in energy results. The magnitude of this effect depends on the Z of the material absorbing the β particles and upon the β-particle energy. The effect of this bremsstrahlung radiation upon the pulse-height spectrum is difficult to analyze quantitatively; fortunately, the effect is usually negligible unless the source disintegrates by high-energy β-particle emission a large part of the time. We have essentially eliminated the bremsstrahlung problem by considering sources that either emit no β particles or emit them only a small part of the time.

One further complication to the pulse-height spectrum is the sum peak. This can occur when two γ rays are emitted simultaneously by the source. If they both deposit their entire energy simultaneously in the crystal, a photopeak occurs in the spectrum at an energy equal to the sum of the two individual γ-ray energies. The intensity of this peak is lower than the intensity of either of the individual γ-ray photopeaks by a factor of 100 or more, due to the small probability of the γ rays' depositing their energy in the crystal at exactly the same time. A continuous energy distribution also occurs due to various fractions of the two γ-ray energies' being deposited in the crystal simultaneously. This effect can be reduced by increasing the source-to-detector distance, and it is such a small contribution to the spectrum that it can be neglected for almost all practical purposes. Figures 10.9 and 10.10 show the sum peak for ^{24}Na and ^{60}Co.

When a source emits γ rays of more than one energy, the resultant pulse-height spectrum is the sum of the responses to each individual γ ray. Figure 10.11 shows the spectra from ^{65}Zn and ^{54}Mn counted separately, and also the composite spectrum when the two sources were counted together. The photopeak of the 1.12-MeV γ ray from ^{65}Zn and its associated higher-energy Compton distribution are unchanged.

The photopeak of the 0.84-MeV γ ray from ^{54}Mn appears more intense than when measured separately, since it is superimposed on the Compton distribution from the ^{65}Zn γ. The positron photopeak from ^{65}Zn is similarly higher, since it is superimposed on the Compton distribution from

the ^{54}Mn γ. The backscatter peak and Compton distribution below the ^{54}Mn photopeak are the sum of individual backscatter peaks and Compton distribution from the ^{54}Mn and ^{65}Zn γ rays.

One can easily see that when the source emits several γ rays the resultant spectrum can become quite complex.

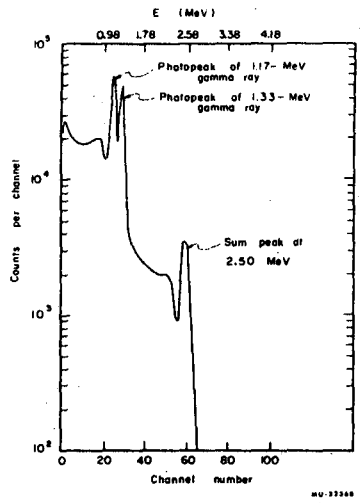

Fig. 10.10. Gamma-ray spectrum of ^{60}Co.

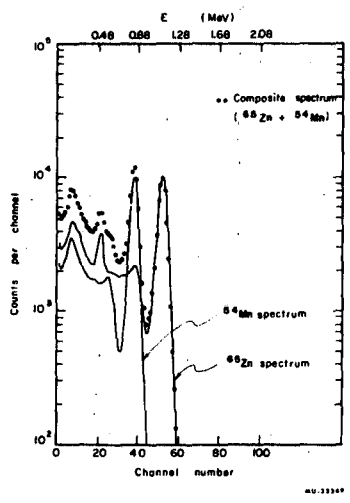

Fig. 10.11. Gamma-ray spectra of ^{65}Zn and ^{54}Mn. and composite spectrum.

REFERENCES

RIN J 63 J. C. Ringle, A Technique for Measuring Neutron Spectra in the Range 2.5–30 MeV Using Threshold Detectors, UCRL-10732, Oct. 1963.

ROU J 69a J. T. Routti, High Energy Neutron Spectrometry With Activation Detectors Incorporating New Methods for the Analysis of Fe(Li) Gamma-Ray Spectra and the Solution of Fredholm Integral Equations (Ph.D. thesis), UCRL-18514, April 1968.

ROU J 69b J. T. Routti, SAMPO--A Fortran IV Program for Computer Analysis of Gamma Spectra from Ge(Li) Detectors, and for Other Spectra with Peaks, UCRL-19452, Oct. 1969.

ROU J 69c J. T. Routti and S. G. Prussin, Photopeak Method for the Computer Analysis of Gamma-Ray Spectra from Semiconductor Detectors, Nucl. Instr. Meth. *72*, 127 (1969).

SMI A 65 A. R. Smith, Threshold Detector Application to Neutron Spectroscopy at the Berkeley Accelerators, in *Proceedings of the USAEC First Symposium on Accelerator Radiation Dosimetry and Experience, Brookhaven National Laboratory, November 3-5, 1965,* CONF, 651109, p. 365.

Background Reading

G. Bertolini and A Coche, eds., *Semiconductor Detectors* (John Wiley and Sons, New York 1968).

J. Birks, *The Theory and Practice of Scintillation Counting* (Pergamon Press, Oxford, 1964).

G. T. Chapman, Chairman, *Proceedings of the Total Absorption Gamma-Ray Spectrometry Symposium, Gatlinburg, Tennessee, May 10-11, 1960,* U.S. Atomic Energy Commission Report TID-5594, 1960 (unpublished).

C. E. Crouthamel, *Applied Gamma-Ray Spectrometry* (Pergamon Press, Ltd., New York, 1960).

J. R. Devoe, Ed., *International Conference on Modern Trends in Activation Analysis, Gaithersburg, Maryland, 1968* (U.S. Government Printing Office, Washington, 1969).

R. C. Kock, *Activation Analysis Handbook* (Academic Press, New York, 1960).

G. D. O'Kelley, Detection and Measurement of Nuclear Radiation, National Academy of Sciences Report NAS-NS-3105, April 1962 (unpublished).

W. J. Price, *Nuclear Radiation Detection* (McGraw-Hill Book Co. Inc., New York 1964), Chaps. 7 and 8.

P. Pringsheim, *Fluorescence and Phosphorescence* (Interscience Publishers, Inc., New York, reprinted 1961), Chap. VII.

S. M. Shafroth, Ed., *Scintillation Spectrometry of Gamma Radiation* (Breach Science Publishers, London, 1967).

K. Siegbahn, Ed., *Alpha, Beta, and Gamma-Ray Spectroscopy* (North-Holland Publishing Co., Amsterdam, 1965).

DETERMINATION OF NEUTRON SPECTRA FROM THRESHOLD DETECTOR DATA

JORMA T. ROUTTI AND ALAN R. SMITH

Experiment 11

Purpose

This experiment illustrates some of the problems that can arise in the determination of accelerator neutron-energy spectra by using threshold detectors (or other energy-sensitive neutron detectors). The use of the open-loop computer program TELLY in conjunction with an interactive cathode-ray-tube (CRT) display enables the student to "see" in a graphic way the influences of the various energy responses or input data errors (or both) on computed spectral results.

Theory

There are several experimental methods for determining neutron spectra. In health physics, activation detectors, nuclear emulsions, and Bonner spheres are widely used.

The neutron spectrum to be studied is characterized by energy and intensity ranges extending over many orders of magnitude, by very small flux values beyond any considerable thickness of shielding, and by omnidirectionality. The use of activation detectors has proven to be one of the best techniques to measure such neutron fields. The relative merits and experimental aspects of such detectors—including threshold detectors, moderating spheres, and nuclear emulsions—have been adequately discussed in earlier studies, many of which were presented in the First Symposium on Accelerator Radiation Dosimetry and Experience (CONF 65).

The use of activation detectors does not, however, yield directly the neutron energy spectrum. A mathematical unfolding procedure is required to obtain the spectrum from the set of measured data.

Several numerical methods have been porposed for the solution of neutron spectra from activation measurements. Many of these techniques are difficult to apply to high-energy neutron spectroscopy. Some of the problems arise from the mathematical characteristics of the equations to be solved, others are related to specific solution methods. These problems are often compounded by large uncertainties in the response functions of the detectors and in the measured data. However, critical use of an appropriate solution technique can yield reliable neutron spectra, the resolution of which, although limited, is quite adequate to aid shielding design and operational safety.

Measurement of radioactivity induced by neutrons provides information on the flux. Study of several activation reactions with different known

energy-dependent response functions, or cross sections, enables us to obtain knowledge of the energy distribution of the neutron flux. Specifically, in activation-detector spectroscopy we search for a solution for a neutron spectrum $\phi(E)$ from a set of activation equations of the form

$$A_j = C_j \int_{E_{min}}^{E_{max}} \sigma_j(E)\, \phi(E)\, dE, \quad \text{for } j = 1 \cdots, m. \tag{1}$$

Here A_j is the saturation activity of the j th detector, $\sigma_j(E)$ is the corresponding response function, and C_j is a normalizing constant between count-rate and neutron flux units. The normalizing constants--sometimes difficult to specify--are taken to be equal to unity in the following. E_{min} and E_{max} define the energy range of the neutron spectrum, and m gives the number of detectors, normally between 4 and 15. Equation 1 is a degenerate case of a Fredholm integral equation of the first kind,

$$A(E') = \int_{E_{min}}^{E_{max}} K(E',E)\ \phi(E)\, dE, \tag{2}$$

which arises in several unfolding problems.

The composition of the kernel of this integral equation is of great importance in several solution methods. In practical applications accurate knowledge of the response functions is greatly desired, and experimentally verified numbers should be preferred. In many cases calculated response functions are more readily available, and are used when experimental data are not complete enough.

For health physics purposes at Berkeley seven activation detectors are widely used (GIL W 68), and their response functions are given in Fig. 11.1. In most cases fluxes as small as 1 n/cm^2 sec may be detected with these detectors.

Routti (ROU J 69a) has discussed in some detail the mathematical problems of finding a solution to the degenerate Fredholm equations obtained when activation detectors are used. In general no unique solution may be found without recourse to *a priori* physical information. Thus added constraints of nonnegativity, reasonable smoothness, and rough ideas of spectrum shape often produce adequate solutions.

An iterative technique, TELLY, which employs the on-line facilities of the CDC-6600 computer, has been developed at LBL and used for the analysis of high-energy neutron spectroscopy with few threshold detectors (GIL W 68). A cathode-ray-tube display is used with light-pen input. The user draws a

spectrum with the light pen on the screen after which the responses are computed for each detector. The solution is then altered by the user in order to get a better match between the computed and the measured responses. After a number of trials the responses are matched with an accuracy reflecting the experimental errors. The precedure also allows the user to apply any prior knowledge of the solution. Examples of TELLY solution spectra are shown in Fig. 11.2.

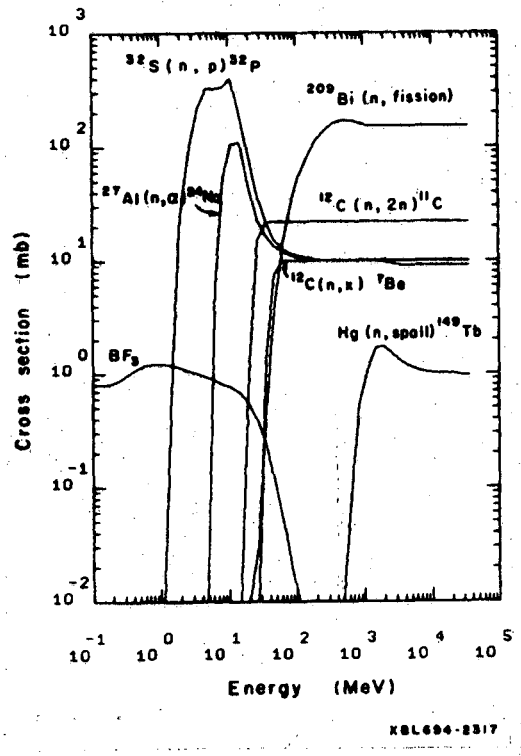

Fig. 11.1. Response functions of high-energy neutron-activation detectors.

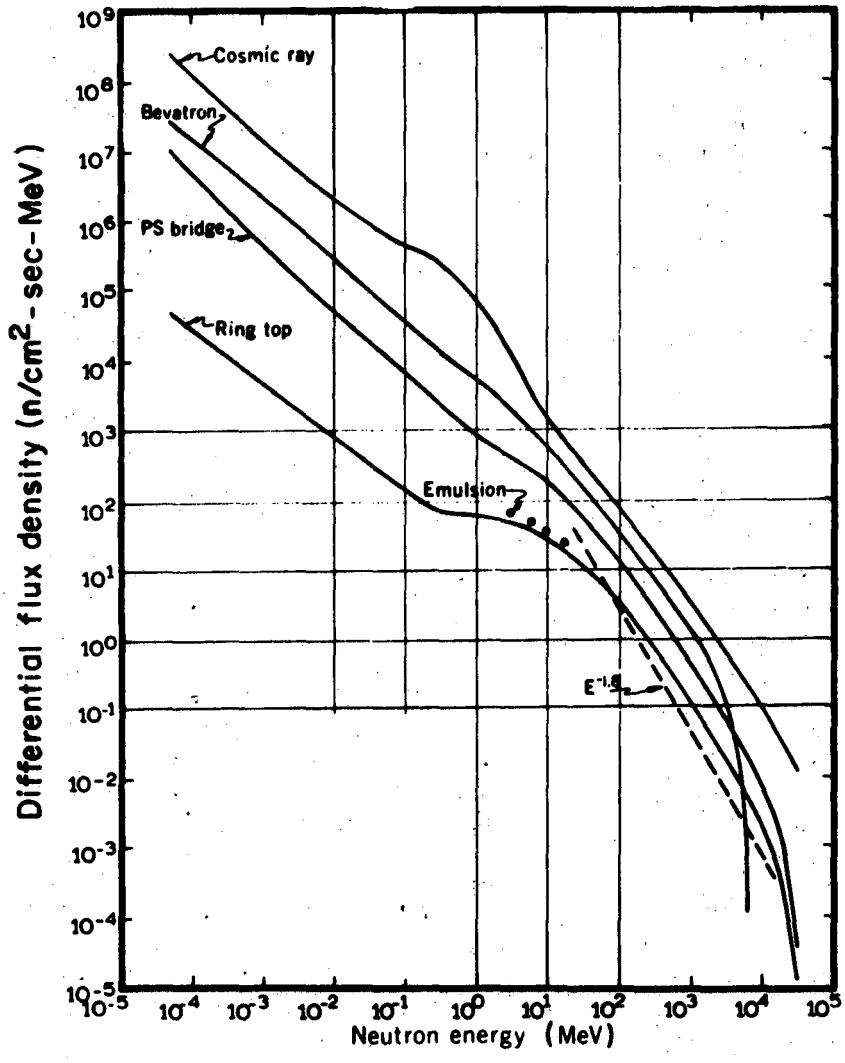

Fig. 11.2. Typical neutron spectra obtained from the TELLY program; Relative intensities of spectra in this figure are aribtrary.

With an increasing number of detectors with overlapping response curves it becomes increasingly difficult to make decisions on the direction of the next iteration. This and the slow speed restrict the applicability of TELLY to study of systems with relatively few response functions. In such cases, however, it performs quite well. Routti (ROU J 69b) has described a generalized least-squares method that permits combination, in a very flexible form, of prior information on the neutron spectrum and information contained in the measurement of the response. The method and computer program LOUHI have been subjected to vigorous mathematical tests, which show it to be capable of providing an adequate solution. LOUHI is best suited for use with a large computer and is of the closed-loop form requiring no intervention on the part of the operator in finding the required solution. Although LOUHI is now used in routine operations at Berkeley (because of its efficient use of computer time), the open-loop program TELLY is used in this experiment because of its graphic readout feature.

Both program types have been used with the same experimental data. TELLY was developed first and used for the analysis of most of the data; its procedures are described below in detail. We have more recently developed closed-loop methods that overcome the difficulty in finding a solution when more than a few measured responses are used. These techniques may also use as much *a priori* physical knowledge as is available, such as nonegativity, non-oscillatory behavior, and cutoff energy of the neutron spectrum. The solution spectrum that matches the measured responses under these constraints is then computed automatically. In all cases investigated the solutions thus found were essentially identical with those obtained by use of TELLY. In either technique, of course, it is essential to be able to match the responses within reasonable experimental accuracy. This has been found to be the case, both with the measured data and with calculated responses corresponding to a wide variety of test spectra.

Laboratory Procedure

TELLY enables the user to construct a neutron-energy spectrum that matches experimentally observed responses from a set of energy-sensitive neutron detectors. The program computes counting rates that would be observed from a given neutron spectral distribution. TELLY employs an open-loop technique to solve the problem, in the sense that the user must supply modifications to an input neutron spectrum in order to achieve the match with a set of observed count rates. The spectral shapes are modified by using a light pen. One simply draws a desired modification on the CRT display, and almost instantly can observe the changes in calculated detector count rates brought about by this spectral alteration.

The program works as follows: The energy region from 48 eV to 36 GeV is divided into 72 intervals of nearly equal width on a logarithmic energy scale. Response functions for each detector are explicitly specified for the 72 intervals.

An input spectrum is also specified for the same intervals. The program first displays this spectrum on the CRT. It then combines the spectrum, interval by interval, with each function in turn, to produce the counting rates that would be observed if the detectors were exposed to this flux distribution. The counting rates are also displayed on the CRT. The light pen can now be used to modify the CRT spectral shape, and thus generate a new set of detector count rates. Such trial count rates are compared with experimental count rates and this comparison is referred to response function shapes, to indicate the direction to be taken in successive spectral modifications. The process is continued until we have obtained the desired degree of match between observed and calculated count rates. That spectral distribution which produces the best match is then assumed to represent the experimental spectral distribution.

TELLY also computes the biological dose delivered by the trial spectra in each of the 72 energy intervals. Printed output includes a 72-point listing of differential flux spectrum, integral flux spectrum, and dose integral, and a log-log plot of the differential flux spectrum. For flux-to-dose conversion, we have adopted the analytic expressions relating neutron energy to dose equivalent suggested by Thomas (THO R 65), as shown in Table 11.I.

Table 11.I. Analytic expressions for dose equivalent vs neutron energy.

Energy range (MeV)	n/cm^2 sec equivalent to 1 mrem/h
$< 10^{-2}$	232
$10^{-2} - 10^{0}$	$7.20\ E^{-3/4}$
$10^{0} - 10^{1}$	7.20
$> 10^{1}$	$12.8\ E^{-1/4}$

About 2 hours of on-line computer time will be available to demonstrate the use of TELLY. Actual experimental data, including moderated BF_3 counter and aluminum, carbon, and bismuth fission threshold detectors, will be used in this study. The CRT displays will allow the student to explore the sensitivity of computed spectra to the presence or absence of any of the several detector responses, as well as the influence of errors in either input data or response functions.

Instructions concerning operation of the interactive CRT facility will be given at the beginning of the laboratory session, to enable the students to "run the show." Given sufficient student interest, additional on-line time can be scheduled for TELLY, as well as for the closed-loop program LOUHI.

REFERENCES

CONF-65 *Proceedings of the USAEC First Symposium on Accelerator Radiation Dosimetry and Experience, Brookhaven National Laboratory, 1965.*

GIL W 68 W. S. Gilbert, D. Keefe, J. B. McCaslin, H. W. Patterson, A. R. Smith, L. D. Stephens, K. B. Shaw, G. R. Stevenson, R. H. Thomas, R. D. Fortune, and K. Goebel, 1966 CERN-LRL-RHEL Shielding Experiment at the CERN Proton Synchrotron, UCRL-17941, Sept. 1968.

ROU J 69a J. T. Routti, Mathematical Considerations of Determining Neutron Spectra from Activation Measurements, in *Proceedings of the Second International Symposium on Accelerator Dosimetry and Experience, Stanford, November 5-7, 1969* CONF-691101.

ROU J 69b J. T. Routti, High-Energy Neutron Spectroscopy With Activation Detectors, Incorporating New Methods for the Analysis of Ge(Li) Gamma-Ray Spectra and the Solution of Fredholm Integral Equations (Ph.D. thesis), UCRL-18514, April 1969.

THO R 65 R. H. Thomas, The Radiation Field Observed Aroung High-Energy Nuclear Accelerators, in *Proceedings of XI International Congress of Radiology, Rome, September 22-28, 1966.*

Background Reading

G. Di Cola and A. Rota, Calculation of Differential Fast-Neutron Spectra from Threshold-Foil Activation Data by Least-Squares Series Expansion Methods, Nucl. Sci. Eng. *23*, 344 (1965).

Raymond Gold, Limitations in the Orthonormal Expansion of Neutron Spectra with Activation Measurements, Nucl. Sci. Eng. *20*, 493 (1964).

Raymond Gold, An Iterative Unfolding Method for Response Matrices, Argonne National Laboratory Report ANL-6984, 1964.

C. R. Greer, J. A. Halbleib, and J. V. Walker, A Technique for Unfolding Neutron Spectra from Activation Measurements, Sandia Laboratories Report SC-RR-67-746, Dec. 1967.

D. M. Hargreaves and G. R. Stevenson, Unfolding Neutron Energy Spectra Using the ALFIE Routine, Rutherford High Energy Laboratory Report RHEL/M 147, July 1968.

Arthur D. Kohler, Jr., An Improved Method of Neutron Spectroscopy Using Threshold Detectors (M.S. thesis), UCRL-11760, Dec. 1964.

W. N. McElroy, S. Berg, and G. Gigas, Neutron-Flux Spectral Determination by Foil Activation, Nucl. Sci. Eng. *27*, 533 (1967).

Keran O'Brien, Robert Sanna, Mary Alberg, James E. McLaughlin, and Sam A. Rothenberg, High-Energy Accelerator Shield Leakage Neutron Spectra, Nucl. Sci. Eng. *27*, 338 (1967).

David L. Phillips, A Technique for the Numerical Solution of Certain Integral Equations of the First Kind, J. Assoc. Comput. Mach. *9*, 84 (1962).

John C. Ringle, A Technique for Measuring Neutron Spectra in the Range 2.5 to 30 MeV Using Threshold Detectors (Ph.D. thesis), UCRL-10732, Oct. 1963.

N. E. Scofield, Iterative Unfolding, in *Proceedings of Symposium on Applications of Computers to Nuclear and Radiochemistry, Gatlinburg, Tennessee, 1962*, NAS-NS-3107.

Laodamas Sklavenitis, Sur la mesure at l'analyse des rayonnements de haute energie par détecteurs a activation, application à la dosimetrie (Ph.D. thesis), Saclay Report CEA-R-3376, Oct. 1967.

G. R. Stevenson, Neutron Spectrometry from 0.025 eV to 25 GeV, Rutherford High-Energy Laboratory Report RHEL/R 154, Nov. 1967.

Otto N. Strand and Ed. R. Westwater, Statistical Estimation of the Numerical Solution of a Fredholm Integral Equation of the First Kind, J. Assoc. Comput. Mach. *15*, 100 (1968).

Y. S. Su, Study of Scintillation Spectrometry: Unfolding Methods, Nucl. Instr. Methods *54*, 109 (1967).

A. N. Tihonov, Soviet Mathematics Doklady, Academy of Sciences of the URSS *151*, 510 (1963).

S. Twomey, On the Numerical Solution of Fredholm Integral Equations of the First Kind by the Inversion of the Linear System Produced by Quadrature, J. Assoc. Comput. Mach. *10*, 97 (1963).

FISSION-TRACK DETECTORS

HAROLD A. WOLLENBERG AND ALAN R. SMITH

Experiment 12

Purpose

The student is to be introduced to the practical techniques involved in the use of fission-track detectors. The effective fission cross section of neutrons emitted from a PuBe source is determined. If practicable, fission-track detectors may be exposed in a high-energy proton beam, or in the vicinity of an accelerator experiment's target assembly, to provide a measure of the effective flux and energy of the nucleons.

Theory

The fission-track method offers a reliable and accurate way to measure the flux of neutron and proton fields at energies above 50 to 100 MeV as well as low and intermediate energies.

The passage of an energetic, massively charged particle through a good insulating solid substance scatters away electrons from the particle track. The subsequent mutual repulsion of remaining positively charged ions forces them away from the path of the particle, leaving a cylindrical damaged region which can be enhanced by etching and made visible when viewed through an ordinary microscope. The response of a substance to charged particles depends on its specific ionization, dJ/dx, which is a function of (a) particle velocity, (b) the effective charge of the ionizing particle, (c) the ionization energy of the other electrons of the substance, and (d) the mass of the electron. For a given substance there is a critical value of specific ionization above which tracks form and below which there is no preferential etching of the solid. Thus if a thin foil of material which undergoes fission, spallation, or fragmentation when exposed to high energy nucleons is placed in close contact with suitable materials such as plastic, glass, or mica, the reaction products may be detected in the insulating material. Charged particles enter the insulator and may then be "materialized" by chemical etching. The number of tracks may be counted under a microscope, and the track density obtained used to provide a measure of the particle fluence incident upon the detector.

We prefer to use mica as a detector for two reasons: first, the diamond-shaped etch pits in mica are easier to distinguish than are the etch pits in plastic or glass; second, the etch pits in mica are caused only by fragments heavier than about mass 30, and are therefore related more closely to fission or other high-threshold energy interactions than are etch pits in plastic--where fragments of mass < 39 are registered. Mica and polycarbonate plastic detectors are compared on Table 12.I, and their characteristic etch pits are shown on Figs. 12.1 a and 12.1 b.

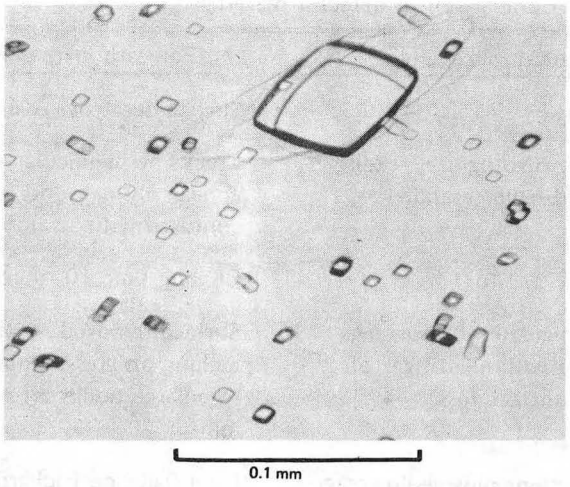

Fig. 12.1. (a) Diamond-shaped fission-track etch pits in a muscovite detector, exposed with a ^{232}Th foil to 3.6X10'' neutrons/cm^2 from a Pu-Be source. The large pit, from spontaneous fission of ^{238}U in the mica, was developed after a 16-h etch in 48% HF prior to the exposure. The smaller pits, from fission induced in the foil, were developed after a 30-min etch.

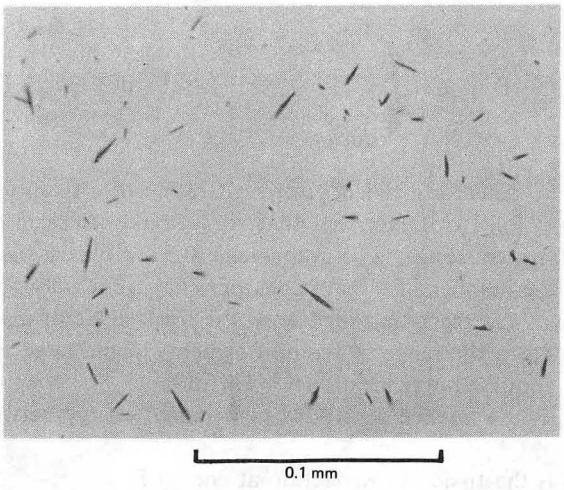

Fig. 12.1 (b) Fission tracks in Lexan polycarbonate plastic, developed after a 15-min etch in 28% KOH; the same exposure conditions as (a).

Table 12.1. Comparison of detector materials.

Natural muscovite	Polycarbonate plastic
Very durable	Surface scratches easily
Tracks easy to recognize, readily distinguished from scratches	Tracks perpendicular to surface appear as small dots, easily confused with scratches
Etching time 1/2 to 4 h	Etching time 10 to 15 min
Track size regulated by varying etching time without danger of appreciable surface loss	Surface removed readily as etching progresses; not possible to enlarge tracks after 15 to 20 min
Uranium content plus geologic age yield background tracks from spontaneous and induced fission.	Essentially no background tracks.

Foils of Th, U, Bi, Pb, Au, and Ta are suitable targets for high-energy nuclear detection (WOL H 69). In the experiment described here the fission of thorium is used to detect neutrons of a few MeV (RAG P 67).

The observed density of fission tracks per cm^2, D, is given by

$$D = \epsilon N \int_{E_{min}}^{E_{max}} \Phi(E)\, \sigma(E)\, dE, \qquad (1)$$

where ϵ is the detector efficiency for registration of a fission track from the target foil (for target foils that are infinitely thick in comparison with fission-fragment range; ϵ has the value 0.5 for binary fission),

N is the number of target nuclei per cm^2 from among which a fission fragment can reach and register in the track detector material (directly related to the range of fission fragments in the target material, for example, about 10 mg/cm^2 in a ^{232}Th foil),

$\Phi(E)$ is the fluence density of neutrons of energy between E and E + dE,

$\sigma(E)$ is the fission cross section at energy E,

and E_{min}, E_{max} are the minimum- and maximum-energy neutrons in the spectrum.

It is often convenient to express the integral of Eq. (1) in the form

$$\int \Phi(E)\, \sigma(E)\, dE = \Phi\, \langle \sigma \rangle , \qquad (2)$$

where Φ is the total neutron fluence ($\int \Phi(E)\, dE$) and $\langle \sigma \rangle$ is an effective cross section. Effective cross sections are usually determined by exposing the detector to a known neutron fluence.

Equipment

PuBe neutron source, 8.3×10^7 n/sec.

Thorium foils.

Lexan polycarbonate and muscovite mica detectors.

HF and KOH etching solutions.

Microscope with calibrated stage.

Laboratory Procedure

Prior to irradiation the mica detector should be pre-etched for approximately 15 hours. This allows the background fission-fragment tracks from spontaneous fission of ^{238}U contained in the mica to be developed to a size much larger than those produced during irradiation in conjunction with a fission foil.

The thorium foil detector assembly is exposed to a PuBe source for approximately 15 hours. After exposure, mica is etched in 48% HF at room temperature for at least 30 min. Lexan is etched in 28% KOH at 65° C for 15 to 20 min. Upon removal from the etching solutions mica should be washed in distilled water, Lexan in detergent solution followed by water. The etched detectors are scanned under a microscope (X500 is a convenient magnification). A sufficient number of fields should be scanned to give good statistical accuracy.

The neutron fluence, Φ, may be calculated from

$$\Phi = Qt/4\pi r^2 , \qquad (3)$$

where Q is the neutron source output in neutrons per sec,

t is the irradiation time,

and r is the effective source-to-detector distance (1.4 cm in the experiment).

Thus, finally, from Eqs. 1, and 2, and 3 we obtain

$$\langle \sigma \rangle = 4\pi r^2 D/\epsilon NQt, \qquad (4)$$

and substituting $r = 1.4$ cm, $\epsilon = 0.5$, $N = 2.7 \times 10^{19}$ nuclei/cm^2, we obtain finally $\langle \sigma \rangle = 1.82 \times 10^6$ (D/Qt) barns.

REFERENCES

RAG P 67 P. F. Rago and N. Goldstein, Thorium Fission Cross Sections for Neutrons Between 12.5 and 18 MeV Using Fission-Fragment Damage Tracks in Lexan, Health Phys. *13*, 654 (1967).

WOL H 69 H. A. Wollenberg and A. R. Smith, Energy and Flux Determinations of High Energy Nucleons, in *Proceedings of the Second International Symposium on Accelerator Dosimetry and Experience, held at Stanford, California, November 5-7, 1969.*

Background Reading

P. B. Price and R. M. Walker, Observations of Charged-Particle Tracks in Solids, J. Appl. Phys. *33* [12], 3400 (1962).

L. M. Kleppe and Sister Mary Rogers, Procedures for Finding Fission Tracks in Mica and Mylar, UCRL-17075, Aug. 1966.

R. L. Fleischer, E. L. Hubbard, P. B. Price, and R. M. Walker, Criterion for Registration in Dielectric Track Detectors, Phys. Rev. *156*, [2], (1967).

J. Hudis and S. Katcoff, High Energy Fission Cross Sections of U, Bi Au, and Ag Measured with Mica Track Detectors, Phys. Rev. 1969.